PhD Thesis

The evolution of the Urgonian platform in the Western Swiss Jura realm and its interactions with palaeoclimatic and palaeoceanographic change along the Northern Tethyan Margin (Hauterivian – earliest Aptian)

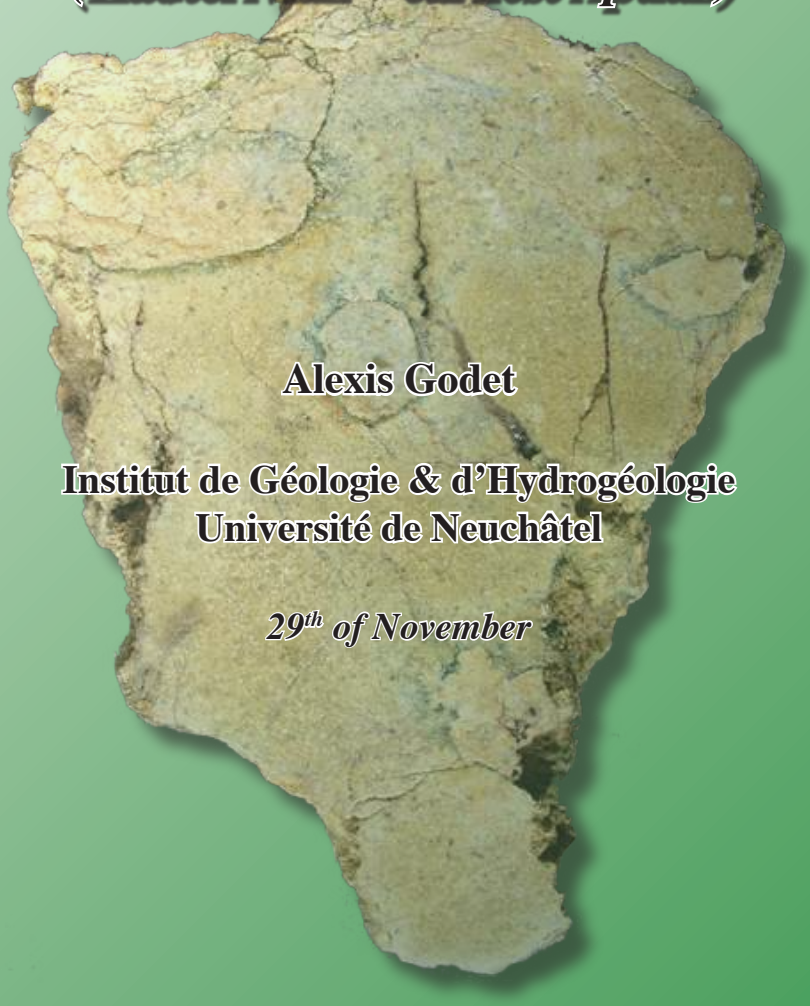

Alexis Godet

Institut de Géologie & d'Hydrogéologie
Université de Neuchâtel

29th of November

Jury

Prof. Karl B. Föllmi (PhD supervisor, Univ. Neuchâtel, CH)
Prof. Thierry Adatte (Univ. Neuchâtel, CH)
Prof. Hubert Arnaud (Univ. Grenoble, F)
Prof. Peter Stille (Univ. Strasbourg, F)
Dr. Annie Arnaud-Vanneau (Univ. Grenoble, F)
Dr. Virginie Matera (Univ. Neuchâtel, CH)
Dr. Eric de Kaenel (DeKaenel Paleoresearch, Neuchâtel, CH)

Université de Neuchâtel

FACULTE DES SCIENCES
Secrétariat-Décanat de la faculté
- Rue Emile-Argand 11
- CP 158
- CH-2009 Neuchâtel

IMPRIMATUR POUR LA THESE

The evolution of the Urgonian platform in the western Swiss Jura realm and its interactions with palaeoclimatic and palaeoceanographic change along the northern Tethyan margin (Hauterivian - earliest Aptian)

Alexis GODET

UNIVERSITE DE NEUCHATEL

FACULTE DES SCIENCES

La Faculté des sciences de l'Université de Neuchâtel,
sur le rapport des membres du jury

Mmes V. Matera, A. Arnaud-Vanneau (Grenoble),
MM. K. Föllmi (directeur de thèse), T. Adatte, E. de Kaenel (Neuchâtel),
H. Arnaud (Grenoble) et P. Stille (Strasbourg)

autorise l'impression de la présente thèse.

Neuchâtel, le 12 décembre 2006

Le doyen :
J.-P. Derendinger

UNIVERSITE DE NEUCHATEL
FACULTE DES SCIENCES
Secrétariat-décanat de la faculté
Rue Emile-Argand 11 - CP 158
CH-2009 Neuchâtel

The evolution of the Urgonian platform in the Western Swiss Jura realm and its interactions with palaeoclimatic and palaeoceanographic change along the Northern Tethyan Margin (Hauterivian – earliest Aptian)

Thèse présentée à la Faculté des Sciences
Institut de Géologie & d'Hydrogéologie, Université de Neuchâtel
Pour l'obtention du grade de docteur ès Sciences

Par

Alexis Godet

Acceptée sur proposition du jury :

Prof. Karl B. Föllmi *(directeur de thèse, Univ. Neuchâtel, CH)*
Prof. Thierry Adatte *(rapporteur, Univ. Neuchâtel, CH)*
Prof. Hubert Arnaud *(rapporteur, Univ. Grenoble, F)*
Prof. Peter Stille *(rapporteur, Univ. Strasbourg, F)*
Dr. Annie Arnaud-Vanneau *(rapporteur, Univ. Grenoble, F)*
Dr. Virginie Matera *(rapporteur, Univ. Neuchâtel, CH)*
Dr. Eric de Kaenel *(rapporteur, DeKaenel Paleoresearch, Neuchâtel, CH)*

Soutenue le 29 Novembre 2006

Université de Neuchâtel
2006

TABLE OF CONTENTS

ACKNOWLEDGMENTS 9

KEYWORDS 11

ABSTRACT 11

MOTS-CLÉS 12

RÉSUMÉ 12

CHAPTER A. GENERAL INTRODUCTION *15*

A.1. THE EARLY CRETACEOUS TIMES IN THE TETHYAN REALM 17

A.1.1. Carbonate platforms - witnesses of environmental change 17
A.1.2. The climate during the Early Cretaceous: controlling factors and main perturbations 18
A.1.3. General statements 22
A.1.4. References 22

A.2. THE HISTORICAL SUCCESSION IN THE NEUCHÂTEL AREA 27

A.2.1. Original definition and evolution of the concept 27
A.2.2. The controversy arising from previous biostratigraphical data and sequence stratigraphy schemes 30
A.2.3. Aims of the present thesis 31
A.2.4. References 32

CHAPTER B. DATING THE EARLY CRETACEOUS (HAUTERIVIAN – BARREMIAN) SEDIMENTARY SUCCESSION IN THE VICINITY OF NEUCHÂTEL *35*

B.1. THE WESTERN SWISS JURA : GEOLOGICAL SETTING 39

B.1.1. Paleogeography 39
B.1.2. Structural setting 40
B.1.3. References 40

B.2. A CONTINUOUS SEDIMENTARY RECORD? 43

B.2.1. Definition of the microfacies 43
B.2.2. Key surfaces 48
B.2.3. The Eclépens section 49
B.2.3.1. Description of the section 49

B.2.3.2. Sequence stratigraphy of the Eclépens section 52
B.2.4. Identification of the main sequence boundaries in the Western Swiss Jura 53
B.2.4.1. The Gorges de l'Areuse section 53
B.2.4.2. The Neuchâtel composite section 56
B.2.4.3. The Vaumarcus section 57
B.2.4.4. The Buttes section 60
B.2.5. Correlation of the different sections – Conclusions 60
B.2.6. References 63

B.3. Biostratigraphy of the Urgonian from the Western Swiss Jura 65

B.3.1. Introduction 65
B.3.2. Orbitolinids 65
B.3.3. Dasycladacean algae 66
B.3.4. Rudists 66
B.3.5. Echinoids 68
B.3.6. Brachiopods 68
B.3.7. Dinoflagellates 69
B.3.8. Ammonites 70
B.3.9. Calcareous nannofossils 70
B.3.10. Main conclusions 73
B.3.11. References 74

B.4. Geochemical and paleoenvironmental constraints on the rise of the Urgonian platform in the Western Swiss Jura 77

B.4.1. Introduction 78
B.4.2. Geographical and geological setting 79
B.4.3. Methods: $^{87}Sr/^{86}Sr$ stratigraphy 80
B.4.3.1. Brachiopod sampling and preparation 80
B.4.3.2. Analyses performed to constrain the diagenetic state of the shells 80
B.4.3.3. Strontium isotope measurement 81
B.4.3.4. Phosphorus analyses 81
B.4.4. Results 81
B.4.4.1. Preservation of the shells and rostra 81
B.4.4.2. $^{87}Sr/^{86}Sr$ results from the Western Swiss Jura and the Vocontian Trough 82
B.4.4.3. Evolution of the Phosphorus content in the Western Swiss Jura 83
B.4.5. Discussion 85
B.4.5.1. $^{87}Sr/^{86}Sr$ dating 85
B.4.5.2. Environmental constraints on the rise of the Urgonian formation of the Western Swiss Jura 87
B.4.5.2.1. Changes in the type of ecological association: evidence from microfacies 87
B.4.5.2.2. Environmental parameters constraining the type of carbonate factory: example from Phosphorus Mass Accumulation Rates and detrital inputs 88
B.4.6.Conclusions 89
B.4.7.Acknowledgements 89
B.4.8.References 90

B.5. K-Ar dating of glauconitic-rich levels from the Western Swiss Jura 95
B.5.1. Introduction 95
B.2.5.2. Methods and results 95
B.2.5.2.1. Glaucony separation 95
B.2.5.2.2. Mineralogy of separated grains by means of XRD 96
B.2.5.2.3. Potassium and Argon measurements 97
B.2.5.3. Discussion 98
B.2.5.4. Conclusions and outlook 98
B.5.5. References 99

B.6. Correlation of the Urgonian Formations from the Western Swiss Jura with other regions of the Tethys 101

B.7. The Western Swiss Jura: Main Conclusions 107

Chapter C. Formal definition of the Eclépens Formation from the Western Swiss Jura 109

C.1. Introduction 111
C.2. Geological and geographical settings 112
C.3. The Eclépens Formation: Formal definition 112
C.3.1. "Urgonien Jaune" and "Urgonien Blanc": main problems 112
C.3.2. Sedimentological definition of the lower and upper boundaries 114
C.3.3. Sedimentological features of the Eclépens Formation 115
C.4. Correlation of the Western Swiss Jura with other areas of the Northern Tethyan margin 118
C.5. Acknowledgments 118
C.6. References 118

Chapter D. From the platform to the basin: environmental constraints on the rise of the Urgonian platform 123

D.1. Enrichment of redox-sensitive trace metals (U, V, Mo, As) associated with the late Hauterivian Faraoni oceanic anoxic event 127

D.1.1. Introduction 127
D.1.2. Studied sections and palaeogeogra-phic setting 128
D.1.3. Methods 129
D.1.4. Results 133
D.1.4.1. Redox-sensitive trace elements 133
D.1.4.1.1. The Fiume-Bosso section 133
D.1.4.1.2. The Veveyse de Châtel-St. Denis section 134
D.1.4.1.3. The Angles section 135
D.1.4.2. Total organic carbon (TOC) 136
D.1.5. Discussion 136
D.1.5.1. Comparison between the three sections 136

D.1.5.2. Behaviour of U, V, Mo, Co, and As 137
D.1.5.3. Redox conditions during the Faraoni event 138
D.1.5.4. Local oxygen-deficient conditions below the Faraoni Level 138
D.1.5.5. Enrichment factors 138
D.1.5.6. Chemostratigraphic tools 139
D.1.5.7. Initiating factors of the Faraoni event 140
D.1.6. Conclusions 140
D.1.7. Acknowledgements 141
D.1.8. References 141

D.2. Evolution of the marine stable carbon-isotope record during the Early Cretaceous: A focus on the Late Hauterivian and Barremian in the Tethyan realm 145

D.2.1. Introduction 146
D.2.2. Geological setting 146
D.2.2.1. The sections of Fiume Bosso and Gorgo a Cerbara 146
D.2.2.2. The section of the Veveyse de Châtel-Saint-Denis 147
D.2.2.3. The section of Angles 147
D.2.3. Methods 147
D.2.4. Note on the ammonite biostratigraphy used 147
D.2.5. Results 148
D.2.5.1. The sections of Fiume Bosso and Gorgo a Cerbara 148
D.2.5.2. The section of the Veveyse de Châtel-Saint-Denis 148
D.2.5.3. The section of Angles 149
D.2.6. Discussion 151
D.2.6.1. Stable isotopes and diagenesis 151
D.2.6.2. Evolution of the $\delta^{13}C$ record during the late Hauterivian and Barremian 153
D.2.6.3. Evolution of the $\delta^{18}O$ record during the late Hauterivian and Barremian 155
D.2.6.4. Possible mechanisms driving the evolution of the $\delta^{13}C$ values during the late Hauterivian and Barremian 157
D.2.6.5. Quantification of the carbonate platform exportation and its influence on the pelagic record 158
D.2.7. Conclusions 160
D.2.8. Acknowledgments 160
D.2.9. References 160

D.3. The late Hauterivian Faraoni oceanic anoxic event in the western Tethys: Evidence from phosphorus burial rates 165

D.3.1. Introduction 166
D.3.2. Geological setting 166
D.3.3. Methods 167
D.3.3.1. Phosphorus analyses 167
D.3.3.2. Age model 168
D.3.4. Results 171
D.3.4.1. The Fiume-Bosso section 171

D.3.4.2. The Veveyse de Châtel-St. Denis section 171
D.3.4.3. The Angles section 171
D.3.4.4. The Gorgo a Cerbara section 171
D.3.5. Discussion 172
D.3.5.1. Phosphorus accumulation 172
D.3.5.2. The C/P molar ratio 176
D.3.5.4. The Faraoni oceanic anoxic event 177
D.3.5.5. The attenuated $\delta^{13}C$ signature during the late Hauterivian and early Barremian 180
D.3.5.6. The carbonate platform drowning episode during the latest Hauterivian and early Barremian: consequence of the Faraoni event? 182
D.3.6. Conclusions 182
D.3.7. Acknowledgments 183
D.3.8. References 183

D.4. Platform-induced clay-mineral fractionation along a northern Tethyan basin-platform transect: implications for the interpretation of Early Cretaceous climate change (Late Hauterivian-Early Aptian) 189

D.4.1. Introduction 190
D.4.2. Geological setting and location of the studied sections 190
D.4.3. Methods 191
D.4.3.1. Rock-Eval analysis 191
D.4.3.2. XRD analysis 192
D.4.3.2.1 Bulk-rock analysis 192
D.4.3.2.2. Clay mineral analysis 192
D.4.4. Results 193
D.4.4.1. The Angles and Combe-Lambert sections 193
D.4.4.1.1. XRD analysis 193
D.4.4.1.2. Rock Eval analysis 195
D.4.4.2. The Cluses section 195
D.4.4.3. The Eclépens section 197
D.4.5. Discussion 200
D.4.5.1. Reliability of the clay-mineral record 200
D.4.5.1.1. Angles and Combe-Lambert 202
D.4.5.1.2. Cluses and Eclépens 202
D.4.5.2.Climate change during the Late Hauterivian – Early Aptian 203
D.4.5.3. Kaolinite evolution from the Vocontian Trough to the western Swiss Jura: Evidence for differential settling 204
D.4.6. Conclusions 208
D.4.7. Acknowledgements 208
D.4.8. References 209

D.5. Interactions between environmental change and shallow-water carbonate build-up along the northern Tethyan margin and their impact on the Early Cretaceous carbon-isotope record 213

D.5.1. Introduction 213

D.5.2. Methodology 216
D.5.3. Evolution of the Early Cretaceous northern Tethyan carbonate platform succession in the Helvetic Alps 216
D.5.4. An ammonite-calibrated $\delta^{13}C$ reference record from southeastern France....218
D.5.5. Discussion and interpretations 220
D.5.5.1. Correlation between episodes of platform demise and paleoceanographic change....220
D.5.5.2. Changes in trophic levels and changes in platform ecology and morphology 221
D.5.5.3. Quality and correlation of the northern Tethyan $\delta^{13}C$ record....222
D.5.5.4. Potential mechanisms driving the marine $\delta^{13}C$ record 222
D.5.5.5. Changes in the ecology and geometry of the northern Tethyan carbonate platform and its influence on the northern Tethyan $\delta^{13}C$ record 225
D.5.5.6. Correlation of changes in carbonate platform ecology along the northern Tethyan margin and trends in the northern Tethyan $\delta^{13}C$ record 227
D.5.6. Conclusions 229
D.5.7. Acknowledgements....229
D.5.8. References....230

D.6. The hemipelagic and pelagic record: main conclusions 237

Chapter E. Main Conclusions *239*

E. 1. The Western Swiss Jura 241
E.2. Paleoceanographic impact of the rise of the Urgonian Platform....241
E.3. Integration of the Western Swiss Jura into the geochemical and sedimentological history of the Northern Tethyan margin 243
E.4. Outlook....245
E.5. References 246

Annexe 1. Oxygen and Carbon Stable-Isotope Data ***247***

Annexe 2. XRD Data (Bulk Rock and Clay Fraction) ***253***

Annexe 3. Cathodoluminescence and SEM Plates ***277***

Annexe 4. Other Manuscripts related to the SFN Projects n°2100-067807/1 and 200020-105206/1 ....***303***

An. 4.1. Biostratigraphy, sedimentology and sequence stratigraphy of the latest Hauterivian – Early Barremian drowning episode of the Northern Tethyan margin (Altmann Member, Helvetic nappes, Switzerland).... 305

An.4.1.1. Introduction....306
An.4.1.2. Geological setting....306
An.4.1.3. Materials and methods....308
An.4.1.4. Biostratigraphy 310
An.4.1.5. Microfacies 311
An.4.1.5.1. HF0 (marls; marls - micrite)....311

An.4.1.5.2. HF1 (mudstone or wackestone; spicule-rich biomicrite) 313
An.4.1.5.3. HF2 (packstone; biopelmicrite) 313
An.4.1.5.4. HF3 (packstone; crinoid-rich biopelmicrite) 313
An.4.1.5.5. HF4 (packstone or grainstone; crinoïdal and bryozoan biomicrite or biosparite) 313
An.4.1.5.6. HF5 (grainstone; coarse bio-sparite with rounded grains) 313
An.4.1.5.7. HF6 (grainstone; oosparite or oobiosparite) 313
An.4.1.5.8. HFa (glauconitic-rich sandstone) 314
An.4.1.5.9. HFb (wackestone or packstone; biomicrite) 314
An.4.1.5.10. HFc (phosphatized hardground) 314
An.4.1.6. Macroscopic sedimentological aspects 314
An.4.1.6.1. Highly reduced sections or hiati 314
An.4.1.6.2. Sections with a phosphatized hardground at their base 315
An.4.1.6.3. Sections with phosphatic nodules 315
An.4.1.6.4. Expanded sections 315
An.4.1.6.5. Ammonite biostratigraphy in the Altmann Member 317
An.4.1.7. Sequence- stratigraphic interpretation 317
An.4.1.8. Depositional model 320
An.4.1.9. Conclusions 323
An.4.1.10. Acknowledgments 324
An.4.1.11. References 324

An.4.2. New data on the age of the installation of Urgonian-type carbonates along the northern Tethyan margin: Biostratigraphy of the Chopf Member (Helvetic Alps, eastern Switzerland) 329

An.4.2.1. Version française abrégée 330
An.4.2.1.1. Introduction 330
An.4.2.1.2. Cadre géographique et géolo-gique 330
An.4.2.1.3. Sedimentologie et biostratigra-phie 330
An.4.2.1.4. Discussion 330
An.4.2.1.5. Conclusions 331
An.4.2.2. Introduction 331
An.4.2.3. Geographical and geological setting 332
An.4.2.4. Sedimentology and bio-stratigraphy 332
An.4.2.5. Discussion 334
An.4.2.6. Conclusions 335
An.4.2.7. Acknowledgments 335
An.4.2.8. References 335

An.4.3. The Hauterivian - Barremian of the Western Swiss Jura around Neuchâtel 339

An.4.3.1. Introduction: the formations from the early Cretaceous of the western Swiss Jura 339
An.4.3.1.1. Developments in the historical definition 339
An.4.3.1.2. Recent developments 340
An.4.3.2. First stop: Gorges de l'Areuse 342
An.4.3.2.1. Location 342

An.4.3.2.2. Previous works 342
An.4.3.2.2.1. Description of the section at Boudry.... 343
An.4.3.2.2.2. Microfacies and sequence stratigraphy of the Boudry section 344
An.4.3.2.2.3. Mineralogy of the Boudry section 346
An.4.3.2.3. The "Pierre Jaune de Neuchâtel" – "Urgonien Jaune" transition 347
An.4.3.2.3.1 Description of the section 347
An.4.3.2.3.2. Microfacies and sequence stratigraphy 348
An.4.3.2.3.3. Mineralogy 349
An.4.3.3. Second stop: Eclépens (Holcim quarry)....349
An.4.3.3.1. Location....349
An.4.3.3.2. The "Pierre Jaune de Neuchâtel" – "Urgonien Blanc" succession at Eclépens 349
An.4.3.3.2.1. Description of the section 349
An.4.3.3.2.2. Microfacies and sequence stratigraphy 350
An.4.3.3.2.3. Mineralogy 354
An.4.3.4. Dating the Urgonian Limestones from the Neuchâtel area....354
An.4.3.4.1. Strontium isotopes 354
An.4.3.4.2. K-Ar radiochronology 358
An.4.3.4.3. Clay mineral correlation 358
An.4.3.5. Conclusion 359
An.4.3.6.Acknowledgements 359
An.4.3.7. References....359

***Annexe 5. Paleontological Reports* 361**

***An.5.1. Dinoflagellates by Dr. E. Ghasemi-Nejad*....** 363

***An.5.2. Taxonomic list of nannofossils (summer 2006, Dr. E. de Kaenel)*....** 371

***An.5.3. Results of the blind test on nannofossils from Eclépens*....** 373

***Annexe 6. Abstracts for Congress* 387**

ACKNOWLEDGMENTS

For me, acknowledgements are maybe one of the most difficult parts to write in a manuscript: I am afraid to forget somebody, I do not know by who to begin, things like that. But well, let's jump into this…

With no doubts at all, I am really grateful to Prof. Karl Foellmi for all the things he did for me during these four years spent at Neuchâtel. First, he believed in me and took me in his team, he was always here to answer my questions, and then reminded me to focus my minds. He was also here when the results of my research were discussed, sometimes in a strange and hard way… Karl, just remember this "blind-test day" at Eclépens, in April 2006… For all of that, and also for all I forgot, *"viele Danke!"*

I also want to thank Prof. Thierry Adatte for all the scientific discussions we had, and also for the "non-scientific" ones! Thanks for having shared your knowledge on the Neuchâtel area, I saved many precious hours. Thanks also for having introduced me to the so interesting and delicate art of the XRD analysis.

Virginie, Virginie… The "ICP-Queen" Dr. Virginie Matera was there to answer to my interrogations about chemistry, to help me during laboratory works dealing with ICP-MS… And also to remind me the pleasures "made in Ch'Nord and Belgium"… *Ch'ti, Goudale, Picon and Grimbergen,* sweet names to my mind and throat ;-)

I also want to acknowledge Prof. Peter Stille (Strasbourg, France) and Dr. Eric de Kaenel (Neuchâtel), for having performed strontium-isotopes analysis and K-Ar dating, and nannofossils determinations, respectively, and for having accepted to be part of my jury.

I want to express all my gratitude to Dr. Annie and Prof. Hubert Arnaud from Grenoble, for having shared their knowledge of the sequence stratigraphy and of the Urgonian from the Vercors and the Western Swiss Jura, and for having accepted to be in my jury. I really appreciated the very constructive discussions we had here at Neuchâtel or on the field in the Vercors.

During the last four years, the Swiss National Fund financially supported the reseach of my colleague, Stéphane Bodin, and I (projects n°2100-067807/1 and 200020-105206/1). I would like to thank them for their grant that allowed fieldwork and laboratory analyses, amongst many other things.

Just after this "official part of the acknowledgements", there are some very important persons I want to acknowledge. First, I want to thank Stéphane, my colleague and friend, for all these discussions about the secrets of the Urgonian, of the Vocontian Trough and geology in general, and so many other things. Of course our collaboration was very fruitful from a scientific point of view, but it is also exceptional that our friendship lived, lives and will live outside the University. I know that it was hard for you to support me sometimes, but if I weren't as I am, it wouldn't have been so funny, would it?

These four years at Neuchâtel wouldn't have been so nice and coloured without the presence of Mary-Alix. You knew what to do and to say when I had doubts or when I was down, and we spent so many nice times that I can't find the words to tell you how grateful I am. Just one thing: don't change anything, you are so special and excellent as you are…

The work wouldn't have been so pleasant without the presence of Haydon in the office ("Ahwoken!"). I really want to thank you for having taught me so useful English words (I hope I'll soon have the opportunity to use them, but not in this manuscript!), and also for having supported me during this period. Good luck for your future!

I would never have succeeded without the technical support of several persons. First, Tiffany Monnier helped Stéphane and I during the preparation of samples for the ICP-MS analysis, and Philipp Steinmann explained us how to overcome the capricious Rock Eval. André Villard ("faut gratter Dédé…") gave the best of him to prepare thin sections, easy ones as well as hard ones… Remember the brachiopods' shells Dédé, what a pleasure… I do not forget the work done by Laureline Scherler and Laurent Chalumeau concerning the preparation of samples from Angles in view of XRD analysis. And finally Eli, Gianfranca and Sabine, the three cute ladies of the Institute, I have no words to qualify my gratitude for you… I thank you all.

I hope I won't forget anybody in the following, but I want to express my best feelings to all my other colleagues, especially to Charles, Laure, Stafele, Erwan, Beni, Flurin, Pascal, Raul, Claire, and Laurent… And also to all the students I met during these four years at Neuchâtel.

My life in Neuchâtel wasn't restricted to the Institute of Geology, that's why I want to thank all the people I met at Colombier, and elsewhere, in particular Beat, Jean, Edmond, Mireille, Jo, Martial and "La Reine Claude". I have a very special thought for Rachel and her "Galinette" Gaëlle, for having shared the "key-ring of the cat's paradise" during the last two years, for all the laughters we had together, and for the rides on her "horse of fire!"

What about my friends abroad? Of course we met only once a year, but you were always on the back of my mind: Ingrid, Cécile (I won our challenge, just have a look below ;-)), Maud, Sandrine, Natacha, Pierre, Xavier and Benji. Thanks for having taking me away from my work during the weekends we had together in Montpellier, Merueil and Cavaillon. I am also grateful to Kevino for the so funny card tournaments we had… Last but not least, I want to thank George for having visited me in Switzerland, and then invited me in your country; it was a very nice trip, especially in Transylvania… *"Pe foarte curînd, prietenul meu din Romania!"*

Of course, I would never succeeded with this thesis if Chantal and Daniel never met and never get married, so, my dear parents, thank you for having created me as I am, I couldn't have dreamt of so attentive and bright parents. Thanks for having put your trust in me and for having brought your support, without any failure. The same for my sister Barbara (my so lovely and cute grasshopper!) and my brother Edwin (you are taller than me, but you will always be my little brother)… Even if I do not show it, I love you all from the deepest part of my heart, sincerely…

To all my family, the ones who are still here as well as the one who is already gone, I reserve a special part in my mind: Zezette & Marcel, Louise, Patou & Silvère, Nicole & Hervé, Christiane & Alain, Jean-Marc & Chantal, and also all my cousins, Mathieu, Benjamin, Jordan, Lucas, Axel, Salomé & Arthur, and also Danièle and Jean-Michel. Thanks for the times we had during these last years, sometimes too short.

Have a nice reading!

To "B, C, D, E", your "A" never stopped thinking of you…

KEYWORDS

Western Swiss Jura; Northern Tethyan margin; Urgonian; Barremian; stratigraphy; sedimentology; mineralogy; sequence stratigraphy; C, O and Sr isotopes.

ABSTRACT

During more than twenty years, a controversy appeared about the age of the Urgonian formation (lower Urgonien Jaune and upper Urgonien Blanc) from the Western Swiss Jura. Depending on previous works, these formations are considered to be Late Hauterivian or Late Barremian in age. This divergence mainly results from different calibration of orbitolinids distribution, as well as divergent sequence stratigraphic models. Because these formations, as well as the underlying Pierre Jaune de Neuchâtel, are linked to the historical succession for the Hauterivian stage, we developed new approaches in order to date, as precisely as possible, the Urgonian formations from the Western Swiss Jura.

The high reworking present at the base of the Urgonien Jaune implied that the biostratigraphy did not give an accurate age model. Moreover, biostratigraphical dating can greatly differ as a function of the considered taxon and the involved specialists. Consequently, we developed sedimentological and geochemical approach. The boundary between the Pierre Jaune de Neuchâtel and the Urgonien Jaune is clearly marked by erosional and reworking processes, suggesting the presence of a sedimentary gap. Indeed, strontium-isotope dating performed on rhynchonellids shells rather indicate a Barremian age for both the Urgonien Jaune and the Urgonien Blanc. The comparison of the phosphorus mass accumulation rates between the Western Swiss Jura and (hemi-)pelagic sections from the Northern Tethyan margin helped to precise this age to the Late Barremian, as oligotrophic conditions allowing the rise of the Urgonian carbonate platform in a photozoan mode only occurred during this period. Finally, sequence stratigraphic correlation of the Western Swiss Jura with the Helvetic realm, the Subalpine Chains and the Northern Vercors implied that the base of the Urgonien Jaune is characterized by the stacking of several sequence boundaries. Moreover, there is no evidence for an other break within the geological record in the Western Swiss Jura after the sequence boundary B3 of the late Early Barremian *Coronites darsi* ammonite zone. In addition, these results are coherent with the fact that the rise of the Urgonian platform began from the maximum flooding surface of the depositional sequence B3 upward in the Northern Tethys. Subsequently, the Urgonian of the Western Swiss Jura may correspond to the lower Urgonian and to the lower Schrattenkalk formations of the Northern Vercors and the Helvetic realm, respectively.

The stable isotopes study of several (hemi-)pelagic sections of the Northern Tethyan margin and their mineralogical contents revealed that the Urgonian platform had a role in paleoceanographic changes that occurred during the Late Barremian. Whereas the $\delta^{13}C$ curve exhibits negligible changes during the latest Hauterivian – Early Barremian, it is shifted toward more positive values from the sequence boundary B3 upward. This behaviour may be linked to the production and the export of ^{13}C-enriched material by carbonate platform through the production of aragonite by benthic organisms. Moreover, the correlation of the kaolinite content along a platform to basin transect through the Northern Tethyan margin showed that the main part of the Barremian was characterized by a humid climate, whereas a seasonally-contrasted climate dominated during the Hauterivian. This correlation also highlighted a differential settling of clay particles, as high amounts of kaolinite were measured in shallow-water carbonates of the Neuchâtel area, whereas hemipelagic limestones from the Vocontian Trough were depleted in this mineral.

Thanks to this multidisciplinary approach, the Western Swiss Jura is better integrated within the history of the Northern Tethyan margin. Finally, interactions between carbonate platforms and basinal environments are clearly highlighted.

MOTS-CLÉS

Jura Suisse occidental ; marge nord téthysienne ; Urgonien ; Barrémien ; stratigraphie ; sédimentologie ; minéralogie ; stratigraphie séquentielle ; isotopes du carbone, de l'oxygène et du strontium.

RÉSUMÉ

Durant les vingt dernières années, une controverse concernant l'âge des formations urgoniennes du Jura neuchâtelois (Urgonien Jaune et Urgonien Blanc) est apparue. En fonction des groupes de travail, ces formations sont attribuées soit au Barrémien supérieur, soit à l'Hauterivien supérieur. Cette différence repose principalement sur des calibrations différentes des échelles d'orbitolinidés, ainsi que sur des découpage séquentiels divergents. Puisque ces formations, ainsi que la Pierre Jaune de Neuchâtel sous-jacente, sont liées à la succession historique de l'Hauterivien, et comme elles représentent la partie proximale de la plateforme carbonatée qui s'est développée sur la marge nord téthysienne durant le Crétacé inférieur, nous proposons de développer de nouvelles approches afin de préciser l'âge de l'Urgonien du Jura Suisse occidental.

A la base de l'Urgonien Jaune, la présence de remaniement induit des résultats biostratigraphiques plus ou moins contradictoires : les âges obtenus par cette approche peuvent parfois grandement différer selon le taxon employé. C'est pourquoi nous développâmes une approche combinant sédimentologie et géochimie. La limite Pierre Jaune de Neuchâtel – Urgonien Jaune est à la fois érosive et marquée par le remaniement, suggérant la présence d'une lacune sédimentaire. De plus, les isotopes du strontium mesurés sur des coquilles de rhynchonellidés indiqueraient un âge Barrémien. La comparaison de l'évolution du phosphore entre la fosse Vocontienne et le Jura neuchâtelois permet de préciser ce premier résultat, puisque des conditions oligotrophiques permettant la mise en place de la plateforme Urgonienne (caractérisée par un écosystème photozoaire) n'apparaissent que dans le Barrémien supérieur. Finalement, la corrélation par stratigraphie séquentielle de coupes du Jura neuchâtelois avec les successions sédimentaires des nappes Helvétiques, des Chaînes Subalpines et du Vercors septentrional implique que plusieurs limites de séquence sont présentes à la base de l'Urgonien Jaune. Qui plus est, il n'y aurait pas d'interruption de l'enregistrement sédimentaire au-dessus de la limite de séquence B3 de la zone à *Coronites darsi* (Barrémien inférieur terminal), située dans la partie basale de l'Urgonien Jaune. Finalement, ces résultats sont en accord avec l'âge de la mise en place de la plateforme urgonienne, qui est datée de la surface d'inondation maximale de la séquence B3 dans d'autres régions nord téthysiennes. Ainsi, l'Urgonien Blanc du Jura neuchâtelois correspondrait à la masse Urgonienne inférieure du Vercors, et au Schrattenkalk inférieur des nappes helvétiques.

L'évolution des isotopes stables du carbone ainsi que de l'assemblage minéralogique de plusieurs coupes du domaine (hémi-)pélagique de la marge nord téthysienne révèle que la plateforme urgonienne a joué un rôle non négligeable dans le développement de changements paléocéanographiques qui se déroulèrent dans cette partie de la Téthys durant le Barrémien. Alors que l'évolution du $\delta^{13}C$ est relativement monotone durant l'Hauterivien supérieur et le Barrémien inférieur, elle montre un changement vers des valeurs plus positives à partir de la limite de séquence B3. Ce comportement serait lié à la production et à l'export de matériel enrichi en ^{13}C par des organismes benthiques présents sur les plateformes. De plus, la corrélation des teneurs en kaolinite le long d'un profil allant de la plateforme jusqu'au bassin montre que la majeure partie du Barrémien était caractérisée par un climat humide, alors que l'Hauterivien serait plutôt dominé par un climat à saisons contrastées. Cette corrélation met également en évidence une sédimentation différentielle des particules argileuses, en particulier de la kaolinite dont les plus fortes teneurs sont observées en domaine proximal alors que les calcaires hémipélagiques de la

fosse Vocontienne montrent des taux nettement inférieurs.

Grâce à cette approche multidisciplinaire, le Jura Suisse occidental est désormais mieux intégré dans l'histoire de la marge nord téthysienne. Finalement, cette étude contribue à la mise en évidence d'une interaction entre plateforme et bassin dans la mise en place de changements paléocéanographiques.

CHAPTER A.

GENERAL INTRODUCTION

Hardground at the base of the Marnes d'Uttins (quarry of Eclépens, VD, Switzerland)

A.1. THE EARLY CRETACEOUS TIMES IN THE TETHYAN REALM

A.1.1. Carbonate platforms - witnesses of environmental change

Carbonate platforms are biologically induced sedimentary edifices which display a wide range of faunistic and floristic diversities. They develop in different geological settings, close to as well as remote from continents (*e.g.*, Bosence, 2005). The type of organisms present in these ecosystems plays a role in the architecture of the platform: heterozoan associations (mainly bryozoans, sponges and crinoids during the Early Cretaceous; Föllmi *et al.*, 1994; James, 1997) led to the formation of ramp morphologies, whereas photozoan assemblages composed of light-dependant organisms (corals, rudists, stromatoporoids and green algae during the Early Cretaceous; Föllmi *et al.*, 1994; Pomar, 2001) are rather present in marginally rimmed platforms with patch reefs and oolitic shoals. Variations in the style of morphology of carbonate platforms are presented in Fig. A.1. As carbonate platforms can be considered as "living organisms", their growth, decline and even death are controlled by several factors, such as the light, the trophic level, the turbidity of seawater and the temperature (*e.g.*, Scott, 1995; Mutti and Hallock, 2003). Changes in the above-mentioned parameters may be triggered by climate change through variations of the carbon dioxide content in the atmosphere (pCO_{2atm}): elevated pCO_{2atm} may enhance greenhouse conditions and subsequently the temperature, then rainfalls and continental runoff may become more important. Finally, the delivery of nutrients (*e.g.*, phosphorus) and detritus into the oceans may augment, thus limiting the development of carbonate platform (Fig. A.2). This feedback mechanism illustrates how carbonate platforms may record global (or local) climate change.

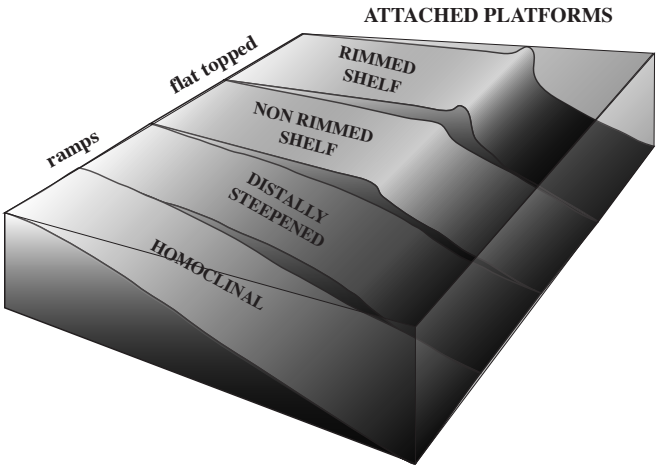

Fig. A.1: Sketch of the different types of carbonate platforms. Heterozoan assemblages rather develop ramp morphology, whereas photozoans build flat-topped edifices (redrawn after Pomar, 2001).

The monitoring of actual carbonate platforms highlights their increasing decline: 58 % of the world's coral reefs are at risk (Bryant *et al.*, 1998). Even if direct human pollution, such as input in the ocean of pesticides or waste waters, may be responsible for the main part of the decreasing activity of reefs, climate warming may have also a non-negligible influence through variations of the CO_2 content in the atmosphere and the hydrosphere, triggered by human activity. Effectively, the actual carbon cycle shows that industries using fossil fuels release 6.3 billions of tonnes of carbon per year, whereas at the same time, oceans and forests absorb about 3.1 GtC. yr^{-1} (Fig. A.3). Consequently the increased input of CO_2 in the atmosphere may trigger drastic change, in particular on the benthic ecosystems that constitute a carbonate platform.

During the Phanerozoic, the evolution of carbonate platforms was punctuated by periods of both rise as well as decline: for example, the Oligocene – Miocene boundary interval (ca. 23 Ma ago, after Gradstein *et al.*, 2004) is marked by the demise of the Malta - Ragusa carbonate

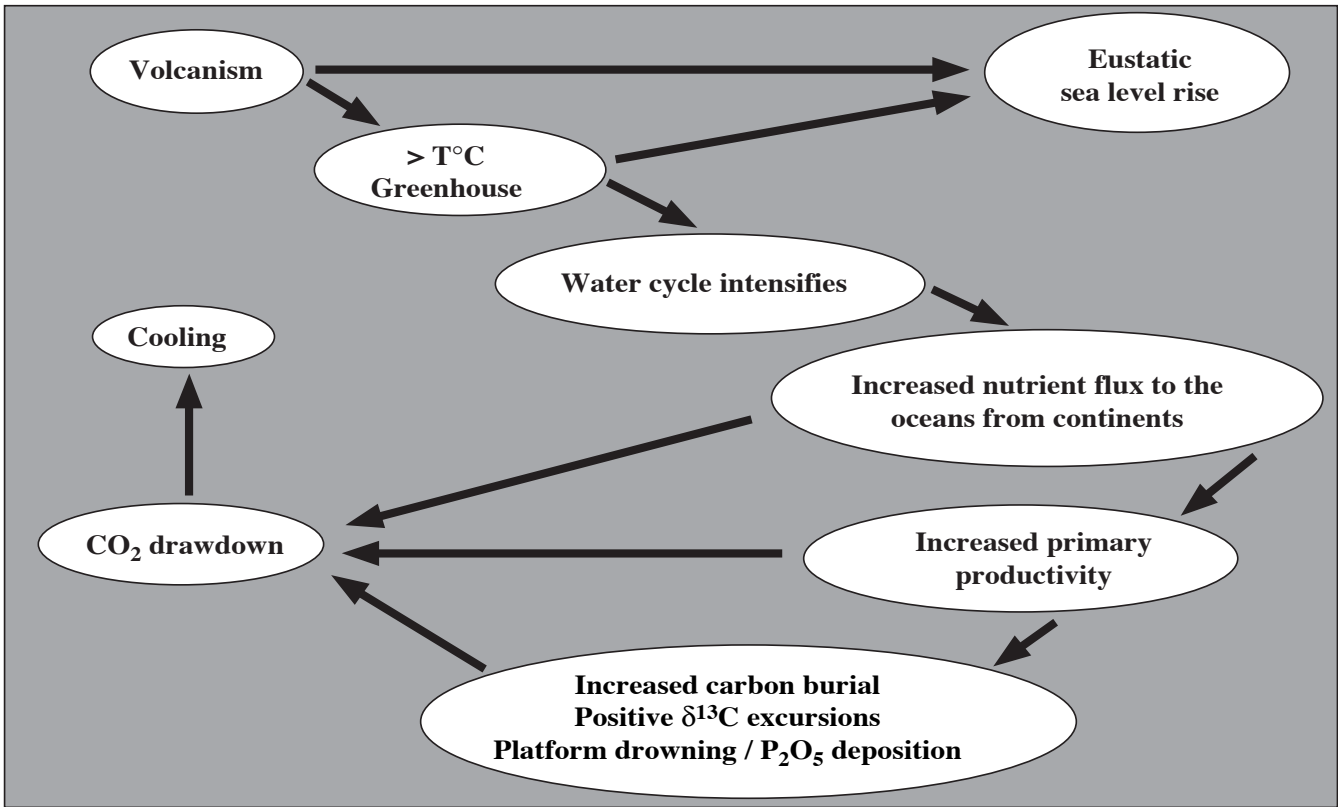

Fig. A.2: Schematic representation of feedback mechanisms between volcanism, continental runoff, platfrom drowning and $\delta^{13}C$ positive excursions (after van de Schootbrugge, 2001; modified after Föllmi et al., 1994).

platform in the Mediterranean Sea (John *et al.*, 2003), and also by the extinction or major turnover of coral associations in the Caribbean Sea (Edinger and Risk, 1994). During the Cretaceous (from 145.5 to 65.5 Ma ago, after Gradstein *et al.*, 2004), the evolution of carbonate factories is very well documented in different parts of the world, in particular in the Tethys, an ancient ocean that bordered the African and European coasts and extended eastward to Australia and southeast Asia (Fig. A.4). In Switzerland, the evolution of the carbonate platform presently exposed in the helvetic Alps lasted from the latest Jurassic to the Cenomanian; during this period, the platform underwent two major transitions from heterozoan to photozoan associations, and several episodes of drowning (Föllmi *et al.*, 1994, in press).

The Cretaceous was very favourable to the development of carbonate platforms, in particular because of the relatively high sea level that prevailed during this period implying larger shallow marginal areas than today (*e.g.*, Haq *et al.*, 1987; Ford and Golonka, 2003; Philip, 2003). These vast sedimentary archives are characterized by geometries which are the direct consequence of sea-level change and the composition and productivity rates of complex and vulnerable ecosystems. They are very appropriate for the reconstruction of environmental change either related to climate or paleoceanographic change.

A.1.2. The climate during the Early Cretaceous: controlling factors and main perturbations

Why do so many geological studies focus on the Cretaceous? Maybe because the climatic conditions that prevailed during this period are considered to gather similarities with the ones predicted by models for the actual Earth system with an increasing pCO_{2atm}. Thus, studying the history of the Earth during the Cretaceous may help to predict its future.

A varying set of paleontological, geochemical and sedimentological proxies is classically used to trace climate and/or environmental change. To test if the latter are linked to changes in the pCO_{2atm}, $\delta^{13}C$ analysis is performed in many cases in order to trace unbalances within the carbon cycle, and consequently to highlight relationships

	1980 to 1989	1990 to 1999
Atmospheric increase	3.3 ± 0.1	3.2 ± 0.1
Fossil emissions	5.4 ± 0.3	6.3 ± 0.4
Ocean-atmosphere flux	-1.7 ± 0.6 (-1.9 ± 0.6)	-2.4 ± 0.7 (-1.7 ± 0.5)
Land-atmosphere flux	-0.4 ± 0.7 (-0.2 ± 0.7)	-0.7 ± 0.8 (-1.4 ± 0.7)
Land use change	2.0 ± 0.8	2.2 ± 0.8
Residual terrestrial sink ***(unknown sink?)***	-2.4 ± 1.1	-2.9 ± 1.1

All values in GtC.yr^{-1}.
After Joos et al. (2003), and references therein.

Fig. A.3: Scheme of the actual carbon cycle. Note that biosphere - hydrosphere - atmosphere exchanges are at the equilibrium, whereas the anthropogenic output create a disbalance of the global assessment.

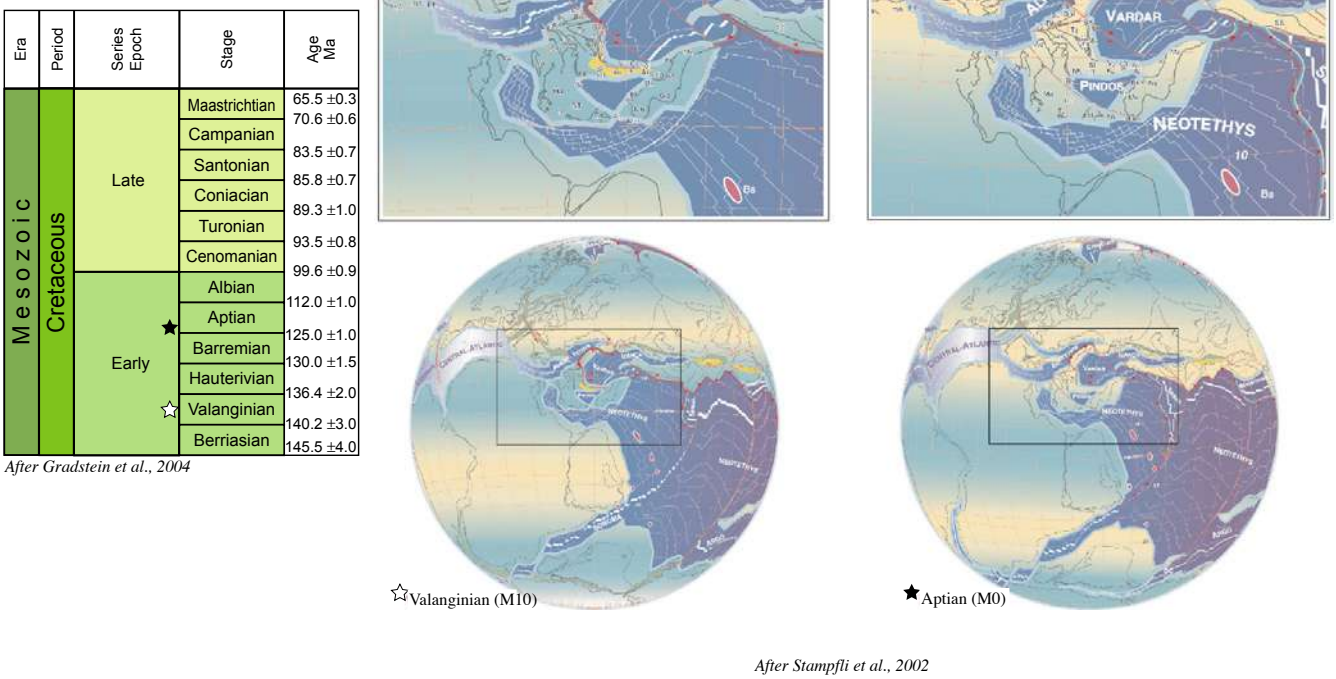

Fig. A.4: Paleogeographic maps of the Valanginian and the Aptian stages, centered on the western Tethys (after Stampfli et al., 2002). The stratigraphic chart for the Cretaceous period is reported on the left hand on the figure (after Gradstein et al., 2004).

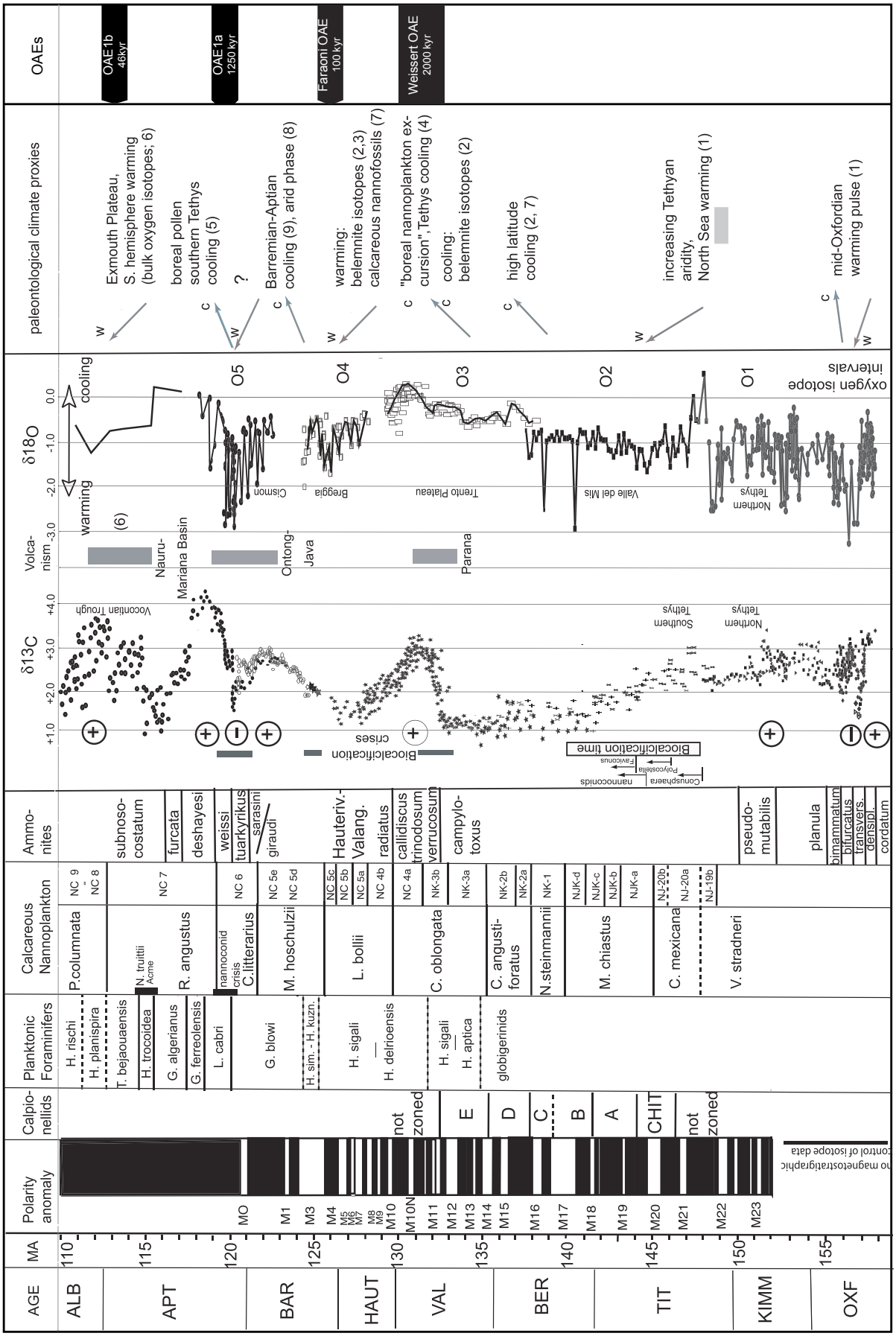

References for paleontological climate proxies: (1) Abbink *et al.*, 2001; (2) Price *et al.*, 2000; (3) Van de Schootbrugge *et al.*, 2000; (4) Melinte & Mutterlose, 2001; (5) Hochuli *et al.*, 1999; (6) Clarke & Jenkyns, 1999; (7) Mutterlose & Kessels, 2000; (8) Ruffell and Batten, 1990; (9) Pucéat *et al.*, 2003; w: warming; c: cooling

Fig. A.5: $\delta^{13}C$ and $\delta^{18}O$ curves for the time span from the Oxfordian (Late Jurassic) to the Early Albian (Early Cretaceous), for the western Tethys (after Weissert and Erba, 2004, and references therein for the magnetostratigraphy, and calpionellids, benthic foraminifers, planktonic foraminifers and nannofossils biozonations). The location and duration of the OAEs are after Erba (2004), except for the Faraoni OAE (Bodin et al., 2006).

between the organic (C_{org}) and carbonate carbon (C_{carb}) burial rates (*e.g.*, Weissert, 1989; Weissert *et al.*, 1998). For instance, positive excursions within the $\delta^{13}C$ record may reflect times of enhanced organic matter preservation. A good case study of this relationship was published by Schlanger and Jenkyns (1976), who linked the preservation of organic matter in Aptian-Albian and Cenomanian-Turonian sediments to the expansion of the oxygen minimum zone in the global ocean, triggered by the Late Cretaceous transgression and also by the decrease of the oceanic circulation due to an equable global climate. These Oceanic Anoxic Events (OAE's) are mirrored, both in carbonates and organic matter, by pronounced positive excursions of the $\delta^{13}C$ (*e.g.*, Weissert and Bréhéret, 1991; Menegatti *et al.*, 1998; Moullade *et al.*, 1998; Fig.1 in Leckie *et al.*, 2002; Erba, 2004; Weissert and Erba, 2004; Fig. A.5). A potential starting point for OAE's is the injection of a high amount of ^{12}C-enriched CO_2 into the oceans via enhanced

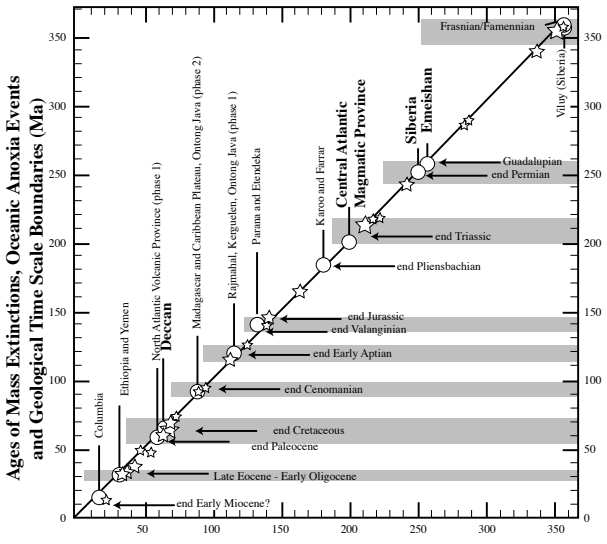

and impact craters >25 kn diameter (modified from Courtillot and Renne, 2003)

Fig. A.6: Correlation of the age of major volcanic events (white circles, including continental flood basalts and oceanic plateaus) and impact craters (>25 km diameter; white stars), with the time of mass extinctions (gray shaded areas). After Keller, 2005 (modified from Courtillot and Renne, 2003).

volcanic activity and/or methane hydrate release (*e.g.*, Dickens *et al.*, 1995; Hesselbo *et al.*, 2000; Weissert, 2000).

Volcanism has often been considered as the main contributor of ^{12}C in order to explain negative spikes or excursions of the $\delta^{13}C$ (Larson, 1991; Larson and Erba, 1999), but mass-balance calculations tend to show that volcanism, alone, cannot account for the amplitude of these negative excursions. One consequence of increased pCO_{2atm} due to volcanism may be an enhanced greenhouse effect, which triggers an increase of the temperatures and ultimately the destabilisation of methane hydrates in the ocean. The relatively good correlation between the timing of mass extinctions, the appearance of OAE's and the installation of Large Igneous Provinces (LIP's) may support this hypothesis (Wignall, 2001; Wignall, 2001; Courtillot and Renne 2003; Keller, 2005; see also Fig. A.6).

Moreover, the evolution of the $^{87}Sr/^{86}Sr$ record during the Early Cretaceous reveals a long-term increase from the Berriasian to the earliest Aptian, then a decrease starts after a small plateau and lasts until the latest Aptian; subsequently the $^{87}Sr/^{86}Sr$ record evolves toward more radiogenic values until the latest Cenomanian (Fig. A.7; see also Veizer *et al.*, 1999; Leckie *et al.*, 2002; McArthur *et al.*, 2004). Change within the $^{87}Sr/^{86}Sr$ ratio reflects variation in the proportion of land-derived material enriched in ^{87}Sr, and of fresh volcanic material where the ^{87}Rb is not yet transformed into ^{87}Sr. Consequently, examining the evolution

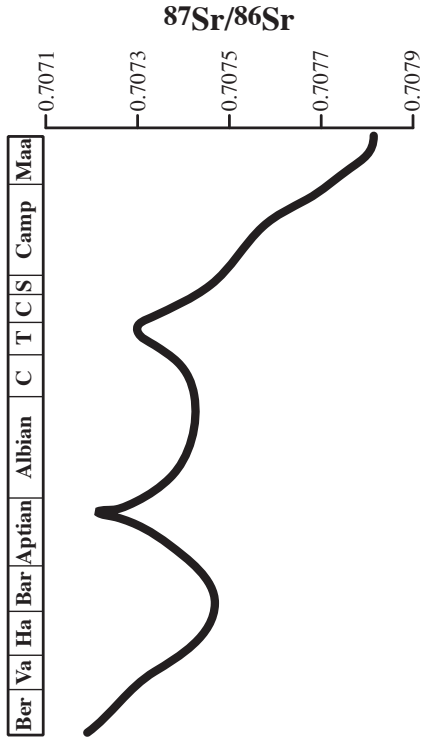

Fig. A.7: $^{87}Sr/^{86}Sr$ evolution during the Early Cretaceous (redrawn from McArthur et al., 2001).

of strontium-isotope curves may help to locate periods of enhanced weathering such as during the first part of the Early Cretaceous.

Another proxy for the intensity of weathering is the mineralogy of representative sections, in particular the estimation of the amount of detritus incoming into the oceans. The presence of siliciclastics in the Tethys and the North Atlantic during the time span from the Valanginian to the Aptian – Albian boundary suggests a relatively warm and humid climate (Weissert, 1990). This hypothesis is supported by the analysis of clay minerals from the Lombardian basin: even if Early Cretaceous sediments are mainly composed of smectite, kaolinite appears episodically during the Valanginian – Hauterivian, the Barremian and especially during the Aptian (Hallam, 1984, 1985; Deconinck and Bernouilli, 1991). The genesis of smectite and kaolinite requires different rates of humidity and the presence of temporal variations in the quantities of these two clay minerals indicate that the climate was subjected to changes during the Early Cretaceous, with implications for the unrolling of major paleoceanographic events such as OAE's and phases of carbonate platform demises.

A.1.3. General statements

During the Early Cretaceous, the evolution of the $\delta^{13}C$ was punctuated by several rapid shifts, which may mirror phases of more or less drastic climate change: the Late Valanginian positive excursion (*e.g.*, Lini *et al.*, 1992; Hennig *et al.*, 1999, Hennig-Fischer, 2003), and also the Early Aptian positive excursion (*e.g.*, Weissert, 1989, Moullade *et al.*, 1998; Erba *et al.*, 1999; Erba, 2004; Erba *et al.*, 2004; Renard *et al.*, 2005) may be triggered by the installation of more humid conditions, as suggested by the presence of bauxite and coals in the Tethyan realm (Hallam, 1984, 1985). Whereas these isotopic events are thought to be associated with OAE's (*e.g.*, Weissert and Erba, 2004), the Faraoni Level, an organic-rich interval defined in the Umbria-Marche basin of Italy and then recovered in other areas of the Tethys (*e.g.*, Cecca *et al.*, 1994, 1995; Baudin, 2005, amongst others), is not mirrored by an increase in the $\delta^{13}C$ values, but rather by an acceleration of the general positive trend that began in the Hauterivian (*e.g.*, van de Schootbrugge *et al.*, 2000; Baudin, 2005). As the Faraoni Level gathers all the sedimentological characteristic of other OAE's, one may wonder why the $\delta^{13}C$ record does not show a fluctuation similar to the ones associated with the Valanginian OAE, OAE1a of the Early Aptian, and OAE2 near the Cenomanian-Turonian boundary.

On the other hand, the sedimentary succession preserved in the Helvetic realm in Switzerland constitutes a very good archive of the carbonate platform that developed from the latest Jurassic to the early Late Cretaceous on the Northern Tethyan margin. Föllmi *et al.* (1994) stated that this platform underwent several crises during this time span; in particular, for the time period studied here, carbonate sedimentation was interrupted by a major phase of condensation and phosphogenesis, from the latest Hauterivian to the Barremian, which is recorded in the so-called Altmann Member. Following Weissert *et al.* (1998), the coincidence in time between the genesis of the Altmann Member and the Faraoni Level may suggest a link between these two events.

A.1.4. References

Abbink, O., Targarona, J., Brinkhuis, H. and Visscher, H. (2001). "Late Jurassic to earliest Cretaceous palaeoclimatic evolution of the southern North Sea." Global and Planetary Change **30** (*3-4*): 231-256.

Baudin, F. (2005). "A Late Hauterivian short-lived anoxic event in the Mediterranean Tethys: the "Faraoni Event"." Comptes Rendus de l'Académie des Sciences de Paris.

Bosence, D. (2005). "A genetic classification of carbonate platforms based on their basinal and tectonic settings in the Cenozoic." Sedimentary Geology **175**: 49-72.

Bryant, D., Burke, L., McManus, J. W. and Spalding, M. (1998). "Reefs at Risk: A Map-Based Indicator of Potential Threats to the World's Coral Reefs", World Resources Institute, Washington D.C., 60 pp.

Cecca, F., Faraoni, P., Marini, A. and Pallini, G. (1995). "Field-trip across the representative sections for the Upper Hauterivian-Barremian

ammonite biostratigraphy in the Maiolica exposed at Monte Nerone, Monte Petrano and Monte Catria (Umbria-Marche, Apennines).” Memorie Descrittive della Carta Geologica d’Italia **51**: 187-211.

Cecca, F., Marini, A., Pallini, G., Baudin, F. and Begouen, V. (1994). “A guide-level of the uppermost Hauterivian (lower Cretaceous) in the pelagic succession of Umbria-Marche Apennines (central Italy): the Faraoni level.” Riv. It. Paleont. Strat. **99** (*4*): 551-568.

Clarke, L. J. and Jenkyns, H. C. (1999). “New oxygen isotope evidence for long-term Cretaceous climate change in the southern Hemisphere.” Geology **8**: 699-702.

Courtillot, V. E. and Renne, P. R. (2003). “On the ages of flood basalt events.” C.R. Geoscience **335**: 113-140.

Deconinck, J.-F. and Bernouilli, D. (1991). “Clay mineral assemblages of Mesozoic pelagic and flysch sediments of the Lombardian Basin (Southern Alps): implications for palaeotectonics, paleoclimate and diagenesis.” Geologische Rundschau **80** (*1*): 1-17.

Dickens, G. R., O’Neil, J. R., Rea, D. K. and Oven, R. M. (1995). “Dissociation of oceanic methane hydrate as a cause of the carbon isotope excursion at the end of the Paleocene.” Paleoceanography **10** (*6*): 965-971.

Edinger, E. N. and Risk, M. J. (1994). “Oligocene - Miocene Extinction and Geographic Restriction of Caribbean Corals: Roles of Turbidity, Temperature, and Nutrients.” Palaios **9**: 576-598.

Erba, E. (2004). “Calcareous nannofossils and Mesozoic oceanic anoxic events.” Marine Micropaleontology **52** (*1-4*): 85-106.

Erba, E., Bartolini, A. and Larson, R. L. (2004). “Valanginian Weissert oceanic anoxic event.” Geology **32** (*2*): 149-152.

Erba, E., Channell, J. E. T., Claps, M., Jones, C. E., Larson, R. L., Opdyke, B., Premoli-Silva, I., Riva, A., Salvini, G. and Torriceli, S. (1999). “Integrated stratigraphy of the Cismon APTICORE (Southern Alps, Italy): A “reference section” for the Barremian-Aptian interval at low latitudes.” Journal of Foraminiferal Research **29** (*4*): 371-391.

Ford, D. and Golonka, J. (2003). “Phanerozoic paleogeography, paleoenvironment and lithofacies maps of the circum-Atlantic margins.” Marine and Petroleum Geology **20** (*3-4, March-April 2003*): 249-285.

Föllmi, K. B., Weissert, H., Bisping, M. and Funk, H. (1994). “Phosphogenesis, carbon-isotope stratigraphy, and carbonate-platform evolution along the Lower Cretaceous northern Tethyan margin.” Geological Society of America Bulletin **106** (*II*): 729-746.

Gradstein, F. M., Ogg, J. G. and Smith, A. M. (2004). “A Geological Time Scale 2004”, Cambridge University Press, 600 pp.

Hallam, A. (1984). “Continental humid and arid zones during the Jurassic and Cretaceous.” Palaeogeography, Palaeoclimatology, Palaeoecology **47**: 195-223.

Hallam, A. (1985). “A review of Mesozoic climates.” J. geol. Soc. London **142**: 433-445.

Haq, B. U., Hardenbol, J. and Vail, P. R. (1987). “The chronology of fluctuating sea level since the Triassic.” Science **235**: 1156-1167.

Hennig Fischer, S. (2003). “Geochemical and sedimentological evidence for environmental changes in the Valanginian (Early Cretaceous) of the Tethys region.” *thesis*, ETH Zürich, 189 + Appendix pp.

Hennig, S., Weissert, H. and Bulot, L. (1999). “C-isotope stratigraphy, a calibration tool between ammonite- and magnetostratigraphy.” Geologica Carpathica **50**: 91-96.

Hesselbo, S. P., Gröcke, D. R., Jenkyns, H. C., Bjerrum, C. J., Farrimond, P., Morgans Bell, H. S. and Green, O. R. (2000). “Massive dissociation of gas hydrate during a Jurassic oceanic anoxic event.” Nature **406** (*27 July 2000*): 392-395.

Hochuli, P. A., Menegatti, A. P., Weissert, H., Riva, A., Erba, E. and Premoli Silva, I. (1999). “Episodes of high productivity and cooling in the early Aptian Alpine Tethys.” Geology **27**: 657-660.

James, N. P. (1997). “The cool-water carbonate depositional realm”. *In:* James, N. P. and Clarke, J. A. D., (*Eds*). Cool-water carbonates. Tulsa, Oklahoma, Society for Sedimentary Geology, **SEPM Special Publication N° 56**: 1-20.

John, C. M., Mutti, M. and Adatte, T. (2003). "Mixed carbonate-siliciclastic record on the North African margin (Malta) - coupling of weathering processes and mid Miocene climate." GSA Bulletin **115** (*2*): 217-229.

Joos, F., Plattner, G. K., Stocker, T. F., Körtzinger, A. and Wallace, D. W. R. (2003). "Trends in Marine Dissolved Oxygen: Implications for Ocean Circulation Changes and the Carbon Budget." EOS, Transactions, American Geophysical Union **84** (*21*): 197 & 201.

Keller, G. (2005). "Impacts, volcanism and mass extinction: random coincidence or cause and effect?" Australian Journal of Earth Sciences **52** (*4-5*): 725-757.

Larson, R. L. (1991). "Geological consequences of superplumes." Geology **19**: 963-966.

Larson, R. L. and Erba, E. (1999). "Onset of the mid-Cretaceous greenhouse in the Barremian-Aptian: Igneous events and the biological, sedimentary and geochemical responses." Paleoceanography **14** (*6*): 663-678.

Leckie, M. R., Bralower, T. J. and Cashman, R. (2002). "Oceanic anoxic events and plankton evolution: Biotic response to tectonic forcing during the mid-Cretaceous." Paleoceanography **17** (*3*).

Lini, A., Weissert, H. and Erba, E. (1992). "The Valanginian carbon isotope event: a first episode of greenhouse climate conditions during the Cretaceous." Terra Nova **4** (*Global Change Spec. Issue (ed. by F.-C. Wezel)*): 374-384.

McArthur, J. M., Howarth, R. J. and Bailey, T. R. (2001). "Strontium Isotope Stratigraphy: LOWESS Version 3: Best Fit to the Marine Sr-Isotope Curve for 0-509 Ma and Accompanying Look-up Table for Deriving Numerical Age." The Journal of Geology **109**: 155-170.

McArthur, J. M., Mutterlose, J., Price, G. D., Rawson, P. F., Ruffell, A. and Thirlwall, M. F. (2004). "Belemnites of Valanginian, Hauterivian and Barremian age: Sr-isotope stratigraphy, composition (87Sr/86Sr, ∂13C, ∂18O, Na, Sr, Mg), and palaeo-oceanography." Palaeogeography, Palaeoclimatology, Palaeoecology **202** (*3-4*): 253-272.

Melinte, M. and Mutterlose, J. (2001). "A Valanginian (Early Cretaceous) 'Boreal nannoplantkon excursion' in sections from Romania." Marine Micropaleontology **43**: 1-25.

Menegatti, A. P., Weissert, H., Brown, R. S., Tyson, R. V., Farrimond, P., Strasser, A. and Caron, M. (1998). "High-resolution $\delta^{13}C$ stratigraphy through the early Aptian "Livello Selli" of the Alpine Tethys." Paleoceanography **13** (*5*): 530-545.

Moullade, M., Kuhnt, W., Bergen, J. A., Masse, J.-P. and Tronchetti, G. (1998). "Correlation of biostratigraphic and stable isotope events in the Aptian historical stratotype of La Bedoule (southeast France)." Comptes Rendus de l'Academie des Sciences - Series IIA - Earth and Planetary Science **327** (*10*): 693-698.

Mutterlose, J. and Kessels, K. (2000). "Early Cretaceous calcareous nannofossils from high latitudes: implications for palaeobiogeography and palaeoclimate." Palaeogeography, Palaeoclimatology, Palaeoecology **160** (*3-4*): 347-372.

Mutti, M. and Hallock, P. (2003). "Carbonate systems along nutrient and temperature gradients: some sedimentological and geochemical constraints." Int. J. Earth Sci. (Geol. Rundsch.) **92**: 465-475.

Philip, J. (2003). "Peri-Tethyan neritic carbonate areas: distribution through time and driving factors." Palaeogeography, Palaeoclimatology, Palaeoecology **196** (*1-2*): 19-37.

Pomar, L. (2001). "Types of carbonate platforms: a genetic approach." Basin Research **13** (*3*): 313-334.

Price, G. D., Ruffell, A., Jones, C. E., Kalin, R. M. and Mutterlose, J. (2000). "Isotopic evidence for temperature variation during the early Cretaceous (late Ryazanian-mid-Hauterivian)." Journal of the Geological Society, London **157**: 335-343.

Pucéat, E., Lécuyer, C., Sheppard, S. M. F., Dromart, G., Reboulet, S. and Grandjean, P. (2003). "Thermal evolution of Cretaceous Tethyan marine waters inferred from oxygen isotope composition of fish tooth enamels." Paleoceanography **18** (*2*): 1029, doi:10.1029/

2002PA000823.

Renard, M., de Rafélis, M., Emmanuel, L., Moullade, M., Masse, J.-P., Kuhnt, W., Bergen, J. A. and Tronchetti, G. (2005). "Early Aptian $\delta^{13}C$ and manganese anomalies from the historical Cassis-La Bédoule stratotype sections (S.E. France): relationship with a methane hydrate dissociation event and stratigraphic implications." Carnets de Géologie / Notebooks on Geology **Article 2005/04 (CG2005_A04)**: 18 p.

Ruffell, A. H. and Batten, D. J. (1990). "The Barremian-Aptian arid phase in western Europe." Palaeogeography, Palaeoclimatology, Palaeoecology **80** (*3-4*): 197-212.

Schlanger, S. O. and Jenkyns, H. C. (1976). "Cretaceous oceanic anoxic events: causes and consequences." Geologie en Mijnbouw **55** (*3-4*): 179-184.

Scott, R. W. (1995). "Global environmental controls on Cretaceous reefal ecosystems." Palaeogeography, Palaeoclimatology, Palaeoecology **119** (*1-2*): 187-199.

Stampfli, G. M., Borel, G. D., Marchand, R. and Mosar, J. (2002). "Western Alps geological constraints on western Tethyan reconstructions". *In:* Rosenbaum, G. and Lister, G. S., (*Eds*). Reconstruction of the evolution of the Alpine-Himalayan Orogen. Journal of the Virtual Explorer, **8**: 77-106.

van de Schootbrugge, B. (2001). "Influence of paleo-environmental changes during the Hauterivian (early Cretaceous) on carbonate deposition along the northern margin of the Tethys: Evidence from geochemical records (C, O and Sr-isotopes, P, Fe, Mn)." *Ph.D. thesis*, Université de Neuchâtel, 291 pp.

van de Schootbrugge, B., Föllmi, K. B., Bulot, L. G. and Burns, S. J. (2000). "Paleoceanographic changes during the early Cretaceous (Valanginian-Hauterivian): evidence from oxygen and carbon stable isotopes." Earth and Planetary Science Letters **181**: 15-31.

Veizer, J., Ala, D., Azmy, K., Bruckschen, P., Buhl, D., Bruhn, F., Carden, G. A. F., Diener, A., Ebneth, S. and Godderis, Y. (1999). "$^{87}Sr/^{86}Sr$, $\delta^{13}C$ and $\delta^{18}O$ evolution of Phanerozoic seawater." Chemical Geology **161** (*1-3*): 59-88.

Weissert, H. (1989). "C-Isotope stratigraphy, a monitor of paleoenvironmental change: a case study from the Early Cretaceous." Surveys in Geophysics **10** (*1*): 1-61.

Weissert, H. (1990). "Siliciclastics in the early Cretaceous Tethys and north Atlantic oceans: documents of periodic greenhouse climate conditions." Mem. Soc. Geol. It. **44**: 59-69.

Weissert, H. (2000). "Deciphering methane's fingerprint." Nature **406** (*27 July 2000*): 356-357.

Weissert, H. and Breheret, J.-G. (1991). "A carbonate carbon-isotope record from Aptian-Albian sediments of the Vocontian trough (SE France)." Bull. Soc. géol. France **162** (*6*): 1133-1140.

Weissert, H. and Erba, E. (2004). "Volcanism, CO_2 and palaeoclimate: a Late Jurassic-Early Cretaceous carbon and oxygen isotope record." Journal of the Geological Society, London **161**: 695-702.

Weissert, H., Lini, A., Föllmi, K. B. and Kuhn, O. (1998). "Correlation of Early Cretaceous carbon isotope stratigraphy and platform drowning events: a possible link?" Palaeogeography, Palaeoclimatology, Palaeoecology **137**: 189-203.

Wignall, P. B. (2001). "Large igneous provinces and mass extinctions." Earth-Science Reviews **53** (*1-2*): 1-33.

A.2.
The historical succession in the Neuchâtel area

A.2.1. Original definition and evolution of the concept

Since the first half of the eighteenth century, and in particular with the arrival of Louis Agassiz, geological research in Neuchâtel has been stimulated and concentrated in the structure of a regional geological society. Within this frame, Auguste de Montmollin presented the results of his own research on the Cretaceous formations of the vicinity of Neuchâtel. In 1835, de Montmollin proposed a stratigraphic scheme, which distinguished five main formations, from the Calcaire Roux (Valanginian) to the upper part of Pierre Jaune de Neuchâtel, and which constitutes his "Terrain Crétacé du Jura"; no age was attributed to these formations. In the same year, Thurmann (1835) introduced the term "Néocomien" instead of the "Terrain Crétacé du Jura" of de Montmollin, and suggested to correlate the Neocomian of Neuchâtel with the chalk or the greensands from other European areas.

In 1847, d'Orbigny defined the Urgonian formation at Orgon (south of France), as a massive calcareous facies rich in rudists. Based on the finding of similar fauna, Desor and Gressly (1859) attributed the term Urgonian to the limestones that follow on the top of the Pierre Jaune de Neuchâtel. The urgonian formation from the Neuchâtel area was then split into two members, the lower and the upper Urgonian, even if Desor and Gressly stated that there were no clear differences in term of fossils content between these two members.

The question of the age of the historical Neocomian has always been a source of struggle. Even if most geologists from the second part of the eighteenth century rapidly agreed that the formations first described by de Montmollin (1835) certainly belong to the Cretaceous, it is only in 1874 that Renevier attributed a Hauterivian age to the formations located between the Valanginian Calcaire roux and the Urgonian (Fig. A.8). On the other hand, the term Barremian, defined by Coquand (1862) was introduced by Baumberger (1901) to characterize the age of the Urgonien Jaune, whereas the Urgonien Blanc would be Aptian in age. By replacing the term "Urgonian" previously used in the vicinity of Neuchâtel (*e.g.*, Jaccard, 1869) by the term "Barremian", Baumberger attributed the name of a stratigraphic stage to a lithostratigraphic division, without any biostratigraphical evidence such as ammonites. His conclusions are only based on the occurrence of similar fauna – especially rudists – between the south of France and the western Switzerland. Moreover, Baumberger (1901) recognized no break in the sedimentation, so that the lower and the upper Pierre Jaune de Neuchâtel would be Early and Late Hauterivian in age, respectively.

The next main step in the evolution of the stratigraphy of the historical succession of the Hauterivian stage was made by Remane *et al.*, who published in 1989 a synthesis in which all the available data, as well as new ones concerning the stratigraphy of this succession, were compiled. Thanks to this major contribution, some discrepancies were elucidated, in particular the stratigraphic position of the Marnes de la Russille. The latter were previously thought to

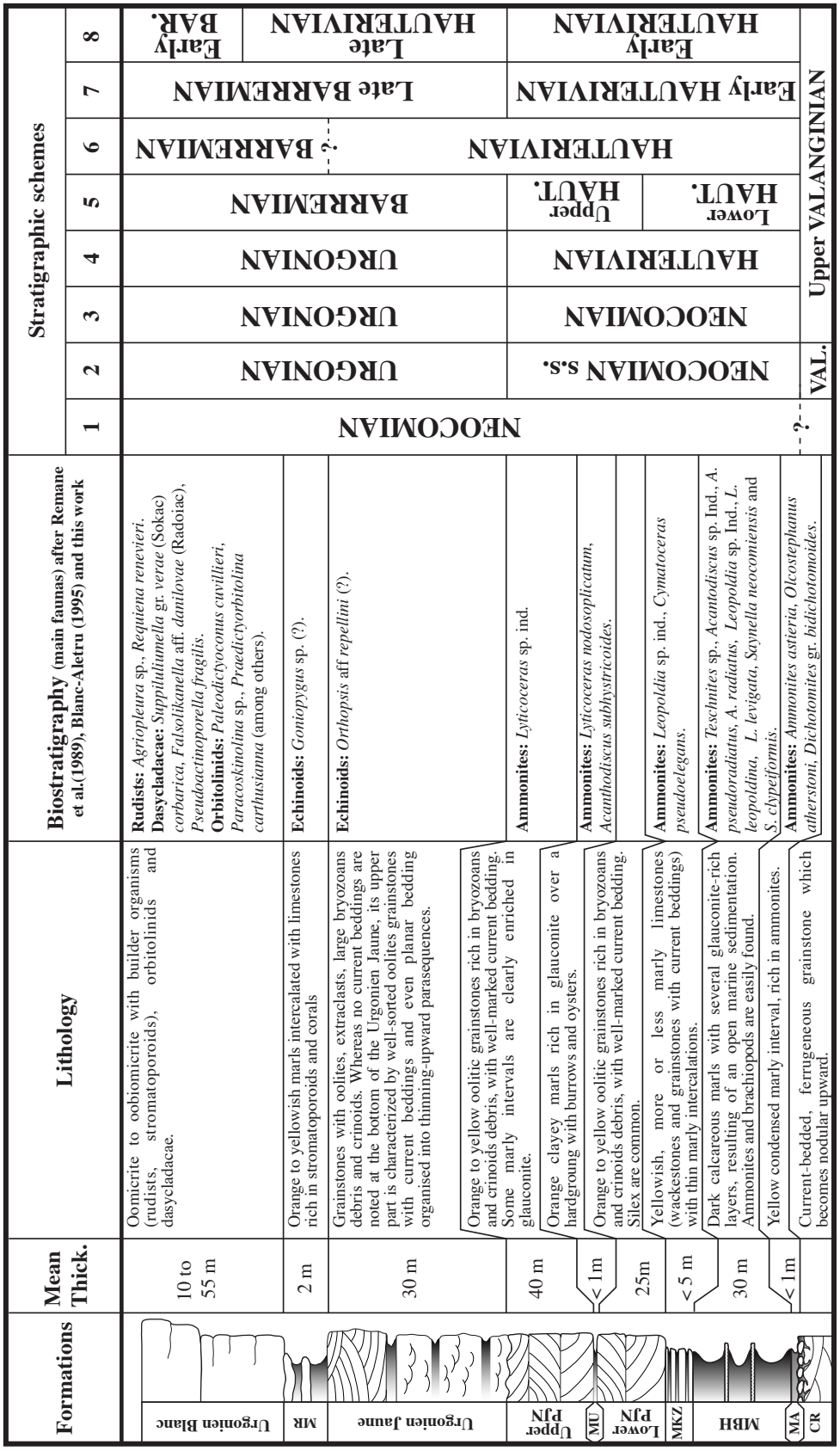

Legend:

• *Abreviations of the names of the formations:* **CR:** Calcaire Roux; **MA:** Marnes à Astieria; **MBH:** Marnes Bleues d'Hauterive; **MKZ:** Megelkalk zone; **PJN:** Pierre Jaune de Neuchâtel; **MU:** Marnes d'Uttins; **MR:** Marnes de la Russille.

• *Numbers on the top of the different stratigraphic schemes:* **1:** Thurmann, 1835; **2:** Desor and Gressly, 1853; **3:** Jaccard, 1869; **4:** Renevier, 1874; **5:** Baumberger, 1901; **6:** Remane, 1989 (modified); **7:** Arnaud-Vanneau and Arnaud, 1990; **8:** Clavel et al., 1995.

*Fig. A.8: Historical succession of the Hauterivian stage defined in the Neuchâtel area. A rapid description of the lithologies, as well as the main indicative fauna, are given. The different stratigraphic schemes (right hand of the figure) correspond to: **1:** Thurmann, 1835; **2:** Desor and Gressly, 1853; **3:** Jaccard, 1869; **4:** Renevier, 1874; **5:** Baumberger, 1901; **6:** Remane, 1989 (modified); **7:** Arnaud-Vanneau and Arnaud, 1990; **8:** Clavel et al., 1995. Abreviations of the names of the formations: **CR:** Calcaire Roux; **MA:** Marnes à Astieria; **MBH:** Marnes Bleues d'Hauteriva; **MKZ:** Mergelkalk Zone; **PJN:** Pierre Jaune de Neuchâtel; **MU:** Marnes d'Uttins; **MR:** Marnes de la Russille.*

separate the upper Pierre Jaune de Neuchâtel from the Urgonien Jaune, whereas Remane *et al.* (1989) located this unit higher in the succession, between the Urgonien Jaune and the Urgonien Blanc (Conrad and Masse, 1989). However, it seems that some divergences began to arise in this synthesis itself: Conrad and Masse (1989; p. 322: *"«L'Urgonien inférieur» (Jaune), jusqu'ici attribué au Barrémien inférieur, est placé dans l'Hauterivien.* […] *Les foraminifères permettent de placer les derniers bancs de «l'Urgonien supérieur» (blanc) dans le Barrémien. C'est donc dans cette formation que doit se situer la limite Hauterivien-Barrémien."*) concluded that the Hauterivian – Barremian boundary may fall somewhere within the Urgonien Blanc,

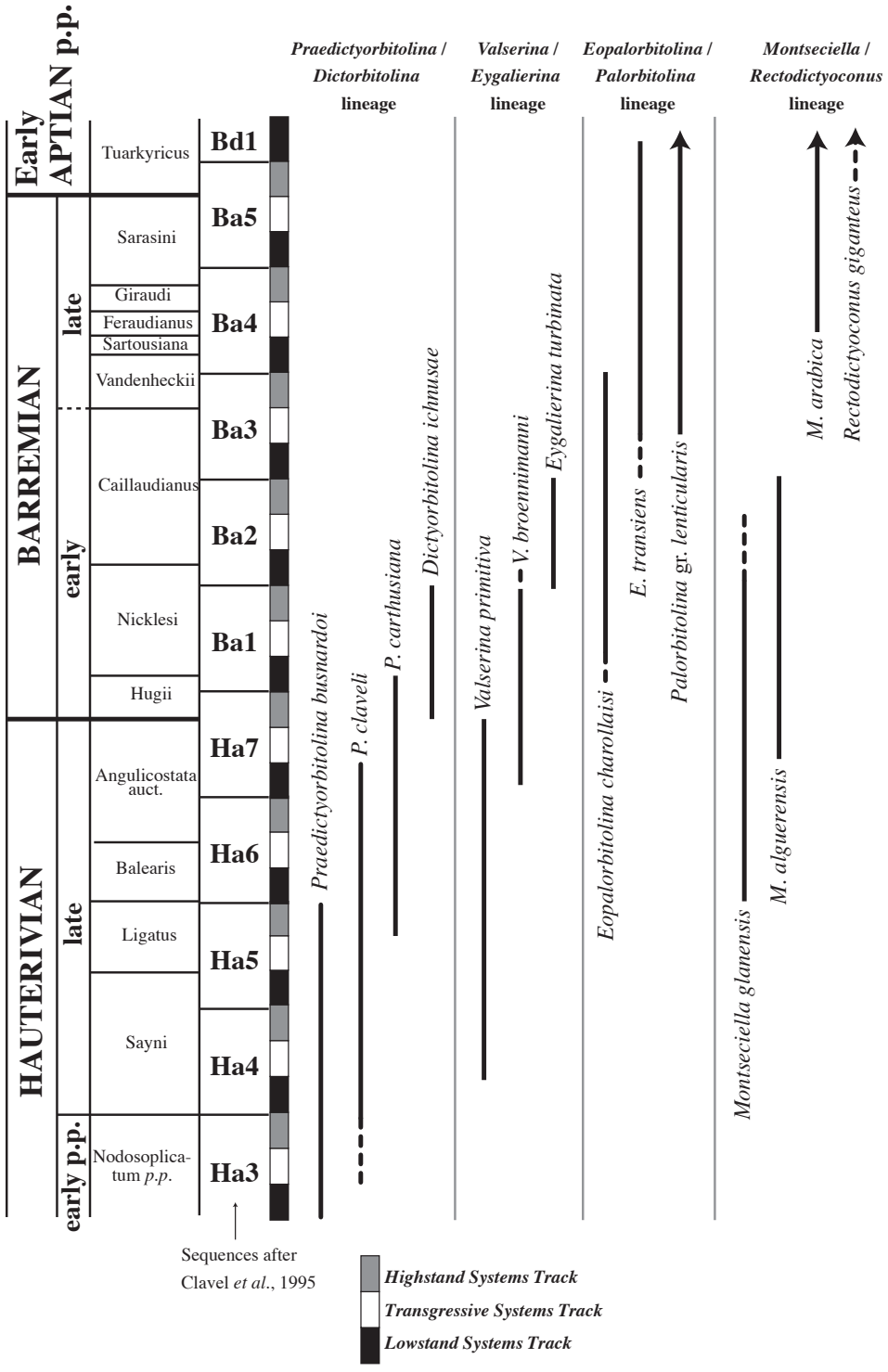

Fig. A.9: Calibration against ammonite zones of the four phylogenetic lineages of orbitolinids defined by Schroeder et al. (2002, redrawn).

whereas Arnaud-Vanneau and Masse (1989; p. 272: *"La découverte de Zweidler (1985) de Paracoskinolina reicheli à la base des calcaires à rudistes d'Eclépens* […] *permet donc de la dater* [*i.e.*, the base of the Urgonien Blanc] *du Barrémien, probablement même du Barrémien supérieur."*) attributed the main part of the same formation to the Barremian or even to the Late Barremian. Their conclusion is mainly based on the presence of *Paracoskinolina reicheli* at the base of the Urgonien Blanc at Eclépens (Zweidler, 1985).

A.2.2. The controversy arising from previous biostratigraphical data and sequence stratigraphy schemes

In a series of papers published since the beginning of the 1980's, and especially after 1989, two main schools of thought emerged concerning the age of the Urgonian formation.

On the one hand, the research team mainly based at Geneva analysed sections from the Vocontian Trough to the Vercors and the Western Swiss Jura. They succeeded in establishing an orbitolinid biozonation (*e.g.*, Schroeder *et al.*, 1968, 2000, 2002), which is based on the evolution of four phylogenetical lineages of these benthic foraminifers calibrated against ammonites from the Ardeche region (Fig. A.9). Consequently, other benthic organisms such as rudists were calibrated against the ammonite biozonation with the help of this biostratigraphic scheme (Masse *et al.*, 1998). Along with the biostratigraphical approach, sequence stratigraphy was performed in sections from the south of France to the Western Swiss Jura. The results highlighted the progradation of the urgonian platform, from the Early Hauterivian to the Early Barremian (Clavel *et al.*, 1995;

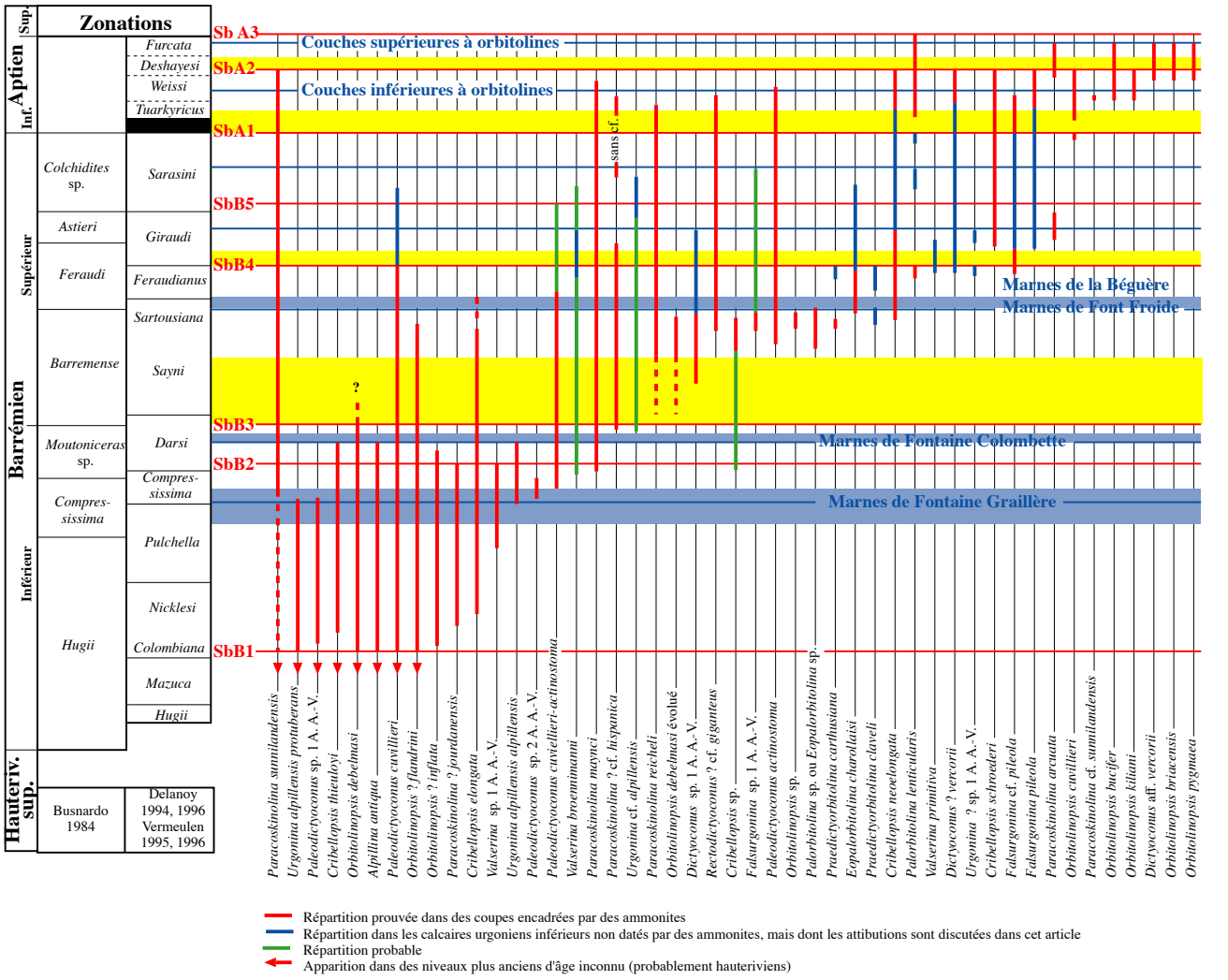

Fig. A.10: Stratigraphic repartition of the main orbitolinids types used by Arnaud et al. (1998), especially in the Vercors area.

Charollais *et al.*, 2003). As a consequence, the above - mentioned authors attributed a "continuous" character to the sedimentation during the Early Cretaceous in the Western Swiss Jura, implying that the Hauterivian – Barremian boundary may fall within the Urgonien Blanc (Clavel *et al.*, 1995).

On the other hand, the same tools – *i.e.* orbitolinids and sequence stratigraphy – were used by Arnaud-Vanneau and Arnaud (1990) and by Arnaud *et al.* (1998). Contrary to Schroeder *et al.* (2002), Arnaud *et al.* (1998) use the association of orbitolinids present in rocks rather than the phylogenetical lineages (Fig. A.10). Their orbitolinids zonation were calibrated with respect to ammonite zonation, in sections from the Vercors where ammonite-dated formations surround orbitolinids-bearing sediments, such as the section at the Gorges du Nant. These authors concluded that a significant hiatus is located at the top of the Pierre Jaune de Neuchâtel which implies that sediments from the Late Hauterivian to the latest Early Barremian are absent. They thus postulated that both the Urgonien Jaune and the Urgonien Blanc are Late Barremian in age, and the time-line responsible for this sedimentary gap may correspond to the sequence boundary B3 (Arnaud *et al.*, 1998; Arnaud, 2005).

A.2.3. Aims of the present thesis

Due to the discrepancies relative to the age of the Urgonian formations from the Western Swiss Jura, the following questions need to be answered.

First, with regards to the two proposed ages for the Urgonian from the vicinity of Neuchâtel, the biostratigraphic frameworks proposed by Arnaud *et al.* (1998) and by Schroeder *et al.* (2002) for the orbitolinids evolution differ by one stage (from the Late Hauterivian to the Early Barremian, ca. 6 My after Gradstein *et al.*, 2004). One can thus be doubtful about the validity of the calibrations of the orbitolinid biozonations. Moreover, other benthic organisms, especially rudists, were calibrated to either of these orbitolinid zonations and were used for biostratigraphic purposes (*e.g.*, Masse *et al.*, 1993) and the quality of these applications stand and fall with the quality of the time calibrations of the orbitolinids.

Because of the lack of an accurate stratigraphic framework which is beyond any doubt, the correlation of the "Hauterivian-Barremian" succession of the Neuchâtel area with other regions of the Tethys is still impossible or at least imprecise. It seems of great importance to solve this problem, in order to try to document, in this very proximal part of the Northern Tethyan margin, the major paleoceanographic events that took place in the Tethys during the studied period.

Last but not least, we should keep in mind that the historical type locality for the Hauterivian stage is within this sedimentary succession and it is awkward not to be certain which part of the sedimentary rocks of this historical succession were deposited during the Hauterivian and where the Hauterivian-Barremian boundary is to be placed.

The objectives of this thesis are thus to find answers which resolve the above-mentioned dilemma, or at least to provide new perspectives which would allow to integrate the studied area into a more global scheme. This research was part of a common project with Stéphane Bodin, and proposed by Prof. Karl B. Föllmi. Our two thesises began in October 2002. Along with the research on the Neuchâtel area, Stéphane Bodin focused on the expression of paleoceanographic events close to the Hauterivian – Barremian boundary in the Helvetic realm; together, we were able to have a sight on two parts of the Northern Tethyan margin, and to compare, discuss our results to see the similarities as well as the discrepancies. A third part of the project consisted in the analysis of (hemi-)pelagic sections from different locations (Switzerland, Italy and France), in order to constrain the paleoceanographic conditions that were responsible for the Faraoni OAE. In the following, the research on the Western Swiss Jura and on the mineralogy of pelagic sections was entirely assumed by myself. The laboratory work (*i.e.*, ICP-MS and spectrophotometry) was done together. Stéphane performed all the work concerning the Helvetic Alps and developed the models based on the trace-element and total phosphorus data (cf. parts D.1 and D.3).

A.2.4. References

Arnaud, H. (2005). "The South-East France Basin (SFB) and Its Mesozoic Evolution". *In:* Adatte, T., Arnaud-Vanneau, A., Arnaud, H., Blanc-Aletru, M.-C., Bodin, S., Carrio-Schaffhauser, E., Föllmi, K. B., Godet, A., Raddadi, M. C. and Vermeulen, J., (*Eds*). The Hauterivian-Lower Aptian sequence stratigraphy from Jura Platform to Vocontian Basin: A multidisciplinary approach. Géologie Alpine, **Série Spéciale «Colloques et Excursions» N°7**: 5-28.

Arnaud, H., Arnaud-Vanneau, A., Blanc-Aletru, M. C., Adatte, T., Argot, M., Delanoy, G., Thieuloy, J.-P., Vermeulen, J., Virgone, A., Virlouvet, B. and Wermeille, S. (1998). «Répartition stratigraphique des orbitolinidés de la plate-forme urgonienne subalpine et jurassienne (SE de la France).» Géologie Alpine **74**: 3-89.

Arnaud-Vanneau, A. and Arnaud, H. (1990). «Hauterivian to Lower Aptian carbonate shelf sedimentation and sequence stratigraphy in the Jura and northern Subalpine chains (southeastern France and Swiss Jura)». *In:* Tucker, M. E., Wilson, J. L., Crevello, P. D., Sarg, J. R. and Read, J. F., (*Eds*). Carbonate Platforms: Facies, Sequences and Evolution. Blackwell Scientific Publications, Special Publication of the International Association of Sedimentologists, **9**: 203-233.

Arnaud-Vanneau, A. and Masse, J.-P. (1989). «Les foraminifères benthiques des formations carbonatées de l'Hauterivien-Barrémien pro parte du Jura vaudois et neuchâtelois (Suisse).» Mémoires de la Société neuchâteloise des Sciences naturelles **XI**: 257-276.

Baumberger, E. (1901). «Uber Facies und Transgressionen der untern Kreid am Nordrande mediterrano - helvetischen Bucht im westlichen Jura.» Wiss. Beil. Ber. Töchterschule Basel: 1-44.

Charollais, J., Clavel, B., Schroeder, R., Busnardo, R., Decrouez, D. and Cherchi, A. (2003). «La migration de la plate-forme urgonienne entre le Jura plissé et les Chaines subalpines septentrionales (France, Suisse): Evolution of the Urgonian platform between the Jura and the Septentrional Subalpine Chains (France, Switzerland).» Geobios **36** (*6 SU -*): 665-674.

Clavel, B., Charollais, J., Schroeder, R. and Busnardo, R. (1995). «Réflexions sur la biostratigraphie du Crétacé inférieur et sur sa complémentarité avec l'analyse séquentielle: exemple de l'Urgonien jurassien et subalpin.» Bull. Soc. géol. France **166** (*6*): 663-680.

Conrad, M. A. and Masse, J. P. (1989). «Corrélations des séries carbonatées de l'Hauterivien et du Barrémien pro-parte dans le nord-ouest vaudois (Suisse).» Mémoires de la Société neuchâteloise des Sciences naturelles **XI**: 307-322.

Coquand, H. (1862). «Sur la convenance d'établir dans le groupe inférieur de la formation crétacée un nouvel étage entre le néocomien proprement dit (couche à Toxaster complanatus et à Ostrea Couloni) et le néocomien supérieur (étage urgonin d'Alc. d'Orbigny).» Bulletin de la Société Géologique de France **(2), 19**: 531-541.

d'Orbigny, A. (1847). «Paléontologie française. Terrains crétacés IV. Brachiopodes», Paris, 269 pp.

de Montmollin, A. (1835). «Mémoire sur le terrain Crétacé du Jura.» Mémoires de la Société des Sciences Naturelles de Neuchâtel **tome I**: 49-65.

Desor, E. and Gressly, A. (1859). «Etudes géologiques sur le Jura neuchâtelois.» Mémoires de la Société des Sciences Naturelles de Neuchâtel **t. IV**: 1-159.

Gradstein, F. M., Ogg, J. G. and Smith, A. M. (2004). «A Geological Time Scale 2004», Cambridge University Press, 600 pp.

Jaccard, A. (1869). «Description géologique du Jura vaudois et neuchâtelois.» Mat. Carte Géol. Suisse **6**: 336 pp.

Masse, J. P., Gourrat, C., Orbette, D. and Schmuck, D. (1998). «Hauterivian Rudist faunas of southern Jura (France).» Geobios **M.S. n°22**: 225-233.

Remane, J., Busnardo, R. and Charollais, J., *(coord.)* (1989). «Révision de l'étage Hauterivien (région - type et environs, Jura franco - suisse)», Mémoires de la Société neuchâteloise des Sciences naturelles **XI**, Neuchâtel (Suisse), 322 pp.

Renevier, E. (1874). «Tableau des terrains sédimentaires formés pendant les époques de la phase organique du globe terrestre avec leurs

représentants en Suisse et dans les régions classiques, leurs synonymes et les principaux fossiles de chaque étage.» Bull. Soc. vaud. Sci. nat. **13**: 218-252.

Schroeder, R., Charollais, J. and Conrad, M. A. (1968). «Essai de biozonation au moyen des orbitolinidae dans les calcaires urgoniens de la Haute-Savoie et de l'Ain, France.» C.R. Acad. Sc. Paris Série D **267** (*22 juillet 1968*): 390-393.

Schroeder, R., Clavel, B., Cherchi, A., Busnardo, R., Charollais, J. and Decrouez, D. (2002). «Lignées phylétiques d'Orbitolinidés de l'intervalle Hauterivien supérieur - Aptien inférieur; leur importance stratigraphique.» Revue Paléobiol., Genève **21** (*2*): 853-863.

Schroeder, R., Clavel, B., Conrad, M. A., Zanetti, L., Busnardo, R., Charollais, J. and Cherchi, A. (2000). «Corrélations biostratigraphiques entre la coupe d'Organyà (Pyrénées Catalanes, NE de l'Espagne) et le Sud-Est de la France pour l'intervalle Valanginien-Aptien.» Treb. Mus. Geol. Barcelona **9**: 5-41.

Thurmann, J. (1835). «Résumé des travaux de la Société des Monts-Jura.» Bulletin de la Société Géologique de France **7**: 207-211.

Zweidler, D. (1985). «Genèse des gisements d'asphalte des formations de la Pierre Jaune de Neuchâtel et des calcaires urgoniens du Jura (Jura neuchâtelois et nord vaudois, Suisse).» *Ph.D. thesis*, Université de Neuchâtel, 108 pp.

Chapter B.

Dating the Early Cretaceous (Hauterivian – Barremian) sedimentary succession in the vicinity of Neuchâtel

Lower Pierre Jaune de Neuchâtel (quarry of Eclépens, VD, Switzerland)

Forewords

The controversy about the age of the Urgonian from the Western Swiss Jura principally resides in the different stratigraphic calibrations of the time-diagnostic faunas used by the different research teams, and in particular on the zonation of orbitolinids. It was our first goal to verify the problems associated with the used biostratigraphies (we first wanted to be sure of this problem) and therefore we specifically collected rudists, echinoids, and brachiopods, as well as samples for the identification of orbitolinids and dasycladacean algae in a selection of sections. The identification of these fossils by different experts resulted in biostratigraphic ages for the Urgonien Jaune and Urgonien Blanc which are incompatible. Consequently, we decided to use stratigraphic tools which were previously not used in this region.

In the following chapter, these approaches are presented. First, sections considered to be representative of the sedimentary succession of the Western Swiss Jura were prospected, in order to define and locate the major breaks within the sedimentary record (part B.2). Then, in the absence of ammonites, several taxons of fauna and flora were examined (part B.3), in order to calibrate the previously defined key surfaces global biostratigraphic schemes. As this approach was not efficient enough to provide a precise age to both the Urgonien Jaune and the Urgonien Blanc, chemostratigraphy (strontium isotopes), as well as changes in oceanic trophic levels (approximated by variations in the phosphorus mass accumulation rates) were applied to decipher between Hauterivian and Barremian ages (part B.4). We also tried to performed direct dating of glauconies, using the K-Ar chronometer (part B.5). Finally, with the sequence stratigraphic framework we obtained, we correlated the Western Swiss Jura with other parts of the Tethys: the Helvetic Alps and the Subalpine Chains (part B.6).

B.1. The Western Swiss Jura : geological setting

B.1.1. Paleogeography

During the Hauterivian and the Barremian, the southern border of the European continent was separated from Africa by the Tethys ocean (Fig. B.1; see also Fig. A.4). At that time, the Western Swiss Jura was situated at subtropical latitudes, at approximately 30°N, and represented a rather confined domain of the Northern Tethyan margin, wedged between the Central, Armorican and Rhenish-Bohemian Massifs, and connected southward with the Vocontian Trough and northward with the Paris Basin (Fig. B.1 and B.2).

During the Hauterivian and the Barremian, the change in the type of carbonate factory that prevailed on the Northern Tethyan margin seems to have influenced the morphology of the coast. From the Late Barremian onward, the rise of the Urgonian platform implied progradation of the deposits in a southward direction. This advance of the Urgonian platform also influenced the shape of the Vocontian Trough, an epicontinental basin connected to the Ligurian Tethys, and surrounded by carbonate platforms, such as the Bas-Dauphine platform (Baudin *et al.*, 1999). Indeed, the size of Vocontian Trough decreased between the Hauterivian and the Late Barremian, as a consequence of the progradation of the Jura

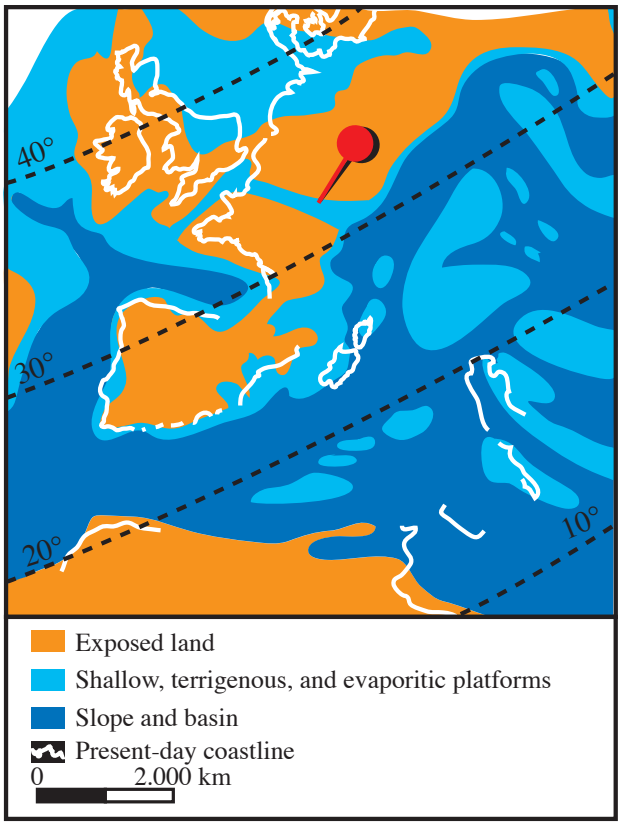

Fig. B.1: Paleogeographical map of the Western Tethys for the base of the Aptian stage (redrawn after Masse et al., 1993).

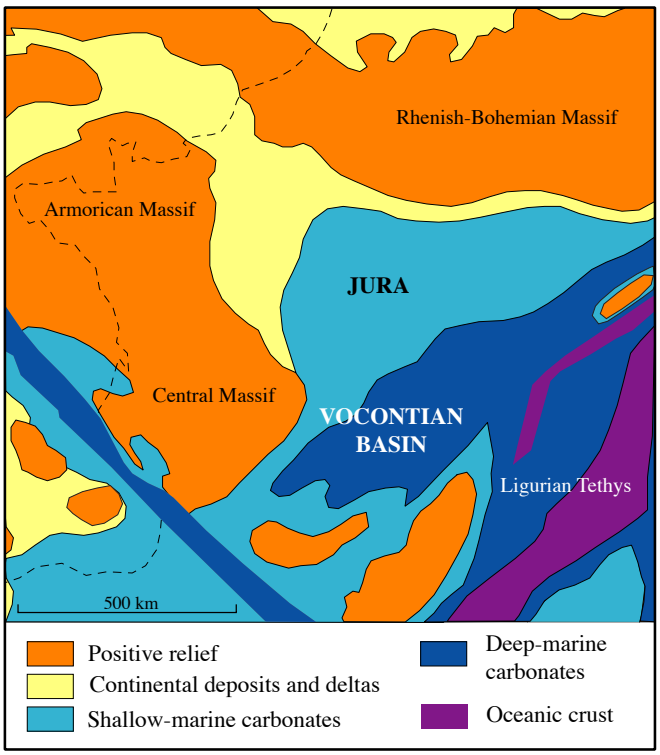

Fig. B.2: Paleogeography in the Early Cretaceous (modified after Strasser et al., 2004; based on Ziegler, 1998).

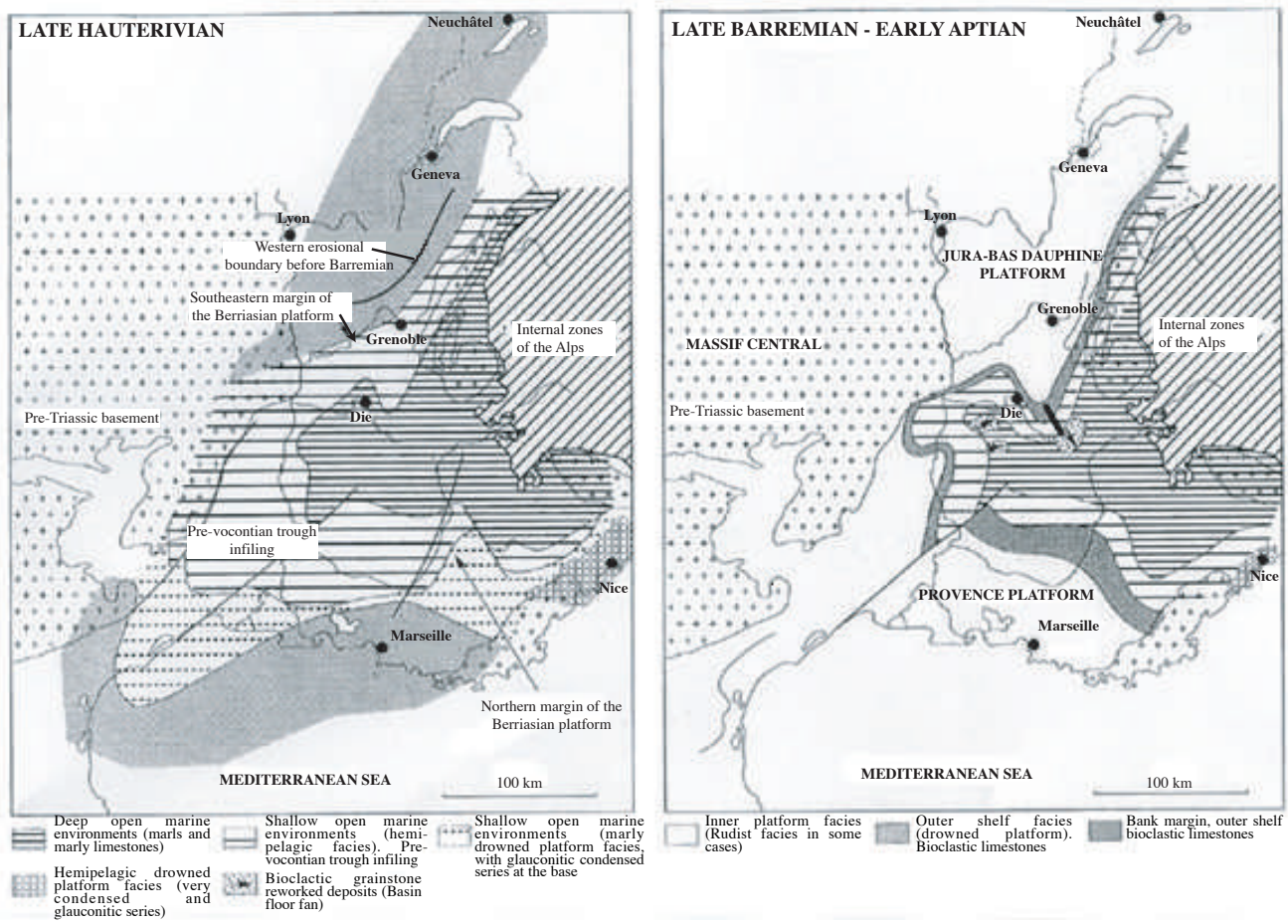

Fig. B.3: Paleogeography of the southeastern France during the Late Hauterivian and the Late Barremian - Early Aptian times (after Arnaud).

– Bas Dauphine and of the Provencal platforms on its northern and southern borders, respectively.

B.1.2. Structural setting

The here-studied sections all belong to the structural domain of the folded Jura (after Trümpy, 1980; Fig. B.3). Following the uplift of the Alps during the Cenozoic, the folding of the Jura mountains began in the Late Serravallian (Late Miocene; Burkhard and Sommaruga, 1998). The northwesternward motion of the African plate implied the formation of NE-SW oriented thrust systems dipping southward. Moreover, several N-S directed tear-faults cut the Jura massif.

B.1.3. References

Baudin, F., Bulot, L. G., Cecca, F., Coccioni, R., Gardin, S. and Renard, M. (1999). "Un équivalent du «Niveau Faraoni» dans le Bassin du Sud-Est de la France, indice possible d'un événement anoxique fini-hauterivien étendu à la Téthys méditerranéenne.» Bull. Soc. géol. France **170**(*4*): 487-498.

Burkhard, M. and Sommaruga, A. (1998). Evolution of the western Swiss Molasse basin: structural relations with the Alps and the Jura belt. *In:* A. Mascle, C. Puigdefàbregas, H. P. Luterbacher and M. Fernàndez, (*Eds*). Cenozoic foreland Basins of Western Europe. Geological Society Special Publications, **134**: 279-298.

Masse, J.-P., Bellion, Y., Benkhelil, J., Dercourt, J., Guiraud, R. and Ricou, L. E. (1993). Lower Aptian Palaeoenvironments (114 to 112 Ma). *In:* J. Dercourt, L. E. Ricou and B. Vrielynck, (*Eds*). Atlas Tethys Palaeoenvironmental Maps. Paris, Gauthier-Villars: Maps. BEICIP-FRANLAB, Rueil-Malmaison.

Strasser, A., Hillgärtner, H. and Pasquier, J.-B. (2004). «Cyclostratigraphic timing of sedimentary processes: An example from the Berriasian of the Swiss and French Jura Mountains.» SEPM Special Publication **N°81**: 135-151.

Trümpy, R. (1980). «Geology of Swizerland: A guide-book. Part A: An Outline of the Geology

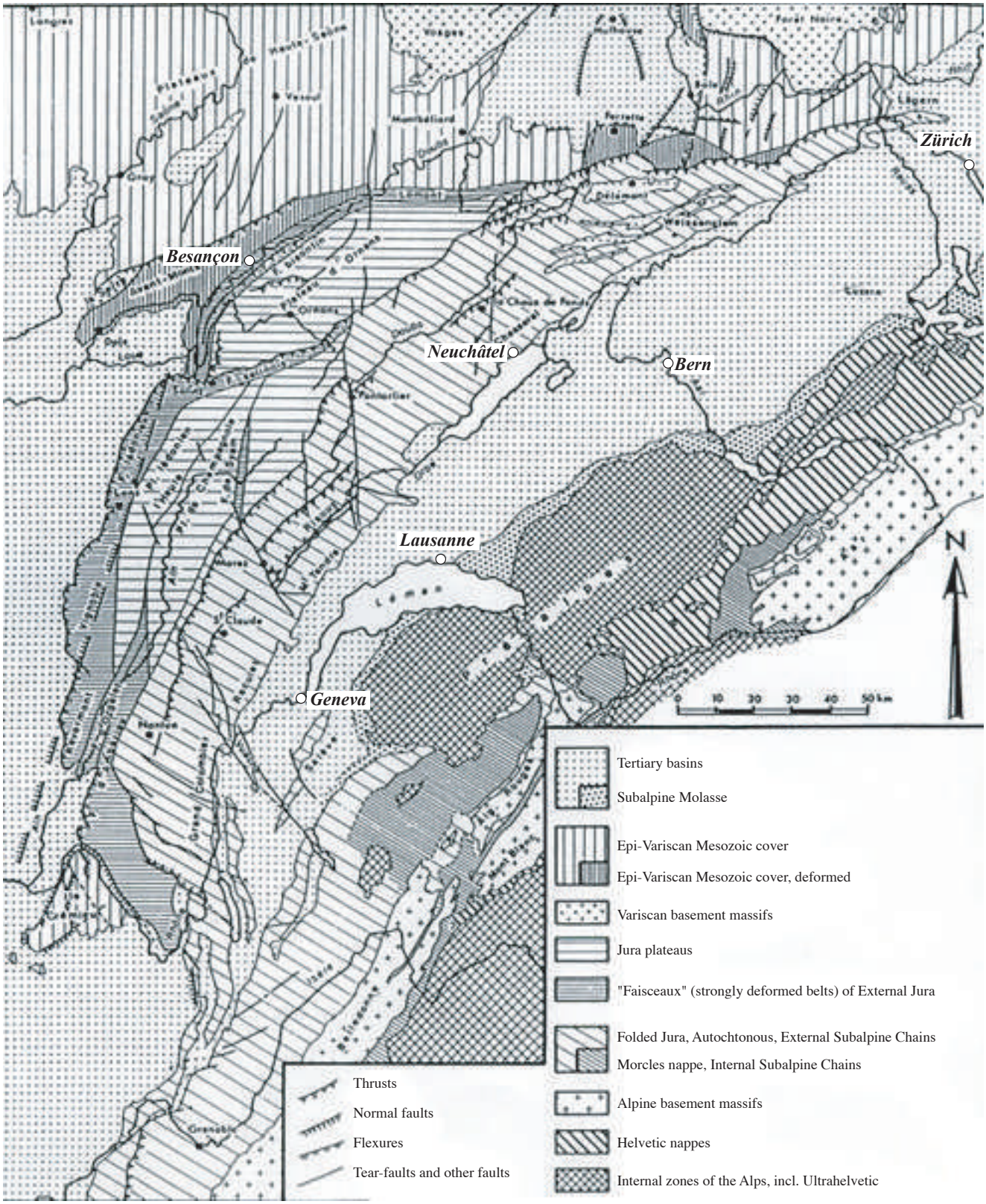

Fig. B.4: Tectonic map of the French and Swiss Jura (after Trümpy, 1980).

of Switzerland», Wepf & Co. Publishers, Basel - New York, 334.

Ziegler, P. A. (1988). «Evolution of the Arctic-North Atlantic and the Western Tethys.» American Association of Petroleum Geologists **Memoir 43**: 198 p.

B.2. A CONTINUOUS SEDIMENTARY RECORD?

In the numerous publications of the team of scientists based at Geneva (*e.g.*, Clavel *et al.*, 1995; Schroeder *et al.*, 2002; Charollais *et al.*, 2003), the integrity of the continuity of the sedimentary record in the Neuchâtel area seems to represent a question of major importance, as these several authors do not recognize any gap or condensation event throughout the sedimentary archive in this region. Consequently, they attribute a Late Hauterivian age to the Urgonien Jaune and situate the Hauterivian-Barremian boundary somewhere within the Urgonien Blanc. On the other hand, Arnaud-Vanneau and Arnaud (1990, 1991) are convinced that a major hiatus is located at the top of the Pierre Jaune de Neuchâtel, which implies a Late Barremian age for both the Urgonien Jaune and the Urgonien Blanc; their conclusions mainly rest on the orbitolinid zonation obtained by Arnaud-Vanneau (1980) in the Vercors area, as well as the integration of this biostratigraphical scheme in a sequence-stratigraphic framework that they constructed in this part of the Urgonian platform (*e.g.*, Arnaud, 1981; Arnaud *et al.*, 1998).

We first intended to check for any clue for a sedimentary break within the geological succession. For this purpose, a sedimentary approach was applied to a set of sections (general location in Fig. B.5), including facies analysis, identification of erosive surfaces and of glauconitisation episodes. The field work was then completed by the analysis of the microfacies in thin sections, in order to identify transgressive and regressive trends, and to define a sequence stratigraphic scheme, which would allow for the recognition of the main sequence boundaries; the latter may constitute good candidates for the identification of possible hiati.

In the following paragraph, we will describe how the sequence stratigraphic approach was applied to a representative section of the studied succession in the Western Swiss Jura, the Eclépens section. The latter crops out approximately fifty kilometres southwesternward from Neuchâtel, in the canton of Vaud (Fig B.6), and belongs to a cement quarry exploited by the Holcim (CH) company. The quality and the continuity of the outcrop are excellent, compared to other studied sections; the Eclépens section allows the observation of the last eight meters of the lower Pierre Jaune de Neuchâtel, of the upper Pierre Jaune de Neuchâtel, and of both the Urgonien Jaune and the Urgonien Blanc (Fig. B.7).

B.2.1. Definition of the microfacies

The types of microfacies used in order to define the main transgressive and regressive trends follow the one defined by Arnaud-Vanneau (1980), and already used in the Western Swiss Jura by Zweidler (1985), Rumley (1993) and Blanc-Aletru (1995). If we consider a rimmed platform, the type of grains and organisms constitutive of the sediments will depend on the light and water depth, on the oxygenation, the nutrient and detritus supply, on the salinity and on the disturbance by waves. As these parameters evolve along a transect through a standard platform, they may imply a transversal distribution of the microfacies. Twelve microfacies are classically used: from F0 to F11, from basinal settings

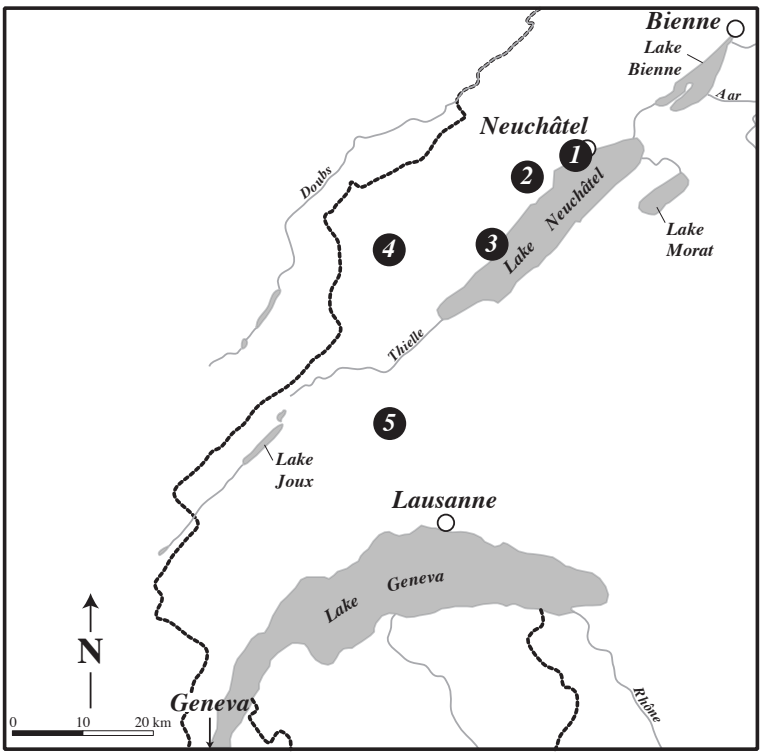

Sections: ***1:*** Pourtalès Hospital, Crêt-Taconnet and Railway Station; ***2:*** Boudry and Gorges de l'Areuse; ***3:*** Vaumarcus; ***4:*** Buttes; ***5:*** Eclépens.

Fig. B.5: Location of the different studied sections within the Western Swiss Jura (modified after Blanc-Aletru, 1995).

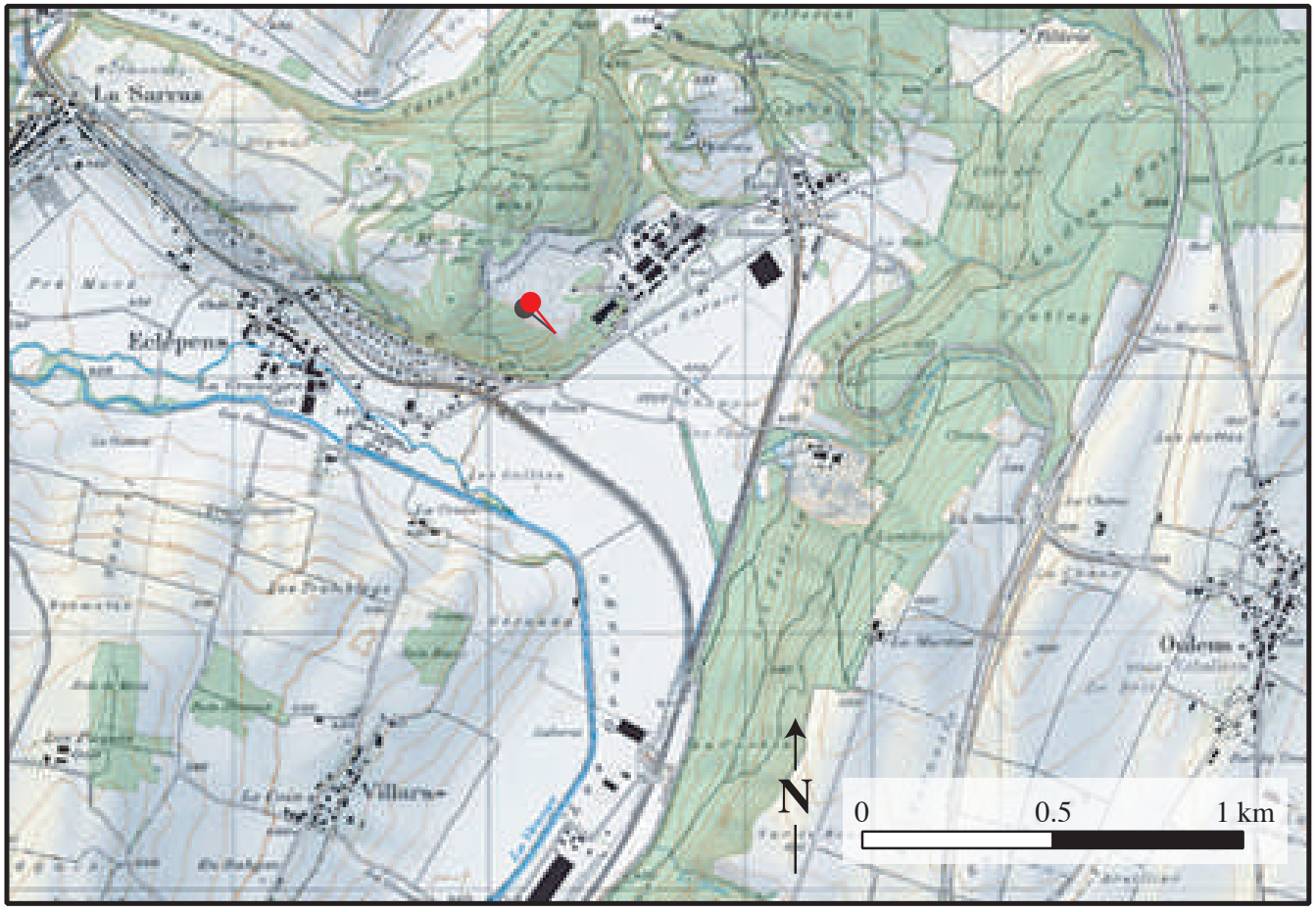

Fig. B.6: Location of the Eclépens section (grey pin. Swiss coordinates: 531'256/167'183). Topographic map at 1/25'000 scale.

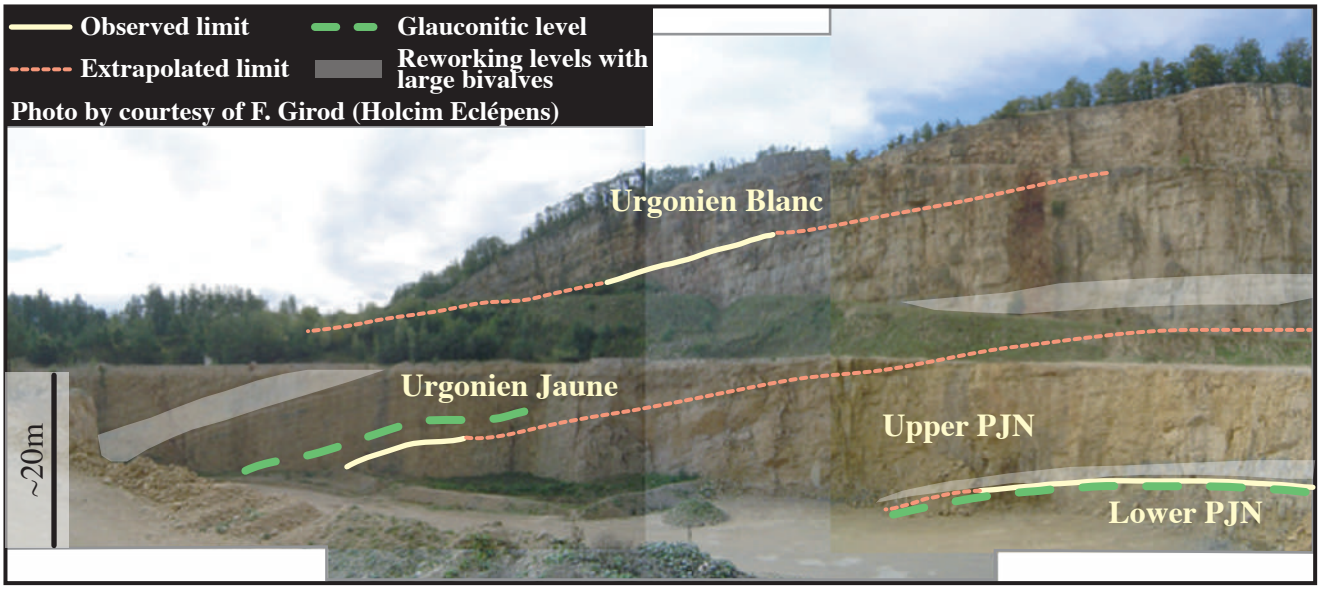

Fig B.7: General overview of the Eclépens section. Note the good continuity and exposure of the outcrop.

to relatively confined, sometimes emerged environments of the supratidal domain (Arnaud Vanneau and Arnaud, 2005; Fig. B.8). As the Western Swiss Jura represents the very proximal part of the northern Tethyan margin, we will refrain from describing microfacies F0, F1, F10 and F11, as they were not recognized in any sections. Following Blanc-Aletru (1995), we used the microfacies FT to characterise the main phases of transgression. The microfacies described in the following are illustrated in Fig. B.9.

Microfacies FT: facies of transgression

Basically, this family of microfacies is characterized by high reworking at the scale of the outcrop and/or of the thin section. In the latter case, intra- and extraclasts are common and usually enrolled in a micritic (carbonate and/or clay) matrix. The direct consequence of this reworking is the diversity of tiny bioclasts (*e.g.*, bivalves, brachiopods, crinoids, oolites), which are highly fractured and often angular. Another important feature of the microfacies FT is the high amount of detrital, sharp quartz grains and of glauconite, for which its dark-green colour and badly-rounded shape suggest a sub-autochtonous origin.

Microfacies F2: biomicrite with sponge spicules

This microfacies corresponds to a wackestone with sponge spicules, quartz and glauconite (5 and 2 %, respectively). The amount of peloids and angular echinoid fragments is low. The fauna exhibits low diversity, and is usually characterized by small-sized, circumlittoral foraminifera (*e.g.*, *Gaudryina* sp.).

Due to the high amount of matrix (wackestone texture), microfacies F2 characterizes the slope of the distal part of the platform, under storm-weather wave base.

Microfacies F3: biopelsparite / biopelmicrite with small echinoid remains

F3 is characterised by a packstone to grainstone texture, with small, rounded crinoidal remains, annelids and high amount of circumlittoral foraminifera. The sphericity of the grains points out to a transport by currents, and thus characterizes the part of the outer platform above the storm-weather wave base.

Microfacies F4: biosparite / biomicrite with crinoids and bryozoans remains

These packstones to grainstones contain crinoidal remains in majority, and also bryozoans and rare ooids; foraminifera are absent from F4. This type of microfacies is rather rare on the external slope of the standard platform, but relatively common on drowned platforms, in which case glauconite becomes very common.

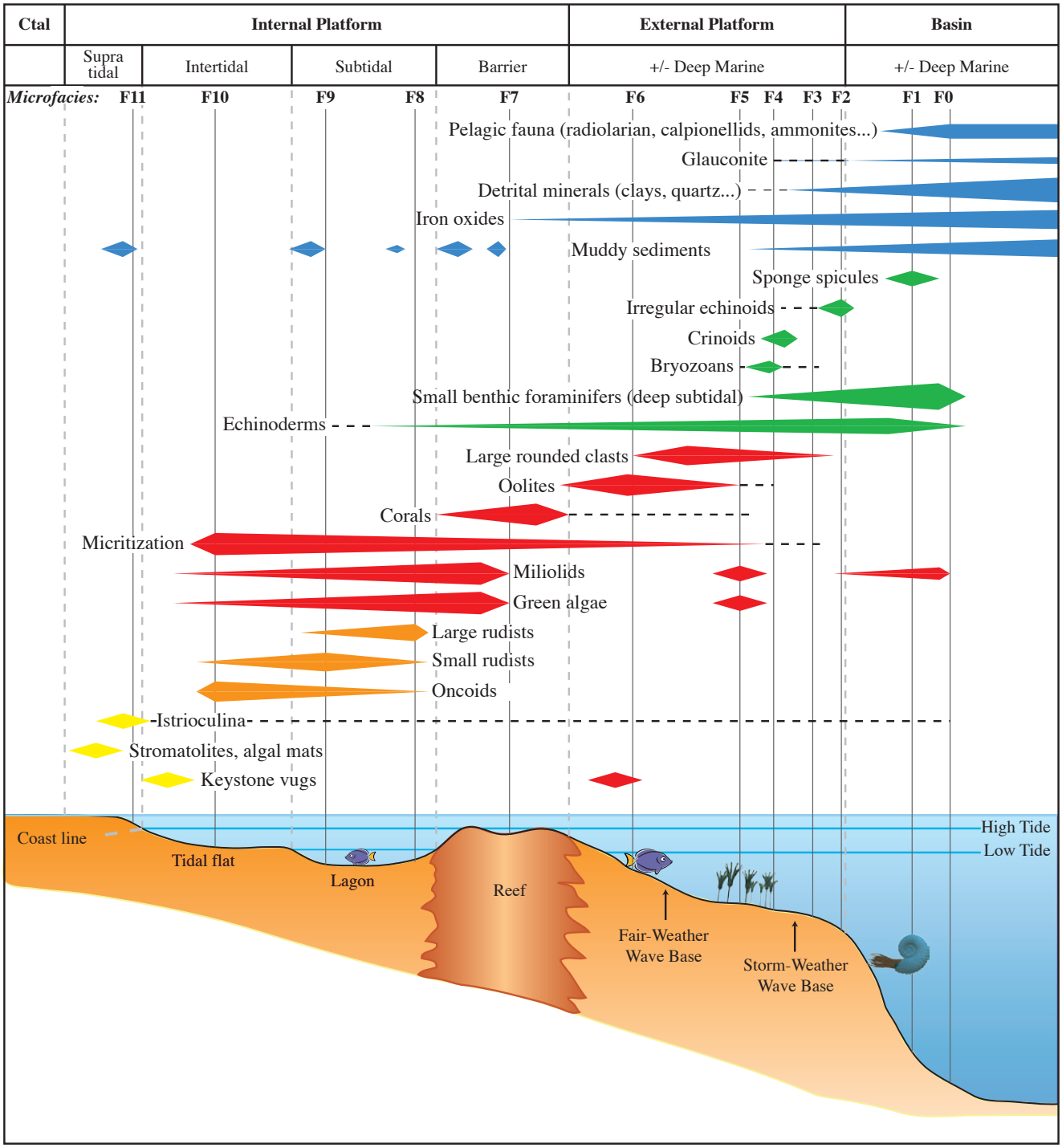

Fig B.8: Repartition of the microfacies along a standard platform profile. The distribution of the main clasts constitutive of carbonated rocks (redrawn after Fig. 21 in Arnaud-Vanneau and Arnaud, 2005).

Microfacies F5: biosparite with large subspherical bioclasts

Microfacies F5 corresponds to a grainstone with large, rounded clasts of bryozoans and crinoids; lithoclasts and peloids may also be found, as well as ooids. The main feature of the faunistic assemblage of F5 is the potential presence of orbitolinids.

The absence of a matrix suggests constant current action; consequently, this type of microfacies corresponds to the upper part of the outer platform, above the fair-weather wave base.

Microfacies F6: ooparite

Ooids are the main component of these grainstones; some crinoidal or bryozoan remains

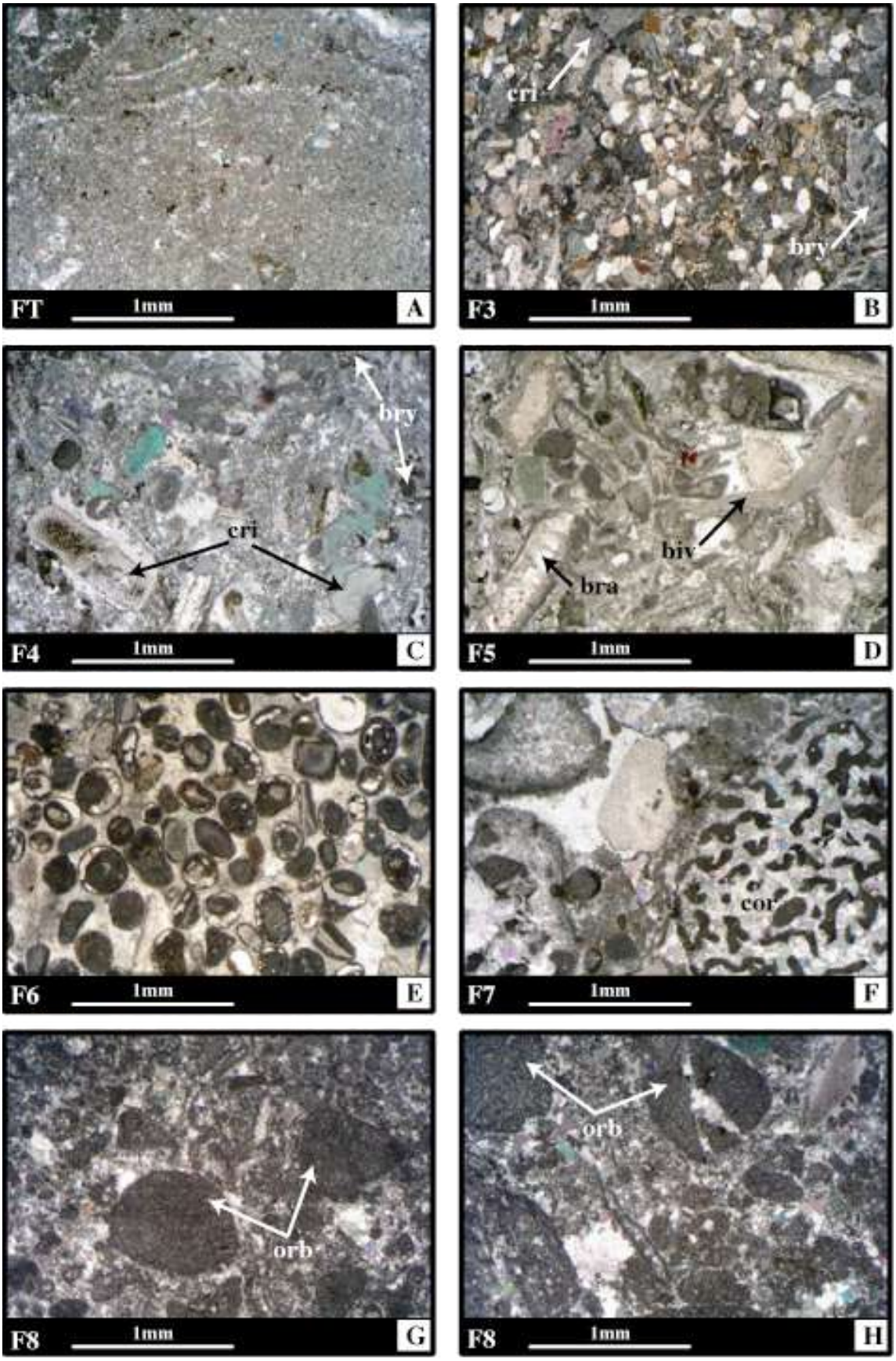

Fig B.9: Micrographs of the microfacies recognized in the studied sections. **A:** *FT, biomicrite with spicules of sponges and cnidarians remains;* **B:** *F3, biopelsparite with crinoidal remains and small foraminifera;* **C:** *F4, bioparite and biomicrite with crinoids and bryozoans;* **D:** *F5, bioparite with large subspherical bioclasts; E: F6, ooparite (note the presence of oomoldic porosity; sample ECII50, Eclépens);* **F:** *F7, biosparites and biomicrites with cnidariand and corals build-up;* **G and H:** *F8, biosparites and biomicrites with large benthic foraminifera and large rudists. Abbreviations: biv = bivalve; bra = brachiopod; bry = bryozoan; cor = coral; cri = crinoid; orb = orbitolinid.*

can be found, but they usually represent less than 5 % of the rock. The nature of the nuclei of the ooids is variable and may consist of quartz grains, bioclasts (*e.g.*, bivalves, crinoids) or foraminifera.

These oolitic deposits are characteristic of the uppermost part of the outer platform, where shallow-water environments are dominated by tidal currents.

Microfacies F7a and F7b: bioparite and biomicrite with cnidarians and coral build-up

The presence of corals or reef-related organisms (such as large bivalves and gastropods, regular echinoids), characterizes the microfacies F7a. Ooids can also be found in these grainstones to packstones. The presence of large benthic foraminifera such as orbitolinids would rather characterize microfacies F7b.

This type of microfacies characterizes the platform border, and especially infralittoral environments with low hydrodynamism where coral build-ups are preserved, or in high-energy infralittoral environments; in the latter case F7 corresponds to the break-up of the reefs.

Microfacies F8: biosparite and biomicrite with large benthic foraminifera and rudists

Rudists, foraminifera, unidentified micritized remains and rare, partially micritized crinoidal remains are found in these wackestones to packstones.

The micritization of the grains mirrors environments with low energy, where the beginning of the confinement allows for important bacterial processes. Sediments with microfacies F8 are thus deposited in the external part of the lagoon, protected by the reef from oceanic influences and storm currents.

Microfacies F9: biosparite and biomicrite with Miliolidae and small rudists

Because of the increasing confinement, the biodiversity decreases and the micritization of grains augments. Consequently, the main constituents of these microfacies are peloids (micritized bioclasts), Miliolidae and fragmented rudists, especially Requinidae. Some oncoids are sometimes also found.

Microfacies F9 thus characterizes the internal part of the lagoon, always submerged and particularly calm.

B.2.2. Key surfaces

The principles of sequence stratigraphy rest on the recognition of several types of key surfaces (Vail *et al.*, 1977, 1987):

The flooding surface, which lays on the bottom and the top of a packet of sediments corresponding to a parasequence.

The sequence boundary (Sb), which corresponds to the maximum of sea-level fall.

The transgressive surface (TS), which reflects the beginning of the sea-level rise.

The maximum flooding surface (mfs), which develops during the maximum of sea-level rise.

In Fig. B.10, the organisation of the sediments during the development of one depositional sequence is presented, as well as the position of the above-mentioned surfaces during one transgression – regression cycle.

Based on field observations and microfacies evolution, sequence and parasequence boundaries are defined; they are usually characterized by a shift from shallow to deeper environments on the microfacies evolution curve.

Sequence boundaries are usually irregular surfaces reflecting the erosion of the bed on which they occur. The identification of the regime of erosion – aerial or submarine – may allow to differentiate type 1 from type 2 sequence boundaries (*e.g.* Vail *et al.*, 1987). Sedimentological evidences for both types of sequence boundary are the following:

Type 1 sequence boundary: in this case, the sea-level fall exceeds the shelf edge, leading to the emersion of the platform. Consequently, karst features may occur, as well as meteoric

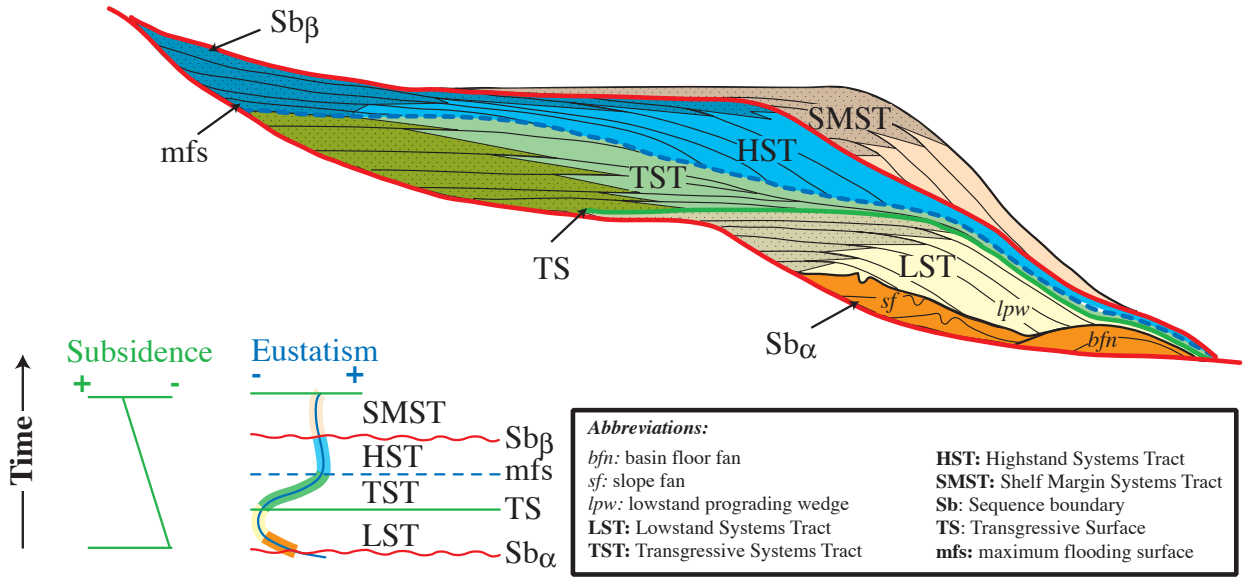

Fig. B10: Depositional model of a complete type 1 sequence and of the lowstand deposits of a type 2 sequence, with the corresponding systems tracts and sea-level curve (after Vail et al., 1977, 1987).

diagenetic overprints, such as phreatic cements and dolomitization (*e.g.*, Sarg, 1988).

Type 2 sequence boundary: as the platform is still under the influence of shallow marine waters, reworking and winnowing processes may dominate the sedimentation on the outer shelf, whereas the inner platform may undergo the same diagenetic changes as in the case of a type 1 sequence boundary.

A third type of sequence boundary was added by Schlager in 1999, and occurs when sea-level fall is less rapid than the subsidence rate, so that the highstand systems tract is immediately followed by a transgressive systems tract. In this case, the platform undergoes a drowning phase, for which the sedimentological features are the presence of high amount of glauconite and / or phosphate associated with hardgrounds.

B.2.3. The Eclépens section

Based on thin-section analysis and field observations (Fig. B.11), a sequence stratigraphic scheme of the section at Eclépens is proposed.

B.2.3.1. Description of the section

The first eight meters of this section are composed of obliquely stratified, oolitic grainstones, with some bioclasts (bivalves, brachiopods, bryozoans), crinoidal remains and siliceous lenses, which is characteristic of the lower Pierre Jaune de Neuchâtel (*e.g.*, Remane, 1989). Then, this succession characteristic of dynamic sedimentation pattern is topped by an erosive surface (truncation of oblique stratifications at the top), which is also perforated, encrusted by oysters and enriched in glauconite; this boundary is interpreted as an hardground and is directly followed by a twenty centimetres-thick interval of clay which exhibits a high content of glauconite (up to 25 %), and which is thought to correspond to the Marnes d'Uttins. The latter is followed by the sediments of the upper Pierre Jaune de Neuchâtel, which starts with a two meters-thick bed of marly limestone (oolitic wackestone texture) with large bivalves (*Panopea*) and brachiopods (mainly terebratulids), and which gradually evolves into an oolitic grainstone deposited in a high energy environment, as suggested by the presence of numerous oblique stratifications characteristic of oolitic submarine shoals. The remainder of the upper Pierre Jaune de Neuchâtel is characterized

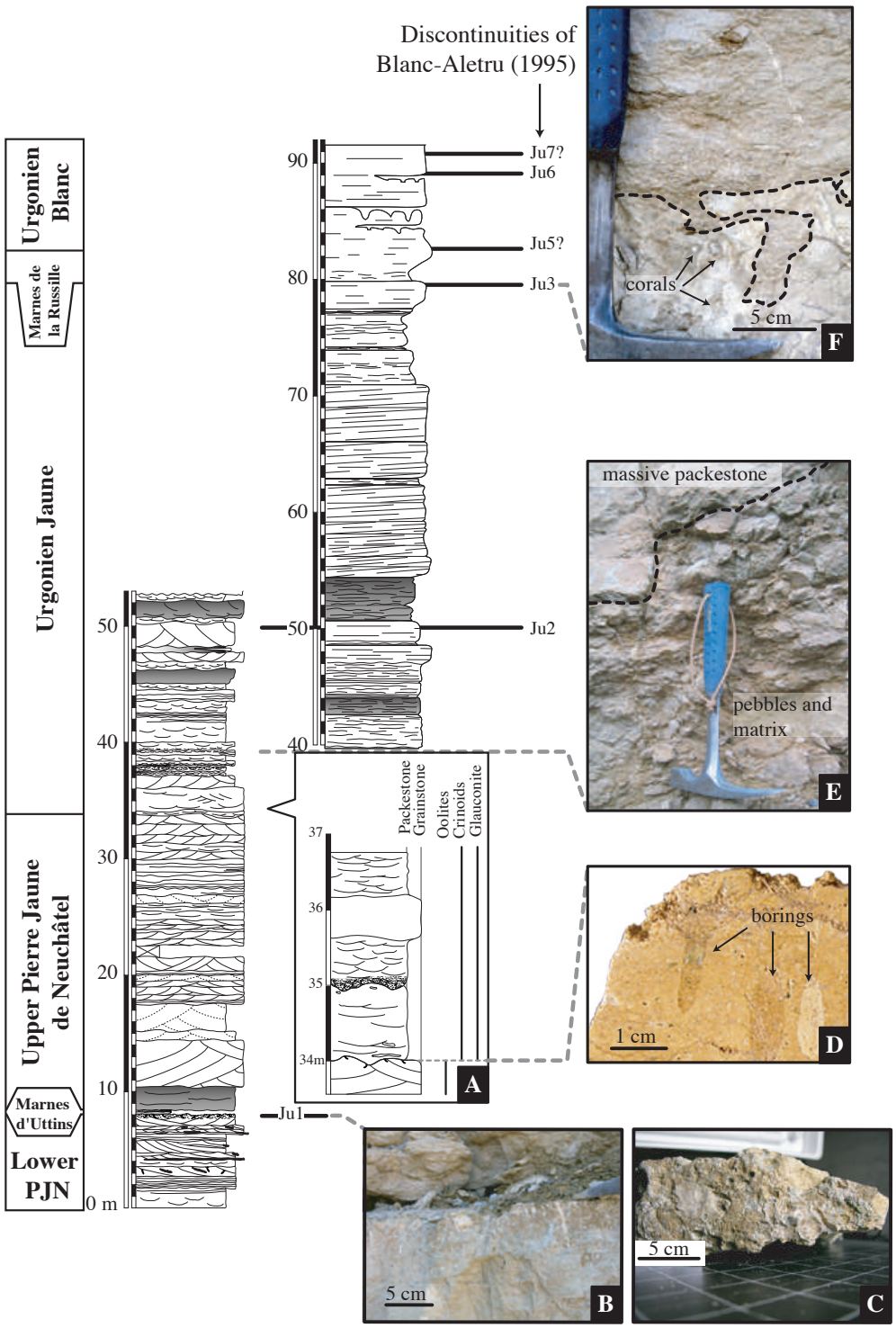

Fig. B.11: Sedimentological log of the Eclépens section. A: close-up on the facies change that occurs at 34m depth is given; B: erosive, perforated hardground with encrusted oysters at the base of the Marnes d'Uttins; C: view of this hardground showing borings and encrusted oystersD: borings on the erosive surface that marks the facies change from an oolitic grainstone to a bioclastic packstone: E: reworking (pebbles of limestones in a marly matrix) at the base of the Urgonien Jaune; F: erosive base of the Marnes de la Russille.

by oolitic packstone to grainstone, with more or less well-expressed oblique stratifications. Contrary to the lower Pierre Jaune de Neuchâtel, this interval, which measures 24m in thickness, contains no cherts.

The boundary between the upper Pierre Jaune and the overlying Urgonien Jaune is associated with an erosive and perforated surface and the abrupt change from an oolitic grainstone to a bioclastic packstone containing glauconite. The latter is rapidly followed by the first levels containing reworked sediments, including nodules and pebbles enrolled in a marly or clayey matrix.

The base of this interval clearly corresponds to an erosive surface: incisions are found in the northern part of the quarry. Moreover, this surface cuts different facies, such as oolitic grainstone and bioclastic, glauconite-rich packstone (Fig. B.12). Then, the sedimentary succession is characterized by 2.9m of bioclastic packstone with clayey layers which are laterally discontinuous. This feature may reflect an increase in reworking processes, as is suggested by the finding of several pebbles of allochtonous material with encrusted oysters on all sides, before the return of bioclastic and glauconitic packstone to grainstone with rare oolites and cross-stratifications.

In the interval between 37 to 40m of the section, the amount of glauconite increases rapidly, as well as the amount of clay. This interval is composed of three beds of bioclastic packstone (ca. 0.3m thick) alternating with marly

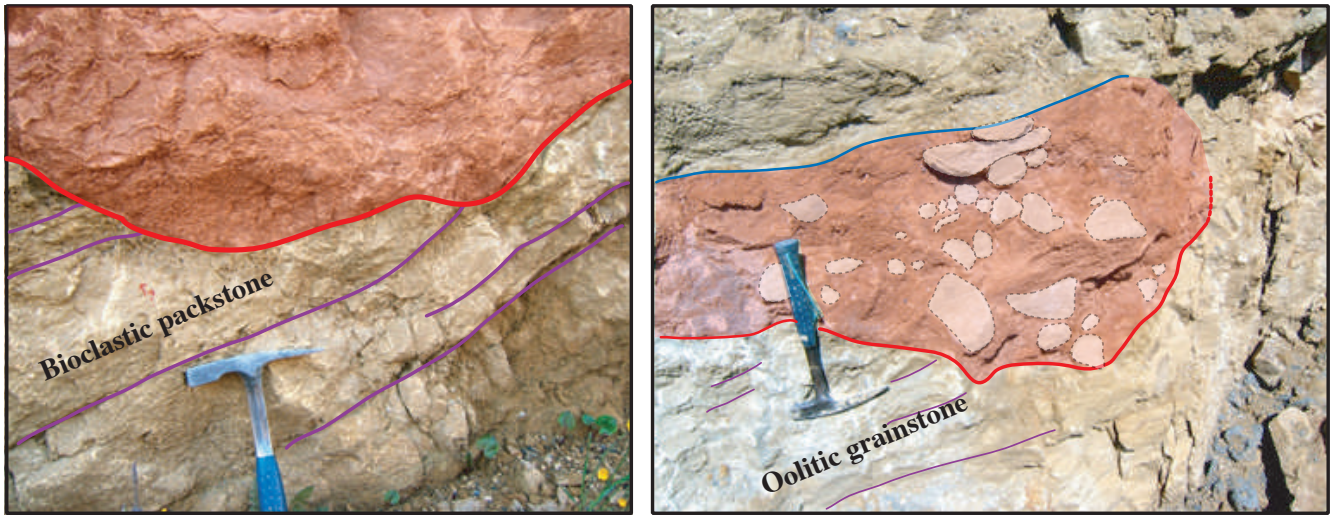

Fig. B.12: Field-pictures of the erosive boundary between the upper Pierre Jaune de Neuchâtel and the Urgonien Jaune. Note the truncation of the underlying oblique stratifications and, on the right hand, the size of pebbles and cobbles.

intervals (thickness ranging from 0.1 to 0.5m). A close-up of this part of the section is given in Fig. B.13, with the main sedimentologic and facies properties of the interval between 34 and 53m.

The upper part of the section was studied in detail by Blanc-Aletru (1995), who performed sedimentological and micropaleontological analysis; in the following, we will thus refrain from an in-depth description of the succession, but only put forward its main features. Blanc-Aletru (1995) proposed a threefold division of the section:

From 50 to 71 m: oolitic facies similar to those of the Pierre Jaune de Neuchâtel are recognized, but they belong to the Urgonien Jaune. At 71 m, Blanc-Aletru (1995) remarked the presence of dissolution in the cortex of the oolites and of an erosive surface, interpreted as a sequence boundary (Ju3 after Blanc-Aletru, 1995).

From 71 to 83 m, Blanc-Aletru (1995) described three subsets:

From 71 to 76 m, mudstones to wackestones with corals fragments, transported foraminifera (with some orbitolinids) and algae, calcareous sponges.

From 76 to 80 m, a transition from bio-ooclastic facies at the base to oolitic grainstones with dissolution of the cortex at the top which are interpreted to be the consequence of a major discontinuity (Ju5 in Blanc-Aletru, 1995).

From 80 to 83 m, the facies is similar to the one described between 71 and 76 m. Blanc-Aletru (1995) attributed these deposits to the Marnes de la Russille.

From 83 to 92 m (top of the section): the facies changes from a wackestone to packstone rich in foraminifera, particularly in orbitolinids (between 83 and 90 m), toward a rudist-bearing facies (90 to 92 m). The presence of karsts is

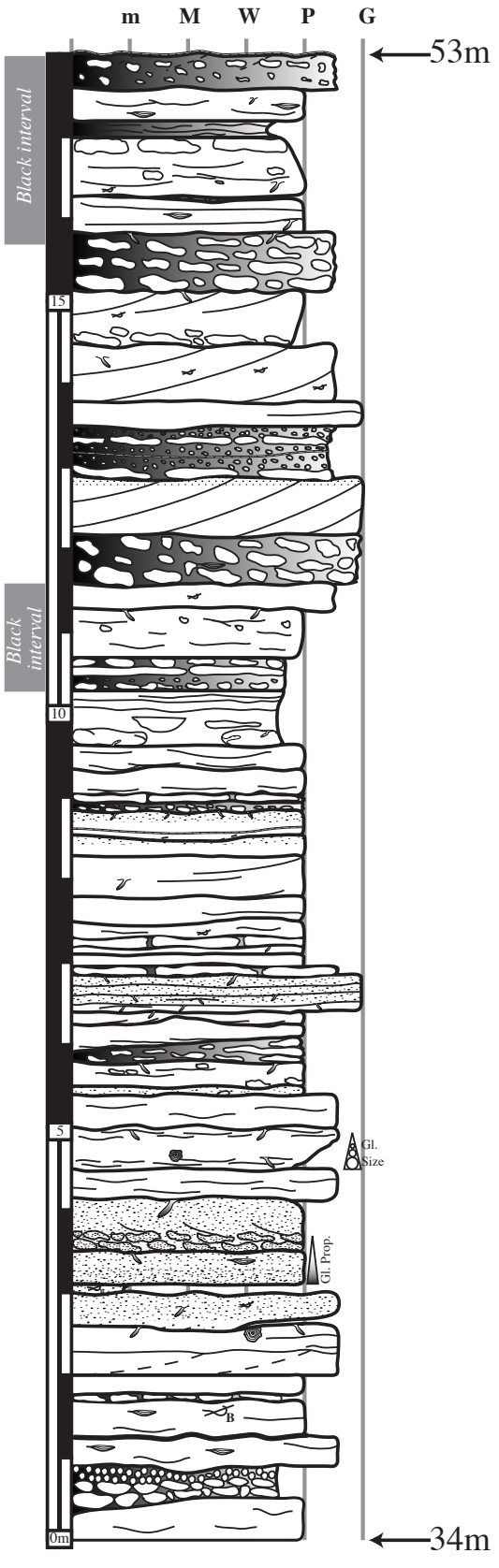

Fig. B.13: Detailed sedimentological log of the interval between 34 and 53 m depth. Note the numerous levels of reworking facies.

noted in this part of the section, which corresponds to the Urgonien Blanc.

B.2.3.2. Sequence stratigraphy of the Eclépens section

The evolution of the microfacies through the entire section, as well as the sequence stratigraphic interpretation, is given in Fig. B.14.

In the lower part of the section, *i.e.* in the Pierre Jaune de Neuchâtel, the microfacies exhibits a shallowing upward evolution from F4 to F6, except for the Marnes d'Uttins interval, which is composed of F3 microfacies. The presence of glauconite, borings and encrusted oysters in this key-surface helps to interpret the hardground of the Marnes d'Uttins as a type 2 sequence boundary. In the following, it will be called SbE1.

As previously said, the Pierre Jaune de Neuchâtel ends with an erosive surface associated with a change in the type of limestone. This surface may represent a second sequence boundary (SbE2), and consequently the marls of the Marnes d'Uttins may correspond to a maximum flooding surface (mfsE1); this implies that the transgressive surface of the first sequence is stacked to the SbE1 or to the mfsE1.

In the interval between 34 and 57 m (see Fig. B.13), the identification of sequence boundary(-ies) is more delicate, in particular due to the reworking processes that imply the mixing of several types of pebbles within marls, and the presence of several sharply erosive surfaces, which may all represent sequence boundaries. In particular, we identify the base of the upper black interval located at approximately 50 m depth as a sequence boundary (SbE3), following Blanc-Aletru (1995). On the other hand, the maximum flooding surface of the sequence 2 (mfsE2) corresponds to a 50 cm-thick marly interval with high content of glauconite and quartz (microfacies FT).

Then in the Urgonien Jaune, several parasequence boundaries are identified from the microfacies evolution: they usually correspond to abrupt shifts from F6 to F3 microfacies. Moreover, the microfacies throughout the Urgonien Jaune displays a general deepening upward stacking pattern; the location of the "deepest" microfacies implies that the Marnes de la Russille correspond to a maximum flooding

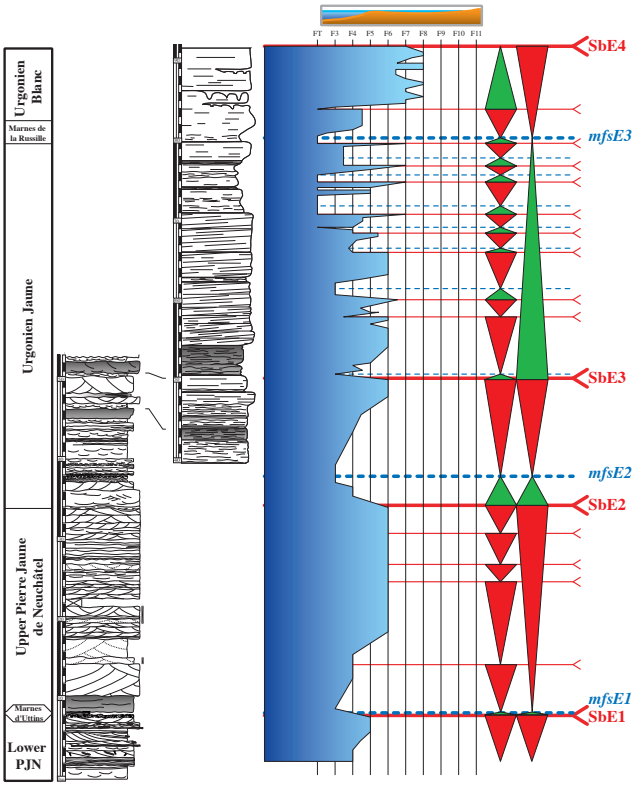

Fig. B.14: Sequence stratigraphy interpretation of the Eclépens section based on the evolution of the microfacies. The triangles on the right hand may correspond to 3rd-order sequences.

surface (mfsE3). This is also supported by the general shallowing upward evolution observed in the Urgonien Blanc, from microfacies F4 / F5 to F8. The karsts which cut through the top of the Urgonien Blanc are interpreted as a type 1 sequence boundary (SbE4), and may reflect the end of the development of the Urgonian platform; the presence of ammonites attributed to the *Deshayesites deshayesi – Deshayesites bowerbanki* zones within similar karsts in the Val de Travers (Renz and Jung, 1978), suggests that this sequence boundary corresponds to the SbA2 of Arnaud (2005), which is coherent with the dating of the end of the development of the Urgonian formations in the Vercors (Arnaud *et al.*, 1998), or in the Helvetic Alps (P. Linder, pers. com.; Föllmi *et al.*, in press).

To summarize, the sedimentary succession in the Eclépens section is mainly characteristic of relatively high-energy dynamics, as suggested by the presence of oblique stratifications within the Pierre Jaune de Neuchâtel, and of reworking processes, in particular in the basal Urgonien Jaune. Several key-surfaces corresponding to sequence boundaries constitute good candidates for temporal gaps: condensation may have occurred within the Marnes d'Uttins, and a part of the sedimentary archives may be missing at the base of the Urgonien Jaune, because of the erosion highlighted by the truncation of underlying oblique stratifications and by the presence of heterometric, polygenic conglomerate just above. Even if the Eclépens section represent a very good location for studying these processes and for performing sequence stratigraphy, we propose now to check if these clues for a sedimentary gap can be found in other sections of the Western Swiss Jura.

B.2.4. Identification of the main sequence boundaries in the Western Swiss Jura

B.2.4.1. The Gorges de l'Areuse section

Located approximately ten kilometres southwesternward from Neuchâtel (Fig. B.15), the Gorges de l'Areuse section represents very proximal environments and allows to focus on the Pierre Jaune de Neuchâtel – Urgonien Jaune boundary. The section, as well as its sequence stratigraphic interpretation, are illustrated in the Fig. B.16. The major part of the Gorges de l'Areuse section is composed of oolitic grainstones organised in cross-stratified beds, which are easily recognizable.

In the top of the section, the good quality of the outcrop allows the description of a typical (para-)sequence. At 6.40 m, an erosive surface with burrows is described, the laminations of the lower bank displaying toplap features. On this surface, which may correspond to the discontinuity "ER" of Blanc-Aletru (1995), a marly interval (about 10 cm) contains some bioclastic pebbles. At 6 m depth, clues for channels were found. Upwards, oolitic banks are present in the following 3 meters. At 3 m depth, a very thin clayey layer (less than 5 cm) separates a grainstone with oolites, crinoids, glauconite and some burrows (sample GA 11) from a packestone / grainstones with oolites and bioclastes (sample GA10). Above this, 3 meters of oolitic grainstones are exposed. Finally, a major discontinuity is observed at the top of that part of

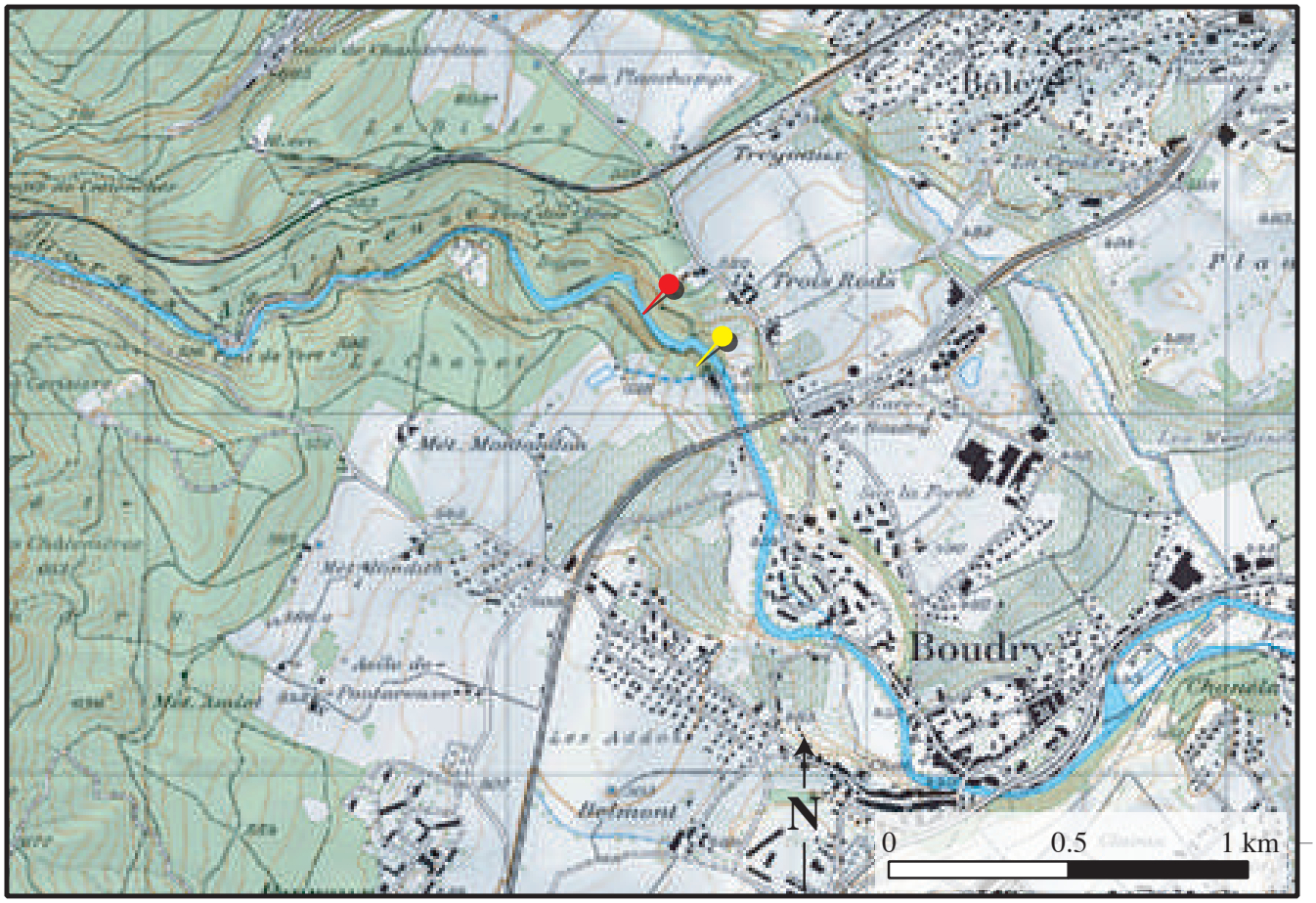

Fig. B.15: Location of the Gorges de l'Areuse (white pin. Swiss coordinates: 553'460/201'179) and Boudry sections (grey pin. Swiss coordinates: 553'545/201'144). Topographic map at 1/25'000 scale.

the section. This erosive surface is perforated and overlaid by a conglomerate with a marly matrix.

This kind of succession is repeated in the bottom of the section almost two times, with marly or clayey intervals more or less well-expressed. The section ends in a little depression, where the last bank of oolitic grainstone with cross stratifications surmounts a 50 cm thick interval of marl.

Thirty-six thin sections were analysed in order to determine the main microfacies that occurred in the upper part of the Gorges de l'Areuse section. The microfacies range from the F3 to the F6 microfacies of Arnaud – Vanneau (1980).

From the determination of the microfacies, a sequence stratigraphic interpretation is proposed:

From the base of the section to 9.10 m, the evolution of the microfacies is very monotonous, only a slight shift from F4 to F6 is noted between 16.30 and 14.60 m; upward, the microfacies F6 dominates.

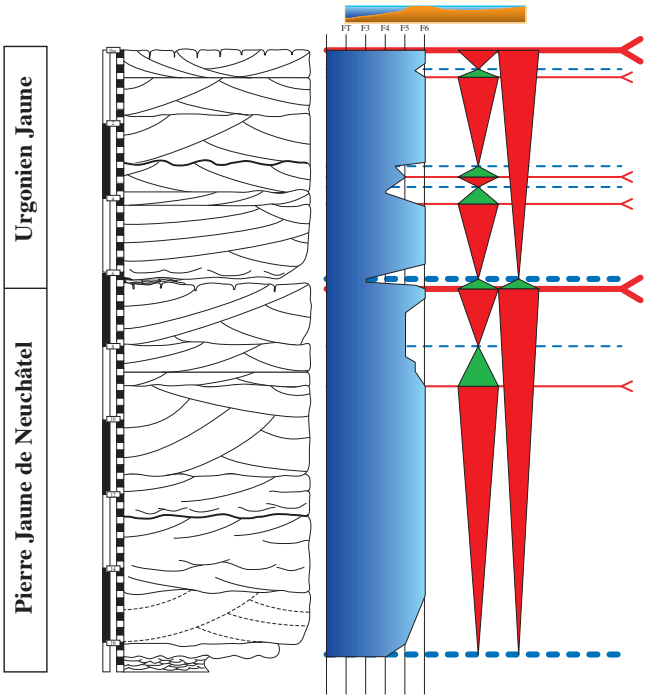

Fig. B.16: Sequence stratigraphy interpretation of the Gorges de l'Areuse section based on the evolution of the microfacies. The triangles on the right hand may correspond to 3rd-order sequences.

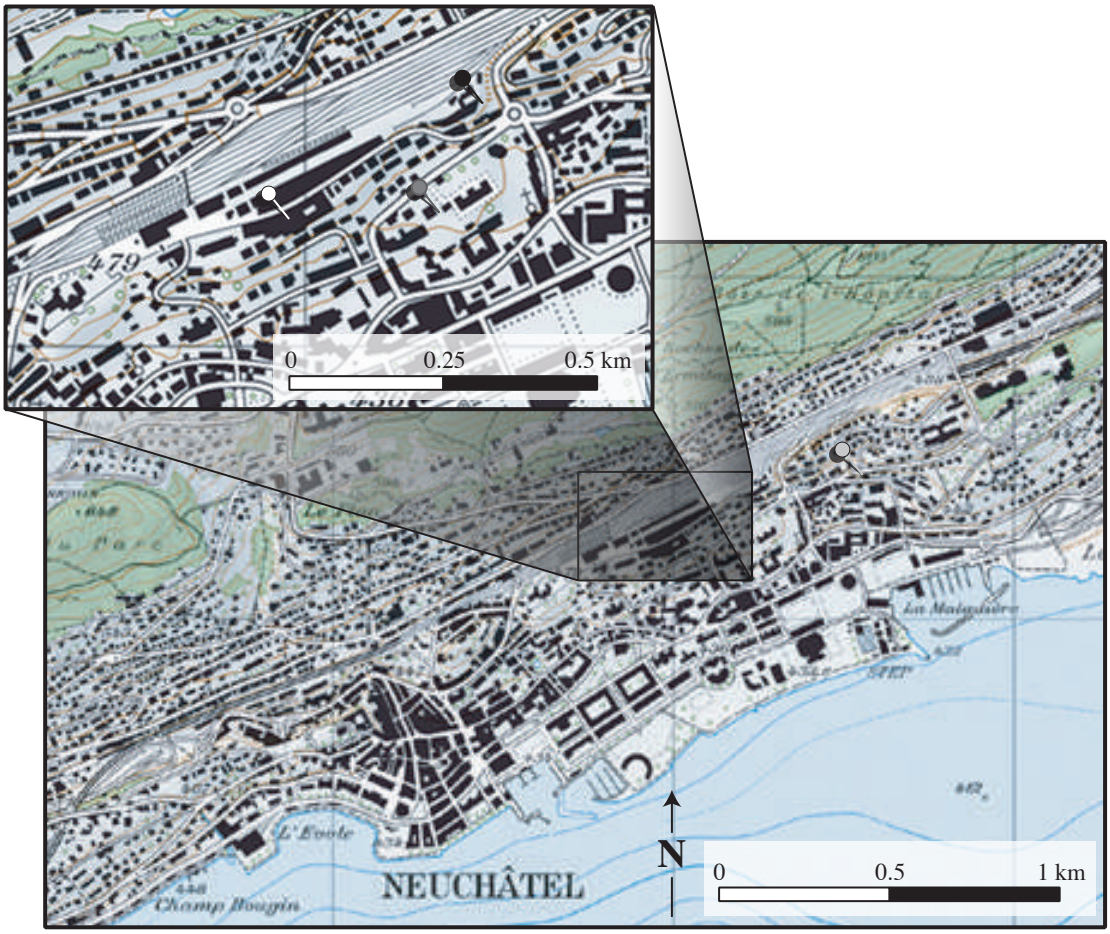

Fig. B.17: Location of the Railway Station, Crêt-Taconnet and Pourtales Hospital sections, and of the Borehole F-607 (black, white, dark grey and light grey pin, respectively. Swiss coordinates: 562'261/205'427, 562'075/205'278, 562'247/205'225, and 562'560/205'390, respectively). Topographic map at 1/25'000 scale.

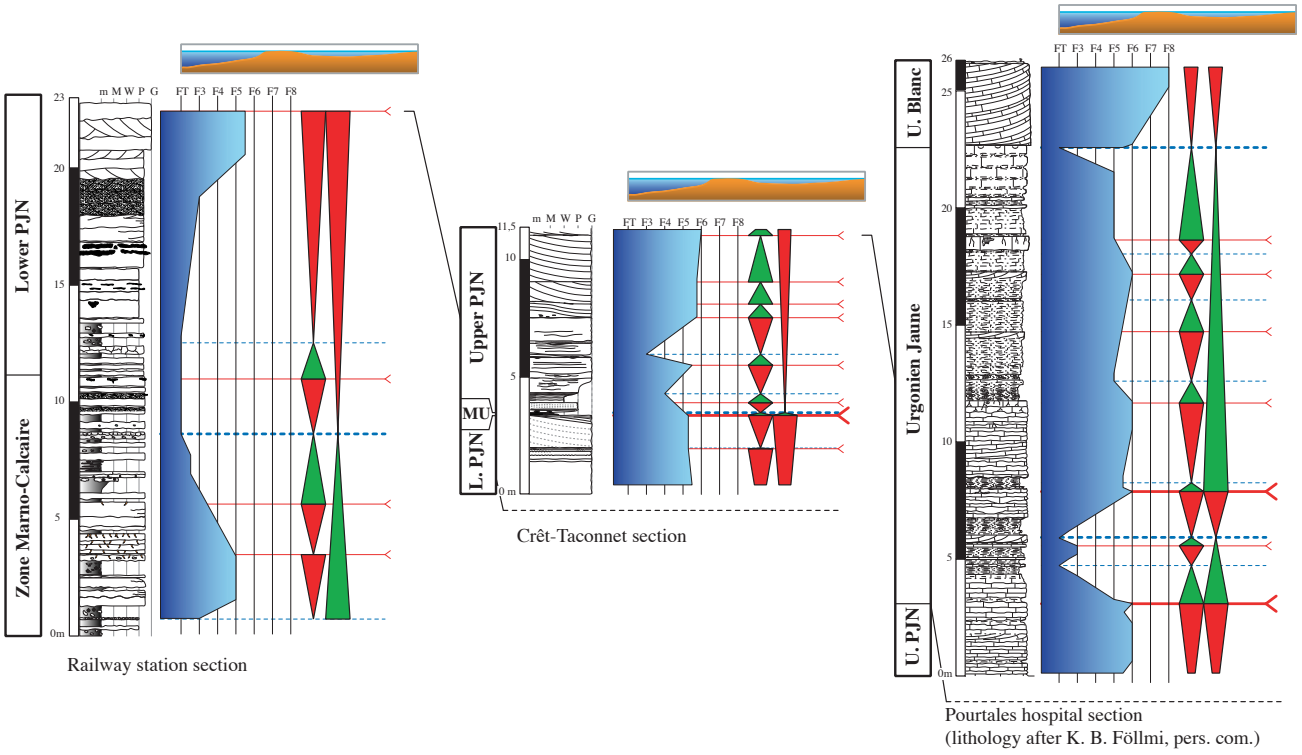

Fig. B.18: Sequence stratigraphy interpretation of the Railway Station, Cret-Taconnet and Pourtales Hospital sections based on the evolution of the microfacies. The triangles on the right hand may correspond to 3rd-order sequences. The black lines between the sections represent the supposed correlations between the three locations.

From 9.10 m to 6.40 m: the evolution of the microfacies is shallowing upward, from F5 to F6. At 6.50 m, the erosive and perforated surface marks a parasequence boundary. In thin section, some ooid cortexes show traces of dissolution (oomoldic porosity). This interval corresponds to a highstand deposit.

From 6.50 m to 6.20 m: the F3 microfacies dominates, implying the presence of a flooding surface. This interval corresponds to a transgressive deposit.

From 6.20 m to 3.10 m: here again, the evolution of the microfacies is shallowing upward, and the thin section from sample GA11 displays dissolution features and recristallisation characteristic of a parasequence boundary. This interval corresponds to a highstand deposit.

From 3.10 m to the top: except the very thin clay layer described between samples GA10 and GA11, the microfacies displays a general shallowing upward evolution. As previously said, the top of the section is characterized by an erosive and perforated surface, which is interpreted as a parasequence boundary whereas the clay level at 3.10 m may represent a flooding surface. So, the last 3 m of the section represents a complete parasequence with a small interval of transgressive deposits and several meter thick highstand deposits.

B.2.4.2. The Neuchâtel composite section

The sections of the Railway Station, Crêt-Taconnet and Pourtalès Hospital were logged in Neuchâtel itself (Fig. B.17), and constitute a composite succession from the Zone Marno-Calcaire (Railway Station) to the base of the Urgonien Blanc (Pourtalès Hospital). They are illustrated in the Fig. B.18, as well as their

Fig. B.19: Location of the Vaumarcus section (between the two pins. Approximated Swiss coordinates: 547'729/191'030). Topographic map at 1/25'000 scale.

respective sequence stratigraphic interpretation.

The Pierre Jaune de Neuchâtel and the Urgonien Blanc display facies similar to that observed at Eclépens. Concerning the Urgonien Jaune, the reworking is less important than at Eclépens, in particular the nodular intervals are less thick; however, the clay content remains important in this part of the succession. Finally, the Railway Station allows the observation of a part of the Zone Marno-Calcaire. The later consists of an alternation of reddish, yellowish to greenish marls with small nodules, with crinoidal limestones (packstone to grainstone) with a more or less important content of glauconite, with rhynchonellids and some burrows.

Four (maximum) flooding surfaces and three (para-)sequence boundaries were recognized:

Within the Zone Marno-Calcaire, a nodular bed of limestones, with a high content of glauconite, of brachiopods and bivalves, may correspond to a (maximum) flooding surface.

Then, in the Crêt-Taconnet section, the disappearance of siliceous lenses and nodules which characterize the lower Pierre Jaune de Neuchâtel, is accompanied by an erosive surface (truncation of the underlying oblique stratifications), and by an increase in the glauconite content. This surface is interpreted as a (para-)sequence boundary.

At the top of the lower Pierre Jaune de Neuchâtel in the Crêt-Taconnet section, a ca. 20 cm-thick marly, greenish interval develops, and may corresponds to the Marnes d'Uttins. Unfortunately, in the lack of ammonites, it is impossible to confirm the presence of this level in the Neuchâtel composite.

At the base of the Pourtalès Hospital section, the microfacies are relatively homogenous (F6), and then rapidly shift toward deeper microfacies (FT to F3). This variation is accompanied by a change in the type of carbonate, from an oolitic grainstone to a bioclastic packstone -grainstone. The corresponding surface is thus interpreted as a (para-)sequence boundary.

Moreover, the above-mentioned shift in the microfacies curve from F6 to FT points out to the presence of a (maximum) flooding surface, approximately three meters above the sequence boundary.

Finally, between the Urgonien Jaune and the Urgonien Blanc of the Pourtalès section, the microfacies rapidly evolves from F5 to FT then to F6-F8; this negative spike may reflect a (maximum) flooding surface.

B.2.4.3. The Vaumarcus section

This section is located approximately 25 km westward from Neuchâtel (Fig. B.19) and allows

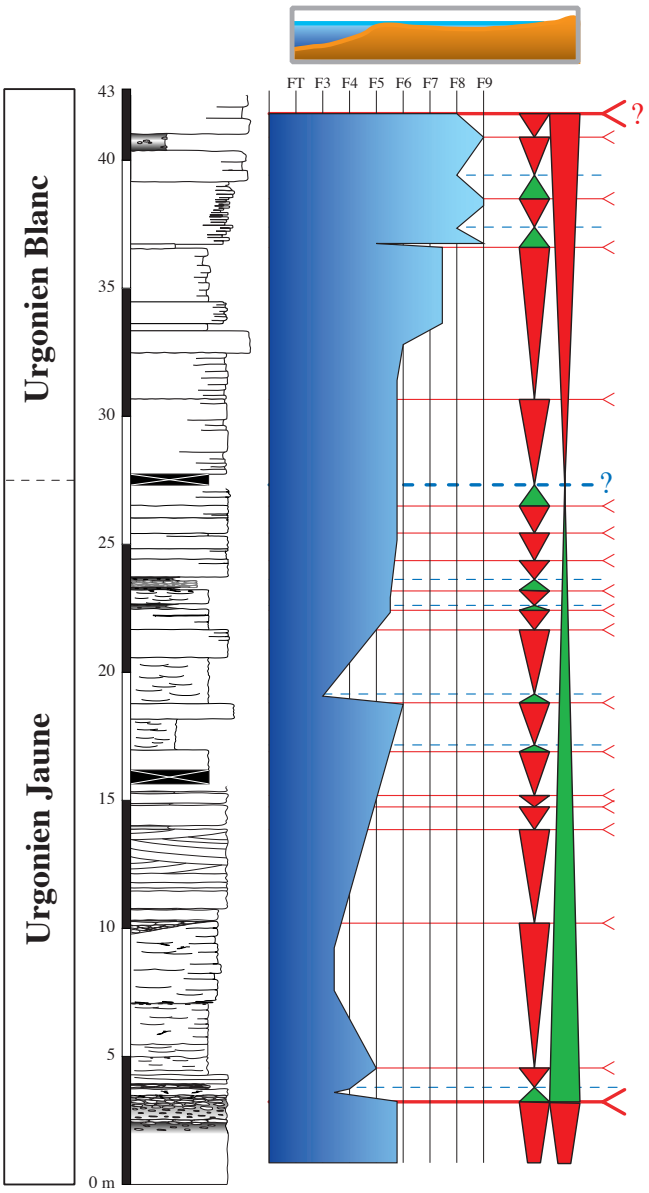

Fig. B.20: Sequence stratigraphy interpretation of the Vaumarcus section based on the evolution of the microfacies. The triangles on the right hand may correspond to 3rd-order sequences.

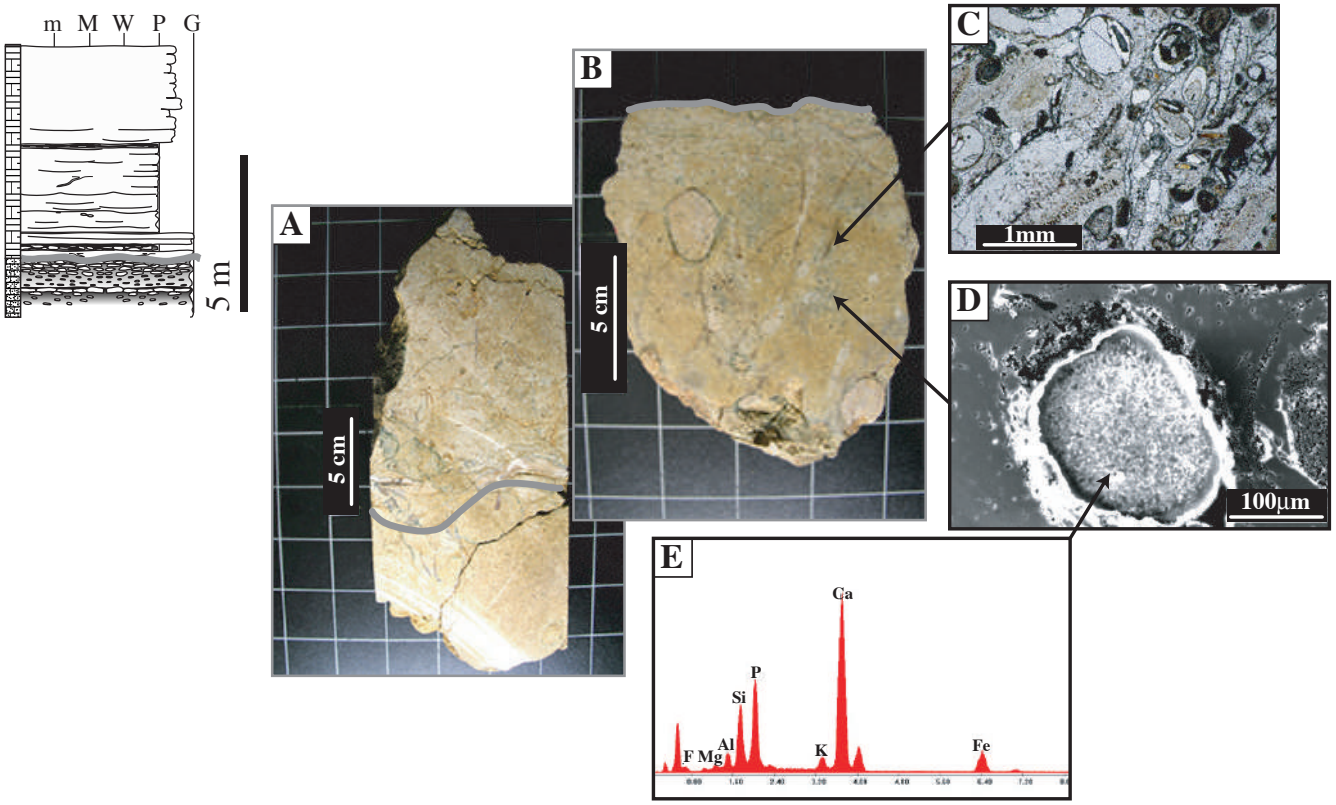

*Fig. B.21: Close-up on the sequence boundary (grey line on the profile, and on pictures A and B) located at the base of the Vaumarcus section. Note the high content of glauconite in the polished slabs (***A** *and* **B***), as well as the presence of oomoldic porosity (***C:** *thin section picture) just under the sequence boundary. The presence of phosphate grains (***D:** *SEM image) has been revealed using EDS (***E:** *analytical spectrum corresponding to D).*

the observation of the last meters of the Pierre Jaune de Neuchâtel (?), and of the entire Urgonien Jaune and Urgonien Blanc (Fig. B.20); the Marnes de la Russille are lacking, certainly due to a bad exposure of the outcrop.

The base of the section is composed of oolitic grainstones characteristic of the microfacies F6, with a well- developed oomoldic porosity (see Fig. B.21 for an example). In this part, sedimentary reworking seems to be important as suggested by the presence of numerous nodules, which are sometimes perforated. On the other hand, an erosive and glauconitised surface is mirrored by a rapid shift in the microfacies curve toward F3; consequently, this first remarkable surface may be a (para-)sequence boundary. Some thin sections of this interval were prospected at the Institute of Microtechnics (University of Neuchâtel), using a Scanning Electronic Microscope (SEM) coupled with a Energy Dispersive Spectrometry (EDS) (Fig. B.21). This approach reveals the presence of sparse phosphate grains, which implies that some condensation may have been associated to this sequence boundary.

Upward, the sedimentary succession exhibits facies typical of the Urgonien Jaune, *i.e.* bioclastic and oolitic packstone to grainstone with more or less glauconite. Moreover, erosional features are noted, such as erosive surfaces and channels. Some meter-thick interval are composed of well-sorted, clean oolitic grainstones with planar or slightly tilted stratifications; the stacking pattern is thinning upward. This type of interval are interpreted as very shallow parasequences, maybe deposited near the shore.

At 28 m depth, the first facies of the Urgonien Blanc appear, with white oolitic and peloidal grainstone; because of the unobservable area, the position of a maximum flooding surface may be extrapolated within this interval. Through the Urgonien Blanc, the microfacies evolves gently from F6 to F9. At the top of the observed sedimentary succession, the location of a sequence boundary is suggested by comparison with the La Lance section located just a few kilometres from Vaumarcus (Blanc-Aletru, 1995).

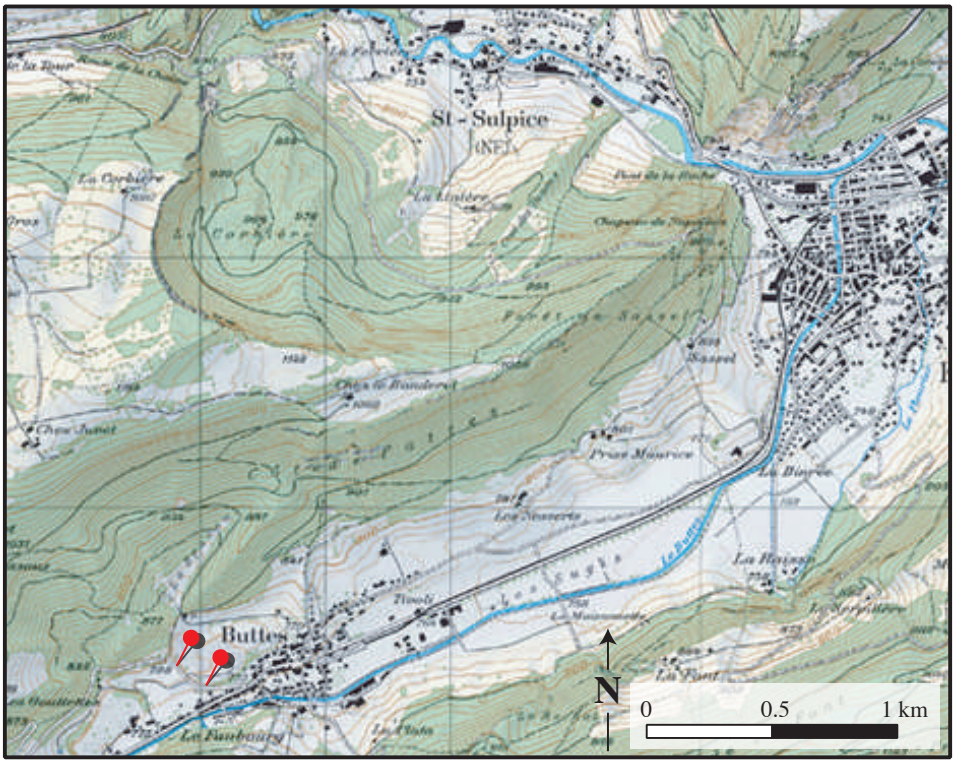

Fig. B.22: Location of the Buttes section (between the two pins. Approximated Swiss coordinates: 531'990/193'287). Topographic map at 1/25'000 scale.

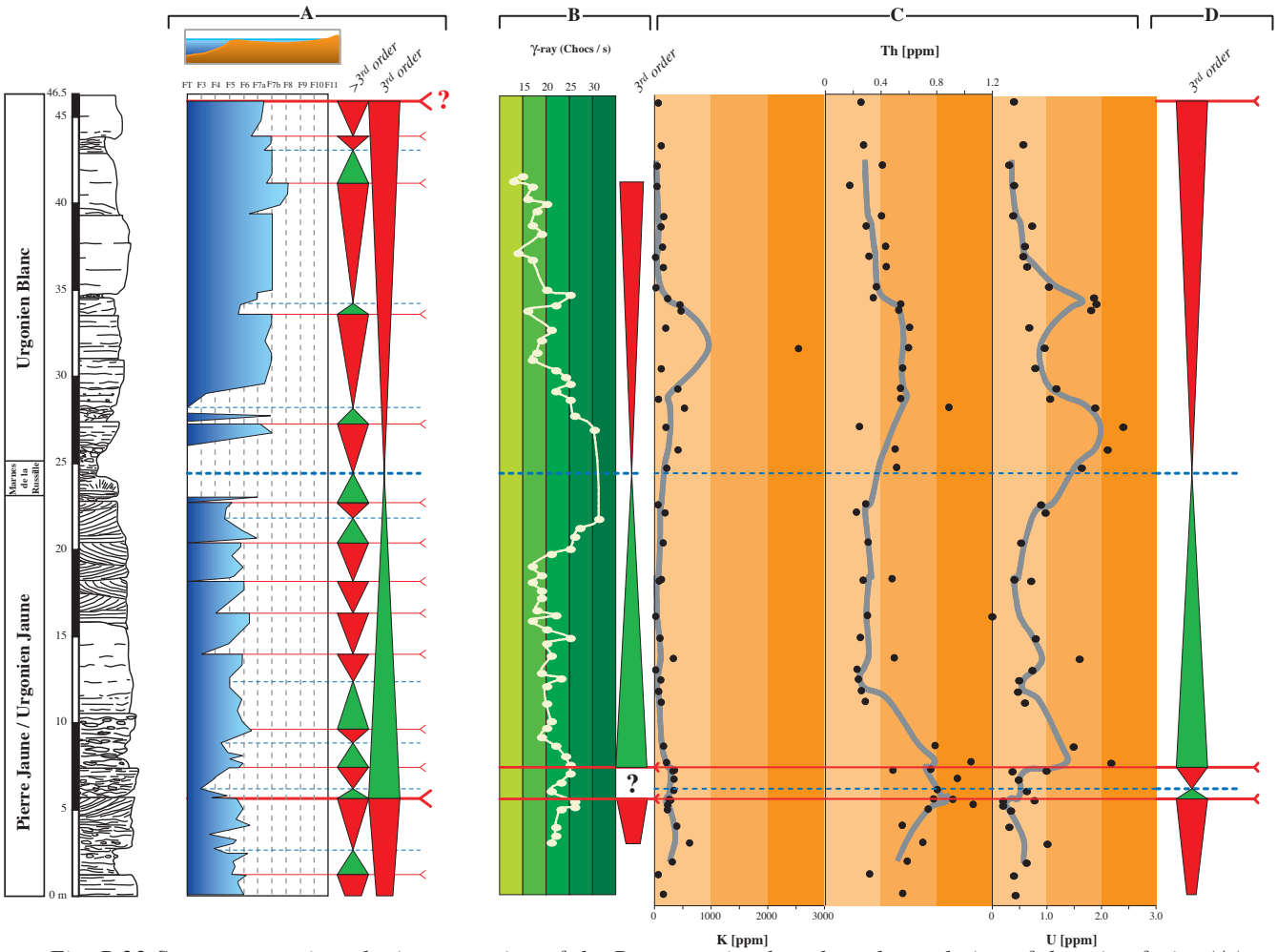

*Fig. B.23 Sequence stratigraphy interpretation of the Buttes section based on the evolution of the microfacies (**A**) as well as on the γ–ray prospecting (**B**). Potassium, Thorium and Uranium curves are also reported (**C**). On the right hand, a sequence stratigraphy scheme is proposed, which integrates both approaches (**D**).*

B.2.4.4. The Buttes section

Located 35 km westward from Neuchâtel (Fig. B.22), this section covers the sedimentary succession from the uppermost Pierre Jaune de Neuchâtel to the top of the Urgonien Blanc. The displayed facies are relatively similar to the ones observed at Vaumarcus, and were already described by Blanc-Aletru (1995); we will thus refrain from an in-depth description of the section and rather focus on the approach we applied.

The Buttes section was prospected in collaboration with Mohamed Chaker Raddadi (University of Grenoble, France), which field of interest is the recognition of key surfaces by means of measurements of natural radioactivity (γ-Ray; *e.g.*, Raddadi *et al.*, 2005). For this, sixty-one in-place analyses were performed using a portable scintillometer which was carried along the sedimentary profile, as shown on the Fig. B.23. Moreover, uranium, potassium and thorium contents were obtained by ICP-MS at the Institute of Geology (University of Neuchâtel); the results are also reported in Fig. B.23, as well as the sequence stratigraphic interpretation based both on this approach and on the microfacies analysis in thin sections.

Thanks to microfacies, one major sequence boundary was identified at 6 m depth; it corresponds to a shift from F6 to F3. Then, several shallowing-upward parasequences are stacked. The maximum flooding surface may correspond to the interval of the Marnes de la Russilles between 23 and 25m, which is dominated by microfacies FT. Finally, the microfacies within the Urgonien Blanc exhibits a shallowing-upward tendency; a final sequence boundary is assigned to the top of this last formation.

Concerning the γ-Ray, the curve shown in Fig. B.23 is well correlated with the sequence stratigraphic interpretation based on the microfacies, as the highest values of the γ-Ray corresponds to a sequence boundary or a maximum flooding surface; this statement is in agreement with the conclusions of Raddadi *et al.* (2005), who studied Late Barremian – earliest Aptian shallow-water carbonates from the Vercors area, and concluded that the maximum in the γ-Ray values were correlated with sequence boundaries or maximum flooding surface. Moreover, these authors supposed that the high γ-Ray values were principally linked to uranium, which may be contained within echinoderm remains.

However, the first peak in the γ-Ray values is immediately followed by a second peak, with the same amplitude; consequently, we assumed that a second sequence boundary may be located just above the first one, and that the position of a maximum flooding surface may be extrapolated between the two sequence boundaries.

From these two approaches, we concluded that the sedimentary succession at Buttes was composed of, at least, three highstand systems tracks and two transgressive systems tracks. The transition between the Pierre Jaune de Neuchâtel and the Urgonien Jaune exhibits a scheme relatively similar to Eclépens, as γ-Ray data revealed the presence of, at least, one stacked depositional sequence at the base of the Urgonien Jaune. In absence of any clear and decisive sedimentological evidence for such a "condensation" of several sequence boundaries, we may consider an alternative hypothesis: in shallow-water environments, several parasequence boundaries may be stacked as the consequence of long-term sea-level fall superimposed to short-term fluctuations. The sedimentological expression of such processes may be a "sequence boundary zone" (*e.g.*, Strasser *et al.*, 1999, 2004), in which several peaks of the γ-Ray may be recorded.

B.2.5. Correlation of the different sections – Conclusions

In order to identify the main sequence boundaries and to discriminate parasequence from sequence boundaries, all the here-described sections where correlated by means of sequence stratigraphy. Other sections where included in order to obtain a stratigraphic scheme as precise as possible; they are the Boudry section which completes the Gorges de l'Areuse section upwards (after Blanc-Aletru, 1995), and the borehole F-607 which cuts through the Pierre Jaune de Neuchâtel down to the Calcaire Roux (after Rumley, 1993).

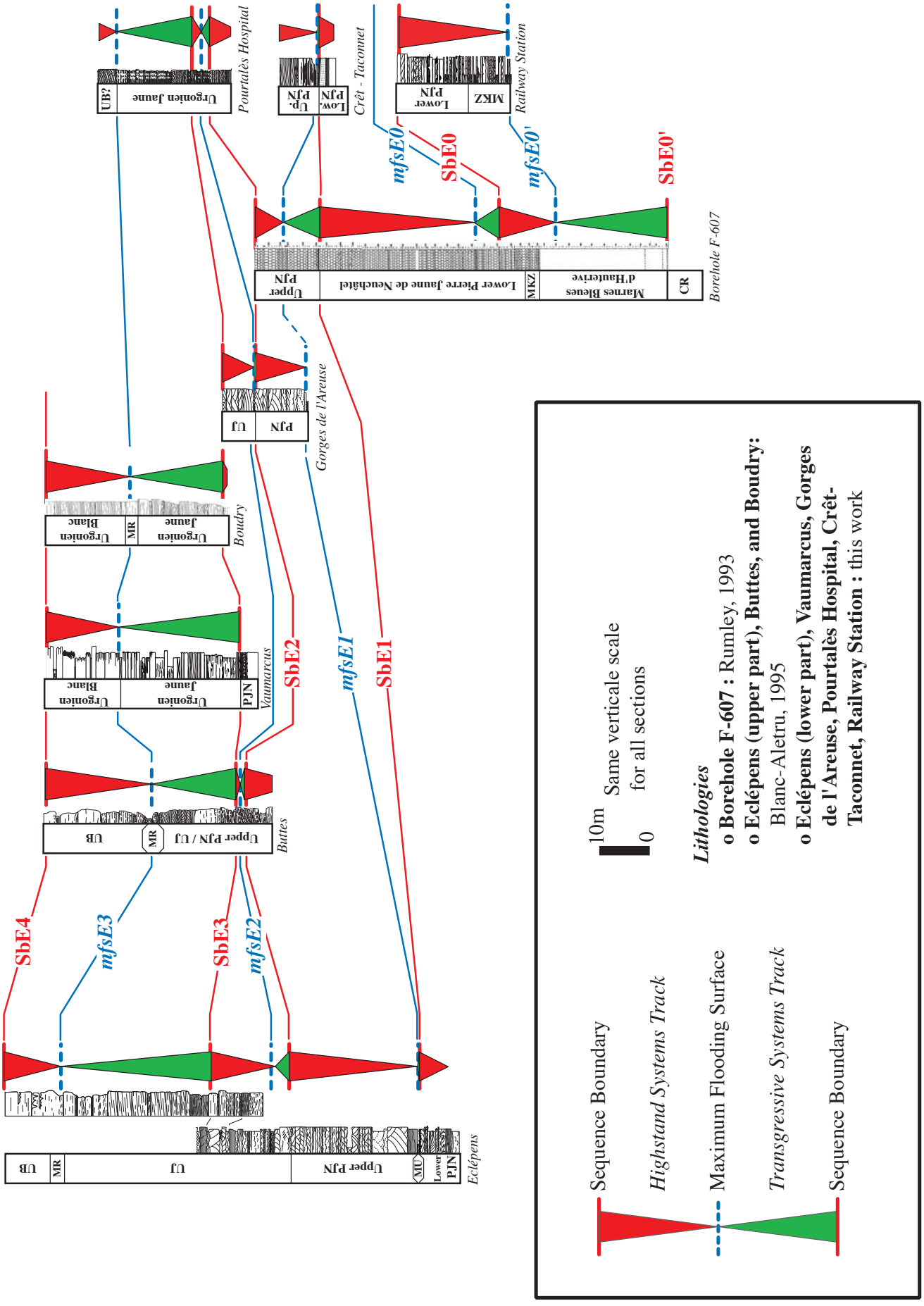

Fig. B.24: Correlation of the different sections prospected in the Western Swiss Neuchâtel, by means of sequence stratigraphy.

A proposition of correlation is given in Fig. B.24; it highlights the importance of the sequence boundaries and maximum flooding surfaces defined at Eclépens. The recognition of these key surfaces in the other sections is based on several field and thin sections observations, as well as their stratigraphic position:

SbE1: it may be recognized at Eclépens, borehole F-607 and Crêt-Taconnet. It always corresponds to an erosive surface associated with encrusted oysters and an increase in the glauconite content. The maximum flooding surface that follows on top is thus the mfs E1 in the borehole F-607 and the Crêt-Taconnet section. Unfortunately, no ammonite finding allows the correspondence between the SbE1 and mfs E1 with the Marnes d'Uttins in these sections.

SbE2: the facies change from an oolitic grainstone to a bioclastic packstone which corresponds to this sequence boundary has been undoubtedly recognized in the Eclépens and other sections (Buttes, Gorges de l'Areuse and Pourtalès Hospital). The ***SbE3***, which consists of an erosive surface coupled with reworking processes such as a polygenic and heterometric conglomerate, has been correlated between these sections as well.

SbE4: even if karstification features were not documented in all the sections where the Urgonien Blanc crops, we assumed that this sequence boundary is always associated with the end of this formation. Moreover, the position of the mfsE3 is based on both the identification of the SbE3 and SbE4, as well as on the first appearance of corals – a criteria which characterizes the Marnes de la Russille (*e.g.*, Remane, 1989; Blanc-Aletru, 1995).

On the other hand, the study of the borehole F-607 and of the Neuchâtel composite section reveals the presence of two other sequence boundaries within the interval from the top of the Calcaire Roux to the lower Pierre Jaune de Neuchâtel.

SbE0': this sequence boundary is located at the top of the Calcaire Roux and consists of an hardground surmounted by marls (Marnes à Astiera), in which ammonite findings suggest that the main part of the Late Valanginian is condensed within this horizon (*e.g.*, Adatte and Rumley, 1989).

SbE0: it has been recognized in the borehole F-607 and probably also at the top of the Railway Station section. It corresponds to a rapid but slight deepening of the microfacies, from F5/F6 (with oomoldic porosity; Railway Station) or F4 (borehole F-607), to FT (borehole F-607).

Thanks to the ammonites described in the literature (*e.g.*, Busnardo and Thieuloy, 1989), some of these sequence boundaries can be dated and correlated with the sequence stratigraphic scheme defined in the Vercors (Arnaud *et al.*, 1998; Arnaud, 2005), in particular:

The fauna collected at Cressier and Valangin constrain the age of the basal Marne Bleue d'Hauterive to the *Acanthodiscus radiatus* ammonite zone, which implies that the SbE0' and mfsE0' corresponds to the SbH1 and mfsH1 of Arnaud (2005), respectively.

In the marls of the Marnes d'Uttins, the ammonite assemblage indicates an Early Hauterivian age (*Lyticoceras nodosoplicatum* ammonite zone); this implies that the SbE1 and mfs E1 may correspond to the SbH3 and mfsH3 of Arnaud (2005), respectively. Consequently, the SbE0 and the mfsE0 may be the equivalents of the SbH2 and mfsH2 of Arnaud (2005), respectively.

In the absence of ammonites or a robust stratigraphic framework, the dating of the other sequence boundaries still remains uncertain. The presence of Early Aptian ammonites in marls which fill the uppermost karst indicates that the underlying formations are older than the *Deshayesites deshayesi – Deshayesites bowerbanki* zones (Renz and Jung, 1978).

On the other hand, the sequence stratigraphy approach highlights that the base of the Urgonien Jaune holds at least two sequence boundaries, SbE2 and SbE3. Moreover, the transgressive systems track deposits of the sequence E3 decreases in thickness landward; this implies than the Eclépens section, which represents the most distal studied succession, may also be most

appropriate to precise the dating of the sequences E2 and E3.

B.2.6. References

Adatte, T. and Rumley, G. (1989). Sedimentology and mineralogy of the Valanginian and Hauterivian in the stratotypic region (Jura mountains, Switzerland). *In:* J. Wiedmann, (*Ed.*). Cretaceous of the Western Tethys: proceedings of the 3rd International Cretaceous Symposium, Tübingen 1987. Stuttgart, E. Schweizerbart'sche Verlagsbuchhandlung (Nägele u. Obermiller): 329-351.

Arnaud, H. (1981). «De la plate-forme urgonienne au bassin vocontien: le Barrémo-Bédoulien des Alpes Occidentales entre Isère et Buëch (Vercors méridional, Diois et Dévoluy).» Géologie Alpine **11**(*3 vol.*): 804 pp.

Arnaud, H. (2005). The South-East France Basin (SFB) and Its Mesozoic Evolution. *In:* T. Adatte, A. Arnaud-Vanneau, H. Arnaud, M.-C. Blanc-Aletru, S. Bodin, E. Carrio-Schaffhauser, K. B. Föllmi, A. Godet, M. C. Raddadi and J. Vermeulen, (*Eds*). The Hauterivian-Lower Aptian sequence stratigraphy from Jura Platform to Vocontian Basin: A multidisciplinary approach. Géologie Alpine, **Série Spéciale «Colloques et Excursions» N°7**: 5-28.

Arnaud, H., Arnaud-Vanneau, A., Blanc-Aletru, M. C., Adatte, T., Argot, M., Delanoy, G., Thieuloy, J.-P., Vermeulen, J., Virgone, A., Virlouvet, B. and Wermeille, S. (1998). «Répartition stratigraphique des orbitolinidés de la plate-forme urgonienne subalpine et jurassienne (SE de la France).» Géologie Alpine **74**: 3-89.

Arnaud Vanneau, A. and Arnaud, H. (2005). Carbonate facies and microfacies of the Lower Cretaceous carbonate platforms. *In:* T. Adatte, A. Arnaud-Vanneau, H. Arnaud, M.-C. Blanc-Aletru, S. Bodin, E. Carrio-Schaffhauser, K. B. Föllmi, A. Godet, M. C. Raddadi and J. Vermeulen, (*Eds*). The Hauterivian-Lower Aptian sequence stratigraphy from Jura Platform to Vocontian Basin: A multidisciplinary approach. Géologie Alpine, **Série Spéciale «Colloques et Excursions» N°7**: 39-68.

Arnaud-Vanneau, A. (1980). «Micro-paléontologie, paléoécologie et sédimentologie d'une plate-forme carbonatée de la marge passive de la Téthys: l'Urgonien du Vercors septentrional et de la Chartreuse (Alpes occidentales).» Géologie Alpine **Grenoble Mém HS 10**: 874 p.

Arnaud-Vanneau, A. and Arnaud, H. (1990). Hauterivian to Lower Aptian carbonate shelf sedimentation and sequence stratigraphy in the Jura and northern Subalpine chains (southeastern France and Swiss Jura). *In:* M. E. Tucker, J. L. Wilson, P. D. Crevello, J. R. Sarg and J. F. Read, (*Eds*). Carbonate Platforms: Facies, Sequences and Evolution. Blackwell Scientific Publications, Special Publication of the International Association of Sedimentologists, **9**: 203-233.

Arnaud-Vanneau, A. and Arnaud, H. (1991). «Sédimentation et variations relatives du niveau de la mer sur les plates-formes carbonatées du Berriasien-Valanginien inférieur et du Barrémien dans les massifs subalpins septentrionaux et le Jura (Sud-Est de la France).» Bulletin de la Société Géologique de France **t. 162**(*n°3*): 535-545.

Blanc-Aletru, M. C. (1995). Importance des discontinuités dans l'enregistrement sédimentaire de l'Urgonien jurassien. Micropaléontologie, Sédimentologie, Minéralogie et Stratigraphie Séquentielle. Géologie Alpine. Ph.D. Thesis Grenoble, Laboratoire de Géologie de l'Université I de Grenoble. Mémoire HS n°24: 299 pp.

Busnardo, R. and Thieuloy, J.-P. (1989). «Les ammonites de l'Hauterivien jurassien: révision des faunes de la région du stratotype historique de l'étage Hauterivien.» Mémoires de la Société neuchâteloise des Sciences naturelles **XI**: 101-147.

Charollais, J., Clavel, B., Schroeder, R., Busnardo, R., Decrouez, D. and Cherchi, A. (2003). «La migration de la plate-forme urgonienne entre le Jura plissé et les Chaines subalpines septentrionales (France, Suisse): Evolution of the Urgonian platform between the Jura and the Septentrional Subalpine Chains (France, Switzerland).» Geobios **36**(*6 SU* -): 665-674.

Clavel, B., Charollais, J., Schroeder, R. and Busnardo, R. (1995). «Réflexions sur la biostratigraphie du Crétacé inférieur et sur sa complémentarité avec l'analyse séquentielle: exemple de l'Urgonien jurassien et subalpin.» Bull. Soc. géol. France **166**(*6*): 663-680.

Föllmi, K. B., Godet, A., Bodin, S. and Linder, P. «Interactions between environmental change and shallow-water carbonate build-up along the northern Tethyan margin and their impact on the early Cretaceous carbon-isotope record.» Paleoceanography **in press**.

Raddadi, M. C., Arnaud Vanneau, A., Poupeau, G., Carrio-Schaffauser, E., Arnaud, H. and Rivera, A. (2005). «Interpretation of gamma-ray logs: The distribution of uranium in carbonate platform.» Comptes Rendus Géosciences **336**(*16*): 1457-1461.

Remane, J. (1989). «The historical type Hauterivian of the Jura mountains: original definition, actual concept, lithostratographic subdivision.» Mémoires de la Société neuchâteloise des Sciences naturelles **XI**: 9-18.

Renz, O. and Jung, P. (1978). «Aptian to Maastrichtian in the SwissJura Mountains.» Eclogae Geologicae Helvetiae **71**(*1*): 1-18.

Rumley, G. (1993). Sédimentologie, minéralogie et stratigraphie de l'Hauterivien dans le Jura neuchâtelois et vaudois (Suisse).» Université de Neuchâtel, 207 pp.

Sarg, J. F. (1988). Carbonate Sequence Stratigraphy. *In:* SEPM, (*Ed.*). Sea-Level Changes - An Integrated Approach. **SEPM, Special Publication n°42**: 155-181.

Schlager, W. (1999). Type 3 Sequence Boundaries. *In:* SEPM, (*Ed.*). Advances in Carbonate Sequence Stratigraphy: Application to Reservoirs, Outcrops and Models. SEPM Special Publication, **n°63**: 35-45.

Schroeder, R., Clavel, B., Cherchi, A., Busnardo, R., Charollais, J. and Decrouez, D. (2002). «Lignées phylétiques d'Orbitolinidés de l'intervalle Hauterivien supérieur - Aptien inférieur; leur importance stratigraphique.» Revue Paléobiol., Genève **21**(*2*): 853-863.

Strasser, A., Hillgärtner, H. and Pasquier, J.-B. (2004). «Cyclostratigraphic timing of sedimentary processes: An example from the Berriasian of the Swiss and French Jura Mountains.» SEPM Special Publication **N°81**: 135-151.

Strasser, A., Pittet, B., Hillgärtner, H. and Pasquier, J.-B. (1999). «Depositional sequences in shallow carbonate-dominated sedimentary systems: concepts for a high-resolution analysis.» Sedimentary Geology **128**: 201-221.

Vail, P. R., Colin, J.-P., Jan du Chêne, R., Kuchly, J., Mediavilla, F. and Trifilieff, V. (1987). «La stratigraphie séquentielle et son application aux corrélations chronostratigraphiques dans le Jurassique du bassin de Paris.» Bulletin de la Société Géologique de France (8) **t. III**(*n°7*): 1301-1321.

Vail, P. R., Mitchum, R. M. J., Todd, R. G., Widmeri, J. W., Thompson, S., Sangree, J. B., Bubb, J. N. and Hatelid, W. G. (1977). Seismic stratigraphy and global changes of sea level. Seismic stratigraphy. Application to hydrocarbon exploration. Am. Assoc. Pet. Geol. Mem., Tulsa, **26**: 49-212.

Zweidler, D. (1985). Genèse des gisements d'asphalte des formations de la Pierre Jaune de Neuchâtel et des calcaires urgoniens du Jura (Jura neuchâtelois et nord vaudois, Suisse).» Université de Neuchâtel, 108 pp.

B.3. BIOSTRATIGRAPHY OF THE URGONIAN FROM THE WESTERN SWISS JURA

B.3.1. Introduction

Even if sequence stratigraphy is a powerful tool to correlate sections within the same basin (or even between different basins), it needs a strong age control in order to date the different sequence boundaries or maximum flooding surfaces identified within the sedimentary succession. It is for this purpose that biostratigraphy is classically used as a necessary tool, as this method may deliver precious information about the age of the deposits.

In the Western Swiss Jura, several sections were prospected for their paleontological contents; orbitolinids, dasycladacean algae, rudists, echinoids, brachiopods, dinoflagellates, ammonites and nannofossils were identified in the Pierre Jaune, Urgonien Jaune and the Urgonien Blanc of the Pourtalès Hospital, Vaumarcus, La Russille, Cressier and Eclépens sections. In the following, we describe the identified fauna and flora, as well as the implication of their finding on the age of the Urgonian limestones from the Neuchâtel area.

B.3.2. Orbitolinids

Orbitolinids were mainly found in the Urgonien Blanc. Their presence was already mentioned in previous studies, in particular by Zweidler (1985), Arnaud-Vanneau and Arnaud (1990), and Blanc-Aletru (1995). As the distribution of these benthic foraminifera along a profile of a carbonate platform is mainly restricted to the upper outer shelf and, especially, to the inner shelf (cf. Fig. B.8), their

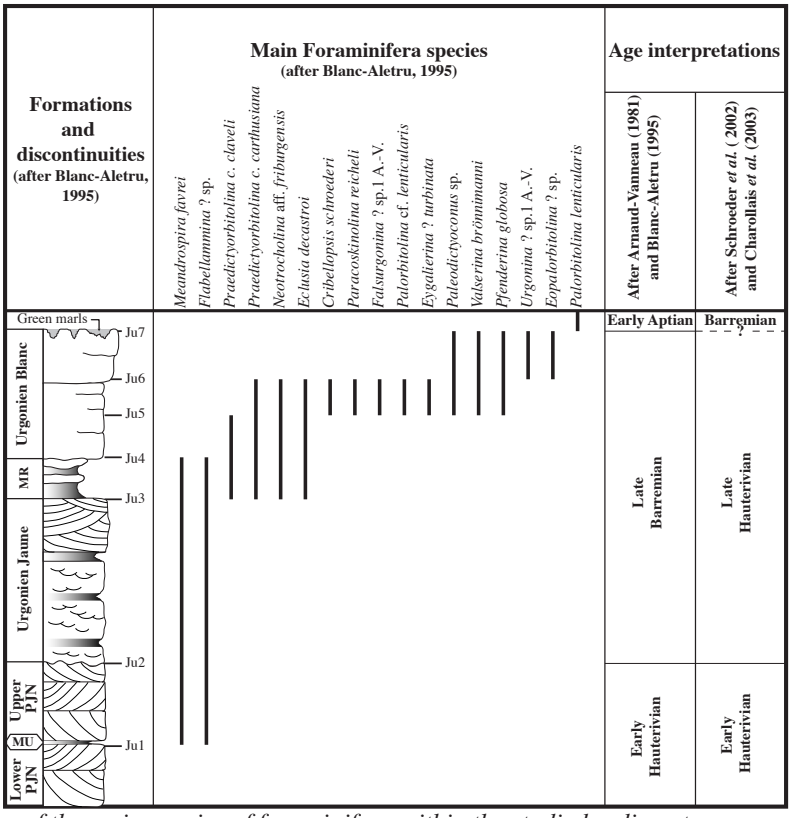

Fig. B.25: Repartition of the main species of foraminifera within the studied sedimentary succession in the Western Swiss Jura (after Blanc-Aletru, 1995).

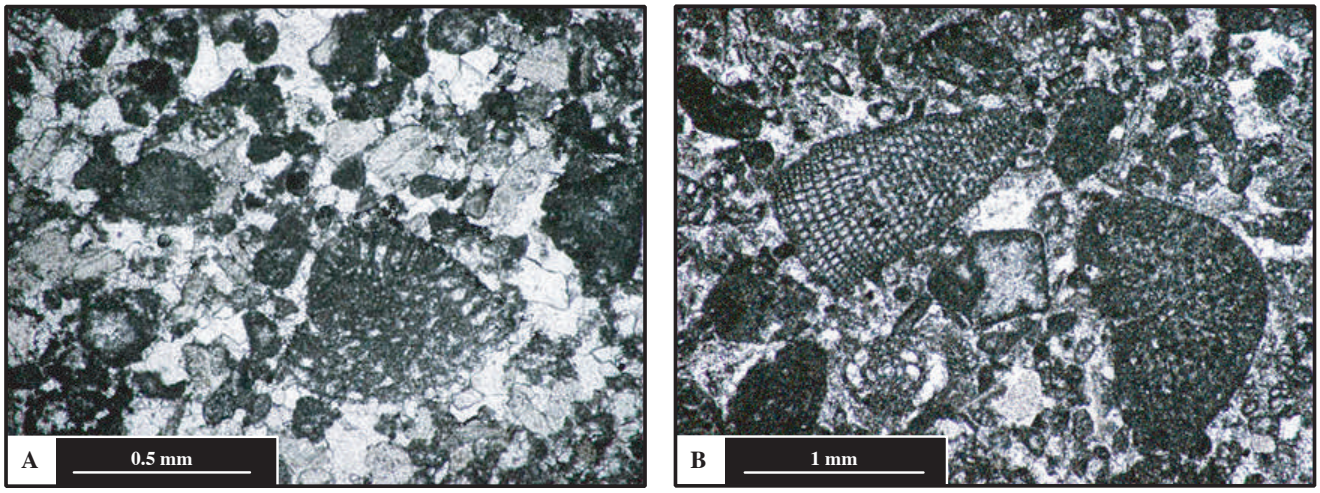

Fig. B.26: Photomicrographs of orbitolinids from the Urgonien Blanc of the Vaumarcus section. **A:** *Paleodictyoconus cuvilieri;* **B:** *Paracoskinolina sp. (specimen on the left). Determinations by Dr. Annie Arnaud-Vanneau, University of Grenoble, France.*

abundance within the Urgonien Blanc seems to be normal, whereas the few specimens observed in the Urgonien Jaune may be transported (see part B.2). The Fig. B.25 summarizes the different species of orbitolinids recognized by Blanc-Aletru (1995) in the Western Swiss Jura, as well as the age deduced from these foraminifera.

Despite the strong diagenesis that micritized the carbonates of the Urgonien Blanc, some species were recognized in thin sections from the Vaumarcus section: even if the specimens of *Paracoskinolina* sp. and *Paleodictyoconus cuvillieri* do not provide age-diagnostic information (Fig. B.26; determination by Dr. Annie Arnaud-Vanneau, University of Grenoble, France), the results of Blanc-Aletru (1995) showed that the complete assemblage of orbitolinids is coherent with a Late Barremian age for the Urgonian from the Western Swiss Jura. Moreover, Zweidler (1985) reported the presence of *Paracoskinolia reicheli* in the Urgonien Blanc of Eclépens; this species may constrain the age of this formation to the latest Barremian. On the other hand, if we consider all the species recognized by Blanc-Aletru (1995), and if we check for their stratigraphic distribution using the zonation proposed by Schroeder *et al.* (2000, 2002), then the age of the Urgonien Blanc should be shifted from the Late Barremian to the Late Hauterivian, revealing the main discrepancy existing between the two classically used zonations of orbitolinids.

B.3.3. Dasycladacean algae

Dasycladacae were identified in thin sections from the Vaumarcus and Pourtalès Hospital sections. The determinations were performed by Prof. Jean-Pierre Masse (University of Provence, Marseille, France) in their majority; Prof. Ioan Bucur (University of Cluj-Napoca, Romania) was also contacted to confirm one determination made on a photomicrograph. Green algae were mainly found within the Urgonien Blanc, even if some specimens were also described in the Urgonian Jaune; in the latter case, they are usually rounded and corroded by reworking processes, and sometimes also impregnated by iron oxyde-hydroxide (see Fig. B.27).

In the Urgonien Blanc from Vaumarcus, *Pseudoactinoporella fragilis* (CONRAD), *Falsolikanella* aff. *danilovae* (RADOICIC) et *Suppiluliumella* gr. *verae* (SOKAC and NIKLER) - *corbarica* (JAFREZZO) were identified. In the absence of other species such as *Similiclypeina paucicalcarea* (CONRAD) and *Salpingoporella muehlbergi* (LORENZ), this assemblage may rather indicate an Early Hauterivian age (after Masse, 1993).

B.3.4. Rudists

Rudists were only found in the upper part of the Urgonien Blanc. They consist of rather small and isolated specimens. In some samples from the Vaumarcus section, Prof. Jean-Pierre Masse

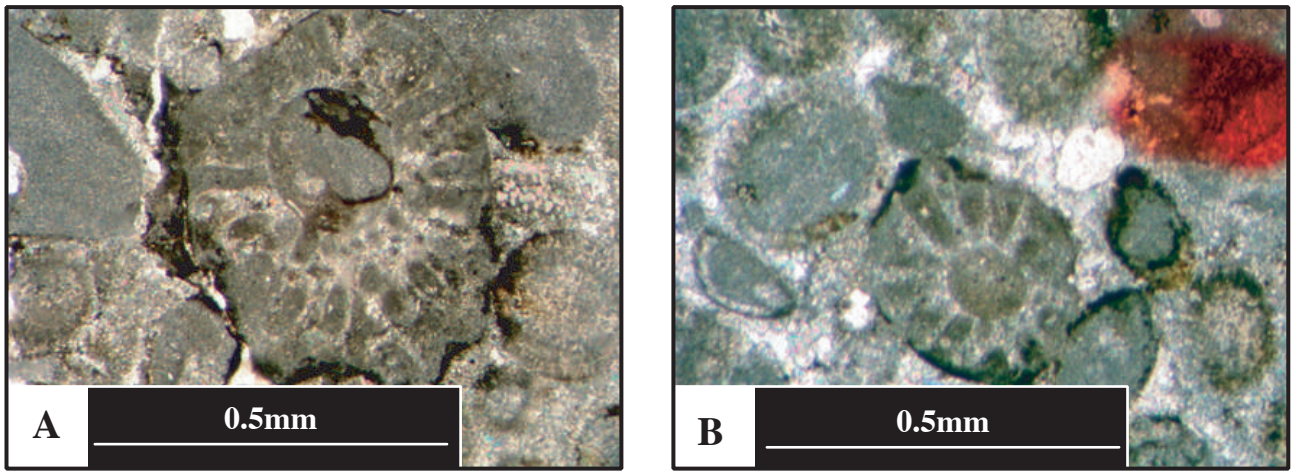

Fig. B.27: Photomicrographs of dasycladacean algae from the Urgonien Jaune of the Pourtalès Hospital section. **A:** *Pseudoactinoporella fragilis (?);* **B:** *Salpingoporella pygmaea (?). Determinations by Dr. Ioan Bucur, University of Cluj-Napoca, Romania (note that these determinations were made from these pictures).*

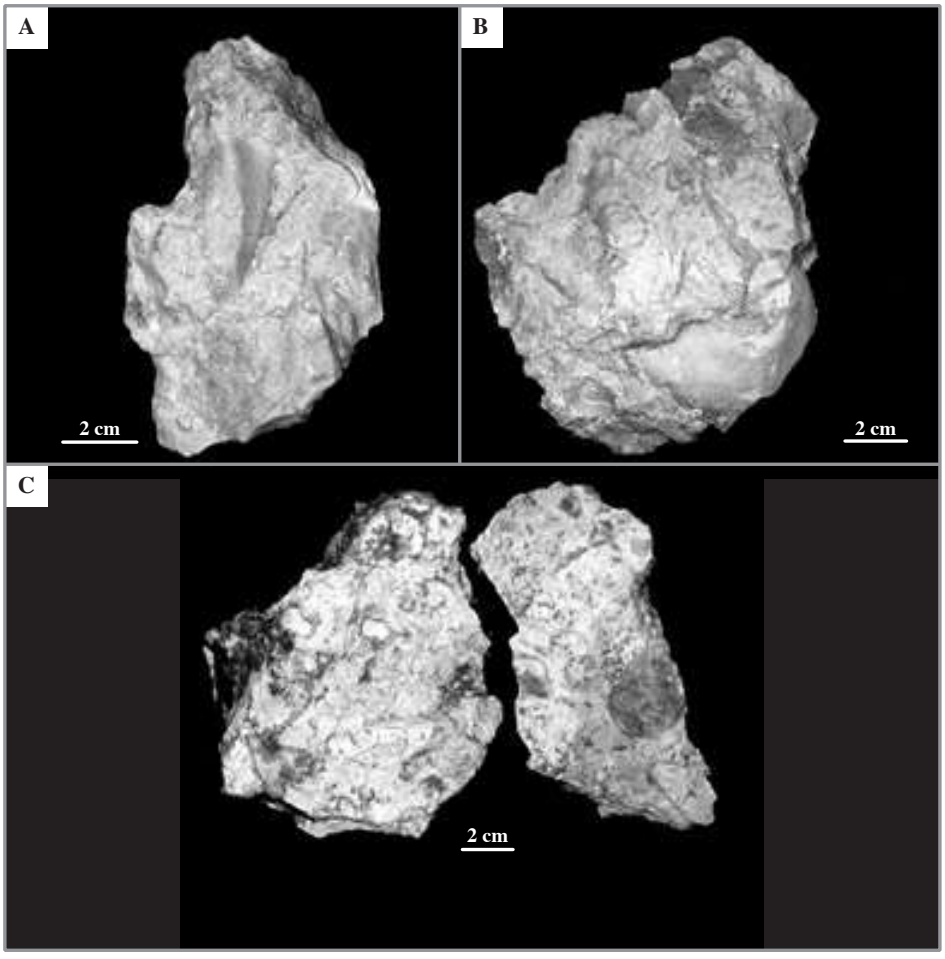

Fig. B.28: Rudists from the Urgonien Blanc of the Vaumarcus section. **A:** *Agriopleura sp.;* **B:** *Requiena renevieri;* **C:** *HCl-leached surface showing sections of numerous specimens. All determinations by Prof. Jean-Pierre Masse, University of Provence, Marseille, France.*

(University of Provence, Marseille, France) recognized small specimens of *Requiena renevieri*, and also some *Agriopleura* sp. (Fig. B.28); this assemblage is classically attributed to the latest Hauterivian – earliest Barremian (*e.g.,* Masse *et al.*, 1998).

B.3.5. Echinoids

Only two well-preserved specimens of echinoids were collected in the Vaumarcus and the La Russille sections. They were identified by Dr. Aurélien Virgone (Total, Pau, France) as *Goniopygus delphinensis* and *Orthopsis* aff. *repellini* (Fig. B.29). Both species imply that the Early Barremian may be missing from the sedimentary record from the Western Swiss Jura, and that the Urgonien Blanc may be Late Barremian – earliest Aptien in age.

Sample LRU12b, Marnes de la Russille, La Russille section

Goniopygus delphinensis

Sample VA60, uppermost Urgonien Jaune, Vaumarcus section

Orthopsis aff. *repellini*

Fig. B.29: Echinoids from the Marnes de La Russille and uppermost Urgonien Jaune of the La Russille and Vaumarcus sections, respectively. All determinations by Dr. Aurélien Virgone, TOTAL, Pau, France.

B.3.6. Brachiopods

The majority of the brachiopods collected in view of $^{87}Sr/^{86}Sr$ analysis were entrusted to Dr. Danièle Gaspard (University of Paris Sud, Orsay, France), in view of their identification. The majority

Samples from the Marne Bleue d'Hauterive of the Cressier section

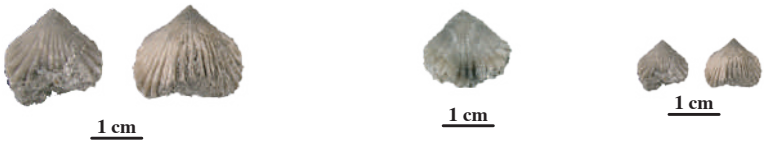

Plicarostrum hauteriviense (BURRI)

Sample from the Marnes de La Russille of the La Russille section

Rhynchonella gilieroni (PICTET) = *Lamellaerhynchia gilieroni* (PICTET) - var. *longirostris* (PICTET)

Fig. B.30: Rhynchonellids from the Marne Bleue d'Hauterive and the Marnes de la Russille of the Cressier and La Russille sections, respectively. All determinations by Dr. Danièle Gaspard, University Paris Sud, Orsay, France.

of the specimens collected in the Marne Bleue d'Hauterive (Cressier section) were attributed to the Early Hauterivian species *Plicarostrum hauteriviense* (BURRI; see Fig. B.30). Then, some rhynchonellids from the Urgonien Jaune (Pourtalès Hospital section) and the Marnes de la Russille (La Russille section) were identified as *Rhynchonella gillieroni* (PICTET) = *Lamellaerhynchia gillieroni* (PICTET) var. *longirostris* (Fig. B.30). The latter species is classically attributed to the interval from the Valanginian to the Early Barremian (Gaspard, 1989, 1999), but this attribution rests mainly on the distribution of orbitolinids in contemporaneous sediments, and consequently needs a calibration with respect to the more classically used ammonite zonation (D. Gaspard, pers. com., 2006).

B.3.7. Dinoflagellates

A selection of marls sampled in the lower part of the Urgonien Jaune were analysed by Dr. Ebrahim Ghasemi-Nejad (University of Tehran, Iran) for their palynological content. In two samples of marls from the Eclépens section, the preservation and abundance of dinoflagellate cysts was good enough to allow the identification of a Late Barremian – earliest Aptian assemblage (Fig. B.31; see also Annexe 5.1 for the complete report of Dr. Ebrahim Ghasemi-Nejad). Moreover, these analyses highlighted the high reworking present

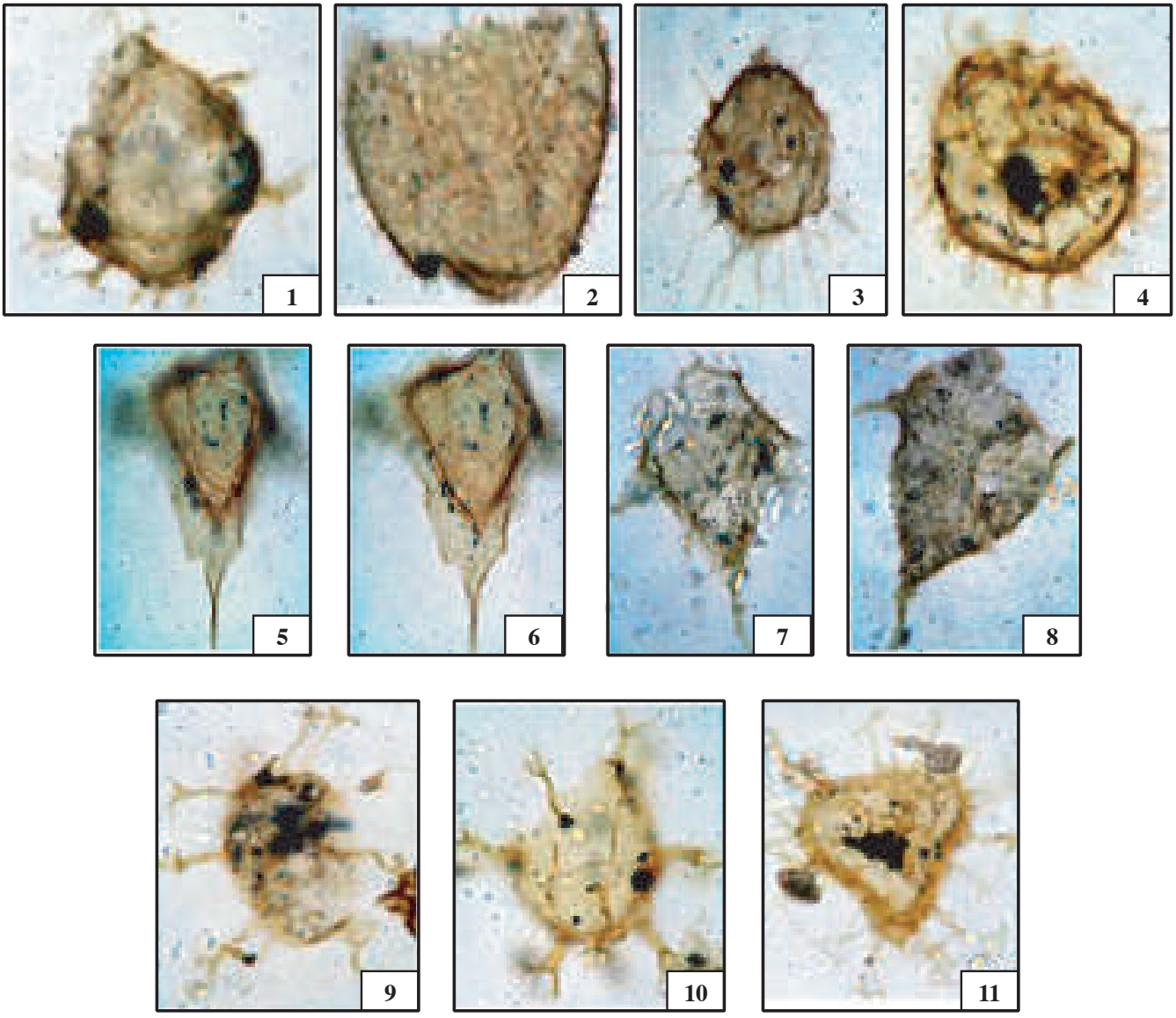

Fig. B.31: Dinoflagellate cysts from marls samples from the lower part of the Urgonien Jaune of the Eclépens section (samples $EC_{II}72$ and $EC_{II}79$). **1, 2:** *Achomosphaera cf. sagena;* **3, 4:** *Hystrichodinium cf. pulchrum;* **5, 6:** *Muderongia mcwhaei;* **7, 8:** *Muderongia tetrancantha;* **9, 10, 11:** *Oligosphaeridium complex. All determinations and photomicrographs by Dr. Ebrahim Ghasemi-Nejad, University of Tehran, Iran.*

at the base of the Urgonien Jaune, as Jurassic species were also identified in these samples from Eclépens.

However, Dr. Peter Hochuli (University of Zürich, Switzerland) prospected the same samples. He concluded that the preservation and abundance of the dinocysts were not so good as suggested by Dr. Ebrahim Ghasemi-Nejad, and also that the floral association rather pointed out to a Hauterivian age; this conclusion is mainly based on a different calibration of the range of appearance of the species *Muderongia mcwhaei* and *Muderongia tetrancantha*. Whereas Dr. Peter Hochuli stated that the last occurrence of *M. mcwhaei* happened in the latest Hauterivian (Montiel, 1998), Dr. Ebrahim Ghasemi-Nejad used it as a marker for the Aptian stage. As the first occurrence of *M. mcwhaei* is reported in the Early Aptian in the Austral area (Oosting *et al.*, 2006), one may wonder if a time lag of about 5 to 7 Ma has occurred for these events between the Tethyan and the Autral realms, and if M. mcwhaei may be considered as a "Lazarus taxon", in which case the validity of its stratigraphic distribution may be called into question. Finally, Dr. Peter Hochuli concluded that there were only Hauterivian markers in samples from the Urgonien Jaune from Eclépens, thought Dr. Ebrahim Ghasemi-Nejad recognized the species *Muderongia tetracantha*, which last occurrence is reported in the earliest Barremian in Stover *et al.* (1996).

B.3.8. Ammonites

As the carbonates preserved in the Western Swiss Jura correspond to rather shallow environment, the presence of ammonites within such facies is rare. Previous studies reported the occurrence of such fossils in the Marne Bleue d'Hauterive and the Marnes d'Uttins, whereas they are absent from the Pierre Jaune de Neuchâtel and the Urgonian.

In the Eclépens section, one ammonite was found within the Marnes d'Uttins (Fig. B.32). It has been determined as an *Acanthodiscus subhystricoides* (KILIAN and REBOUL) by Dr. Jean-Pierre Thieuloy (University of Grenoble, France), a species classically attributed to the *L. nodosoplicatum* ammonite zone of the Early Hauterivian.

B.3.9. Calcareous nannofossils

Nannoplankton biostratigraphy was already used to precise the age of the Calcaire Roux, Zone Marno-calcaire and Marne Bleue d'Hauterive; the latter formation was clearly attributed to the Early Hauterivian (Manivit, 1989). More recently, other attempts to use calcareous nannofossils were carried out by Dr. Bas van de Schootbrugge (Johann Wolfgang Goethe University, Frankfurt am Main, Germany) during his PhD thesis at Neuchâtel, in collaboration with Dr. Katarina von Salis (previously at the ETH Zürich, Switzerland),

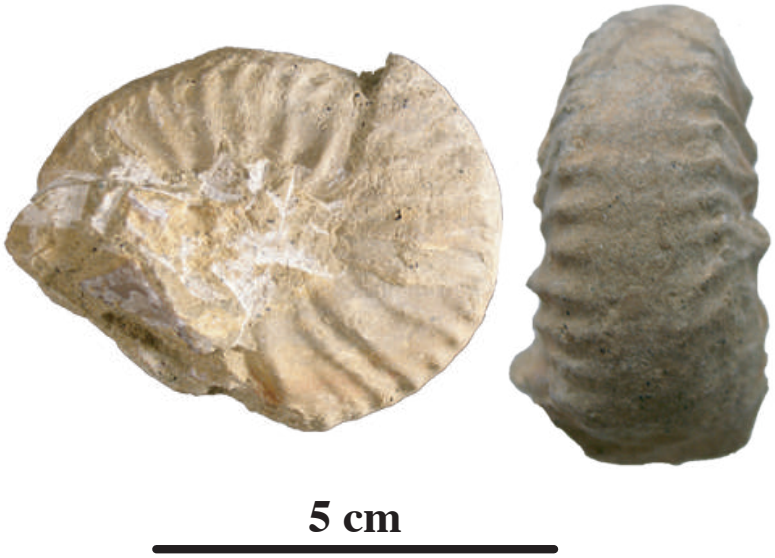

Fig. B.32: Specimen of Acanthodiscus subhystricoides (KILIAN and REBOUL) from the Marnes d'Uttins of the Eclépens section. Determination by Dr. Jean-Pierre Thieuloy, University of Grenoble, France.

then by Dr. Silvia Gardin (University Paris VI, Paris, France) in the frame of this PhD thesis, who looked at samples from the Marnes de la Russille collected in the La Russille and Vallorbe sections. Unfortunately, the results of these attempts were not constructive.

During the summer 2005, Dr. Eric de Kaenel analysed, in the frame of this PhD thesis, some marls sampled near the base of the Urgonien Jaune at Eclépens. The abundance and the preservation of calcareous nannofossils allowed to attribute two samples to the latest Barremian – earliest Aptian, as shown in Fig. B.33, even if numerous Hauterivian species pointed out to the importance of the reworking in this part of the Eclépens section (see Annexe 5.2 for the taxonomic list of species). In particular, the appearance of *H. irregularis* approximates the Barremian-Aptian boundary and defines the base of the NC6 nannofossil zone (*e.g.,* Herrle and Mutterlose, 2003). This event was calibrated to the magnetostratigraphy in several sections from North Italy (Channell and Erba, 1992), where *H. irregularis* first occurs just below the CM0/CM1n boundary. In the Gorgo a Cerbara section (North Italy), the proposed boundary stratotype, the LO of *H. irregularis* is recorded just below the M0 magnetic chron. In this section, a specimen of the ammonite *Deshayesites* sp. has also been recorded in the M0 chron (Channell *et al*., 2000). Moreover, the appearance of *N. truitti* has also been calibrated (Channell *et al*., 2000), and lies between the FO of *H. irregularis* and the CM0/CM1n boundary.

Finally, the appearance of large morphotypes of *Assipetra infracretacea* (>7.5 μm) and *Assipetra terebrodentarius* (> 7.0 μm) has been calibrated to the lower part of the magnetic chron M0 (Tremolada and Erba, 2002) and postdates the appearances of *H. irregularis* and *N. truitti*. In sample $EC_{II}79$, the presence of a large specimen of *A. terebrodentarius* (6.9 μm) may indicate that the age of this sample corresponds to the lower magnetic chron M0 or basal Aptian (*D. oglanlensis* ammonite zone).

The determinations and age attribution made by Dr. Eric de Kaenel were subsequently confirmed during an informal meeting organized by Prof. Karl B. Föllmi during the 7th International Symposium on the Cretaceous housed in Neuchâtel in September 2005. The following experts in calcareous nannofossils biostratigraphy were present: Prof. Elisabetta Erba (University of Milan, Italy), Dr. Silvia Gardin (University of Paris VI, Paris, France), Prof. Jörg Mutterlose (University of Bochum, Germany), and Dr. Jens O. Herrle (University of Liverpool, United-Kingdom). All of them concluded that the species identified and illustrated by Dr. Eric de Kaenel implied a latest Barremian – earliest Aptien age for the base of the Urgonien Jaune at Eclépens.

Prof. Elisabetta Erba and Dr. Silvia Gardin analysed other marls sampled near the base of the Urgonien Jaune at Eclépens by Dr. Marc-André Conrad and Prof. Jean Charollais (both attached to the University of Geneva, Switzerland); these new samples were attributed to the Late Hauterivian.

In order to solve this discrepancy between the two sets of samples analysed for their calcareous nannofossil content, a blind test was organised by Prof. Karl B. Föllmi in March 2006, in the presence of Prof. Jean Charollais, Dr. Roger Jan du Chêne (University of Paris VI, Paris, France), Dr. Marc Weidmann, Stéphane Bodin and Alexis Godet (both from the University of Neuchâtel, Switzerland). Prof. André Strasser (University of Fribourg, Switzerland) accepted to act as a neutral expert, by collecting the samples, sending them to three experts (Prof. Elisabetta Erba, Dr. Silvia Gardin and Dr. Eric de Kaenel), and collecting their reports. In the beginning of October 2006, the results of this blind test pointed out to a Hauterivian age for the eight samples collected in March 2006 (see Annexe 5.3 for the entire report by Prof. André Strasser). One striking feature of this blind test is the finding of Albian flora by Dr. Eric de Kaenel in two samples, whereas the uppermost part of the Urgonien Blanc cannot be younger than the *Deshayesites deshayesi – Deshayesites bowerbanki* ammonite zones of the Early Aptian (Renz and Jung, 1978). Moreover, whereas the results from Prof. Elisabetta Erba and Dr. Silvia Gardin are in relatively good agreement, the identifications made by Dr. Eric de Kaenel are significantly different; this implies that the results of this test are not unequivocal.

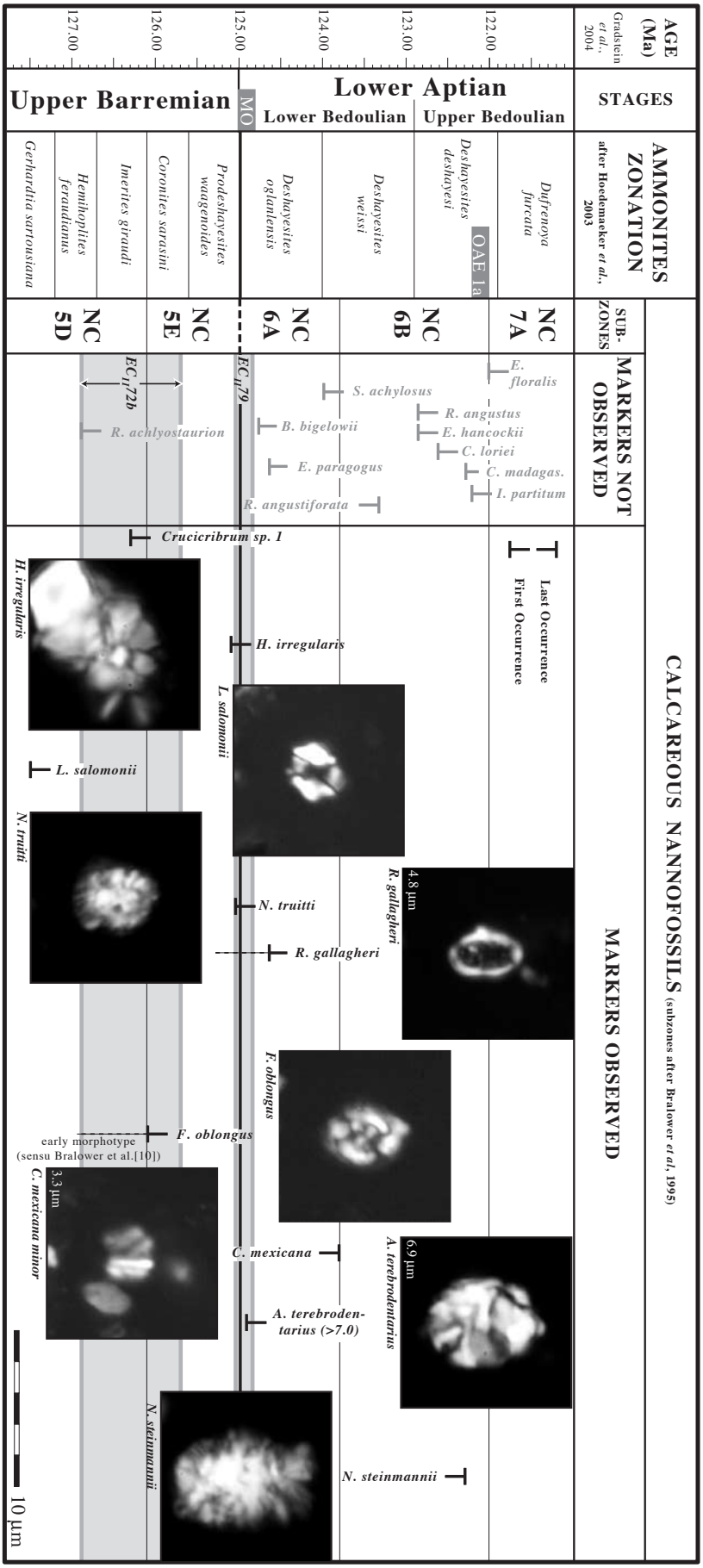

Fig. B.33: Repartition of the calcareous nannofossils found in marls from the lower part of the Urgonien Jaune (samples $EC_{II}72b$ and $EC_{II}79$), calibrated against ammonite biostratigraphy and nannofossil biozonation. ***All determinations and photomicrographs by Dr. Eric de Kaenel, Neuchâtel, Switzerland.***

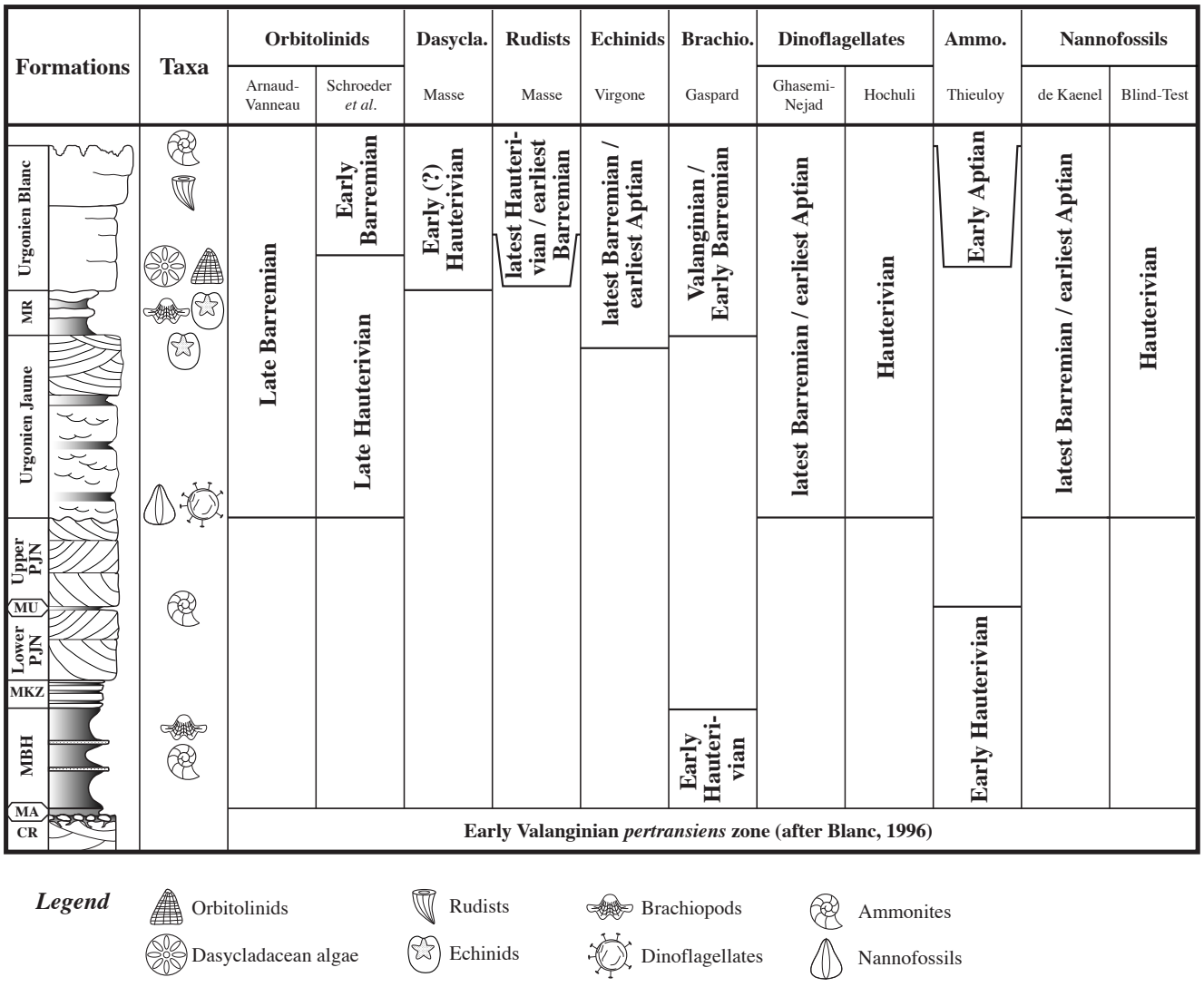

Abreviations of the names of the formations: **CR:** Calcaire Roux; **MA:** Marnes à Astieria; **MBH:** Marne Bleue d'Hauterive; **MKZ:** Megelkalk zone; **PJN:** Pierre Jaune de Neuchâtel; **MU:** Marnes d'Uttins; **MR:** Marnes de la Russille.

Fig. B.34: Repartition of the identified fauna and flora along a stratigraphic profile of the studied succession. The different attribution in terms of age are reported on the right-hand side on the figure.

B.3.10. Main conclusions

Although the studied formations are not devoid of age-diagnostic fauna and flora, it seems presently difficult to conclude a precise age for the Urgonien Jaune and the Urgonien Blanc using these biostratigraphical data. As shown in Fig. B.34, different ages can be proposed, as a function of the used taxa and fossil groups. Only the orbitolinids (calibrated by Schroeder *et al.*, 2002), the rudists, the brachiopods, and the green algae give a coherent stratigraphic scheme, but of great importance is to note that the biostratigraphic distributions of rudists and rhynchonellids are calibrated against the ammonite zonation by using the phyletic evolution of orbitolinids described, for example, by Schroeder *et al.* in 2002 (see Masse *et al.*, 1998; Gaspard, pers. comm., 2006). Moreover, it seems ambiguous to obtain a (late) Early Hauterivian age by the dasycladacae, whereas the rudists sampled in the same section just a few meters above are attributed to the latest Hauterivian – earliest Barremian, without any break within the sedimentary record between them.

Concerning the discrepancies occurring between the different specialists who dealt with dinoflagellates and calcareous nannofossils, several hypotheses may be emitted. First, the problem of the preparation of the marly samples in view of the analysis of nannofossils can be evoked in order to explain the high diversity reported by Dr. Eric

de Kaenel, whereas in the same samples, Prof. Elisabetta Erba and Dr. Silvia Gardin observed a significantly less diversified assemblage (see Annexe 5.3). Moreover, the calibration of the bioevents used to differentiate Hauterivian from Barremian sediments seems to be different, depending on the involved specialists. Then, the taxonomic criteria used by the different experts may be compared. Finally, it is quite surprising that no reworking is reported within the calcareous nannofossils assemblages, whereas numerous evidences for such processes were reported from field observations of the basal Urgonien Jaune (see part B.2). The same remarks can be emitted to explain the discrepancies in the dinoflagellate dating given by Dr. Ebrahim Ghasemi Nejad and Dr. Peter Hochuli.

As the results obtained by biostratigraphy do not seem to be conclusive enough to give a coherent and precise age for the Urgonien Jaune and the Urgonien Blanc from the Western Swiss Jura, we propose to look for alternative and independent methods, such as sequence stratigraphy, chemostratigraphy, and clay mineralogy, which may help to add valuable information on the age and correlations of the Urgonian Jaune and Urgonien.

B.3.11. References

Arnaud-Vanneau, A. and Arnaud, H. (1990). "Hauterivian to Lower Aptian carbonate shelf sedimentation and sequence stratigraphy in the Jura and northern Subalpine chains (southeastern France and Swiss Jura)". *In:* Tucker, M. E., Wilson, J. L., Crevello, P. D., Sarg, J. R. and Read, J. F., (*Eds*). Carbonate Platforms: Facies, Sequences and Evolution. Blackwell Scientific Publications, Special Publication of the International Association of Sedimentologists, **9**: 203-233.

Blanc, E. (1996). "Transect plate-forme-Bassin dans les séries du Berriasien supérieur et du Valanginien Inférieur (Domaines Jurassien et N-Vovontien). Chronostratigraphie et transfert des sédiments." *Ph.D. thesis*, Université de Grenoble, 321 pp.

Blanc-Aletru, M. C. (1995). Importance des discontinuités dans l'enregistrement sédimentaire de l'Urgonien jurassien. Micropaléontologie, Sédimentologie, Minéralogie et Stratigraphie Séquentielle. Géologie Alpine. Ph.D. Thesis Grenoble, Laboratoire de Géologie de l'Université I de Grenoble. Mémoire HS n°24: 299 pp.

Channell, J. E. T. and Erba, E. (1992). "Early Cretaceous polarity chrons CM0 to CM11 recorded in northern Italian land sections near Brescia." Earth and Planetary Science Letters **108** (*4*): 161-179.

Channell, J. E. T., Erba, E., Muttoni, G. and Tremolada, F. (2000). "Early Cretaceous magnetic stratigraphy in the APTICORE drill core and adjacent outcrop at Cismon (Southern Alps, Italy), and correlation to the proposed Barremian - Aptian boundary stratotype." GSA Bulletin **112** (*9*): 1430-1443.

Gaspard, D. (1989). "Explosion de brachiopodes au Crétacé inférieur dans la mer épicontinentale jurassienne." Revue de Paléobiologie **Vol. Spéc. n°3**: 81-102.

Gaspard, D. (1999). "Distribution of Lower Cretaceous brachiopods in Europe (Berriasian to Aptian)." Bulletin de la Société Géologique de France **170** (*3*): 311-326.

Herrle, J. O. and Mutterlose, J. (2003). "Calcareous nannofossils from the Aptian-Lower Albian of southeast France: palaeoecological and biostratigraphic implications." Cretaceous Research **24** (*1*): 1-22.

Manivit, H. (1989). "Nannoplancton de l'Hauterivien marneux du Jura." Mémoires de la Société neuchâteloise des Sciences naturelles **XI**: 223-231.

Masse, J.-P. (1993). "Early Cretaceous Dasycladales biostratigraphy from Provence and adjacent regions (South of France, Switzerland, Spain). A reference for Mesogean correlations". *In:* al., F. B. e., (*Ed.*). Studies on Fossil Benthic algae. Modena, Boll. Soc. Paleont. Ital., **Spec. Vol. 1**: 311.324.

Masse, J. P., Gourrat, C., Orbette, D. and Schmuck, D. (1998). "Hauterivian Rudist faunas of southern Jura (France)." Geobios **M.S. n°22**: 225-233.

Monteil, E. (1998). "Tethyan dinoglagellate cysts". *In:* De Graciansky, P. C., Hardenbol, J., Jacquin, T. and Vail, P. R., (*Eds*). Mesozoic and Cenozoic Sequence Chronostratigraphy Framework of European Basins. Tulsa, Oklahoma, U.S.A., **SEPM Special Publication 60**: Chart 5 -

Cretaceous Biochronostratigraphy.

Oosting, A. M., Leereveld, H., Dickens, G. R., Henderson, R. A. and Brinkhuis, H. (2006). "Correlation of Barremian-Aptian (mid-Cretaceous) dinoflagellate cyst assemblages between the Tethyan and Austral realms." Cretaceous Research **xx** (*in press*): 1-22.

Renz, O. and Jung, P. (1978). "Aptian to Maastrichtian in the SwissJura Mountains." Eclogae Geologicae Helvetiae **71** (*1*): 1-18.

Schroeder, R., Clavel, B., Cherchi, A., Busnardo, R., Charollais, J. and Decrouez, D. (2002). "Lignées phylétiques d'Orbitolinidés de l'intervalle Hauterivien supérieur - Aptien inférieur; leur importance stratigraphique." Revue Paléobiol., Genève **21** (*2*): 853-863.

Schroeder, R., Clavel, B., Conrad, M. A., Zanetti, L., Busnardo, R., Charollais, J. and Cherchi, A. (2000). "Corrélations biostratigraphiques entre la coupe d'Organyà (Pyrénées Catalanes, NE de l'Espagne) et le Sud-Est de la France pour l'intervalle Valanginien-Aptien." Treb. Mus. Geol. Barcelona **9**: 5-41.

Stover, L. E., Brinkhuis, H., Damassa, S. P., de Verteuil, L., Herlby, R. J., Monteil, E., Partridge, A. D., Powell, A. J., Riding, J. B., Smelror, M. and Williams, G. L. (1996). "Mesozoic-Tertiary dinoflagellates, acritarchs and prasinophytes". *In:* Jansonius, J. and Mc Gregor, D. C., (*Eds*). Palynology: principles and applications. American Association of Stratigraphic Palynologists Foundation, **2**: 641-750.

Tremolada, F. and Erba, E. (2002). "Morphometric analyses of Aptian Assipetra infracretacea and Rucinolithus terebrodentarius nannoliths: implications for Taxonomy, biostratigraphy and paleoceanography." Marine Micropaleontology **44**: 77-92.

Zweidler, D. (1985). "Genèse des gisements d'asphalte des formations de la Pierre Jaune de Neuchâtel et des calcaires urgoniens du Jura (Jura neuchâtelois et nord vaudois, Suisse)." *Ph.D. thesis*, Université de Neuchâtel, 108 pp.

B.4.
Geochemical and paleoenvironmental constraints on the rise of the Urgonian platform in the Western Swiss Jura

Alexis Godet[1], Stéphane Bodin[1], Peter Stille[2], Virginie Matera[1], Bas van de Schootbrugge[3], Thierry Adatte[1] and Karl B. Föllmi[1]

[1]Institut de Géologie, Université de Neuchâtel, rue Emile Argand 11, CP 158, 2009 Neuchâtel, Switzerland; [2]Centre de Géochimie de la Surface, Université Louis Pasteur, 67084 Strasbourg, France; [3]Institut für Geologie und Paläontologie, J.W. Goethe Universität, 60054 Frankfurt am Main, Germany

Manuscript for Eclogae Geologicae Helvetiae

Abstract

We present a new strontium isotope data set obtained from well-preserved rhynchonellid shells collected in a selection of sections in the Urgonian formations cropping out in the western Swiss Jura in order to precise its age. We calibrate these results with a new $^{87}Sr/^{86}Sr$ data set obtained from belemnites from the Vocontian Trough, which are precisely dated by ammonite stratigraphy (Early Hauterivian to Late Barremian). Our data allow to discriminate between the Hauterivian and Barremian and to attribute a Barremian age to the Urgonian formations. This age correlation is backed up by a comparison of changes in phosphorus contents (in ppm) and phosphorus mass accumulation rates (PMAR) measured in the Urgonian formations and in (hemi-) pelagic sections from the northern Tethyan realm, respectively. Sediments of Late Hauterivian age are characterized by relatively high PMAR, whereas sediments of Late Barremian age show low PMAR. On the northern Tethyan margin, this difference in PMAR is interpreted as the manifestation of a change in trophic levels, with Hauterivian sediments being characterized by mesotrophic, heterozoan platform ecosystems, whereas in the Late Barremian a shift toward oligotrophic conditions may have favoured the installation of photozoan benthic ecosystems, which include corals and rudists, and with this the widespread development of the Urgonian carbonate platform, as recorded in the sedimentary archive of the Western Swiss Jura.

Keywords

Western Swiss Jura; Urgonian; Early Cretaceous; strontium isotopes; rhynchonellids; trophic changes.

Résumé

Afin d'approfondir nos connaissances sur l'âge des formations urgoniennes du Jura Suisse occidental, nous présentons de nouvelles données du rapport isotopique du strontium mesuré sur des coquilles bien préservées de rhynchonellidés, provenant de diverses coupes de la région neuchâteloise. La comparaison de ces résultats avec l'évolution du rapport $^{87}Sr/^{86}Sr$ (obtenue à partir de belemnites récoltées dans des coupes datées par ammonites de la fosse vocontienne) permet seulement de différencier des âges hauteriviens et barrémiens. Cependant, les changements passés du niveau trophique océanique, estimé par les taux d'accumulation du phosphore (PMAR) mesurés dans des coupes (hémi-)pélagiques de la marge nord téthysienne, permettent d'affiner l'âge des formations urgoniennes neuchâteloise : alors que l'Hauterivien supérieur est caractérisé par des valeurs relativement élevées du PMAR (conditions mésotrophiques), l'évolution vers des environnements oligotrophiques décrite dans le Barrémien supérieur a pu favoriser la mise en place de constructions carbonatées à coraux et rudistes, ainsi que le développement, à plus grande échelle, de la plateforme urgonienne dans un mode photozoan, telle qu'elle est présente dans l'enregistrement sédimentaire du Jura Suisse occidental.

B.4.1. Introduction

The evolution of the Northern Tethyan Margin during the Early Cretaceous is marked by a series of changes in the style of carbonate production (Föllmi *et al*., 1994; in press). During the Hauterivian – earliest Aptian, for example, the sedimentary succession preserved in the Helvetic realm documents the development of a carbonate platform both in a heterozoan mode dominated by crinoids and bryozoans (essentially during the Hauterivian) as well as in a photozoan mode characterized by corals, rudists, stromatoporoids and chaetitids (from the late Barremian onwards). These periods of platform growth were interrupted by two episodes of drowning, which are documented by the Lidernen Member (middle of *L. nodosoplicatum* to late *P. ligatus* ammonite zones; van de Schootbrugge, 2001) and the Altmann Member (late *B. balearis* to middle *C. darsi* ammonite zones; Bodin *et al*., 2006b). The ages of these changes are well constrained by ammonite biostratigraphy.

The dating of contemporaneous sediments in the Western Swiss Jura is, unfortunately, not as well constrained, principally because ammonites are almost entirely lacking in this proximal area of the Northern Tethyan Margin. The historical succession for the Hauterivian stage was defined in the region of Neuchâtel (*e.g*., de Montmollin, 1835; Thurmann, 1835; Desor and Gressly, 1859; Renevier, 1874), and was originally proposed to be composed, from the base to the top, by the Marnes à Astieria, the Marne Bleue d'Hauterive (MBH), the Pierre Jaune de Neuchâtel (PJN) - which is separated in a lower and upper part by the Marnes d'Uttins - , the Urgonien Jaune (UJ) and the Urgonien Blanc (UB; Fig. B.35). Whereas the MBH and the Marnes d'Uttins were dated with the help of ammonite biostratigraphy as belonging to the *A. radiatus* and the *L. nodosoplicatum* zones, respectively, the Urgonian formations were subsequently attributed by Baumberger (1901) to the Barremian without any robust biostratigraphic evidence. This proposition remained accepted during most of the twentieth century. During the

Legend:

• *Abreviations of the names of the formations:* **CR:** Calcaire Roux; **MA:** Marnes à Astieria; **MBH:** Marne Bleue d'Hauterive; **MKZ:** Megelkalk zone; **PJN:** Pierre Jaune de Neuchâtel; **MU:** Marnes d'Uttins; **MR:** Marnes de la Russille.

• *Numbers on the top of the different stratigraphic schemes:* **1:** Thurmann, 1835; **2:** Desor and Gressly, 1853; **3:** Jaccard, 1869; **4:** Renevier, 1874; **5:** Baumberger, 1901; **6:** Remane, 1989 (modified); **7:** Arnaud-Vanneau and Arnaud, 1990; **8:** Clavel *et al*., 1995; **9:** this work.

Fig. B.35: Sedimentary description of a theoretical succession of the Early Cretaceous from the Western Swiss Jura. The main fauna and flora are reported, as well as the different stratigraphic schemes proposed since the definition of the historical succession of the Hauterivian stage.

last twenty-five years, however, two divergent stratigraphic schemes have emerged. The first school of thought proposed that a significant hiatus is associated with the boundary between the upper PJN and the UJ, and attributed a Late Barremian age for both the UJ and the UB (*e.g.*, Arnaud-Vanneau and Arnaud, 1990; Arnaud *et al.*, 1998). This conclusion is mainly based on a comparison between the Vercors and the Western Swiss Jura, on orbitolinid biostratigraphy (Arnaud-Vanneau, 1980), and on a sequence stratigraphic correlation of the sedimentary successions (Arnaud, 1981, 2005a). A second stratigraphic school proposed that sedimentation processes were relatively continuous in the Western Swiss Jura during this period, which implies that the UJ would be Late Hauterivian in age and the Hauterivian-Barremian boundary would be located within the UB (*e.g.*, Clavel *et al.*, 1987, 1995; Charollais *et al.*, 2003). This is deducted again from orbitolinid biostratigraphy – which in this case was developed by R. Schroeder (*e.g.*, Schroeder *et al.*, 1990; Schroeder, 1994) and albeit fundamentally different from the one proposed by Arnaud-Vanneau (1980) - and from other time-diagnostic benthic organisms such as dasycladacean green algae and rudists (*e.g.*, Masse *et al.*, 1998). The zonations of both these groups are, however, calibrated against the orbitolinid zonation of R. Schroeder. This biostratigraphical approach is also completed by a sequence-stratigraphic analysis of sections along a transect from the Western Swiss Jura to the Provence (*e.g.*, Clavel *et al.*, 1995).

With this contribution, we propose a new, non-paleontological approach with which we evaluate the stratigraphic context of the upper PJN and Urgonian formation from the Neuchâtel area. This is not quite trivial, as the above-mentioned formations belong to the historical succession of the Hauterivian stage. Moreover, determining the age of deposition of both the UJ and the UB may help to constrain the stratigraphic distribution of several kinds of time-diagnostic shallow-water benthic organisms. It may furthermore bring more insight in the way and timing of the installation of Urgonian-type shallow-water platforms, which are a truly global phenomenon in the subtropical waters of the Tethys (*e.g.*, Ager, 1981).

We present a new chemostratigraphic correlation based on $^{87}Sr/^{86}Sr$ measurements performed on well-preserved rhynchonellid shells (brachiopods), which were sampled in different sections from the Western Swiss Jura. These results are compared to a new series of $^{87}Sr/^{86}Sr$ data obtained from belemnites sampled in stratigraphic order in the sections of the Vergons, La Charce, Angles and Combe-Lambert (all from the Vocontian Trough, SE France). These sections are well dated by ammonite biostratigraphy (*e.g.*, Bulot *et al.*, 1992; Delanoy, 1997; Vermeulen, 2002).

Finally, several major paleoceanographic events occurred in the Northern Tethyan realm during the Late Hauterivian – Early Aptian, such as the Faraoni Anoxic Event (*e.g.*, Cecca *et al.*, 1994; Bodin *et al.*, 2006a REDOX), or the carbonate platform drowning episodes D2 and D3, which both are documented in the Helvetic realm in the so-called Lidernen Bed and Altmann Member (Föllmi *et al.*, 1994, in press; Bodin *et al.*, in press). Changes in environmental parameters such as climate, nutrient and detrital inputs, and seawater temperature may have triggered the above-mentioned variations in the type of carbonate factory and the ecological crises documented by these drowning episodes. We propose to trace back these paleoceanographic and environmental changes in the western Jura realm and to especially determine which expression these drowning episodes found in the platform succession of the western Jura mountains. Our tool here is a quantification of total phosphorus contents, which serve here as a proxy of nutrient availablity, and to compare stratigraphic changes therein with changes in hemipelagic sections from the Vocontian Basin and elsewhere in the Tethyan realm (Bodin *et al.*, 2006).

B.4.2. Geographical and geological setting

The studied area belongs to the folded Jura realm and is located in NW Switzerland (Trümpy, 1980). An excellent and well-exposed section crops out in the quarry of Eclépens (canton of Vaud), which exploited by the Holcim (CH) company (Fig. B.36). It is located approximately 45km southwesternward from Neuchâtel, on the SE side of the Mormont hill, and allows the continuous observation of the succession from the last eight meters of the lower PJN up to the top of the UB.

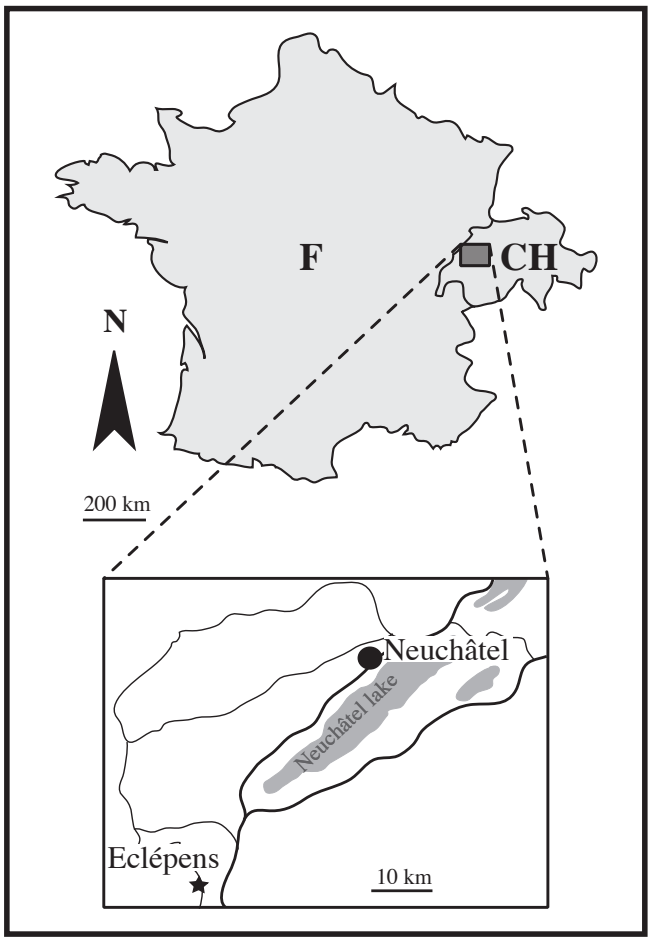

Fig. B.36: Location of the studied area.

B.4.3. Methods: $^{87}Sr/^{86}Sr$ stratigraphy

B.4.3.1. Brachiopod sampling and preparation

We sampled well-preserved rhynchonellid shells. We refrained from using terebratulids, because of the presence of perforations in their shells («punctae»), which may be filled by diagenetic calcite (*e.g.*, Veizer *et al.*, 1999). Whenever possible, the brachiopods were collected from marly layers, which may correspond to sedimentation under low-energy conditions; from this we assume that the potential that the sampled brachiopods reworking from older intervals is low.

Rhynchonellid shells were cleaned using metallic brushes and needles, until the main part of the adhered sediments was removed. They were then washed in an ultrasonic bath, in order to remove fine particles adhered on their surface. In the following, the brachiopods were sawn, and one half of the shells was used to prepare thin sections for Scanning Electron Microscopy (SEM) and cathodoluminescence investigations (see part B.4.3.2.). The second half was polished using a dental microdrill in order to remove the primary layer, which may have been subjected to stronger diagenetic overprint relative to the secondary layer (*e.g.*, Carpenter and Lohmann, 1995). Subsequently, samples were rinsed with ultrapure water. Following the procedure of Voigt *et al.* (2003), powder was obtained from the dried shells using a microdrilling Dremel device equipped with a carburized titanium drill, which was washed with 10% HCl and ultrapure water between each sample treatment in order to avoid any contamination. Each powdered sample was split into two aliquots for $^{87}Sr/^{86}Sr$ and elemental analyses, respectively.

B.4.3.2. Analyses performed to constrain the diagenetic state of the shells

The preservation of the brachiopod shells was checked for any diagenetic alteration by the following three approaches.

Thin sections were first examined using an optic microscope, and in the following the microstructure of a selection of shells was observed using a Scanning Electron Microscope (Phillips SX 50M) at the Institute of Microtechnics of the University of Neuchâtel.

Secondly, evidence for recristallisation or mineralogical changes was searched for on the same set of thin sections, by means of cathodoluminescence microscopy (CL8200 MK4, CITL), at the Institute of Geology and Paleontology of the University of Fribourg.

Finally, the concentration of Sr, Ca, Mg and Mn was measured using a quadrupole ICP-MS (Perkin-Elmer ELAN 6100, Perkin-Elmer Corp., Wellesley, MA, USA), at the Geological Institute of the University of Neuchâtel, in order to compare the results with values obtained for brachiopods from the Holocene (*e.g.*, Fig. 3 in Korte *et al.*, 2003; Fig. 4 in Shields *et al.*, 2003, and references therein). About 5 mg of powder of brachiopods were solubilized in 10 mL of HCL, using the procedure of Boyle and Keigwin (1985/86). The same procedure was applied to belemnites collected in hemipelagic sections from the Vocontian Trough (Bodin *et al.*, in prep.).

B.4.3.3. Strontium isotope measurement

Strontium-isotope analyses were performed at the Centre de Géochimie de la surface (CNRS) in Strasbourg (France) on brachiopods from the Western Swiss Jura and belemnites from the stratotype section of Angles (Vocontian Trough, SE France; see Bodin *et al.*, in prep for further information concerning this material). The procedure is similar to the one described by Stille *et al.* (1994). Powdered samples were treated with 0.5 M acetic acid in order to remove Sr-rich calcite overgrowths and rinsed with distilled water prior to dissolution in 6 N HCl. Chemical separations were performed using ammonium citrate and 4.0 and 6.0 M HCl as eluent through AG 50W-X12 (200-400) ion exchange resin in 1 ml quartz columns for Sr and bulk rare-earth element separation. The blank at the time of analysis was < 1 ng for Sr. Sr was measured using triple Re filament assemblies and single oxidized Ta filaments. Sr isotope measurements were performed on a fully automatic VG Sector mass spectrometer with a 6 cups multicollector. The ratio $^{86}Sr/^{88}Sr$=0.1194 was used for fractionation correction. The average $^{87}Sr/^{86}Sr$ of 15 NBS-987 standard measurements performed at the time of analysis was 0.710257 (1σ). 80-100 ratios for Sr were collected to achieve adequate precision.

B.4.3.4. Phosphorus analyses

Total phosphorus analyses were performed on bulk rock samples. The latter were sawed in order to eliminate the altered parts and the veins of the rock. Then, powders were obtained using an agate crusher. Around 100 mg of powder were mixed with 1 ml of $MgNO_3$ and left to dry in an oven at 45°C for 2 hours. The samples were then ashed in a furnace at 550°C during two hours. After cooling, 10 ml of 1N HCl were added and placed under constant shaking for 14 hours. The solutions were filtrated with a 63μm filter, diluted ten times, and analyzed using the ascorbic acid method of Eaton *et al.* (1995). For this process, the solution was mixed with ammonium molybdate and potassium antimonyl tartrate, which in an acid medium react with orthophosphate to form phosphomolybdic acid. This acid is reduced with ascorbic acid to form an intense blue color. The intensity of the blue color is determined with a photospectrometer (Perkin Elmer UV/Vis Photospectrometer Lambda 10). The concentration of PO_4 in mg/L is obtained by calibration with known standard solutions. Individual samples were measured three times and precision was better than 5%. Replicate analyses of samples have a precision better than 10%.

B.4.4. Results

B.4.4.1. Preservation of the shells and rostra

Our SEM observations on a selection of thin sections of representative brachiopods (n=6) showed no trace of dissolution or recristallisation, and in all cases the lamellar microstructure of the secondary layer was well discernable (Fig. B.37; compare with Veizer *et al.*, 1999; Fig. 2 in Korte *et al.*, 2003; Shields *et al.*, 2003).

The prospecting on the complete set of samples (n=19) by cathodoluminescence microscopy revealed the systematic absence of luminescence in the secondary layer, whereas the shell infills displayed an orange luminescent colour (Fig. B.37), which is likely due to an activation by the presence

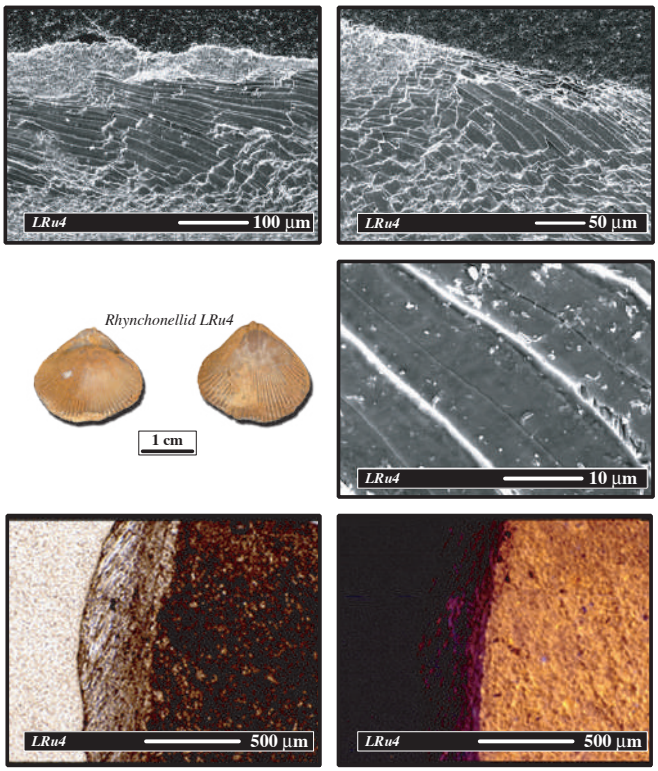

Fig. B.37: The SEM micrographs of the rhynchonellid LRu4 (La Russille section; upper part of the figure) shows a good preservation of the primary fibreous structure of the secondary layer. On cathodoluminesence micrographs of the same sample (lower part of the figure), the secondary layer is non-luminescent, suggesting no recristallisation of the primary low-Mg calcite.

of Mn (*e.g.*, Barbin and Gaspard, 1995). This implies that the secondary layers were precipitated in equilibrium with the sea water, and that they did not undergo recristallisation (*e.g.*, Popp *et al.*, 1986; Brand *et al.*, 2003; Shields *et al.*, 2003).

Finally, determination of Sr, Ca, Mg and Mn in brachiopods (Table B.1) allowed to trace two types of diagram where the fields of stability for well-preserved brachiopods are defined. (Sr/Ca)*1000 to Mn and Sr/Mg to Mn/Mg cross-plots revealed that the samples from the Western Swiss Jura fall within the stability fields defined from data from the literature, except for two samples that may have undergone a stronger diagenesis compared to the rest of the selected fossils (see Fig. B.38 and references therein). Moreover, the Mn contents of the here-analyzed fossils are coherent with the range of values postulated for well-preserved, modern brachiopods by Brand *et al.* (2003).

The preservation of the belemnites rostra was constrained by ICP-MS analyses of Mn, Fe, by the measurement of carbon and oxygen stable isotopes, and by microscopic observation of the microstructure of the rostra (Bodin *et al.*, in prep). These approaches helped to conclude that the diagenetic impact on the belemnites was low enough to perform strontium isotopes measurements (see Bodin *et al.*, in prep. For an in-depth discussion on the diagenetic state of the here-analysed belemnites).

B.4.4.2. $^{87}Sr/^{86}Sr$ results from the Western Swiss Jura and the Vocontian Trough

A total of 50 belemnites from the Vocontian Trough (Fig. B.39) and 19 brachiopods from the Western Swiss Jura (Fig. B.40) were analysed for their $^{87}Sr/^{86}Sr$ content (Table B.2). The brachiopod $^{87}Sr/^{86}Sr$ ratios of the Western Swiss Jura exhibit an increasing trend as a function of the stratigraphic succession, from 0.707410 in the MBH up to 0.707540 for the uppermost sample in the UB (Fig. B.40). In the hemipelagic setting of the Vocontian Trough, an ammonite- and time-calibrated belemnite $^{87}Sr/^{86}Sr$ data set is obtained for the time span from the *A. radiatus* (Early Hauterivian) to the

Sample	Formation	[Mn] ppm	Mn/Mg	Sr/Mg	Sr/Ca*1000	$^{87}Sr/^{86}Sr$
C+160b	*MBH*	257.59	0.24	0.63	2.71	0.707410
C+100	*MBH*	56.19	0.12	0.67	1.75	0.707423
C-120	*MBH*	28.29	0.03	0.61	2.19	0.707431
C-40a	*MBH*	10.55	0.02	0.96	2.17	0.707434
C(0;-30)	*MBH*	19.40	0.02	0.63	2.31	0.707413
C-40b	*MBH*	14.56	0.02	0.73	2.26	0.707417
MC1a	*MU*	67.03	0.07	0.47	1.90	0.707507
MC1c	*MU*	190.35	0.19	0.31	1.35	0.707541
MC3a	*MU*	60.56	0.06	0.52	1.96	0.707464
MC4	*MU*	51.81	0.03	0.26	2.15	0.707448
ECb10	*UJ*	37.90	0.01	0.19	2.36	0.707461
F2a†	*UJ*					0.707437
F2b	*UJ*	69.79	0.11	0.86	1.92	0.707477
LRu4	*MR*	25.08	0.02	0.67	2.14	0.707468
LRu12a	*MR*	44.76	0.04	0.44	1.68	0.707513
LRu12b†	*MR*					0.707443
E125Br	*UB*	46.61	0.01	0.14	1.79	0.707509
E120Br	*UB*	59.05	0.05	0.42	2.00	0.707490
VA61	*UB*	28.87	0.01	0.09	0.88	0.707540

†Due to the tiny size of the brachiopod and the subsequent small amount of powder, it was impossible to perform ICP-MS analyses.

*Table B.1: ICP-MS and $^{87}Sr/^{86}Sr$ results for rhynchonellids from the Western Swiss Jura (**MBH:** Marne Bleue d'Hauterive; **MU:** Marnes d'Uttins; **UJ:** Urgonien Jaune; **MR:** Marnes de la Russille; **UB:** Urgonien Blanc). The grey shading indicates slightly altered samples.*

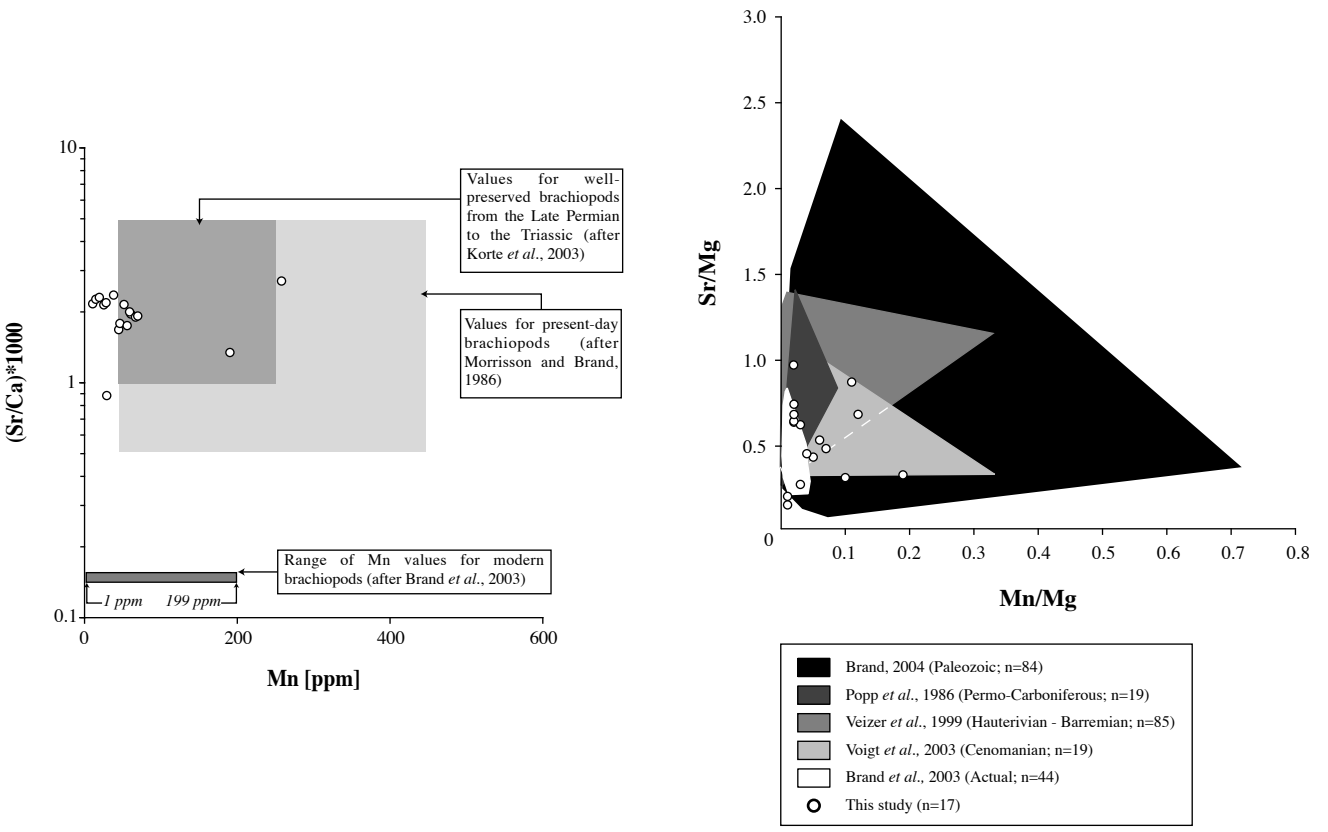

*Fig. B.38: (Sr/Ca)*1000 to Mn, and Sr/Mg to Mn/Mg cross plots of the here-analysed rhynchonellids from the Western Swiss Jura.*

D. weissi (Early Aptian) ammonite zone. In order to plot the belemnite $^{87}Sr/^{86}Sr$ ratios against time, we used the timescale of Gradstein *et al.* (2004) and approximated the time span for each substage, and thus the extent of each ammonite zone, assuming that the latter were of equal duration (except for the *S. angulicostata* and *P. mortilleti* zone, which were thought to represent half the period of the other Late Hauterivian zones). Finally, the belemnite $^{87}Sr/^{86}Sr$ values were distributed within each ammonite zone, according to the stratigraphic position of the belemnite samples within the sedimentary succession relative to the time scale attributed by ammonite biostratigraphy (Fig. B.39 and B.40).

During the Hauterivian, the belemnite $^{87}Sr/^{86}Sr$ record shows a rapid increase, before a maximum is reached in the Early Barremian (mean value of 0.707507 in the *K. nicklesi* zone). In the following, the strontium-isotope curve shifts gently toward less radiogenic values (mean value of 0.707418 in the *M. sarasini* zone). The evolution and the numerical values of the belemnite $^{87}Sr/^{86}Sr$ record are coherent with previous studies carried out on bulk rock, brachiopods, conodonts and belemnites from the Hauterivian – early Aptian interval, as shown on Fig. B.39 (*e.g.*, Veizer *et al.*, 1999; Jones and Jenkyns, 2001; McArthur *et al.*, 2004). However, the high values observed in Resolution Guyot (Jones and Jenkyns, 2001) may be linked to meteoric diagenesis, which may have had an impact on the shallow-water carbonates analyzed by these authors.

B.4.4.3. Evolution of the Phosphorus content in the Western Swiss Jura

The conversion of Phosphorus contents (in ppm) into Phosphorus Mass Accumulation Rates greatly depends on the chosen age model. In the Western Swiss Jura, the different stratigraphic framework proposed by Clavel *et al.* (1995) and by Arnaud-Vanneau and Arnaud (1990) are shifted by one stratigraphic stage, and they also disagree about the duration of the Urgonien Jaune and the Urgonien Blanc. Whereas Arnaud-Vanneau and Arnaud (1990) thought that they may correspond to one depositional sequence, Clavel *et al.* (1995)

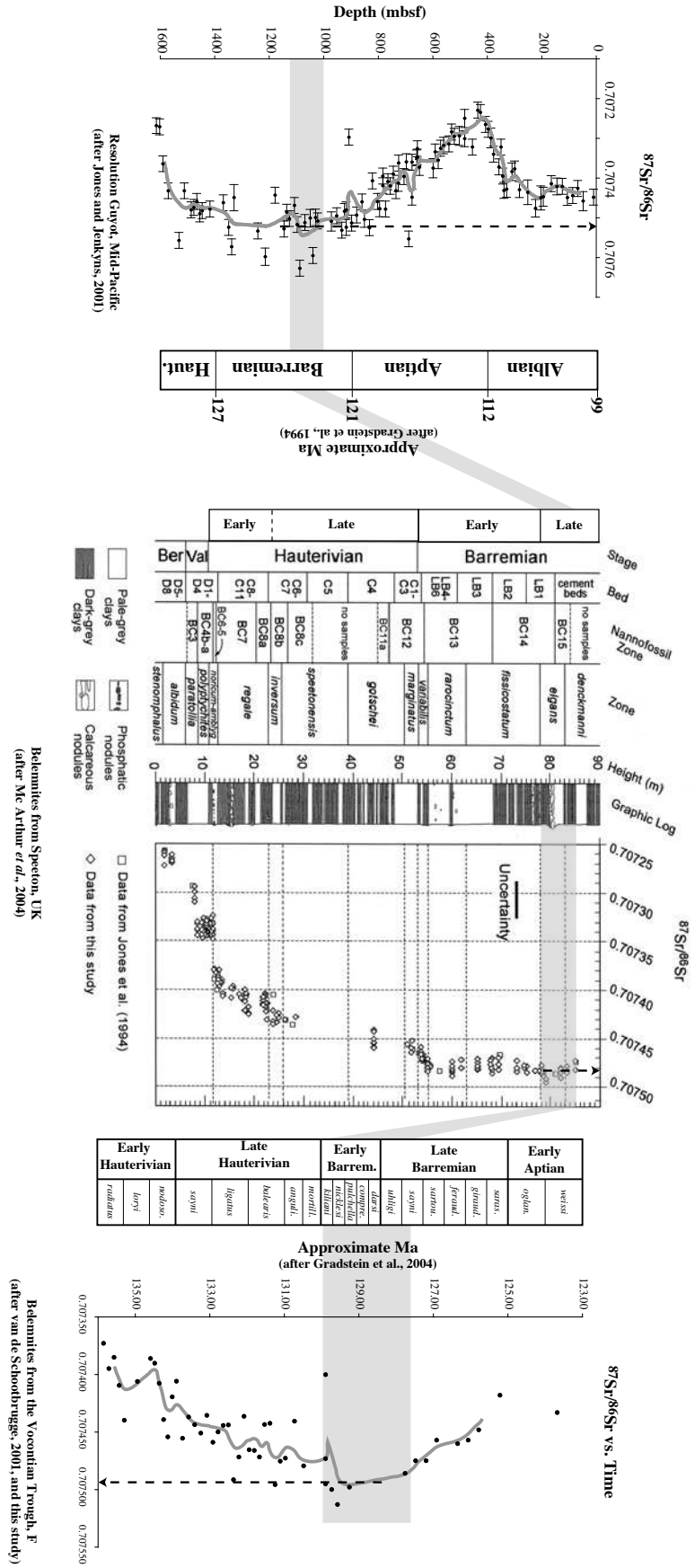

Fig. B.39: Comparison of the $^{87}Sr/^{86}Sr$ curves from Resolution Guyot (Mid-Pacific; Jones and Jekyns, 2001), Speeton (United-Kingdom; Mc Arthur et al., 2004) and the Vocontian Trough (data after van de Schootbrugge et al., 2001, and from this study). Note that the highest values for these three studies are relatively similar (0.707493 and 0.707513 for Mc Arthur et al., 2004, and this study, respectively), expect for Resolution Guyot which maximum reaches 0.707627. Moreover, the maximal plateau is located around the Early – Late Barremian boundary for Speeton and Resolution Guyot, whereas more data are needed to better constrain its stratigraphic position within the sedimentary succession of the Vocontian Trough.

Sample	Stage	Ammonite zone	$^{87}Sr/^{86}Sr$
LC 256c	Early Hauterivian	*Radiatus*	0.707373
LC 258c	Early Hauterivian	*Radiatus*	0.707395
LC 262c	Early Hauterivian	*Radiatus*	0.707385
LC 264c	Early Hauterivian	*Radiatus*	0.707410
LC 272c	Early Hauterivian	*Radiatus*	0.707440
LC 284c	Early Hauterivian	*Loryi*	0.707406
LC 286c	Early Hauterivian	*Loryi*	0.707386
LC 294c	Early Hauterivian	*Nodosoplicatum*	0.707390
LC 301c	Early Hauterivian	*Nodosoplicatum*	0.707408
LC 303c	Early Hauterivian	*Nodosoplicatum*	0.707439
LC 313c	Early Hauterivian	*Nodosoplicatum*	0.707454
LC 315c	Early Hauterivian	*Nodosoplicatum*	0.707419
LC 316c	Early Hauterivian	*Nodosoplicatum*	0.707406
LC 326c	Late Hauterivian	*Sayni*	0.707455
VG 76c	Late Hauterivian	*Sayni*	0.707437
LC 329c	Late Hauterivian	*Sayni*	0.707444
VG 79c	Late Hauterivian	*Sayni*	0.707451
VG 82c	Late Hauterivian	*Sayni*	0.707436
VG 91C	Late Hauterivian	*Sayni*	0.707459
VG 99C	Late Hauterivian	*Ligatus*	0.707450
VG 109c	Late Hauterivian	*Ligatus*	0.707444
VG 117c	Late Hauterivian	*Ligatus*	0.707444
VG 128c	Late Hauterivian	*Ligatus*	0.707492
VG 130c	Late Hauterivian	*Ligatus*	0.707472
VG 133c	Late Hauterivian	*Ligatus*	0.707436
VG 150c	Late Hauterivian	*Ligatus*	0.707465
AN1b	Late Hauterivian	*Balearis*	0.707466
AN 3c	Late Hauterivian	*Balearis*	0.707472
AN 8C	Late Hauterivian	*Balearis*	0.707443
AN 9C	Late Hauterivian	*Balearis*	0.707442
AN 15C	Late Hauterivian	*Balearis*	0.707496
AN 20c	Late Hauterivian	*Balearis*	0.707475
AN 34C	Late Hauterivian	*Balearis*	0.707473
VG 181c	Late Hauterivian	*Angulicostata*	0.707441
VG 197c	Late Hauterivian	*Angulicostata*	0.707479
AN76b	Early Barremian	*Kiliani*	0.707495
AN85b	Early Barremian	*Kiliani*	0.707473
AN92b	Early Barremian	*Kiliani*	0.707400
AN103b	Early Barremian	*Nicklesi*	0.707500
AN104b	Early Barremian	*Nicklesi*	0.707513
AN111.1b	Early Barremian	*Pulchella*	0.707498
AN151.3b	Late Barremian	*Sayni*	0.707486
AN158b	Late Barremian	*Sayni*	0.707475
AN161.1b	Late Barremian	*Sartousiana*	0.707475
AN162b	Late Barremian	*Sartousiana*	0.707457
AN165b	Late Barremian	*Feraudianus*	0.707460
SDL362b	Late Barremian	*Giraudi*	0.707457
SDL366b	Late Barremian	*Giraudi*	0.707448
SDL373b	Late Barremian	*Sarasini*	0.707418
COM109b	Early Aptian	*Weissi*	0.707433

Table B.2: $^{87}Sr/^{86}Sr$ results for belemnites sampled in the La Charce, Vergons, Angles, Saut-du-Loup and Combe-Lambert sections from the Vocontian Trough. The preservation of these samples is discussed in van de Schootbrugge et al. (2000; non-shaded samples), and in Bodin et al. (in prep; light-grey shaded samples).

concluded that the Urgonian from the Western Swiss Jura may be constituted of at least three 3rd order sequences. From this, we preferred to present total phosphorus evolution (in ppm) rather than PMAR, in order to avoid a perturbation of the trend due to a wrong estimation of the sedimentation rate. However, whatever the used age model, the PMAR trends might be approximately the same, only the absolute values would be different.

Through the Marne Bleue d'Hauterive, phosphorus curve exhibits high contents above 0.6 ppm (Fig. B.41). Then, a decreasing trend starting near the Marne Bleue d'Hauterive – zone Marno-calcaire boundary reaches it minimum approximately five meter above the base of the lower Pierre Jaune de Neuchâtel. Following on top, the phosphorus curve describes an increasing trend throughout the lower Pierre Jaune de Neuchâtel, with maximal values around 1 ppm. Finally, the sedimentary succession from the base of the Urgonien Jaune to the top of the Urgonien Blanc is characterized by low phosphorus values (around 0.1 ppm), which describe a decreasing trend upward.

B.4.5. Discussion

B.4.5.1. $^{87}Sr/^{86}Sr$ dating

The evolution of the $^{87}Sr/^{86}Sr$ ratio can successfully be used to attribute a numerical age to sedimentary rocks, especially if the strontium-isotopes curve exhibits fluctuations (*e.g.*, McArthur *et al.*, 2001). For the time span from the Early Hauterivian to the earliest Aptian, the behaviour of our belemnite $^{87}Sr/^{86}Sr$ record is contrasted enough to differentiate Hauterivian from Early Barremian samples: in Fig. B.40, the belemnite $^{87}Sr/^{86}Sr$ record increases slowly from the Early Hauterivian to the middle Early Barremian (*Nicklesia pulchella* ammonite zone), data for the late Early and earliest Late Barremian interval are unfortunately lacking, and from the early Late Barremian onwards it decreases upward until the earliest Aptian (see also Jones and Jenkyns, 2001; Mc Arthur *et al.*, 2004).

A comparison of the strontium-isotope ratios measured on belemnites with the results from rhynchonellids reveals that the values obtained for brachiopods from the MBH and the Marnes d'Uttins are similar with the $^{87}Sr/^{86}Sr$ measured in belemnites from the *A. radiatus* / *C. loryi* and the *L. nodosoplicatum* ammonite zones, respectively. As the MBH and the Marnes d'Uttins are attributed to these ammonite zones (*e.g.*, Busnardo and Thieuloy, 1989; Remane, 1989), this correlation points to the reliability of strontium-isotope stratigraphy for this

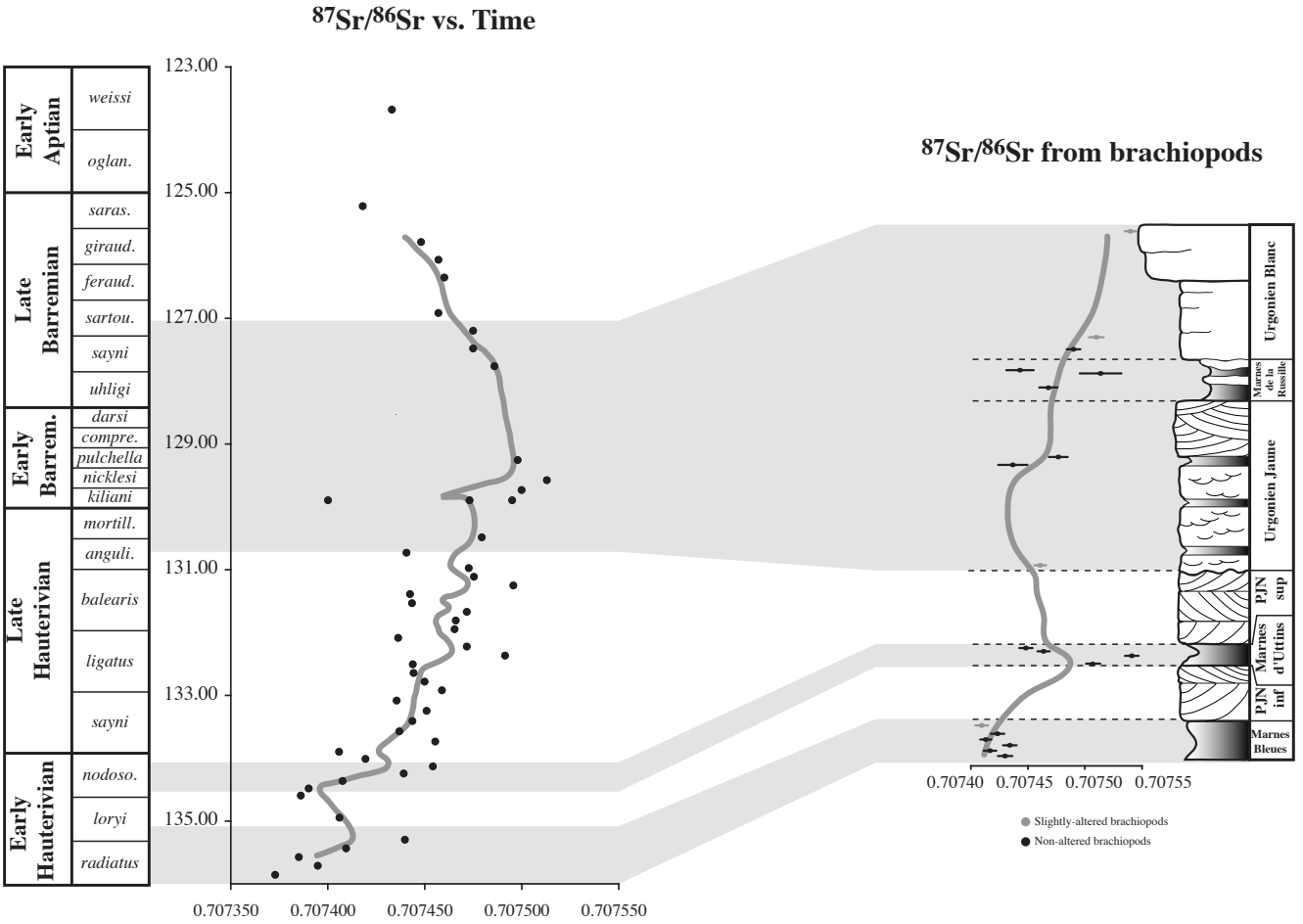

Fig. B.40: Comparison of the strontium-isotopes ratios measured on rhynchonellids from the Western Swiss Jura, with the ammonite-calibrated $^{87}Sr/^{86}Sr$ curve obtained from belemnites from the Vocontian Trough (data for the main part of the Hauterivian after van de Schootbrugge, 2001). The light-grey shading highlights the different correlatable parts of both curves.

interval.

In the following, brachiopods from the UJ, the Marnes de la Russille and the base of the UB display generally slightly higher $^{87}Sr/^{86}Sr$ ratios, and a positive trend is visible which is similar to the increase observed in the Vocontian Trough from the Early Hauterivian to the top of the Early Barremian. Moreover, if we consider the average value above 0.70747 given by brachiopods from the Marnes de la Russille and the value of 0.70754 for the upper part of the UB, these sediments may belong to the Barremian stage, as such high values are only observed within this stage in the Vocontian Trough. However, more values from the belemnites from the *Kotetishvilia compressissima* to the Heinzia sayni are needed, in order to better constrain the attribution of the Urgonion from the Western Swiss Jura to the Barremian stage.

Some problems are inherent with the correlation proposed here, such as the problem of the sampling resolution, which influences the temporal resolution of the here-presented $^{87}Sr/^{86}Sr$ curves. Effectively, the interval from the UJ to the top of the UB may be constituted by third-order transgressive and highstand deposits (*e.g.*, Arnaud-Vanneau and Arnaud, 1990; Godet *et al.*, 2005), with several episodes of sediment reworking documented from the lower part of the Urgonien Jaune. More precisely, the main part of the Urgonian limestone from the Western Swiss Jura may correspond to the B3 depositional sequence (see parts B.6 and C), and thus may represent a time span of less than one million years (see Arnaud, 2005b), whereas the positive trend observed in the Late Hauterivian - Early Barremian from the Vocontian Trough envelops approximately 4 Ma (Fig. B.40).

However, a discrepancy occurs between the value measured on brachiopod sample VA61

(uppermost UB) and values from the Vocontian Trough, as VA61 holds a $^{87}Sr/^{86}Sr$ ratio of 0.707540, which is higher than any value measured on Barremian belemnites. Classically, enrichment in radiogenic isotopes is explained by post-depositional, progressive alteration of low-Mg calcitic material in the presence of meteoric waters (e.g, Brand, 1991). The presence of karsts at the top of the UB, as well as the rapid decrease of the $\delta^{18}O$ (from -6 to -8‰) and the good correlation between the $\delta^{18}O$ and the $\delta^{13}C$ within the UB at Eclépens (data from van de Schootbrugge, 2001), support this hypothesis. An alternative explanation may consist in an increase of the paleosalinity: recent studies used the $^{87}Sr/^{86}Sr$ ratio as a proxy for seawater salinity, and showed that it increases along with the salinity (*e.g.*, Ingram and DePaolo 1993; Widerlund and Andersson 2006). Moreover, Brand *et al.* (2003) claimed that the strontium-isotope system in modern brachiopods is not affected by changes in temperatures or paleoceanographic conditions, but only and slightly by variations in salinity. During the Late Barremian – earliest Aptian period, the Urgonian platform that developed on the northern Tethyan margin consisted of a marginally rimmed platform with patch reefs and oolitic shoals (Arnaud-Vanneau, 1980). Such an architecture may imply an increase in salinity because of the restricted connection between the back-reef settings and the open ocean. Clay-minerals studies also point out the impact of the rise of the Urgonian platform on clay-mineral distributions: the development of a rimmed-platform during the Late Barremian – earliest Aptian implied a differential settling of kaolinite particles, with high contents in proximal settings and a decrease toward hemipelagic environments (see part D.4). However, an increase of the salinity may only partially explain the more radiogenic values of the $^{87}Sr/^{86}Sr$ of the brachiopod VA61: an offset of 0.000101 of the $^{87}Sr/^{86}Sr$ ratio may correspond to an increase of salinity of approximately 33 ‰ (after data from Table 2 in Ingram and DePaolo, 1993). Moreover, there is no clue for an arid climate on the Northern Tethyan margin during this period; for instance clay minerals associated with arid conditions such as palygorskite and sepiolite are missing (see also Rat and Pascal, 1979); on the contrary, clay assemblages are dominated by kaolinite in the Urgonien Jaune and Urgonien Blanc of the Eclépens section (see part D.4). Even if a change in the paleosalinity may have been triggered by restricted conditions in the internal parts of the Urgonian platform, late-stage meteoric diagenesis may have had the most important influence on the strontium-isotope system of VA61.

B.4.5.2. Environmental constraints on the rise of the Urgonian formation of the Western Swiss Jura

Carbonate factories include ecological associations that are dependent on a series of environmental parameters, to which belong seawater oxygenation, temperature, light, turbidity, and nutrient inputs (*e.g.*, Mutti and Hallock, 2003). The two latter factors may control the dominance of heterozoan versus photozoan communities in tropical to sub-tropical climate zones (*e.g.*, James, 1997). Recently, our analysis of the evolution of clay minerals along a transect through the Northern Tethyan margin showed that the Hauterivian was dominated by a seasonal contrasted climate, whereas more humid, inter-tropical conditions prevailed during the latest Hauterivian and the main part of the Barremian (Godet *et al.*, 2006 Cret Res). Outgoing from such a climate change, the rate of continental weathering may have changed as well and with that the input of nutrients into the ocean. This then has an impact on trophic levels and consequently, variations therein may have triggered changes in the type of carbonate factory (*e.g.*, Föllmi, 1996).

B.4.5.2.1. Changes in the type of ecological association: evidence from microfacies

In the Western Swiss Jura, the outcropping carbonates display shallow-water facies characteristic of different depositional settings. Ecological assemblages are not uniform throughout the sedimentary succession and are related to different types of carbonate factories.

The microfacies analysis of thin sections from the PJN points out to the dominance of oolitic grainstones, with some bioclasts of crinoids and bryozoans; this association corresponds to a heterozoan assemblage (*e.g.*, James, 1997). On the other hand, the main part of the UB is

composed of bioclastic packstones to grainstones with bivalves, large benthic foraminifera (orbitolinids), green algae (dasycladaceae), rudists, corals and stromatoporoids; this faunal and floral ecosystem reflects a production of carbonates in a photozoan mode (*e.g.*, Föllmi *et al.*, 1994). The characterization of the UJ in terms of carbonate factories still remains difficult, as sedimentary reworking is important within this formation.

Such an evolution is also described in the Early Cretaceous succession from the Helvetic Alps (*e.g.*, Föllmi *et al.*, 1994, 2006; Funk *et al.*, 1993). In particular, a major change occurred from the Late Hauterivian to the Late Barremian, as the heterozoan carbonate factory developed in this area of the Northern Tethyan Margin (upper Kieselkalk formation; late *P. ligatus* – mid *B. balearis* ammonite zone) underwent a major drowning phase (Altmann members; mid *B. balearis* – mid *C. darsi* ammonite zone), then recovered in a transitional mode (heterozoan / photozoan association: Drusberg formation; mid *C. darsi* - *Gerhardtia sartousiana* ammonite zone) and finally evolved towards a true photozoan mode from the *Gerhardtia sartousiana* ammonite zone onward (Bodin *et al.*, 2006b, d). Moreover in the Vercors area, the rise of the Urgonian platform in a photozoan mode, marked by the first appearance of rudists, corals and orbitolinids, began close to the Early – Late Barremian transition, above the Sequence Boundary (Sb) B3 (latest *Coronites darsi* ammonite zone; Arnaud *et al.*, 1998; Arnaud, 2005b). Finally, in the Gard (south of France), the finding of ammonites in hemipelagic facies below rudist-bearing limestones suggests a Late Barremian age for the installation of the Urgonian platform in this area (Cotillon *et al.*, 1979). The consistent appearance of photozoan Urgonian platform carbonates in the Late Barremian along the northern Tethyan margin renders it very likely that the Urgonian formations from the western Jura mountains also appeared during this time frame.

B.4.5.2.2. Environmental parameters constraining the type of carbonate factory: example from Phosphorus Mass Accumulation Rates and detrital inputs

As phosphorus represents an essential and often limiting element for living organisms, it has been used in previous studies to constrain nutrient levels in past oceans (*e.g.*, Föllmi, 1996; van de Schootbrugge *et al.*, 2003; Bodin *et al.*, 2006c). In particular, the calculation of Phosphorus Mass Accumulation Rates (PMAR, in $mg.cm^{-2}.kyr^{-1}$) allows for an approximation of variations of nutrient input into the oceanic realm as a function of time.

For the time span from the latest Valanginian to the earliest Aptian, the comparison of the Phosphorus contents and PMAR between the Western Swiss Jura and the Vocontian Trough highlights several similarities (Fig. B.41). First, the Phosphorus contents record from the Western Swiss Jura displays relatively high values during the Early Hauterivian (MBH and MKZ formations), which is compatible with the PMAR evolution from the Vocontian Trough during the time span from the *Acanthodiscus radiatus* to the middle of the *Lyticoceras nodosoplicatum* ammonite zones. Then, the Phosphorus curve displays a slight positive trend during the time of deposition of the lower Pierre Jaune de Neuchâtel (borehole F-607, Fig. B.41). On the contrary, the Phosphorus curve reaches very low values through the Urgonien Jaune and the Urgonien Blanc. In comparison with the Vocontian Trough, this behaviour of the Phosphorus content may imply that both the Urgonien Jaune and the Urgonien Blanc were deposited during the Late Barremian, as the lowest values of the Early Hauterivian – earliest Aptian time span are reached between the earliest *H. uhligi* and the latest *M. sarasini* ammonite zones.

On the other hand, the evolution of the Phosphorus curve in the Western Swiss Jura is coherent with the evolution of the style of carbonate production deducted from the ecological associations of the different studied formations: organisms constituting the heterozoan association characteristic of the PJN, such as crinoids and bryozoans, live in water with higher trophic level compared to corals, rudists and stromatoporoids, which are found within the Marnes de la Russille and the UB, and which may have preferred oligotrophic conditions (e.g Hallock & Schlager 1986; Hallock 1988; Mutti & Hallock, 2003). Consequently, the oceanic trophic level may have constituted a limiting factor on the rise of photozoan carbonate platforms, whereas heterozoan associations are

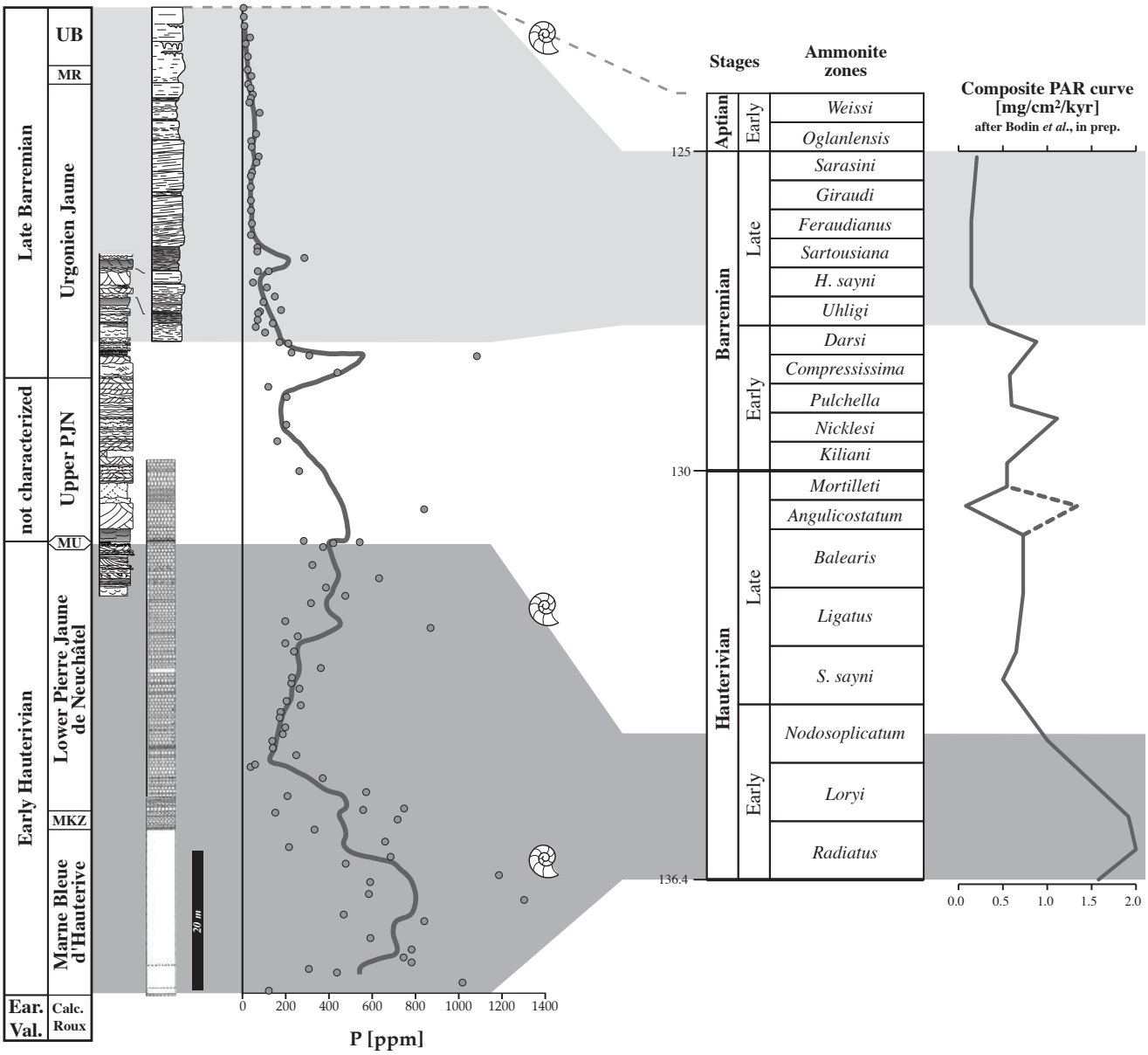

Fig. B.41: Comparison of the Phosphorus Mass Accumulation Rates between the Western Swiss Jura and the Vocontian Trough. The different shadings show the comparable intervals of the Early Hauterivian (dark-grey) and the Late Barremian (light-grey).

expected to develop during period of higher PMAR values. From this comes that during times of relative high PMAR, photozoan associations are not expected to be found within the sedimentary record.

B.4.6.Conclusions

Despite the non-negligible influence of diagenesis, the $^{87}Sr/^{86}Sr$ ratios on rhynchonellid brachiopods allow to attribute a Barremian age the Urgonian Blanc from the Western Swiss Jura.

Moreover, the evolution of the carbonate platform that developed on the northern Tethyan margin during the Hauterivian and the Barremian may have been influenced by changes in nutrient input mirrored by the evolution of the PMAR. The latter implies that the Urgonian platform began to rise under oligotrophic conditions, and that the development of such sedimentary build-up was more or less synchronous at the scale of the Northern Tethyan realm.

B.4.7.Acknowledgements

The first author is grateful to Mireille Leboeuf and Massoud Dadras (Institute of Microtechnics,

Neuchâtel), and to André Strasser (Institute of Geology, Fribourg), for their help with SEM and cathodoluminescence microscopy, respectively. We acknowledge Tiffany Monnier, who performed the preparation of brachiopods samples for the ICP-MS analyses. This research is financially supported by the Swiss National Fund (projects n°2100-067807/1 and 200020-105206/1).

B.4.8.References

Arnaud, H. (1981). "De la plate-forme urgonienne au bassin vocontien: le Barrémo-Bédoulien des Alpes Occidentales entre Isère et Buëch (Vercors méridional, Diois et Dévoluy).» Géologie Alpine **11** (*3 vol.*): 804 pp.

Arnaud, H. (2005a). «Sequence stratigraphy interpretation». *In:* Adatte, T., Arnaud-Vanneau, A., Arnaud, H., Blanc-Aletru, M.-C., Bodin, S., Carrio-Schaffhauser, E., Föllmi, K. B., Godet, A., Raddadi, M. C. and Vermeulen, J., (*Eds*). The Hauterivian-Lower Aptian sequence stratigraphy from Jura Platform to Vocontian Basin: A multidisciplinary approach. Géologie Alpine, **Série Spéciale «Colloques et Excursions» N°7**: 174-179.

Arnaud, H. (2005b). «The South-East France Basin (SFB) and Its Mesozoic Evolution». *In:* Adatte, T., Arnaud-Vanneau, A., Arnaud, H., Blanc-Aletru, M.-C., Bodin, S., Carrio-Schaffhauser, E., Föllmi, K. B., Godet, A., Raddadi, M. C. and Vermeulen, J., (*Eds*). The Hauterivian-Lower Aptian sequence stratigraphy from Jura Platform to Vocontian Basin: A multidisciplinary approach. Géologie Alpine, **Série Spéciale «Colloques et Excursions» N°7**: 5-28.

Arnaud, H., Arnaud-Vanneau, A., Blanc-Aletru, M. C., Adatte, T., Argot, M., Delanoy, G., Thieuloy, J.-P., Vermeulen, J., Virgone, A., Virlouvet, B. and Wermeille, S. (1998). «Répartition stratigraphique des orbitolinidés de la plate-forme urgonienne subalpine et jurassienne (SE de la France).» Géologie Alpine **74**: 3-89.

Arnaud-Vanneau, A. (1980). «Micropaléontologie, paléoécologie et sédimentologie d'une plate-forme carbonatée de la marge passive de la Téthys: l'Urgonien du Vercors septentrional et de la Chartreuse (Alpes occidentales).» Géologie Alpine **Grenoble Mém HS 10**: 874 p.

Arnaud-Vanneau, A. and Arnaud, H. (1990). «Hauterivian to Lower Aptian carbonate shelf sedimentation and sequence stratigraphy in the Jura and northern Subalpine chains (southeastern France and Swiss Jura)». *In:* Tucker, M. E., Wilson, J. L., Crevello, P. D., Sarg, J. R. and Read, J. F., (*Eds*). Carbonate Platforms: Facies, Sequences and Evolution. Blackwell Scientific Publications, Special Publication of the International Association of Sedimentologists, **9**: 203-233.

Barbin, V. and Gaspard, D. (1995). «Cathodoluminescence of recent articulate brachiopod shells. Implications for growth stages and diagenesis evaluation.» Geobios **18** (*Supplément 1*): 39-45.

Baumberger, E. (1901). «Uber Facies und Transgressionen der untern Kreid am Nordrande mediterrano - helvetischen Bucht im westlichen Jura.» Wiss. Beil. Ber. Töchterschule Basel: 1-44.

Bodin, S., Fiet, N., Matera, V., Godet, A., Clément, A., Janssen, N. M. M. and Föllmi, K. B. «An integrated approach to palaeoceanographic changes during the Early Cretaceous in the western Tethyan realm and their links to carbonate-platform factory changes and drowning.» Earth and Planetary Science Letters **(in prep.)**.

Bodin, S., Godet, A., Matera, V., Steinmann, P., Vermeulen, J., Gardin, S., Adatte, T., Coccioni, R. and Föllmi, K. B. (2006a). «Enrichment of redox-sensitive trace metals (U, V, Mo, As) in carbonates associated with the late Hauterivian Faraoni oceanic anoxic event.» International Journal of Earth Sciences (Geologisches Rundschau) **In press**.

Bodin, S., Godet, A., Vermeulen, J., Arnaud, H., Strasser, A., Fiet, N., Adatte, T. and Föllmi, K. B. (2006c). «The late Hauterivian Faraoni oceanic anoxic event in the western Tethys: Evidence from phosphorus burial rates.» Palaeogeography, Palaeoclimatology, Palaeoecology **235**: 245-264.

Bodin, S., Godet, A., Vermeulen, J., Linder, P. and Föllmi, K. B. (2006b). «Biostratigraphy, sedimentology and sequence stratigraphy of the latest Hauterivian - early Barremian drowning episode of the Northern Tethyan margin (Altmann Member, Helvetic Nappes, Switzerland).» Eclogae Geologicae Helveticae, in press.

Bodin, S., Vermeulen, J., Godet, A. and Föllmi, K. B. (2006d). «New data on the age of the installation of Urgonian-type carbonates along

the northern Tethyan margin: biostratigraphy of the Chopf Member (Helvetic Alps, eastern Switzerland).» Comptes Rendus Géosciences **338**: 727-733.

Boyle, E. A. and Keigwin, L. D. (1985/86). «Comparison of Atlantic and Pacific paleochemical records for the last 215,000 years: changes in deep ocean circulation and chemical inventories.» Earth and Planetary Science Letters **76** (*1-2*): 135-150.

Brand, U. (1991). «Strontium isotope diagenesis of biogenic aragonite and low-Mg calcite.» Geochimica et Cosmochimica Acta **55** (*2*): 505-513.

Brand, U., Logan, A., Hiller, N. and Richardson, J. (2003). «Geochemistry of modern brachiopods: applications and implications for oceanography and paleoceanography.» Chemical Geology **198** (*3-4*): 305-334.

Bulot, L. G., Thieuloy, J.-P., Blanc, E. and Klein, J. (1992). «Le cadre stratigraphique du Valanginien supérieur et de l'Hauterivien du Sud-Est de la France; définition des biochronozones et caractérisation de nouveaux biohorizons.» Géologie Alpine **68**: 13-56.

Busnardo, R. and Thieuloy, J.-P. (1989). «Les ammonites de l'Hauterivien jurassien: révision des faunes de la région du stratotype historique de l'étage Hauterivien.» Mémoires de la Société neuchâteloise des Sciences naturelles **XI**: 101-147.

Carpenter, S. J. and Lohmann, K. C. (1995). «$\delta^{18}O$ and $\delta^{13}C$ values of modern brachiopod shells.» Geochimica et Cosmochimica Acta **59** (*18*): 3749-3764.

Cecca, F., Marini, A., Pallini, G., Baudin, F. and Begouen, V. (1994). «A guide-level of the uppermost Hauterivian (lower Cretaceous) in the pelagic succession of Umbria-Marche Apennines (central Italy): the Faraoni level.» Riv. It. Paleont. Strat. **99** (*4*): 551-568.

Charollais, J., Clavel, B., Schroeder, R., Busnardo, R., Decrouez, D. and Cherchi, A. (2003). «La migration de la plate-forme urgonienne entre le Jura plissé et les Chaines subalpines septentrionales (France, Suisse): Evolution of the Urgonian platform between the Jura and the Septentrional Subalpine Chains (France, Switzerland).» Geobios **36** (*6 SU* -): 665-674.

Clavel, B., Charollais, J. and Busnardo, R. (1987). «Données biostratigraphiques nouvelles sur l'apparition des faciès urgoniens du Jura au Vercors.» Eclogae geol. Helv. **80** (*1*): 59-68.

Clavel, B., Charollais, J., Schroeder, R. and Busnardo, R. (1995). «Réflexions sur la biostratigraphie du Crétacé inférieur et sur sa complémentarité avec l'analyse séquentielle: exemple de l'Urgonien jurassien et subalpin.» Bull. Soc. géol. France **166** (*6*): 663-680.

Cotillon, P., Ferry, S., Busnardo, R., Lafargue, D. and Renaud, B. (1979). «Synthèse stratigraphique et paléogéographique sur les faciès urgoniens du Sud de l'Ardèche et du Nord du Gard (France S-E).» Geobios **Mémoire spécial n°3**: 121-139.

de Montmollin, A. (1835). «Mémoire sur le terrain Crétacé du Jura.» Mémoires de la Société des Sciences Naturelles de Neuchâtel **tome I**: 49-65.

Delanoy, G. (1997). «Biostratigraphie des faunes d'Ammonites à la limite Barrémien-Aptien dans la région d'Angles-Barrême-Castellane. Etude particulière de la famille des Heteroceratina Spath, 1922 (Ancyloceratina, Ammonoidea).» Annales du Muséum d'Histoire Naturelle de Nice **Tome XII**: 1-270.

Desor, E. and Gressly, A. (1859). «Etudes géologiques sur le Jura neuchâtelois.» Mémoires de la Société des Sciences Naturelles de Neuchâtel **t. IV**: 1-159.

Eaton, A. D., Clesceri, L. S. and Greenberg, A. E. (1995). «Standard methods for the examination of water and wastewater», **19th edition**, pp.

Funk, H., Föllmi, K. B. and Mohr, H. (1993). «Evolution of the Tithonian-Aptian carbonate platform along the northern Tethyan margin, eastern Helvetic Alps.» *In:* Simo, J. A. T., Scott, R. W. and Masse, J. P., (*Eds*). Cretaceous carbonates platforms. Tulsa, OK, United States., **AAPG (American Association of Petroleum Geologists) Memoir 56**: 387-407.

Föllmi, K. B. (1996). «The phosphorus cycle, phosphogenesis and marine phosphate-rich deposits.» Earth-Science Reviews **40** (*1-2*): 55-124.

Föllmi, K. B., Badertscher, C., de Kaenel, E., Stille, P., John, C. M., Adatte, T. and Steinmann, P. (2005). «Phosphogenesis and organic-carbon

preservation in the Miocene Monterey Formation at Naples Beach, California - The Monterey hypothesis revisited.» GSA Bulletin **117** (*5/6*): 589-619.

Föllmi, K. B., Godet, A., Bodin, S. and Linder, P. (2006). «Interactions between environmental change and shallow-water carbonate build-up along the northern Tethyan margin and their impact on the early Cretaceous carbon-isotope record.» Paleoceanography **in press**.

Föllmi, K. B., Weissert, H., Bisping, M. and Funk, H. (1994). «Phosphogenesis, carbon-isotope stratigraphy, and carbonate-platform evolution along the Lower Cretaceous northern Tethyan margin.» Geological Society of America Bulletin **106** (*II*): 729-746.

Godet, A., Blanc-Aletru, M.-C., Bodin, S., Adatte, T. and Föllmi, K. B. (2005). «The Hauterivian-Barremian of the Western Swiss Jura around Neuchâtel». *In:* Adatte, T., Arnaud-Vanneau, A., Arnaud, H., Blanc-Aletru, M.-C., Bodin, S., Carrio-Schaffhauser, E., Föllmi, K. B., Godet, A., Raddadi, M. C. and Vermeulen, J., (*Eds*). The Hauterivian-Lower Aptian sequence stratigraphy from Jura Platform to Vocontian Basin: A multidisciplinary approach. Géologie Alpine, **Série Spéciale «Colloques et Excursions» n°7**: 79-96.

Godet, A., Föllmi, K. B., Bodin, S., Arnaud-Vanneau, A. and Adatte, T. «Formal definition of the Eclépens Formation from the Western Swiss Jura.» Eclogae geol. Helv. **(in prep.)**.

Gradstein, F. M., Ogg, J. G. and Smith, A. M. (2004). «A Geological Time Scale 2004», Cambridge University Press, 600 pp.

Hallock, P. (1988). «The role of nutrient availability in bioerosion: consequences to carbonate buildups.» Palaeogeography, Palaeoclimatology, Palaeoecology **63**: 275-291.

Hallock, P. and Schlager, W. (1986). «Nutrient Excess and the Deise of Coral Reefs and Carbonate Platforms.» Palaios **1**: 389-398.

Ingram, B. L. and DePaolo, D. J. (1993). «A 4300 year strontium isotope record of estuarine paleosalinity in San Francisco Bay, California.» Earth and Planetary Science Letters **119**: 103-119.

James, N. P. (1997). «The cool-water carbonate depositional realm». *In:* James, N. P. and Clarke, J. A. D., (*Eds*). Cool-water carbonates. Tulsa, Oklahoma, Society for Sedimentary Geology, **SEPM Special Publication N° 56**: 1-20.

Jones, C. E. and Jenkyns, H. C. (2001). «Seawater strontium isotopes, oceanic anoxic events, and seafloor hydrothermal activity in the Jurassic and Cretaceous.» American Journal of Science **301**: 112-149.

Korte, C., Kozur, H. W., Bruckschen, P. and Veizer, J. (2003). «Strontium isotope evolution of Late Permian and Triassic seawater.» Geochimica et Cosmochimica Acta **67** (*1*): 47-62.

Masse, J. P., Gourrat, C., Orbette, D. and Schmuck, D. (1998). «Hauterivian Rudist faunas of southern Jura (France).» Geobios **M.S. n°22**: 225-233.

McArthur, J. M., Howarth, R. J. and Bailey, T. R. (2001). «Strontium Isotope Stratigraphy: LOWESS Version 3: Best Fit to the Marine Sr-Isotope Curve for 0-509 Ma and Accompanying Look-up Table for Deriving Numerical Age.» The Journal of Geology **109**: 155-170.

McArthur, J. M., Mutterlose, J., Price, G. D., Rawson, P. F., Ruffell, A. and Thirlwall, M. F. (2004). «Belemnites of Valanginian, Hauterivian and Barremian age: Sr-isotope stratigraphy, composition (87Sr/86Sr, ∂13C, ∂18O, Na, Sr, Mg), and palaeo-oceanography.» Palaeogeography, Palaeoclimatology, Palaeoecology **202** (*3-4*): 253-272.

Mutti, M. and Hallock, P. (2003). «Carbonate systems along nutrient and temperature gradients: some sedimentological and geochemical constraints.» Int. J. Earth Sci. (Geol. Rundsch.) **92**: 465-475.

Popp, B. N., Anderson, T. F. and Sandberg, P. A. (1986). «Brachiopods as indicators of original isotopic compositions in some Paleozoic limestones.» GSA Bulletin **97**: 1262-1269.

Rat, P. and Pascal, A. (1979). «De l'étage aux systèmes bio-sédimentaires urgoniens.» Geobios **Mémoire spécial n°3**: 384-399.

Remane, J. (1989). «The historical type Hauterivian of the Jura mountains: original definition, actual concept, lithostratographic subdivision.» Mémoires de la Société neuchâteloise des Sciences naturelles **XI**: 9-18.

Renevier, E. (1874). «Tableau des Terrains

Sédimentaires qui représentent les Epoques de la Phase Organique.» Bulletin de la Société Vaudoise des Sciences Naturelles **XIII**: 218-252.

Schroeder, R. (1994). «Description de *Praedictyorbitolina claveli* nov. sp., orbitolinidé (Foraminiferida) de l'Hauterivien supérieur du Jura neuchâtelois et vaudois (Suisse).» Publ. Dép. géol. paléontol. Univ. Genève **14**: 15-24.

Schroeder, R., Clavel, B. and Charollais, J. (1990). «*Praedictyorbitolina carthusiana* nov. gen. nov. sp., orbitolinidé (Foraminiferida) de la limite Hauterivien-Barrémien des Alpes occidentales.» Paläontologische Zeitschrift **64** (*3-4*): 193-202.

Shields, G. A., Carden, G. A. F., Veizer, J., Meidla, T., Rong, J.-Y. and Li, R.-Y. (2003). «Sr, C, and O isotope geochemistry of Ordovician brachiopods: a major isotopic event around the Middle-Late Ordovician transition.» Geochimica et Cosmochimica Acta **67** (*11*): 2005-2025.

Stille, P., Riggs, S., Clauer, N., Ames, D., Crowson, R. and Snyder, S. (1994). «Sr and Nd isotopic analysis of phosphorite sedimentation through one Miocene high-frequency depositional cycle on the North Carolina continental shelf.» Marine Geology **117**: 253-273.

Thurmann, J. (1835). «Résumé des travaux de la Société des Monts-Jura.» Bulletin de la Société Géologique de France **7**: 207-211.

Trümpy, R. (1980). «Geology of Swizerland: A guide-book. Part A: An Outline of the Geology of Switzerland», Wepf & Co. Publishers, Basel - New York, 334 pp.

van de Schootbrugge, B. (2001). «Influence of paleo-environmental changes during the Hauterivian (early Cretaceous) on carbonate deposition along the northern margin of the Tethys: Evidence from geochemical records (C, O and Sr-isotopes, P, Fe, Mn).» *Ph.D. thesis*, Université de Neuchâtel, 291 pp.

van de Schootbrugge, B., Kuhn, O., Adatte, T., Steinmann, P. and Föllmi, K. (2003). «Decoupling of P- and Corg-burial following Early Cretaceous (Valanginian-Hauterivian) platform drowning along the NW Tethyan margin.» Palaeogeography, Palaeoclimatology, Palaeoecology **199** (*3-4 SU* -): 315-331.

Veizer, J., Ala, D., Azmy, K., Bruckschen, P., Buhl, D., Bruhn, F., Carden, G. A. F., Diener, A., Ebneth, S. and Godderis, Y. (1999). «$^{87}Sr/^{86}Sr$, $\delta^{13}C$ and $\delta^{18}O$ evolution of Phanerozoic seawater.» Chemical Geology **161** (*1-3*): 59-88.

Vermeulen, J. (2002). «Etude stratigraphique et paléontologique de la famille des Pulchelliidae (Ammonoidea, Ammonitina, Endomocerataceae).» Géologie Alpine **Mémoire H.S. N°42**: 333 pp.

Voigt, S., Wilmsen, M., Mortimore, R. N. and Voigt, T. (2003). «Cenomanian palaeotemperatures derived from the oxygen isotopic composition of brachiopods and belemnites: evaluation of Cretaceous palaeotemperatures proxies.» Int. J. Earth Sci. (Geol. Rundsch.) **92**: 285-299.

Widerlund, A. and Andersson, P. S. (2006). "Strontium isotopic composition of modern and Holocene mollusc shells as a palaeosalinity indicator for the Baltic Sea." Chemical Geology **232** (*1-2*): 54-66.

B.5.
K-Ar dating of glauconitic-rich levels from the Western Swiss Jura

B.5.1. Introduction

Absolute dating of sedimentary rocks has always been one of the most important debate in geochronology. First attempts of direct dating of sedimentary successions using U-Pb or Pb-Pb methods showed that these approaches may be successful (*e.g.,* Moorbath *et al.*, 1987; Smith and Farquhar, 1989), and may give precisions on the age of early diagenesis, which occurred close to the time of deposition. But, U-Pb and Pb-Pb chronometers applied to carbonates reach several limits, especially if the analyzed rocks underwent late diagenesis or if detrital carbonate particles are present. Moreover, the isotopic behaviour of U and Pb in carbonates in less predictable than in silicate rocks, and the use of several chronometers is needed to constrain the age of deposition (Jahn and Cuvellier, 1994). Furthermore, carbonated rocks rarely hold sufficient contents of U and Pb, which implies complicated chemical procedures in order to concentrate these elements (*e.g.,* Fölling *et al.*, 2000).

As far back as the beginning of the 70's, Rb-Sr or K-Ar chronometers were applied to glauconitic minerals (*e.g.,* Burleigh Harris and Bottino, 1974; Burleigh Harris and Fullagar, 1989). However, the question of the maturity of glauconies is the keystone of the quality of such analyses: light-green glauconitic grains are poorly evolved (Odin and Matter, 1981), and they usually deliver too young radiometric ages, both with Rb-Sr and K-Ar chronometers (Montag and Seidemann, 1981; see also the comments of Odin and Gale, 1982).

Applying K-Ar method to glauconies implies a profound knowledge of the analysed material. In the following, we present how we prepared glauconitic grains from selected marly levels from the Pierre Jaune de Neuchâtel and the Urgonien Jaune, and the K-Ar dates obtained after several attempts. Finally, we will briefly discuss the validity and implications of these results.

B.2.5.2. Methods and results

B.2.5.2.1. Glaucony separation

In the Eclépens section, two clayey layers enriched in glaucony were sampled in view of K/Ar dating. Samples $EC_{II}21$ and $EC_{II}57$ belong to the "Marnes d'Uttins" and to the lowermost part of the "Urgonien Jaune", respectively (see Fig. B.42 for the location of the samples).

The samples were first dried at 40°C during one night, then roughly crushed using a "jaw" crusher. Using a wet granulometric column, the samples were sorted in four size classes (>1mm, 1mm-250μm, 250μm-125μm, 125μm-63μm). Each sieve was washed until the residue was cleaned of all clay particles, then it was transferred in Petri box using deionised water and put in an oven (at 40°C) until all the water is evaporated.

Each granulometric fraction was then examined under a binocular; as the main part of the glauconitic particles was concentrated in the >1mm and the 1mm-250μm fractions, the other granulometric classes were abandoned. All dark green, badly-rounded glauconitic grains were supposed to be of (sub-)autochtonous origin, following the recommendations of previous studies (*e.g.,* Odin and Matter 1981; Odin and Fullagar, 1988); they were separated by hand picking and washed several times using deionised water. The majority of the particles (*i.e.*, quartz, calcite) attached on the surface of glauconititic grains was removed using ultrasonic baths, during at least ten minutes for each sample. Finally, each

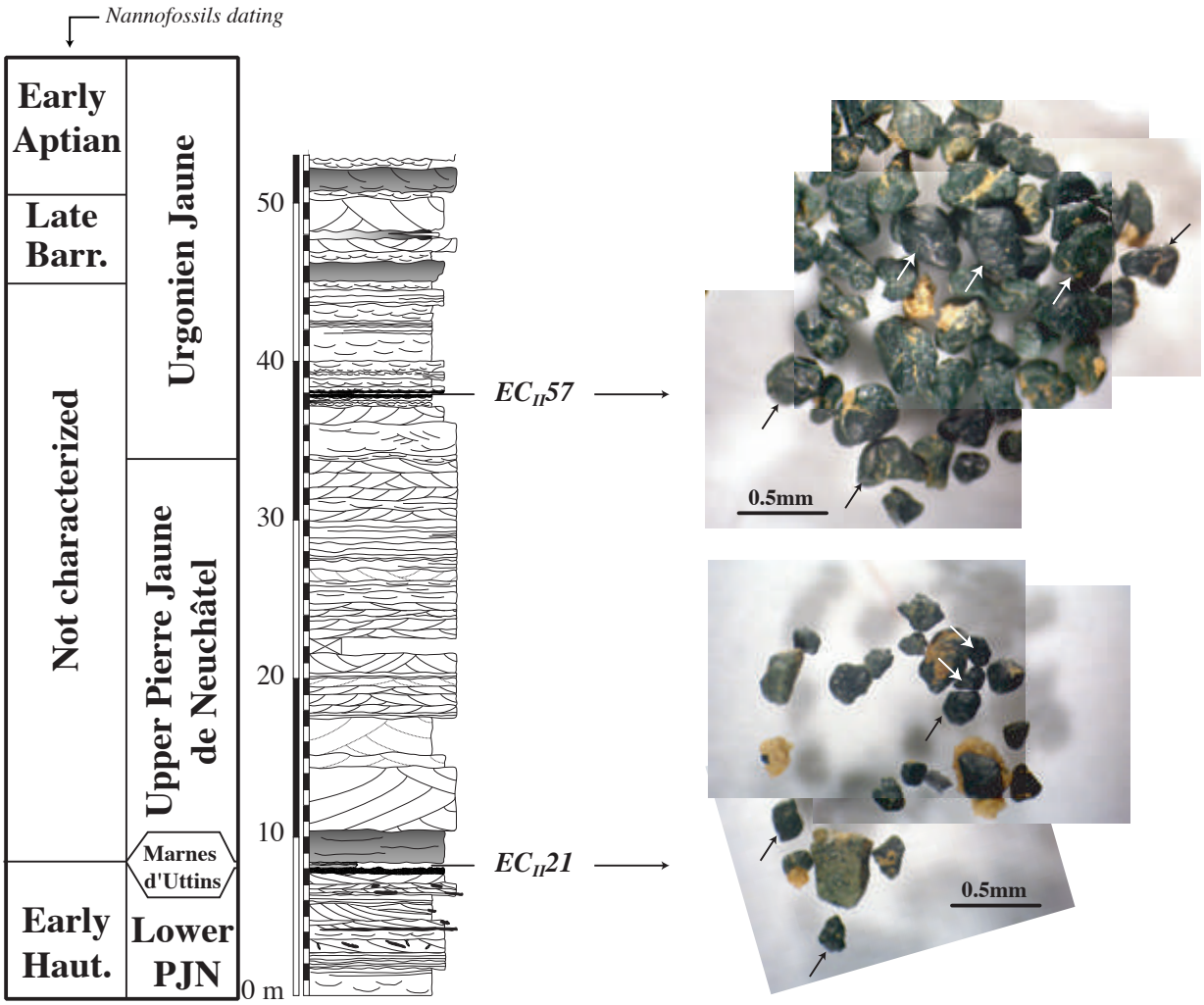

Fig. B.42: Position of the two analysed samples within the lower part of the Eclépens section. On the right hand, photographs of the samples during hand picking are shown; only the dark-green and clean grains were selected (white and black arrows).

sample was split into two aliquots for XRD and K/Ar dating, respectively.

B.2.5.2.2. Mineralogy of separated grains by means of XRD

In view of XRD analyses, the glauconitic grains separated from the samples $EC_{II}21$ and $EC_{II}57$ (1mm – 250μm fraction) were crushed by hand using an agate mortar, in order to produce an homogenous powder. The later was solubilized in deionised water, then deposited on clean glass-plates and put on sample holder in a XDS Scintag 2000 Diffractometer. In order to detect minor amount of clay minerals, the XRD parameters were set as follows:

- Angular range: 2 – 64.97 °2θ.
- Step size: 0.03 °2θ.
- Scan rate: 0.2 °2θ.

The diffractogram of samples $EC_{II}21$ and $EC_{II}57$ (1mm – 250μm fraction) are shown in Fig. B.43. One important thing is to note the presence of calcite, which suggests that the ultrasonic cleaning was not efficient enough to remove all the particles adhered on the glauconite surface. The diffractograms were compared with the values of diffraction peaks of the glauconite (1M) standard JCPDS 09-0439 (dark dotted lines on the Fig. B.43), using the software MacDiff v 4.2.5; the majority of the peaks of $EC_{II}21$ and $EC_{II}57$ are correlatable with the standard's data. Moreover, the position of the 060 peak at 61.2°2θ (61.35°2θ in Tab 7.4 in Moore and Reynolds, 1997), suggests that the separated grains correspond to relatively evolved glaucony.

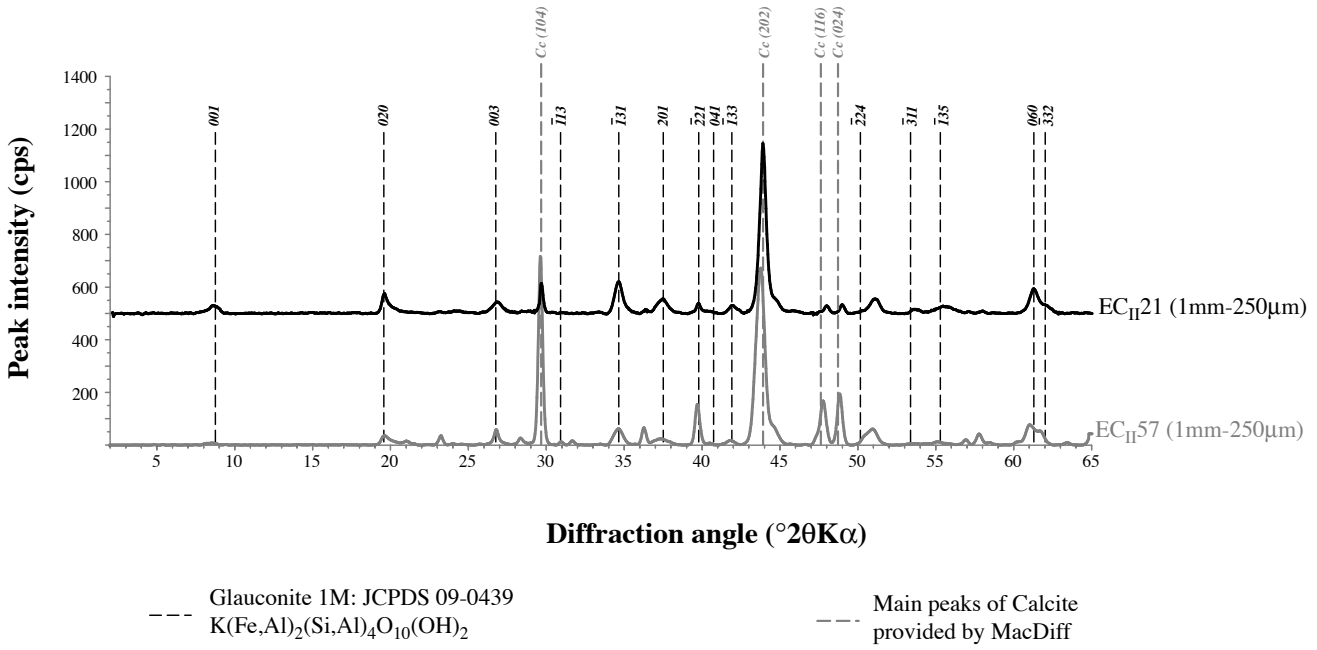

Fig. B.43: Diffractogramms of samples $EC_{II}21$ and $EC_{II}57$. The position of the 001 and 060 peaks (ca. 8.8 and 61.2°2θ, respectively) attests the presence of relatively well-evolved glauconitic minerals.

B.2.5.2.3. Potassium and Argon measurements

This part of the laboratory works was achieved by Dr. Nicolas Fiet (University of Paris Sud, Orsay, France), Prof. J. Kramers (University of Berne, Switzerland), and Prof. P. Stille ("Centre de Géochimie de la Surface, Ecole et Observatoire de la Surface", Strasbourg, France).

A first set of samples was analysed at the "Centre de Géochimie de la Surface, Ecole et Observatoire de la Surface" (Strasbourg, France), by Prof. Peter Stille. The procedure used for samples from Eclépens is similar to the one described by Schaltegger *et al.* (1995). For determination of the K concentration, ca. 50-60 mg of dry sample were heated at 850°C for 24 hours prior to digestion, to oxidize the organic matter. Dissolution was achieved in screwed Savillex vials containing HF and HNO_3 during five days. The dissolved samples were diluted with 2% HNO_3 and their K concentration was measured by atomic absorption spectrometry with an analytical accuracy of ca. ±1%. The Ar isotopic composition was measured on ca. 50 mg of sample, which was previously dried overnight at 110°C, using an Ar extraction method close to that described by Bonhomme *et al.* (1975) and an upgraded AEI MS-20 mass spectrometer. The isotope ratios are corrected for blank and mass discrimination. Analysis of samples replicates implied a precision of ± 2.3 Ma ($EC_{II}21$) and ± 2.6 Ma ($EC_{II}57$).

Samples $EC_{II}21$ and $EC_{II}57$ were also analysed at the "Laboratoire Intéractions et Dynamique des Environnements de Surface, I.D.E.S" of the University Paris Sud (Orsay, France), by Dr. Nicolas Fiet, who separated the glauconitic minerals himself. The procedure is similar to that described by Fiet *et al.* (2006). The K content was determined by atomic flame emission, and radiogenic Ar determination was performed using the technique described by Cassignol and Gillot (1982).

All the results are shown in Fig. B.44. The most important things to note are that the ages are stratigraphically reversed, as sample $EC_{II}21$ yields a younger age than $EC_{II}57$, and that both ages are in the same range of uncertainty. Moreover, the difference between the two batches of analysis exceeds 20 Ma for both samples.

Operator / Laboratory	Attempt	Samples	K_2O (%)	Ar*	Age (Ma)	Error (Ma)
P. Stille, Strasbourg, France	1	$EC_{II}21$	6.47	97.36 %	127.5	±2.3
		$EC_{II}57$	6.03	95.18 %	130.7	±2.6
N. Fiet, Orsay, France	2	$EC_{II}21$	6.08	$6.92*10^{14}$ at/g	105.8	±1.5
		$EC_{II}57$	6.06	$7.03*10^{14}$ at/g	107.9	±1.5

Fig. B.44: Results of the different attempts of K-Ar dating on glauconites from samples $EC_{II}21$ and $EC_{II}57$.

B.2.5.3. Discussion

Grains morphology points out that the here-analyzed glauconitic grains are relatively evolved; the "pop-corn" shape as well as the dark-green colour of the majority of the separated particles indicate that the glauconitization processes reached stage 3 of the Fig. 12 of Odin and Matter (1981). Moreover, XRD analysis reveals the presence of relatively well-evolved glaucony, even if the presence of high energetic peaks of calcite (at 29.45 and 43.15°2θ) tends to minimize the intensity of glaucony peaks. Finally, the high K_2O content (above 6% in all cases) corresponds to evolved glauconies (Odin and Matter, 1981). Consequently, glauconitic minerals from both samples might theoretically give a reliable dating.

However, the obtained ages are reversed and, in certain cases, too young. Two mechanisms may account for low K-Ar ages: Ar loss or K gain (Téllez-Duarte and López-Martínez, 2002), even if the first process is the most common (*e.g.*,, Schaltegger *et al.*, 1995). As the glauconies were sampled in clayey levels, the circulation of fluids within these horizons may have inhibited the closure of the chemical system, and thus allowed the loss of radiogenic Ar. An escape of Ar due to thermal diagenesis is unlikely, as the sedimentary succession at Eclépens underwent a maximum burial depth of approximately 2500 m followed by the rapid exhumation (Burkhard and Sommaruga, 1998). The presence of a major tear-fault (associated to the fault of Pontarlier) within the quarry of Eclépens may also have facilitated the circulation of fluids and the partial resetting of the K-Ar system.

Finally, if we consider the stratigraphic chart of Gradstein *et al.* (2004), the most reliable data set gave a latest Hauterivian – Late Barremian (attempt 1) or a Albian age (attempt 2). Note that the Albian age obtained from the attempt 2 corresponds to a latest Aptian-earliest Albian age on the stratigraphic chart published by Fiet *et al.* (2006). On the other hand, the calculated uncertainties imply that samples $EC_{II}21$ and $EC_{II}57$ are synchronous. This suggests that the main loss of time may be located within the Marnes d'Uttins, or that the glauconies from the samples $EC_{II}57$ may be reworked, and may come from the Marnes d'Uttins that would have been previously eroded in more proximal parts of the margin.

B.2.5.4. Conclusions and outlook

K-Ar dating of selected glauconitic grains from two marly levels of the Eclépens section revealed that the isotopic system may have undergone resetting. The subsequent ages are reversed, are in the same range of analytical error and, in some case, too young to be consistent with the age derived from other approaches. Moreover, the presence of ammonites in the karst on top of the Urgonien Blanc implies that the underlying formations cannot be younger than the *D. deshayesi* / *D. bowerbanki* ammonite zones (Renz and Jung, 1978). This implies that the here-analyzed glauconitic minerals do not hold a reliable age or do not help to differentiate the age of the two analysed samples, at least with respect to the current international stratigraphic chart of Gradstein *et al.* (2004).

B.5.5. References

Bonhomme, M. G., Thuizat, R., Pinault, Y., Clauer, N., Wendling, R. and Winkler, R. (1975). "Méthode de potassium-argon. Appareillage et technique.» Note tech. Inst. de Géologie, Univ. L. Pasteur, Strasbourg **3**: 53 pp.

Burkhard, M. and Sommaruga, A. (1998). Evolution of the western Swiss Molasse basin: structural relations with the Alps and the Jura belt. *In:* A. Mascle, C. Puigdefàbregas, H. P. Luterbacher and M. Fernàndez, (*Eds*). Cenozoic foreland Basins of Western Europe. Geological Society Special Publications, **134**: 279-298.

Burleigh Harris, W. and Bottino, M. L. (1974). «Rb-Sr Study of Cretaceous Lobate Glauconite Pellets, North America.» Geological Society of America Bulletin **85**: 1475-1478.

Burleigh Harris, W. and Fullagar, P. D. (1989). «Comparison of Rb-Sr and K-Ar date of middle Eocene bentonite and glauconite, southeastern Atlantic Coastal Plain.» Geological Society of America Bulletin **101**: 573-577.

Cassignol, C. and Gillot, P.-Y. (1982). Range and effectiveness of unspiked potassium-argon dating: experimental groundwork and applications. *In:* G. S. Odin, (*Ed.*). Numerical Dating in Stratigraphy (Part I). Chichester · New York · Brisbane · Toronto · Singapore, John Wiley & Sons: 159-179.

Fiet, N., Quidelleur, X., Parize, O., Bulot, L. G. and Gillot, P. Y. (2006). «Lower Cretaceous stage durations combining radiometric data and orbital chronology: Towards a more stable relative time scale?» Earth and Planetary Science Letters **246**: 407-417.

Fölling, P. G., Zartman, R. E. and Frimmel, H. E. (2000). «A novel approach to double-spike Pb-Pb dating carbonate rocks: examples from Neoproterozoic sequences in southern Africa.» Chemical Geology **171**: 97-122.

Gradstein, F. M., Ogg, J. G. and Smith, A. M. (2004). «A Geological Time Scale 2004», Cambridge University Press, 600.

Jahn, B.-M. and Cuvellier, H. (1994). «Pb-Pb and U-Pb geochronology of carbonate rocks: an assessment.» Chemical Geology (Isotope Geoscience Section) **115**: 125-151.

Montag, R. L. and Seidemann, D. E. (1981). «A test of the reliability of Rb-Sr dates for selected glauconite morphologies of the upper Cretaceous (Navesink Formation) of New Jersey.» Earth and Planetary Science Letters **52**(*2*): 285-290.

Moorbath, S., Taylor, P. N., Orpen, J. L., Treloar, P. and wilson, J. F. (1987). «First direct radiometric dating of Archaean stromatolitic limestone.» Nature **326**: 865-867.

Moore, D. M. and Reynolds, R. C. J. (1997). «X-Ray diffraction and the Identification and Analysis of Clay Minerals», Oxford University Press, New York, 378 pp.

Odin, G. S. and Fullagar, P. D. (1988). Geological Significance of the Glaucony Facies. *In:* G. S. Odin, (*Ed.*). Green Marine Clay - Oolitic Ironstone Facies, Verdine Facies, Glaucony Facies and Celadonite-Bearing Facies - A Comparative Study. Developments in Sedimentology, Amsterdam - Oxford - New York - Tokyo, Elsevier, **45**: 445.

Odin, G. S. and Gale, N. H. (1982). «Some fundamental considerations in the dating of glauconies: a comment on «A test of the reliability of Rb-Sr dates for selected glauconite morphologies of the Upper Cretaceous (Navesink Formation) of New Jersey», by R.L. Montag and D.E. Seidemann.» Earth and Planetary Science Letters **58**: 443-445.

Odin, G. S. and Matter, A. (1981). «De glauconiarum origine.» Sedimentology **28**: 611-641.

Renz, O. and Jung, P. (1978). «Aptian to Maastrichtian in the SwissJura Mountains.» Eclogae Geologicae Helvetiae **71**(*1*): 1-18.

Schaltegger, U., Zwingmann, H., Clauer, N., Larqué, P. and Stille, P. (1995). «K-Ar dating of a Mesozoic hydrothermal activity in Carboniferous to Triassic clay minerals of northern Switzerland.» Schweizerische Mineralogische und Petrographische Mitteilungen **75**(*2*): 163-176.

Smith, P. E. and Farquhar, R. M. (1989). «Direct dating of Phanerozoic sediments by the ^{238}U-^{206}Pb method.» Nature **241**(*12 October 1989*): 518-521.

Tellez Duarte, M. A. and Lopez Martinez, M. (2002). «K-Ar dating and geological significance

of clastic sediments of the Paleocene Sepultura Formation, Baja California, Mexico.» Journal of South American Earth Sciences **15**(*6*): 725-730.

B.6. Correlation of the Urgonian Formations from the Western Swiss Jura with other regions of the Tethys

Thanks to the new constraints on the age of the Urgonian formations from the Western Swiss Jura, an attempt to correlate this proximal part of the Northern Tethyan margin is proposed here, mainly based on sequence stratigraphy. Effectively, the use of this tool implies the integration of all the previously presented data (*i.e.*, sedimentology, biostratigraphy and strontium-isotopes stratigraphy), and thus the construction of a robust stratigraphic scheme.

Based on chemostratigraphy, we correlated the SbE3 defined at Eclépens with the SbB3 of Arnaud (2005). Moreover, the ammonite assemblage that covers on top the Urgonien Blanc (Renz and Jung, 1978), implies that the SbE4 corresponds to the SbA2.

The identification of these sequence boundaries permits the correlation of the sections from the Western Swiss Jura with the Cluses section, which is located in the French Subalpine Chains near Geneva. Its micropaleontological content was studied in detail by Wermeille (1996) and also by Trabold (1996). The dating of the Cluses section is based on orbitolinids repartition, and as the two above-mentioned authors use the biostratigraphic schemes of Arnaud-Vanneau (1980) and of Schoeder *et al*. (2002), respectively, some discrepancies can be noted between the two studies. In particular, Wermeille (1996) concluded that the Barremian part of the Cluses section begins with the depositional sequence B3, whereas Trabold (1996) thought that the entire Barremian stage was preserved within this sedimentary record. We decided to keep the stratigraphic scheme of Wermeille (1996), as it is the one that is the most comparable with the one we obtained during this work (Fig. B.45).

Whereas Wermeille (1996) observed the SbB4 and the SbB5 in the Cluses section, we concluded that these sequence boundaries may be absent in the Western Swiss Jura, or eroded by the SbA2. Moreover, it seems that several sequence boundaries are located in a narrow interval at the base of the Urgonien Jaune, that is why we propose there the stacking of several sequence boundaries. This conclusion is supported by the comparison of the sequence stratigraphic scheme of the Western Swiss Jura with the one obtained in sections from the Helvetic Alps (Fig. B.46, after Stéphane Bodin, pers. com.; see also Annexe 4.1). As a matter of fact, the age of deposition of the Urgonian equivalent from the Helvetic Alps (Schrattenkalk Formation) is well constrained by ammonite biostratigraphy (see Annexe 4.1 and 4.2) to the *Gerhardtia sartousiana* zone; the correlation between the Western Swiss Jura and the Helvetic regions reveals that the sequence boundaries H4 to B2 of Arnaud (2005) are stacked in the first few meters of the Urgonien Jaune.

The condensation of several depositional sequences at the base of the Urgonien Jaune, as well as the Late Barremian age of the Urgonien Blanc, implies that the rise of the Urgonian formation along the Northern Tethyan margin is not a synchronous phenomenon. In the distal part of the Helvetic ramp, the new dating obtained for the Chopf Member (*G. sartousiana*; cf. Annexe 4.2) implies that the Urgonien Blanc may

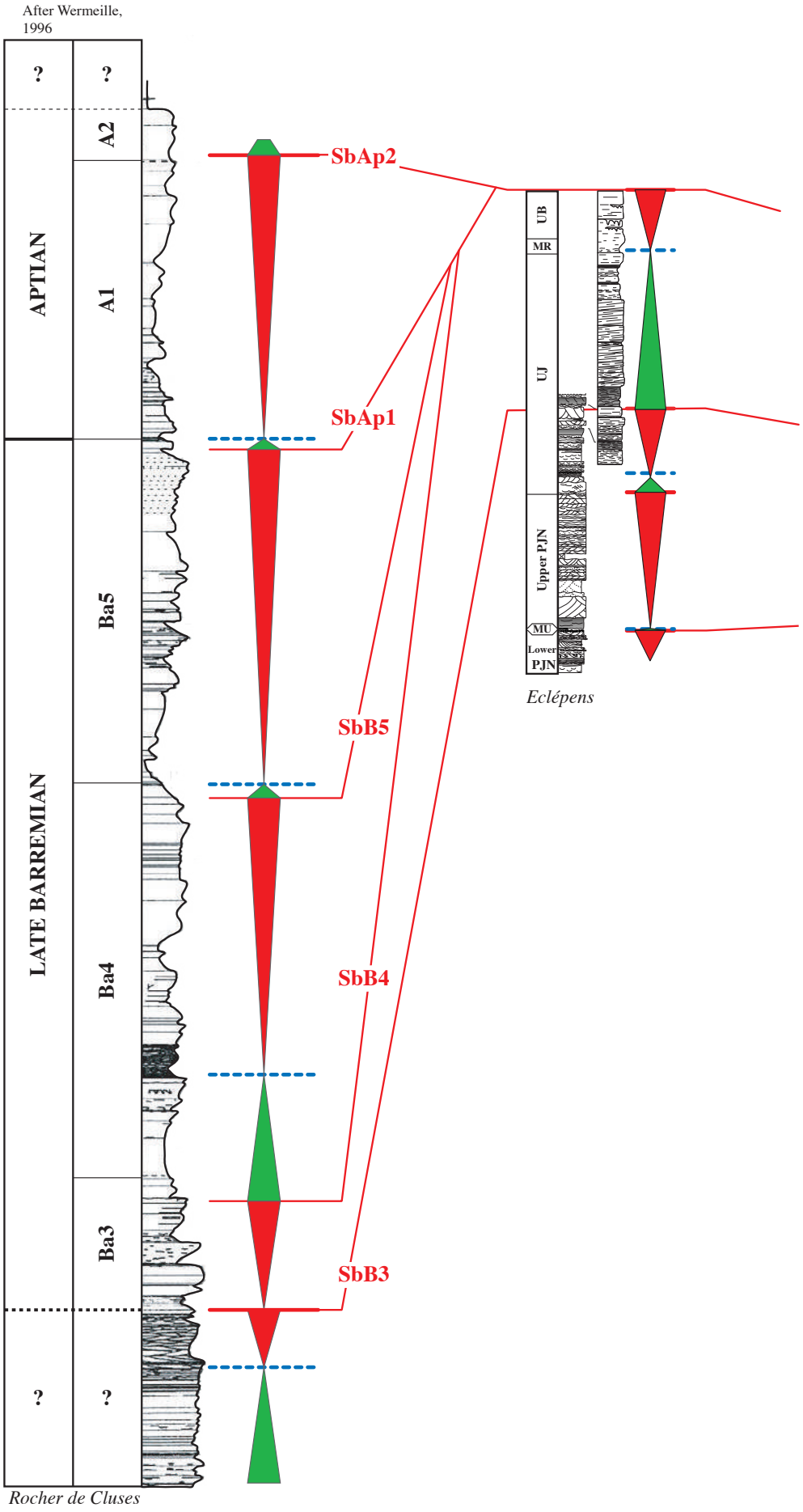

Fig. B.45: Sequence stratigraphy correlation of the section of Cluses (Subalpine Chains; after Wermeille, 1996) with the sections studied in the Western Swiss Jura.

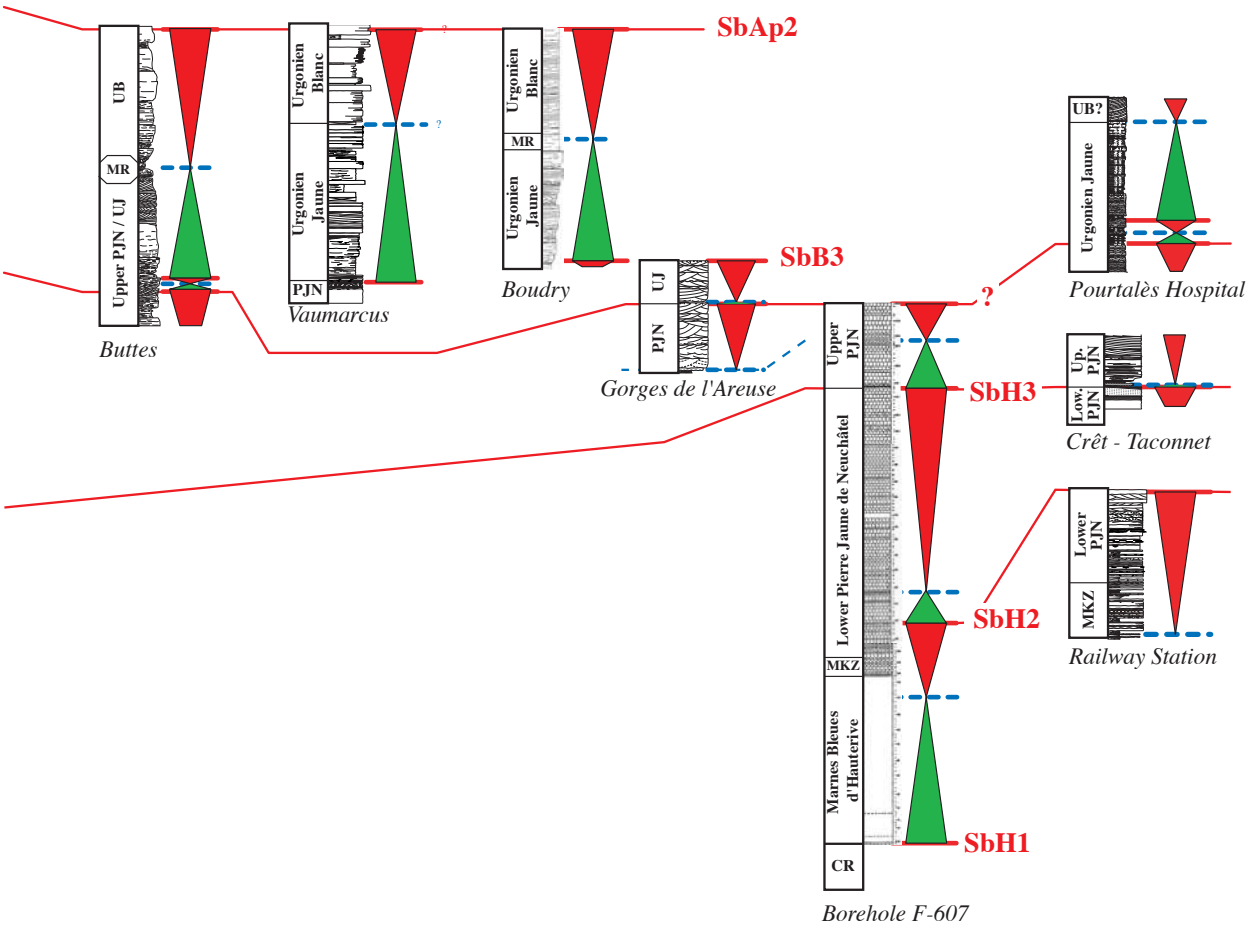

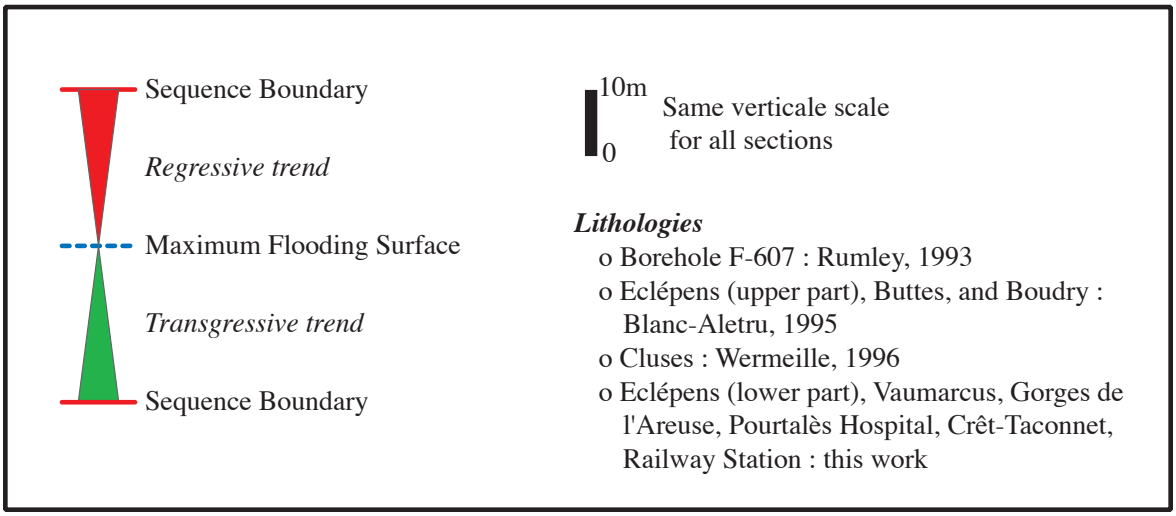

Fig. B.45 (continued): Sequence stratigraphy correlation of the section of Cluses (Subalpine Chains; after Wermeille, 1996) with the sections studied in the Western Swiss Jura.

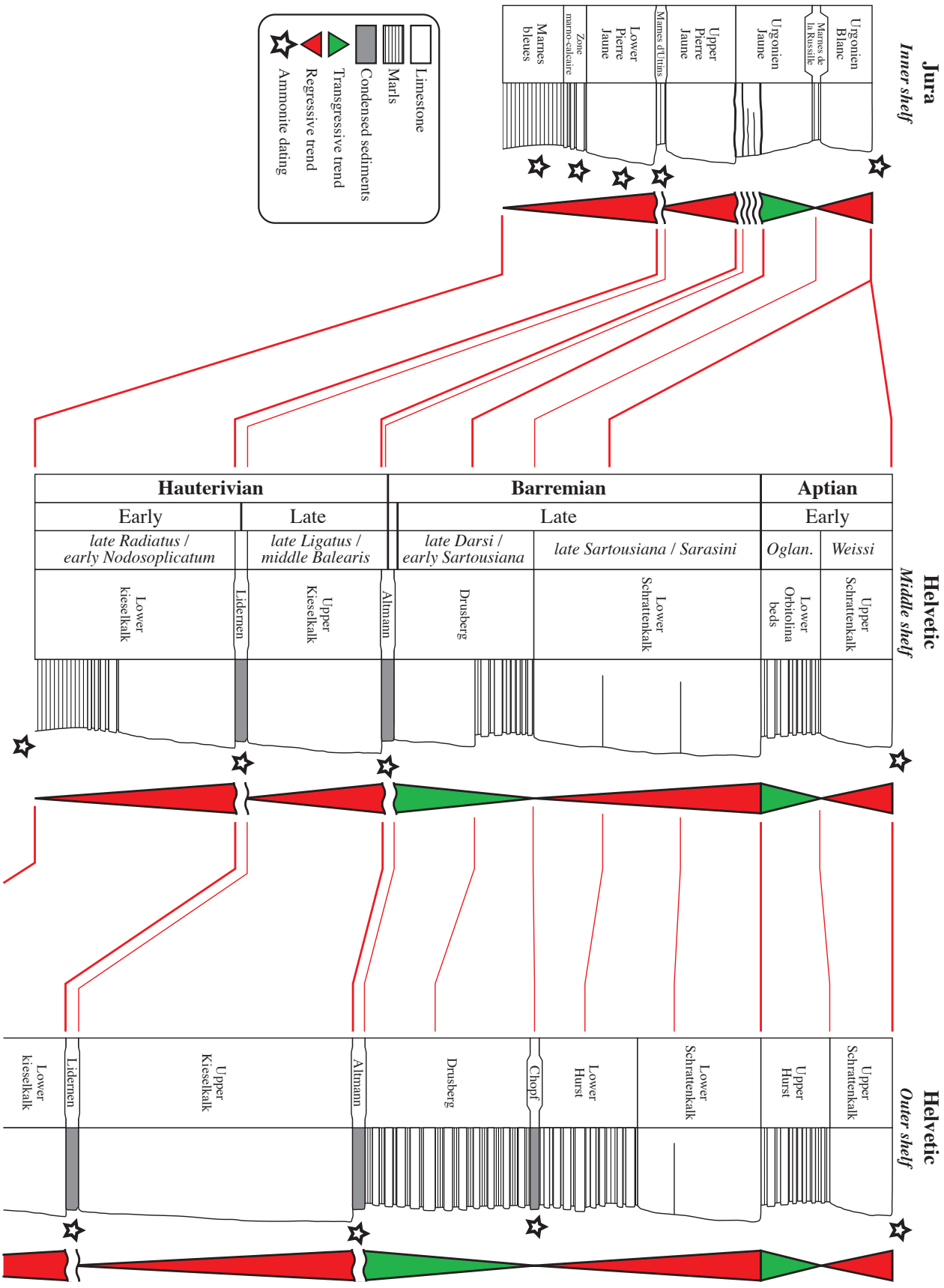

Fig. B.46: Sequence stratigraphy correlation of a synthetic profile of the studied succession in Western Swiss Jura, with the contemporaneous series preserved in the Helvetic realm (after S. Bodin, pers. com.).

rather correspond to the upper than to the lower Schrattenkalk Formation.

References

Arnaud, H. (2005). «The South-East France Basin (SFB) and Its Mesozoic Evolution.» Géologie Alpine **Série Spéciale «Colloques et Excursions» N°7**: 5-28.

Arnaud-Vanneau, A. (1980). «Micropaléontologie, paléoécologie et sédimentologie d'une plate-forme carbonatée de la marge passive de la Téthys: l'Urgonien du Vercors septentrional et de la Chartreuse (Alpes occidentales).» Géologie Alpine **Grenoble Mém HS 10**: 874 p.

Renz, O. and Jung, P. (1978). «Aptian to Maastrichtian in the SwissJura Mountains.» Eclogae Geologicae Helvetiae **71**(1): 1-18.

Schroeder, R., Clavel, B., Cherchi, A., Busnardo, R., Charollais, J. and Decrouez, D. (2002). «Lignées phylétiques d'Orbitolinidés de l'intervalle Hauterivien supérieur - Aptien inférieur; leur importance stratigraphique.» Revue Paléobiol., Genève **21**(2): 853-863.

Trabold, G. L. (1996). «Development of the Urgonian limestones in the Delphino Helvetic Realm (Northern Subalpine Chains, Haute-Savoie, France). Sedimentology, Sequence Stratigraphy and Biostratigraphy.» Université de Genève, Publications du Département de Géologie et Paléontologie **20**: 1-187.

Wermeille, S. (1996). Etude sédimentologique, minéralogique et micropaléontologique des calcaires urgoniens de la région subalpine (Savoie, France). Coupes du Rocher de Cluses, du Borne et d'Andey. Neuchâtel, University of Neuchâtel**:** 129.

B.7. THE WESTERN SWISS JURA: MAIN CONCLUSIONS

Thanks to this multidisciplinary approach, the age of the Urgonian formations from the Western Swiss Jura can now be constrained from the Late Hauterivian (base of the Urgonien Jaune) to the Late Barremian (Urgonien Blanc). This age is in agreement with the timing observed in other regions for the installation and the development of the Urgonian platform in a photozoan mode. It agrees in particularly with the rise of the Schrattenkalk platform in the Helvetic Alps, which is now dated to start in the *Gerhardtia sartousiana* ammonite zone, thanks to the recent finding of ammonites within the Chopf Member (see Annexe 4.2).

Knowing that the Marnes d'Uttins are dated as the *Lyticoceras nodosoplicatum* ammonite zone, and that the base of the Urgonien Blanc belongs to the Late Barremian, we can now constrain the location(s) of the main sedimentary hiatus within the succession. There are two possible candidates:

- If we consider the results of the $^{86}Sr/^{87}Sr$ data and if we focus to the results obtained for brachiopods from the Marnes d'Uttins, we may interpret the scattering of the values as a mixing between Early Hauterivian and younger brachiopods. Following van de Schootbrugge (2001), the Marnes d'Uttins may correspond to an episode of condensation already described in the Helvetic Alps, the Lidernen Beds, as is also indicated by the high amount of glauconite found within this level at Eclépens (see part B.2). The latter may thus contain the main time-gap.

- A second solution is given by the correlation between the Western Swiss Jura and the Helvetic Alps by means of sequence stratigraphy. Following an episode of condensation and phosphogenesis recorded in the so-called Altmann Member, sedimentation processes took up again first in a "mixed-mode" (photozoan and heterozoan: the Drusberg formation), then in a true photozoan mode (Schrattenkalk formation). This scheme is relatively comparable to the one observed in the Western Swiss Jura (see part B.1), and as the end of the Altmann Member is well constrained to the *Coronites darsi* zone by ammonite biostratigraphy, it implies that several sequence boundaries are stacked at and near the base of the Urgonien Jaune. Consequently, the lack of time is located in several key-surfaces, with the first of them corresponding to the basal hardground of the Marnes d'Uttins. Then, the Pierre Jaune de Neuchâtel – Urgonien Jaune limit may probably constitute a second time gap, as this boundary is characterized by a local hardground, a local angular discontinuity and erosion, and also by a sudden facies change. Finally, the basal portion of the Urgonien Jaune is marked by more than ten reworking intervals, each of which may follow a hiatus of non-defined duration.

The new age model obtained in this study allows the integration of the Western Swiss Jura sedimentary succession into a more global scheme. In particular, this will help us to improve our knowledge on the general development of the Urgonian platform along the northern Tethyan margin and to integrate its evolution into a more general paleoceanographic and paleoenvironmental framework.

Reference

van de Schootbrugge, B. (2001). «Influence of paleo-environmental changes during the Hauterivian (early Cretaceous) on carbonate deposition along the northern margin of the

Tethys: Evidence from geochemical records (C, O and Sr-isotopes, P, Fe, Mn).» *Ph.D. thesis*, Université de Neuchâtel, 291 pp.

Chapter C.

Formal definition of the Eclépens Formation from the Western Swiss Jura

Karl B. Föllmi in front of the Marnes de la Russille (quarry of La Sarraz, VD, Switzerland)

C. Formal definition of the Eclépens Formation from the Western Swiss Jura

Alexis Godet[1], Karl B. Föllmi[1], Stéphane Bodin[1], and Thierry Adatte[1]

[1]Institut de Géologie, Université de Neuchâtel, Rue Emile Argand 11, CP 158, 2009 Neuchâtel, Switzerland

Manuscript for Eclogae Geologicae Helvetiae

Abstract

In the Western Swiss Jura, the Early Cretaceous successions, which are traditionally called "Urgonien Jaune" and "Urgonien Blanc" characterise a proximal part of the Urgonian carbonate platform that developed along the Northern Tethyan margin. We propose, with this contribution, (1) to attribute a formal name to these units: the Eclépens Formation, and (2) to designate a type section for this new formation: the Eclépens section (canton of Vaud). In particular, we emphasize the importance of a precise, clear and well-documented definition for its basal boundary. Finally, using sequence stratigraphic arguments, we discuss the validity of this definition by correlating the type section of Eclépens with other sections in the Western Swiss Jura, and also by comparing the occurrence of the Eclépens Formation with equivalent formations in other regions documenting the Northern Tethyan margin.

Résumé

Dans le Jura Suisse occidental, l'"Urgonien Jaune" et l'"Urgonien Blanc" du Crétacé inférieur représentent une des parties les plus internes de la plateforme urgonienne qui s'est développée à cette époque sur la marge nord-téthysienne. Nous proposons, avec cette note, (1) de formaliser le nom de ces unités de la région neuchâteloise et de leurs attribuer le nom de Formation d'Eclépens, et (2) également de leurs assigner une coupe de référence: la coupe d'Eclépens (canton de Vaud). De plus, il nous semble important de définir et de documenter de manière claire et précise la limite basale de cette formation d'Eclépens. Finalement, nous discutons la validité de cette définition à l'aide d'arguments séquentiels, d'une part en corrélant la coupe de référence d'Eclépens avec d'autres affleurements du Jura Suisse occidental, mais également en comparant le Jura neuchâtelois avec d'autres régions de la marge nord-téthysienne.

Keywords

Eclépens Formation; Urgonian limestones; Pierre Jaune de Neuchâtel; Western Swiss Jura; Early Cretaceous; Barremian

C.1. Introduction

In the first half of the nineteenth century, the Hauterivian stage was defined in the vicinity of Neuchâtel (*e.g.*, de Montmollin, 1835; Thurmann, 1835; Renevier, 1874). From the base to the top, the historical stratotype is composed by the "Marne Bleue d'Hauterive", the "Zone Marno-Calcaire", and the "Pierre Jaune de Neuchâtel". Following on top of the latter formation, the "Calcaire Jaune à *Goniopygus peltatus*" and the "Calcaire Blanc à *Requiena ammonia*" of Renevier (1874) were thought to be contemporaneous to the Urgonian of d'Orbigny, (1847), and were subsequently renamed "Urgonien Inférieur" (Jaune) and "Urgonien Blanc", respectively (Baumberger, 1901). They were attributed to the Barremian stage defined by Coquand (1862), without any robust biostraphical evidence, such as ammonites (Baumberger, 1901).

Since the first designation of the Hauterivian historical succession, the definition of the base of the Urgonian formation of the Western Swiss Jura remained relatively blurred until the end of

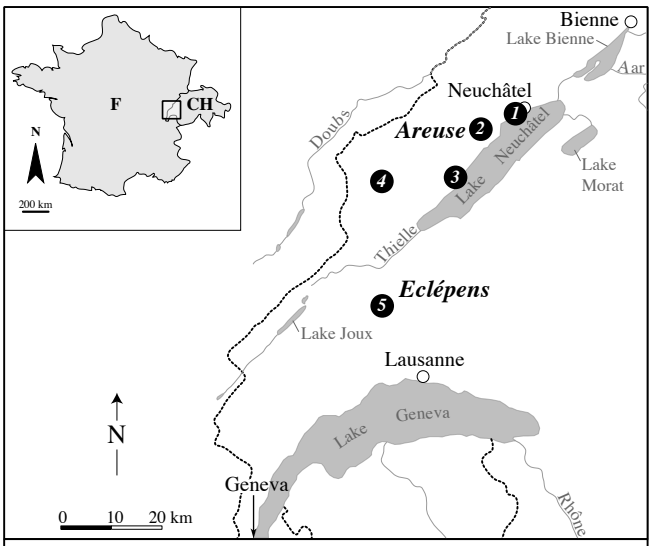

1: sections within the city of Neuchâtel (borehole F-607 (Swiss coordinates: 562'560/205'390), Pourtalès Hospital (562'247/205'225), Crêt-Taconnet (562'075/205278) and Railway Station (562'261/205'427))
2: Boudry (553'545/201'144) and Gorges de l'Areuse (553'460/201'179) sections
3: Vaumarcus section (547'729/191'030)
4: Buttes section (531'990/193'287)
5: Eclépens section (531'256/167'183)

Fig. C.1: Location of the outcrops mentioned in this study.

the twentieth century. The "Marnes de la Russille" (a marly interval rich in coral debris) were first thought to mark the boundary between the "Pierre Jaune de Neuchâtel" and the "Urgonien Jaune" (Jaccard, 1861); however, Conrad & Masse (1989) demonstrated that the "Marnes de la Russille" were rather located between the "Urgonien Jaune" and the "Urgonien Blanc". On the other hand, the "Urgonien Jaune" is classically defined as an oolitic to bioclastic grainstone interrupted by several marly intervals, but without oblique stratifications, compared to the "Pierre Jaune de Neuchâtel" (*e.g.*, Remane, 1989); recent works showed that most sections examined here, oblique stratifications are found in both formations, and thus cannot be used to differentiate them (Godet *et al.*, 2005). Moreover, the same studies lead to the attribution of the Urgonian from the Western Swiss Jura to the late Barremian, as suggested by Arnaud-Vanneau & Arnaud (1990), whereas they were previously thought to be Late Hauterivian – earliest Barremian in age (*e.g.*, Clavel *et al.*, 1995.

With this contribution, we propose to give a new and appropriate definition for the "Pierre Jaune de Neuchâtel" – "Urgonien Jaune" boundary, mainly based on sedimentological evidence from a well - exposed outcrop located in the canton of Vaud, the Eclépens section. In order to avoid confusion with former definitions of formations and age attributions, we suggest a new and more suitable name for both the "Urgonien Jaune", the "Marnes de la Russille" and the "Urgonien Blanc", which will be grouped into a new formation, the Eclépens Formation (Fm). Subsequently, the Eclépens section is designated as the type section (lectostratotype) for the Eclépens Fm. Finally, we will examine the validity and the reproducibility of this definition in several sections from the Western Swiss Jura by means of sequence stratigraphic correlations, as well as the correlation of the Eclépens Fm with analogues in other areas from the northern Tethyan margin.

C.2. Geological and geographical settings

The here studied sedimentary succession actually belongs to the folded Jura (Trümpy, 1980). During the Early Cretaceous, the Western Swiss Jura area was located in very proximal environments of the northern Tethyan margin, where carbonate platform systems developed. The later are now also preserved in the Vercors and the Helvetic areas of the central European Alps(*e.g.*, Arnaud-Vanneau & Arnaud, 1990; Föllmi *et al.*, 1994).

Located in the canton of Vaud, at ca. 50 km southwesternward from Neuchâtel (Swiss coordinates 531'256/167'183; Fig. C.1), the section of Eclépens is exposed in a cement quarry exploited by the Holcim (CH) company. Consequently, the outcrop is continuously refreshed and allows a continuous observation of the sedimentary succession from the uppermost lower "Pierre Jaune de Neuchâtel" to the top of the "Urgonien Blanc" (Fig. C.2).

C.3. The Eclépens Formation: Formal definition

C.3.1. "Urgonien Jaune" and "Urgonien Blanc": main problems

The first publications on the Hauterivian historical stratotype did not clearly define the difference between the "Pierre Jaune de Neuchâtel" and the "Urgonien Jaune"; both may be regrouped into the upper yellow limestone ("calcaire jaune supérieur"; *e.g.*, de Montmollin,

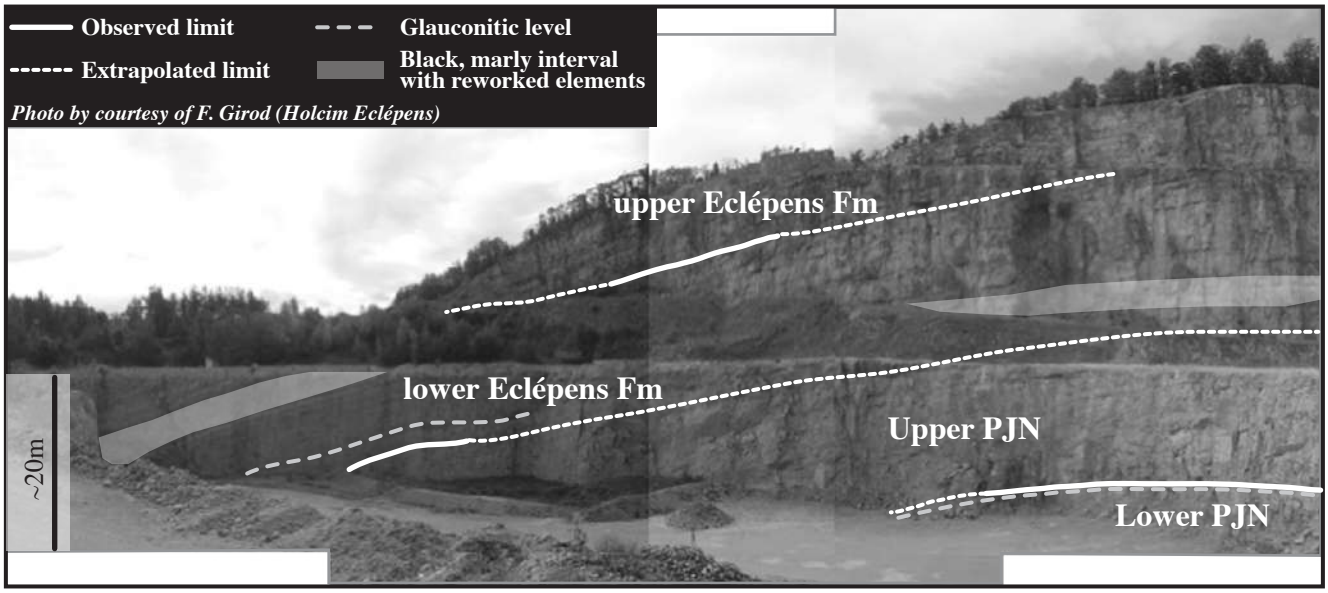

Fig. C.2: Panoramic view of the Eclépens section. The limits between the different formations, as well as the main sedimentological markers, are reported.

1835; Renevier, 1853). On the other hand, the term "Urgonien" qualified, in this historical definition, fossils-rich levels where *Requiena ammonia* appeared. In 1874, Renevier included the "Calcaire jaune à *Goniopygus peltatus*" (*i.e.* "Urgonien Jaune") in its table of the sedimentary succession, but without giving a clear definition of the limit between the "Pierre Jaune de Neuchâtel" and the "Urgonien Jaune". This emphasizes the problem of a precise description of the boundary between the two above-mentioned units, which still implies some significant misunderstandings: for exampled Mouty (1966) signalled the presence of an ammonite (*Leopoldia* sp.) in the Valserine valley (near of Bellegarde, France), but without giving a clear illustration of both the fossil and the sedimentary succession; however, one can deduce from his description of the outcrop that this ammonite was found near the base of the "Urgonien Jaune". Several decades after, this ammonite was re-identified as a *Lyticoceras* / *Cruasiceras* sp., and was thought to belong to the uppermost "Pierre Jaune de Neuchâtel" (Busnardo & Thieuloy, 1989), to the uppermost "Urgonien Jaune" (Clavel & Charollais, 1989), and finally to the top of the "Pierre Jaune de Neuchâtel" or to the base of the "Urgonien Jaune" (both in Charollais *et al.*, 2003). It seems thus that a differentiation between the "Pierre Jaune de Neuchâtel" and the "Urgonien Jaune" only based on the lithofacies is not so trivial (*e.g.*, the disappearance of oblique stratifications in the "Urgonien Jaune"; Remane, 1989), and that some sedimentological criteria are needed to define this boundary as precise as possible.

Finally, the terms "Urgonien Jaune" and "Urgonien Blanc" are, from our point of view, confusing and obsolete: using a colour term for the "Urgonien Jaune" is not appropriate, as the limestones constitutive of this unit can be yellowish, but also black and even whitish. In particular in proximal settings, the uppermost "Urgonien Jaune" is constituted of white, oolitic grainstones relatively similar to the facies found in the "Urgonien Blanc" (*e.g.* the Pourtalès Hospital within the city of Neuchâtel); subsequently, the location of the limit between these two sedimentary units is sometimes hard, especially as the "Marnes de la Russille", which are supposed to mark this boundary, are not preserved everywhere in the studied area. That is why we propose to group the "Urgonien Jaune", "Marnes de la Russille" and "Urgonien Blanc" in one formation clearly defined by its basal and upper limits. Moreover, the term "Urgonien" rather refers to a rudists-bearing facies defined in the south of France (d'Orbigny, 1847); as the rudists are only found in the uppermost "Urgonien Blanc" in the Western Swiss Jura, we propose to avoid the use of a faciologic term to designate a lithostratigraphic unit.

C.3.2. Sedimentological definition of the lower and upper boundaries

Of great importance is to clearly define the base of the Urgonian Formation. For this purpose, several sections from the Western Swiss Jura were analysed in detail, and from this two main statements were derived. First, both the "Pierre Jaune de Neuchâtel" and the "Urgonien Jaune" include yellowish, oolithic limestones with oblique stratification, consequently a differentiation based on this criterium should be abandoned. Secondly, the macrofauna of these formations do not allow for biostratigraphic differentiation, and thus do not help through their rapid identification on the field. On the other hand, precise prospecting within the Eclépens section allows the definition of new criteria to define the limit between the "Pierre Jaune de Neuchâtel" and the "Urgonien Jaune".

At Eclépens, the "Pierre Jaune de Neuchâtel" exhibits its characteristic facies: oolitic grainstones with a variable amount of bioclasts (mainly bivalves, bryozoans and crinoids) are organized into obliquily-stratified bodies. We define the top of this formation by a perforated, well-expressed erosional surface (named ECα), which is surmounted by a 1m-thick bed of crinoidal packstone with glauconite (Fig. C.3). The latter type of facies is rarely or never found within the "Pierre Jaune de Neuchâtel", except near its lower limit where it is accompanied by siliceous lenses; it thus may characterise the first sediments constitutive of the basal Eclépens Fm. Moreover, this limit

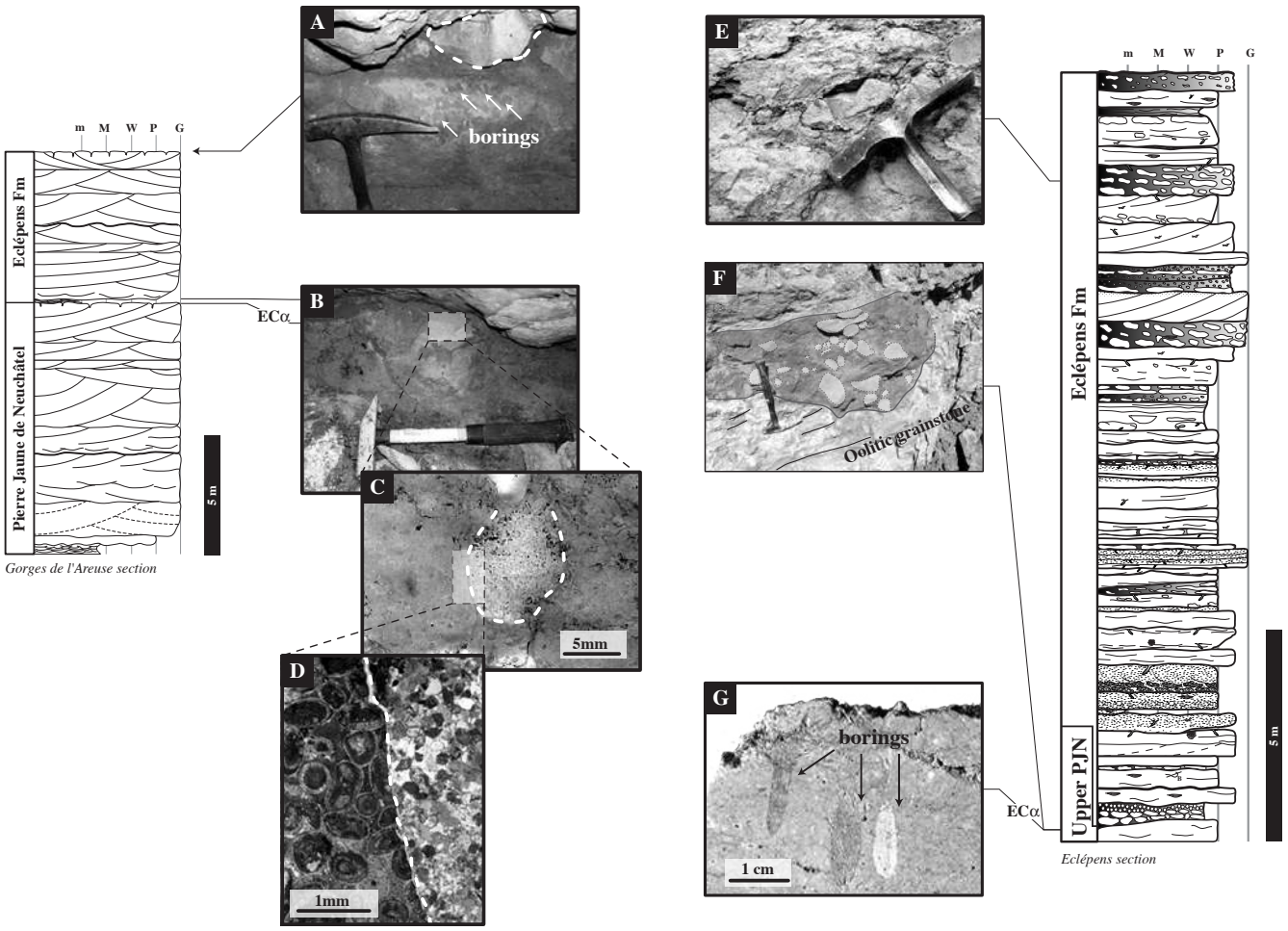

Fig. C.3: Sedimentological characteristics of the limit between the "Pierre Jaune de Neuchâtel" and the Eclépens Fm, in the type section of Eclépens (right-hand side) and the Gorges de l'Areuse section (left-hand side). The latter was deposited in more proximal environments. **A:** *Close-up on the first level of reworking within the Eclépens Fm of the Gorges de l'Areuse section;* **B:** *Field photograph of the perforated surface marking the "Pierre Jaune de Neuchâtel" – Eclépens Fm boundary (sample GA26, Gorges de l'Areuse);* **C and D:** *Thin section and microphotograph of one boring in sample GA26, respectively;* **E:** *Pebble in more or less indurate marly matrix (Eclépens Fm, Eclépens type section);* **F:** *Erosive surface near of the base of the Eclépens Fm, note the presence of large-size pebbles (Eclépens type section);* **G:** *Photograph of a polished slab showing borings characteristic of the "Pierre Jaune de Neuchâtel" – Eclépens Fm boundary (sample EC$_{II}$51b, Eclépens type section).*

is also characterized by local channel infills and angular discordance, as shown in Fig. C.3F. Then, a second erosional surface marks the beginning of the reworking that characterizes the main part of the lower "Urgonien Jaune". Reworking processes are recognizable at the scale of the outcrop (large pebbles or cobbles, which are sometimes perforated and/or encrusted by oysters on all their surfaces), as well as in thin sections (intra- and extraclasts). We thus conclude that the surface ECα marks a change in the type of carbonates that are deposited, as well as in the kind of sedimentary dynamics.

The end of the "Urgonien Blanc" is easily recognizable, as it is marked by a karst filled with orbitolinid-bearing greenish marls. Karstification processes are also well-expressed in the "Urgonien Blanc" of the Vaumarcus and La Lance sections (Blanc-Aletru, 1995), where karst pockets are filled mainly with orbitolinids-bearing, green marls. Based on ammonites finding, this surface that marks the final emersion of the Urgonian platform, is older than the *Deshayesites deshayesi – Deshayesites bowerbanki* ammonite zones of the Early Aptian (Renz & Jung, 1978).

C.3.3. Sedimentological features of the Eclépens Formation

In order to clarify the possible confusions stated in the paragraph 3.1, we propose a new name in relation with a type-locality where this formation is well observable:

Eclépens Formation. Type section (lectostratotype): Eclépens quarry (Swiss coordinates: 531'256 / 167'183). Mean thickness in the Eclépens section: 58m.

The Eclépens Fm corresponds to the sedimentary succession between the two remarkable discontinuities described in paragraph C.3.2; from the base to the top, it comprises the previous "Urgonien Jaune", "Marnes de la Russille" and "Urgonien Blanc" units, and displays a wide range of facies, as shown in Fig. C.4, in which the sedimentary log of its lectostratotype is given, as well as the evolution of the microfacies. We propose then to split the Eclépens Fm into three informal units: the lower Eclépens Fm, the Marnes de la Russille and the upper Eclépens Fm unit.

Just above ECα, the Eclépens Fm is constituted by bioclastic packestones, which exhibit an increasing enrichment in glauconitic minerals. The latter culminates within a 2m-thick interval of marly limestones with more than 30% of glauconite. Then, the sedimentation continues with several intervals of reworked sediments, which are characterized by pebbles and cobbles enrolled in a marly matrix; some of these lithoclastes are perforated or encrusted by oysters. In the Eclépens section, reworking processes are certainly the highest from the base of the Eclépens Fm to 51m depth, where black conglomerates are found. In the upper part of the section, the lower Eclépens Fm unit is rather composed of bio-oosparite organized into oblique-stratified beds.

The transition from the lower to the upper Eclépens Fm units is marked by several marly intervals where the occurrence of cnidarian remains is noticeable, as well as an increased amount of detrital quartz. These layers corresponds to the "Marnes de la Russille" located at the boundary between the former "Urgonien Jaune" and "Urgonien Blanc" (Conrad & Masse, 1989). However, Blanc-Aletru (1995) remarked that the occurrence as well as the faciologic expression of the "Marnes de la Russille" is not systematic and similar in all sections, thus suggesting its invalidity as a formation. In this way, we propose to consider the "Marnes de la Russille" as an informal unit, which marks the transition from the lower toward the upper Eclépens Fm units.

Finally, the highest part of the Eclépens Fm begins with orbitolinid-bearing biopelsparites, which correspond to the external part of the inner platform. Contrary to the lower Eclépens Fm unit, the upper Eclépens Fm unit is characterized by white, massive beds where the amount of micritized grains is higher compared white grainstones constitutive of the uppermost part of the lower Eclépens Fm unit within the Pourtalès Hospital section. The appearance or the frequent occurrence of several kinds of benthic organisms, such as orbitolinids, dasycladacean green algae and rudists is also typical for this part of the Eclépens Fm. In particular, the presence of *Paracoskinolina reicheli* (Guillaume, 1956) and *Praedyctiorbitolina carthusiana carthusiana* (Schroeder, Clavel and Charollais, 1990) is noted in this unit (Zweidler,

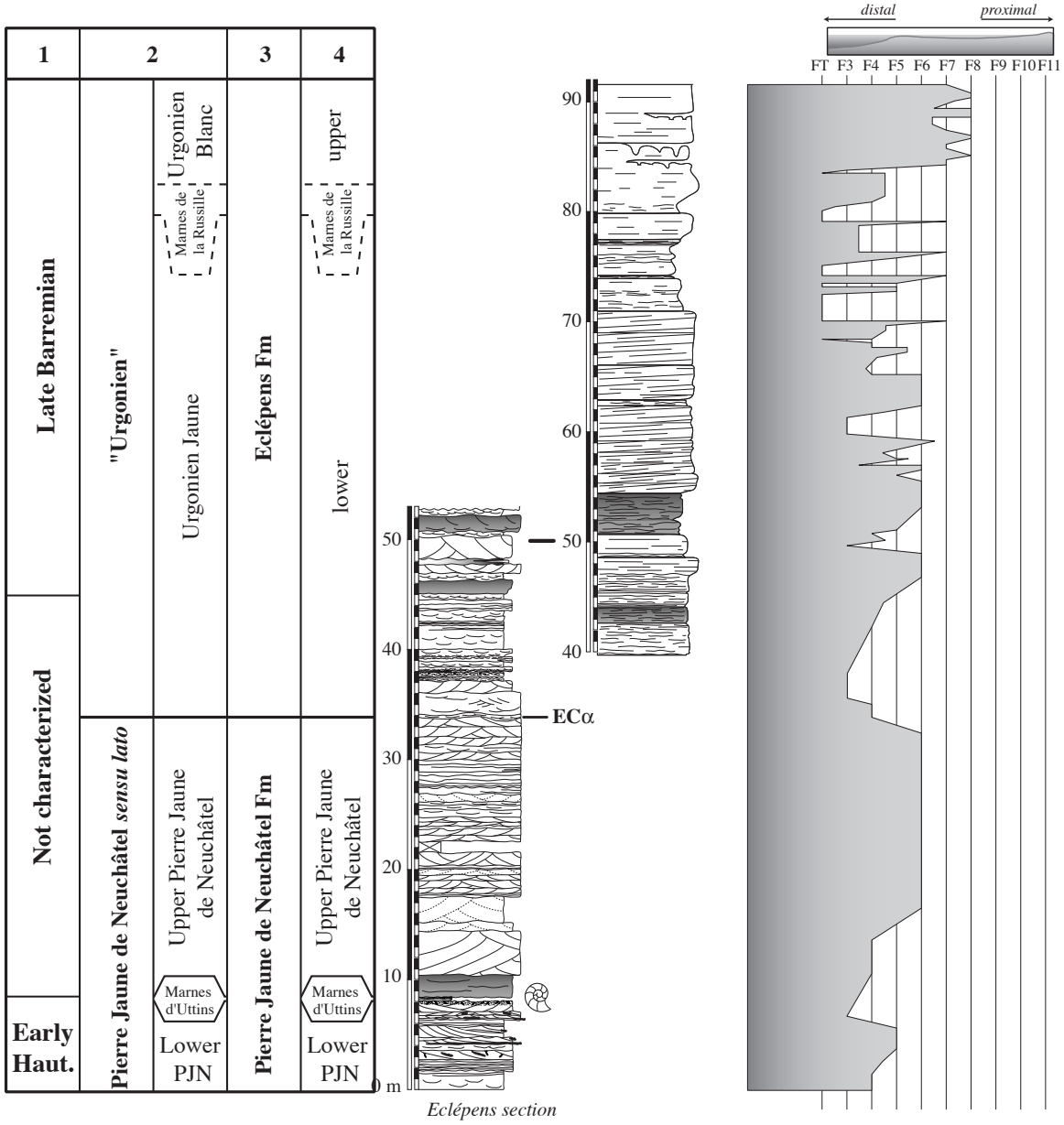

The numbers on the top of the columns refer to:

1. Ammonites and chemistratigraphic dating.
2. Former lithostratigraphic scheme.
3. Formal formations proposed in this contribution.
4. Informal units proposed in this contribution.

Microfacies types after Arnaud-Vanneau, 1980.
Upper part of the section (log and microfacies) after Blanc-Aletru, 1995.
Lower part of the section (log and microfacies) after Godet *et al*., 2005.

Fig. C.4: Sedimentological log of the entire Eclépens section. The age of the here-proposed formations are reported on the left-hand side (after Godet et al., 2005), as well as the correspondence between former and new lithostratigraphic scheme. On the right-hand side, the evolution of the microfacies from the base to the top shows a gradual shift toward more proximal settings.

1985; Blanc-Aletru, 1995). Moreover, rudists appear in the uppermost part of this unit, where microfacies correspond to the most restricted environments; the most characteristic genera are *Pachytraga tubiconcha* (Astre), *Requiena ammonia* (Goldfuss), *Requiena renevieri* (Paquier) and *Agriopleura* sp. (Blanc-Aletru, 1995; Masse *et al*., 1998; Masse, pers. com.). This unit ends with the development of a karst (*cf*. paragraph C.3.2).

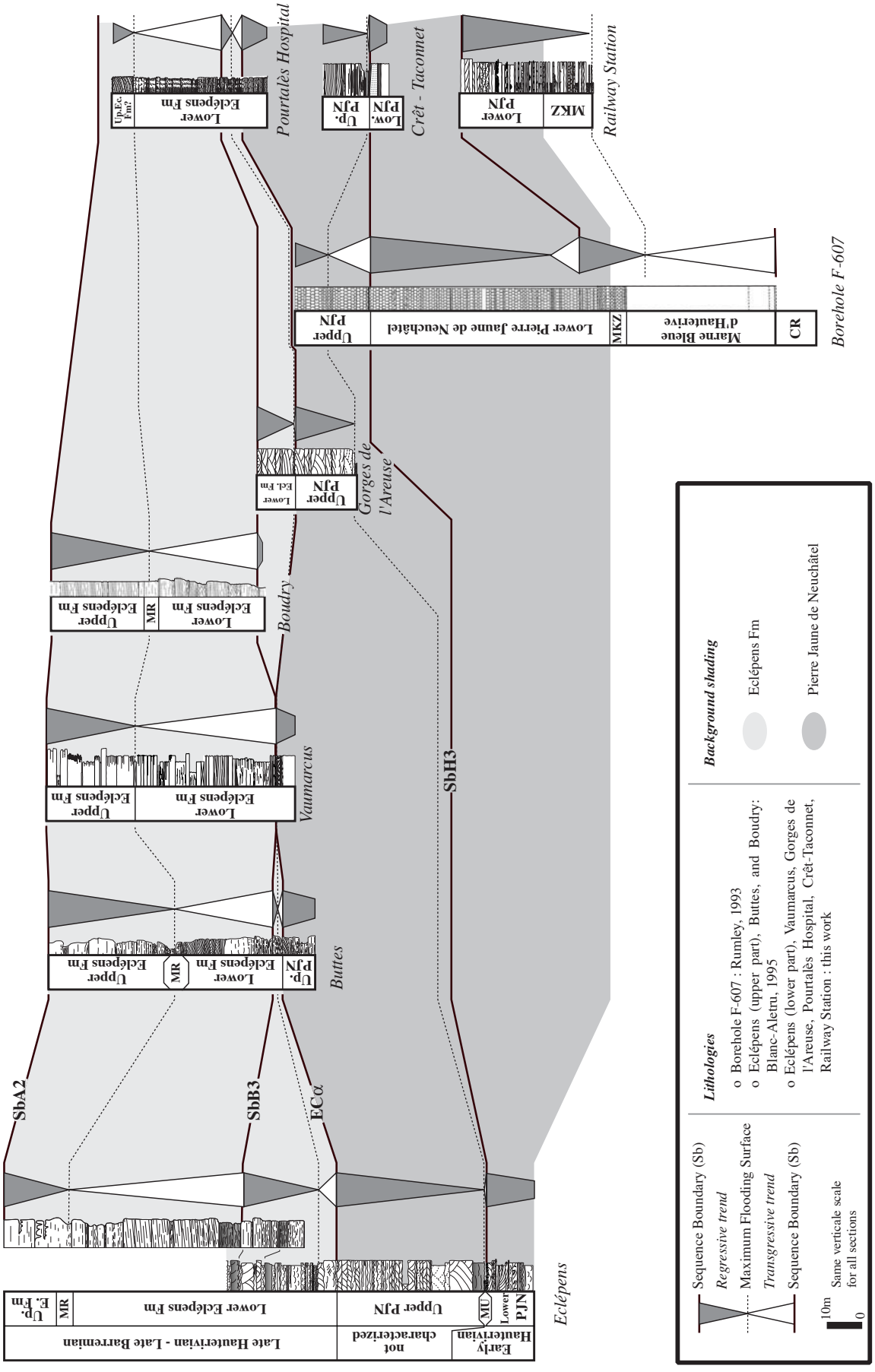

Fig. C.5: Sequence stratigraphic correlation of sections from the Western Swiss Jura. Regressive and transgressive trends are deduced from microfacies analysis in thin sections.

C.4. Correlation of the Western Swiss Jura with other areas of the Northern Tethyan margin

In the Western Swiss Jura, the age of the Eclépens section is well-constrained by several approaches. Measurements of $^{87}Sr/^{86}Sr$ on brachiopods shells (rhynchonellids) sampled in the upper and lower Eclépens Fm units display relatively high values (from 0.707437 to 0.707540; mean value of 0.707482 for all samples from the Eclépens Fm), which may imply a Barremian age for this formation, at least (Godet *et al.*, 2005). Moreover, the evolution of the oceanic trophic level, approximated by the Phophorus Mass Accumulation Rates measured in (hemi-)pelagic sections from the northern Tethys as well as in sections from the Western Swiss Jura, implies that the limestones constitutive of the upper Eclépens Fm unit correspond to oligotrophic conditions and cannot be deposited elsewhere than during the Late Barremian (Godet *et al.*, in prep for Eclogae). From these two approaches comes a relatively good control on the age of the Eclépens Fm (Fig. C.4). Mainly based on microfacies analysis in thin sections, a sequence stratigraphic correlation of a selection of representative sections of the Western Swiss Jura is proposed in Fig. C.5. The latter allows the recognition of the ECα limit, and thus emphasizes the validity of this sedimentological criterion to characterize the "Pierre Jaune de Neuchâtel" – Eclépens Fm boundary. It also permits the identification of the sequence boundaries (Sb) B3 and A2 of Arnaud (2005) in the lowermost and uppermost parts of the Eclépens Fm, whereas recent ammonite finding (Godet *et al.*, 2005)implies that the basal hardground of the "Marnes d'Uttins" corresponds to the SbH3 of Arnaud (2005).

On the other hand, recent findings of ammonites within the Helvetic area helped to more precisely date the deposition of the Schrattenkalk Fm (*i.e.*, the equivalent of the Urgonian limestones). Ammonites found within the Altmann Member indicate that the Helvetic carbonate platform underwent a major phase of drowning, from the *Spathicrioceras angulicostatum* to the *Coronites darsi* ammonite zone (Bodin *et al.*, 2006a Eclogae). Moreover, in the distal part of the Helvetic platform, ammonites belonging to the Chopf Member (a phosphatic, glauconite-rich interval) implies that the deposition of the Schrattenkalk Fm began in the *Gerhardtia sartousiana* ammonite zone (Bodin *et al.*, 2006b).

An attempt to correlate the regressive and transgressive trends between the Western Swiss Jura (Godet *et al.*, 2005), the middle Helvetic shelf (Funk *et al.*, 1993; Bodin *et al.*, 2006a Eclogae; Föllmi *et al.*, 2006 Paleoceanography), the Subalpine Chains (Wermeille, 1996) and the northern Vercors (*e.g.*, Arnaud-Vanneau *et al.*, 2005), is presented in Fig. C.6. From this it appears that:

(1) In the Western Swiss Jura, several sequence boundaries may be stacked at the base of the Eclépens Fm in order to explain its Late Barremian age. An additional sedimentary gap can also be suspected within the "Marnes d'Uttins".

(2) The correlation of the SbB3 and A2 within this transect through the northern Tethyan margin implies that the upper Eclépens Fm unit, as well as the Lower Schrattenkalk Member, correspond to the Lower Urgonian Fm of the Vercors. On the other hand, the Upper Urgonian Fm of the Vercors may corresponds to the Upper Schrattenkalk Fm, whereas it is missing from the sedimentary succession of the Western Swiss Jura.

C.5. Acknowledgments

The financial support of the Swiss National Fund is gratefully acknowledged (projects n°2100-067807/1 and 200020-105206/1)

C.6. References

Arnaud, H. (2005). "The South-East France Basin (SFB) and Its Mesozoic Evolution". *In:* Adatte, T., Arnaud-Vanneau, A., Arnaud, H., Blanc-Aletru, M.-C., Bodin, S., Carrio-Schaffhauser,

Fig. C.6 (opposite): Sequence stratigraphic correlation of the Eclépens Fm and its possible equivalents between the Northern Vercors (Gorges du Nant section; Arnaud-Vanneau et al., 2005), the Subalpine Chains (Rocher de Cluses section; Wermeille, 1996), the Western Swiss Jura (composite section; Godet et al., 2005; this work), and the Helvetic Realm (composite section; Funk et al., 1993; Bodin et al., 2006a, b; Föllmi et al., 2006).

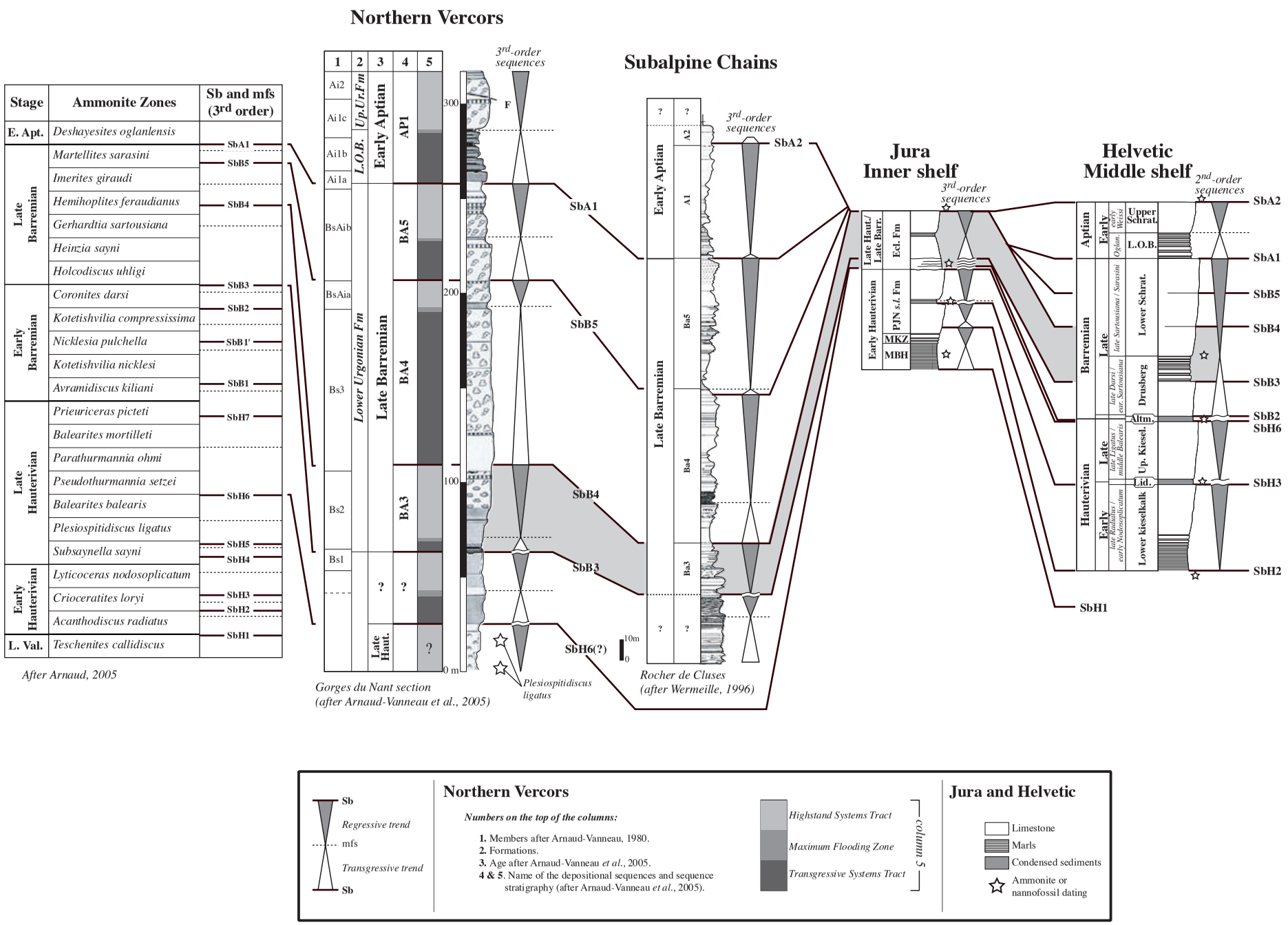
Northern Vercors
Subalpine Chains
Jura
Inner shelf
Helvetic
Middle shelf
3rd-order sequences
2nd-order sequences
Stage
Ammonite Zones
Sb and mfs (3rd order)
E. Apt.
Late Barremian
Early Barremian
Late Hauterivian
Early Hauterivian
L. Val.
Deshayesites oglanlensis
Martellites sarasini
Imerites giraudi
Hemihoplites feraudianus
Gerhardtia sartousiana
Heinzia sayni
Holcodiscus uhligi
Coronites darsi
Kotetishvilia compressissima
Nicklesia pulchella
Kotetishvilia nicklesi
Avramidiscus kiliani
Prieuriceras picteti
Balearites mortilleti
Parathurmannia ohmi
Pseudothurmannia setzei
Balearites balearis
Plesiospitidiscus ligatus
Subsaynella sayni
Lyticoceras nodosoplicatum
Crioceratites loryi
Acanthodiscus radiatus
Teschenites callidiscus
SbA1
SbB5
SbB4
SbB3
SbB2
SbB1'
SbB1
SbH7
SbH6
SbH5
SbH4
SbH3
SbH2
SbH1
After Arnaud, 2005
Ai2
Ai1c
Ai1b
Ai1a
BsAib
BsAia
Bs3
Bs2
Bs1
Up.Ur.Fm
L.O.B.
Lower Urgonian Fm
Early Aptian
Late Barremian
Late Haut.
AP1
BA5
BA4
BA3
300
200
100
0 m
F
Gorges du Nant section
(after Arnaud-Vanneau et al., 2005)
Plesiospitidiscus ligatus
Early Aptian
Late Barremian
A2
A1
Ba5
Ba4
Ba3
10m
0
Rocher de Cluses
(after Wermeille, 1996)
Late Haut./ Late Barr.
Early Hauterivian
Ecl. Fm
PJN s.l. Fm
MKZ
MBH
Aptian
Barremian
Hauterivian
Early
Late
Upper Schrat.
L.O.B.
Lower Schrat.
Drusberg
Altm.
Up. Kiesel.
Lid.
Lower kieselkalk
Oglan. / early Weissi
late Sartousiana / Sarasini
late Darsi / exc. Sartousiana
late Ligatus / middle Balearis
late Radiatus / early Nodosoplicatum
SbA2
SbA1
SbB5
SbB4
SbB3
SbB2
SbH6
SbH3
SbH2
SbH1
Sb
Regressive trend
mfs
Transgressive trend
Sb
Northern Vercors
Numbers on the top of the columns:
1. Members after Arnaud-Vanneau, 1980.
2. Formations.
3. Age after Arnaud-Vanneau et al., 2005.
4 & 5. Name of the depositional sequences and sequence stratigraphy (after Arnaud-Vanneau et al., 2005).
Highstand Systems Tract
Maximum Flooding Zone
Transgressive Systems Tract
column 5
Jura and Helvetic
Limestone
Marls
Condensed sediments
Ammonite or nannofossil dating

E., Föllmi, K. B., Godet, A., Raddadi, M. C. and Vermeulen, J., (*Eds*). The Hauterivian-Lower Aptian sequence stratigraphy from Jura Platform to Vocontian Basin: A multidisciplinary approach. Géologie Alpine, **Série Spéciale "Colloques et Excursions" N°7**: 5-28.

Arnaud Vanneau, A., Arnaud, H., carrio-Schaffauser, E. and Raddadi, M. C. (2005). "Urgonian deposits and Barremian-early Aptian sequence stratigraphy in the Vercors massif". *In:* Adatte, T., Arnaud-Vanneau, A., Arnaud, H., Blanc-Aletru, M.-C., Bodin, S., Carrio-Schaffhauser, E., Föllmi, K. B., Godet, A., Raddadi, M. C. and Vermeulen, J., (*Eds*). The Hauterivian-Lower Aptian sequence stratigraphy from Jura Platform to Vocontian Basin: A multidisciplinary approach. Géologie Alpine, **Série Spéciale "Colloques et Excursions" N°7**: 97-126.

Arnaud-Vanneau, A. (1980). "Micropaléontologie, paléoécologie et sédimentologie d'une plate-forme carbonatée de la marge passive de la Téthys: l'Urgonien du Vercors septentrional et de la Chartreuse (Alpes occidentales)." Géologie Alpine **Grenoble Mém HS 10**: 874 p.

Arnaud-Vanneau, A. and Arnaud, H. (1990). "Hauterivian to Lower Aptian carbonate shelf sedimentation and sequence stratigraphy in the Jura and northern Subalpine chains (southeastern France and Swiss Jura)". *In:* Tucker, M. E., Wilson, J. L., Crevello, P. D., Sarg, J. R. and Read, J. F., (*Eds*). Carbonate Platforms: Facies, Sequences and Evolution. Blackwell Scientific Publications, Special Publication of the International Association of Sedimentologists, **9**: 203-233.

Baumberger, E. (1901). "Uber Facies und Transgressionen der untern Kreid am Nordrande mediterrano - helvetischen Bucht im westlichen Jura." Wiss. Beil. Ber. Töchterschule Basel: 1-44.

Blanc-Aletru, M. C. (1995). "Importance des discontinuités dans l'enregistrement sédimentaire de l'Urgonien jurassien. Micropaléontologie, Sédimentologie, Minéralogie et Stratigraphie Séquentielle." *Ph.D thesis thesis*, Laboratoire de Géologie de l'Université I de Grenoble, 299 pp.

Bodin, S., Godet, A., Vermeulen, J., Linder, P. and Föllmi, K. B. (2006a). "Biostratigraphy, sedimentology and sequence stratigraphy of the latest Hauterivian - early Barremian drowning episode of the Northern Tethyan margin (Altmann Member, Helvetic Nappes, Switzerland)." Eclogae Geologicae Helveticae, in press.

Bodin, S., Vermeulen, J., Godet, A. and Föllmi, K. B. (2006b). "New data on the age of the installation of Urgonian-type carbonates along the northern Tethyan margin: biostratigraphy of the Chopf Member (Helvetic Alps, eastern Switzerland)." Comptes Rendus Géosciences **338**: 727-733.

Busnardo, R. and Thieuloy, J.-P. (1989). "Les ammonites de l'Hauterivien jurassien: révision des faunes de la région du stratotype historique de l'étage Hauterivien." Mémoires de la Société neuchâteloise des Sciences naturelles **XI**: 101-147.

Charollais, J., Clavel, B., Schroeder, R., Busnardo, R., Decrouez, D. and Cherchi, A. (2003). "La migration de la plate-forme urgonienne entre le Jura plissé et les Chaines subalpines septentrionales (France, Suisse): Evolution of the Urgonian platform between the Jura and the Septentrional Subalpine Chains (France, Switzerland)." Geobios **36** (*6 SU* -): 665-674.

Clavel, B. and Charollais, J. (1989). "Corrélation des formations hauteriviennes du Jura méridional au Jura neuchâtelois." Mémoires de la Société neuchâteloise des Sciences naturelles **XI**: 299-305.

Clavel, B., Charollais, J., Schroeder, R. and Busnardo, R. (1995). "Réflexions sur la biostratigraphie du Crétacé inférieur et sur sa complémentarité avec l'analyse séquentielle: exemple de l'Urgonien jurassien et subalpin." Bull. Soc. géol. France **166** (*6*): 663-680.

Conrad, M. A. and Masse, J. P. (1989). "Corrélations des séries carbonatées de l'Hauterivien et du Barrémien pro-parte dans le nord-ouest vaudois (Suisse)." Mémoires de la Société neuchâteloise des Sciences naturelles **XI**: 307-322.

Coquand, H. (1862). "Sur la convenance d'établir dans le groupe inférieur de la formation crétacée un nouvel étage entre le néocomien proprement dit (couche à Toxaster complanatus et à Ostrea Couloni) et le néocomien supérieur (étage urgonin d'Alc. d'Orbigny)." Bulletin de la Société Géologique de France (2) **19**: 531-541.

D'Orbigny, A. (1847). "Paléontologie française.

Terrains crétacés IV. Brachiopodes", Paris, 269 pp pp.

de Montmollin, A. (1835). "Mémoire sur le terrain Crétacé du Jura." Mémoires de la Société des Sciences Naturelles de Neuchâtel **tome I**: 49-65.

Funk, H., Föllmi, K. B. and Mohr, H. (1993). "Evolution of the Tithonian-Aptian carbonate platform along the northern Tethyan margin, eastern Helvetic Alps." *In:* Simo, J. A. T., Scott, R. W. and Masse, J. P., (*Eds*). Cretaceous carbonates platforms. Tulsa, OK, United States., **AAPG (American Association of Petroleum Geologists) Memoir 56**: 387-407.

Föllmi, K. B., Godet, A., Bodin, S. and Linder, P. "Interactions between environmental change and shallow-water carbonate build-up along the northern Tethyan margin and their impact on the early Cretaceous carbon-isotope record." Paleoceanography **in press**.

Föllmi, K. B., Weissert, H., Bisping, M. and Funk, H. (1994). "Phosphogenesis, carbon-isotope stratigraphy, and carbonate-platform evolution along the Lower Cretaceous northern Tethyan margin." Geological Society of America Bulletin **106** (*II*): 729-746.

Godet, A., Blanc-Aletru, M.-C., Bodin, S., Adatte, T. and Föllmi, K. B. (2005). "The Hauterivian-Barremian of the Western Swiss Jura around Neuchâtel". *In:* Adatte, T., Arnaud-Vanneau, A., Arnaud, H., Blanc-Aletru, M.-C., Bodin, S., Carrio-Schaffhauser, E., Föllmi, K. B., Godet, A., Raddadi, M. C. and Vermeulen, J., (*Eds*). The Hauterivian-Lower Aptian sequence stratigraphy from Jura Platform to Vocontian Basin: A multidisciplinary approach. Géologie Alpine, **Série Spéciale "Colloques et Excursions" n°7**: 79-96.

Guillaume, H. (1956). "Une nouvelle espèce crétacée du genre *Dictyoconus* Blanckenhorn." Eclogae geol. Helv. **49** (*1*): 141-147.

Jaccard, A. (1861). "Sur quelques points de la géologie du Jura." Actes Soc. helv. Sci. nat. **74**.

Masse, J. P., Gourrat, C., Orbette, D. and Schmuck, D. (1998). "Hauterivian Rudist faunas of southern Jura (France)." Geobios **M.S. n°22**: 225-233.

Mouty, M. (1966). "Le Néocomien dans le Jura méridional." *Ph.D. thesis thesis*, Université de Genève, Laboratoire de Géologie, 256 pp.

Remane, J. (1989). "The historical type Hauterivian of the Jura mountains: original definition, actual concept, lithostratographic subdivision." Mémoires de la Société neuchâteloise des Sciences naturelles **XI**: 9-18.

Renevier, E. (1853). "Note sur le terrain néocomien qui borde le pied du Jura, de Neuchâtel à la Sarraz." Bulletin de la Société Vaudoise des Sciences Naturelles **Bulletin n°31, tome III**: 261-277.

Renevier, E. (1874). "Tableau des terrains sédimentaires formés pendant les époques de la phase organique du globe terrestre avec leurs représentants en Suisse et dans les régions classiques, leurs synonymes et les principaux fossiles de chaque étage." Bull. Soc. vaud. Sci. nat. **13**: 218-252.

Renz, O. and Jung, P. (1978). "Aptian to Maastrichtian in the SwissJura Mountains." Eclogae Geologicae Helvetiae **71** (*1*): 1-18.

Schroeder, R., clavel, B. and Charollais, J. (1990). "*Praedictyorbitolina carthusiana* n. gen. n. sp., Orbitolinidé (Foraminiferida) de la limite Hauterivien-Barrémien des Alpes occidentales." Paläontologische Zeitschrift **64** (*3/4*): 193-202.

Thurmann, J. (1835). "Résumé des travaux de la Société des Monts-Jura." Bulletin de la Société Géologique de France **7**: 207-211.

Trümpy, R. (1980). "Geology of Swizerland: A guide-book. Part A: An Outline of the Geology of Switzerland", Wepf & Co. Publishers, Basel - New York, 334 pp.

Wermeille, S. (1996). "Etude sédimentologique, minéralogique et micropaléontologique des calcaires urgoniens de la région subalpine (Savoie, France). Coupes du Rocher de Cluses, du Borne et d'Andey." *Unpublished diploma thesis*, University of Neuchâtel, 129 pp.

Zweidler, D. (1985). "Genèse des gisements d'asphalte des formations de la Pierre Jaune de Neuchâtel et des calcaires urgoniens du Jura (Jura neuchâtelois et nord vaudois, Suisse)." *Ph.D. thesis*, Université de Neuchâtel, 108 pp.

CHAPTER D.

FROM THE PLATFORM TO THE BASIN: ENVIRONMENTAL CONSTRAINTS ON THE RISE OF THE URGONIAN PLATFORM

Jean Vermeulen working on the Barremian stratotype (Angles section, France)

Forewords

The Late Hauterivian – earliest Aptian period was marked by a series of episodes of important paleoceanographic and paleoenvironmental change, such as the occurrence of an oceanic anoxic event recorded in (hemi-)pelagic environments (Faraoni level in Italy, France, Switzerland…), and a coeval platform drowning event in shallow-water settings (Altmann Member in the Helvetic Alps). Even if a link between these two kinds of phenomena and their respective depositional settings was already suggested in several papers, we are now able to integrate the Western Swiss Jura within such an interconnected scheme, and explain how this shallow-water carbonate platform may have interacted with the unfolding of more global mechanisms.

In the following chapter, the results of our multi-proxy analyses of several hemi- to pelagic sections are presented. These section are located in the Umbria-Mache Basin of Italy (Fiume-Bosso and Gorgo a Cerbara sections), the Ultrahelvetic Realm of Switzerland (Veveyse de Châtel Saint Denis section), and in the Vocontian Trough of the southeastern France (Angles and Combe-Lambert sections).

First, we characterized the anoxic nature of the Faraoni event by means of redox-sensitive trace-elements behaviour (part D.1). We subsequently checked for the expression of this potential anoxic event within the stable isotope record, and estimated the impact of the evolution of the Northern Tethyan margin carbonate platform on the $\delta^{13}C$ record (part D.2). Using temporal fluctuations in phosphorus mass accumulation coupled with the above-mentioned tools, we proposed a model for the development of the Faraoni anoxic event (part D.3). In order to reconstruct the importance of climate change in triggering the Faraoni anoxia, we studied the evolution of clay minerals along a transect perpendicular to the northern Tethyan margin, and explored the impact the morphology of the carbonate platform may have had on the deposition of clay particles (part D.4). Finally, we checked if the evolution of the carbonate platform which developed on the northern Tethyan margin account for fluctuations within the $\delta^{13}C$ record during the entire Early Cretaceous (part D.5).

D.1.
Enrichment of redox-sensitive trace metals (U, V, Mo, As) associated with the late Hauterivian Faraoni oceanic anoxic event

Stéphane Bodin[1], Alexis Godet[1], Virginie Matera[1], Philipp Steinmann[1], Jean Vermeulen[2], Silvia Gardin[3], Thierry Adatte[1], Rodolfo Coccioni[4], Karl B. Föllmi[1]

[1]Institut de Géologie, Université de Neuchâtel, Rue Emile Argand 11, CP 158, 2009 Neuchâtel, Switzerland; [2]Grand Rue, 04330 Barrême, France; [3]CNRS-UMR 5143 "Paléodiversité et Paléolenvironnement", case 104, Université Paris 6, 4 Place Jussieu, 75252 Paris Cedex 05, France; [4]Istituto di Geologia e Centro di Geobiologia dell'Università, Campus Scientifico, Località Crocicchia, 61029 Urbino, Italy

Published in International Journal of Earth Sciences (Geologisches Rundschau).

Abstract

The Faraoni Level is a short-lived oxygen-deficient event that took place during the latest Hauterivian. In order to improve our understanding of the palaeoenvironmental conditions that occurred during this event, we have analysed the contents of several redox-sensitive trace elements(U, V, Mo, As, Co, Cd, Cu, Zn, Ni, Pb, Cr) from bulk limestone samples of late Hauterivian – early Barremian age from three reference sections. U, V, Mo and As show consistent and significant enrichments during the Faraoni event whereas the other redox-sensitive trace elements analysed here are not systematically enriched. In order to explain this discrepant behaviour, we propose that the Faraoni Level was deposited during a period of anoxic conditions near the sediment-water interface. The distinctive peaks in U, V, Mo and As contents are traceable throughout the three studied sections and represent a good correlation tool which helps to identify the Faraoni Level and its equivalents in the western Tethyan realm and outside of the Tethys. For example, a peak in U contents in upper Hauterivian sediments of the northwestern Pacific realm (ODP leg 185, site 1149) may well be an expression of the Faraoni event in this particular basin.

Keywords

Hauterivian, Barremian, Chemostratigraphy, Western Tethys, Trace metals.

D.1.1. Introduction

Since the first description by Cecca *et al*. (1994) of an organic-rich guide level – the so-called Faraoni Level – in upper Hauterivian (late *Spathicrioceras angulicostatum* ammonite zone) pelagic carbonates of the Umbria-Marche Basin (Italy), it has been shown that correlatable organic-rich levels occur throughout the western Tethyan realm. Equivalents of the Faraoni Level have been identified on the Trento Plateau in Italy (Cecca *et al*. 1996; Coccioni *et al*. 1998), in the Vocontian Trough in France (Baudin *et al*. 1999), and in the Swiss Préalpes (Busnardo *et al*. 2003).

It is for this reason that Baudin *et al*. (2002) associated this level with a short-lived oxygen-deficient event in the western Tethyan realm. And following Baudin (2005), the Faraoni Level and its equivalent can be qualified as an anoxic event (compare this reference for a detailed biostratigraphic definition of this event). With the Valanginian event (Erba *et al*. 2004), the Faraoni event is one of the first palaeoceanographic events which led to major change in the carbon cycle during the early Cretaceous.

The environmental circumstances leading to this short-lived oxygen-deficient event in the late Hauterivian are still not clear. In contrast to the anoxic events in the Valanginian, the early Aptian, and near the Cenomanian/Turonian boundary (*e.g*. Schlanger and Jenkyns 1976; Schlanger *et al*. 1987; Lini *et al*. 1992; Jones and Jenkyns 2001; Sanfourche and Baudin 2001), the Faraoni Level is not accompanied by a major carbon isotope excursion towards more positive values, but rather by a small long-term increase culminating around the Faraoni event (Föllmi *et al*. 1994; Erba *et al*. 1999; van de Schootbrugge *et al*. 2000; Company *et al*. 2005; Godet *et al*. 2006). Furthermore, no major volcanic episode has, of yet, been identified for the late Hauterivian. This means that the classical model postulated for the origin of oceanic anoxic events in general, *i.e*. increased volcanism leading to an increase in atmospheric CO_2, climate warming, increased weathering and nutrient availability, higher productivity and consequently higher preservation rates of organic matter (*e.g*. Jenkyns 1999; Jenkyns 2003) can not be applied in this case.

The Faraoni event corresponds in time to the onset of drowning episode D3 during the evolution of a carbonate platform system located along the northern Tethyan margin (Föllmi *et al*. 1994). But, in contrast to the Valanginian and the Aptian – Albian drowning episodes (D1, D4 and D5), the drowning episode D3 - not being mirrored by a distinct positive excursion in carbon isotopes, is also in need of an alternative explanation (van de Schootbrugge *et al*. 2000, 2003). It is therefore important to identify the palaeoenvironmental conditions leading to the Faraoni event, whilst also respecting the coeval drowning event on the northern Tethyan carbonate platform, which may have been linked to this anoxic event.

We investigated three (hemi-) pelagic key sections representing a north-south transect through the western Tethys and including micritic carbonates and marls of the Hauterivian—Barremian transition with regards to their redox-sensitive trace-element concentrations. The studied trace elements are uranium (U), vanadium (V), molybdenum (Mo), arsenic (As), cobalt (Co), cadmium (Cd), cupper (Cu), zinc (Zn), nickel (Ni), lead (Pb) and chromium (Cr). Their behaviour around the Faraoni Level is quite distinct and helps us to improve our understanding of redox conditions and changes therein in this basin during the Faraoni event.

In this paper, the term "Faraoni Level" and "Faraoni Level equivalent" refers to the interval composed of organic-rich sediments and the intervening carbonate beds that are associated with the Faraoni oceanic anoxic event. The term "Faraoni Level" is used when the lithological characteristics are the same as in the type area (*e.g*., Cecca *et al*., 1994), whereas the term "Faraoni Level equivalent" is used when the lithology is different from that of the type area (*i.e*., lacking a distinct enrichment in organic matter). The redox classification of sedimentary environments used here is adapted from Algeo and Maynard (2004) and references therein. Thus, oxic, suboxic and anoxic environments are characterized by >2.0, 2.0-0.2, and <0.2 ml O_2 l^{-1} H_2O respectively. Anoxia and euxinia are distinguished by the absence or presence of free H_2S in the water column respectively.

D.1.2. Studied sections and palaeogeographic setting

The studied sections were chosen according to the following criteria: (1) presence of the Faraoni Level or its equivalent; (2) good age control based on biostratigraphy (ammonites, nannofossils); (3) presence of pelagic carbonates and (4); representative of different areas of the western Tethys (Fig. D.1).

The first studied section is the Fiume-Bosso section, located between Urbino and Gubbio, near Cagli (central Italy; see also Cecca *et al*. 1994).

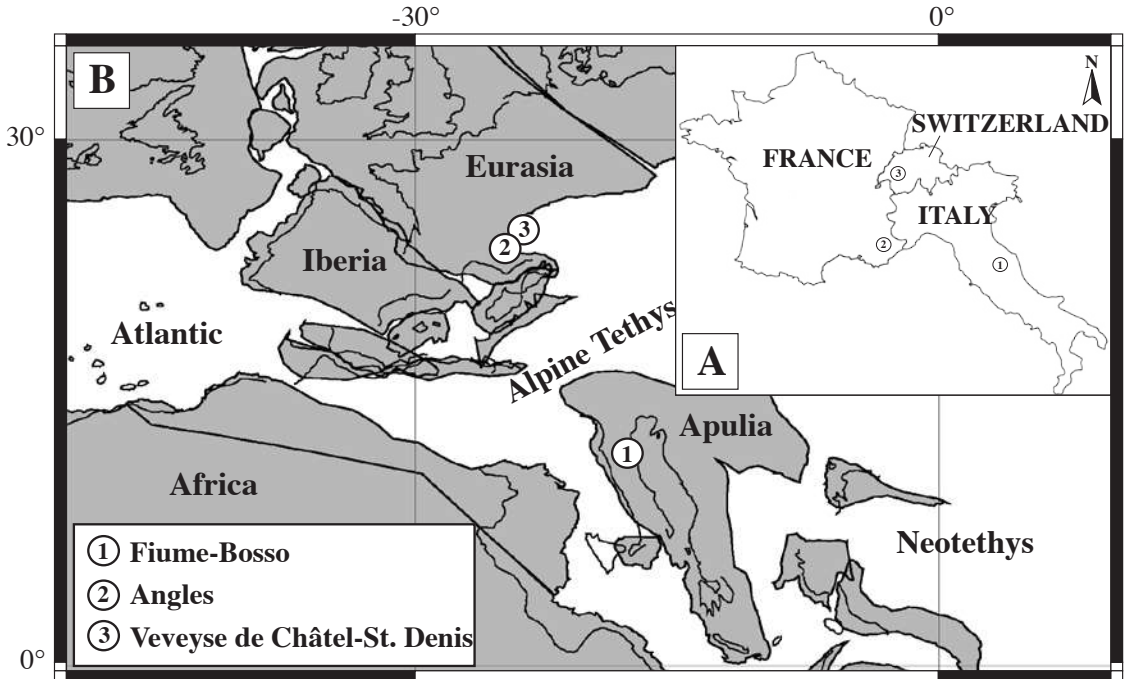

Fig. D.1: A. Actual location of the three studied sections. B. Paleogeographic position of the three studied sections at the Hauterivian – Barremian boundary. Palaeomap modified from Hay et al. (1999). Modified from Bodin et al. (2006).

This section represents the type section for the Faraoni Level (Cecca *et al.* 1994). The lithology consists of pelagic limestone and chert, which locally includes thin organic-rich marl layers and laminae, characteristic of the Maiolica Formation. The Faraoni Level is composed by a succession of three laminated black-shale layers and intervening calcareous beds.

The Veveyse de Châtel-St. Denis (VCD) is the second studied section. It is situated in the canton of Fribourg, along the Veveyse river, in western Switzerland (see Busnardo *et al.* (2003) for a detailed geographic description). Its lithology consists of a succession of alternating pelagic marls and marly limestones, which are rich in macrofossils. The equivalent of the Faraoni Level (identified by ammonite dating) is represented by the "couches à poissons" (an alternation of more or less organic-rich shale and marly limestone, rich in fish fossils) (Busnardo *et al.* 2003).

The third studied section is along the «route d'Angles», near Barrême in southeastern France, and is situated in the Vocontian Trough (see Busnardo 1965, for a detailed geographic description). Its lithology consists of a fossiliferous, hemi-pelagic succession of regularly alternating marlstone and limestone. Ammonite dating indicates that the Faraoni Level equivalent is situated around the bed AN 53. Black shale has not been distinguished within this interval, which is characterized by an alternation of limestone and laminated shale. In the sedimentary interval attributed to the *P. mortilleti* zone, no marls were sampled due to poor outcrop quality.

During the late Hauterivian, the Angles and the VCD sections were situated along the northern Tethyan margin. The VCD section is part of the Ultrahelvetic realm, which is considered as the deeper offshore prolongation of the Vocontian Trough to the northeast (Trümpy 1960). The Fiume-Bosso section, which is the deepest section, was situated in the southern part of the Tethys, in the Umbria-Marche Basin, remote from any continent.

D.1.3. Methods

ICP-MS analyses were performed on bulk rock samples from limestone and marlstone for all three sections. The limestone samples were sawed in order to eliminate altered parts and rock veins. Then, powders were obtained for both limestone and marls using a mechanic agate crusher. A

portion of approximately 250 mg was transferred into a digestion vessel (PTFE) and 10 ml of concentrated nitric acid (suprapur, Merck) were added. The sample was digested in a microwave oven (MSL-Ethos plus, Milestone) using the heating program recommended by the EPA 3051 method. After cooling, the resulting solution was filtered (0.45 μm) and diluted to 100 ml with ultrapure water. For the limestone, dissolution percentages determined after filtration were about 91% of initial sample weight in the Angles section, 83% in the VCD section, and 98% in the Fiume-Bosso section. Moreover, no correlation was observed between the concentration of the different analysed samples and the dissolution percentage obtained during digestion procedure (*e.g.*, U in Fig. D.2). This shows that the studied elements are present in the soluble authigenic phase and are not due to partial leaching of the detrital insoluble fraction.

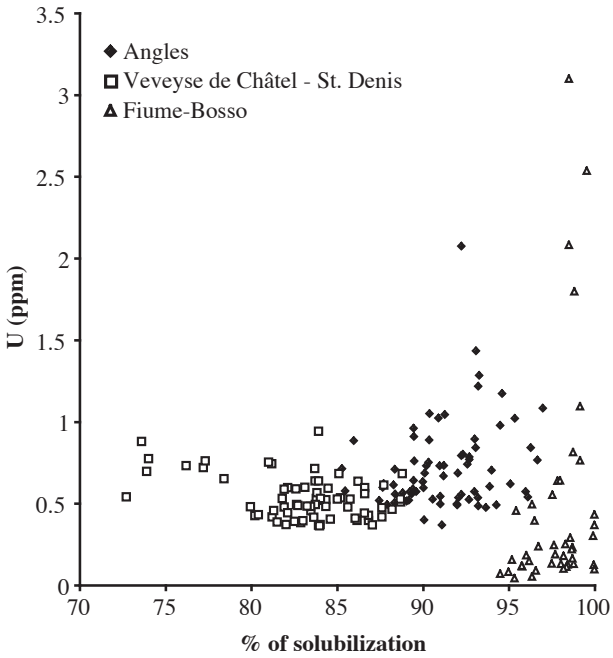

Fig. D.2: U (ppm) versus percentage of dissolution in the three studied sections. No correlation is observed. See text for discussion.

In the marls, the dissolution percentages were close to 50%. Mineralogical analyses indicate that clay and quartz grains constitute the insoluble part of the rock. No trace of carbonate is found, allowing us to postulate that the entire authigenic portion of the rock is dissolved with this method.

A second dilution (1/20) was then performed prior to analysis. To correct for matrix-induced ion signal variation and instrumental drift, rhodium was used as the internal standard. The element concentrations of the acid digests were determined by ICP-MS (ELAN 6100, Perkin Elmer) using a semi-quantitative mode (Totalquant). Totalquant (TQ) is a simple, rapid and accurate panoramic method based on full mass-spectra scan methods and was successfully applied to the analysis of various biological and environmental samples (Jitaru *et al.* 2003) like, for instance, in sediments (Bayon *et al.* 1998). TQ enables spectral interpretation of a full mass spectrum by comparison with an internal response table which includes assignment of element intensities based on internal response factors and an interpretation of interferences based on implemented algorithms for numerical calculation of interference corrections. The response table is usually updated before analysis by determination of a blank and one standard solution. Two Certified Reference Materials (CRM) (NIST-1640 natural water, LKSD-1 lake sediment from Canadian Centre for Mineral and Energy Technology – CANMET – Canada) were measured to evaluate the accuracy which is achieved in panoramic analysis with the Elan 6100. Here we present the results obtained for the four principal trace elements discussed in this study (V, Mo, As, and U). The mean recovery rates were determined for V, Mo, and As (no certified concentration values for U are available for the two CRM) and were, for the NIST-1640 CRM (N=11) 101% for V; 99% for Mo, and 101% for As, and Relative Standard Deviation (RSD) was better than ± 9% for V; ± 6% for Mo and ± 7% for As; for the LKSD-1 CRM (N=12 digestions) mean recovery rates were 90% for V; 89% for Mo, and 110% for As (for this CRM, recovery rates are based on certified concentration values obtained by partial extraction using concentrated HNO_3 and HCl whereas we used concentrated HNO_3 digestion); analytical precision (RSD) was about ± 8% for V; ± 9% for Mo, and ± 12% for As.

Furthermore, multiple digestions (N=10) of a sample corresponding to the Faraoni Level of the Angles section (bed AN 53-2) were analyzed. The RSD of these analyses were about ± 15% for V; ± 12% for Mo; ± 12% for As and ± 3% for U. A detection limit lower than 1 μg/kg was observed for the four trace elements studied.

Fiume-Bosso		Sample	U	V	Mo	As	Co	Cd	Cu	Zn	Ni	Pb	Cr
late Hauterivian	no ammonite zonation	FB 59	0.15	0.81		0.39	2.61	0.06	2.61	8.96	13.30	0.90	1.81
		FB 65	0.05	0.58		0.25	1.51	0.14	3.69	7.21	12.31	1.27	2.13
		FB 71	0.09	0.64		0.23	3.02	0.12	5.20	7.43	12.24	1.48	2.38
		FB 79		0.63		0.16	0.99	0.09	2.26	6.01	12.10	1.02	2.09
		FB 89	0.07	0.71		0.08	1.43	0.14	5.06	9.05	13.76	0.89	2.18
		FB 94	0.11	0.79		0.09	1.87	0.26	3.11	10.22	13.58	1.23	2.36
		FB 99	0.08	0.80		0.17	2.06	0.35	4.22	19.28	14.69	5.07	3.19
		FB 104	0.18	1.25	0.03	0.31	2.26	0.10	6.74	20.41	16.34	2.00	1.85
		FB 109	0.64	1.10	0.01	0.16	1.70	0.07	3.91	4.64	15.09	6.63	1.62
		FB 115	0.12	0.91		0.33	1.92	0.14	3.48	8.91	15.30		1.83
		FB 123	0.15	0.93	0.10	0.12	2.28	0.21	5.24	31.52	15.04		1.70
	angulicos.	FB 128a	0.19	0.91	0.03	0.22	1.64	0.28	2.92	17.02	13.45	2.87	3.10
		FB 134a	0.24	1.08	0.16	0.51	2.07	0.08	5.70	17.88	15.64	1.53	1.77
		FB 136	0.23	0.73	0.03	0.46	1.48	0.10	4.78	24.86	13.74	0.91	1.95
		FB 139	0.39	1.08		0.21	1.23	0.16	2.56	5.23	11.14	1.80	2.01
	catulloi	FB 371	0.55	2.04	0.09	0.18	1.08	0.09	2.64	8.95	10.37		1.99
		FB 373a	0.49	4.60	0.42	0.50	1.36	0.37	1.56	22.37	12.40		1.62
		FB 373d	0.76	5.21	0.55	0.29	0.96	0.27	1.68	9.14	11.67		1.97
		FB 375	2.53	11.61	0.31	0.42	0.94	0.19	1.84	16.43	10.12		2.44
		FB 378	3.10	10.36	0.32	0.23	0.92	0.29	3.27	7.42	11.36		2.16
		FB 380a	1.09	7.74	0.29	0.31	0.89	0.04		13.40	13.22		2.18
		FB 380b	1.80	7.35	0.40	0.27	0.79	0.18		28.41	10.03		1.97
		FB 382a	2.08	6.96	0.15	0.32	1.01	0.09	1.36	7.07	11.37		2.29
		FB 382c	0.81	2.78	0.20	3.73	2.25	0.14		26.70	11.24		1.70
		FB 385	0.64	3.01	0.14	3.37	1.49	0.09	2.16	8.69	11.87		1.84
		FB 387b	0.37	2.08	0.14	0.39	1.79	0.17	3.54	9.88	11.96		3.19
		FB 391	0.24	0.84	0.03	0.29	2.35	0.26	3.01	8.32	11.93		1.79
		FB 396b	0.43	0.82	0.08	0.44	2.02	0.08	1.92	7.97	11.82		1.49
		FB 402b	0.12	0.63	0.12	0.20	1.37	0.14	2.12	20.70	12.44		
		FB 410	0.22	1.13	0.16	0.43	2.33	0.13	2.65	10.22	15.59	0.98	
early Barremian	no ammonite zonation	FB 417	0.13	0.89		0.24	1.05	0.11	1.48	5.95	12.97		
		FB 424	0.09	0.65	0.05	0.19	1.37	0.16	2.65	5.80	12.72		
		FB 430a	0.30	0.89		0.26	1.51	0.25	2.32	9.71	13.31	0.83	
		FB 433	0.11	1.00	0.01	0.22	0.97	0.12	1.88	6.88	11.71		
		FB 440a	0.13	1.73	0.02	0.28	1.93	0.18	3.58	12.15	15.39	1.03	1.60
		FB 448b	0.18	0.86	0.01	0.12	1.11	0.11	2.01	6.24	12.77		
		FB 451a	0.25	0.89	0.04	0.35	1.35	0.10	2.26	5.09	12.06		
		FB 454b	0.13	0.85	0.03	0.12		0.13	2.14	7.02	12.78		
		FB 459b	0.11	0.68		0.13	1.21	0.13	2.46	5.20	11.97		
		FB 464a	0.14	1.09	0.03	0.37	1.04	0.10	1.93	9.53	7.96		
		FB 469	0.16	0.93	0.04	0.32	1.25	0.10	2.72	6.54	12.49		
		FB 473b	0.29	0.85		0.21	1.14	0.06	1.85	5.73	13.86		
		FB 480a	0.13	0.85	0.10	0.24	1.27	0.10	2.88	17.81	12.31		1.96
		FB 487	0.10	0.85	0.04	0.29	1.86	0.23	3.18	3.34	17.36		
		FB 494b	0.23	1.08	0.04	0.24	1.22	0.09	1.71	41.15	16.10		
		FB 499a	0.45	1.82	0.17	1.76	1.45	0.11	2.84	66.11	15.79	2.32	1.42

VCD		Sample	U	V	Mo	As	Co	Cd	Cu	Zn	Ni	Pb	Cr
late Hauterivian	sayni	VCD 1A	0.64	8.74	0.27	1.38	2.28		7.55	26.45	11.68	2.22	7.73
		VCD 3A	0.52	6.28	0.02	0.45	2.08	0.02	7.44	23.04	16.91		6.58
		VCD 4A	0.59	4.92	0.25	0.56	1.79	0.03	8.04	14.88	18.34		4.97
		VCD 6A	0.43	5.02		0.25	1.99		7.26	19.28	17.01		5.01
		VCD 9A	0.42	4.36	0.10	0.13	1.37		6.41	12.55	14.31		5.11
		VCD 13A	0.72	6.27	0.33	0.46	1.91	0.01	7.98	15.41	17.41		6.14
		VCD 15A	0.54	6.17	0.08	0.64	2.06		7.40	12.24	16.34		4.59
		VCD 18A	0.77	6.40	0.19	0.46	1.29		7.08	15.07	14.44		4.85
		VCD 21A	0.76	5.82	0.34	0.66	1.76	0.03	9.08	17.76	16.73		6.02
		VCD 24A	0.48	5.79	0.41	0.70	1.64		6.70	13.81	16.87		5.56
		VCD 27A	0.65	8.14	0.21	1.24	1.92	0.04	6.92	19.41	13.19	4.67	5.97
		VCD 29A	0.43	6.98	0.15	0.91	2.12	0.08	9.10	31.52	14.93	2.84	5.92
	ligatus	SDII 1	0.48	6.60	0.29	1.21	2.16	0.07	7.63	20.81	14.79	3.49	5.12
		SDII 3	0.59	4.09	0.24	0.88	1.77	0.03	6.29	23.44	12.49	2.53	2.88
		SDII 5	0.52	5.17	0.07	0.82	1.51	0.05	5.43	21.42	20.02	4.22	4.50
		SDII 6	0.52	4.95	0.15	0.37	1.28	0.04	5.76	17.89	11.12	2.34	4.07
		SDII 7c	0.45	5.57	0.18	0.36	1.44	0.08	4.70	21.01	11.31	2.27	3.62
		SDII 10	0.53	6.33	0.19	0.85	1.93	0.03	8.60	23.37	15.30	5.20	4.51
		SDII 11	0.48	7.77	0.47	0.66	2.25	0.02	6.69	22.48	14.73		5.72
		SDII 13a	0.40	6.06	0.31	0.67	1.79	0.04	6.33	20.49	12.03	5.22	3.97
		SDII 14	0.51	4.33	0.15	0.55	1.76		6.25	15.62	12.48		2.43
		SDII 15	0.53	5.89		0.79	2.12		6.01	15.90	13.55		4.14
	balearis	SDII 16b	0.59	6.38		0.56	1.77		45.52	29.02	12.91		3.53
		SDII 18	0.54	5.26	0.26	0.67	1.93		5.45	17.30	12.72		4.04
		SDII 19	0.38	5.66	0.04	0.76	2.43	0.28	6.72	93.62	14.17	6.48	3.42
		SDII 21	0.68	4.92	0.14	0.47	1.64		4.05	17.02	12.65		4.36
		SDII 23	0.71	4.76		0.47	1.96		5.12	16.02	13.27		3.78
		SDII 25	0.57	5.54	0.02	0.62	1.37		9.60	14.59	11.24	1.87	3.76
		SDII 27	0.40	4.72		0.51	1.68		7.00	19.06	9.74	1.96	4.03
		SDII 28	0.53	5.32	0.06	1.53	3.94		10.82	31.10	19.45	4.59	4.16
		SDII 30	0.48	4.64		0.32	1.89		6.18	28.28	10.29	1.81	3.75
		SDII 33	0.74	7.73	0.12	0.95	2.79	0.07	11.08	37.47	16.66	3.37	8.04
		SDII 34	0.53	5.25		0.88	3.06		5.57	13.85	13.84	2.69	4.61
		SDII 36	0.53	4.46	0.01	1.28	2.60		5.38	27.48	13.70	3.48	2.30
		SDII 40	0.61	6.17		0.70	1.47		6.60	22.08	10.30	1.49	5.37
		VCDII 51A	0.42	4.33	0.10	0.61	2.40	0.09	6.76	22.40	10.58	2.24	4.39
	angulicostata	SDII 42	0.47	5.82		0.60	1.69		5.42	16.23	10.90	2.10	4.11
		VCDII 50A	0.64	4.96		0.47	1.35	0.03	6.25	13.85	9.02	1.34	3.57
		SDII 43	0.64	7.88	0.21	0.53	1.26	0.11	9.11	22.73	11.26	2.24	6.28
		VCDII 49A	0.60	6.28		1.01	3.11	0.14	7.24	38.48	13.49	1.64	4.93
		VCDII 48A	0.60	8.57		1.00	2.66	0.17	7.31	47.85	12.39	2.68	6.31
		VCDII 46A	0.75	5.33		0.45	1.71	0.03	7.64	24.44	10.43	1.25	3.61
		VCDII 44A	0.56	5.88		0.58	1.00		4.70	12.86	8.48		3.79
		VCDII 42A	0.53	5.15		0.54	1.86	0.05	5.89	13.90	8.57	0.89	4.19
		VCDII 40A	0.73	8.04	0.26	1.14	2.32	0.07	7.46	16.68	11.50	1.47	6.77
		SDII 51	0.49	6.52		0.44	0.99		7.19	19.08	10.36	1.47	5.11
		VCDII 37A	0.60	5.06		0.48	1.39		3.93	13.15	8.45	0.86	3.95
		VCDII 35A	0.39	4.82	0.01	0.44	1.32	0.02	4.59	13.49	7.57	1.16	3.06
		VCDII 33A	0.40	4.83		0.57	1.77		5.47	14.92	8.82	1.51	3.25
		VCDII 30A	0.39	4.39		0.48	1.11		4.59	10.09	13.62	0.96	3.33
		VCDII 27A	0.37	5.02		0.68	1.85		3.90	22.87	9.85	0.89	2.66
		VCDII 25A	0.70	8.50	0.04	1.03	3.63		10.99	36.43	16.85	2.43	8.37
		VCDII 22A	0.88	6.95	0.01	1.20	2.84	0.12	9.23	47.93	14.57	3.26	4.65

Table D.1: Redox-sensitive trace elements analyses in limestones for the three studied sections (expressed in ppm). The dark grey band indicates the Faraoni Level or its equivalent. No value is indicated when below the limit of detection.

VCD		Sample	U	V	Mo	As	Co	Cd	Cu	Zn	Ni	Pb	Cr
late Hauterivian	angulicostata	VCDII 19A	0.59	7.16		1.15	2.34		7.02	21.65	14.25	2.73	5.43
		VCDII 16A	0.94	11.69	1.22	2.54	1.51		5.44	13.43	11.39	1.13	3.60
		VCDII12A	0.68	6.79	0.75	1.13	1.66	0.05	5.27	13.92	6.94	1.19	3.28
		VCDII10A	0.53	3.96		0.73	1.45	0.02	5.45	14.87	7.66	1.59	2.40
		VCDII8A	0.46	4.48		0.51	1.57	0.03	6.46	17.02	7.54	1.28	3.81
		SD 42	0.44	6.50		0.75	1.88	0.05	5.53	20.46	12.37	4.58	5.72
		VCDII6A	0.41	4.14		0.74	1.63		4.41	15.89	8.05	1.44	2.15
		SD 38	0.48	6.45	0.31	0.89	1.62	0.04	5.81	17.32	11.00	1.47	3.83
		SD 36	0.43	5.24		0.38	1.22	0.03	6.02	20.50	11.61		2.94
		SD 32	0.41	5.88		0.51	1.12	0.05	4.66	16.93	12.01	1.30	4.07
		SD 29	0.37	5.39	0.07	0.88	1.91		5.25	17.39	10.62	2.20	4.09
		SD 27	0.49	1.88			1.24	0.01	5.65	15.35	12.01	2.43	
		SD 24	0.50	1.79			2.02		5.72	18.61	11.17	1.30	
Barremian	hugii	SD 21	0.36	2.17			0.97		5.69	7.73	11.63	1.61	
		SD 19	0.44	2.69			1.25		5.97	11.26	11.74	1.92	
		SD 16	0.37	2.54			1.42		5.60	16.38	18.00	2.43	
		SD 12	0.49	2.67			1.22		7.72	12.33	11.73	1.44	
		SD 8	0.37	1.96			1.99		6.60	18.12	10.74	1.56	
		SD 5	0.42	4.14		0.05	2.36		5.82	14.32	12.02	1.84	
		SD 1	0.46	5.18		0.30	2.61		6.08	25.27	14.83	3.05	

Angles		Sample	U	V	Mo	As	Co	Cd	Cu	Zn	Ni	Pb	Cr
late Hauterivian	balearis	AN 2	0.57	7.78	0.60	0.82	1.04	0.02	5.54	16.12	13.14	1.52	6.69
		AN 4	0.50	4.88	0.26	0.65	1.36	0.02	4.47	17.42	12.63	2.00	3.87
		AN 6	0.60	5.04	0.20	0.77	1.49	0.03	4.68	21.93	13.41	2.35	3.68
		AN 8	0.71	5.03	0.33	0.44	1.01	0.06	5.91	35.59	12.25	1.25	4.79
		AN 10	0.88	4.87	0.14	0.77	1.79	0.02	5.79	15.46	13.57	1.54	4.44
		AN 13	0.64	3.64	0.11	0.29	0.97	0.01	3.72	13.18	11.18		3.29
		AN 15.1	0.57	2.62	0.19	0.39	1.23	0.03	3.58	11.36	11.29	1.05	2.75
		AN 16	0.52	2.75	0.14	0.36	1.28		3.64	7.65	11.24	1.28	2.33
		AN 18	0.55	3.89	0.40	0.45	1.32	0.05	4.88	30.37	11.16		3.70
		AN 20	0.49	3.43	0.45	0.25	0.80	0.04	3.11	17.93	8.95	0.91	3.41
		AN 23	0.91	4.13	0.16	0.41	1.36	0.07	6.66	17.79	12.45	1.48	3.61
		AN 26	0.76	2.92	0.18	0.30	0.83		4.32	14.90	9.81	0.98	3.79
		AN 27.2	0.62	4.64	0.25	0.66	1.15	0.11	6.85	26.72	11.30	1.91	4.43
		AN 29	0.55	2.70	0.44	0.73	1.11	0.03	3.35	13.45	10.79	1.55	2.63
		AN 31	0.67	3.04	0.17	0.61	1.17	0.02	4.61	20.26	11.28	1.24	3.18
		AN 33	0.47	2.71	0.11	0.40	1.06		3.42	6.85	10.55	1.16	3.11
		AN 35	1.02	4.02	0.13	0.50	1.05	0.09	5.49	16.32	11.66	1.62	2.99
	angulicostatum	AN 38	0.48	2.45	1.02	1.49	5.15	0.39	5.92	75.44	24.32	6.24	2.39
		AN 40	0.63	4.15	0.57	0.61	0.98	0.20	4.40	23.53	10.43	1.99	3.30
		AN 43	0.73	3.97	0.24	0.57	1.25	0.09	5.67	18.99	11.65	1.93	3.81
		AN 46	0.49	2.85	0.06	0.35	1.08	0.04	3.60	15.65	11.06	0.96	2.90
		AN 49.1	0.73	4.18	0.10	0.43	1.13	0.11	3.93	48.61	10.54	1.13	3.00
		AN 50	0.49	3.45	0.36	0.35	0.77	0.06	3.22	14.54	9.72	1.21	2.65
		AN 51	1.05	4.62	0.59	0.74	1.16	0.08	5.34	26.19	12.53	1.58	3.48
		AN 52	1.43	8.93	4.87	4.80	2.36	2.12	6.41	420.80	26.63	5.73	2.14
		AN 53.2	1.28	7.43	4.61	3.45	1.42	0.05	3.83	13.13	23.69	4.81	1.99
	mortilleti	AN 55	2.07	4.75	0.14	0.20	0.71	0.03	3.16	25.79	8.58	1.02	2.35
		AN 62.1	0.78	4.79	0.44	0.64	1.03		3.52	17.13	10.21	1.08	2.45
		AN 65.1	0.98	4.38	0.16	0.54	1.56		3.93	12.59	11.89	2.06	1.87
		AN 68	0.79	4.61	0.20	0.46	0.98	0.06	4.69	24.61	10.37	1.03	3.13
		AN 71	0.89	4.22	0.06	0.47	0.99		3.70	15.91	10.74	1.22	2.40
early Barremian	kiliani	AN 72	1.17	4.61		0.31	1.05	0.12	4.14	23.89	11.19	1.91	2.22
		AN 75	0.53	3.57	0.05	0.38	1.03	0.02	3.44	16.25	10.10	1.15	2.76
		AN 78	0.54	5.00	0.17	0.62	2.17	0.04	4.18	29.54	11.93	1.57	3.40
		AN 81	0.73	5.30	0.04	0.50	1.30	0.08	4.84	33.86	10.64	1.51	2.83
		AN 84	0.52	4.88	0.18	0.42	1.28	0.04	3.50	26.82	11.05	1.35	2.44
		AN 87	0.59	7.34	0.61	0.88	1.57	0.04	5.15	17.40	12.42	2.05	5.31
		AN 89	0.56	5.17	0.21	0.61	1.25	0.03	3.89	14.02	9.25	1.26	3.48
		AN 90	0.56	4.98	0.29	0.86	1.79		4.52	18.55	13.17	2.06	3.59
		AN 92	0.40	4.08	0.20	0.58	1.34	0.04	4.55	12.24	11.60	2.37	3.18
		AN 93	0.37	3.59	0.03	0.46	1.25	0.02	3.62	16.10	11.02	1.36	3.52
	nicklesi	AN 95	0.51	3.95	0.21	0.87	1.47	0.06	5.80	17.18	10.65	1.74	3.31
		AN 97	0.49	3.13	0.07	0.42	1.11	0.06	3.85	15.57	11.56	1.26	2.64
		AN 98	0.53	3.49	0.21	0.75	1.50	0.11	11.51	29.09	10.91	1.40	2.71
		AN 101	0.71	4.92	0.23	0.92	1.33	0.04	6.11	23.13	12.82	2.21	3.65
		AN 103	0.57	6.88	0.65	1.02	2.01	0.06	6.03	30.35	12.74	2.42	4.53
		AN 104	0.52	5.15	0.37	1.10	1.30	0.06	6.05	24.55	11.33	2.22	4.06
		AN 105	0.52	4.47	0.63	1.22	1.49	0.05	6.94	33.44	11.80	2.28	3.79
		AN 108	0.89	5.81	0.71	1.08	1.49	0.08	6.21	37.61	11.22	2.20	3.37
	pulchella	AN 109.4	0.49	4.14	0.69	1.14	1.72	0.02	5.75	29.79	11.49	2.08	3.04
		AN 110.1b	0.68	5.48	1.11	1.36	1.73	0.04	5.34	52.45	13.14	2.66	3.08
		AN 110.3c	0.62	3.99	0.33	0.67	1.38	0.08	4.04	47.02	10.42	0.91	2.64
		AN 110.4	1.04	5.03	0.47	1.07	1.09	0.07	5.29	21.30	11.21	1.77	2.88
		AN 111.2	0.80	5.36	0.12	0.87	0.88	0.05	4.58	20.12	8.83	1.50	2.58
		AN 111.5	1.22	7.64	0.72	1.12	1.20	0.09	5.10	65.66	10.84	1.86	3.26
		AN 112.2	0.74	6.66	0.17	0.55	1.33	0.07	4.41	23.15	10.43	1.24	2.52
	compressissima	AN 112.7	0.59	5.55	0.42	0.63	1.04	0.08	4.12	150.20	10.55	1.83	2.41
		AN 114.2	0.68	4.61	0.41	0.88	0.93	0.04	4.68	24.82	10.13	1.43	1.80
		AN 115	0.77	6.43	0.62	1.21	1.05	0.03	5.45	24.46	13.81	9.36	2.57
		AN 117	0.60	4.16	0.30	0.74	1.27	0.05	5.44	24.94	10.40	1.36	1.87
		AN 119	0.57	3.10	0.23	0.34	1.00	1.25	4.83	80.29	10.27		1.55
		AN 121	0.54	3.38	0.12	0.32	1.34	0.06	3.29	18.69	10.94	0.99	1.86
		AN 123	0.57	4.26	0.27	0.53	1.38	0.08	4.57	30.62	11.74	1.10	2.53
	darsi	AN 125	0.96	6.99	0.73	1.06	1.95	0.05	7.09	41.84	14.53	1.94	3.81
		AN 127	1.02	4.27	0.32	0.36	0.76	0.03	5.15	18.56	8.52		1.98
		AN 128	0.76	3.24	0.34	0.42	0.84	0.07	4.39	14.86	9.74		1.69
		AN 129	0.75	4.25	1.70	2.58	1.76	0.09	6.48	23.92	12.89	1.88	2.28
		AN 131	0.84	8.34	0.73	0.95	1.25	0.03	7.52	21.95	13.50	1.47	1.90
		AN 133	0.84	3.10	0.39	1.08	1.00	0.10	6.30	21.42	12.97	1.45	2.01
		AN 136.2	0.61	4.88	0.47	1.94	2.27	0.07	8.46	29.82	14.45	3.71	2.89
		AN 138	0.70	3.41	0.57	1.10	0.97	0.21	6.72	44.43	11.66	1.36	1.17
		AN 139d	1.08	3.54	0.16	0.63	0.94	0.17	4.86	26.74	11.87	1.95	3.74

Table D.1 (continued): Redox-sensitive trace elements analyses in limestones for the three studied sections (expressed in ppm). The dark grey band indicates the Faraoni Level or its equivalent. No value is indicated when below the limit of detection.

Fiume-Bosso		Sample	U	V	Mo	As	Co	Cd	Cu	Zn	Ni	Pb	Cr
late Hauterivian	angu.	FB 133	2.01	69.51	2.96	15.55	39.00	1.62	93.32	287.33	136.27	39.08	38.66
		Fb 138	3.97	27.74	1.00	19.77	41.14	1.20	139.33	235.05	99.30	26.68	33.83
		FB 372	9.47	84.72	1.90	14.29	58.25	3.38	214.15	528.47	223.99	50.01	53.08
	catulloi	FB 374	12.83	345.94	61.83	177.42	84.54	10.48	270.70	1068.19	533.54	49.22	66.55
		FB 377	6.29	68.15	15.97	8.13	9.42	4.32	23.68	220.95	99.15	4.49	8.79
		FB 379	15.40	306.71	19.28	28.51	67.00	4.23	273.71	701.05	428.86	33.57	71.43
		FB 381b	9.92	151.09	28.26	33.44	29.64	5.06	61.67	313.80	268.18	14.52	22.21
		FB 384	12.04	169.53	5.48	40.58	106.59	3.83	211.07	612.52	277.61	51.44	66.48
		FB 397	2.85	20.43	0.30	8.25	67.51	0.90	164.07	248.47	143.25	34.58	33.69

VCD		Sample	U	V	Mo	As	Co	Cd	Cu	Zn	Ni	Pb	Cr
late Hauterivian	angulicostata	VCDII 10b	1.38	12.59	0.45	1.89	4.14	0.13	14.62	50.26	19.43	2.25	12.93
		VCDII 11b	1.29	8.27	0.29	1.87	3.84	0.21	13.77	49.12	21.39	3.79	8.43
		VCDII 14b	0.82	5.47	0.57	1.95	3.00	0.05	10.19	20.06	19.01	1.90	7.22
		VCDII 17b	3.27	15.21	1.59	6.74	3.46	0.60	15.77	53.27	23.53	3.95	8.34
		VCDII 18b	1.26	11.67	0.12	2.37	4.93	0.05	16.14	51.92	27.56	4.30	13.63
		VCDII 20b	1.45	11.60		3.44	7.42	0.20	18.30	86.81	37.34	9.23	11.95
		VCDII 25b	1.08	8.15		1.85	5.13	0.43	19.39	112.65	28.29	4.37	9.33
		VCDII 26b	1.05	8.56		2.68	4.41	0.13	15.84	56.10	23.71	5.68	9.18
		VCDII 27b	1.31	11.47	0.21	1.94	4.38	0.07	20.00	49.23	28.48	3.75	13.25
		VCDII 28b	1.06	13.37	0.15	2.16	5.01	0.16	16.50	61.06	21.64	4.25	12.78
		VCDII 29b	0.91	7.75	0.06	1.47	3.00	0.13	14.43	36.53	20.36	3.41	7.89
		VCDII 30b	1.03	6.84	0.03	1.44	4.01	0.07	17.12	41.84	22.74	3.64	8.05
		VCDII 31b	1.17	6.99	0.19	2.09	5.13	0.06	15.28	36.51	26.18	5.04	8.26
		VCDII 32b	1.24	9.64	0.03	1.52	4.43	0.17	19.81	47.95	28.04	3.25	13.09
		VCDII 33b	1.50	11.92	0.17	2.30	4.63	0.10	24.18	65.32	34.76	6.90	13.59

Angles		Sample	U	V	Mo	As	Co	Cd	Cu	Zn	Ni	Pb	Cr
late Hauterivian	angulicostatum	AN37b	1.92	21.45	0.57	2.86	5.76	0.56	42.80	100.62	50.60	12.67	26.37
		AN38b	1.59	14.64	0.44	3.13	5.71	0.38	38.98	81.97	38.78	13.09	16.89
		AN39b	1.62	16.99	1.15	4.12	6.64	1.28	36.73	167.87	42.80	14.17	16.63
		AN40b	2.17	16.34	0.71	3.86	6.89	0.56	44.88	139.18	42.11	22.05	16.67
		AN41b	2.56	22.10	0.73	4.47	8.67	0.84	58.35	205.46	55.25	20.63	23.53
		AN42b	2.28	15.30	0.16	2.99	5.63	0.58	39.87	110.99	42.70	10.33	17.90
		AN43b	1.59	12.39	0.27	1.73	3.39	0.35	24.57	74.26	29.27	7.90	12.99
		AN44b	1.58	12.78	0.28	2.41	3.88	0.34	28.36	72.99	27.64	10.51	14.37
		AN45b	2.32	31.12	0.57	4.80	13.38	0.32	57.41	111.72	55.01	16.73	30.66
		AN46b	2.15	12.78	0.25	3.45	7.80	0.39	48.73	103.01	68.49	9.22	15.47
		AN48b	1.85	18.98	0.37	3.35	6.26	0.49	44.40	114.71	37.86	10.54	21.80
		AN51b	3.54	19.23	2.97	2.06	1.82	0.06	8.39	31.71	33.60	3.61	8.42
		AN52b	3.73	27.35	1.78	4.71	4.19	0.45	19.08	91.12	51.41	7.13	17.08
		AN53.1b	2.98	18.84	3.30	1.52	1.69	0.06	10.16	19.16	38.32	3.13	7.90
Barr.	kilian.	AN72b	1.59	10.45	0.37	3.20	3.72	0.22	25.72	136.80	24.11	7.30	8.84
		AN73b	1.61	10.84	0.31	2.94	6.00	0.50	22.91	138.40	32.25	7.44	10.76
		AN75b	1.48	13.92	0.19	3.39	5.66	0.29	26.22	128.48	33.94	8.73	14.48

Table D.2: Redox-sensitive trace-element analyses in marlstones for the three studied sections (expressed in ppm). The dark grey band indicates the Faraoni Level or its equivalent. No value is indicated for values below the limit of detection.

The content and the type of organic matter were determined using Rock-Eval pyrolysis (Rock-Eval 6; Behar *et al.* 2001). The parameter TOC (total organic carbon in weight %) was obtained using the standard temperature cycle. Two standards (an in-house standard and the «IFP 160000» standard from the Institut Français du Pétrole, Paris, France) were passed at the beginning and at the end of a batch of approximately 15 samples.

D.1.4. Results

D.1.4.1. Redox-sensitive trace elements

The data for U, V, Mo, As, Co, Cd, Cu, Zn, Ni, Pb and Cr are shown in Tables D.1 and D.2 for limestone and marl for the three sections.

D.1.4.1.1. The Fiume-Bosso section

In limestone samples, the data obtained for U, V, Mo, and As contents show comparable variations, with a consistently low background level, contrasted by a maximum in concentrations in and close to the Faraoni Level (Fig. D.3, Table D.1). The average values for the background level correspond to approximately 0.2, 0.9, 0.03 and 0.3 ppm and the maximum values to approximately 3.1, 11.6, 0.5 and 3.0 ppm, for the U, V, Mo, and As contents, respectively.

The data obtained in the marlstones show equally a clear enrichment of U, V, Mo, and As around the Faraoni Level (Table D.2). The maximum values reach 15.4 ppm for U, 345.9 ppm for V, 61.8 ppm for Mo, and 177.4 ppm for As, whereas background level are equal

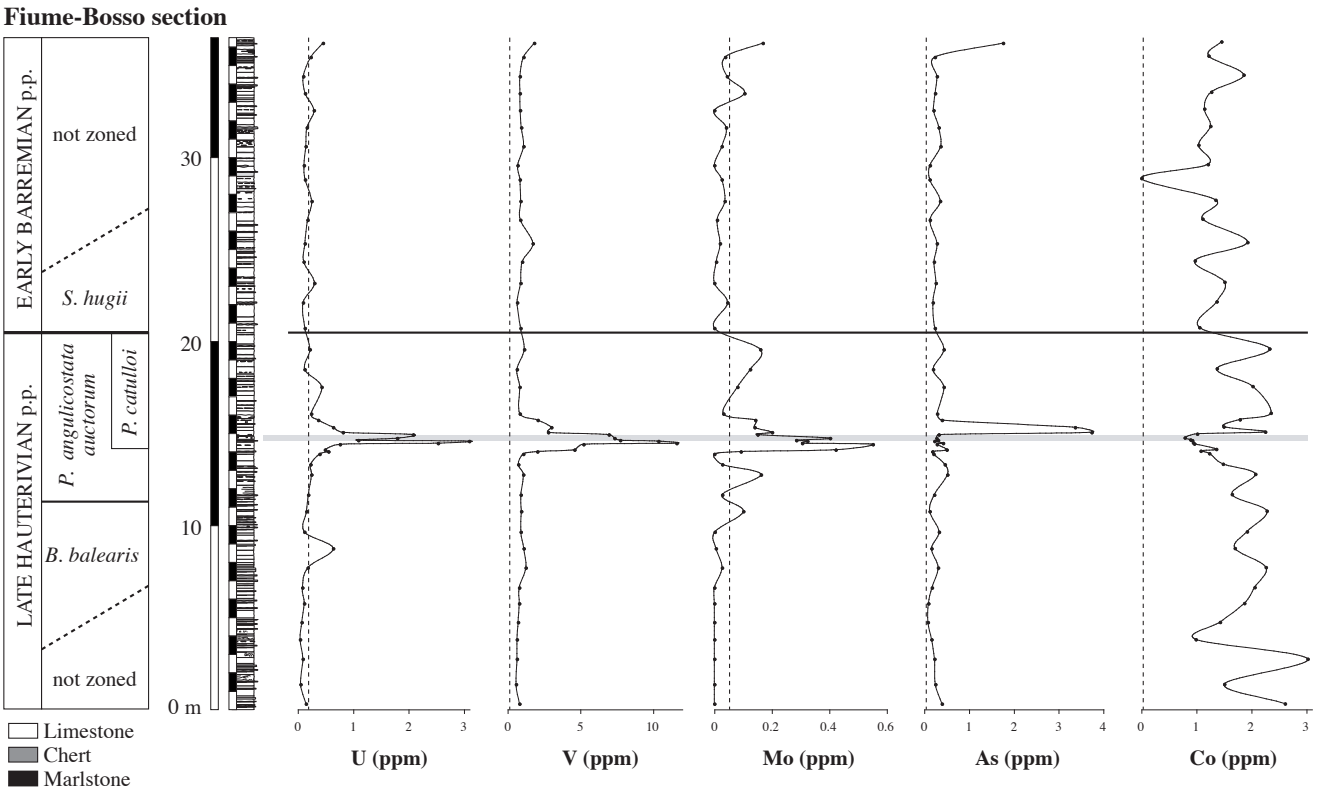

Fig. D.3: Redox sensitive trace elements distributions for the Fiume-Bosso section. The grey band indicates the position of the Faraoni Level and the dashed line the limit of quantification for each element.

to approximately 2.9, 54.1, 2.3, and 13.2 ppm respectively.

Despite a small negative shift in the upper part of the section, the global trend of Co in limestone samples seems to be more or less constant (Table D.1), fluctuating around 1.8 ppm. The Faraoni Level is marked by a short negative shift towards 0.9 ppm. In the shale, the Co curve shows a small positive shift within the Faraoni Level. A maximum of 106.6 ppm is present just above the Faraoni Level (Table D.2) whereas the background level values correspond to approximately 50 ppm.

For the other elements, only Cd and Zn show a small positive shift in limestone levels within the Faraoni Level. In the upper part of the section, a positive shift (up to 66.1 ppm) of Zn is remarked. In the Faraoni shale samples, a positive shift of Cd, Cu, Zn, Ni is present, with very high maximum values (10.5, 273.7, 1068.2, and 533.5 ppm respectively). On the other hand, it appears that Pb and Cr record a negative shift.

D.1.4.1.2. The Veveyse de Châtel-St. Denis section

In this section, the data obtained in limestone samples for U, V, Mo, and As contents show a behaviour similar to that of the Fiume-Bosso section, with the difference that peaks are less pronounced in comparison to the background level (Fig. D.4, Table D.1). We also note that the background levels are generally higher in the lower part of the section, below the "couches à poissons" (Faraoni Level equivalent), with the exception of Mo, which shows an interval of increased values only in the first 40 m of the measured section. Interestingly, U and V present a double peak in contents around the level of the "couches à poissons", with the higher peak representing the "couches à poissons" itself. The average values of the background levels correspond to approximately 0.5, 5.4, 0.09. and 0.8 ppm and the maximum values are approximately 0.9, 11.7, 1.2, and 2.5 ppm, for U, V, Mo and As contents, respectively. The data obtained in the marls show equally a clear enrichment of U, V, Mo, and As around the Faraoni Level (Table D.2).

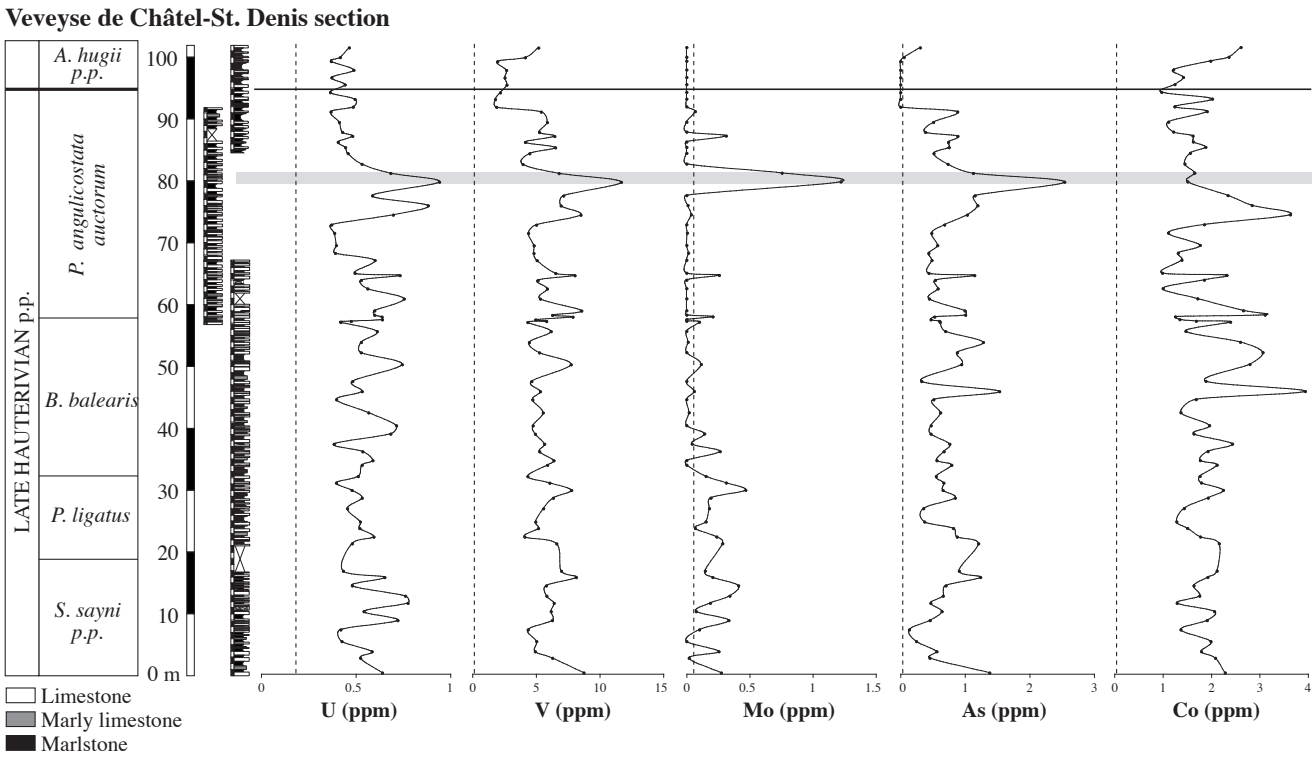

Fig. D.4: Redox sensitive trace elements distributions for the Veveyse de Châtel-St. Denis section. The grey band indicates the position of the "couche à poissons" (Faraoni Level equivalent) and the dashed line the limit of quantification for each element.

Co contents in limestone show a small overall decrease from the bottom to the top of the section, with a mean value of about 1.7 ppm. A peak is distinguished 5 m below the equivalent of the Faraoni Level, reaching 3.6 ppm. In the marls, a peak reaching 7.4 ppm is distinguished 3 m below the Faraoni Level.

In this section, the Cu, Zn, Ni, and Pb show a small positive shift in the limestone 5 m below the Faraoni Level equivalent. They correspond to the peaks of U, V, and Co. Cu and Zn show equally a peak approximately 40 m below the Faraoni Level, at the beginning of the *B. balearis* zone. On the other hand, in the marls, only Cd is enriched within the Faraoni Level equivalent, whereas enrichment of Cd, Zn, Ni and Pb characterizes again the beds situated 5 m below this level.

D.1.4.1.3. The Angles section

In the limestone samples, the trends in U, V, Mo, and As contents are comparable to the other two sections, with peak values at the level of the Faraoni Level equivalent (Fig. D.5, Table D.1). Whereas the background levels are low and rather constant for U, Mo, and As, V contents show a more variable evolution, with a series of positive excursions above the Faraoni Level equivalent. The average values for the background levels are at about 0.7, 4.5, 0.2, and 0.6 ppm and the maximum values correspond to approximately 2.1, 8.9, 4.9, and 6.3 ppm, for U, V, Mo, and As contents, respectively. The data obtained in the marl samples show equally a clear enrichment of U, V, Mo, and As around the Faraoni Level equivalent (Table D.2).

The overall trend in Co contents in limestone is more or less constant, with average values oscillating around 1.3 ppm. A peak with a value of 5.1 ppm is distinguished approximately 6 m below the equivalent of the Faraoni Level (bed AN 38). In the same bed, a small peak is present in the Mo and the As curves. Within the equivalent of the Faraoni Level, a small peak of Co reaching 2.4 ppm is distinguished. The data obtained in the marls show equally a clear enrichment of U, V, Mo, and As around the Faraoni Level equivalent (Table D.2). In the marl samples, a remarkable peak in Co contents characterizing the Faraoni Level equivalent has not been observed.

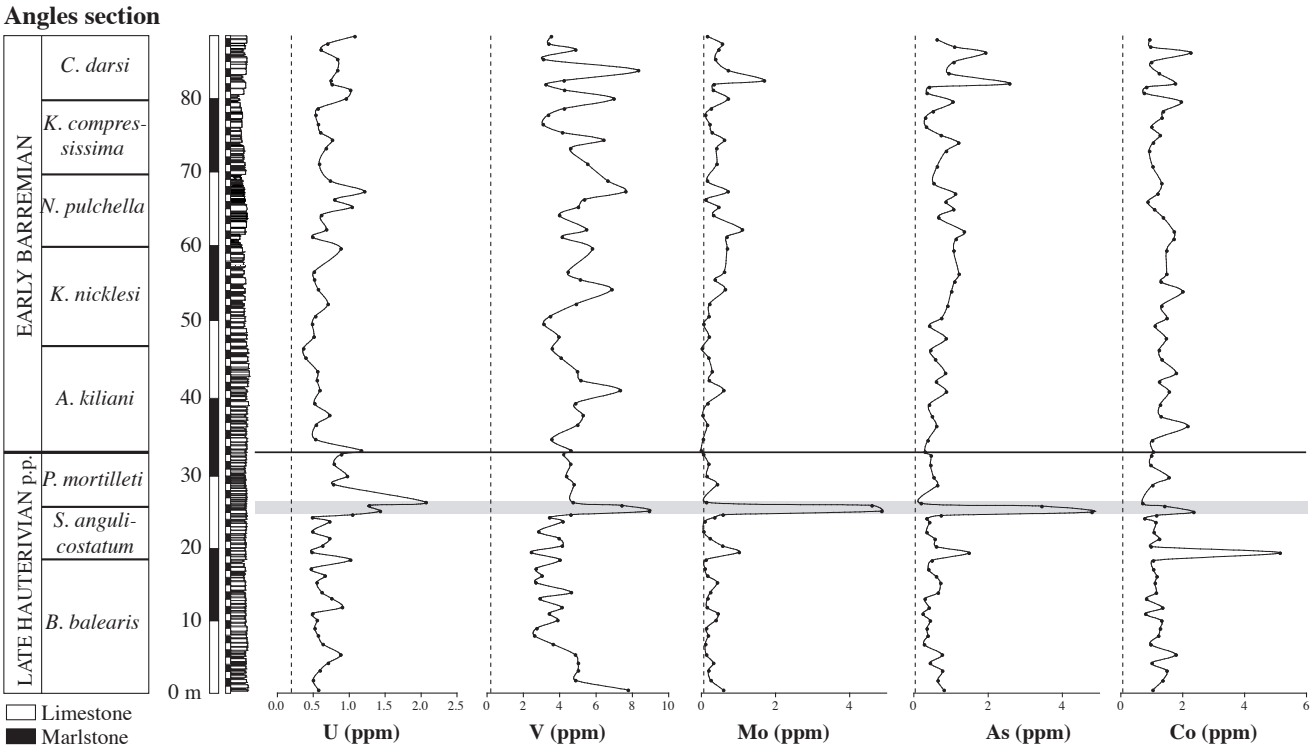

Fig. D.5: Redox sensitive trace elements distributions for the Angles section. The grey band indicates the position of the Faraoni Level equivalent and the dashed line the limit of quantification for each element.

A maximum of 13.4 ppm is seen within bed AN 45b.

In this section, a clear peak of Cd, Zn, Ni, and Pb occurs within the limestone beds of the Faraoni Level equivalent. Moreover, a peak of Ni and Pb marks bed AN 38. On the other hand, no significant peak of these elements has been found in the Faraoni Level equivalent marls. We notice, however, that all these elements are more concentrated in the marls below the Faraoni equivalent than above.

D.1.4.2. Total organic carbon (TOC)

In the limestone samples, measured TOC values are not higher than 0.1%. We will therefore restrict our discussion to the results obtained in the marl samples (see Fig. D.6). In the Fiume-Bosso section, a maximum TOC value of 14.8% has been measured in the thin marl level interval just below the Faraoni Level. Within the Faraoni Level, the average value of TOC is close to 3.25%. These values are not significantly different from those obtained in marl samples above and below the Faraoni Level.

In the VCD section, no major variations have been measured (Fig. D.6). The average value is close to 0.5% and the Faraoni Level equivalent TOC value is equal to 0.31%. In the Angles section, no major variation has been observed as well. The TOC values are however higher and reach 2.63 %. TOC values in the Faraoni Level equivalent are close to 1.25%.

D.1.5. Discussion

D.1.5.1. Comparison between the three sections

Trends in U, V, Mo, and As contents are all characterized by pronounced positive peaks marking the Faraoni Level and its equivalent, and are very distinct relative to the measured intervals below and above this level, representing the upper Hauterivian and the lower Barremian. This positive peak is present in both limestone and marl samples, despite differing background level values. For the trends in Co, Cd, Cu, Zn, Ni, Pb, and Cr contents, no significant overall variations are observed and no specific enrichments are recorded for the Faraoni Level and its equivalent apart from local variations.

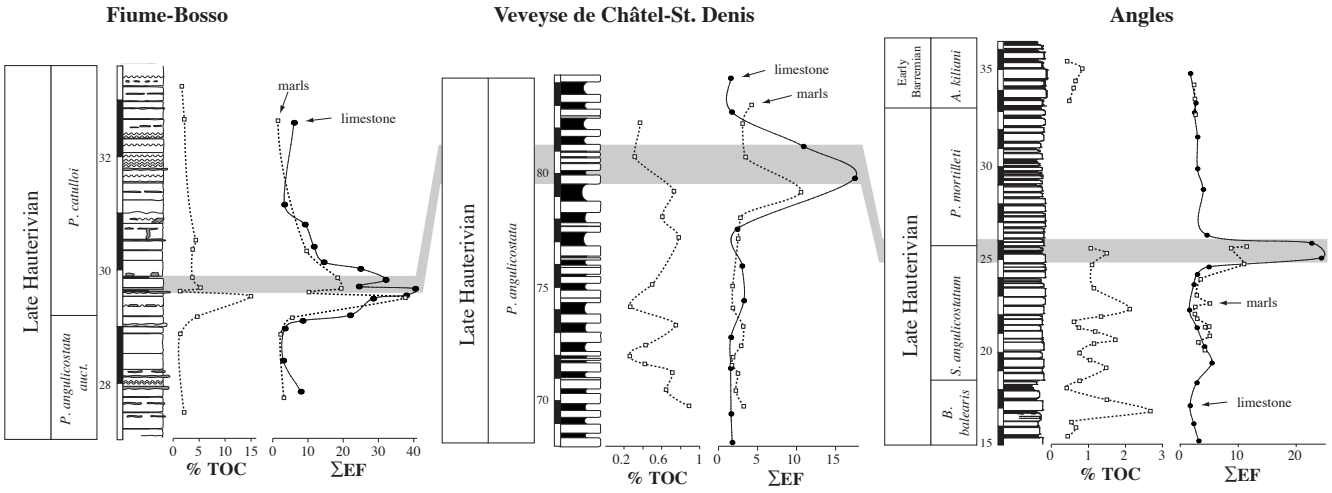

Fig. D.6: Correlation of the Faraoni Level for the three different sections. For each section, the TOC analyses in marls as well as the Trace Element Index (ΣEF) in both limestone and marls are figured. See text for ΣEF calculation details. The lithologic legend for each section is the same as in previous figures.

D.1.5.2. Behaviour of U, V, Mo, Co, and As

Enrichments in U, V, and Mo are well known for numerous black shales of the Phanerozoic (*e.g.*, Brumsack and Gieskes 1983; Brumsack 1989; Coveney *et al.* 1991; Sun and Püttmann 1997; Nijenhuis *et al.* 1999; Warning and Brumsack 2000; Yarincik *et al.* 2000; Mangini *et al.* 2001; Tribovillard *et al.* 2004; Wilde *et al.* 2004; Brumsack, 2006). U and V enrichments are usually associated to anoxic to euxinic bottom-water conditions during the time of deposition (*e.g.*, Hastings *et al.* 1996; Morford and Emerson 1999; Mangini *et al.* 2001). Under mildly reducing and anoxic conditions, U and V may be removed from the ocean by the formation of organo-metal ligands in humic acids; by crystalline precipitation (UO_2 and V_2O_3 or $V(OH)_3$), and V may also be removed by surface-adsorption processes (Algeo and Maynard 2004). For Mo, Algeo and Maynard (2004) propose adsorption onto humic substances as a main possible mechanism to transfer this element from the water column into the sediment, and under euxinic conditions, by a rapid uptake by authigenic/syngenetic sulfides.

Overall, the solubility of these three elements decreases in the reduced state, and their precipitation and enrichment in sediments is favoured during periods of anoxia (*e.g.* Yarincik *et al.* 2000; Mangini *et al.* 2001; Algeo and Maynard 2004).

Co shows a more complex behaviour in the three sections studied here. This element should behave similar to U, V and Mo, and indeed, in oxygen-depleted waters, Co forms an insoluble sulfide (CoS) that is trapped in sediments (Algeo and Maynard 2004). These sulfides are taken up in solid solution by authigenic Fe sulfides (Huerta-Diaz and Morse 1992). But, because of the slow kinetics of this uptake, significant Co enrichment in the sedimentary environment is limited to euxinic conditions (Sun and Püttmann 1997; Algeo and Maynard 2004).

Sedimentary enrichments in As are less well documented from the geological record. As is usually mobile under slightly reducing conditions through the reductive dissolution of the As bearing phases (Fe (hydr)oxides). Furthemore, Bostick and Fendorf (2003) detailed the mechanisms of As uptake in more anoxic environments and demonstrated the surface precipitation of As on iron sulphide minerals. This hypothesis is supported by Huerta-Diaz and Morse (1992) who noted a close link between As and pyrite in sediments underneath anoxic water. Hence, the presence of abundant marcasite nodules within the Faraoni Level in central Italy (Cecca *et al.* 1994) is compatible with the enrichment in As.

An increased input of trace metals in the ocean in association with large igneous province (LIP) activity has been forwarded as an alternative explanation for trace-metal enrichment in mid-

Cretaceous organic-rich sediments, which were formed during oceanic anoxic events (*e.g.*, Sinton and Duncan 1997; Larson and Erba 1999; Leckie *et al*. 2002; Erba 2004; Snow *et al*. 2005). For the late Hauterivian, however, there is no evidence for LIP volcanism so far (*e.g.*, Larson 1991; Courtillot and Renne 2003), although a certain degree of volcanic activity has been documented at Rio Grande, documenting the end of the Paraná continental flood basalts (Stewart *et al*. 1996). The volume of lava emitted during this episode is one order of magnitude lower compared to other LIP's. Moreover, Brumsack (2006) pointed out that trace-metal enrichment (with the exception of extreme enrichment of Ag, Cu, Ni, V and Zn) in sediments associated with the Cenomanian – Turonian boundary oceanic anoxic event may be explained by seawater as the mere source for these elements (see also Arthur *et al*. 1988; Piper 1994). The trace-metal enrichments calculated for the Faraoni event (Table D.3) are on the same order of magnitude as those calculated for present-day coastal upwelling zones and anoxic basins (*e.g.*, Brumsack, 2006). We therefore exclude volcanic activity as a major source of trace-metal enrichment during the Faraoni event.

D.1.5.3. Redox conditions during the Faraoni event

The behaviour of the redox-sensitive elements, measured in and around the Faraoni Level and its equivalents, allows us to precise the redox conditions that were present during the Faraoni event. The enrichment of U, V, Mo, and As are interpreted as a signature of anoxic and euxinic conditions (Algeo and Maynard 2004). The conservative behaviour of Co during the Faraoni event with regards to its background level is characteristic of dysoxic to anoxic facies according to these authors. The Faraoni Level is therefore clearly the expression of an anoxic event (with eventually locally weakly euxinic conditions such as is indicated at Angles with regard to a small increase of the Co content). The fact that the other redox-sensitive trace elements studied here are not systematically enriched within the Faraoni Level underlines the limit of our comprehension of this system. Partial diagenetic remobilization or differences in sediment uptake processes may be evoked to explain the non-systematic presence of enrichments in the other studied trace elements. Such remobilization processes are thus thought to be responsible of the slight shift of Mo and As peak within the Angles section. Further investigations are however needed to resolve this problem.

Using total sulphur versus TOC plots, Baudin *et al*. (2002) argued for dysoxic rather than for truly anoxic conditions for the Faraoni Level. This observation together with the conservative behaviour of Co may hint at the possibility that the anoxic conditions were not so strong and closer to the dysoxia/anoxia threshold that to the anoxia/euxinic threshold (O_2 close to 0.2 ml/l of H_20), with the exception of the section at Angles, where conditions may have been more severe.

D.1.5.4. Local oxygen-deficient conditions below the Faraoni Level

In the Angles and the VCD sections, isolated maxima in trace-metal contents are recognized, notably below the Faraoni Level equivalent. In the VCD section, U, V, Zn, Ni, and Co contents show a peak 5 m below the Faraoni equivalent. In the Angles section, Mo, As, Ni, Pb, and Co contents show a peak 6 m below the Faraoni Level equivalent. These peaks are not correlated in time between the two sections and could have resulted from local changes in bottom-water oxygen conditions, resulting in local anoxia or euxinia.

D.1.5.5. Enrichment factors

For each separated lithology (*i.e.* limestones or marls), enrichment factors (EFs) were calculated for U, V, Mo, and As according to the following equation (see Table D.3 and Fig. D.6):

$$EFs = [Me]_{peak} / [Me]_{background}$$

In this equation, $[Me]_{background}$ represents the average value of the background level of the different curves and $[Me]_{peak}$ is the maximum value of the different peaks. The EFs thus obtained are coherent with those obtained by Morford and Emerson (1999) (for U, V, and Mo, and based on references therein) for anoxic conditions, representing another clue for anoxic conditions during the Faraoni event.

(ppm)	Background level average	Maximum value of the peak	Enrichment factors
Fiume-Bosso			
U	0.17	3.1	**18.24**
V	0.9	11.6	**12.89**
Mo	0.03	0.55	**18.33**
As	0.3	3	**10.00**
Veveyse			
U	0.53	0.94	**1.77**
V	5.411	11.7	**2.16**
Mo	0.09	1.22	**13.56**
As	0.75	2.54	**3.39**
Angles			
U	0.69	2.1	**3.04**
V	4.55	8.9	**1.96**
Mo	0.24	4.87	**20.29**
As	0.65	4.8	**7.38**

Table D.*3: Background level values, maximum value of the peak and enrichment factors of U, V, Mo, and As for the three studied sections (see text for calculation details).*

In order to compare the different sections, an enrichment factor index (□EF) is calculated by adding the EFs of U, V, and Mo (see Fig. D.6). A clear peak is thus obtained for the three sections for both lithologies, underlining the higher uptake of U, V, and Mo in the sediment during the Faraoni event.

A remarkable feature of the Faraoni Level is the alternation between limestones and laminated shales, which is interpreted, in a first approximation, as the results of variations in oxygen content (see Westphal *et al*. 2004 for a review). The higher values of redox-sensitive trace elements in the Faraoni shales compared with the Faraoni limestones seem to confirm this hypothesis. However, if we look at the enrichment factors index (□EF) calculated for both marls and limestones (Fig. D.6), such a dichotomy is not found. The variation of these indices is more or less the same within the same section. On the contrary, it seems that the limestones are a little bit more enriched in redox-sensitive trace elements than the marls during the Faraoni event compared to "normal" conditions. The higher redox-sensitive trace element content of the marlstones (compared to the limestones) is thus not induced by difference of synsedimentary redox conditions between marlstones and limestones (as already shown by Westphal *et al*. 2004), but is rather the result of synsedimentary condensation or early diagenetic processes. This underlines the importance of the lithology effect on analyses and the need to consider "mono-lithologic" analyses when discussing temporal variations.

In Fig. D.6, where the TOC is plotted versus the □EF, we remark that TOC is only clearly enriched in the Faraoni Level of the Fiume-Bosso section, whereas □EF shows a positive shift in all three sections. This allows us to postulate that the enrichment of redox-sensitive trace elements is a more conservative tracer of anoxic conditions than TOC contents. This latter may be more easily removed during diagenetic processes.

D.1.5.6. Chemostratigraphic tools

The distinct enrichment of the redox-sensitive elements U, V, Mo and As in the sedimentary environment during the Faraoni event appears to be unique for the examined time interval of the Late Hauterivian – Early Barremian and is therefore useful as a tracer of the Faraoni event within the Tethyan realm.

Outside the Tethyan realm, a distinct enrichment in U contents occurs in sediments of the Late Hauterivian of the Izu-Mariana margin, northwestern Pacific, in ODP hole 1149b, (ODP leg 185; Plank *et al*. 2000, upper part of the lithologic unit IV, interval 185-1149B-19R-1, see Fig. F27 and F72). This peak is associated with a layer containing elevated quantities of euhedral barite, along with dolomite rhombs and phosphatic fish remains. Plank *et al*. (2000) argue that this peculiar mineral assemblage indicates an episode of enhanced organic-matter accumulation, which they correlate with the Faraoni event. According to the data presented here, the enrichment in U represents a further strong argument in favour of this assumption. This suggests that the Faraoni event was not restricted to the western Tethyan realm, but may also be recorded in sediments of the northwestern Pacific. Further investigations - especially in sediments of the southern hemisphere - are required to confirm the global character of this event.

In the Fiume-Bosso section, the enrichment in U, V, and Mo contents began slightly before and ended slightly after the Faraoni Level s.s. This may indicate that the Faraoni anoxic event may have started slightly earlier and lasted longer than the time associated with the formation of the Faraoni Level itself. This would signify that the organic-rich facies of the Faraoni Level in

the Italian sections does not reflect the entire period of oxygen depletion, but rather the time of important organic matter preservation and/or accumulation during the culmination of this event. This may be taken into account when tracing the equivalent of the Faraoni Level by using trace-metal enrichment in sections were ammonites are absent or extremely rare. The here described trace-metal enrichments trace the Faraoni anoxic event rather than the Faraoni Level itself.

D.1.5.7. Initiating factors of the Faraoni event

As recognized by Baudin *et al*. (2002) and Baudin (2005), the Faraoni Level and its equivalent can be qualified as an anoxic event. An important difference between the Faraoni event and other Cretaceous OAE's consists, however, in the fact that the anoxic event is not mirrored by a major shift in the carbon isotope record (*e.g*., Erba *et al*. 1999; van de Schootbrugge *et al*. 2000; Company *et al*. 2005; Godet *et al*. 2006), but only by a small positive excursion (0.5‰). Godet *et al*. (2006) explain this attenuated signal by a buffering effect on the carbon-isotope record exerted by the large size of the oceanic dissolved inorganic carbon reservoir. Furthermore, the classical scenario invoking an episode of intensified volcanism and reinforced greenhouse conditions (*e.g*., Jenkyns 1999, 2003) is difficult to apply to this peculiar event. As previously said, there is no evidence for large igneous province (LIP) volcanism during the late Hauterivian so far, even if a certain degree of volcanism has been documented in Rio Grande. This volcanic activity is however one order of magnitude lower than that associated with LIP (*e.g*., Larson 1991; Courtillot and Renne 2003). We therefore consider the Rio Grande volcanism as not responsible for the Faraoni event, even if slightly stronger greenhouse conditions may have been induced by this volcanic episode.

As discussed by Baudin *et al*. (2002), the Faraoni Level corresponds to the maximum flooding surface (mfs) of the Ha6 sequence (Haq *et al*. 1987; Hardenbol *et al*. 1998). For the VCD section, Busnardo *et al*. (2003) attributed the "couches à poissons" to the transgressive surface (ts) of the Ha6 sequence, but A. Strasser (Fribourg, personal communication) correlates the same horizon also to the mfs of the Ha6 sequence (see also Bodin *et al*. in press). The Ha6 mfs corresponds to the maximum of a second-order transgression (Haq *et al*. 1987; Hardenbol *et al*. 1998), which led to the connection of the Tethyan and the Boreal realms, as is suggested by belemnite migration patterns observed by Mutterlose and Bornemann (2000) and the presence of boreal nannoplankton in the Angles section around the Faraoni Level (Godet *et al*. 2006). This second-order transgression may have lead to the flooding of large epicontinental areas. Bodin *et al*. (in press) pointed out the role of this mechanism as the main trigger for the onset of anoxic conditions during the Faraoni anoxic event, by increased nutrient delivery, and the related increase in primary productivity (see also Company *et al*. 2005). Baudin *et al*. (2002) also proposed increased primary productivity as the prime factor leading to the origin of the Faraoni event along the line of the scenario proposed here.

D.1.6. Conclusions

Redox-sensitive trace elemental analysis is a fruitful method to better understand and constrain anoxic events. Indeed, the multi-element analysis discussed here provides additional insight into the oxygenation conditions during the Faraoni anoxic event and serves as a promising correlation tool, especially if biostratigraphic information is lacking.

By comparing the behaviour of the redox-sensitive trace elements with the specific enrichments in U, V, and Mo contents, the Faraoni Level appears to be the expression of anoxic conditions at least near the sediment-water interface. This interpretation is supported by the enrichment of As, which is largely controlled by its sorption onto sulfide minerals in anoxic environments (Bostick and Fendorf 2003). The lack of systematic enrichment of Cd, Cu, Zn, Ni, Pb, and Cr may be related to diagenetic removal or unknown synsedimentary differences in uptake processes.

In the sections analysed, the distinct enrichments in U, V, and Mo are a feature characteristic of the Faraoni Level, and are

unique with regards to the time interval of the late Hauterivian and the early Barremian. We therefore propose to use this feature to correlate the Faraoni Level throughout the entire Tethys, and especially in sections where organic-rich intervals are lacking such as in the section of Angles, and to search for expressions of the Faraoni event also in other basins. For example, a distinct enrichment in U in sediments of late Hauterivian age in the northwestern Pacific may well be correlated with the Faraoni event (Plank *et al*. 2000, see Fig F27 and F72).

According to the general behaviour of the redox-sensitive trace elements in the three analyzed sections, the Faraoni Level may be the expression of a climax situation during a longer period of steadily increasing anoxia induced by a second-order sea level rise. The mobilization of nutrients during this sea level rise may have played an important role in the onset of the Faraoni event.

D.1.7. Acknowledgements

We thank B. van de Schootbrugge, H. Mort, P. Linder, and C. Rambeau for their help in the field, J. Charollais, H. Mort, and F. Baudin for stimulating discussions, T. Monnier for help in the laboratory work and the team of the "Reserve Géologique de Haute-Provence" for providing the authorization for field work and sampling in this region. We also thank E. Erba and J. Hölemann for constructive criticism of the manuscript. Financial support from the Swiss National Science Foundation is gratefully acknowledged (projects 2100-067807/1 and 200020-105206/1).

D.1.8. References

Algeo, T. J. and Maynard, J. B. (2004). "Trace-element behavior and redox facies in core shales of Upper Pennsylvanian Kansas-type cyclothems." Chemical Geology **206**(*3-4*): 289-318.

Arthur, M. A., Jenkyns, H. C., Brumsack, H.-J. and Schlanger, S. O. (1988). Stratigraphy, geochemistry, and paleoceanography of organic carbon-rich Cretaceous sequences. *In:* R. N. Ginsburg and B. Beaudoin, (*Eds*). Cretaceous resources, events and rhythms: Background and plans for research. Digne, France, Kluwer Academic Publishers, **Proc. of ARW**: 75-119.

Baudin, F. (2005). «A Late Hauterivian short-lived anoxic event in the Mediterranean Tethys: the «Faraoni Event».» Comptes Rendus Geoscience **337**: 1532-1540.

Baudin, F., Bulot, L. G., Cecca, F., Coccioni, R., Gardin, S. and Renard, M. (1999). «Un équivalent du «Niveau Faraoni» dans le bassin du Sud-Est de la France, indice possible d'un événement anoxique fini-hauterivien étendu à la Téthys méditerranéenne.» Bulletin de la Société Géologique de France **170**(*4*): 487-498.

Baudin, F., Cecca, F., Galeotti, S. and Coccioni, R. (2002). «Palaeoenvironmental controls of the distribution of organic matter within a C_{org}-rich marker bed (Faraoni level, uppermost Hauterivian, central Italy).» Eclogae geologicae Helvetiae **95**(*1*): 1-13.

Bayon, M. M., Alonso, J. I. G. and Medel, A. S. (1998). «Enhanced semiquantitative multi-analysis of trace elements in environmental samples using inductively coupled plasma mass spectrometry.» Journal of Analytical Atomic Spectrometry **13**(*4*): 277-282.

Behar, F., Beaumont, V. and Penteado, H. L. D. (2001). «Rock-Eval 6 technology: Performances and developments.» Oil and Gas Science and Technology **56**(*2*): 111-134.

Bodin, S., Godet, A., Föllmi, K. B., Vermeulen, J., Arnaud, H., Strasser, A., Fiet, N. and Adatte, T. (2006). «The Late Hauterivian Faraoni oceanic anoxic event in the western Tethys: Evidence from phosphorus burial rates.» Palaeogeography, Palaeoclimatology, Palaeoecology **235**: 238-257.

Boning, P., Brumsack, H.-J., Bottcher, M. E., Schnetger, B., Kriete, C., Kallmeyer, J. and Borchers, S. L. (2004). «Geochemistry of Peruvian near-surface sediments.» Geochimica et Cosmochimica Acta **68**(*21*): 4429-4451.

Bostick, B. C. and Fendorf, S. (2003). «Arsenite sorption on troilite (FeS) and pyrite (FeS2).» Geochimica et Cosmochimica Acta **67**(*5*): 909-921.

Brumsack, H.-J. (1989). «Geochemistry of recent TOC-rich sediments from the Gulf of California and the Black Sea.» Geol. Rundsch. **78**: 851-882.

Brumsack, H.-J. (2006). «The trace metal content of recent organic carbon-rich sediments: Implications for Cretaceous black shale formation.» Palaeogeography, Palaeoclimatology, Palaeoecology.

Brumsack, H.-J. and Gieskes, J. M. (1983). «Interstitial water trace-element chemestry of laminated sediments of the Gulf of California (Mexico).» Marine Chemistry **14**: 89-106.

Busnardo, R. (1965). «Le stratotype du Barrémien.» Mémoires du Bureau de Recherche Géologiques et Minières. **34**: 101-116.

Busnardo, R., Charollais, J., Weidmann, M. and Clavel, B. (2003). «Le Crétacé inférieur de la Veveyse de Châtel (Ultrahelvétique des Préalpes externes; canton de Fribourg, Suisse).» Revue Paléobiol., Genève **22**(*1*): 1-174.

Cecca, F., Galeotti, S., Coccioni, R. and Erba, E. (1996). «The equivalent of the «Faraoni Level» (uppermost Hauterivian, Lower Cretaceous) recorded in the eastern part of Trento Plateau (Venetian southern Alps, Italy).» Riv. Ital. Paleontol. Stratigr. **102**(*3*): 417-424.

Cecca, F., Marini, A., Pallini, G., Baudin, F. and Begouen, V. (1994). «A guide-level of the uppermost Hauterivian (Lower Cretaceous) in the pelagic succession of Umbria-Marche Apennines (Central Italy): the Faraoni Level.» Riv. Ital. Paleontol. Stratigr. **99**: 551-568.

Coccioni, R., Baudin, F., Cecca, F., Chiari, M., Galeotti, S., Gardin, S. and Salvini, G. (1998). «Integrated stratigraphic, palaeontological, and geochemical analysis of the uppermost Hauterivian Faraoni Level in the Fiume Bosso section, Umbria-Marche Apennines, Italy.» Cretaceous Research **19**(*1*): 1-23.

Company, M., Aguado, R., Sandoval, J., Tavera, J. M., Jiménez de Cisneros, C. and Vera, J. A. (2005). «Biotic changes linked to a minor anoxic event (Faraoni Level, latest Hauterivian, Early Cretaceous).» Palaeogeography, Palaeoclimatology, Palaeoecology **224**: 186-199.

Courtillot, V. E. and Renne, P. R. (2003). «On the ages of flood basalt events.» Comptes Rendus Geosciences **335**(*1*): 113-140.

Coveney, J. R. M., Lynn Watney, W. and Maples, C. G. (1991). «Contrasting depositional models for Pennsylvanian black shale discerned from molybdenum abundances.» Geology **19**: 147-150.

Erba, E. (2004). «Calcareous nannofossils and Mesozoic oceanic anoxic events.» Marine Micropaleontology **52**: 85-106.

Erba, E., Bartolini, A. and Larson, R. L. (2004). «Valanginian Weissert oceanic anoxic event.» Geology **32**(*2*): 149-152.

Erba, E., Channell, J. E. T., Claps, M., Jones, C. E., Larson, R. L., Opdyke, B., Premoli-Silva, I., Riva, A., Salvini, G. and torriceli, S. (1999). «Integrated stratigraphy of the Cismon APTICORE (Southern Alps, Italy): A «reference section» for the Barremian-Aptian interval at low latitudes.» Journal of Foraminiferal Research **29**(*4*): 371-391.

Föllmi, K. B., Weissert, H., Bisping, M. and Funk, H. (1994). «Phosphogenesis, carbon-isotope stratigraphy, and carbonate-platform evolution along the Lower Cretaceous northern Tethyan margin.» Geological Society of America Bulletin **106**(*6*): 729-746.

Godet, A., Bodin, S., Föllmi, K. B., Vermeulen, J., Gardin, S., Fiet, N., Adatte, T., Berner, Z., Stüben, D. and Van de Schootbrugge, B. (2006). «Evolution of the marine stable carbon-isotope record during the early Cretaceous: A focus on the late Hauterivian and Barremian in the Tethyan realm.» Earth and Planetary Science Letters **242**: 254-271.

Haq, B. U., Hardenbol, J. and Vail, P. R. (1987). «Chronology of fluctuating sea levels since the Triassic.» Science **235**: 1156-1167.

Hardenbol, J., Thierry, J., Farley, M. B., de Graciansky, P.-C. and Vail, P. R. (1998). Mesozoic and Cenozoic Sequence Chronostratigraphic Framework of European Basins. *In:* P.-C. de Graciansky, J. Hardenbol, T. Jacquin and P. R. Vail, (*Eds*). Mesozoic and Cenozoic Sequence Stratigraphy of European Basins. Special Publication Society for Sedimentary Geology, **60**: 3-13.

Hastings, D. W., Emerson, S. R. and Mix, A. C. (1996). «Vanadium in foraminiferal calcite as a tracer for changes in the areal extend of reducing sediments.» Paleoceanography **11**(*6*): 665-678.

Hay, W. W., DeConto, R., Wold, C. N., Wilson, K. M., Voigt, S., Schulz, M., Wold-Rossby, A.,

Dullo, W.-C., Ronov, A. B., Balukhovsky, A. N. and Soeding, E. (1999). Alternative global Cretaceous paleogeography. *In:* E. Barrera and C. Johnson, (*Eds*). The Evolution of Cretaceous Ocean/Climate Systems. Geological Society of America Special Paper: 332.

Huerta-Diaz, M. A. and Morse, J. W. (1992). «Pyritization of trace metals in anoxic marine sediments.» Geochimica et Cosmochimica Acta **56**(*7*): 2681-2702.

Jenkyns, H. C. (1999). «Mesozoic anoxic events and palaeoclimate.» Zentralblatt Geologie und Paläontologie, 1 **Heft 7-9**: 943-949.

Jenkyns, H. C. (2003). «Evidence for rapid climate change in the Mesozoic-Palaeogene greenhouse world.» Philosophical Transactions of the Royal Society, London, A **361**: 1885-1916.

Jitaru, P., Tirez, K. and De Brucker, N. (2003). «Panoramic analysis for monitoring trace metals in natural waters by ICP-MS.» Atomic Spectroscopy **24**(*1*): 1-10.

Jones, C. E. and Jenkyns, H. C. (2001). «Seawater strontium isotopes, oceanic anoxic events, and seafloor hydrothermal activity in the Jurassic and Cretaceous.» American Journal of Science **301**: 112-149.

Larson, R. L. (1991). «Latest pulse of Earth: Evidence for a mid-Cretaceous superplume.» Geology **19**: 547-550.

Larson, R. L. and Erba, E. (1999). «Onset of the mid-Cretaceous greenhouse in the Barremian-Aptian: Igneous events and the biological, sedimentary and geochemical responses.» Paleoceanography **14**(*6*): 663-678.

Leckie, R. M., Bralower, T. J. and Cashman, R. (2002). «Oceanic anoxic events and plankton evolution: Biotic response to tectonic forcing during the mid-Cretaceous.» Paleoceanography **17**(*3*): 1-29.

Lini, A., Weissert, H. and Erba, E. (1992). «The Valanginian carbon isotope event; a first episode of greenhouse climate conditions during the Cretaceous.» Terra Nova **4**(*3*): 374-384.

Mangini, A., Jung, M. and Laukenmann, S. (2001). «What do we learn from peaks of uranium and of manganese in deep sea sediments?» Marine Geology **177**(*1-2*): 63-78.

Morford, J. L. and Emerson, S. R. (1999). «The geochemistry of redox sensitive trace metals in sediments.» Geochimica et Cosmochimica Acta **63**(*11-12*): 1735-1750.

Mutterlose, J. and Bornemann, A. (2000). «Distribution and facies patterns of Lower Cretaceous sediments in northern Germany: a review.» Cretaceous Research **21**(*6*): 733-759.

Nijenhuis, I. A., Bosch, H.-J., Sinninghe Damste, J. S., Brumsack, H.-J. and De Lange, G. J. (1999). «Organic matter and trace element rich sapropels and black shales: a geochemical comparison.» Earth and Planetary Science Letters **169**(*3-4*): 277-290.

Piper, D. Z. (1994). «Seawater as the source of minor elements in black shales, phosphorites and other sedimentary rocks.» Chemical Geology **114**: 95-114.

Plank, T., Ludden, J. N., Escutia, C. and al. (2000). Proceeding of the Ocean Drilling Program, Initial Reports, 185 [Online]. Available from World Wide Web: <http://www-odp.tamu.edu/publications/185_IR/185ir.htm>.

Sanfourche, J. and Baudin, F. (2001). «La genèse des évènements anoxiques de la période moyenne du Crétacé. Examen de l'hypothèse du meromictisme océanique.» Annale de la Société Géologique du Nord **8**(*2*): 107-119.

Schlanger, S. O., Arthur, M. A., Jenkyns, H. C. and Scholle, P. A. (1987). The Cenomanian-Turonian oceanic anoxic event, I. Stratigraphy and distribution of organic-rich beds and the marine 13C excursion. *In:* J. Brooks and A. J. Fleet, (*Eds*). Marine Petroleum Sources Rocks. Geological Society, London, Special Publications, **26**: 371-399.

Schlanger, S. O. and Jenkyns, H. C. (1976). «Cretaceous oceanic anoxic events: causes and consequences.» Geologie en Mijnbouw **55**: 179-184.

Sinton, C. W. and Duncan, R. A. (1997). «Potential links between ocean plateau volcanism and global ocean anoxia at the Cenomanian-Turonian boundary.» Economic Geology **92**: 836-842.

Snow, L. J., Duncan, R. A. and Bralower, T. J. (2005). «Trace element abundances in the Rock Canyon Anticline, Pueblo, Colorado,

marine sedimentary section and their relationship to Caribbean plateau construction and oxygen anoxic event 2.» Paleoceanography **20**: PA3005, 1-14.

Stewart, K., Turner, S., Kelley, S., Hawkesworth, C., Kirstein, L. and Mantovani, M. (1996). «3-D, ^{40}Ar-^{39}Ar geochronology in the Paraná continental flood basalt province.» Earth and Planetary Science Letters **143**(*1-4*): 95-109.

Sun, Y. and Püttmann, W. (1997). «Metal accumulation during and after deposition of the Kupferschiefer from the Sangerhausen Basin, Germany.» Applied Geochemistry **12**(*5*): 577-592.

Tribovillard, N., Riboulleau, A., Lyons, T. and Baudin, F. (2004). «Enhanced trapping of molybdenum by sulfurized marine organic matter of marine origin in Mesozoic limestones and shales.» Chemical Geology **213**(*4*): 385-401.

Trümpy, R. (1960). «Paleotectonic evolution of the Central and Western Alps.» Bulletin of the Geological Society of America **71**: 843-908.

Van de Schootbrugge, B., Föllmi, K. B., Bulot, L. G. and Burns, S. J. (2000). «Paleoceanographic changes during the early Cretaceous (Valanginian-Hauterivian): evidence from oxygen and carbon stable isotopes.» Earth and Planetary Science Letters **181**: 15-31.

Van de Schootbrugge, B., Kuhn, O., Adatte, T., Steinmann, P. and Föllmi, K. B. (2003). «Decoupling of P- and Corg-burial following Early Cretaceous (Valanginian-Hauterivian) platform drowning along the NW Tethyan margin.» Palaeogeography, Palaeoclimatology, Palaeoecology **199**(*3-4*): 315-331.

Warning, B. and Brumsack, H.-J. (2000). «Trace metal signatures of eastern Mediterranean sapropels.» Palaeogeography, Palaeoclimatology, Palaeoecology **158**(*3-4*): 293-309.

Westphal, H., Munnecke, A., Pross, J. and Herrle, J. O. (2004). «Multiproxy approach to understanding the origin of Cretaceous pelagic limestone-marl alternations (DSDP site 391, Blake-Bahama Basin).» Sedimentology **51**(*1*): 109-126.

Wilde, P., Lyons, T. W. and Quinby-Hunt, M. S. (2004). «Organic carbon proxies in black shales: molybdenum.» Chemical Geology **206**(*3-4*): 167-176.

Yarincik, K. M., Murray, R. W., Lyons, T. W., Peterson, L. C. and Haug, G. H. (2000). «Oxygenation history of bottom waters in the Cariaco Basin, Venezuela, over the past 578,000 years: Results from redox-sensitive metals (Mo, V, Mn, and Fe).» Paleoceanography **15**(*6*): 593-604.

D.2.
Evolution of the marine stable carbon-isotope record during the Early Cretaceous: A focus on the Late Hauterivian and Barremian in the Tethyan realm

Alexis Godet[1], Stéphane Bodin[1], Karl B. Föllmi[1], Jean Vermeulen[2], Silvia Gardin[3], Nicolas Fiet[4], Thierry Adatte[1], Zsolt Berner[5], Doris Stüben[5], and Bas van de Schootbrugge[6]

[1]Institut de Géologie, Université de Neuchâtel, rue Emile Argand 11, 2007 Neuchâtel, Switzerland; [2]Grand Rue, 04330 Barrême, France; [3]CNRS-UMR 5143 «Paléobiodiversité et Paléoenvironnement», case 104, Université Paris 6, 4 Place Jussieu, 75252 Paris Cedex 05, France; *[4]UMR 8148 – I.D.E.S., Bât. 504, University of Paris XI Orsay, 91405 Orsay Cedex, France; [5]Institut für Mineralogie und Geochemie, Universität Karlsruhe, 76131 Karlsruhe, Germany; [6]Institut für Geologie und Paläontologie, J.W. Goethe Universität, 60054 Frankfurt am Main, Germany*

Published in Earth and Planetary Science Letters, 2006, volume 242, issue 3-4, pages 254 - 271.

Abstract

In order to improve our understanding of the relationships between the late Hauterivian oceanic anoxic Faraoni event, contemporaneous platform drowning along the northern Tethyan margin and global environmental change in general, we established high-resolution $\delta^{13}C$ and $\delta^{18}O$ curves for the late Hauterivian and the entire Barremian stage. These data were obtained from whole-rock carbonate samples from the Veveyse de Châtel St. Denis section (Switzerland), the Fiume-Bosso section and the nearby Gorgo a Cerbara section (central Italy), and the Angles section (Barremian stratotype, France).

We observe an increase of 0.3‰ in mean $\delta^{13}C$ values within sediments from the middle Hauterivian *Subsaynella sayni* ammonite zone to the Hauterivian-Barremian boundary; $\delta^{13}C$ values remain essentially stable during the early Barremian. During the latest early Barremian and most of the late Barremian, $\delta^{13}C$ values increase slowly (until the *Imerites giraudi* zone) and the latest Barremian is characterized by a negative trend in $\delta^{13}C$ values, with minimal values at the Barremian-Aptian boundary. During the earliest Aptian, $\delta^{13}C$ mean values start to rise again and attain +2.25‰.

We interpret the evolution of the $\delta^{13}C$ record as resulting from the interaction between changes in the carbon cycle in the Tethyan basin and the adjacent platforms and continents. In particular, changes towards warmer and more humid conditions on the continent and coeval phases of platform drowning along the northern Tethyan margin may have contributed to enhance the oceanic dissolved inorganic carbon (DIC) reservoir which may have pushed the $\delta^{13}C$ record towards more negative values and exerted a general attenuation on the $\delta^{13}C$ record. From this may have come the general change from a heterozoan to a photozoan carbonate platform community, which influenced the evolution in $\delta^{13}C$ values by increasing the export of aragonite and diminishing export of dissolved organic carbon into the basins.

Keywords

Hauterivian; Barremian; Tethys; oceanic anoxic Faraoni event; carbon and oxygen isotopes; paleoceanography.

D.2.1. Introduction

Correlated stratigraphic records of stable carbon isotopes measured in marine whole-rock carbonates or on isolated marine carbonate shells and skeletons provide very valuable insight into temporal changes in the global carbon cycle and in paleo-environmental conditions in general. The Cretaceous carbon cycle was perturbed by a series of short-lived oceanic anoxic events (OAEs) and contemporaneous phases of carbonate platform destruction, which are marked in the carbon isotope records of bulk carbonate ($\delta^{13}C_{carb}$) and organic matter ($\delta^{13}C_{org}$) record (*e.g.*, Weissert, 1989; Lini *et al.*, 1992; Föllmi *et al.*, 1994; Jenkyns *et al.*, 1994; Weissert *et al.*, 1998; Veizer *et al.*, 1999; Jenkyns, 2003; Erba *et al.*, 2004; Weissert and Erba, 2004; compare also Schlanger and Jenkyns, 1976; Jenkyns, 1980; Jones and Jenkyns, 2001). An exception to these observed links between environmental change and corresponding variations in the $\delta^{13}C$ record seems to be exemplified by the Faraoni anoxic event, a black-shale interval recovered in Tethyan (hemi-) pelagic sections of latest Hauterivian age (Cecca *et al.*, 1994; Baudin *et al.*, 1999) and which is coeval to the onset of a major platform drowning episode along the northern Tethyan margin (Föllmi et al, 1994). This event does not appear to be associated with an abrupt change in $\delta^{13}C$ values but rather with a long-term increase in the $\delta^{13}C$ record (*e.g.*, van de Schootbrugge *et al.*, 2000).

We investigated four hemipelagic to pelagic sections in the Tethyan realm (Angles (SE France), Fiume-Bosso (central Italy), Gorgo a Cerbara (central Italy) and Veveyse de Châtel-St. Denis (west Switzerland)), in order to more precisely constrain the $\delta^{13}C$ and $\delta^{18}O$ record around the Faraoni anoxic event and during the associated platform drowning event, which itself extends well into the early Barremian. We associate the obtained trends with changes in the oceanic carbon cycle, which was influenced by a number of mechanisms, amongst which we count the paleo-ecology of Tethyan carbonate platforms and their influence on the isotope signature of inorganic carbon species. In particular, we suggest that the change between photozoan and heterozoan dominated carbonate-platform ecosystem (Föllmi *et al.*, 1994) may influence the isotope signature of the adjacent open ocean.

D.2.2. Geological setting

D.2.2.1. The sections of Fiume Bosso and Gorgo a Cerbara

The lower Cretaceous sedimentary succession of the Umbria Marche basin (Italy) is composed of the Maiolica (late Tithonian to early Aptian) and the Marne a Fucoidi (early Aptian to late Albian) formations (Coccioni *et al.*, 1998).

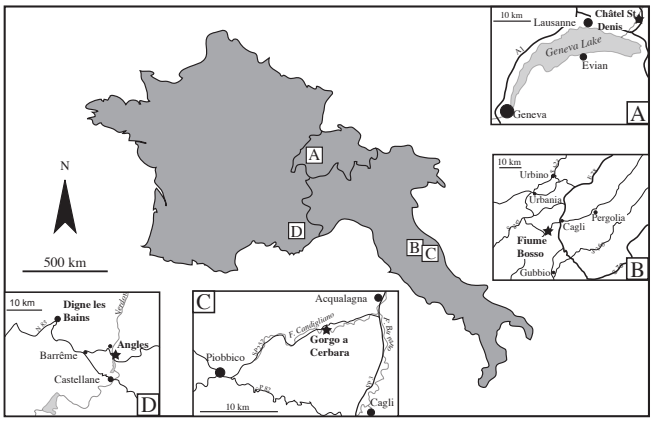

Fig. D.7: location of the different studied sections.

The section of Fiume Bosso (FB) is located between Urbino and Gubbio, near Cagli (central Italy, Fig. D.7; see also Cecca *et al.*, 1994a). It represents the type section for the Faraoni level (Cecca *et al.*, 1994a). The section is composed of white to grey limestone of the Maiolica Formation which is regularly intercalated with siliceous lenses and layers and contains rare marly and shaly, organic-rich intervals; it was deposited in a pelagic environment near the central zone of the Tethys (paleo-latitude ≈ 17°N for the middle Cretaceous after Scotese *et al.*, 1998). The magnetostratigraphy and ammonite biostratigraphy of this section were provided by Channel *et al.* (1995) and by Cecca *et al.* (1994a), respectively. Coccioni *et al.* (1998 employed an accurate age model for the middle part of the measured section, where they recognized the *Pseudothurmannia angulicostata* auct., *Pseudothurmannia catulloi* and *Spitidiscus hugii* ammonite zones (Fig. D.8).

The section of Gorgo a Cerbara (GC) is located

approximately 4 km east of Piobbico, along the Candigliano River (Fig. D.7; cf. Cecca *et al.*, 1994b). This outcrop represents the type locality for the Barremian-Aptian boundary (*e.g.*, Coccioni *et al.*, 1992) and consists of a lithology which is comparable to that of the FB section. As the GC section covers the entire Barremian stage (*e.g.*, Fiet and Gorin, 2000), it complements the FB section upward.

D.2.2.2. The section of the Veveyse de Châtel-Saint-Denis

The section at Veveyse de Châtel-Saint-Denis (VCD) is located in the canton of Fribourg, Switzerland (Fig. D.7) and is part of the tectonic unit "Ecaille de Riondonnaire" (Ultrahelvetic realm, northern Tethyan shelf margin; Trümpy, 1960; Busnardo *et al.*, 2003).

The measured VCD section consists of bioturbated limestones alternating with marls, and covers the time interval from the late Hauterivian (*S. sayni* zone) to the early Barremian (*Avramidiscus hugii* zone; Busnardo *et al.*, 2003). This section lacks chert and the amount of marls is higher, in comparison with the FB and GC sections.

D.2.2.3. The section of Angles

The section at route d'Angles (RA) is located in the Alpes de Haute Provence region of France (Fig. D.7) and represents the stratotype of the Barremian stage (Busnardo, 1965). The sediments of this hemipelagic section were deposited in the Vocontian Trough (*e.g.*, Baudin *et al.*, 1999).

For this section, we used the biostratigraphical scheme of Vermeulen (2002), who developed an ammonite zonation from the *Balearites balearis* zone (late Hauterivian) up to the *Martellites sarasini* zone (late Barremian); the upper part of the section (early Aptian) is not yet completely prospected, but is thought to belong to the *Deshayesites oglalensis* zone. Lithologically, the Angles section is composed of poorly bioturbated grey limestones alternating with dark marls.

D.2.3. Methods

We measured all sections in detail sampling each separate limestone bed and, where appropriate, the marl and black-shale levels. The carbonate samples were sawn in order to eliminate weathered surfaces and recrystallized areas or veins. Rock powder was obtained by using a mechanic agate crusher.

The samples of the FB, VCD, and RA sections were analyzed at the stable isotope laboratory of the Department of Mineralogy and Geochemistry at the University of Karlsruhe, Germany, using an Optima (Micromass, UK) ratio mass spectrometer equipped with an online carbonate preparation line (MultiCarb) with separate vials for each sample. Subsequent replicate sample analyses for $\delta^{13}C$ were within 0.05 to 0.06‰ and for $\delta^{18}O$ ranged from 0.06 to 0.12‰. Carbonates samples from the GC section were analyzed at the Stable Isotope Laboratory of Hydrology (UMR 8148-IDES, University of Paris Sud, Orsay, France), using a VG SIRA 10 triple collector instrument. The powdered carbonate samples were reacted with anhydrous orthophosphoric acid at 25 °C (Mc Crea, 1950). Using internal carbonate standards, the reference material NBS 19 as well as replicate analyses of samples, the reproducibility of C and O analyses was better than ± 0.05 ‰ and ± 0.08 ‰ respectively.

D.2.4. Note on the ammonite biostratigraphy used

During the last ten years, the ammonite zonation of the early Cretaceous has become more and more precise, due to the prospecting of several key sections such as the outcrops at Rio Argos (Spain) or Angles (France), and the correlation of the obtained biozonations (*e.g.*, Hoedemaeker and Rawson, 2000; Hoedemaeker *et al.*, 2003). As a consequence, the ammonite zonation currently proposed by the Kilian Group (Hoedemaeker *et al.*, 2003) is not identical with the biostratigraphy published for the FB, VCD and RA sections: the Pseudothurmannia mortilleti zone used by Vermeulen (2002) in the latest Hauterivian does not exist in the biostratigraphy of the FB section (Coccioni *et al.*, 1998), but corresponds to the upper part of the P. angulicostata auct. zone used at FB.

In table D.4, we propose a correlation between the different biostratigraphical schemes used for the

Stages	Coccioni *et al.*, 1998	Hoedemaeker & Rawson, 2000	Vermeulen, 2002	Nannofossils events (Angles section, this work)
Aptian *p.p*			*D. oglanlensis*	*Assipetra* spp. bloom
Late Barremian			*M. sarasini*	FO *R. irregularis*
			I. giraudi	
			H. feraudianus	
			G. sartousiana	
			H. sayni	FO *F. oblonga*
			H. uhligi	
Early Barremian			*C. darsi*	
			K. compressissima	
			N. pulchella	
		K. nicklesi	*K. nicklesi*	LO *C. oblongata*
	S. hugii	*A. hugii*	*A. kiliani*	
Late Hauterivian	*P. angulicostata* auct.	*P. angulicostata* auct.	*P. mortilleti*	
			S. angulicostatum	LO *L. bollii*
	B. balearis	*B. balearis*	*B. balearis*	
	P. ligatus	*P. ligatus*		
	S. sayni	*S. sayni*		

Table D.4: Synthesis of the different ammonite biostratigraphies used in the Fiume Bosso, Veveyse de Châtel Saint Denis and Angles sections (Coccioni et al., 1998; Busnardo et al., 2003; Vermeulen, 2002, respectively). Nannofossils bioevents from Angles are also reported (S. Gardin, this work).

VCD, FB and RA sections. For the VCD section, we use the zonation of Hoedemaeker and Rawson (2000) instead of scheme adopted by Busnardo *et al*. (2003), in order to facilitate the comparison between all studied sections.

D.2.5. Results

D.2.5.1. The sections of Fiume Bosso and Gorgo a Cerbara

The carbon isotope curve obtained for the FB section (Fig. D.8) shows a rather regular behavior for the lower part of the measured section, with $\delta^{13}C$ mean values increasing from 1.7 up to 2.15‰ (P. catulloi zone). The Faraoni level itself is characterized by a positive shift of approximately 0.15‰. In the upper part of the measured section, $\delta^{13}C$ mean values range between 1.8‰ and 1.9‰.

The $\delta^{18}O$ curve displays variations with a similar frequency, and with a range of mean values from –2.45 to –2.15‰.

The $\delta^{13}C$ record in sediments of the GC section displays a slight increase from approximately 2.2 to 2.7‰ (Fig. D.9). The general trend towards more positive values is superimposed by two negative excursions in sediments corresponding to the middle of the CM3 and to the interval around the Barremian – Aptian boundary.

The $\delta^{18}O$ curve shows a slight decrease from the base of the section up to sediments corresponding to the end of the CM3; in the following, the $\delta^{18}O$ record evolves slowly towards heavier values.

D.2.5.2. The section of the Veveyse de Châtel-Saint-Denis

In the lower part of the measured section (S. sayni zone up to the base of the Pseudothurmannia angulicostata zone), a slow and steady increase from 0.85 to 1.15‰ characterizes the main trend of

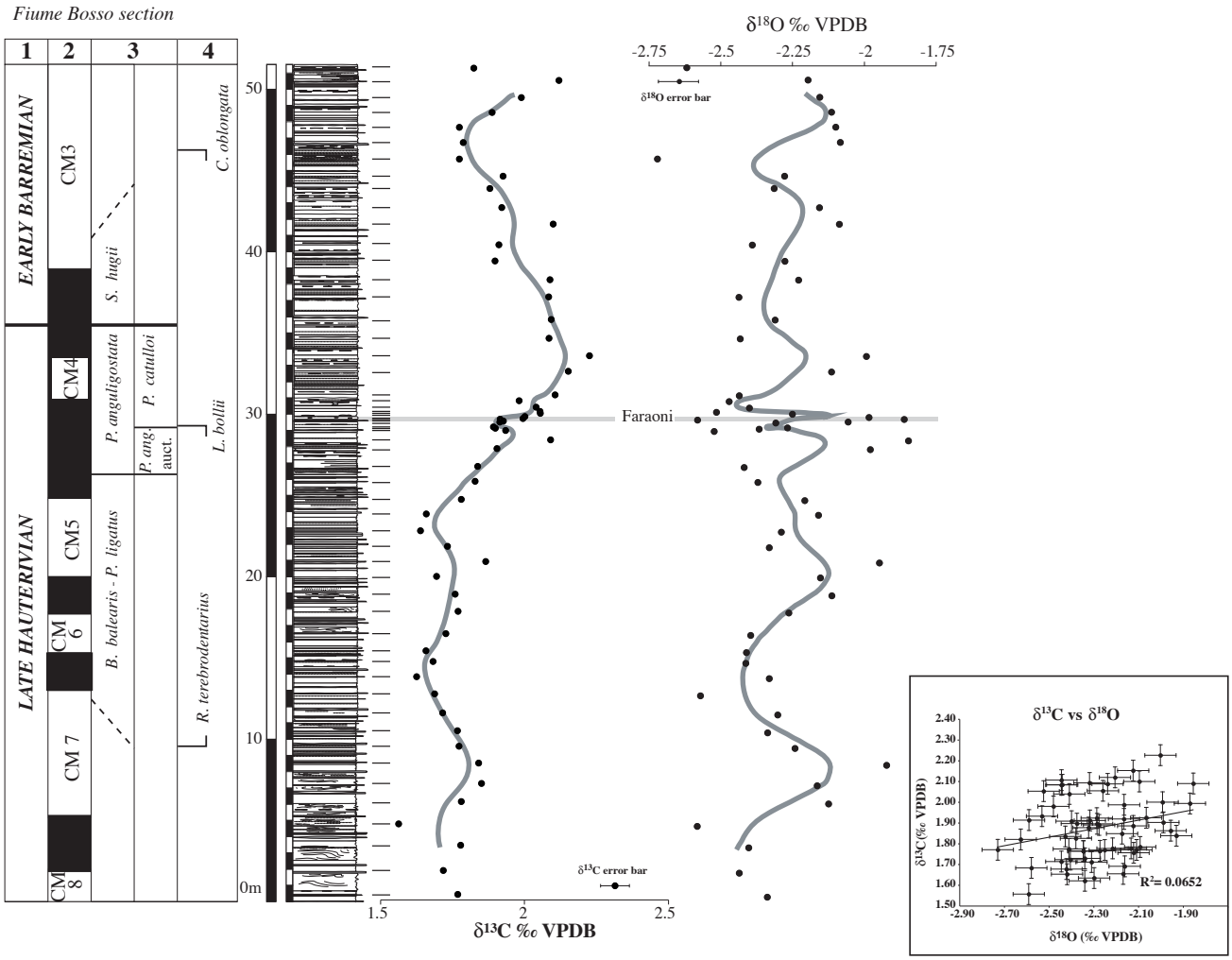

*Fig. D.8: δ[13]C and δ[18]O curves obtained from whole-rock carbonate samples (n = 59) of the Fiume Bosso section. Numbers on top of the columns refer to **1:** stages; **2:** magnetostratigraphy from Channell et al. (1995); **3:** ammonite zonation after Coccioni et al. (1998); **4:** nannofossil bioevents (this work). The grey line represents the five point moving average curve.*

the curve (Fig. D.10). In the overlying sediments of the P. angulicostata zone, the positive gradient in $\delta^{13}C$ curve becomes steeper, with a positive shift of about 0.5‰ in sediments in the vicinity of the "Couche à Poissons", which is considered as an equivalent of the Faraoni level (Busnardo *et al.*, 2003). The $\delta^{13}C$ curve reaches a maximum of approximately 1.35‰ in sediments just below the Hauterivian-Barremian boundary. In the uppermost part of the measured section the $\delta^{13}C$ curve shows a slight decreasing trend with values diminishing from 1.35 to 1.05‰.

The $\delta^{18}O$ curve is characterized by a general trend toward heavier values, from approximately –2.7‰ to –2.1‰, which seems to be superimposed by a shorter interval in sediments of the early *P. angulicostata* zone, where the trend in $\delta^{18}O$ is stable or even directed towards lighter values.

D.2.5.3. The section of Angles

The $\delta^{13}C$ curve displays a slight increase for sediments belonging to the B. balearis and Spathicrioceras angulicostatum zones (from 1 to 1.4‰; Fig. D.11); the data corresponding to the Faraoni equivalent display an acceleration of the general increase before a stabilization of the signal. After a decrease of 0.2‰ in the P. mortilleti and the *A. kiliani* zones, the $\delta^{13}C$ curve displays an irregular evolution from the *K. nicklesi* to *K. compressissima* zone. Sediments attributed to the *C. darsi* zone show an increase in $\delta^{13}C$ values from 1.3 to 1.8‰, whereas sediments from the *Holcodiscus uhligi* to *Gerhardtia sartousiana* zones display a more stable albeit a slightly increasing set of values. The $\delta^{13}C$ curve shows an increase for sediments of the Hemihoplites *feraudianus* zone, followed by a decrease from 2.25 to 1.75‰ for sediments

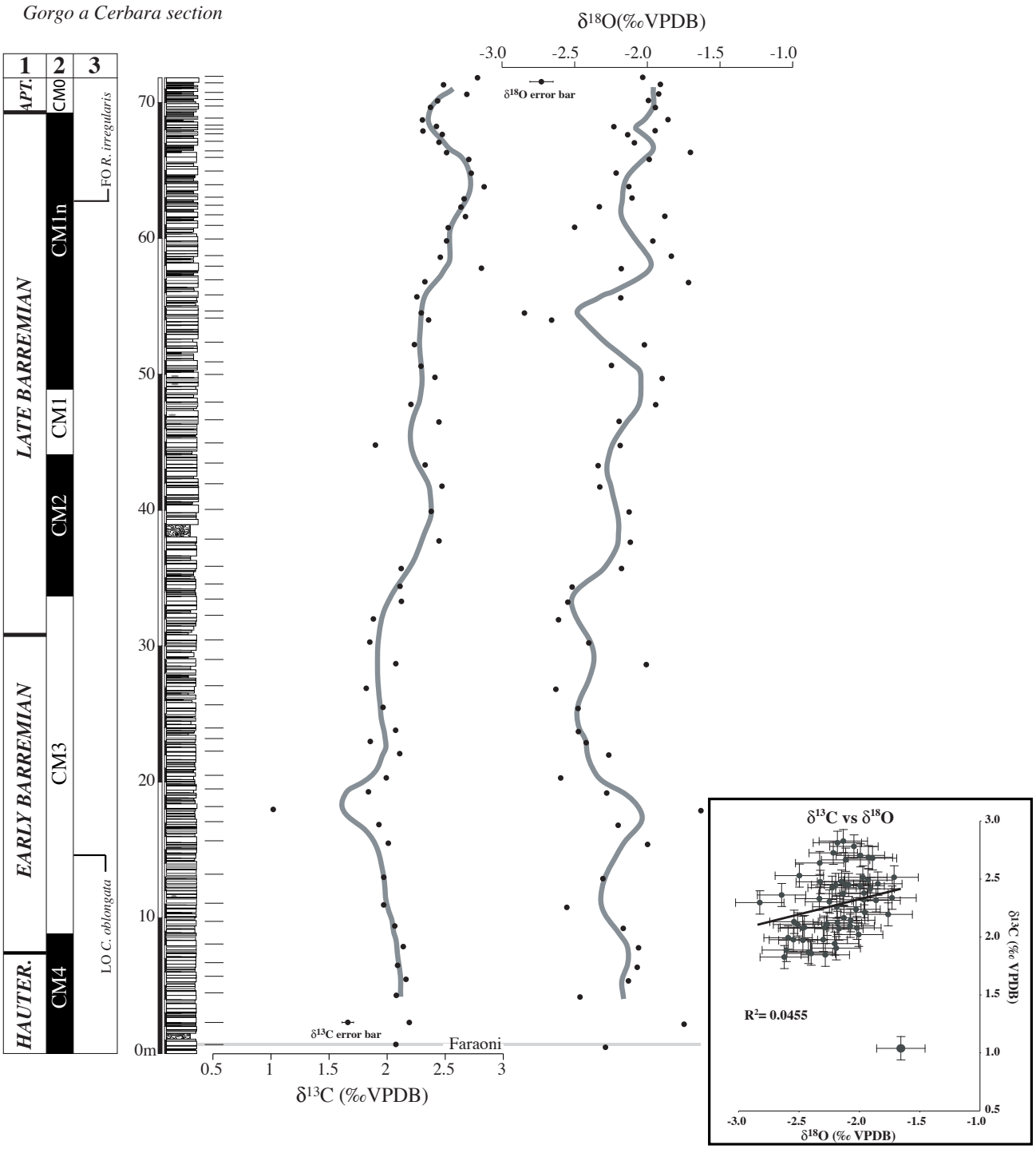

*Fig. D.9: $\delta^{13}C$ and $\delta^{18}O$ curves obtained from whole-rock carbonate samples (n = 60) of the Gorgo a Cerbara section. Numbers on top of the columns refer to **1:** stages; **2:** magnetostratigraphy after Lowrie and Alvarez (1984), Erba (1996) and Channell et al. (1995), as reported in Fiet and Gorin (2000); **3:** bioevents after Cecca et al. (1995). The grey line represents the five point moving average curve.*

belonging to the *I. giraudi* and *M. sarasini* zones. The $\delta^{13}C$ trend increases again to 2.25‰ in sediments of the D. oglanlensis zone, thereby marking a minimum precisely at the Barremian – Aptian boundary.

The evolution of the $\delta^{18}O$ curve is more variable, with a double negative peak from –3 to –4.15‰ near the base of the measured section. Then, the $\delta^{18}O$ record slowly increases in sediments belonging to the latest Hauterivian and remains rather stable for sediments in the remainder of the Hauterivian and the lower part of the early Barremian. In sediments from the N. pulchella to the *H. sayni* zone, the $\delta^{18}O$ trend is negative, with a minimal value of about –4.15‰ reached

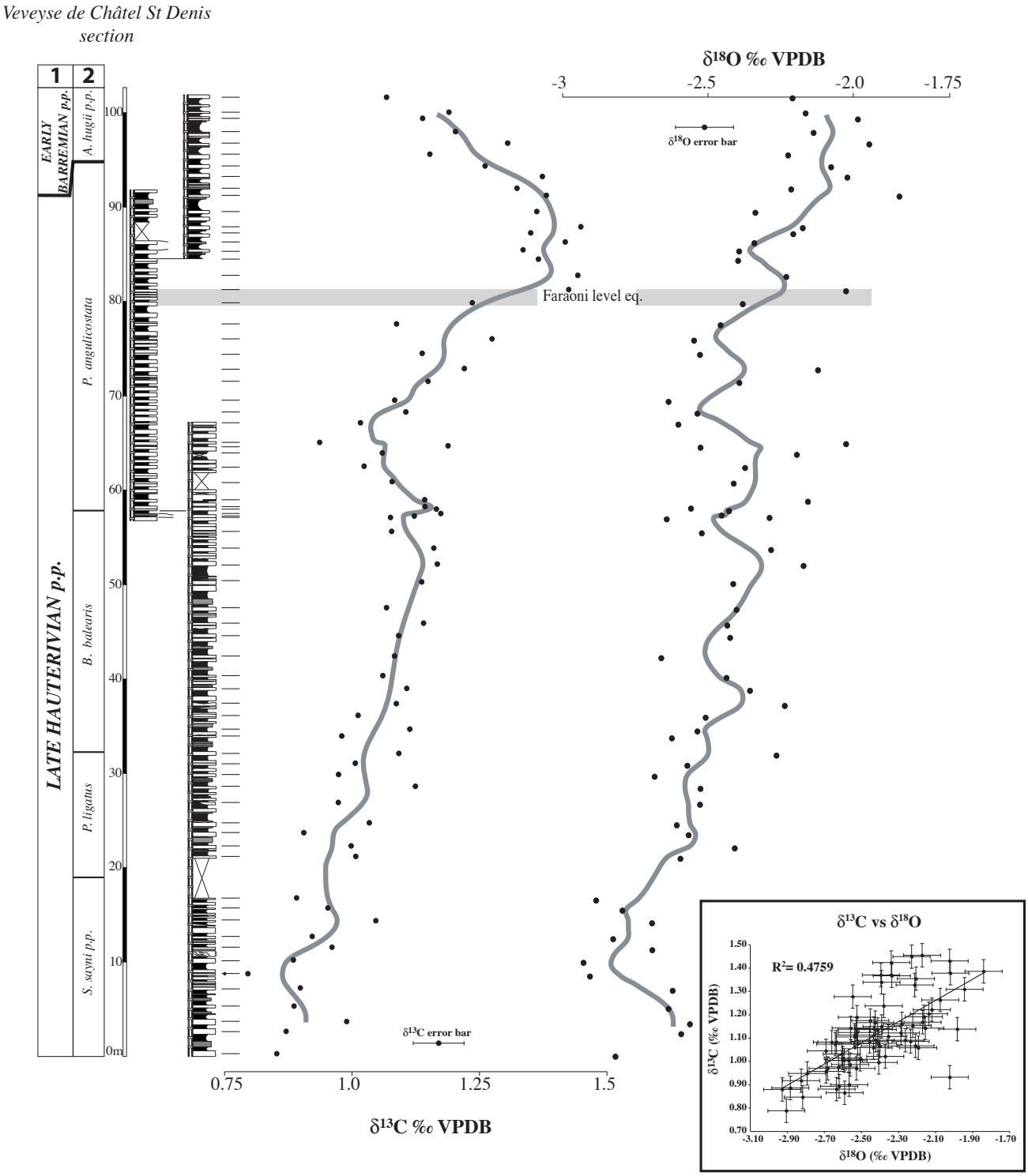

*Fig. D.10: δ[13]C and δ[18]O curves obtained from whole-rock carbonate samples (n = 41) of the Veveyse de Châtel Saint Denis section. Numbers on top of the columns refer to **1:** stages; **2:** ammonite zonation modified after Busnardo et al. (2003). The grey line represents the five point moving average curve.*

in sediments of the *H. sayni* zone. The subsequent positive trend in $\delta^{18}O$ values lasts until the base of the *I. giraudi* zone, where the $\delta^{18}O$ curve reaches a value of –2.75‰. The uppermost part of the $\delta^{18}O$ curve displays a decrease toward the lowest values of the measured section (–4.18‰).

D.2.6. Discussion

D.2.6.1. Stable isotopes and diagenesis

$\delta^{18}O$-$\delta^{13}C$ cross plots reveal a lack of correlation between the trends in oxygen and carbon isotopes for all sections (R^2 = 0.0652, 0.0686, 0.4759, and 0.041 for the FB, GC, VCD and RA sections,

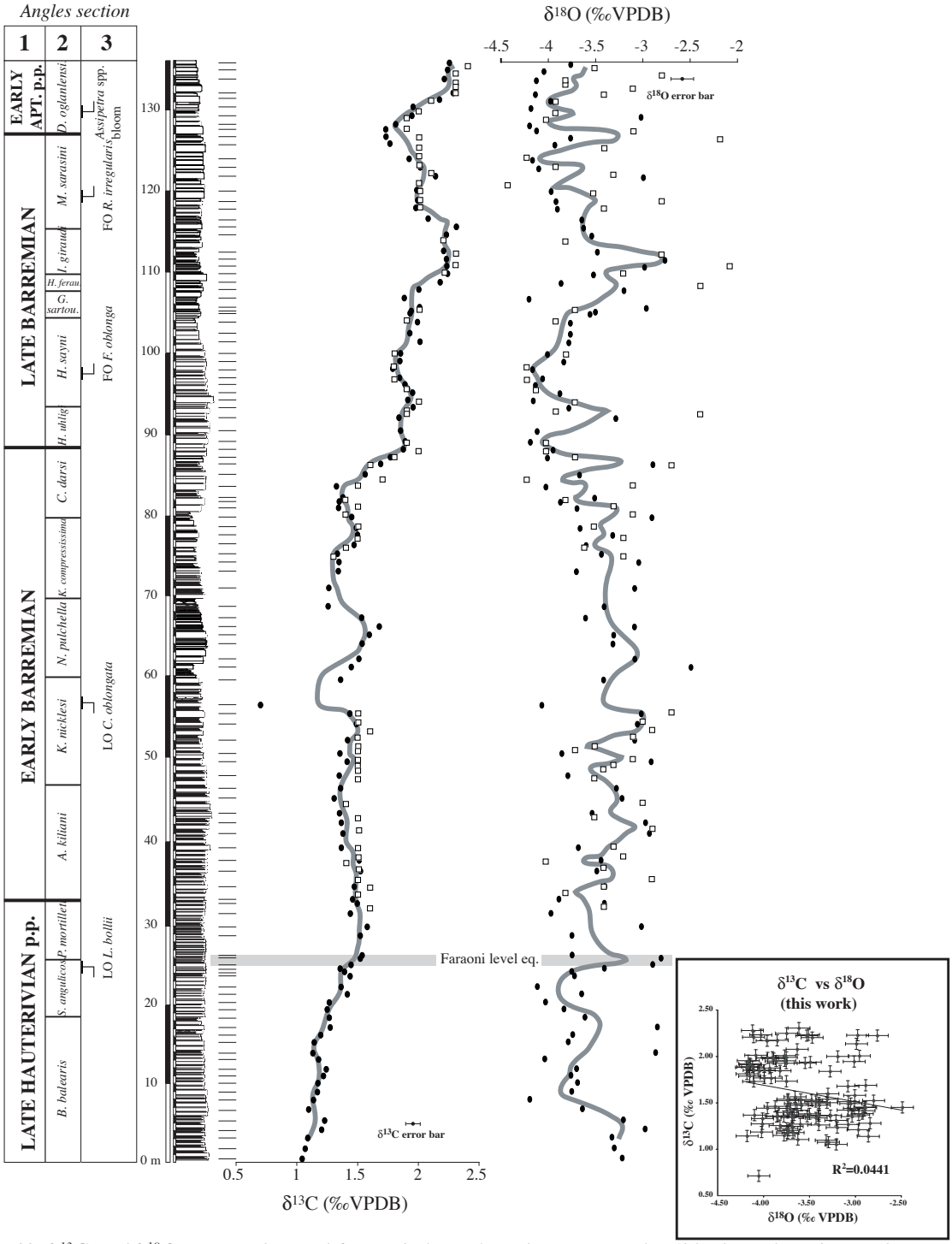

*Fig. D.11: δ[13]C and δ[18]O curves obtained from whole-rock carbonate samples (black circles: this study, n = 116; white square: data from Wissler et al., 2002) of the Angles section. Numbers on top of the columns refer to **1:** stages; **2:** ammonites zonation after Vermeulen (2002); **3:** nannofossils bioevents (this work). The grey line represents the five point moving average curve. Note the complementarity of the data of Wissler et al. (2002) and of this study.*

respectively; Fig. D.8 to D.11); the good correlation between the $\delta^{18}O$ and the $\delta^{13}C$ record at VCD may reflect the comparable evolution of both proxies during the late Hauterivian, as previously described by van de Schootbrugge *et al.* (2000). Moreover, the results obtained are coherent with values for open marine carbonates from previous studies (*e.g.*, Weissert and Erba, 2004; van de Schootbrugge *et al.*, 2000; Fig. 8 in Weissert, 1989). We assume therefore that for the four studied sections, diagenetic transformations had little impact on the carbon isotopic system.

The oxygen isotope record of the RA section, however, appears to be affected by slight diagenetic

change: the $\delta^{18}O$ values are systematically lighter by approximately 1-1.2‰ in comparison with the other sections analyzed here or even to the Hauterivian part of the Vergons section (van de Schootbrugge *et al.*, 2000). This is consistent with the burial history of the RA section, which is part of the Digne thrust system and has been exposed to higher burial temperatures during alpine deformation (*e.g.*, van de Schootbrugge *et al.*, 2000). Thus, paleotemperatures can not be deduced from the absolute $\delta^{18}O$ values of RA, whereas trends in $\delta^{18}O$ may be used for correlation, as diagenesis did not totally reset the isotopic system as shown by the value of R^2 at RA and by the preservation of the clay mineral assemblage (Bodin *et al.*, 2006).

The $\delta^{18}O$ records for the Italian and Swiss sections show rather high and probably only mildly altered oxygen isotopic values, which is again consistent with their tectonic history. We will refrain from an indepth discussion of the trends discerned and only mention the long-term trend in $\delta^{18}O$ values.

D.2.6.2. Evolution of the $\delta^{13}C$ record during the late Hauterivian and Barremian

The integration of geochemical, biostratigraphic and magnetostratigraphic data allows us to correlate and to describe general trends in the evolution of the $\delta^{13}C$ record for the time span between the S. sayni and the D. oglanlensis. In Fig. D.12, several time lines support our correlation between the Umbria-Marche basin, the Ultrahelvetic realm, and the Vocontian trough: (1) the top of the *B. balearis* ammonite zone between the VCD, FB, and RA sections; (2) the Faraoni level, which is considered to result from a synchronous anoxic event; this level is well approximated by the LO of nannofossil *L. bollii* at FB, RA, GC and Cismon; (3) the Hauterivian-Barremian boundary which is defined by means of ammonites in the VCD, RA, and FB sections; (4) the early / late Barremian boundary which is defined by ammonites at RA and by magnetostratigraphy, ammonites and nannofossils at GC and Cismon; and (5) the Barremian-Aptian boundary, which is defined by magnetostratigraphy and nannofossil biostratigraphy (FO of *R. irregularis*) in the GC section and the Cismon core, and by ammonite and nannofossil biostratigraphy in the RA section.

The trend in $\delta^{13}C$ values for the late Hauterivian appears to be marked by a stable long-term trend towards slightly higher values, which becomes more accentuated during the *P. angulicostata* zone. A maximum in $\delta^{13}C$ values for the late Hauterivian is reached in the upper *P. angulicostata* zone (VCD section), just above the Faraoni level. This implies that this level is placed within the slope of a positive increase in $\delta^{13}C$, with an amplitude of 0.5-0.8‰. This positive shift was already observed in the Vergons section, near the RA section (Baudin *et al.*, 1999; van de Schootbrugge *et al.*, 2000), and is thought to be characteristic of the Faraoni level. The short-lived negative excursion observed within the organic-rich Faraoni level of the FB section (Fig. D.8), which exhibits TOC values of up to 25% (Coccioni *et al.*, 1998), is interpreted here to reflect a local, early diagenetic signal due to the mineralization of organic carbon during bacterial sulfate reduction (*e.g.*, Raiswell and Fisher, 2004).

The evolution of the $\delta^{13}C$ record during the early Barremian is illustrated by a trend toward more negative values in the *A. kiliani* zone (RA section), which is followed by an irregular long-term trend with no discernible gradient. The top of the early Barremian (*C. darsi* zone) is again marked by a positive gradient of about 0.4% (RA section).

The $\delta^{13}C$ record during the late Barremian shows an irregular long-term trend towards more positive values followed by a negative gradient. The Barremian-Aptian boundary is marked by a minimum in $\delta^{13}C$ values in both the RA and GC sections.

We also compared our results with the $\delta^{13}C$ record established for the Cismon Apticore (Fig. D.12; Erba *et al.*, 1999) and from this correlation it appears that the identification of the early – late Barremian boundary in the RA, GC and Cismon sections is not coherent. At RA, this boundary is defined by ammonites, and corresponds to the end of a positive shift of the $\delta^{13}C$, whereas at GC this boundary is located in the upper part of the CM3 chron (Channell *et al.*, 1995), just below the beginning of a positive shift**,** which seems comparable to the positive

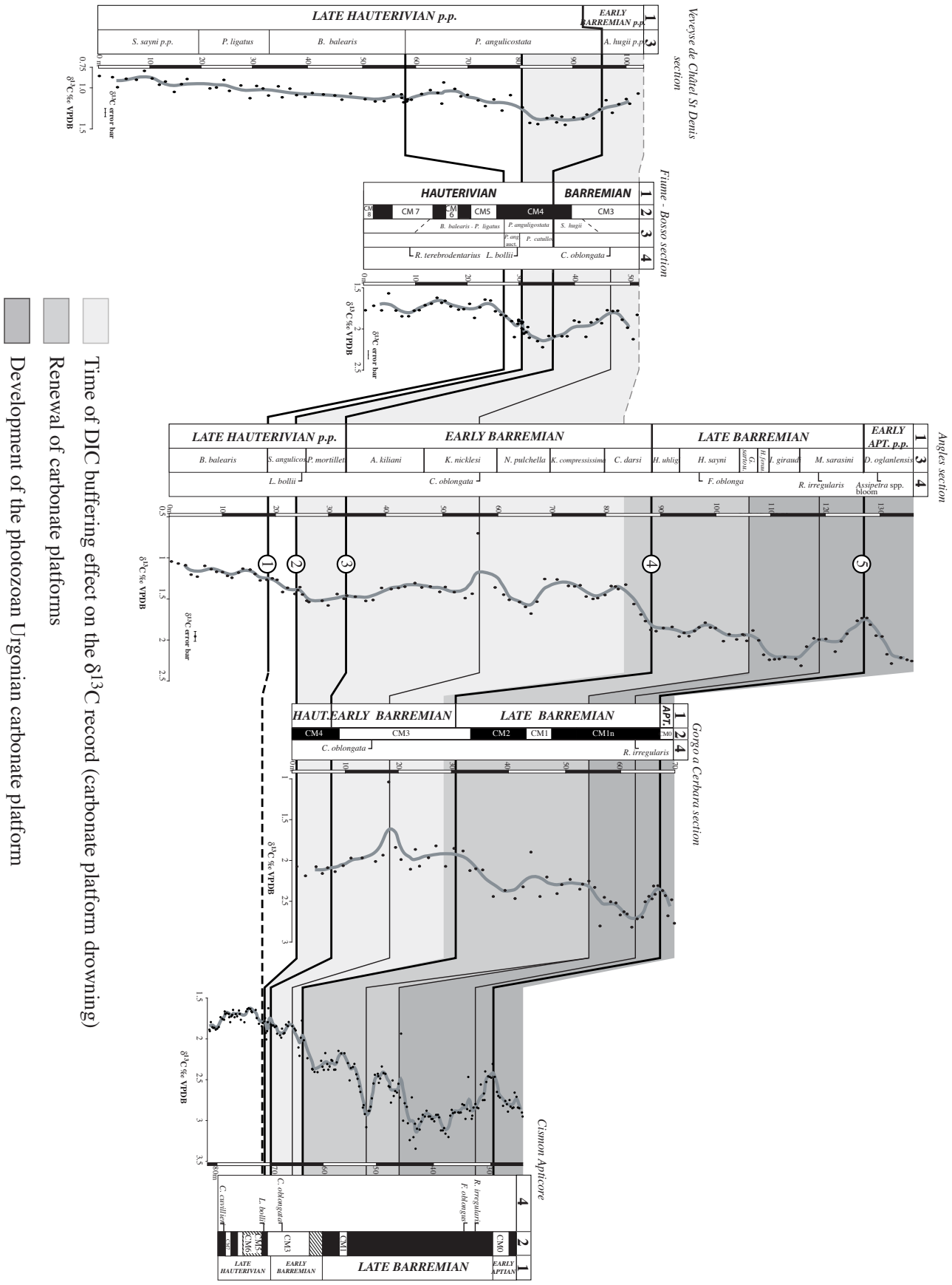

*Fig. D.12: Correlation of the Veveyse de Châtel Saint Denis, Fiume Bosso, Angles, Gorgo a Cerbara and Cismon Apticore $\delta^{13}C$ curves. Numbers on top of the columns of each section refer to **1:** stages; **2:** magnetostratigraphy of the FB (Channell et al., 1995), CG (Lowrie and Alvarez, 1984; Channell et al., 1995; Erba, 1996) sections and Cismon Apticore (Erba et al., 1999); **3:** ammonite zonation of the VCD (Busnardo et al., 2003), FB (Coccioni et al., 1998) and RA (Vermeulen, 2002) sections; **4:** nannofossils bioevents of the FB, RA (this work), CG (Cecca et al., 1995) sections and Cismon Apticore (Erba et al., 1999). Numbers on the time-lines refer to the numbering used in the text.*

shift observed at RA. At Cismon, the location of the early-late Barremian boundary with respect to the positive shift of the $\delta^{13}C$ curve is identical to RA; however a discrepancy occurs between the magnetostratigraphic records from GC and Cismon, as the early-late Barremian boundary is located several meters above the boundary between the CM3 and CM2 magnetozones at Cismon.

The correlation of the RA and GC sections with the Cismon record shows a further discrepancy: Wissler *et al*. (2002) already called into question the continuity of the record at RA and, in particular, proposed the presence of a significant hiatus in sediments attributed to the *I. giraudi* zone, and inferred the absence of up to 50% of the entire Barremian stage in the stratotype of the Barremian. In the RA section, the *I. giraudi* zone is characterized by a positive shift ($\Delta\delta^{13}C$ = 0.35‰), which is also easily recognizable at GC and Cismon with amplitudes of 0.28 and 0.45‰, respectively. On the other hand, just below the above-mentioned positive shift, the $\delta^{13}C$ curve at Cismon displays a negative excursion, which is not recorded at RA. Based on these observations, it seems that either condensation or omission may have occurred in sediments belonging to the G. sartousiana or the *H. feraudianus* zones of the RA section. These phenomena may be linked to the maximum flooding surface of the B3 sequence, which is expressed by a glauconitic level within the G. sartousiana zone, or to the sequence boundary B4, a major sequence boundary in south-eastern France located in the *H. feraudianus* zone (Arnaud *et al*., 1998).

Alternatively, normal (syn-sedimentary?) faults led to the formation of a decametric graben in the H. sayni zone of the Angles section. It is therefore possible that a hiatus, coinciding with the first positive excursion of the Cismon section, is present within this zone. Further investigations are needed to solve this question.

D.2.6.3. Evolution of the $\delta^{18}O$ record during the late Hauterivian and Barremian

In Fig. D.13, the correlation of the $\delta^{18}O$ curves from the RA, VCD, and GC sections allows to define major trends in the evolution of the $\delta^{18}O$ during the late Hauterivian and the Barremian. We do not consider the FB section because it covers a relatively short time-period, and does not add essential information with regards to the long-term trend in $\delta^{18}O$ values. The late Hauterivian and a part of the early Barremian (until the *K. nicklesi* zone; data from the VCD and the RA sections) are characterized by an increase of approximately 1.1‰. The later is followed by a decreasing trend which lasted until the base of the *H. sayni* zone, with values reaching – 4.1‰ at Angles. The beginning of the late Barremian is characterized by a positive trend ($\Delta\delta^{18}O$ = 1.1‰) with a maximum located near the base of the *I. giraudi* zone (RA section). Finally, the $\delta^{18}O$ record shows a decreasing trend for the latest Barremian and the earliest Aptian.

The increasing trend during the late Hauterivian may be linked to the installation of a marine passage between the boreal and the tethyan realms. Indeed, Mutterlose and Bornemann (2000) described the arrival of tethyan faunas in lower Cretaceous sediments from northern Germany, in particular in the latest Hauterivian. This implies that a connection came into place between the Tethys and the boreal region during the late Hauterivian (Fig. 20 in Mutterlose and Bornemann, 2000), which through the exchange of water masses may have led to relatively high $\delta^{18}O$ values observed in the late Hauterivian – early Barremian. This hypothesis is also supported by the presence of boreal nannofossil species at Angles in sediments of the P. mortilleti and A. kiliani zones. Alternatively, the $\delta^{18}O$ trend may reflect an increased salinity which would be in agreement with the enhanced evaporation and the subsequent increased continental weathering deduced from the kaolinite evolution during the latest Hauterivian and the early Barremian (Bodin *et al*., 2006).

The return to more negative values in sediments from the *N. pulchella* to the *H. sayni* zones at RA (*i.e*., middle of CM3 to the base of CM2 at GC) may indicate the end of the interaction between boreal and tethyan water masses, and consequently the return to warmer oceanic temperatures; this would be in agreement with a short-term eustatic minimum (Haq *et al*., 1987).

Finally, the $\delta^{18}O$ curve forms a maximum which is located in the I. giraudi zone (RA section). This appears to be synchronous with a short-term

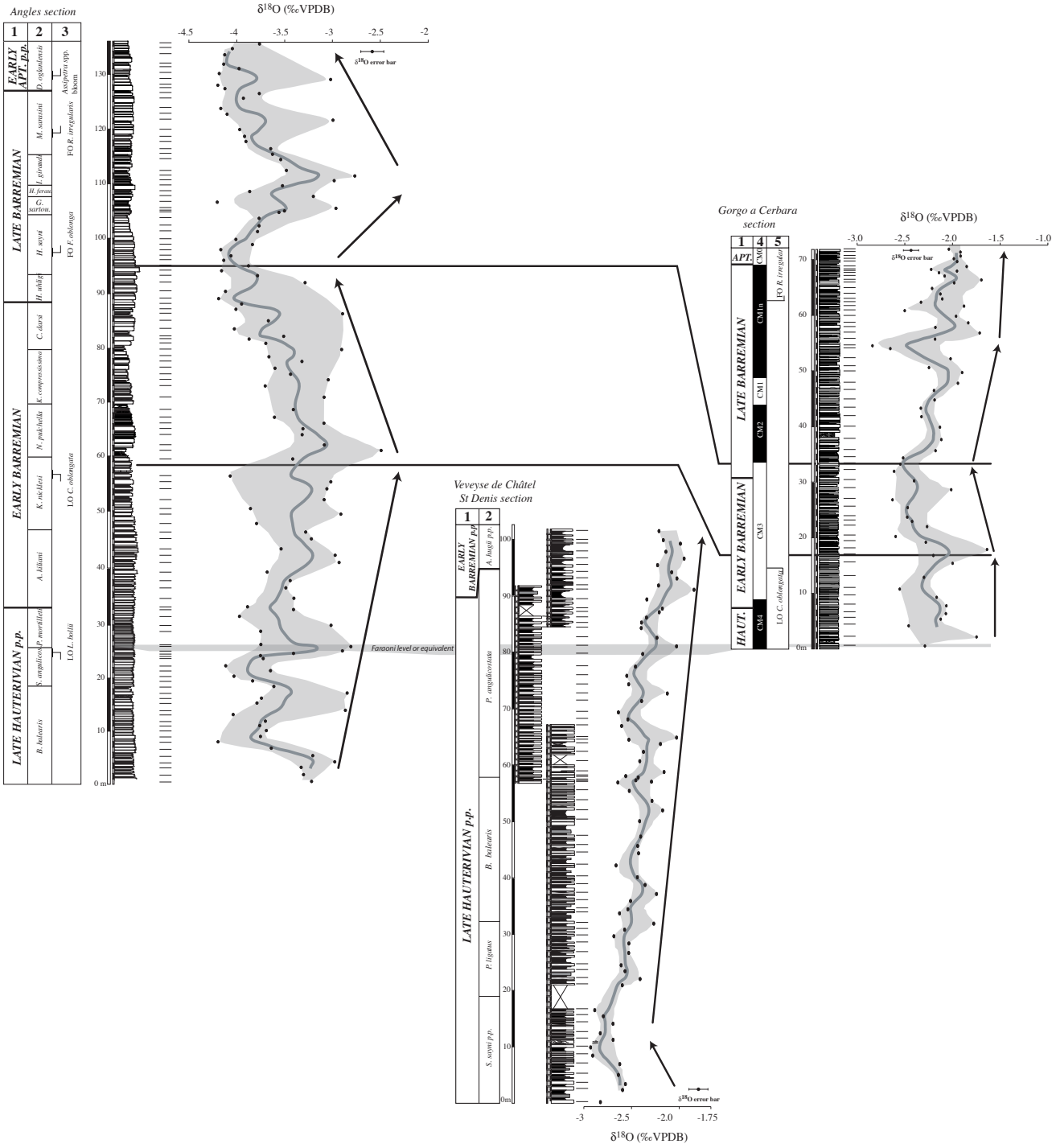

*Fig. D.13: Correlation of the $\delta^{18}O$ curves from the Angles, Veveyse de Châtel Saint Denis and Gorgo a Cerbara sections. Numbers on top of the columns of each section refer to **1:** stages; **2:** ammonite zonations of the RA (Vermeulen, 2002) and VCD (modified after Busnardo et al., 2003) sections; **3:** nannofossils bioevents (this work); **4:** magnetostratigraphy of GC (Lowrie and Alvarez, 1984; Channell et al., 1995; Erba, 1996; Fiet and Gorin, 2001); **5:** nannofossils bioevents of the CG section (Cecca et al., 1995). The dark grey lines represent the five points moving average curves. The light grey areas represent the scattering of the minima and maxima values.*

eustatic maximum that would have led to the arrival of cooler water in the Tethys and a corresponding positive shift of the $\delta^{18}O$ curve. However, boreal nannofloras were not detected in this interval and therefore the trend towards higher values may also be due to climate cooling, in the absence of water-mass exchange between the Tethyan and the boreal realms.

These observed trends are in agreement with the trends of the $\delta^{18}O$ curve obtained from belemnites by Podlaha *et al.* (1998), Veizer *et al.* (1999), or by van de Schootbrugge *et al.* (2000), who observed the heaviest $\delta^{18}O$ values of the

entire early Cretaceous during the Hauterivian, whereas the Barremian is characterized by an initial warming phase followed by a cooling phase. Moreover, the trend we observe is coherent with published early Cretaceous $\delta^{18}O$ curve (Weissert and Erba, 2004). This thermal evolution during the Barremian is also reported from fish tooth enamels analysis by Pucéat *et al.* (2003), although the low-resolution of their study - probably due to the scarcity of fish teeth in sediments - does not allow a precise correlation between their results and the curves presented therein. Finally, the shift toward more negative values recorded at Angles from the I. giraudi zone to the top of the section, may correspond to the lower part of the negative shift recorded by rudists in the latest Barremian-earliest Aptian (Steuber *et al.*, 2005).

D.2.6.4. Possible mechanisms driving the evolution of the $\delta^{13}C$ values during the late Hauterivian and Barremian

In a classical sense, the evolution of the carbonate $\delta^{13}C$ record is interpreted as an approximation of the ratio between carbonate carbon and organic carbon burial fluxes in marine environments and their associated changes (*e.g.*, Scholle and Arthur, 1980; Weissert, 1989; Weissert *et al.*, 1998). External factors such as the release of methane from clathrate dissociation in slope environments (*e.g.*, Dickens *et al.*, 1995, 2002)), atmosphere-ocean exchange of CO_2 (including volcanic activity; *e.g.*, Weissert and Erba, 2004), and the influx of terrestrial organic matter may also influence this record as well (*e.g.*, Cerlings *et al.*, 2003).

A new approach in the interpretation of marine carbonate $\delta^{13}C$ records is given by a linkage in the style and intensity of shallow-water carbonate production and the rate of export of shallow-water carbonates into the basin environment, levels of dissolved inorganic carbon (DIC) in open oceans, and the $\delta^{13}C$ record (*e.g.*, Bartley and Kah, 2004; Swart and Eberli, 2005).

The latest Hauterivian is characterized by an increase in the $\delta^{13}C$ record ($\Delta\delta^{13}C$ = 0.5 – 1‰), which reaches a maximum just before the Hauterivian-Barremian boundary. The Faraoni level and its equivalents are localized in the middle of this positive gradient. Even if the $\delta^{13}C$ excursion does not have the same amplitude as the excursions associated with the oceanic anoxic events during the Valanginian, Aptian, and late Cenomanian (*e.g.* Lini *et al.*, 1998; Herrle *et al.*, 2004; Keller *et al.*, 2004, respectively), the trend towards more positive values could still be explained by a shift in the burial ratio of organic carbon and carbonate carbon, as is suggested by the Faraoni anoxic event and the coeval onset in platform demise along the northern Tethyan margin. It remains, however, to be seen in how far this event has had an impact on the global carbon cycle. The Faraoni level is mainly known from the western Tethyan realm (Baudin *et al.*, 1999, 2002). Recently, a possible equivalent was described from the northwestern Pacific realm (Planck *et al.*, 2000), which would imply that the extent of this event is more important than previously assumed. If indeed the Faraoni oceanic anoxic event is implied in this small positive shift in $\delta^{13}C$ values, an explanation for the attenuated isotope signature needs to be found. In following Bartley and Kah (2004) we suggest that the attenuating effect may have been related to the increased size of the oceanic DIC reservoir.

Two principal processes may have enhanced the DIC reservoir during the late Hauterivian: (1) clay mineral studies in sections of late Hauterivian and Barremian age of the northern and the southern Tethyan margin in western Europe show systematic increases in kaolinite contents in the late Hauterivian, which may indicate a change of the climate towards warmer and more humid conditions for this time period (Ruffell and Batten, 1990; Deconinck and Bernouilli, 1991; Bodin *et al.*, 2006). Such climate conditions are favorable for increasing rates of DIC mobilization via biogeochemical weathering and throughput of DIC into the ocean by enhanced river transport (Holmden *et al.*, 1998). During the late Hauterivian, the threefold evolution of ammonite fauna linked to sea-level fluctuations (Company *et al.*, 2005) may reflect the enhanced and facilitated export of DIC; (2) a widespread platform drowning event that started during the latest Hauterivian along the northern Tethyan margin may also have contributed to an increase in the oceanic DIC reservoir through the decrease in shallow-water carbonate production – a potential sink of DIC- and a corresponding increase in ocean alkalinity (*e.g.*,

van de Schootbrugge *et al.*, 2003). The increased oceanic DIC reservoir may have been sustained throughout most of the early Barremian, paralleled by persisting drowning conditions on the northern Tethyan platform, and this may explain the rather steady evolution in the $\delta^{13}C$ record throughout the early Barremian.

The positive shift in the $\delta^{13}C$ record close to the early–late Barremian transition ($\Delta\delta^{13}C$ = 0.5-0.7‰) is more difficult to be explained in terms of changes in the burial ratio of organic and carbonate carbon, since to our knowledge no major change in organic carbon output has been documented from this time interval. We propose to link this shift to an important change in the shallow-water platform carbonate factory, which is documented from the northern Tethyan margin and elsewhere: the platform drowning episode that started in the latest Hauterivian and ended near the early-late Barremian boundary (S. Bodin, pers. com.) marks the transition between carbonate production dominated by heterozoans ("green water" or foramol facies; Föllmi *et al.*, 1994; Mutti and Hallock, 2003) and photozoans ("blue water" or chlorozoan facies). This transition is documented by the widespread installation of the so-called "Urgonian" facies in France and Switzerland, which is, for example, also documented from the Cupido and Coahuila carbonate platforms of northeastern Mexico, where peritidal shelf-lagoonal carbonate deposits are formed during the late Barremian and Aptian (Bralower *et al.*, 1999; Lehman *et al.*, 1999; see also Ager, 1981), and from the Jebel Akhdar in northeastern Oman where the installation and subsequent progradation of shallow-water carbonate platforms is observed during the Barremian (Masse *et al.*, 1997; Hillgärtner *et al.*, 2003).

The principal carbonate mineral produced by heterozoan assemblages, which – in the helvetic realm - are dominated by crinoidal remains, is calcite, whereas photozoan assemblages also produced aragonite during the early Cretaceous (corals and associated rudists, green algae, etc.; *e.g.*, Stanley and Hardie, 1998; Steuber, 2002). Aragonite tends to be enriched in ^{13}C relative to calcite and $\delta^{13}C_{aragonite}$ may reach values of up to 5‰ (*e.g.*, Romanek *et al.*, 1992; Swart and Eberli, 2005). If produced by green algae, aragonite consists of a fine-grained material that is readily transported and exported into adjacent basins, where it is either dissolved in the water column or integrated into peri-platform sediments (*e.g.*, Droxler *et al.*, 1983; Swart and Eberli, 2005). The increased export of meta-stable, ^{13}C-enriched particulate inorganic carbon (PIC) in the form of aragonite with the renewal of photozoan assemblages may have influenced the $\delta^{13}C$ record from the early-late Barremian transition, in particular through the installation of the Urgonian-type platforms in the *G. sartousiana* zone. This is coherent with the Phosphorus Mass Accumulation Rate evolution during this period (Bodin *et al.*, 2006): the onset of photozoans may be coeval with oligotrophic conditions, which is in agreement with Mutti and Hallock (2003). Moreover, the arrival of photozoan carbonate platforms around the Tethys in the middle late Barremian may have led to a decrease in the oceanic DIC reservoir implicitly diminishing the DIC buffering effect. This we relate to the possible reduction in the throughput of DIC via the platform because of its transformation and storage by carbonate-producing organisms and because of the rather closed architecture of the platform, which is usually rimmed towards the basin by patch reefs and/or oolithic shoals. Consequently, the oceanic C-system would have become more sensitive to paleoceanographic and / or paleoecological perturbations, in particular to the export of material that holds a more positive $\delta^{13}C$ signature.

The negative excursion in $\delta^{13}C$ values of approximately 0.5‰ at the Barremian-Aptian boundary is in our view related to a widespread decrease in kaolinite and an increase of detrital input in general registered along the northern Tethyan margin and elsewhere, and a corresponding temporary disappearance of the Urgonian facies (*e.g.*, Ruffell and Batten, 1990; Weissert, 1990). The corresponding increase in continentally derived DIC and decrease in shallow-water carbonate production may have contributed to this negative excursion. The involvement of increased methane release from slope environments cannot be excluded either (*e.g.*, Dickens *et al.*, 1995; Jenkyns, 2003), even though direct evidence is lacking.

D.2.6.5. Quantification of the carbonate

platform exportation and its influence on the pelagic record

In order to quantify the impact of the export of aragonite and/or calcite from the platform to the basin, we calculated theoretical $\delta^{13}C$ values that would result from an increasing input of platform-derived calcite or aragonite into the pelagic environment.

Concerning the platform, we estimated the volume of carbonates produced by using the surface covered by neritic carbonates during the early Aptian (Philipp, 2003), and assuming a sedimentation rate of 5 cm.ky^{-1} (Föllmi *et al.*, 1994; Hillgärtner *et al.*, 2003). Using paleomaps of the Tethyan realm, Philip (2003) estimated that the deposition of neritic carbonates was mainly limited to intertropical seas, and that they covered an area of approximately 4.63×10^6 km^2 in the early Aptian. Presently, reefs are estimated to represent an area of only 247,000 km^2 (Burke *et al.*, 1998). The importance of late early Cretaceous shallow-water carbonate production relative to today points to a potentially significant influence on the oceanic carbon-cycle during the early Cretaceous. In this estimation we used a $\delta^{13}C_{calcite}$ value of 1‰ and a $\delta^{13}C_{aragonite}$ value of 5‰ (Swart and Eberli, 2005).

For the pelagic production, we estimated the area covered by the Tethys as the average of the late Tithonian and early Aptian areas (Fourcade *et al.*, 1993; Masse *et al.*, 1993). Then, the volume of carbonate produced per ky and per km^2 was estimated from the sedimentation rate recorded during the late Barremian in the RA section, assuming that $CaCO_3$ represents on average, approximately 73% of the total pelagic sedimentation (Munnecke *et al.*, 2001).

For both parts of the model we quantify both the quantity of ^{12}C and ^{13}C produced, then we calculate a theoretical $\delta^{13}C$ (noted $\delta^{13}C_{theo}$) that takes into account the influence of the platforms. So the variable parameters are the rate of export (τ) under particulate or dissolved form, and the $\delta^{13}C$ that would be recorded in the basin without any influence from the platforms ($\delta^{13}C_{ini}$).

The results (Fig. D.14) show that during time

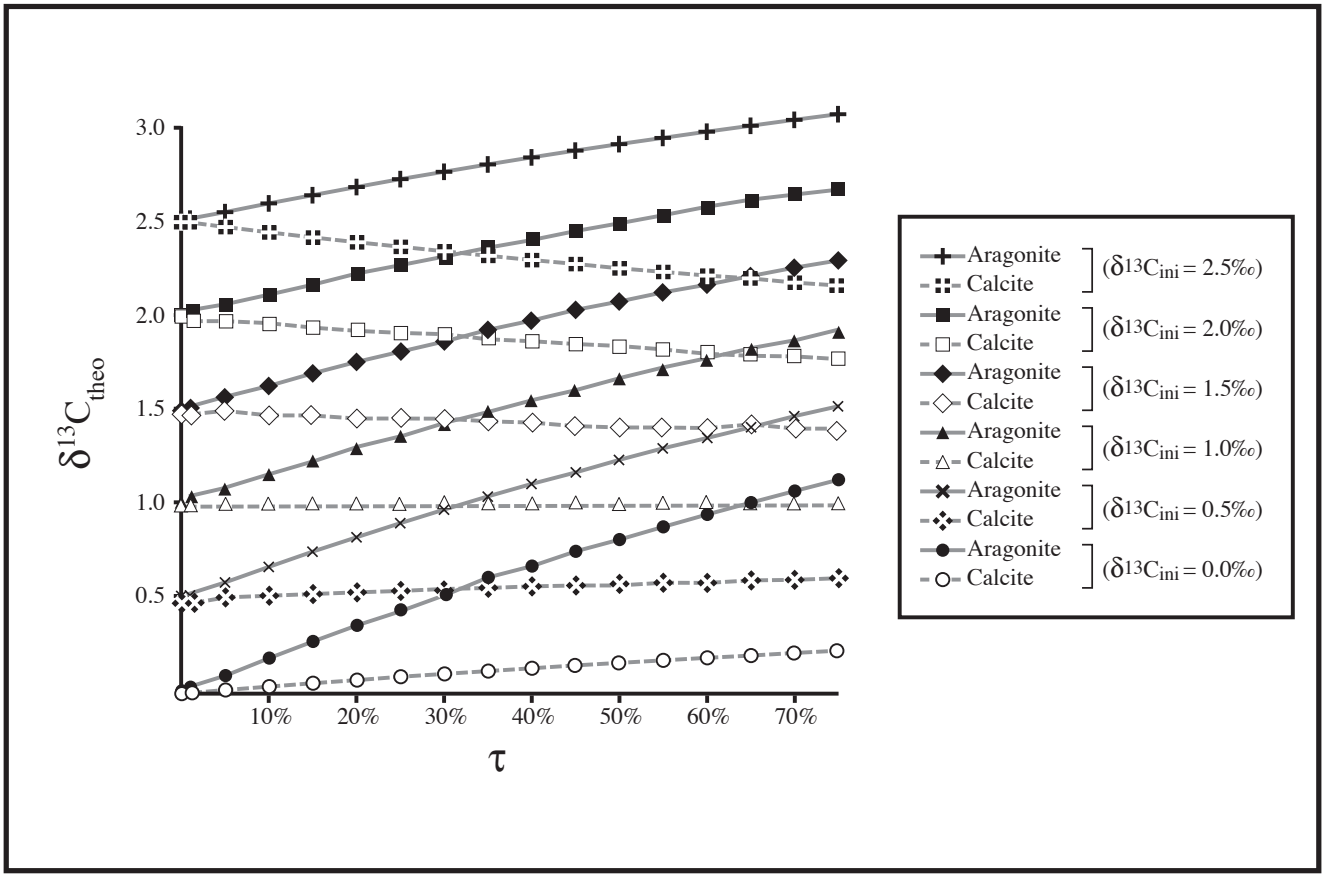

Fig. D.14: Predicted $\delta^{13}C$ values recorded in pelagic settings ($\delta^{13}C_{theo}$), as a function of the exportation rate (τ), of the $\delta^{13}C$ in the basin without platform influence ($\delta^{13}C_{ini}$) and of the mineralogy of the exported material ($\delta^{13}C_{calcite}$ = 1‰; $\delta^{13}C_{aragonite}$ = 5‰, after Swart and Eberli, 2005).

of aragonite production, the $\delta^{13}C$ increases; even with a τ of 20% and with a $\delta^{13}C_{ini}$ of 2‰, the $\delta^{13}C_{theo}$ reaches a value of 2.20‰. Such a shift is recorded in RA sediments attributed to the G. sartousiana zone, which corresponds to the onset of the Urgonian platform. In comparison, storms can remove up to 50 % of present-day reefs (Kleypas *et al.*, 2001).

In contrast, the $\delta^{13}C_{theo}$ values decrease in the theoretical case that platform carbonate is mainly produced as calcite. With a $\delta^{13}C_{ini}$ value of 2‰ and a τ of 30%, the $\delta^{13}C_{theo}$ value corresponds to 1.90‰. This suggests that photozoan carbonate factories such as the Urgonian platforms and their potential to produce and export aragonite into the pelagic realm may have had a considerable effect on the pelagic $\delta^{13}C$ signal, whereas shallow-water carbonate production in the heterozoan mode would be less influential.

D.2.7. Conclusions

The carbon and oxygen stable isotope records of selected sections representative for the northern and southern Tethyan margins give a consistent image of environmental change during the late Hauterivian and Barremian. The late Hauterivian is characterized by a long-term increase in the $\delta^{13}C$ record, which becomes accentuated during the latest part of this stage. This trend is explained here in a classical sense, with a shift in the burial ratio of organic and inorganic carbon in favor of organic carbon, which culminated in the widespread deposition of organic-rich sediments during the Faraoni oceanic anoxic event during the latest Hauterivian. This anoxic event is coeval with the onset of a platform drowning episode along the northern Tethyan margin, which lasted until the latest early Barremian. This was also a period of relative climate stability albeit with a tendency towards warmer conditions as is shown by the $\delta^{18}O$ record. The general stability of the $\delta^{13}C$ record during the early Barremian is explained by a buffering effect of the increased oceanic DIC reservoir, which is sustained by increased continental DIC input and diminished carbonate sedimentation rates along the northern Tethyan margin.

Near the transition from the early to the late Barremian, a shift toward more positive values is seen in the $\delta^{13}C$ record, which is explained here by the installation of widespread photozoan-type shallow-water carbonates of the so-called Urgonian platforms. This type of carbonate production likely favored the production of aragonite, which may have been a source of heavy $\delta^{13}C$ material in the adjacent basins, once exported into those realms.

The negative excursion in $\delta^{13}C$ values at the Barremian-Aptian boundary is explained by a widespread decrease in the production of photozoan carbonates and an increase in detritus, which both may have contributed to an increase in the transfer of DIC towards the ocean.

D.2.8. Acknowledgments

We acknowledge the Swiss National Science Foundation (projects 2100-067807/1 and 200020-105206/1) for its financial support and the “Réserve Géologique de Haute Provence” for its permission to sample the RA section. The authors would like to thank Rodolfo Coccioni (University of Urbino, Italy) and Jean Charollais (University of Geneva, Switzerland) for their advice and help in the field, and Elisabetta Erba (University of Milan, Italy) for providing the Cismon Apticore isotope data. We are also grateful to Haydon Mort, Pascal Linder, and Claire Rambeau (University of Neuchâtel, Switzerland) for their assistance during the sampling of the different sections, and to Gesine Preuss (University of Karlsruhe, Germany) for her technical support during the isotope analytical work. The quality of the English was improved by Haydon Mort, and this manuscript benefited from the constructive comments of three anonymous reviewers.

D.2.9. References

Ager, D. V. (1981). The Nature of the Stratigraphical Record. New York, John Wiley and Sons.

Arnaud, H., Arnaud-Vanneau, A., Blanc-Aletru, M. C., Adatte, T., Argot, M., Delanoy, G., Thieuloy, J.-P., Vermeulen, J., Virgone, A., Virlouvet, B. and Wermeille, S. (1998). «Répartition stratigraphique des orbitolinidés de la plate-forme urgonienne subalpine et jurassienne (SE de la France).» **Géologie Alpine** 74: 3-89.

Bartley, J. K. and Kah, L. C. (2004). «Marine carbon reservoir, C_{org} - C_{carb} coupling, and the evolution of the Proterozoic carbon cycle.» **Geology** 32(*2*): 129-132.

Baudin, F., Bulot, L. G., Cecca, F., Coccioni, R., Gardin, S. and Renard, M. (1999). «Un équivalent du «Niveau Faraoni» dans le Bassin du Sud-Est de la France, indice possible d'un événement anoxique fini-hauterivien étendu à la Téthys méditerranéenne.» **Bull. Soc. géol. France** 170(*4*): 487-498.

Baudin, F., Cecca, F., Galeotti, S. and Coccioni, R. (2002). «Palaeoenvironmental controls of the distribution of organic matter within a Corg-rich marker bed (Faraoni level, uppermost Hauterivian, central Italy).» **Eclogae geol. Helv.** 95: 1-13.

Bodin, S., Godet, A., Adatte, T. and Föllmi, K. B. (2005). «Palaeoceanographic and palaeoclimatic changes of the northern tethyan realm during the Hauterivian-Barremian: New insight from the Angles section (SE France).» **Géologie Alpine** Série Spéciale «Colloques et Excursions» N°7.

Bodin, S., Godet, A., Vermeulen, J., Arnaud, H., Strasser, A., Fiet, N., Adatte, T. and Föllmi, K. B. (2006). The late Hauterivian Faraoni oceanic anoxic event in the western Tethys: Evidence from phosphorus burial rates. Causes and consequences of organic carbon burial through time. A. Negri, T. Wagner and P. A. Meyers. Special volume of Palaeogeography, Palaeoclimatology, Palaeoecology.

Bralower, T. J., CoBabe, E., Clement, B., Sliter, W. V., Osburn, C. L. and Longoria, J. (1999). «The record of global change in mid-Cretaceous (Barremian-Albian) sections from the Sierra Madre, northeastern Mexico.» **Journal of Foraminiferal Research** 29(*4*): 418-137.

Burke, L., Bryant, D., McManus, J. W. and Spalding, M. (1998). Reefs at Risk: A Map-Based Indicator of Potential Threats to the World's Coral Reefs. Worls Resources Institute. Washington D.C.: 3-11.

Busnardo, R. (1965). «Le stratotype du Barrémien. I.- Lithologie et macrofaune.» **Mém. Bur. Rech. Géol. Min.** 34: 101-116.

Busnardo, R., Charollais, J., Weidmann, M. and Clavel, B. (2003). «Le Crétacé inférieur de la Veveyse de Châtel (Ultrahelvétique des Préalpes externes; canton de Fribourg, Suisse).» **Revue Paléobiol., Genève** 22(*1*): 1-174.

Cecca, F., Faraoni, P., Marini, A. and Pallini, G. (1995). «Field-trip across the representative sections for the Upper Hauterivian-Barremian ammonite biostratigraphy in the Maiolica exposed at Monte Nerone, Monte Petrano and Monte Catria (Umbria-Marche, Apennines).» **Memorie Descrittive della Carta Geologica d'Italia** 51: 187-211.

Cecca, F., Marini, A., Pallini, G., Baudin, F. and Begouen, V. (1994a). «A guide-level of the uppermost Hauterivian (lower Cretaceous) in the pelagic succession of Umbria-Marche Apennines (central Italy): the Faraoni level.» **Riv. It. Paleont. Strat.** 99(*4*): 551-568.

Cecca, F., Pallini, G., Erba, E., Premoli-Silva, I. and Coccioni, R. (1994b). «Hauterivian-Barremian chronostratigraphy based on ammonites, nannofossils, planktonic foraminifera and magnetic chrons from the Mediterranean domain.» **Cretaceous Research** 15(*4*): 457-467.

Cerlings, T. E., Wang, Y. and Quade, J. (1993). «Expansion of C4 ecosystems as an indicator of global ecological change in the late Miocene.» **Nature** 361: 344-345.

Channell, J. E. T., Cecca, F. and Erba, E. (1995). «Correlations of Hauterivian and Barremian (Early Cretaceous) stage boundaries to polarity chrons.» **Earth and Planetary Science Letters** 134: 125-140.

Coccioni, R., Baudin, F., Cecca, F., Chiari, M., Galeotti, S., Gardin, S. and Salvini, G. (1998). «Integrated stratigraphic, palaeontological, and geochemical analysis of the uppermost Hauterivian Faraoni Level in the Fiume Bosso section, Umbria-Marche Apeninnes, Italy.» **Cretaceous Research** 19: 1-23.

Coccioni, R., Erba, E. and Premoli Silva, I. (1992). «Barremian-Aptian calcareous plankton biostratigraphy from the Gorgo Cerbara section (Marche, central Italy) and implications for plankton evolution.» **Cretaceous Research** 13: 517-537.

Company, M., Aguado, R., Sandoval, J., Tavera, J. M., de Cisneros, C. J. and Vera, J. A. (2005). «Biotic changes linked to a minor anoxic event (Faraoni Level latest Hauterivian,

Early Cretaceous).» **Palaeogeography, Palaeoclimatology, Palaeoecology** 224: 186-199.

Deconinck, J.-F. and Bernouilli, D. (1991). «Clay mineral assemblages of Mesozoic pelagic and flysch sediments of the Lombardian Basin (Southern Alps): implications for palaeotectonics, paleoclimate and diagenesis.» **Geologische Rundschau** 80(*1*): 1-17.

Dickens, G. R., Fewless, T., Thomas, E. and Bralower, T. J. (2002). Excess barite accumulation during the Paleocene-Eocene Thermal Maximum: Massive input of dissolved barium from seafloor gas hydrate reservoirs. Causes and Consequences of Globally Warm climates in the Early Paleogene. S. L. Wing, P. D. Gingerich, B. Schmitz and E. Thomas, Geological Society of America. Special Paper 369: 11-23.

Dickens, G. R., O'Neil, J. R., Rea, D. K. and Oven, R. M. (1995). «Dissociation of oceanic methane hydrate as a cause of the carbon isotope ecxcursion at the end of the Paleocene.» **Paleoceanography** 10(*6*): 965-971.

Droxler, A. W., Schlager, W. and Whallon, C. C. (1983). « Quaternary aragonite cycles and oxygen isotope record in Bahamian carbonate ooze.» **Geology** 11: 235-239.

Erba, E. (1996). «The Aptian stage.» **Bulletin de l'Institut Royal des Sciences Naturelles de Belgique** 66-Supplement: 31-43.

Erba, E., Bartolini, A. and Larson, R. L. (2004). «Valanginian Weissert oceanic anoxic event.» **Geology** 32(*2*): 149-152.

Erba, E., Channell, J. E. T., Claps, M., Jones, C. E., Larson, R. L., Opdyke, B., Premoli-Silva, I., Riva, A., Salvini, G. and Torriceli, S. (1999). «Integrated stratigraphy of the Cismon APTICORE (Southern Alps, Italy): A «reference section» for the Barremian-Aptian interval at low latitudes.» **Journal of Foraminiferal Research** 29(*4*): 371-391.

Fiet, N. and Gorin, G. (2000). «Lithological expression of Milankovitch cyclicity in carbonate-dominated, pelagic, Barremian deposits in central Italy.» **Cretaceous Research** 21(*4*): 457-467.

Fourcade, E., Azema, J., Cecca, F., Dercourt, J., Guiraud, R., Sandulescu, M., Ricou, L. E., Vrielynck, B., Cottereau, N. and Petzold, M. (1993). Late Tithonian Palaeoenvironments (138 to 135 Ma). Atlas Tethys Palaeoenvironmental Maps. J. Dercourt, L. E. Ricou and B. Vrielynck. Paris, Gauthier-Villars: Maps. BEICIP-FRANLAB, Rueil-Malmaison.

Föllmi, K. B., Weissert, H., Bisping, M. and Funk, H. (1994). «Phosphogenesis, carbon-isotope stratigraphy, and carbonate-platform evolution along the Lower Cretaceous northern Tethyan margin.» **Geological Society of America Bulletin** 106(*II*): 729-746.

Haq, B. U., Hardenbol, J. and Vail, P. R. (1987). «The chronology of fluctuating sea level since the Triassic.» **Science** 235: 1156-1167.

Herrle, J. O., Kößler, P., Friedrich, O., Erlenkeuser, H. and Hemleben, C. (2004). «High-resolution carbon isotope records of the Aptian to Lower Albian from SE France and the Mazagan Plateau (DSDP Site 545): a stratigraphic tool for paleoceanographic and paleobiologic reconstruction.» **Earth and Planetary Science Letters** 218(*1-2*): 149-161.

Hillgärtner, H., Van Buchem, F. S. P., Gaumet, F., Razin, P., Pittet, B., Grötsch, J. and Droste, H. (2003). «The Barremian-Aptian evolution of the eastern Arabian carbonate platform margin (northern Oman).» **Journal of Sedimentary Research** 73(*5*): 756-773.

Hoedemaeker, P. J. and Rawson, P. F. (2000). «Report on the 5th International Workshop of the Lower Cretaceous Cephalopod Team (Vienna, 5 September 2000).» **Cretaceous Research** 21(*6*): 857-860.

Hoedemaeker, P. J., Reboulet, S., Aguirre-Urreta, M. B., Alsen, P., Aoutem, M., Atrops, F., Barragan, R., Company, M., Gonzalez, C. and Klein, J. (2003). «Report on the 1st International Workshop of the IUGS Lower Cretaceous Ammonite Working Group, the 'Kilian Group' (Lyon, 11 July 2002).» **Cretaceous Research** 24(*1*): 89-94.

Holmden, C., Creaser, R. A., Muehlenbachs, K., Leslie, S. A. and Bergström, S. M. (1998). «Isotopic evidence for geochemical decoupling between ancient epeiric seas and bordering oceans: Implications for secular curves.» **Geology** 26(*6*): 567-570.

Jenkyns, H. C. (1980). «Cretaceous anoxic events: from continents to oceans.» **Journal of the**

Geological Society, London 137: 171-188.

Jenkyns, H. C. (2003). «Evidence for rapid climate change in the Mesozoic-Paleogene greehouse world.» **Phil. Trans. R. Soc. Lond.** 361: 1885-1916.

Jenkyns, H. C., Gale, A. S. and Corfield, P. M. (1994). «Carbon and oxygen isotope stratigraphy of english chalk and Italian Scaglia and its palaeoclimatic significance.» **Geol. Mag.** 131: 1-34.

Jones, C. E. and Jenkyns, H. C. (2001). «Seawater strontium isotopes, oceanic anoxic events, and seafloor hydrothermal activity in the Jurassic and Cretaceous.» **American Journal of Science** 301: 112-149.

Keller, G., Berner, Z., Adatte, T. and Stueben, D. (2004). «Cenomanian-Turonian and $d^{13}C$, and $d^{18}O$, sea level and salinity variations at Pueblo, Colorado.» **Palaeogeography, Palaeoclimatology, Palaeoecology** 211(*1-2*): 19-43.

Kleypas, J. A., Buddemeir, R. W. and Gattuso, J.-P. (2001). «The future of coral reefs in an age of global change.» **Int. J. Earth Sci. (Geol. Rundsch.)** 90: 426-437 DOI 10.1007/s005310000125.

Lehman, C., Osleger, D. A., Montanez, I. P., Arnaud-Vanneau, A. and Banner, J. (1999). «Evolution of Cupido and Coahuila carbonate platforms, Early Cretaceous, northeastern Mexico.» **GSA Bulletin** 111(*7*): 1010-1029.

Lini, A., Weissert, H. and Erba, E. (1992). «The Valanginian carbon isotope event: a first episode of greenhouse climate conditions during the Cretaceous.» **Terra Nova** 4(*Global Change Spec. Issue (ed. by F.-C. Wezel)*): 374-384.

Lowrie, W. and Alvarez, W. (1984). «Lower Cretaceous magnetic stratigraphy in Umbrian pelagic limestone sections.» **Earth and Planetary Science Letters** 71: 315-328.

Masse, J.-P., Bellion, Y., Benkhelil, J., Dercourt, J., Guiraud, R. and Ricou, L. E. (1993). Lower Aptian Palaeoenvironments (114 to 112 Ma). Atlas Tethys Palaeoenvironmental Maps. J. Dercourt, L. E. Ricou and B. Vrielynck. Paris, Gauthier-Villars: Maps. BEICIP-FRANLAB, Rueil-Malmaison.

Masse, J.-P., Borgomano, J. and Maskiry, S. A. (1997). «Stratigraphy and tectonosedimentary evolution of a late Aptian-Albian carbonate margin: the northeastern Jebel Akhdar (Sultanate of Oman).» **Sedimentary Geology** 113(*3-4*): 269-280.

Mc Crea, J. M. (1950). «On the isotope chemistry of carbonates and a paleotemperature scale.» **J. Chem. Phys.** 18: 849-857.

Munnecke, A., Westphal, H., Elrick, M. and Reijmer, J. J. G. (2001). «The mineralogical composition of precursor sediments of calcareous rhythmites: a new approach.» **Int. J. Earth Sci. (Geol. Rundsch.)** 90: 795-812.

Mutterlose, J. and Bornemann, A. (2000). «Distribution and facies patterns of Lower Cretaceous sediments in northern Germany: a review.» **Cretaceous Research** 21(*6*): 733-759.

Mutti, M. and Hallock, P. (2003). «Carbonate systems along nutrient and temperature gradients: some sedimentological and geochemical constraints.» **Int. J. Earth Sci. (Geol. Rundsch.)** 92: 465-475.

Philip, J. (2003). «Peri-Tethyan neritic carbonate areas: distribution through time and driving factors.» **Palaeogeography, Palaeoclimatology, Palaeoecology** 196(*1-2*): 19-37.

Plank, T., Ludden, J. N., Escutia, C. and al. (2000). Proceeding of the Ocean Drilling Program, Initial Reports, 185 [Online]. Available from World Wide Web: <http://www-odp.tamu.edu/publications/185_IR/185ir.htm>.

Podlaha, O. G., Mutterlose, J. and Veizer, J. (1998). «Preservation of $d^{18}O$ and $d^{13}C$ in belemnite rostra from the Jurassic / early Cretaceous successions.» **American Journal of Science** 298: 324-347.

Pucéat, E., Lécuyer, C., Sheppard, S. M. F., Dromart, G., Reboulet, S. and Grandjean, P. (2003). «Thermal evolution of Cretaceous Tethyan marine waters inferred from oxygen isotope composition of fish tooth enamels.» **Paleoceanography** 18(*2*): 1029, doi:10.1029/2002PA000823.

Raiswell, R. and Fisher, Q. J. (2004). «Rates of carbonate cementation associated with sulphate reduction in DSDP/ODP sediments: implcations for the formation of concretions.» **Chemical Geology** 211: 71-85.

Romanek, C. S., Grossman, E. L. and Morse, J. W. (1992). «Carbon isotopic fractionation in synthetic aragonite and calcite: Effects of temperature and precipitation rate.» **Geochimica**

et Cosmochimica Acta 56(*1*): 419-430.

Ruffell, A. H. and Batten, D. J. (1990). «The Barremian-Aptian arid phase in western Europe.» **Palaeogeography, Palaeoclimatology, Palaeoecology** 80(*3-4*): 197-212.

Schlanger, S. O. and Jenkyns, H. C. (1976). «Cretaceous oceanic anoxic events: causes and consequences.» **Geologie en Mijnbouw** 55(*3-4*): 179-184.

Scholle, P. A. and Arthur, M. A. (1980). «Carbon Isotope Fluctuations in Cretaceous Pelagic Limestones: Potential Stratigraphic and Petroleum Exploration Tool.» **The American Association of Petroleum Geologists Bulletin** 64: 67-87.

Scotese, C. R., Gahagan, L. M. and Larson, R. L. (1988). «Plate tectonic reconstructions of the Cretaceous and Cenozoic ocean basins.» **Tectonophysics** 155(*1-4*): 27-48.

Stanley, S. M. and Hardie, L. A. (1998). «Secular oscillations in the carbonate mineralogy of reef-building and sediment-producing organisms driven by tectonically forced shifts in seawater chemistry.» **Palaeogeography, Palaeoclimatology, Palaeoecology** 144: 3-19.

Steuber, T. (2002). «Plate tectonic control on the evolution of Cretaceous platform-carbonate production.» **Geology** 30(*3*): 259-262.

Steuber, T., Rauch, M., Masse, J.-P., Graaf, J. and Malkoč, M. (2005). «Low-latitude seasonnality of Cretaceous temperatures in warm and cold episodes.» **Nature** 437(*27 October 2005*): 1341-1344.

Swart, P. K. and Eberli, G. «The Nature of the $d^{13}C$ of Periplatform Sediments: Implications for stratigraphy and the global carbon cycle.» **Sedimentary Geology, in press**.

Trümpy, R. (1960). «Paleotectonic evolution of the central and western Alps.» **Bulletin of the Geological Society of America** 71(*6*): 846-908.

van de Schootbrugge, B., Föllmi, K. B., Bulot, L. G. and Burns, S. J. (2000). «Paleoceanographic changes during the early Cretaceous (Valanginian-Hauterivian): evidence from oxygen and carbon stable isotopes.» **Earth and Planetary Science Letters** 181: 15-31.

van de Schootbrugge, B., Kuhn, O., Adatte, T., Steinmann, P. and Follmi, K. (2003). «Decoupling of P- and Corg-burial following Early Cretaceous (Valanginian-Hauterivian) platform drowning along the NW Tethyan margin.» **Palaeogeography, Palaeoclimatology, Palaeoecology** 199(*3-4 SU -*): 315-331.

Veizer, J., Ala, D., Azmy, K., Bruckschen, P., Buhl, D., Bruhn, F., Carden, G. A. F., Diener, A., Ebneth, S. and Godderis, Y. (1999). «$^{87}Sr/^{86}Sr$, $\delta^{13}C$ and $\delta^{18}O$ evolution of Phanerozoic seawater.» **Chemical Geology** 161(*1-3*): 59-88.

Vermeulen, J. (2002). «Etude stratigraphique et paléontologique de la famille des Pulchelliidae (Ammonoidea, Ammonitina, Endomocerataceae).» **Géologie Alpine** Mémoire H.S. N°42: 3-333.

Weissert, H. (1989). «C-Isotope stratigraphy, a monitor of paleoenvironmental change: a case study from the Early Cretaceous.» **Surveys in Geophysics** 10(*1*): 1-61.

Weissert, H. (1990). «Siliciclastics in the early Cretaceous Tethys and north Atlantic oceans: documents of periodis greenhouse climate conditions.» **Mem. Soc. Geol. It.** 44: 59-69.

Weissert, H. and Erba, E. (2004). «Volcanism, CO_2 and paleaoclimate: a Late Jurassic-Early Cretaceous carbon and oxygen isotope record.» **Journal of the Geological Society, London** 161: 695-702.

Weissert, H., Lini, A., Föllmi, K. B. and Kuhn, O. (1998). «Correlation of Early Cretaceous carbon isotope stratigraphy and platform drowning events: a possible link?» **Palaeogeography, Palaeoclimatology, Palaeoecology** 137: 189-203.

Wissler, L., Weissert, H., Masse, J.-P. and Bulot, L. G. (2002). «Chemostratigraphic correlation of Barremian and lower Aptian ammonite zones and magnetic reversals.» **Int. J. Earth Sci. (Geol. Rundsch.)** 91(*2*): 272-279.

D.3. The late Hauterivian Faraoni oceanic anoxic event in the western Tethys: Evidence from phosphorus burial rates

Stéphane Bodin[1], Alexis Godet[1], Karl B. Föllmi[1], Jean Vermeulen[2], Hubert Arnaud[3], André Strasser[4], Nicolas Fiet[5], Thierry Adatte[1]

[1]Institut de Géologie, Université de Neuchâtel, Rue Emile Argand 11, 2007 Neuchâtel, Switzerland; [2]Grand Rue, 04330 Barrême, France; [3]Laboratoire de Géodynamique des Chaînes Alpines, Maison des Géosciences, 38041 Grenoble Cedex, France; [4]Department of Geosciences, Geology-Palaeontology, Perolles, CH-1700 Fribourg, Switzerland; [5]UMR 8148 – I.D.E.S., Bât. 504, University of Paris XI Orsay, 91405 Orsay Cedex, France

Manuscript published in Palaeogeography, Palaeoclimatology, Palaeoecology, 2006, volume 235, issue 1-3, pages 238-257.

Abstract

In uppermost Hauterivian sediments of the western Tethys, a short-lived anoxic event (Faraoni event) is documented both in form of an interval enriched in organic matter (pelagic realm) as well as a condensed interval enriched in glauconite and phosphate (shelf realm). This latter interval represents the onset of a drowning episode on the Helvetic carbonate platform along the northern tethyan margin, which lasted throughout the early Barremian. This drowning episode marks a turning point in the way the platform carbonate factory functioned: during the Hauterivian, carbonate production was dominated by heterozoans, whereas during the late Barremian a photozoan assemblage developed that is preserved in the so-called Urgonian limestone. The late Hauterivian Faraoni oceanic anoxic event is of particular interest, because it is not accompagnied by a major positive shift in $\partial^{13}C$, unlike other oceanic anoxic events during the Cretaceous (Valanginian, early Aptian, Cenomanian-Turonian boundary).

We have analyzed four (hemi-)pelagic sections with regards to their phosphorus content in order to better understand the palaeoceanographic conditions related to this anoxic event and the associated changes in the shallow-water carbonate factory. The sections are located in Angles (SE France), Fiume-Bosso and Gorgo a Cerbara (central Italy), and Veveyse de Châtel-St. Denis (west Switzerland). We calculated phosphorus mass accumulation rates by using a cyclostratigraphic approach in order to obtain an adequate age model. We observe a comparable and correlatable long-term trend for the four sections, which suggests that the phosphorus mass accumulation rates and temporal changes therein are representative for the western tethyan pelagic realm. The Faraoni event is marked by a minimum in phosphorus accumulation and a positive shift in the C_{org}/P_{tot} ratios, which is interpreted as a reflection of the decreased capacity of storing and preserving phosphorus in oxygen-depleted sediments. Moreover, the onset in the decrease in phosphorus accumulation coincides with a sea level rise, while the Faraoni level itself corresponds to a maximum flooding interval. This phase of sea-level rise may have been important in the establishment of marine connections between the boreal and tethyan realms, and as such in the exchange of nutrient-enriched waters. The model for the origin of the Faraoni oceanic anoxic event proposed here incorporates these aspects together with a positive feedback loop generated by phosphorus regeneration, and a negative feedback loop related to changes in the ocean oxygen cycle.

The subsequent long-term changes in phosphorus burial rates during the Barremian suggest that the Faraoni event marks the onset of a long period of environmental instability with regards to platform growth, leading to periodic phases of eutrophication and drowning of the northern tethyan carbonate platform. This environmental crisis ended during the late Barremian with the onset of the deposition of the Urgonian limestone under oligotrophic conditions.

Keywords

Faraoni anoxic event; Hauterivian; Barremian; Tethys; phosphorus accumulation rate; platform drowning

D.3.1. Introduction

The early Cretaceous is characterized by marked environmental and palaeoceanographic changes, which are documented by episodic oceanic anoxic events, repeated platform drowning phases, and pronounced excursions in the stable carbon (C) isotope record (*e.g.*, Lini *et al.*, 1992; Föllmi *et al.*, 1994; Weissert *et al.*, 1998; Herrle, 2002). One of the less well-understood events of this period is the so-called Faraoni event (Baudin *et al.*, 1999; Cecca *et al.*, 1994), which is a short-lived oceanic event that occurred during the latest Hauterivian. In comparison to the other anoxic events, the Faraoni event is a rather atypical event for which the environmental circumstances are still not clear: in contrast to the anoxic events during the Valanginian, the early Aptian, and near the Cenomanian-Turonian boundary (*e.g.*, Schlanger and Jenkyns, 1976; Schlanger *et al.*, 1987; Weissert, 1989; Lini *et al.*, 1992; Jones and Jenkyns, 2001; Weissert and Erba, 2004), the Faraoni level is not accompanied by a major carbon isotope excursion towards more positive values but instead by a minor long-term increase (Föllmi *et al.*, 1994; Erba *et al.*, 1999; Van de Schootbrugge *et al.*, 2000). Furthermore, no major volcanic episode has, of yet, been identified for the late Hauterivian. This means that the classical model postulated for the origin of oceanic anoxic events in general, (*i.e.*, increased volcanism leading to an increase in atmospheric CO_2, climate warming, increased weathering and nutrient availability, higher productivity and consequently higher preservation rates of organic matter (*e.g.*, Jenkyns, 1999, 2003) can not be applied in this case.

The Faraoni event marks the onset of a long-lasting drowning episode on the Helvetic carbonate platform of the northern tethyan margin (D3 in Föllmi *et al.*, 1994), which is documented by a hiatus or by the presence of condensed glauconite and phosphate-rich sediments – the so-called Altmann Beds (Funk, 1969). This drowning episode is associated with a fundamental change in the carbonate factory of this platform system: during the Hauterivian, carbonate production occurred mainly by heterozoan assemblages, which are documented – for example - by the Kieselkalk Formation (Funk, 1969; Föllmi *et al.*, 1994), whereas during the late Barremian, photozoan assemblages dominated and their debris accumulated in the widespread "Urgonian" limestone (= Schrattenkalk Formation in the Helvetic realm).

For this period and for the early Cretaceous in general, only a limited amount of data has been obtained with regards to its phosphorus (P) record (Föllmi, 1995, 1996; van de Schootbrugge *et al.*, 2003). P is an important and often limiting biophile element (Broecker and Peng, 1982; Ingall and Jahnke, 1994; Tyrrell, 1999), which is closely linked to the Carbon (C) cycle through two interfaces: (1) biogeochemical weathering, during which atmospheric CO_2 is transformed into HCO_3^- and P is mobilized; and (2) photosynthesis, which is often limited by P and by which CO_2 is transformed into organic C (*e.g.*, Föllmi *et al.*, 2004). A reconstruction of changes in the P cycle during this critical period may, for these reasons, help to improve our understanding of the mechanisms leading to the Faraoni anoxic event and the associated platform drowning episode.

Four pelagic or hemi-pelagic sections located in Angles (SE France), Fiume-Bosso (central Italy), Gorgo a Cerbara (central Italy) and Veveyse de Châtel-St. Denis (west Switzerland) were analyzed. By monitoring the P record in these key sections and integrating sequence stratigraphy and cyclostratigraphy, we are able to reconstruct a general trend in P accumulation for the western Tethyan realm during the late Hauterivian and Barremian. In using the C_{org}/P_{org} and C_{org}/P_{tot} ratios, we also show that a decrease in the capacity of storing and preserving P in the sedimentary reservoir during the unfolding of the Faraoni event may have helped to sustain this anoxic event.

D.3.2. Geological setting

Four pelagic or hemi-pelagic sections in different basins within the western Tethys were selected. These sections are well dated and include the Faraoni level or its equivalent. The first studied section is the Fiume-Bosso section, located between Urbino and Gubbio, near Cagli (central Italy, Fig. D.15; see also Cecca *et al.*, 1994). It represents the type section for the

Faraoni level (Cecca *et al.*, 1994). The lithology is characteristic of the Maiolica Formation and consists of a succession of pelagic limestone beds containing abundant cherts, and locally intercalated thin organic-rich marl layers and/or laminae. The section of Gorgo a Cerbara is situated in the same area and its lithology is similar to the one of the Fiume-Bosso section. It is situated approximately 4 km east of Piobbico city along the Candigliano River (Fig. D.15; see Cecca *et al.*, 1995). This type section for the Barremian/Aptian boundary is complementary to the Fiume-Bosso section and covers the whole Barremian.

The section of the Veveyse de Châtel-St. Denis (VCD) is the third studied section. It is situated in the canton of Fribourg, along the Veveyse river, in western Switzerland (see Busnardo *et al.*, 2003, for a detailed geographic description). Its lithology consists of a succession of alternating pelagic marl and marly limestone, which are rich in macrofossils.

The fourth studied section outcrops along the "Route d'Angles", near St. André-Les-Alpes, in the Vocontian basin (S-E of France, see Busnardo (1965) for a detailed geographic description). Its lithology consists of a fossiliferous, hemi-pelagic succession of regularly alternating marl and limestone.

The palaeogeographic location of these four sections is shown in Fig. D.15. During the early Cretaceous, the Angles and the VCD sections were situated along the northern tethyan margin. The VCD section is part of the Ultrahelvetic realm, which is considered as the deeper offshore prolongation of the Vocontian basin to the northeast (Trümpy, 1960). The Fiume-Bosso and the Gorgo a Cerbara sections were located in the southern part of the tethyan realm, remote from any continent, and were surrounded by carbonate shelves. The four sections represent a N-S transect across the western Tethys.

D.3.3. Methods

D.3.3.1. Phosphorus analyses

Total phosphorus analyses were performed on bulk rock samples from the limestone intervals for all four sections. The samples were sawed in order to eliminate the altered parts and the veins of the rock. Then, powders were obtained using an agate crusher. Around 100 mg of powder were mixed with 1 ml of $MgNO_3$ and left to dry in an oven at 45°C for 2 hours. The samples were then ashed in a furnace at 550°C during two hours. After cooling,

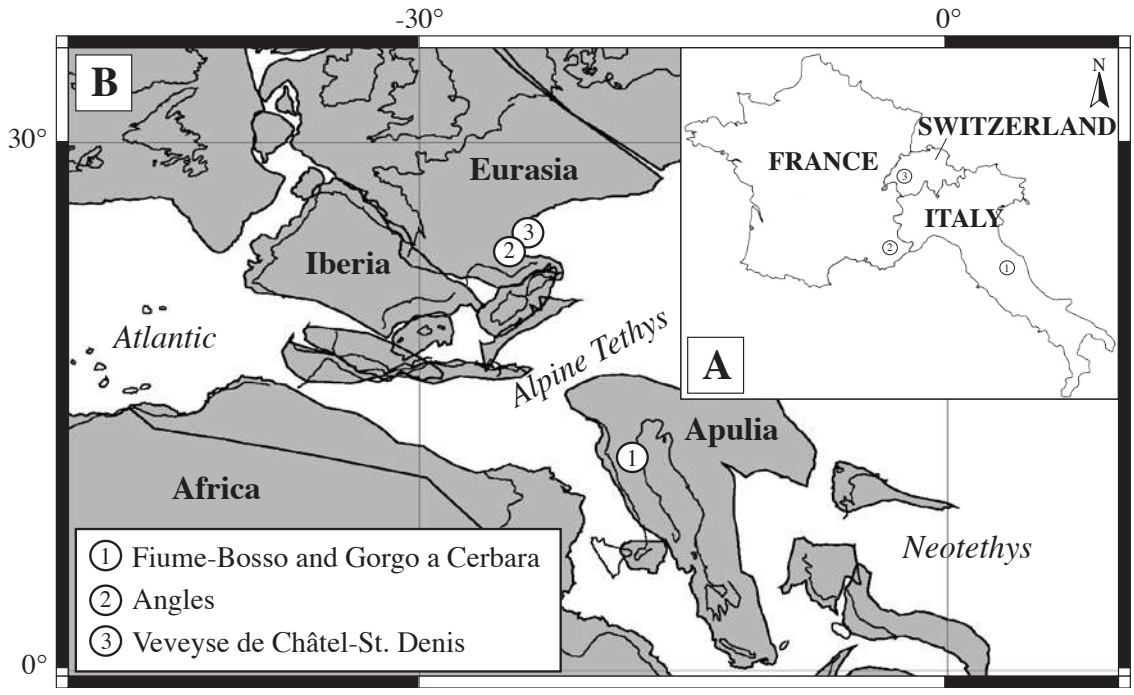

Fig. D.15: A. Localization of the four studied sections. B. Palaeogeographic map at the Hauterivian-Barremian transition (127 Myr B.P.) showing the localization of the four sections (modified from Hay et al., 1999).

10 ml of 1N HCl were added and placed under constant shaking for 14 hours. The solutions were filtrated with a 63μm filter, diluted ten times, and analyzed using the ascorbic acid method of Eaton *et al*. (1995). For this process, the solution was mixed with ammonium molybdate and potassium antimonyl tartrate, which in an acid medium react with orthophosphate to form phosphomolybdic acid. This acid is reduced with ascorbic acid to form an intense blue color. The intensity of the blue color is determined with a photospectrometer (Perkin Elmer UV/Vis Photospectrometer Lambda 10). The concentration of PO4 in mg/L is obtained by calibration with known standard solutions. Individual samples were measured three times and precision was better than 5%. Replicate analyses of samples have a precision better than 10% in the case of low P concentration (such as in samples of the Fiume-Bosso and Gorgo a Cerbara sections) and better than 7% in the two other sections.

Total P content in marls was determined using the same method as for the limestone. P content of the organic matter was determined by using a sequential extraction technique, adapted from the SEDEX method developed by Ruttenberg (1992) and modified by Anderson and Delaney (2000). As for total phosphorus, the solutions were diluted ten times, colorated using the ascorbic acid method of Eaton *et al*. (1995) and analyzed with a photospectrometer (Perkin Elmer UV/Vis Photospectrometer Lambda 10).

C_{org}/P_{org} and C_{org}/P_{tot} ratios were determined in the marls within and around the Faraoni level for three sections (Fiume-Bosso, Angles and VCD). The C concentration was obtained by Rock-Eval pyrolysis (Behar *et al*., 2001) using the standard temperature cycle. Two standards (an in-house standard and the «IFP 160000» standard from the Institut Français du Pétrole, Paris, France) were analyzed at the beginning and at the end of a batch of ca. 15 samples. C/P is expressed in mol/mol unit (Fig. D.16). The results for TOC and phosphorus are shown in Table D.5.

D.3.3.2. Age model

In order to avoid problems of condensation and to better compare the different sections, we decided to calculate phosphorus accumulation rates (PAR). The PAR is expressed in mg of P per cm^2 per kyr. This is a multiplication of the concentration in P (mg/g), the density (g/cm^3), and the sedimentation rate (cm/kyr). As all the samples are pelagic or hemi-pelagic mudstones, the density was assumed to be constant and equal to 2.5 g/cm^3 for all analyzed samples.

An age model was obtained for the four sections by a cyclostratigraphic approach (Table D.6). For the Angles section, following the study of Giraud *et al*. (1995) in the late Hauterivian (*angulicostata* zone) sediment of Vergons, we considered that each limestone-marl couplet represents a duration of 20 kyr. We estimated as such an average sedimentation rate for the successions of sediments that correspond to the time envelopes of complete ammonite zones (Vermeulen, 2002). It appears that in the Angles section, the *sartousiana* and the *feraudianus* zones are not complete due to the presence of hiati and/or condensed sediments (Delanoy, 1997; Vermeulen, 2002; see also Wissler *et al*., 2002). For the sediments attributed to these two ammonite zones, we decided to use the time envelopes for the corresponding sedimentary intervals from the Saut-du-Loup section, which is situated in the same area (close to Barrême) and appears to be more complete (Vermeulen, 1980). For the Fiume-Bosso and the Gorgo a Cerbara sections, we followed the method described in Fiet and Gorin (2000) to discriminate 100-kyr bundles in Barremian carbonate-dominated pelagic deposits of central Italy, and then determine sedimentation rates based on the eccentricity bundles. Finally, in the VCD section, the same method as for the Angles section was applied. The ammonite zones have been defined by Busnardo *et al*. (2003) and their limits are dated approximately by Hardenbol *et al*. (1998). By counting the limestone-marl alternations between these limits, an average time span of 20 kyr is suggested for one limestone-marls couplet. Occasionally it is observed that five couplets group into bundles, which would then correspond to 100 kyr. These frequencies imply that sedimentation was controlled by orbital cycles in the Milankovitch frequency band.

We find a duration of 500 kyr for the interval between the base/onset of the Faraoni level and the Hauterivian-Barremian boundary in three sections

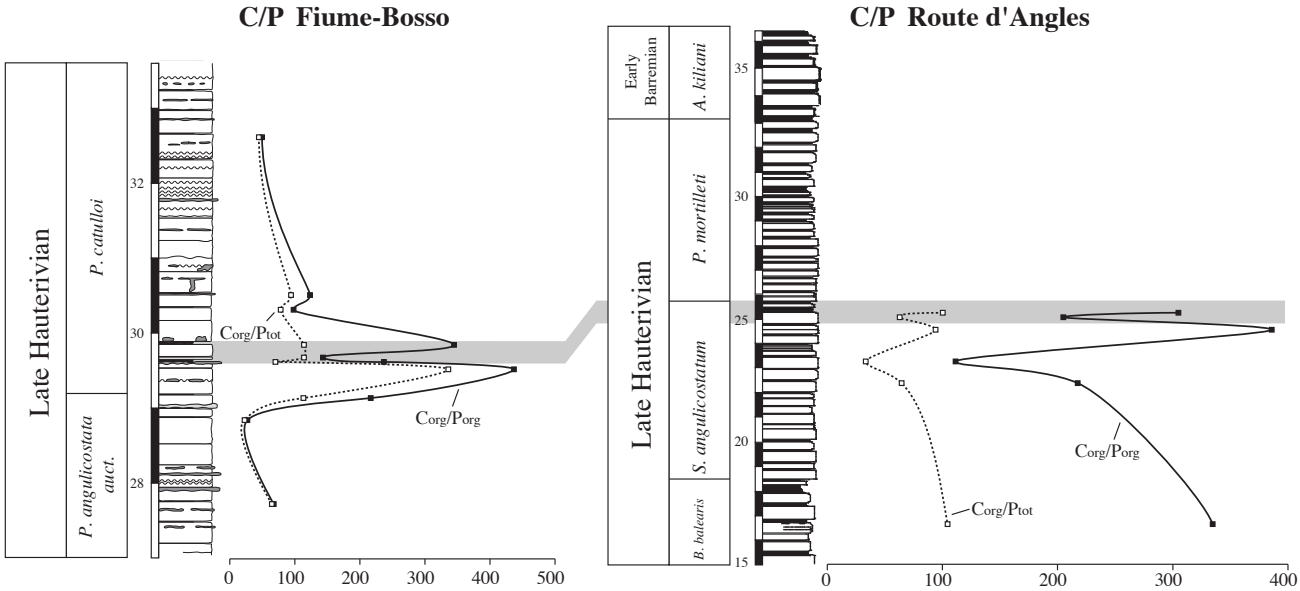

Fig. D.16: C/P_{org} and C/P_{tot} ratios (expressed in mol/mol) in the Fiume-Bosso and Angles sections. The grey band traces the Faraoni level.

(Fiume-Bosso, Gorgo a Cerbara and Angles). In the VCD section, the calculated duration is equal to 420 kyr. This slight difference reflects the limits of the cyclo-stratigraphy approach. In the Angles section, the duration of the Barremian is estimated to be equal to 4.52 Myr (with the integration of the duration of the *sartousiana* and *feraudianus* zones from the Saut-du-Loup section). This duration is in relative good agreement with those obtained by Fiet and Gorin (2000) for the Barremian of the Gorgo a Cerbara section (5.11 ± 0.34 Myr) and the estimation of the age of the Barremian proposed by Gradstein *et al*. (2004) (between 130 ±1.5 and 125 ±1.0 Myr B.P.). However, a discrepancy exists with the study of Wissler *et al*. (2004), who found a duration of 4 Myr between the top of Chron M3 and the base of Chron M0, which is not in good agreement with our estimation of 3.15 Myr for the same time interval at Gorgo a Cerbara.

Ech	TOC [%]	[P_{org}] (ppm)	[P_{tot}] (ppm)	C_{org} (mmol/g)	P_{org} (mmol/g)	P_{tot} (mmol/g)	C_{org}/P_{org}	C_{org}/P_{tot}
Fiume-Bosso								
FB 133	2.11	786.7	809.0	1.760	0.0254	0.0261	69.3	67.4
FB 138	1.12	1001.1	1280.2	0.931	0.0323	0.0413	28.8	22.5
FB 372	4.51	540.5	1011.8	3.752	0.0174	0.0327	215.0	114.9
FB 374	14.81	871.0	1130.2	12.329	0.0281	0.0365	438.5	337.9
FB 377	1.12	120.8	404.4	0.931	0.0039	0.0131	238.6	71.3
FB 379	4.99	897.6	1091.0	4.152	0.0290	0.0352	143.3	117.9
FB 381b	3.65	274.3	813.8	3.037	0.0089	0.0263	343.0	115.6
FB 384	3.69	954.8	1195.6	3.073	0.0308	0.0386	99.7	79.6
FB 386	4.25	902.6	1163.7	3.537	0.0291	0.0376	121.4	94.2
FB 397	2.02	1014.7	1094.5	1.679	0.0328	0.0353	51.3	47.5
Angles								
AN32b	2.63	202.8	668.7	2.191	0.0065	0.0216	334.6	101.5
AN46b	2.13	251.3	894.1	1.769	0.0081	0.0289	218.1	61.3
AN48b	1.11	256.9	942.4	0.926	0.0083	0.0304	111.6	30.4
AN51b	1.09	72.8	311.6	0.908	0.0024	0.0101	386.3	90.3
AN52b	1.49	186.5	645.2	1.244	0.0060	0.0208	206.6	59.7
AN53.1b	1.09	92.0	289.7	0.906	0.0030	0.0094	304.9	96.9
Veveyse								
VCDII 11B	0.37	127.2	263.0	0.305	0.0041	0.0085	74.2	35.9
VCDII 14B	0.31	103.5	258.4	0.258	0.0033	0.0083	77.2	30.9
VCDII 17B	0.73	154.4	380.4	0.604	0.0050	0.0123	121.1	49.2
VCDII 18B	0.61	159.2	410.4	0.505	0.0051	0.0132	98.3	38.1
VCDII 20B	0.78	146.0	315.3	0.645	0.0047	0.0102	137.0	63.4

Table D.5: TOC (%), P_{org} (ppm), P_{tot} (ppm) and calculated C/P_{org} and C/P_{tot} ratios for the marls samples of the Fiume-Bosso, Angles and VCD sections around the Faraoni level.

Angles

Ammonite Zone	20 kyr bundles	Duration
B. balearis *(at least)*	35	700000
S. angulicostatum	21	420000
P. mortilleti	24	480000
A. kiliani	25	500000
K. nicklesi	20	400000
N. pulchella	20	400000
K. compressissima	20	400000
C. darsi	17	340000
H. uhligi	12	240000
H. sayni	28	560000
G. sartousiana	20	400000
H. feraudianus	23	460000
I. giraudi	16	320000
M. sarasini	25	500000
D. oglanlensis *(at least)*	20	400000
late Hauterivian *(at least)*	80	1600000
Lower Barremian	102	2040000
Upper Barremian	124	2480000
Lowermost Aptian *(at least)*	20	400000
Barremian	226	4520000
Begining of Faraoni level to H/B boundary	25	500000

Fiume-Bosso

Ammonite Zone	100 kyr bundles	Duration
B. balearis *(at least)*	8	800000
P. angulicostata auct.	8	800000
P. catulloi (subzone)	5.5	550000
S. hugii *(at least)*	3	300000
Begining of Faraoni level to H/B boundary	5	500000

Veveyse de Châtel-St. Denis

Ammonite Zone	20 kyr bundles	Duration
S. sayni *(at least)*	34	680000
P. ligatus	25	500000
B. balearis	36	720000
P. angulicostata auct.	52	1040000
T. hugii (at least)	12	240000
Begining of Faraoni level to H/B boundary	21	420000

Gorgo a Cerbara

Magneto-chron	100 kyr bundles	Duration
M-4 *(at least)*	6	600000
M-3	17.5	1750000
M-2	6	600000
M-1	3.5	350000
M-1n	22	2200000
M-0	3.3	330000
late Hauterivian *(at least)*	5	500000
Lower Barremian	16	1600000
Upper Barremian	33.3	3330000
Lowermost Aptian *(at least)*	4	400000
Barremian	49.3	4930000
Begining of Faraoni level to H/B boundary	5	500000

Table D.6: Calculated duration of the different ammonite or magnetochron zones within the four sections. The values obtained for the first and the last ammonite zone or magnetochron for each section is a minimum value.

D.3.4. Results

D.3.4.1. The Fiume-Bosso section

The PAR values vary between 0.09 and 0.44 mg/cm^2/kyr (Fig. D.17). In the lower part of the section (below the *angulicostatum* auctorum zone), the long-term trend appears more or less constant (approximately 0.21 mg/cm^2/kyr) despite high-frequency fluctuations. Then, within the *angulicostatum* auctorum zone, the values begin to decrease and reach a minimum (0.13 mg/cm^2/kyr) around the Faraoni level. Above the Faraoni level, the values increase and reach a maximum in the sediments approximately 10 meters above the Faraoni level. In the upper part of the section we observe again a decrease in the PAR trend.

The C_{org}/P_{org} ratios measured in marly intervals within and around the Faraoni level show two closely spaced excursions toward values between 300 and 450 near and within the Faraoni level whereas background values vary between 50 and 100 (Fig. D.16). The C_{org}/P_{tot} ratios show approximately the same behaviour as the C_{org}/P_{org} ratios but with lower absolute values. Near or within the Faraoni level, values are higher than 114 (with the exception of one sample) whereas the other samples have values between 20 and 100.

D.3.4.2. The Veveyse de Châtel-St. Denis section

The VCD section displays the highest PAR values of this work (Fig. D.18). They vary between 0.98 and 3.48 mg/cm^2/kyr, with a mean value of 1.82 mg/cm^2/kyr. In the lower part of the section (*sayni* zone), a first decrease in PAR is observed, with values reaching a minimum at the *sayni-ligatus* boundary. A strong increase follows and PAR values reach a maximum within the *balearis* zone. The sediments attributed to the late *balearis* – early *angulicostata auct.* zones are marked by generally low PAR values and a decreasing trend. A short positive shift is distinguished in the middle of the *angulicostata auct.* zone. We note that the sediments considered to represent the equivalent of the Faraoni level are marked by a negative shift in PAR. Finally, the upper part of the section shows an increase in PAR values.

The C/P ratios are very low, with an average value close to 100 for the C_{org}/P_{org} ratios and close to 45 for the C_{org}/P_{tot} ratios. No specific trend is distinguished.

D.3.4.3. The Angles section

The sediment succession of the Angles section studied here represents the time interval between the *balearis* zone (late Hauterivian) and the *oglanlensis* zone (earliest Aptian). This specific section yielded the most contrasted PAR curve (Fig. D.19). PAR values vary between 0.57 and 1.96 mg/cm^2/kyr, with an average value of 1.08 mg/cm^2/kyr. After a more or less constant trend in sediments attributed to the *balearis* zone (mean value of 1.28 mg/cm^2/kyr), a first decrease is observed in sediments of the *angulicostatum* zone (Vermeulen, 2002), and a minimum in PAR values is reached within the Faraoni level (0.57 mg/cm^2/kyr). Higher up in the section, the trend in PAR values increases again up to the sediments of the latest *nicklesi* zone. A small positive shift is observed in sediments of the middle *kiliani* zone. In sediments from the *pulchella* to the *darsi* zones, the values are firstly rapidly decreasing, and then more or less constant with a positive shift in sediments dating from the beginning of the *compressissima* zone. In the following, the PAR values are increasing up to the end of the *darsi* zone. Finally, in the sediments near the top of the section dated as late Barremian – earliest Aptian, the long-term trend appears more or less constant (around 0.98 mg/cm^2/kyr) despite some high-frequency fluctuations (especially in sediments of the *sartousiana – feraudianus* zones).

The C_{org}/P_{org} ratios are clearly enriched around the Faraoni level (with a twofold peak and a maximum value of 386). Approximately 8m below the Faraoni level, a further peak near 330 is distinguished (Fig. D.16). The same behaviour is seen for the C_{org}/P_{tot} ratios, but with a maximum value of 102 for the enriched samples.

D.3.4.4. The Gorgo a Cerbara section

The PAR values vary between 0.08 and 0.77 mg/cm^2/kyr (Fig. D.20). Sediments belonging to the early Barremian and the early-late Barremian boundary transition are characterized by two

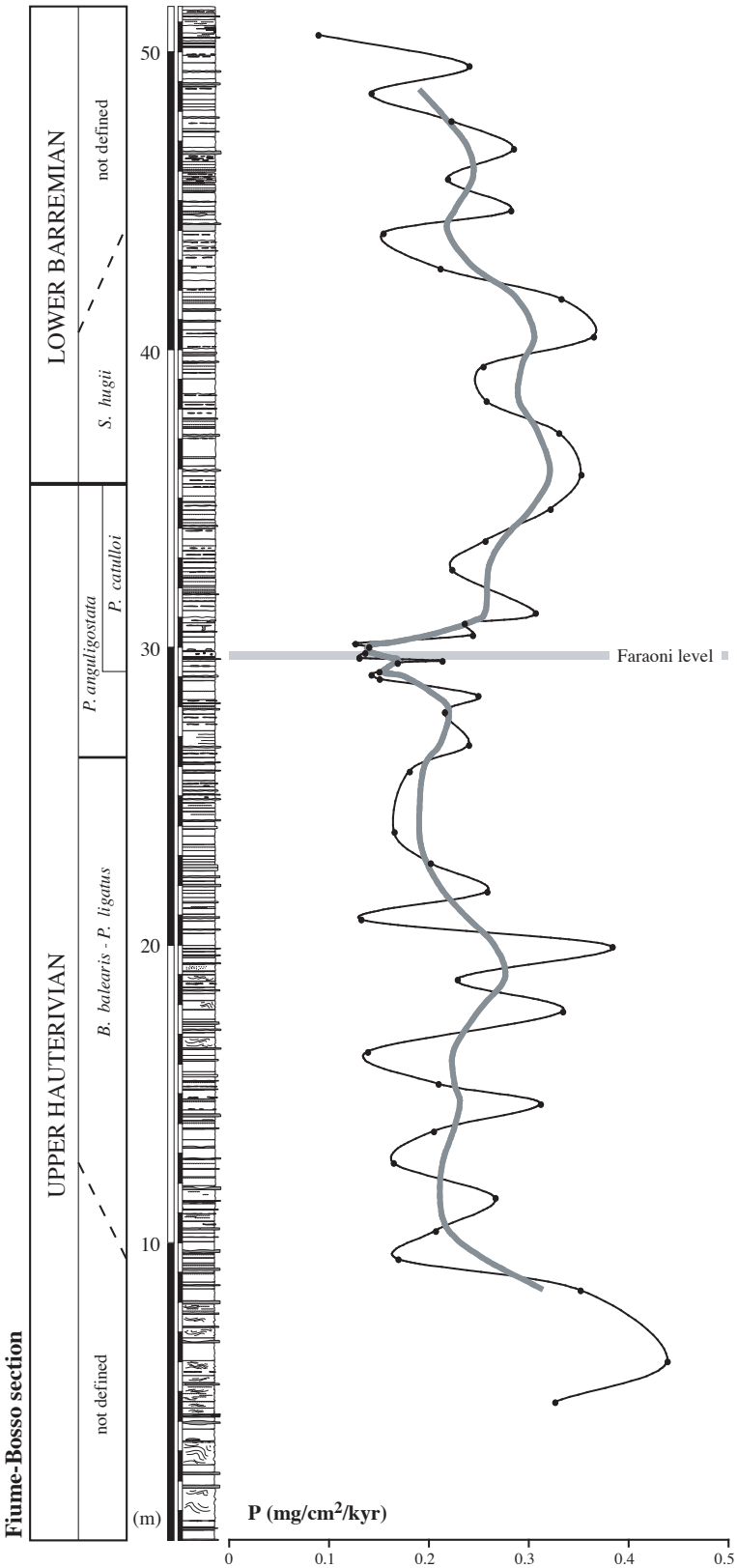

Fig. D.17: Fiume-Bosso PAR values. The trend curve is calculated using a five point moving average formula. Biostratigraphy after Coccioni et al. (1998).

strong positive shifts (the values exceed 0.60 mg/cm^2/kyr in both shifts). In sediments attributed to the late Barremian, a slightly diminishing trend of around 0.30 mg/cm^2/kyr is distinguished, along with higher frequency fluctuations.

D.3.5. Discussion

D.3.5.1. Phosphorus accumulation

The flux of dissolved, bio-available, P into

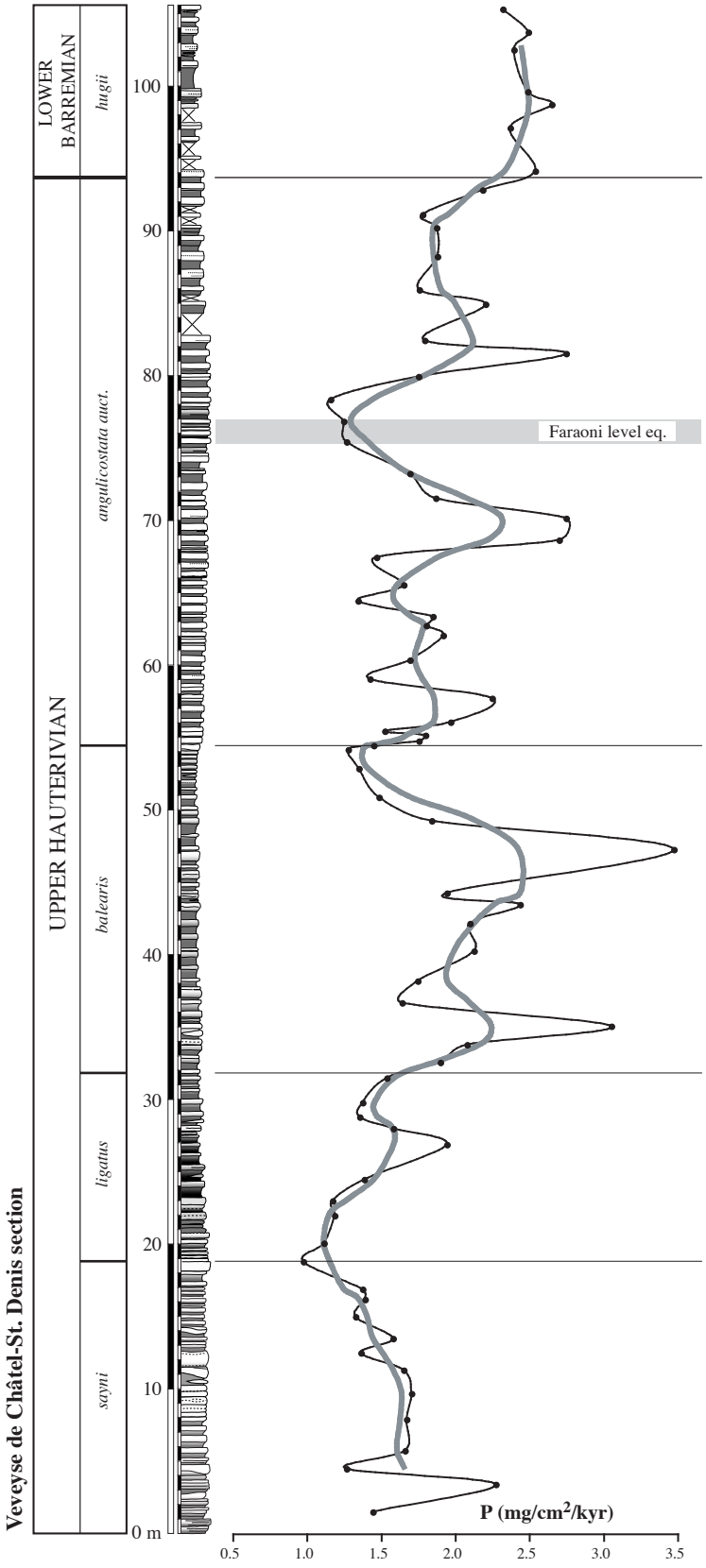

Fig. D.18: Veveyse PAR values. The trend curve is calculated using a five point moving average formula. Biostratigraphy modified after Busnardo et al. (2003).

the ocean is mainly controlled by continental runoff and atmospheric transport (Föllmi, 1996; Delaney, 1998; Benitez-Nelson, 2000; Compton *et al.*, 2000). The removal of bio-available P from the ocean reservoir is given by the difference between the rate of P sedimentation and its return

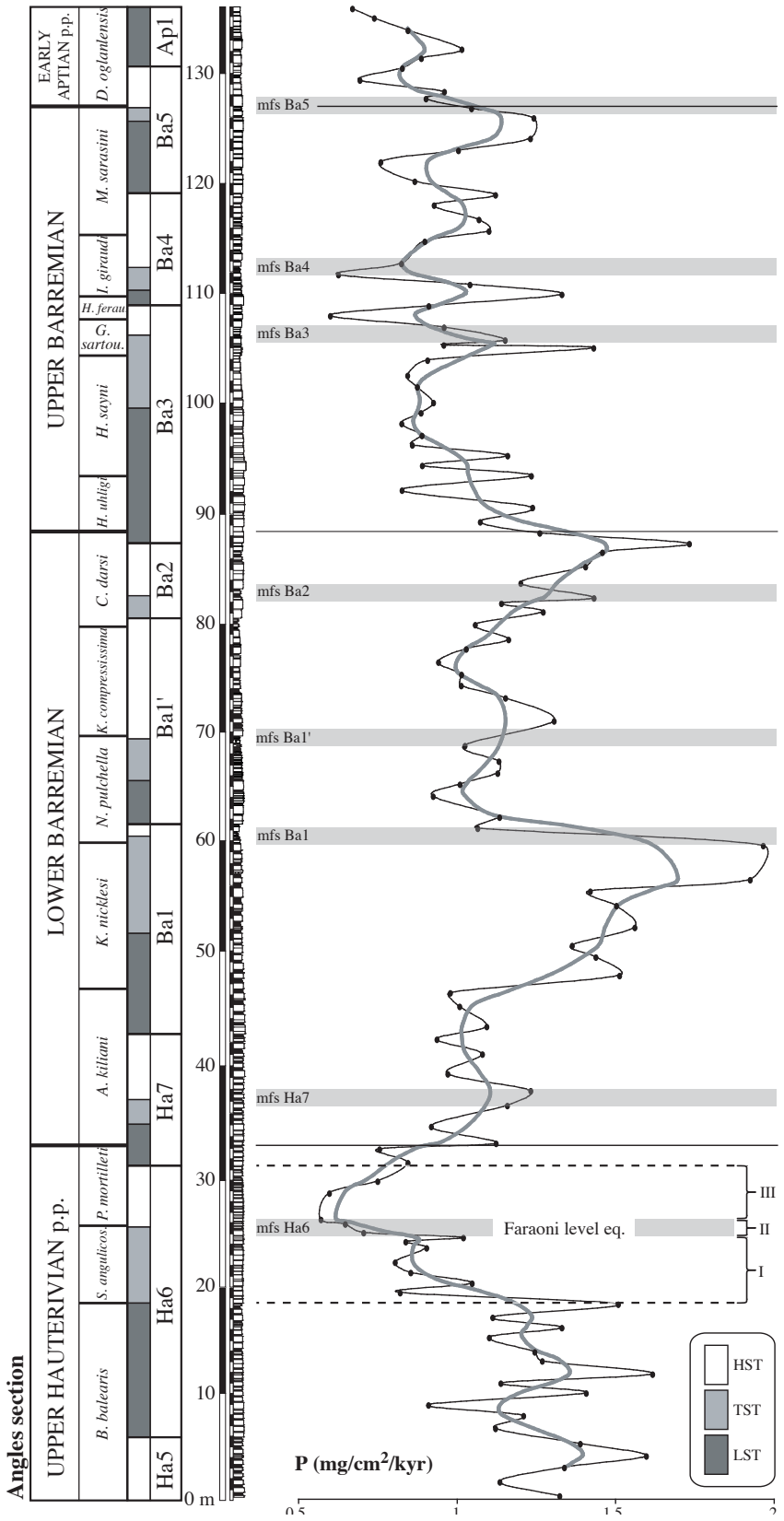

Fig.D.19: Angles PAR values. The trend curve is calculated using a five point moving average formula. Biostratigraphy after Vermeulen (2002). I, II and III refers to the model stages developed in Fig.7.

flux from the sedimentary reservoir. The transfer of bio-available P into the sedimentary reservoir occurs either by sedimentation of organic matter bound P, P adsorbed on clay particles and Fe- and Mn-oxyhydroxides, P in fish debris, or by direct (microbial?) precipitation of dissolved inorganic

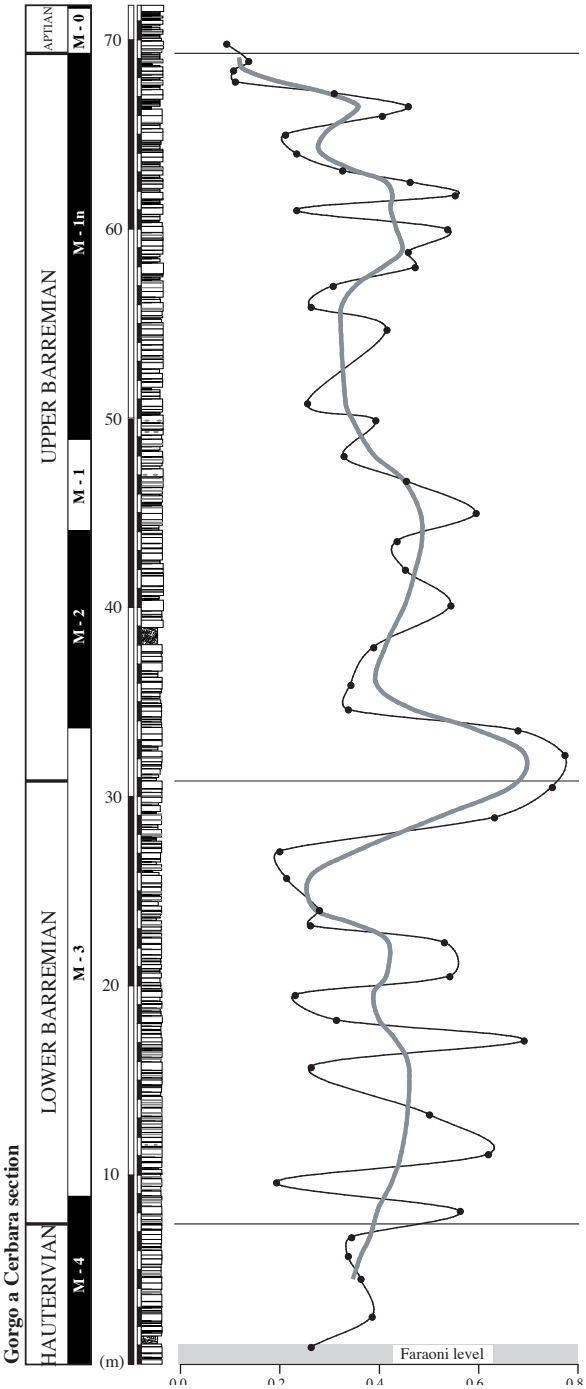

Fig.D.20: Gorgo a Cerbara PAR values. The trend curve is calculated using a five point moving average formula. Modified after Fiet and Gorin, 2000.

P (*e.g.*, Ruttenberg, 1993; Filippelli and Delaney, 1996; Föllmi, 1996). Early diagenetic regeneration of P and its removal from the sediments is an important process (Broecker and Peng, 1982; Colman and Holland, 2000; Tamburini *et al.*, 2002, 2003; but see also Anderson *et al.*, 2001). The efficiency of P storage in the sedimentary reservoir is redox dependent and P regeneration becomes more important in oxygen-depleted bottom waters (Ingall and Jahnke, 1994; Van Cappellen and Ingall, 1996; Colman and Holland, 2000; Emeis *et al.*, 2000). The redox-sensitive capacity of P storage in the sedimentary reservoir may result in a positive feedback mechanism between water-column anoxia, enhanced benthic phosphorus regeneration, and increased marine productivity (Ingall and Jahnke, 1994, 1997; Van Cappellen and Ingall, 1996; Colman and Holland, 2000).

The rate of P accumulation integrated over larger areas and time scales exceeding the actual residence time of P (approximately 10 kyr; Ruttenberg, 1993; Filippelli and Delaney, 1996; Colman and Holland, 2000) is therefore driven by two main processes: (1) the combined river and atmospheric input of P, which is linked to the rates of continental weathering, erosion, and runoff; and (2) the degree of bottom-water oxygenation. As such, an increase in PAR indicates either an increase in the intensity of continental weathering and erosion rate, for example induced by a more humid climate and/or an increase in bottom-water oxygenation. On the other hand, a decrease in PAR indicates either a decrease in continental weathering rates, related for example to a change to a drier climate, or a spread of dysaerobic to anoxic bottom-waters, or the combined effect of both processes.

D.3.5.2. The C/P molar ratio

In the Fiume-Bosso and Angles sections, the marls associated with the Faraoni level are marked by an increase of the C_{org}/P_{org} molar ratio in preserved organic matter to values of maximal 400. The marls in and around the equivalent of the Faraoni level of the VCD section yielded very low TOC values (< 0.5%) and an interpretable C/P molar ratio could not be obtained. The measured C_{org}/P_{org} molar ratios deviate from the Redfield ratio (106:1; Redfield, 1958), which implies that the preserved organic matter is depleted in phosphorus relative to carbon. Ingall *et al*. (1993), Ingall and Jahnke (1994, 1997), Van Cappellen and Ingall (1996), and Slomp *et al*. (2004) associated increased C_{org}/P_{org} molar ratios in organic matter with the degradation of organic matter and the relative loss of organic phosphorus under the influence of water column anoxia, which would concur with the overall minimal values in P accumulation rates during the Faraoni anoxic event. Interestingly, a twofold spike in C_{org}/P_{org} molar ratio is present in both sections, which may suggest that the unfolding of anoxic conditions may not have been uniform, but stepwise, with an intermittent return to more normal conditions. Within the Faraoni level, the C_{org}/P_{tot} molar ratio appears to trace well the lower spike in the twofold spike in the C_{org}/P_{org} ratio; the upper spike is less markedly traced.

Following Anderson *et al*. (2001), it appears that the $C_{org}/P_{reactive}$ molar ratio ($P_{reactive} = P_{oxide\text{-}associated} + P_{authigenic} + P_{org}$) is a more robust measure of the degree of P lost to the ocean than C_{org}/P_{org} molar ratio, due to the possible diagenetic transfer of organic phosphorus into an authigenic phase. In ancient marine sedimentary rocks, the chemical distinction between the $P_{authigenic}$ and $P_{detritic}$ phases is, however, difficult (*e.g*., Filippelli and Delaney, 1995) and we decided, therefore, to analyze P_{tot} and to calculate the C_{org}/P_{tot} ratio ($P_{tot} = P_{reactive} + P_{detritic}$). Silt- and sand-sized detrital material is quasi absent in the here analyzed (hemi-)pelagic sections and the presence of detrital phosphate seems minimal but cannot be totally excluded. The here presented C_{org}/P_{tot} ratio is therefore a minimal value and the ratio approaching the effective quantity of organic phosphorus that was transferred into an authigenic phase and remained as such within the marly bed lies somewhere between the C_{org}/P_{tot} and C_{org}/P_{org} molar ratios.

At Fiume Bosso, pre- and post Faraoni sediments show C_{org}/P_{tot} and C_{org}/P_{org} molar ratios which are almost identical and mostly substantial lower than the Redfield ratio, whereas the organic-rich Faraoni sediment have higher C_{org}/P_{tot} and C_{org}/P_{org} molar ratios. The low and almost identical pre- and post-Faraoni C_{org}/P_{tot} and C_{org}/P_{org} molar ratios suggest that practically all P is conserved as P_{org} and that the organic matter is depleted in C_{org} relative to P_{org}, most likely by bacterial degradation (*e.g*., Reimers *et al*., 1990). The Faraoni sediment show systematically lower C_{org}/P_{tot} than C_{org}/P_{org} ratios, which are all slightly to markedly higher than the Redfield ratio, with the exception of one sample (Fig. D.16). This suggests that during early diagenesis of the organic-rich sediments of the Faraoni level, P_{org} was preferentially mobilized (relative to C_{org}) and a transfer of P_{org} took place both into an authigenic phase as well as out of the organic-rich layer, most likely back into the bottom water. This systematic stratigraphic change in C_{org}/P_{tot} and C_{org}/P_{org} molar ratios in and around the Faraoni sediments suggests that under normal conditions, a preferential loss of C_{org} relative to P_{org} took place, whereas under more anoxic conditions during the deposition of the Faraoni level, a preferential loss of P_{org} relative to C_{org} is observed, which is related both to a transfer of Porg into an authigenic phase, as well as out of

the initial layer back into the seawater.

For the Angles section, the C_{org}/P_{tot} molar ratios are systematically lower than the C_{org}/P_{org} molar ratios, both within the sediments of the Faraoni equivalent, as well as around this level. This may indicate that in all analyzed marl samples, P_{tot} is a composite of P_{org} and $P_{authigenic+detritic}$. The C_{org}/P_{org} molar ratios are all higher than the Redfield ratio, whereas the C_{org}/P_{tot} molar ratios are lower or near the Redfield ratio. This may signify that systematically a transfer took place of P_{org} into an authigenic P phase, whereas – in contrast to the Fiume Bosso section – a diagenetic transfer of P back to the seawater is less likely. In addition, due to the paleogeographic position of Angles close to the European continent, a more significant influx of $P_{detritic}$ than at Fiume-Bosso can not be excluded. Moreover, in the Angles section, TOC values are generally low (mean value close to 1.5%) and the Faraoni level is not as much enriched as could be expected from a basinal record (cf. Fiume-Bosso results, Table D.5). This may hint at the possibility of late-stage diagenetic alteration of organic matter coupled with the preferential loss of C_{org}. These two mechanisms could thus also be responsible of the negative shift of the Angles C_{org}/P_{tot} molar ratios relative to the C_{org}/P_{org} molar ratios.

D.3.5.3. Comparison of the PAR curves between the four sections

The PAR of the Fiume-Bosso and the Gorgo a Cerbara sections are characterized by low average values whereas the VCD section shows PAR values which are about eight times higher than those of the Fiume-Bosso and Gorgo a Cerbara sections. This difference in absolute PAR values is likely related to the different paleogeographic positions of the sections. The paleogeographical location of the Fiume-Bosso and Gorgo a Cerbara sections is remote from any continental source, and the low PAR, which are comparable to the PAR values from the ODP and DSPD compilation from Föllmi (1995), indicate generally low detrital influx rates. Moreover, the values of the VCD section, which are high also compared to those of the Angles section, indicate that along the northwestern tethyan margin the Ultrahelvetic realm received more detrital material than the Vocontian Basin during the time period studied. In the field, the more marly facies of the Ultrahelvetic carbonates supports this observation.

The good overall correlation between the PAR trend calculated for the four sections, as well as with the PAR trend given by Föllmi (1995) and van de Schootbrugge *et al*. (2003), suggests that the evolution in PAR during the late Hauterivian and the Barremian is similar over wide areas within the western Tethys (Fig. D.21). PAR values show a first minimum close to the *sayni – ligatus* zone boundary, which was already described by van de Schootbrugge *et al*. (2003) for the Tethyan realm. In the absence of known anoxia events during this time, this may be explained by low nutrient influx rates into the Tethyan realm during the early late Hauterivian. PAR values show subsequently a general increase until the *balearis* zone, which is followed by a general decrease towards the Faraoni level. In the Fiume-Bosso, Angles and VCD sections, the Faraoni level itself is marked by a minimum in PAR values. In sediments above the Faraoni level, PAR values increase again in all four sections. The early Barremian is thus characterized by relative high values in the four studied sections as well as in the global curve of Föllmi (1995). Following Bréhéret (1994) and Erba *et al*. (1999), the early Barremian in the western tethyan realm is characterized by the deposition of black shales that appear contemporaneous with the positive peaks in PAR. Finally, in the late Barremian, PAR values are more or less constant (with a slight decrease), even if the global curve of Föllmi (1995) shows a slight increase (Fig. D.21). In the Italian sections, extreme fluctuations are observed during the late Hauterivian and the early Barremian. Moreover, in these sections, many thin and isolated black-shale horizons are found during this time interval, arguing for local and short-lived anoxic conditions during the late Hauterivian – early Barremian within the Umbria-Marche basin.

D.3.5.4. The Faraoni oceanic anoxic event

The latest Hauterivian minimum in PAR values observed in the Fiume-Bosso, Angles and VCD sections coincides with the Faraoni level, which may hint at a causal relationship between

late Hauterivian PAR behaviour and the Faraoni anoxic event. If this is the case, then the decrease in PAR values during the late Hauterivian may well be the consequence of a progressive loss of oxygen in oceanic bottom waters, with the Faraoni anoxic event as a result of the culminating effect of the loss of oxygen, which may have started in the late *balearis* zone. This could also explain the presence of the pronounced negative shift in the VCD section during the *angulicostata auct*. zone below the Faraoni level. Eventual anoxic conditions may have developed earlier than in shallower regions, which were bathed in oxygen-depleted bottom waters only later, due, for example, to the progressive vertical expansion of an oxygen minimum zone. The minimum in PAR is probably related to a general diminution both in the capacity of transferring P into the sedimentary reservoir as well as in the capacity of preserving P within the sedimentary reservoir, as is indicated by the C/P molar ratios in Fiume Bosso – both in dependency of oxygen contents in the bottom waters.

For the Angles section, a detailed study of the trends in stacking patterns has been made, which was used for a sequence-stratigraphic interpretation (Fig. D.19). This allows us to compare the PAR curve with the inferred sequence-stratigraphic trends. It appears that almost every maximum in PAR values is related to a maximum flooding surface (mfs), except for of the Faraoni level and the mfs Ba4, which are characterized by a minimum in PAR values. Interestingly, the sea-level lowstands are not characterized by high PAR values. These observations correlate well with the observations of Föllmi (1995) who noted a positive correlation between sea level and phosphorus burial during greenhouse climates. A clear difference in the nutrient cycle between greenhouse and icehouse conditions is thus underlined in the Barremian sediments of the Angles section. Below the Faraoni level, the onset of the PAR decrease coincides with the transgressive surface (ts) of Ha6 and the minimum in PAR values with the mfs Ha6.

This relationship suggests the presence of a link between the Faraoni anoxic event and the late Hauterivian phase of sea-level rise (Ha6), which represent an important transgression during the late Hauterivian and early Barremian (Haq *et al*., 1987; Hardenbol *et al*., 1998). During this transgression, straits connecting the tethyan and boreal realms were opened and/or became broader and deeper, as is suggested by belemnite migration patterns observed by Mutterlose and Bornemann (2000) and the presence of boreal nannoplancton in the Angles section around the Faraoni level (Silvia Gardin, pers. comm.). This may have led to the increased influx of colder and eventually more nutrient-rich waters into the Tethys, as was also proposed for the middle Hauterivian transgression (van de Schootbrugge *et al*., 2003).

During greenhouse conditions, a link between sea-level change and nutrient influx has already been noted by different authors (*e.g*., Jenkyns *et al*., 1994; Föllmi, 1995; Hilbrecht *et al*., 1996; Gale *et al*., 2000; Jarvis *et al*., 2002; van de Schootbrugge *et al*., 2003), and different mechanisms have been proposed:

(1) Jarvis *et al*. (2002) invoked reworking of sediments and soils by flooding of land areas to explain the increase in nutrient fluxes during transgression. The peculiar palaeogeography of the Cretaceous world, characterized by the presence of extensive shallow epicontinental seas during high sea level, may have favoured this process.

(2) An additional mechanism may have been provided by intensified sea surface-water evaporation due to the enhanced surface of epicontinental seas: intensified evaporation may have lead to increased wind velocities (*e.g*., Iruthayaraj and Morachan, 1978), which may have resulted in stronger coastal upwelling and in increased availabity of nutrients during sea-level rise

(3) A third mechanism which relates sea-level with nutrient supply is climate: Transgression, climate warming, and enhanced evaporation may accelerate the global water cycle and intensify precipitation on the continent, which again favours biogeochemical weathering and the release of biophile elements (*e.g*., Föllmi, 1996).

(4) A positive feedback between water-column

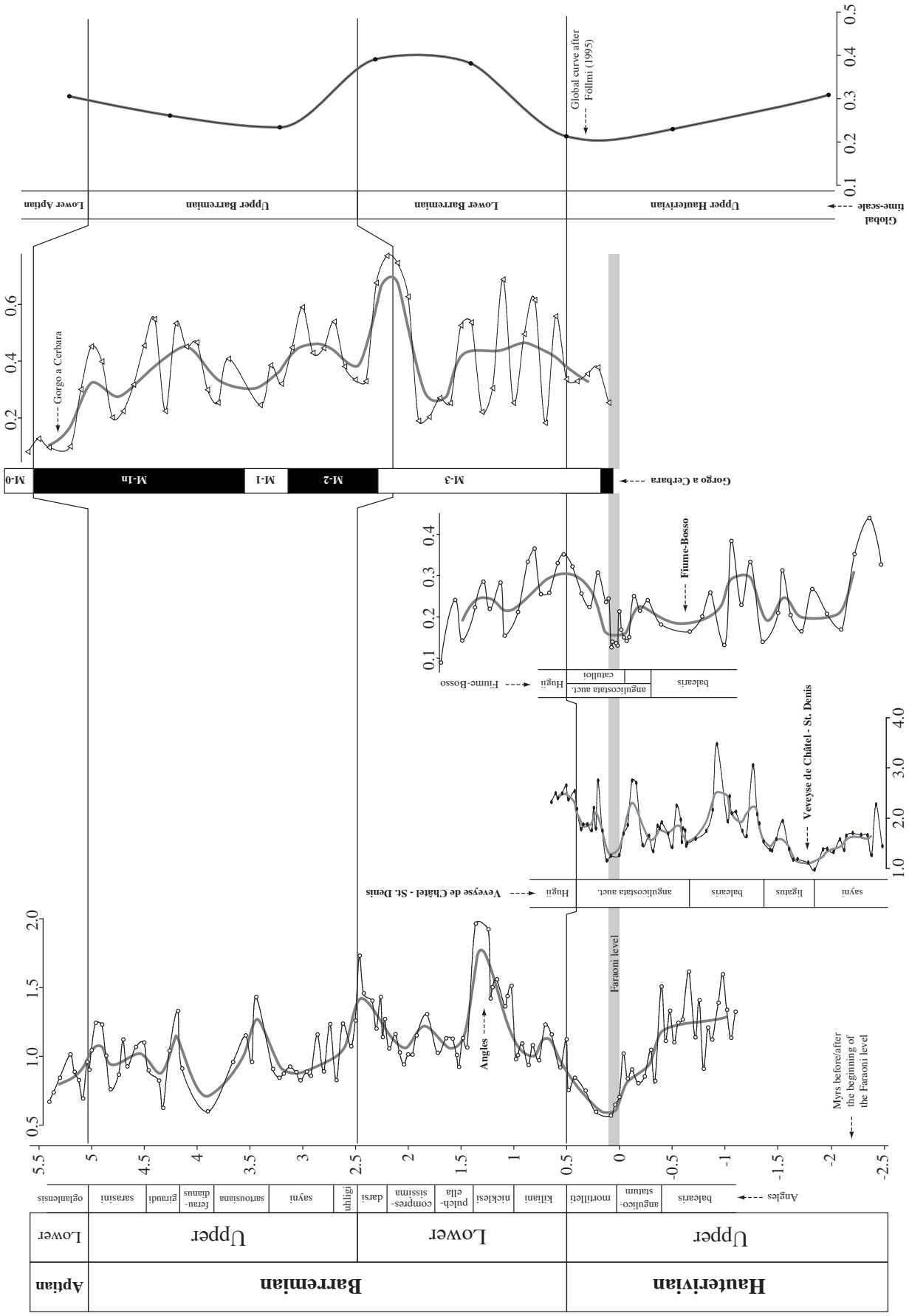

Fig. D.21: Correlation of the PAR values from the four studied sections and the global curve established by Föllmi (1995). The absolute PAR values being different for the four sections, the curves are not to scale to better compare the different variations of the PAR values. The absolute ages, in regard to the beginning of the Faraoni level, were obtained using cyclo-stratigraphic interpretations (see text for explanation).

anoxia, enhanced benthic phosphorus regeneration, and marine productivity during transgressions should also be taken into account (Ingall and Jahnke, 1994, 1997). This mechanism, however, appears to be balanced by the phosphorus-oxygen negative feedback loop described by Holland (1994) and Lenton and Watson (2000). In this model, the amount of phosphorus dissolved in the water is influenced by changes in the levels of dissolved oxygen in the water column. The decrease of the burial of organic and iron-bound phosphorus under oxygen-depleted conditions in ocean bottom waters tends to increase the ocean nutrient inventory and provide negative feedback against declining oxygen by increasing the population of oxygen-producing organisms.

In taking into account the observed link between the minima in the PAR record accompanying the oceanic anoxic Faraoni event, we propose the following model (Fig. D.22):

(1) The third-order sea-level rise during the late Hauterivian (Ha6 transgression: Haq *et al*., 1987; Hardenbol *et al*., 1998) led to a combination of the above-mentioned mechanisms (*i.e*., reworking of sediments and soils on flooded land areas, stronger evaporation rates, stronger winds and stronger upwelling, stronger biogeochemical weathering), which - together with enhanced tethyan-boreal connection and the influx of colder and eventually nutrient-rich waters - resulted in increased nutrient input into the Tethys. The resulting increase in primary productivity and corresponding export production induced a decrease in oceanic oxygen levels and the expansion of the oxygen minimum zone. The spreading of oxygen-depleted ocean bottom waters may have resulted in enhanced P regeneration from the sediments, which also contributed to a further fertilisation of the ocean. During this time interval, true anoxic conditions were not reached on a global scale and short-lived anoxic conditions were only locally present. During the late Hauterivian sea-level rise, the phosphorus-oxygen negative feedback loop described by Holland (1994) and Lenton and Watson (2000) may have been overwhelmed by the coupled positive feedback mechanism leading to higher nutrient concentrations, and may have been too weak to balance the decrease in oceanic oxygen levels.

(2) During the period of most rapid sea-level rise (mfs Ha6), these coupled mechanisms reached their climax and resulted in the Faraoni oceanic anoxic event. This event may be considered as the result of a steady-state situation, in which the positive feedback mechanisms leading to increased nutrient availability are balanced by the negative feedback mechanisms (phosphorus-oxygen negative feedback coupled with organic matter preservation). The limestone–black shale alternation, which is characteristic of the Faraoni level in the four investigated sections and elsewhere may then be explained by high-frequency oscillations superimposed on this steady-state situation.

(3) During subsequent sea-level highstand (highstand systems track of Ha6), the rapid filling of shallow-water areas by sediments may have diminished the importance of the tethyan-boreal connection, and the associated nutrient influx. Also the other mechanisms leading to nutrient mobilisation may have become less efficient, due, for example, to less intense biochemical weathering in a transport-limited weathering system (Stallard and Edmond, 1983), or to a progressively diminishing return flux of P from the sediments. As such the phosphorus-oxygen negative feedback mechanism may have become stronger than the positive feedback mechanisms leading to enhanced P availability. This then may have resulted in an increase in oceanic oxygen levels, the diminution of the OMZ and thus the termination of the oceanic anoxic conditions.

In this model, the Faraoni level is considered as the turning point during the evolution of this oceanic oxygen depletion event. Indeed, the increased transfer of organic matter into the sedimentary reservoir should be considered as the response of the Earth system by which it counteracts the decrease of oceanic oxygen levels.

D.3.5.5. The attenuated $\delta^{13}C$ signature during the late Hauterivian and early Barremian

One of the remarkable features of the Faraoni oceanic anoxic event is its poor expression in the $\delta^{13}C$ record. The $\delta^{13}C$ record of the late

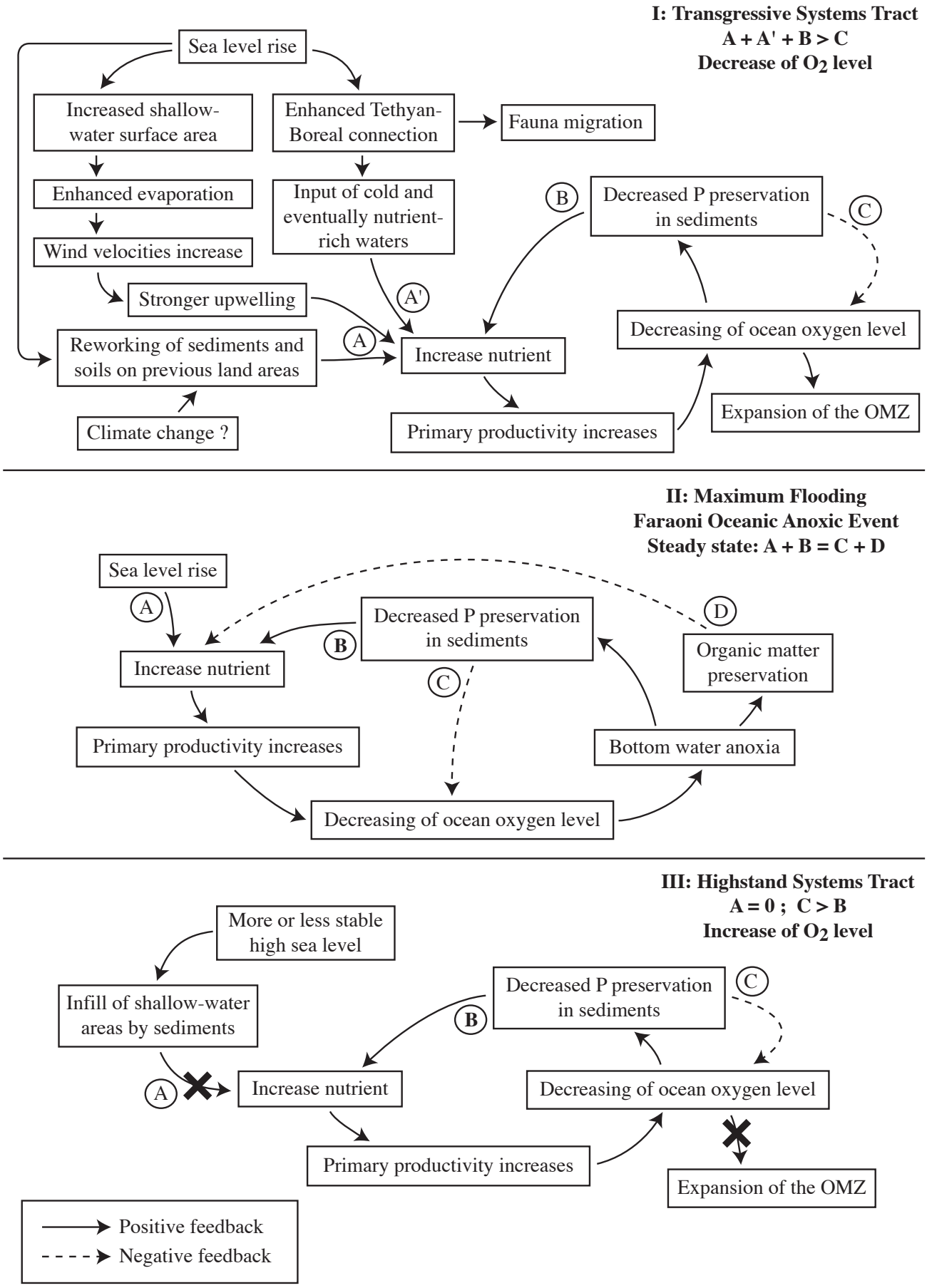

Fig. D.22: Three step (transgressive systems tract, maximum flooding, highstand systems tract) box model of the unfolding of the Faraoni event. See text for explanation.

Hauterivian is characterized by a long-term steady increase of approximately 1‰ which culminates in a maximum near the Hauterivian-Barremian boundary, followed by a small decrease in the earliest Barremian (van de Schootbrugge *et al*., 2000; Godet *et al*., in press). Unlike the oceanic anoxic events of the Valanginian, early Aptian and latest Cenomanian, the Faraoni anoxic event is not related to a well-expressed positive excursion in $\delta^{13}C$. The accumulation of organic-rich sediments accompanied by an episode of carbonate platform drowning is an expression of important changes in the carbon cycle, which normally would find an expression in the $\delta^{13}C$ record. Either the Faraoni anoxic event is the result of regional, rather than global environmental change, limited to the Tethyan realm, and the changes in the carbon household within this realm were not sufficiently important to influence global $\delta^{13}C$ signatures, or a buffering mechanism capable to attenuate the $\delta^{13}C$ record played a role. This buffering mechanism maybe related to different mechanisms, such as the enhanced productivity of shallow-water carbonates outside the western tethyan realm or the increased size of the oceanic dissolved inorganic carbon reservoir (*e.g*., van de Schootbrugge *et al*., 2003; Bartley and Kah, 2004).

D.3.5.6. The carbonate platform drowning episode during the latest Hauterivian and early Barremian: consequence of the Faraoni event?

The Faraoni oceanic anoxic event is contemporaneous with the onset of a platform drowning event along the northern tethyan margin that started during the latest Hauterivian and ended near the boundary between the early and late Barremian (D3 in Föllmi *et al*., 1994). Interestingly, the time covered by this drowning episode is mirrored by contrasted variations in PAR in the Western Tethys, *i.e*. by a negative shift associated with the late Hauterivian Faraoni event and by two major positive shifts during the early Barremian. These two latter peaks in PAR may reflect an increase of nutrient input induced by change towards probably more humid climate in the western tethyan realm. These climate changes and related changes in nutrient input came after the Faraoni oceanic anoxic event and may have prolonged the drowning episode, which onset is related to the environmental changes during the Faraoni event. Subsequently, during the late Barremian, platform growth took up again leading to the deposition of the "Urgonian" limestone was promoted to a large extend by photozoans. The unfolding of this important phase in the evolution of helvetic platform growth may have been related to an overall decrease in P availability as is documented by our P-accumulation curve.

D.3.6. Conclusions

Monitoring phosphorus accumulation in pelagic and hemi-pelagic sediments of the western Tethys during the late Hauterivian and Barremian allows us to better understand the associated palaeoceanographic changes, and especially the unfolding of the late Hauterivian Faraoni oceanic anoxic event. Our results correlate well with those previously obtained by van de Schootbrugge *et al*. (2003) for the late Hauterivian. Good correlation is also seen with the DSDP-ODP based curve of Föllmi (1995).

Based on the general evolution of the PAR curve and its correlation with inferred sea-level variations, we propose a new model for the origin of the Faraoni event, which incorporates increased nutrient mobilization on the continent and an improved tethyan-boreal connection, which is linked to a positive feedback loop generated by a decrease in the capacity of phosphorus preservation in the sedimentary reservoir, and a negative feedback loop related to changes in the ocean oxygen cycle.

Moreover, the Faraoni event is linked to the onset of an important platform drowning event along the northern tethyan margin. An extended increase in nutrient input during the early Barremian may have extended the drowning episode well into the Barremian.

Finally, during the late Barremian, the recorded low PAR values are in agreement with the worldwide development of the Urgonian facies, reflecting oligotrophic conditions on the shelf.

D.3.7. Acknowledgments

The authors acknowledge Rodolfo Coccioni, Pascal Linder, Haydon Mort, Claire Rambeau, Virginie Matera and Philipp Steinmann for their help in the field and/or stimulating discussions. Special thanks go to the team of the "Reserve Géologique de Haute-Provence" for providing an authorization for fieldwork. We thank Helmut Weissert and an anonymous reviewer for their critical reviews. Financial support from the Swiss National Science Foundation Project 2100-067807/1 and 200020-105206/1 is gratefully acknowledged.

D.3.8. References

Anderson, L. D. and Delaney, M. L. (2000). «Sequential extraction and analysis of phosphorus in marine sediments: Streamlining of the SEDEX procedure.»**Limnol. Oceanogr.** 45(*2*): 509-515.

Anderson, L. D., Delaney, M. L. and Faul, K. L. (2001). «Carbon to phosphorus ratios in sediments: Implications for nutrient cycling.» **Global Biogeochemical Cycles** 15(*1*): 65-79.

Bartley, J. K. and Kah, L. C. (2004). «Marine carbon reservoir, C_{org} - C_{carb} coupling, and the evolution of the Proterozoic carbon cycle.» **Geology** 32(*2*): 129-132.

Baudin, F., Bulot, L. G., Cecca, F., Coccioni, R., Gardin, S. and Renard, M. (1999). «Un équivalent du «Niveau Faraoni» dans le bassin du Sud-Est de la France, indice possible d'un événement anoxique fini-hauterivien étendu à la Téthys méditerranéenne.» **Bulletin de la Société Géologique de France** 170(*4*): 487-498.

Behar, F., Beaumont, V. and Penteado, H. L. D. (2001). «Rock-Eval 6 technology: Performances and developments.» **Oil and Gas Science and Technology** 56(*2*): 111-134.

Benitez-Nelson, C. R. (2000). «The biogeochemical cycling of phosphorus in marine systems.» **Earth-Science Reviews** 51(*1-4*): 109-135.

Broecker, W. S. and Peng, T.-H. (1982). Tracers in the sea, Lamont-Doherty Geological Observatory, Columbia University, Palisades, New-York, Eldigio Press.

Bréhéret, J.-G. (1994). The Mid-Cretaceous organic-rich sediments from the Vocontian zone of the French Southeast basin. Hydrocarbon and Petroleum Geology of France. A. Mascle. 4: 295-320.

Busnardo, R. (1965). «Le stratotype du Barrémien.» **Mémoires du Bureau de Recherche Géologiques et Minières.** 34: 101-116.

Busnardo, R., Charollais, J., Weidmann, M. and Clavel, B. (2003). «Le Crétacé inférieur de la Veveyse de Châtel (Ultrahelvétique des Préalpes externes; canton de Fribourg, Suisse).» **Revue Paléobiol., Genève** 22(*1*): 1-174.

Cecca, F., Faraoni, P., Marini, A. and Pallini, G. (1995). «Field-trip across the representative sections for the Upper Hauterivian - Barremian ammonite biostratigraphy in the Maiolica exposed at Monte Nerone, Monte Petrano and Monte Catria (Umbria-Marche, Apennines).» **Memorie Descrittive della Carta Geologica d'Italia** 51: 187-211.

Cecca, F., Marini, A., Pallini, G., Baudin, F. and Begouen, V. (1994). «A guide-level of the uppermost Hauterivian (Lower Cretaceous) in the pelagic succession of Umbria-Marche Apennines (Central Italy): the Faraoni Level.» **Riv. Ital. Paleontol. Stratigr.** 99: 551-568.

Coccioni, R., Baudin, F., Cecca, F., Chiari, M., Galeotti, S., Gardin, S. and Salvini, G. (1998). «Integrated stratigraphic, palaeontological, and geochemical analysis of the uppermost Hauterivian Faraoni Level in the Fiume Bosso section, Umbria-Marche Apennines, Italy.» **Cretaceous Research** 19(*1*): 1-23.

Colman, A. S. and Holland, H. D. (2000). The global diagenetic flux of phosphorus from marine sediments to the oceans; redox sensitivity and the control of atmospheric oxygen levels. Marine authigenesis; from global to microbial. C. R. Glenn, L. Prévôt-Lucas and J. Lucas, SEPM Special Publication n° 66: 53-75.

Compton, J., Mallinson, D., Glenn, C. R., Filippelli, G. M., Föllmi, K. B., Shields, G. and Zanin, Y. (2000). Variations in the global phosphorus cycle. Marine authigenesis; from global to microbial. C. R. Glenn, L. Prévôt-Lucas and J. Lucas, SEPM Special Publication n° 66: 21-33.

Delaney, M. L. (1998). «Phosphorus

accumulation in marine sediments and the oceanic phosphorus cycle.» **Global Biogeochemical Cycles** 12(*4*): 563-572.

Delanoy, G. (1997). «Biostratigraphie des faunes d'ammonites à la limite Barrémien-Aptien dans la région d'Angles-Barrême-Castellane.» **Annales du Muséum d'Histoire Naturelle de Nice (Nice)** tome XII: 1-270.

Eaton, A. D., Clesceri, L. S. and Greenberg, A. E. (1995). Standard methods for the examination of water and wastewater.

Emeis, K.-C., Struck, U., Leipe, T., Pollehne, F., Kunzendorf, H. and Christiansen, C. (2000). «Changes in the C, N, P burial rates in some Baltic Sea sediments over the last 150 years - relevance to P regeneration rates and the phosphorus cycle.» **Marine Geology** 167: 43-59.

Erba, E., Channell, J. E. T., Claps, M., Jones, C. E., Larson, R. L., Opdyke, B., Premoli-Silva, I., Riva, A., Salvini, G. and Torriceli, S. (1999). «Integrated stratigraphy of the Cismon APTICORE (Southern Alps, Italy): A «reference section» for the Barremian-Aptian interval at low latitudes.» **Journal of Foraminiferal Research** 29(*4*): 371-391.

Fiet, N. and Gorin, G. (2000). «Lithological expression of Milankovitch cyclicity in carbonate-dominated, pelagic, Barremian deposits in central Italy.» **Cretaceous Research** 21(*4*): 457-467.

Filippelli, G. M. and Delaney, L. M. (1996). «Phosphorus geochemistry of equatorial Pacific sediments.» **Geochimica et Cosmochimica Acta** 60(*9*): 1479-1495.

Filippelli, G. M. and Delaney, M. L. (1995). «Phosphorus geochemestry, diagenesis, and mass balances of the Miocene Monterey Formation at Shell Beach, California.» **U.S. Geological Survey Bulletin (1995)**: G1-G11.

Funk, H. (1969). «Typusprofile der helvetischen Kieselkalk Formation und der Altmann Schichten.» **Eclogae geologicae Helvetiae** 62(*1*): 191-203.

Föllmi, K. B. (1995). «160 m.y. record of marine sedimentary phosphorus burial: Coupling of climate and continental weathering under greenhouse and icehouse conditions.» **Geology** 23: 859-862.

Föllmi, K. B. (1996). «The phosphorus cycle, phosphogenesis and marine phosphate-rich deposits.» **Earth-Science Reviews** 40(*1-2*): 55-124.

Föllmi, K. B., Tamburini, F., Hosein, R., Van de Schootbrugge, B., Arn, K. and Rambeau, C. (2004). Phosphorus, a servant faithful to Gaia? Biosphere remediation rather than regulation. Scientist Debate Gaia: The Next Century. S. H. Schneider, J. R. Miller, E. Crist and P. J. Boston: 79-92.

Föllmi, K. B., Weissert, H., Bisping, M. and Funk, H. (1994). «Phosphogenesis, carbon-isotope stratigraphy, and carbonate-platform evolution along the Lower Cretaceous northern Tethyan margin.» **Geological Society of America Bulletin** 106(*6*): 729-746.

Gale, A. S., Smith, A. B., Monks, N. E. A., Young, J. A., Howard, A., Wray, D. S. and Huggett, J. M. (2000). «Marine biodiversity through the late Cenomanian - Early Turonian: palaeoceanographic controls and sequence stratigraphic biases.» **Journal of Geological Society of London** 157: 745-757.

Giraud, F., Beaufort, L. and Cotillon, P. (1995). «Contrôle astronomique de la sédimentation carbonatée dans le Crétacé inférieur du Bassin vocontien (SE France).» **Bull. Soc. Geol. France** 166(*4*): 409-421.

Godet, A., Bodin, S., Föllmi, K. B., Vermeulen, J., Gardin, S., Fiet, N., Adatte, T., Berner, Z., Stüben, D. and van de Schootbrugge, B. (2006). «Evolution of marine stable carbon-isotope record during the early Cretaceous: A focus on the late Hauterivian and Barremian in the Tethyan realm.» **Earth and Planetary Science Letters** in press.

Gradstein, F. M., Ogg, J. G., Smith, A. G., Bleeker, W. and Lourens, L. J. (2004). «A new Geologic Time Scale with special reference to Precambrian and Neogene.» **Episodes** 27(*2*): 83-100.

Haq, B. U., Hardenbol, J. and Vail, P. R. (1987). «Chronology of fluctuating sea levels since the Triassic.» **Science** 235: 1156-1167.

Hardenbol, J., Thierry, J., Farley, M. B., de Graciansky, P.-C. and Vail, P. R. (1998). Mesozoic and Cenozoic Sequence Chronostratigraphic Framework of European Basins. Mesozoic and

Cenozoic Sequence Stratigraphy of European Basins. P.-C. de Graciansky, J. Hardenbol, T. Jacquin and P. R. Vail. 60: 3-13.

Hay, W. W., DeConto, R., Wold, C. N., Wilson, K. M., Voigt, S., Schulz, M., Wold-Rossby, A., Dullo, W.-C., Ronov, A. B., Balukhovsky, A. N. and Soeding, E. (1999). Alternative global Cretaceous paleogeography. The Evolution of Cretaceous Ocean/Climate Systems. E. Barrera and C. Johnson: 332.

Herrle, J. O. (2002). «Paleoceanographic and paleoclimatic implications on Mid-Cretaceous black shale formation in the Vocontian basin and the Atlantic: Evidence from calcareous nannofossils and stable isotopes.» **Mikropaläontologische Mitteilungen** 27: 1-113.

Hilbrecht, H., Frieg, C., Troger, K.-A., Voigt, S. and Voigt, T. (1996). «Shallow water facies during the Cenomanian-Turonian anoxic event: bio-events, isotopes, and sea level in southern Germany.» **Cretaceous Research** 17: 229-253.

Holland, H. D. (1994). «The phosphate-oxygen connection.» **Eos Trans. AGU** 75 (3), Ocean Sci. Meet. Suppl.: 96.

Ingall, E. and Jahnke, R. (1994). «Evidence for enhanced phosphorus regeneration from marine sediments overlain by oxygen depleted waters.» **Geochimica et Cosmochimica Acta** 58(*11*): 2571-2575.

Ingall, E. D., Bustin, R. M. and Van Cappellen, P. (1993). «Influence of water column anoxia on the burial and preservation of carbon and phosphorus in marine shales.» **Geochimica et Cosmochimica Acta** 57(*2*): 303-316.

Ingall, E. D. and Jahnke, R. (1997). «Influence of water-column anoxia on the elemental fractionation of carbon and phosphorus during sediment diagenesis.» **Marine Geology** 139: 219-229.

Iruthayaraj, M. R. and Morachan, Y. B. (1978). «Relationship between evaporation from different evaporimeters and meteorological parameters.» **Agricultural Meteorology** 19(*2-3*): 93-100.

Jarvis, I., Mabrouk, A., Moody, R. T. J. and de Cabrera, S. (2002). «Late Cretaceous (Campanian) carbon isotope events, sea-level change and correlation of the Tethyan and Boreal realms.» **Palaeogeography, Palaeoclimatology, Palaeoecology** 188(*3-4*): 215-248.

Jenkyns, H. C. (1999). «Mesozoic anoxic events and palaeoclimate.» **Zentralblatt Geologie und Paläontologie, 1** Heft 7-9: 943-949.

Jenkyns, H. C. (2003). «Evidence for rapid climate change in the Mesozoic-Palaeogene greenhouse world.» **Philosophical Transactions of the Royal Society, London, A** 361: 1885-1916.

Jenkyns, H. C., Gale, A. S. and Corfield, R. M. (1994). «Carbon- and oxygen-isotope stratigraphy of the English Chalk and Italian Scaglia and its palaeoclimatic significance.» **Geol. Mag.** 131: 1-34.

Jones, C. E. and Jenkyns, H. C. (2001). «Seawater strontium isotopes, oceanic anoxic events, and seafloor hydrothermal activity in the Jurassic and Cretaceous.» **American Journal of Science** 301: 112-149.

Lenton, T. M. and Watson, A. J. (2000). «Redfield revisited, 2, What regulates the oxygen content of the atmosphere?» **Global Biogeochemical Cycles** 14(*1*): 249-268.

Lini, A., Weissert, H. and Erba, E. (1992). «The Valanginian carbon isotope event; a first episode of greenhouse climate conditions during the Cretaceous.» **Terra Nova** 4(*3*): 374-384.

Mutterlose, J. and Bornemann, A. (2000). «Distribution and facies patterns of Lower Cretaceous sediments in northern Germany: a review.» **Cretaceous Research** 21(*6*): 733-759.

Redfield, A. C. (1958). «The biological control of chemical factors in the environment.» **American Scientist** 46: 205-222.

Reimers, C., Kastner, M. and Garrison, R. E. (1990). The role of bacterial mats in phosphate mineralization with particuliar reference to the Monterey Formation. Phophate Deposits of the World, Vol. 3, Neogene to Modern Phosphorites. W. C. Burnett and S. R. Riggs, Cambridge, Cambridge University Press: 300-311.

Ruttenberg, K. C. (1992). «Development of a sequential extraction method for different forms of phosphorus in marine sediments.» **Limnology Oceanography** 37(*7*): 1460-1482.

Ruttenberg, K. C. (1993). «Reassessment of the oceanic residence time of phosphorus.»

Chemical Geology 107(*3-4*): 405-409.

Schlanger, S. O., Arthur, M. A., Jenkyns, H. C. and Scholle, P. A. (1987). The Cenomanian-Turonian oceanic anoxic event, I. Stratigraphy and distribution of organic-rich beds and the marine 13C excursion. Marine Petroleum Sources Rocks. J. Brooks and A. J. Fleet, Geological Society, London, Special Publications. 26: 371-399.

Schlanger, S. O. and Jenkyns, H. C. (1976). «Cretaceous oceanic anoxic events: causes and consequences.» **Geologie en Mijnbouw** 55: 179-184.

Slomp, C. P., Thomson, J. and de Lange, G. J. (2004). «Controls on phosphorus regeneration and burial during formation of eastern Mediterranean sapropels.» **Marine Geology** 203(*1-2*): 141-159.

Stallard, R. F. and Edmond, J. M. (1983). «Geochemestry of the Amazon: 2. The influence of geology and weathering environment on the dissolved load.» **Journal of Geophysical Research** 88: 9671-9688.

Tamburini, F., Föllmi, K. B., Adatte, T., Bernasconi, S. M. and Steinmann, P. (2003). «Sedimentary phosphorus record from the Oman margin: New evidence of high productivity during glacial periods.» **Paleoceanography** 18(*1*): PA 1015.

Tamburini, F., Huon, S., Steinmann, P., Grousset, F. E., Adatte, T. and Föllmi, K. B. (2002). «Dysaerobic conditions during Heinrich events 4 and 5: Evidence from phosphorus distribution in a North Atlantic deep-sea core.» **Geochimica et Cosmochimica Acta** 66(*23*): 4069-4083.

Trümpy, R. (1960). «Paleotectonic evolution of the Central and Western Alps.» **Bulletin of the Geological Society of America** 71: 843-908.

Tyrrell, T. (1999). «The relative influences of nitrogen and phosphorus on oceanic primary production.» **Nature** 400: 525-531.

Van Cappellen, P. and Ingall, E. D. (1996). «Redox stabilization of the atmosphere and oceans by phosphorus-limited marine productivity.» **Science** 271: 493-496.

Van de Schootbrugge, B., Föllmi, K. B., Bulot, L. G. and Burns, S. J. (2000). «Paleoceanographic changes during the early Cretaceous (Valanginian-Hauterivian): evidence from oxygen and carbon stable isotopes.» **Earth and Planetary Science Letters** 181: 15-31.

Van de Schootbrugge, B., Kuhn, O., Adatte, T., Steinmann, P. and Föllmi, K. B. (2003). «Decoupling of P- and Corg-burial following Early Cretaceous (Valanginian-Hauterivian) platform drowning along the NW Tethyan margin.» **Palaeogeography, Palaeoclimatology, Palaeoecology** 199(*3-4*): 315-331.

Vermeulen, J. (1980). Etude de la famille des Pulchelliidae, révision de trois espèces types du Barrémien du Sud-Est de la France.» 101 pp.

Vermeulen, J. (2002). Etude stratigraphique et paléontologique de la famille des Pulchelliidae (ammonoidea, Ammonitina, Endemocerataceae). Grenoble, France.

Weissert, H. (1989). «C-isotope stratigraphy, a monitor of paleoenvironmental change: a case study from the Early Cretaceous.» **Surveys in Geophysics** 10: 1-61.

Weissert, H. and Erba, E. (2004). «Volcanism, CO_2 and palaeoclimate; a Late Jurassic-Early Cretaceous carbon and oxygen isotope record.» **Journal of the Geological Society of London** 161(*4*): 695-702.

Weissert, H., Lini, A., Föllmi, K. B. and Kuhn, O. (1998). «Correlation of Early Cretaceous carbon isotope stratigraphy and platform drowning events: a possible link?» **Palaeogeography, Palaeoclimatology, Palaeoecology** 137: 189-203.

Wissler, L., Weissert, H., Buonocunto, F. P., Ferreri, V. and D'Argenio, B. (2004). Calibration of the Early Cretaceous time scale: a combined chemostratigraphic and cyclostratigraphic approach to the Barremian-Aptian interval, Campania Apennines and Southern Alps (Italy). Cyclostratigraphy: Approach and case histories. B. D'Argenio, A. G. Fischer, I. Premoli-Silva, H. Weissert and V. Ferreri, SEPM Special Publication No. 81: 123-133.

Wissler, L., Weissert, H., Masse, J.-P. and Bulot, L. G. (2002). «Chemostratigraphic correlation of Barremian and lower Aptian ammonite zones and magnetic reversals.» **International Journal of Earth sciences (Geol. Rundsch.)** 91: 272-279.

D.4.
Platform-induced clay-mineral fractionation along a northern Tethyan basin-platform transect: implications for the interpretation of Early Cretaceous climate change (Late Hauterivian-Early Aptian)

Alexis Godet[1], Stéphane Bodin[1], Thierry Adatte[1] and Karl B. Föllmi[1]

[1]Institute of Geology, University of Neuchâtel, rue Emile Argand 11, CP 158 2009 Neuchâtel, Switzerland

Manuscript submitted to Cretaceous Research Special Volume, proceedings of the 7th International Symposium on the Cretaceous

Abstract

High-resolution clay-mineral analyses were performed on Upper Hauterivian to Lower Aptian sediments along a platform-to-basin transect through the northern Tethyan margin from the Neuchâtel area (Switzerland), to the Vocontian Trough (France) in order to investigate links between climate change, carbonate platform evolution, and fractionation patterns in clay minerals during their transport.

During the Hauterivian, the northern Tethyan carbonate platform developed in a heterozoan mode, and the associated ramp-like topography facilitated the export of detrital material into the adjacent basin, where clay-mineral assemblages are dominated by smectite and kaolinite is almost absent, thereby suggesting dry-seasonal conditions. During the Late Hauterivian *Balearites balearis* ammonite zone, a change to a more humid climate is documented by the appearance of kaolinite, which reaches up to 30% of the clay fraction in sediments in the Vocontian Trough. This prominent change just preceded the Faraoni Oceanic Anoxic Event and the onset of the demise of the Helvetic Carbonate Platform, which lasted to the late Early Barremian.

From the Late Barremian onwards, the renewed growth of the northern Tethyan carbonate platform in a photozoan mode and the associated development of a marginally confined platform topography segregated or fractionated the clay-mineral assemblages exported into hemipelagic settings: kaolinite particles were preferentially retained in proximal, platform settings, due to their size, relatively high specific weight, and capacity to flocculate in the marine environment. In the inner platform environment preserved in the Swiss Jura, an average of 32% of kaolinite in the clay fraction is observed during the latest Barremian – earliest Aptian, whereas clay-mineral assemblages of coeval sediments from deeper depositional settings are dominated by smectite and show only minor amounts of kaolinite.

This signifies that besides palaeoclimate conditions, the morphology and ecology of the carbonate platform had a significant effect on the distribution and composition of clay assemblages during the late Hauterivian – early Aptian along the northern Tethyan margin.

Keywords

Kaolinite, smectite, climate change, Early Cretaceous, carbonate platform, Jura mountains, Vocontian Trough, northern Tethyan margin

D.4.1. Introduction

The Early Cretaceous climate was sustained by generally elevated atmospheric pCO_2 (*e.g.*, Berner and Kothavala, 2001), implying reinforced greenhouse conditions, which influenced the water cycle, the intensity of rainfall, and the biogeochemical weathering of continental rocks (*e.g.*, Weissert, 1989; Weissert *et al.*, 1998; Larson and Erba, 1999). The latter may have affected marine biological communities by regulating the input of nutrients in the ocean; episodes of enhanced nutrients transfer to the ocean may have led to increased marine productivity rates and the subsequent generation and preservation of organic-rich sediments under partly anoxic conditions.

An example of such an episode is documented by the Late Hauterivian Faraoni Level, which was first described in the Umbria-Marche basin of Italy (Cecca *et al.*, 1995), and subsequently recovered in sections from other regions of the central and western Tethys (Baudin, 2005). The Faraoni Level displays features similar to other Oceanic Anoxic Events (OAE's; *e.g.* Schlager and Jenkyns, 1976; Scholle and Arthur, 1980) such as the presence of finely laminated black-shale facies with TOC values of more than 10% in Italian sections. However, unlike other Cretaceous OAE's, the Faraoni Level is not associated with a carbon isotope excursion and only marked by an increase of 0.15‰ in sediments from the western Switzerland and southeastern France (Baudin *et al.*, 1999; Godet *et al.*, 2006); by comparison, the OAE1a (Early Aptian) is associated to a negative spike (amplitude of ca. -1.5‰) followed by a positive excursion (amplitude of ca. +2‰; *e.g.*, Föllmi *et al.*, in press). This is explained by a buffering effect on the marine $\delta^{13}C$ record, through accelerated water cycle and increased delivery of Dissolved Inorganic Carbon (DIC) to the ocean more humid climate conditions (*e.g.*, Bartley and Kah, 2004; Godet *et al.*, 2006).

Climate change during the early Cretaceous has been deduced from the temporal evolution of clay-mineral assemblages (*e.g.*, Ruffell and Batten, 1990; Ruffell *et al.*, 2002). Clay minerals are valid indicators of the intensity of geochemical weathering processes on the continent, because such processes are influenced by climate (humidity, average temperature, seasonality; *e.g.*, Chamley, 1981; Ruffell *et al.*, 2002). Geomorphology is in turn an expression of tectonic and climatic processes. Investigations of clay minerals in Barremian sediments of Western Europe (Spain, England, France, and Germany) have led to the interpretation of a relatively stable dry climate, which were probably interrupted by short-term changes from arid to semi-arid conditions, as is indicated by the occurrence of traces of kaolinite (Ruffell and Batten, 1990). Late Jurassic – Early Cretaceous sediments from the Jura Mountains contain relatively high amounts of kaolinite (up to 30%), except in Hauterivian sediments where smectite represents up to 50% of the clay fraction, which suggests seasonally dry conditions for this stage (Persoz, 1982; Adatte and Rumley, 1989).

Here we show the results of our analysis of clay-mineral assemblages from a selection of sections of Hauterivian and Barremian age along a transect through the northern Tethyan margin, which ranges from the hemipelagic Vocontian Trough to the platform environment preserved in the Jura Mountains. We use this data set to reconstruct the evolution of climate during the Hauterivian and Barremian along the northern Tethyan margin. Then, we propose to deduct the potential effect of this type of environmental change on the continental hydrological cycle and intensity in chemical weathering processes; the related transfer of nutrients and DIC into the ocean will be taken into consideration, as well as the corresponding impact on the marine environment and marine carbon isotope system. We also consider the impact of different carbonate platform morphologies associated with photozoan and heterozoan production modes on the spatial distribution of clay minerals, especially kaolinite.

D.4.2. Geological setting and location of the studied sections

The sections of La Charce, Vergons, Angles (stratotype of the Barremian stage), and Combe-Lambert are located in the region of the Alpes de Haute Provence, southeastern France (Figs. D.23, D.24 and D.25). They represent a hemipelagic environment typical for the Vocontian Trough, and

the abundance of ammonites allows for excellent time-calibration (*e.g.*, Bulot *et al.*, 1992; Delanoy, 1997; Vermeulen, 2002). During the Early Cretaceous, the Vocontian Trough constituted an epicontinental basin, which was surrounded by carbonate platforms such as the Bas-Dauphine platform and which was connected to the Ligurian Tethys (*e.g.*, Baudin *et al.*, 1999).

Located in France, approximately 20km southeastward from Geneva (Fig. D.23), the section of Cluses (Fig. D.26) belongs to the Bornes Massif, which constitutes the northeastern part of the French Subalpine Chains (*e.g.* Trabold, 1996). In the absence of ammonites in these facies, which is similar to that of the Helvetic ramp, the dating of the Cluses section is mainly based on orbitolinids and echinoids (Trabold, 1996; Wermeille, 1996).

Finally, the Eclépens section is located between Neuchâtel and Lausanne (Switzerland), and belongs to the Western Swiss Jura (Figs. D.23 and D.27). This region hosts the historical succession of the Hauterivian stage - first described by de Montmollin (1835), which is composed, from the base to the top, by the "Marne à Astiera", the "Marne Bleue d'Hauterive", and the "Pierre Jaune de Neuchâtel" (PJN). Whereas the age of these formations is well-constrained

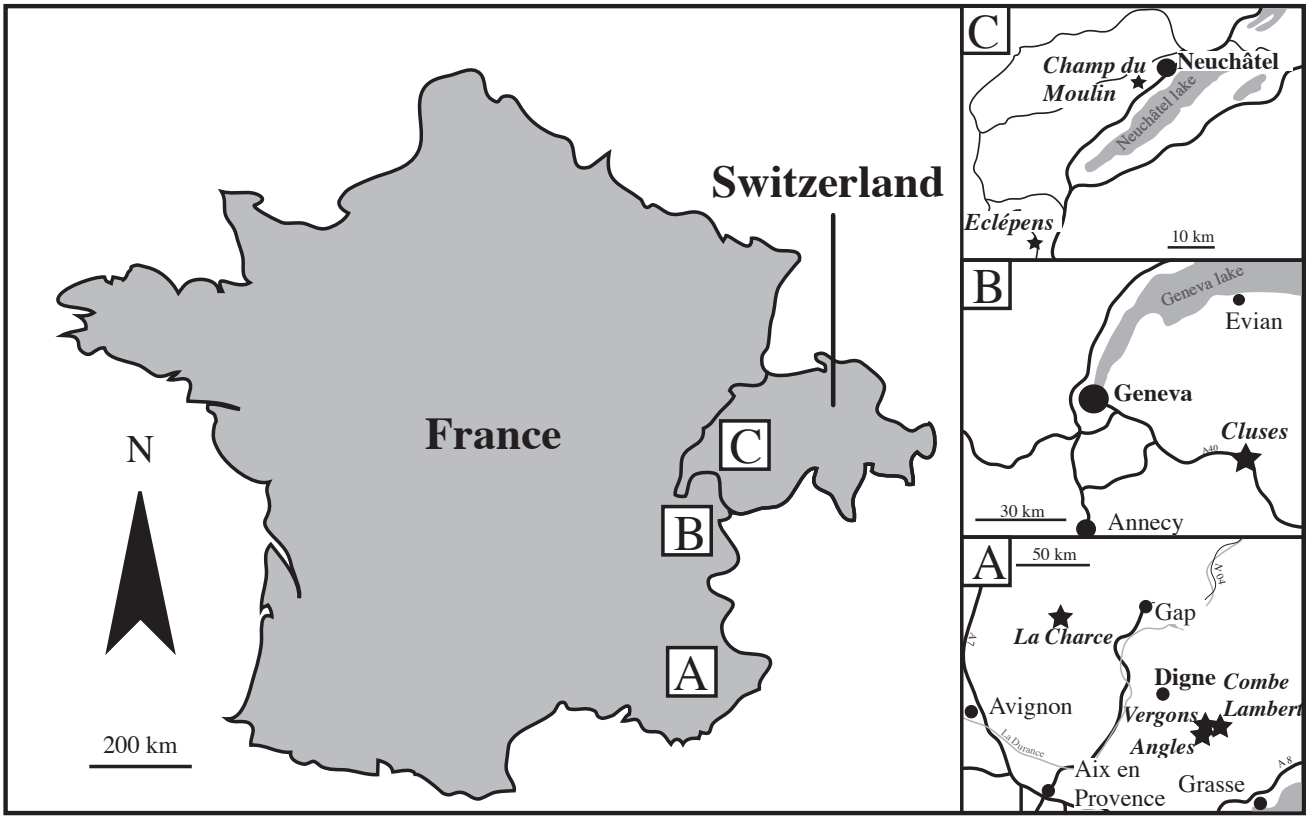

Fig. D.23: Location of the studied sections.

by ammonite biostratigraphy, the overlying "Urgonien Jaune" (UJ) and "Urgonien Blanc" (UB) are lacking ammonites; based on recent nannofossils finding near the base of the UJ, these formations are attributed to the Late Barremian – earliest Aptian (Godet *et al.*, 2005). The study of Blanc-Aletru (1995) on the upper part of the section (UJ and UB) are complementary to the results of this work.

D.4.3. Methods

D.4.3.1. Rock-Eval analysis

Organic matter analyses were performed using a Rock Eval 6 equipment at the Institute of Geology of the University of Neuchâtel, on a batch of 26 marls around the Faraoni Level equivalent at Angles. Approximately 100 mg of ground and homogenised sample is subjected to a pyrolysis step followed by the complete oxidation

of the residual sample (Espitalié *et al*. (1985), Lafargue *et al*. (1998) and Behar *et al*. (2001)). A FID detector measures the hydrocarbon released during pyrolysis, while CO_2 and CO are detected by infrared absorbance during both steps. In the here applied standard cycle for «whole rock», pyrolysis starts isothermally at 300°C for 3 minutes, after which the sample is heated to 650°C. The oxidation step starts isothermally at 400°C (3 min) and then heats up to 850°C. Organic carbon decomposition results in 4 main peaks: the S1 peak (hydrocarbons released during the isothermal phase), the S2 peak (hydrocarbons produced between 300 and 650°C), the S3 peak (CO_2 from pyrolysis of OM up to 400°C), and the S4 peak (CO_2 released from residual organic matter below ca. 550°C during the oxidation step). Mineral carbon decomposition is recorded by the S3' peak (pyrolysis-CO_2 released above 400°C), and the S5 peak (oxidation-CO_2 released above ca. 550°C).

These peaks are used to calculate the amount of total organic carbon (TOC) and the amount of mineral carbon (MinC). In addition, the so-called hydrogen index (HI = S2/TOC) and oxygen index (OI = S3/TOC) are calculated. The HI and OI indices are proportional to the H/C and O/C ratios of the organic matter, respectively, and can be used for organic matter classification in Van-Krevelen-like diagrams (Espitalié *et al*., 1985).

Measurements are calibrated using two standards (IFP 160000 and VP143h); the error relative to standard IFP 160000 is approximately 0.77, 0.08, 0.25 and 1.5 % for TOC, MinC, HI and OI, respectively.

D.4.3.2. XRD analysis

X-ray diffraction analyses were performed to identify and quantify the different components of the bulk rock (Angles) and the clay-mineral assemblages (all studied sections). As data for the upper part of Eclépens (Blanc-Aletru, 1995), Cluses (Wermeille, 1996), Vergons and La Charce (van de Schootbrugge, 2001) sections were obtained using the methods described by Kübler (1987) and Adatte *et al*. (1996), the same procedures were performed on samples from Angles, Combe-Lambert and the lower part of Eclépens. This allowed us to better compare the integrity of the dataset and to avoid discrepancies due to the process of quantification. Moreover, the methods described in these aforementioned papers are accurate enough for bulk rock composed of several different mineral phases, even if the procedures mentioned by Środoń (1980) and Hillier (1989) are known to be precise and have been subsequently used to analyse the bulk-rock composition.

Samples were trimmed to avoid altered material. Subsequently, they were roughly crushed in a "jaw" crusher, and an aliquot of the resulting gravels was crushed using an agate mortar to obtain a fine and homogeneous powder (grain size ≤40μm).

D.4.3.2.1 Bulk-rock analysis

About 800 mg of the powder were pressed (20 bar) in a powder holder, and the bulk-sample was analysed by XRD at the Institute of Geology of the University of Neuchâtel (Scintag XRD 2000 Diffractometer), in order to determine bulk-rock mineralogy using procedures described by Ferrero (1965, 1966), Klug and Alexander (1974), Kübler (1983), and Adatte *et al*. (1996). This method allows the semi-quantification of the whole-rock mineralogy (obtained by XRD patterns of random powder samples) by using external standards with an error varying between 5 and 10 % for the phyllosilicates and 5 % for grain minerals. The different minerals recognized and quantified are calcite, "phyllosilicates" group, quartz, sodic plagioclase (albite), and potassic feldspar (microcline); the position of the peaks used for their recognition is given in Table D.7. Organic matter, poorly crystallised minerals (such as pyrite and goethite), ankerite and dolomite were not quantified due to the low intensity of their respective peak. They constitute the unquantified component of the samples.

D.4.3.2.2. Clay mineral analysis

This procedure is based on the method described by Kübler (1987) and Adatte *et al*. (1996). Samples are transferred into glass containers with de-ionised water and agitated by air injection; subsequently they are decarbonatized

by HCl 10% (1.25N) leaching during 20 min. Dissolution of the samples is promoted by ultrasonic disaggregation (3 minutes per sample). The insoluble residue is washed and centrifuged until a neutral suspension is obtained (pH 7-8). Using the Stokes law, two granulometric fractions are separated (<2μm and 2-16μm). The selected fraction is then pipetted and deposited on a glass plate. A first analysis is performed after air-drying at temperature room, a second one after saturation of the sample with ethylen-glycol, in order to identify swelling minerals, and a third one after heating to 350°C for selected samples. The intensities of the identified minerals are measured for a semi-quantitative estimate of the proportion of clay minerals, which is therefore given in relative percent without correction factors for both fractions.

Mica, kaolinite, chlorite, illite / smectite irregular mixed-layers (R0), and ordered mixed-layers (R1) were identified in the studied sections; the position of the peaks used for their recognition is given in Table D.8. Measurements of the amount of smectite and illite layers in the R0 mixed-layers were performed on both limestones and marls, following the procedure of Moore and Reynolds (1997; Table D.9). They reveal the presence of two types of R0 minerals. The first one contains more than 80% of smectite layers, and corresponds to an almost pure smectite characterized by a peak at 5.2 °2θ; it will hereafter be called “smectite”. The second type is characterized by less than 70-60% of smectite layers and by a peak (001) between 9 and 9.5 °2θ: the term R0 I/S will be used hereafter for such. The R1 mixed-layers are corrensite (chlorite / smectite R1 mixed-layer) or rectorite (illite / smectite R1 mixed-layer). The illite cristallinity index (IC) was measured on several diffractograms of marls and limestones, following the methods described by Kübler (1987), and by Kübler and Goy-Eggenberger (2001).

D.4.4. Results

D.4.4.1. The Angles and Combe-Lambert sections

D.4.4.1.1. XRD analysis

For the Angles section, analyses of whole-rock (n=180) and insoluble-residue (n=170) samples were performed both on marl and limestone samples, whereas in sediments from the Combe-Lambert section, only clay minerals were analysed (n=25).

Calcite content shows no major variations, except for samples belonging to the *Balearites balearis* and *Spathicrioceras angulicostatum* (Late Hauterivian), and to the *Holcodiscus uhligi* and *Heinzia sayni* ammonite zones (early Late Barremian), where significant drops in the calcite content are observed (Fig. D.24). The quartz content decreases slightly from the base of the section up to the sedimentary interval attributed to the *Nicklesia pulchella* zone, and then it increases up to the top of the section, which belongs to the Early Aptian. The evolution of phyllosilicates follows that of quartz, with a rapid increase just below the Faraoni Level equivalent (at 24.50m).

From these results, a detrital index (DI), which corresponds to the ratio of the calcite to the quartz and phyllosilicates (in percents), is calculated, assuming that the major part of quartz is of detrital origin, as suggested by the absence of any post-depositional silicification.

High DI values reflect low detrital input. The evolution of the DI can be divided into three parts (Fig. D.24; see also Table D.7):

- From the base of the section to the Faraoni Level equivalent (*S. angulicostatum* – *Pseudothurmannnia mortilleti* boundary), DI values are low.
- From the Faraoni Level equivalent to the sequence boundary (Sb) B4 (approximately at 109m, in sediments of the *Hemihoplites feraudianus* ammonite zone; after Arnaud, 2005), the DI curve increases sharply.
- From the SbB4 to the top of the section, the DI decreases to values comparable to those observed in part I.

In the insoluble residue of the <2μm fraction of sediments from the Angles and the Combe-Lambert sections, mica, kaolinite, “smectite”, chlorite, and R0 I/S were identified (Fig. D.25;

see also Table D.8 and Fig. D.28 for an example of diffractograms).

The evolution of the kaolinite/mica and kaolinite/smectite ratios points out the predominance of kaolinite relative to smectite and mica in certain intervals (Fig. D.25). In particular, the kaolinite content reaches 25% of the total

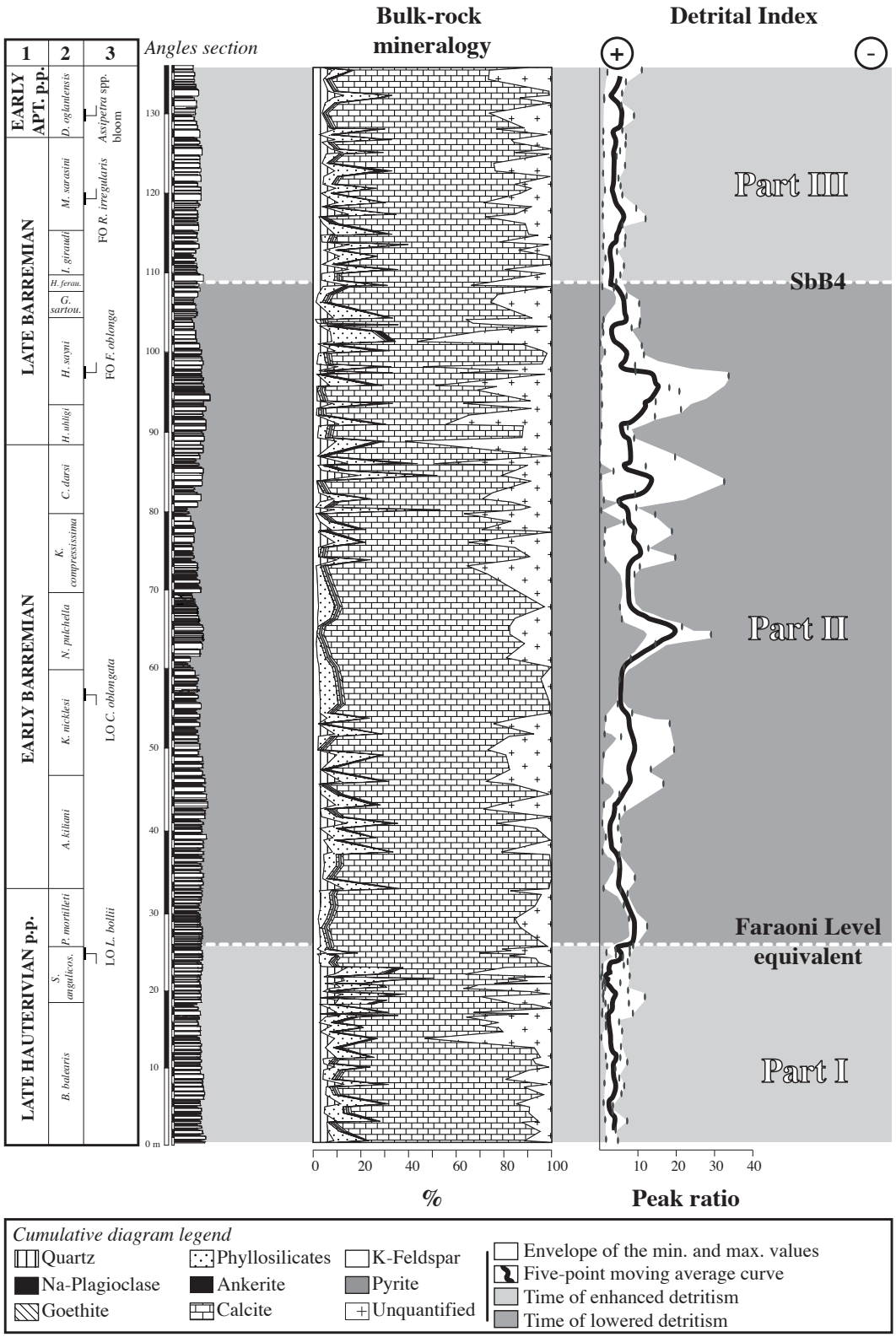

*Fig. D.24: Bulk-rock mineralogy of the Angles section. The detrital index corresponds to the ratio of calcite to quartz and phyllosilicates (in percentage). Numbers on top of the columns (left part of figure) correspond to the **1)** stratigraphic stages, **2)** ammonite zones and **3)** main nannofossils bioevents (after Godet et al., 2006). The sequence boundary B4 (SbB4) is positioned after Arnaud (2005).*

clay-mineral content in selected marly samples of part II of the section, whereas this mineral tends to decrease in content in part III of the section. However, kaolinite remains relatively low in limestone samples, trough the entire section (see Table D.8). Contrary to kaolinite**,** "smectite" is the most abundant mineral in part I and especially in part III of the Angles section, where it reaches a maximum of approximately 80 % in sediments belonging to the *Martelites sarasini* zone. Whereas

Section	Age	Mineral	Peak position (°2θ)	Bulk rock					
				Marls		Limestones		All lithologies	
				Mean value	*Extreme values*	*Mean value*	*Extreme values*	*Mean value*	*Extreme values*
Angles	*Part I*	Calcite	29.43	*51.80*	*19.8 - 78.8*	*82.10*	*68.1 - 91.5*	*66.00*	*19.8 - 91.5*
		Quartz	26.65	*9.50*	*2.5 - 14.4*	*4.30*	*2.6 - 6.5*	*7.10*	*2.5 - 14.4*
		Phyllosilicate	19.80	*16.20*	*7.2 - 32.6*	*3.90*	*0.0 - 8.1*	*10.40*	*0.0 - 32.6*
		K-Feldspars	27.50	*0.70*	*0.0 - 2.2*	*0.00*	*0.0 - 0.3*	*0.40*	*0.0 - 2.2*
		Na-Plagioclases	27.90	*1.00*	*0.0 - 2.1*	*0.10*	*0.0 - 0.6*	*0.60*	*0.0 - 2.1*
		Unquantified	----	*20.70*	*0.4 - 53.2*	*9.60*	*0.1 - 28.5*	*15.50*	*0.1 - 53.2*
		Detrital Index	----	*1.40*	*0.3 - 3.8*	*5.40*	*2.1 - 10.8*	*3.30*	*0.3 - 10.8*
	Part II	Calcite	29.43	*42.20*	*7.4 - 72.7*	*80.90*	*59.9 - 96.9*	*68.70*	*7.4 - 96.9*
		Quartz	26.65	*9.50*	*3.0 - 19.2*	*2.40*	*1.0 - 4.8*	*4.60*	*1.0 - 19.2*
		Phyllosilicate	19.80	*18.80*	*6.9 - 41.3*	*3.00*	*0.0 - 7.7*	*8.00*	*0.0 - 41.3*
		K-Feldspars	27.50	*0.60*	*0.0 - 1.9*	*0.00*	*0.0 - 0.4*	*0.20*	*0.0 - 1.9*
		Na-Plagioclases	27.90	*1.50*	*0.2 - 4.9*	*0.00*	*0.0 - 0.3*	*0.50*	*0.0 - 4.9*
		Unquantified	----	*26.90*	*1.1 - 61.5*	*13.70*	*0.0 - 37.8*	*17.90*	*0.0 - 61.5*
		Detrital Index	----	*1.00*	*0.1 - 2.7*	*6.30*	*1.5 - 30.8*	*4.60*	*0.1 - 30.8*
	Part III	Calcite	29.43	*53.40*	*35.2 - 72.3*	*81.10*	*67.3 - 91.1*	*70.50*	*35.2 - 91.1*
		Quartz	26.65	*11.20*	*8.0 - 15.2*	*4.40*	*2.5 - 7.6*	*7.00*	*2.5 - 15.2*
		Phyllosilicate	19.80	*17.90*	*8.0 - 22.4*	*3.40*	*0.0 - 9.0*	*9.00*	*0.0 - 22.4*
		K-Feldspars	27.50	*0.30*	*0.0 - 1.2*	*0.10*	*0.0 - 0.4*	*0.20*	*0.0 - 1.2*
		Na-Plagioclases	27.90	*0.90*	*0.9 - 2.8*	*0.10*	*0.0 - 0.3*	*0.40*	*0.0 - 2.8*
		Unquantified	----	*15.70*	*0.8 - 33.7*	*11.10*	*0.1 - 28.5*	*12.90*	*0.1 - 33.7*
		Detrital Index	----	*1.30*	*0.6 - 2.6*	*5.50*	*2.1 - 10.7*	*3.90*	*0.6 - 10.7*

Table D.7: Synthesis of the results of bulk-rock analysis performed on samples from Angles. All values in percents.

the evolution of mica is rather monotonous, the chlorite content increases gently from the base to the top, with higher contents in limestones (mean value of 21%) compared to those of marls (mean value of 11%); the repartition of the "smectite" follows the same rule, with higher contents in limestones compared to marls (mean values of 27% and 12%, respectively).

D.4.4.1.2. Rock Eval analysis

A batch of 26 samples of marl belonging to the time span from the *B. balearis* to the *Avramidiscus kiliani* ammonite zone were analysed for their organic geochemistry parameters (Table D.10). The TOC values range from 0.35 to 2.63%, with a maximum reached in the *B. balearis* ammonite zone, under the Faraoni Level equivalent. The HI values are relatively low within the dataset, but an increase in noted around the Faraoni Level equivalent, with a maximum of 345 mgHC/gTOC. Finally, the measured Tmax are somewhat high, with a mean value of 436°C (extreme values of 432 and 440°C).

D.4.4.2. The Cluses section

In contrast to the Angles and Combe-Lambert sections, smectite is absent in the analysed clay-mineral assemblage of this section: only mica, kaolinite, chlorite and mixed-layer clay minerals were identified (n = 194, Fig. D.26; see also Table D.8 and Fig. D.28 for an example of diffractograms). In some samples, the nature of the mixed-layers has been identified: corrensite and rectorite are characterized by peaks at 6.0 and 6.5 °2θ, respectively, and sometimes by a superstructure near 3 °2θ which appears on diffractograms of glycolate-saturated samples. As these minerals are absent in most of the samples, they were not included in the quantification calculation (except for the samples illustrated by their diffractogram in Fig. D.28).

In the Cluses section, some narrow intervals are enriched in kaolinite at the base and the top of the depositional sequence Ba4; then, a major

episode of enrichment in this mineral is noted from the base of the Ba5 sequence upward, with maximum values reaching more than 50%. Kaolinite contents remains also high in sediments of Aptian age. This trend in kaolinite contents is also well expressed in the curves of the kaolinite/mica and kaolinite/(Qz+Fk+Pl) ratios (Fig. D.26; see also Table D.8).

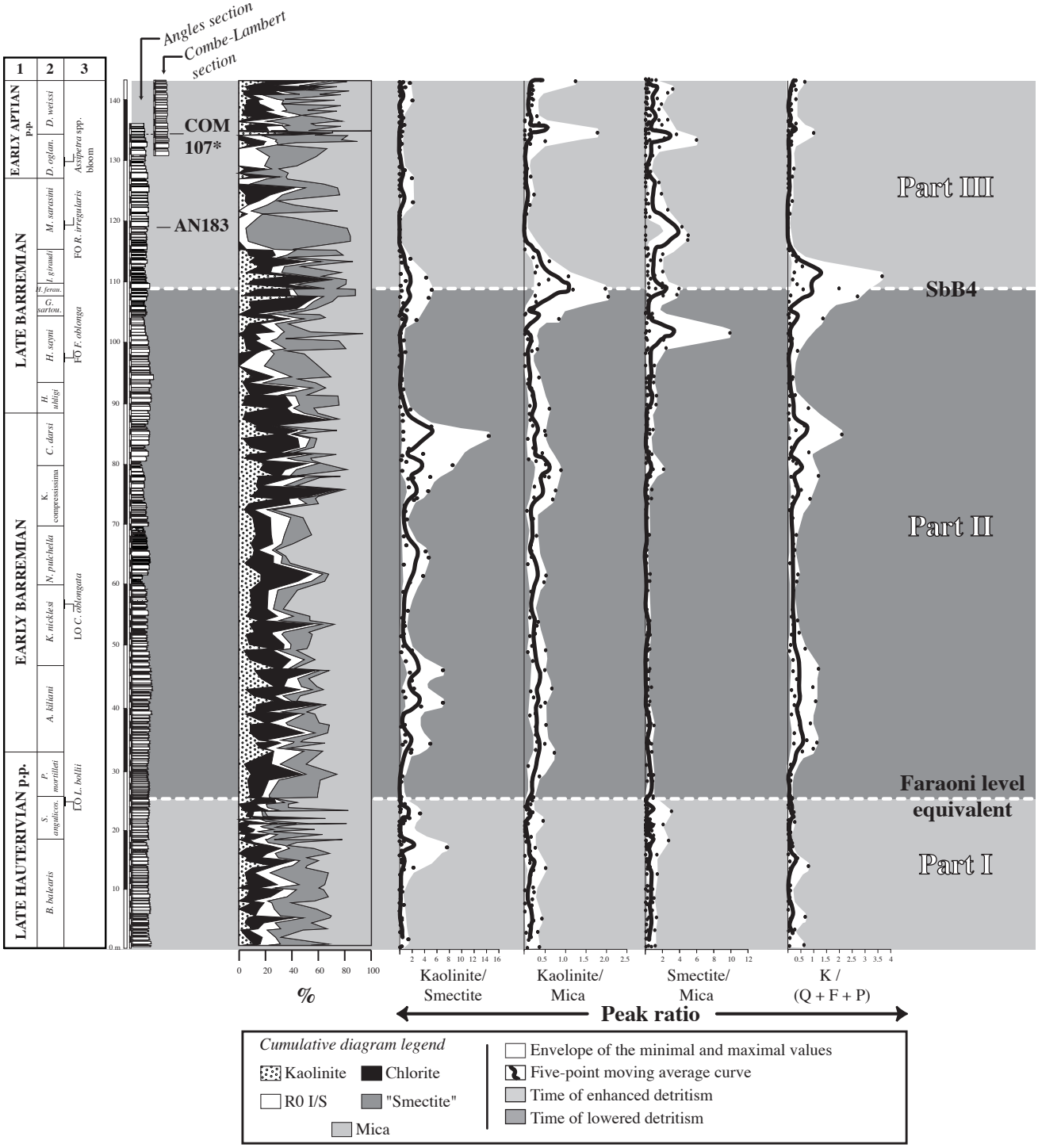

*Fig. D.25: Evolution of the clay-mineral assemblage of the insoluble residue (<2µm fraction) of the Angles and the Combes-Lambert sections. On the right, the curves of the kaolinite/smectite, kaolinite/mica, and kaolinite/(quartz + feldspar + phyllosilicate) ratios point out the dominance of kaolinite during most of the Barremian. Numbers on top of the columns (left part of figure) correspond to the **1)** stratigraphic stages, **2)** ammonite zones and **3)** main nannofossils bioevents (after Godet et al., 2006). Sample numbers refer to the diffractograms C and D displayed in Fig. D.28. Abbreviations of the minerals: K = Kaolinite: Q = Quartz; F = potassic feldspar; P = sodic plagioclase.*

D.4.4.3. The Eclépens section

Mica, kaolinite, "smectite", chlorite, and R0 I/S were identified in the <2μm fraction of sediments from Eclépens (n = 186 in Fig. D.27; see also Table D.8 and Fig. D.28 for an example of diffractograms).

The most characteristic feature of the clay assemblage in this section is the antagonistic behaviour of "smectite" and kaolinite contents: "smectite" contents vary from 50% in the PJN to 0% in the UB, whereas kaolinite is mostly absent in the PJN and only appears in sediments above the boundary between the PJN and the UJ, with values reaching more than 50%.

Section	Age	Mineral	Peak position (°2θ)	Clay fraction (< 2 μm)					
				Marls		Limestones		All lithologies	
				Mean value	*Extreme values*	*Mean value*	*Extreme values*	*Mean value*	*Extreme values*
Angles / Combe-Lambert	*Late Hauterivian*	Illite-Micas	8.8 (*001*)	58	30- 81	41	17 - 68	48	17 - 81
		Kaolinite	12.34 (*001*) / 24.9 (*002*)	6	0 - 25	5	0 - 15	5	0 - 25
		"Smectite"	5.2 (*001* on glycolated sample)	6	0 - 38	28	4 - 58	23	0 - 58
		Chlorite	12.34 (*002*) / 25.2 (*004*)	8	0 - 23	18	6 - 38	13	0 - 38
		R0 I/S	9-9.5 (*001*)	11	0 - 19	9	0 - 17	10	0 - 19
	Barremian	Illite-Micas	8.8 (*001*)	51	25 - 73	36	6 - 74	41	6 - 82
		Kaolinite	12.34 (*001*) / 24.9 (*002*)	20	0 - 51	8	0 - 19	11	0 - 51
		"Smectite"	5.2 (*001* on glycolated sample)	12	2 - 25	23	2 - 78	19	0 - 78
		Chlorite	12.34 (*002*) / 25.2 (*004*)	8	0 - 23	25	0 - 61	19	0 - 61
		R0 I/S	9-9.5 (*001*)	10	1 - 25	9	3 - 21	9	1 - 25
	Earliest Aptian	Illite-Micas	8.8 (*001*)	54	29 - 82	29	0 - 63	39	0 - 71
		Kaolinite	12.34 (*001*) / 24.9 (*002*)	9	3 - 52	3	0 - 23	6	0 - 52
		"Smectite"	5.2 (*001* on glycolated sample)	8	0 - 21	42	12 - 76	28	0 - 76
		Chlorite	12.34 (*002*) / 25.2 (*004*)	19	3 - 56	11	0 - 55	15	0 - 56
		R0 I/S	9-9.5 (*001*)	11	3 - 21	14	0 - 26	12	0 - 26
Cluses	*Not attributed*	Illite-Micas	8.8 (*001*)					94	80 - 100
		Kaolinite	12.34 (*001*) / 24.9 (*002*)					3	0 - 19
		Chlorite	12.34 (*002*) / 25.2 (*004*)					1	0 - 12
		R0 I/S	9-9.5 (*001*)					3	0 - 20
	Barremian	Illite-Micas	8.8 (*001*)					89	23 - 100
		Kaolinite	12.34 (*001*) / 24.9 (*002*)					9	0 - 77
		Chlorite	12.34 (*002*) / 25.2 (*004*)					2	0 - 36
		R0 I/S	9-9.5 (*001*)					1	0 - 12
	Aptian	Illite-Micas	8.8 (*001*)					76	0 - 100
		Kaolinite	12.34 (*001*) / 24.9 (*002*)					20	0 - 100
		Chlorite	12.34 (*002*) / 25.2 (*004*)					3	0 - 45
		R0 I/S	9-9.5 (*001*)					1	0 - 10
Eclépens	*Early Hauterivian*	Illite-Micas	8.8 (*001*)					59	28 - 100
		Kaolinite	12.34 (*001*) / 24.9 (*002*)					3	0 - 15
		"Smectite"	5.2 (*001* on glycolated sample)					25	0 - 60
		Chlorite	12.34 (*002*) / 25.2 (*004*)					2	0 - 8
		R0 I/S	9-9.5 (*001*)					11	0 - 20
	Not attributed	Illite-Micas	8.8 (*001*)					53	22 - 100
		Kaolinite	12.34 (*001*) / 24.9 (*002*)					1.5	0 - 8
		"Smectite"	5.2 (*001* on glycolated sample)					25	0 - 62
		Chlorite	12.34 (*002*) / 25.2 (*004*)					1.5	0 - 6
		R0 I/S	9-9.5 (*001*)					19	0 - 70
	Late Barremian	Illite-Micas	8.8 (*001*)					31	0 - 100
		Kaolinite	12.34 (*001*) / 24.9 (*002*)					32	0 - 100
		"Smectite"	5.2 (*001* on glycolated sample)					18	0 - 67
		Chlorite	12.34 (*002*) / 25.2 (*004*)					5	0 - 16
		R0 I/S	9-9.5 (*001*)					14	0 - 100

No limestone - marl alternation

Table D.8: Synthesis of the results of insoluble residue (<2μm) analysis performed on samples from Angles, Combe-Lambert, Cluses and Eclépens. All values in relative percents.

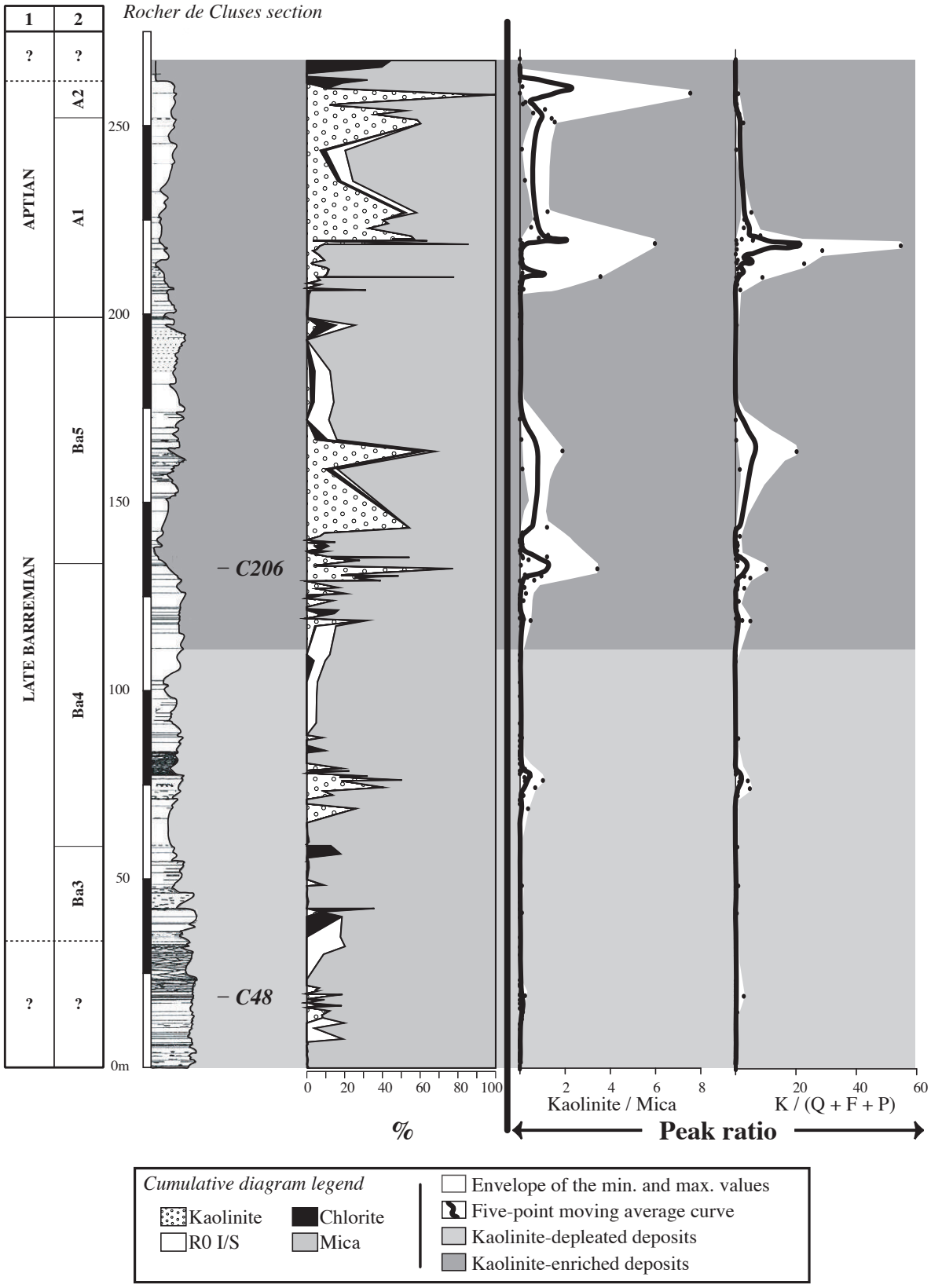

*Fig. D.26: Evolution of the clay-mineral assemblage of the insoluble residue (<2µm fraction) of the Cluses section. On the left part of the figure, the numbers on top of the columns correspond to the **1)** stratigraphic stages and **2)** depositional sequences (after Wermeille, 1996). On the right, the evolution of the kaolinite/mica and kaolinite/(quartz + feldspar + phyllosilicates) ratios reveals the dominance of kaolinite from the upper part of the Ba4 depositionnal sequence (Late Barremian) to the top of the section (A2 sequence, Early Aptian). Sample numbers refer to the diffractograms E and F displayed in Fig. D.28. Abbreviations of the minerals: K = Kaolinite: Q = Quartz; F = potassic feldspar; P = sodic plagioclase.*

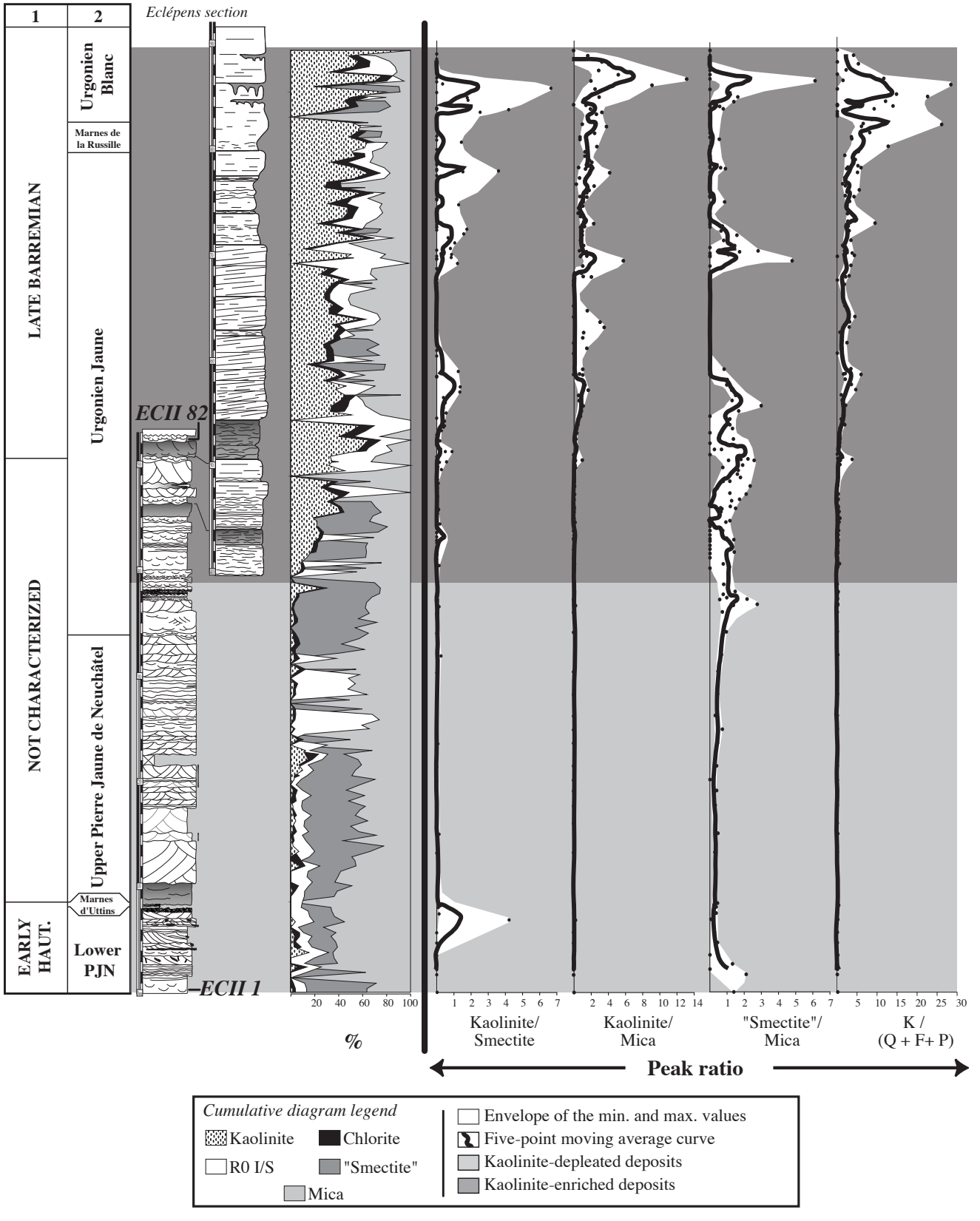

*Fig. D.27: Evolution of the clay-mineral assemblage of the insoluble residue (<2µm fraction) of the Eclépens section. On the left part of the figure, the numbers on top of the columns correspond to the **1)** stratigraphic stages (modified after Godet et al., 2005) and **2)** formations. On the right, the curves of kaolinite/smectite, kaolinite/mica, and kaolinite/(quartz + feldspar + phyllosilicate) ratios point out the dominance of the kaolinite throughout the Urgonian limestone, whereas sediments from the Pierre Jaune de Neuchâtel contain almost no kaolinite. Sample numbers refer to the diffractograms A and B displayed in Fig. D.28. Abbreviations of the minerals: K = Kaolinite: Q = Quartz; F = potassic feldspar; P = sodic plagioclase.*

D.4.5. Discussion

D.4.5.1. Reliability of the clay-mineral record

Clay minerals are formed in terrestrial soils, and have the potential to be subsequently eroded and exported to the ocean. Their genesis depends both on the lithological characteristics of the substratum as well as on the prevailing climate. For example, smectite may form in soils exposed to a dry, seasonally well-contrasted climate or it may be also the result of the weathering of basalts (Chamley, 1989). Clay-mineral assemblages may then fractionate during their transport to the ocean - for example due to sea-level change and the shelf morphology, thereby perturbing the original environmental signal. Once deposited in the sedimentary environment clay-mineral compositions may be further modified by diagenetic processes (*e.g.*, Chamley, 1989; Kübler and Jaboyedoff, 2000). The late diagenetic overprint is dependent on the original sediment composition, the degree of burial diagenesis and eventually also its tectonic history. Deconinck and Debrabant (1985) studied limestones-marls alternations of Berriasian age from the Vergons section (southeastern France), where smectite contained in marl would preferentially transform into illite (and to a lesser extend into chlorite), whereas in limestone smectite would mainly convert into chlorite. Moreover, smectite is very sensitive to high temperatures linked to the burial and / or the tectonic history of the region: Ferry *et al.* (1983) interpreted the transformation of smectite into chlorite in sediments belonging to the Valanginian of the Vocontian Trough as the

Section	Sample	Lithology	Δ2°θ	% smectitic layers	% illitic layers
Angles	AN 2b	marlstone	6.22	61.05	39.07
	AN 6b	marlstone	5.76	76.99	23.11
	AN 10b	marlstone	6.26	59.72	40.40
	AN 15.1b	marlstone	5.93	71.06	29.04
	AN 18b	marlstone	6.93	39.75	60.39
	AN 29b	marlstone	6.69	46.44	53.69
	AN 34b	marlstone	6.51	51.75	48.38
	AN 38b	marlstone	6.51	51.79	48.34
	AN 81b	marlstone	6.15	63.26	36.86
	AN 103b	marlstone	6.21	61.29	38.83
	AN 35	limestone	5.67	80.69	19.40
	AN 49.1	limestone	5.40	91.17	8.92
	AN 156.4	limestone	5.64	81.67	18.43
	AN 156.6	limestone	5.97	69.54	30.56
	AN 181	limestone	5.46	88.79	11.30
	AN 183	limestone	5.70	79.52	20.58
	AN 185	limestone	5.76	77.12	22.98
	AN 190	limestone	5.85	73.81	26.30
	AN 197	limestone	5.37	92.36	7.73
	AN 206	limestone	5.19	100.01	0.07
	Mean values :		*Marlstone*	*58.31*	*41.81*
			Limestone	*83.47*	*16.63*
			All lithologies	**70.89**	**29.22**
Combe-Lambert	COM 108*	marlstone	6.14	63.59	36.52
	COM 122*	marlstone	6.45	53.71	46.42
	COM 104	limestone	6.18	62.37	37.75
	COM 106	limestone	6.03	67.51	32.60
	COM 112	limestone	5.70	79.49	20.61
	COM 122h	limestone	5.94	70.43	29.68
	COM 124	limestone	5.89	72.40	27.70
	Mean values :		*Marlstone*	*58.65*	*41.47*
			Limestone	*70.44*	*29.67*
			All lithologies	**67.07**	**33.04**
Eclépens	ECII 1	limestone	5.57	84.36	15.73
	ECII 3	limestone	5.69	79.67	20.43
	ECII 8	limestone	5.77	76.64	23.46
	ECII52	limestone	6.75	44.75	55.38
	ECII 55	limestone	5.76	77.24	22.86
	ECII 57	limestone	6.00	68.59	31.51
	ECII 60	limestone	6.00	68.61	31.50
	ECII 74	limestone	6.18	62.33	37.78
	ECII 82	limestone	5.70	79.42	20.68
	Mean values :		***All lithologies***	**71.29**	**28.82**

Table D.9: Measurements of the content of smectite layers in samples from Angles, Combe-Lambert and Eclépens. All values in percents.

ID	Depth [m]	Stage	Ammonite Zone	TOC [%]	MINC [%]	HI [mgHC/g TOC]	OI [mgCO_2/g TOC]	Tmax [∘C]
AN29b	15.35	Late Hauterivian	*B. balearis*	0.39	8.03	82	137	435
AN30b	15.82	Late Hauterivian	*B. balearis*	0.65	6.74	94	84	437
AN31b	16.12	Late Hauterivian	*B. balearis*	0.47	7.54	93	95	434
AN32b	16.65	Late Hauterivian	*B. balearis*	2.63	3.20	254	35	434
AN33b	17.35	Late Hauterivian	*B. balearis*	1.49	4.76	207	73	438
AN34b	17.94	Late Hauterivian	*B. balearis*	0.35	9.15	70	129	435
AN35b	18.29	Late Hauterivian	*B. balearis*	0.71	7.51	123	113	437
AN37b	19.00	Late Hauterivian	*S. angulicostatum*	1.44	4.79	191	50	438
AN38b	19.47	Late Hauterivian	*S. angulicostatum*	1.08	5.29	101	83	437
AN39b	19.94	Late Hauterivian	*S. angulicostatum*	0.77	5.87	88	88	435
AN40b	20.41	Late Hauterivian	*S. angulicostatum*	1.14	5.06	104	85	437
AN41b	20.59	Late Hauterivian	*S. angulicostatum*	1.73	3.46	130	55	439
AN42b	21.00	Late Hauterivian	*S. angulicostatum*	1.15	4.99	106	65	437
AN43b	21.29	Late Hauterivian	*S. angulicostatum*	0.73	7.24	95	66	439
AN44b	21.59	Late Hauterivian	*S. angulicostatum*	0.65	6.17	80	84	440
AN45b	21.82	Late Hauterivian	*S. angulicostatum*	1.37	1.81	84	63	437
AN46b	22.35	Late Hauterivian	*S. angulicostatum*	2.13	1.89	181	51	436
AN48b	23.29	Late Hauterivian	*S. angulicostatum*	1.11	4.22	109	140	438
AN51b	24.53	Late Hauterivian	*S. angulicostatum*	1.09	10.18	345	42	434
AN52b	25.06	Late Hauterivian	*S. angulicostatum*	1.49	7.97	256	48	434
AN53.1b	25.18	Late Hauterivian	*S. angulicostatum*	1.09	10.16	342	45	434
AN72b	33.87	Early Barremian	*A. kiliani*	0.50	6.42	65	111	437
AN73b	34.43	Early Barremian	*A. kiliani*	0.65	5.42	109	69	435
AN74b	34.74	Early Barremian	*A. kiliani*	0.66	4.78	105	80	432
AN75b	35.37	Early Barremian	*A. kiliani*	0.82	5.19	151	44	437
AN76b	35.68	Early Barremian	*A. kiliani*	0.39	7.60	94	89	435

Table D.10: Results of the Rock Eval analyses performed on marls from the B. balearis to the A. kiliani ammonite zones (Angles section).

result of increasing thermal diagenesis, which may have affected carbonates more strongly than marls. The diagenetic transformation of smectite is also accompanied by the appearance of mixed-layered minerals, such as in Tithonian – Berriasian sediments of the Vergons section and in sediments from the early Cretaceous of the Daluis section (Deconinck and Debrabant, 1985). All these mechanisms fractionating and transforming clay mineral assemblages may led to a misreading of the original climatic signal. This implies that the integrity of the clay-mineral assemblage is to be

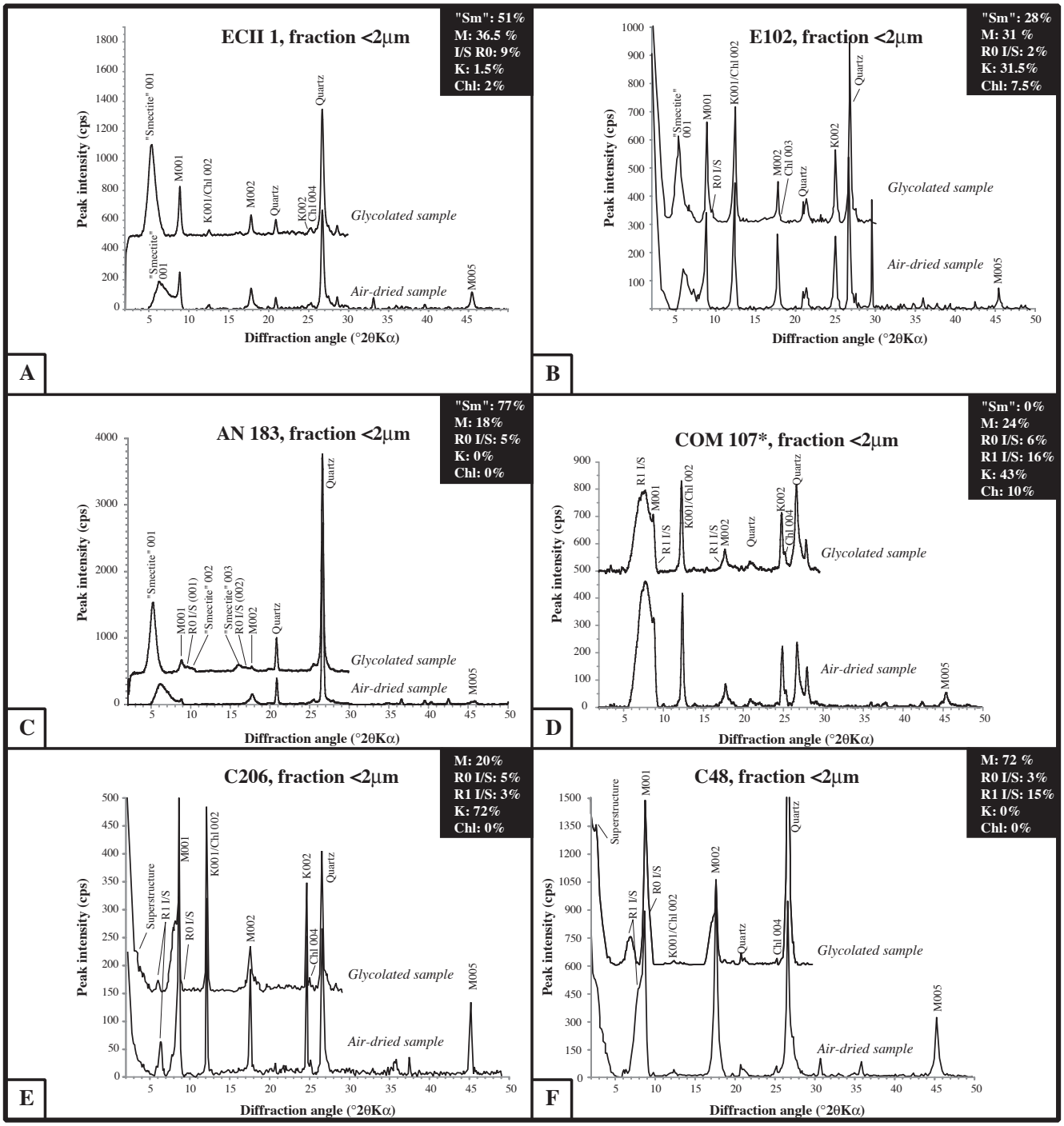

Fig. D.28: Diffractograms characteristic of the studied sections. **A:** *sample ECII1 (oolitic grainstone), Early Hauterivian, base of the Eclépens section;* **B:** *sample E102 (bioclastic packstone), Late Barremian, Eclépens section;* **C:** *sample AN183 (hemipelagic mudstone), M. sarasini ammonite zone (Late Barremian), Angles;* **D:** *sample COM107* (hemipelagic marlstone), boundary between the Deshayesites oglanlensis and D. weissi ammonite zones (Early Aptian), Combe-Lambert;* **F:** *sample C45 (bioclastic packstone), base of the Cluses section;* **E:** *sample C206 (peloidal grainstone to packstone with large benthic foraminifera), top of the depositional sequence Ba4 (Late Barremian), Cluses. Abbreviations of the minerals: "Sm" = "Smectite"; Sm = Smectite; M = Mica; K = Kaolinite; Chl = Chlorite.*

tested before its interpretation as a signal of the prevailing climate and changes therein.

D.4.5.1.1. Angles and Combe-Lambert

During the Cenozoic, the alpine orogenetic phase led to the formation of thrusts sheets in sediments belonging to the Vocontian Trough, and in particular the formation of the "nappe de Dîgne" had an impact on the thermal evolution of the Hauterivian – Barremian succession in the sections of Angles and Combe-Lambert (*e.g.*, van de Schootbrugge *et al.*, 2000). The associated tectonic overprint of clay-mineral assemblages did not completely obliterate their environmental signal: both the preservation of high contents of "smectites" and kaolinite compared to R0 I/S, as well as the absence of regular mixed-layers indicate low to medium diagenetic overprint. This is coherent with the amount of illite layers within the R0 I/S, which reaches an average value of 30% in the Angles and Combe-Lambert sections (all lithologies). On the other hand, the higher proportion of chlorite preserved in limestones compared to marls may have been the consequence of quite strong diagenetic overprint (*e.g.*, Deconinck and Chamley, 1983; Deconinck, 1987). But, as "smectites" display a similar behaviour, a change from humid to dryer conditions between marls and limestones may have controlled, at least in part, the distribution of both chlorite and "smectites" between the two lithologies. This is in agreement with the content of R0 I/S, which remains the same whatever the lithology. The better preservation of "smectite" in limestones compared to marls may also be a function of the lithology: Burkhard (1988) and Huon *et al.* (1994) reported the presence of well-crystallised smectite in micrite from the Doldenhorn nappe (Helvetic Alps), which reached temperatures of 300 to 350°C during at least 10 millions years; this suggests that the fine-grained, carbonated lithology constitutes a protection against thermal diagenesis, which is in contradiction with the conclusions of Ferry *et al.* (1983).

Moreover, the IC values are highly variable, ranging from 0.15 to 0.2 °2θ in limestones, and from 0.35 to 0.4 °2θ in marls, which corresponds to values typical for the diagenetic zones 1 to 3 of Kübler and Jaboyedoff (2000). However, the increase of the IC in marls is certainly due to a higher content of "smectite" and R0 I/S compared to limestones, which may enlarge the peak 001 of the mica. The apparent thickness of this peak may therefore reflect a mixture of detrital illite and of mixed-layers.

On the other hand, Rock-Eval analyses were performed on 26 marl samples belonging to the *B. balearis* (late Hauterivian) to the *A. kiliani* zones (early Barremian) of Angles. In Fig. D.29, T_{max} values reach 440°C (mean value of 436°C), which is consistent with the values obtained in the Vergons section by Baudin *et al.* (1999), who concluded a low degree of thermal diagenesis for this section. This implies that the sedimentary succession may have reached the beginning of the potential oil window and the zone of transition of the smectite to the R0 I/S (Espitalié *et al.*, 1985; see also Fig. 23 in Kübler, 1997).

Finally, a recently published cross plot of $\delta^{13}C$ versus $\delta^{18}O$ measured at Angles (*e.g.*, Wissler *et al.*, 2002; Godet *et al.*, 2006) reveals no clear correlation, and even if $\delta^{18}O$ displays relatively light values (minimum of -4.5‰ in Wissler *et al.*, 2002), the trends observed in the stratigraphic evolution of $\delta^{18}O$ values at Angles can be correlated between the Vocontian Trough, the Ultrahelvetic realm in Switzerland and the Umbria-Marche basin in Italy, which excludes a strong diagenetic overprint at Angles (Godet *et al.*, 2006).

All these parameters constrain the diagenetic overprint at Angles (and by extension at Combe-Lambert) close to the transition between stages 2 and 3 of Kübler and Jaboyedoff (2000). This implies that the main part of the clay-minerals assemblage is well-preserved in this succession, especially the kaolinite may have not suffered from diagenesis.

D.4.5.1.2. Cluses and Eclépens

At Cluses, diagenesis was more pronounced than at Angles and Combe-Lambert, as is suggested by the absence of smectite and the presence of rectorite and corrensite (Wermeille, 1996). However, the preservation of kaolinite suggests

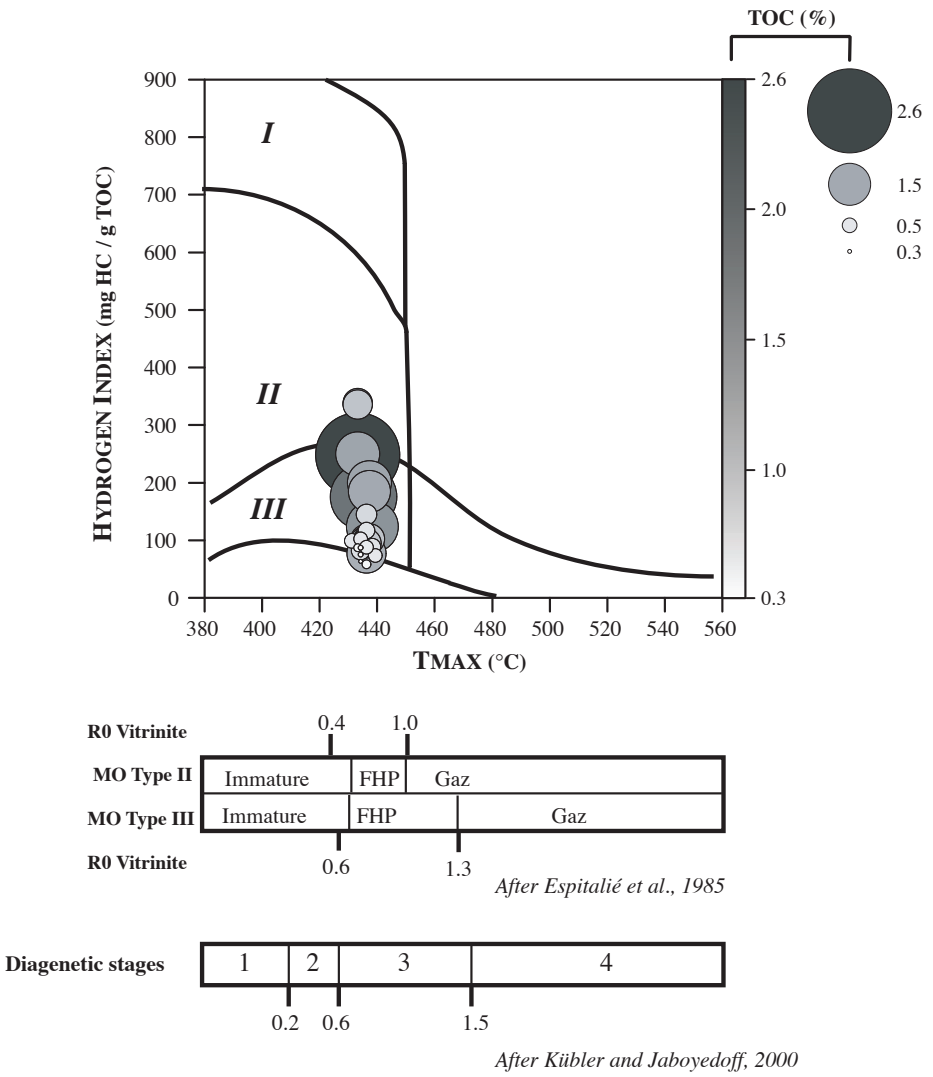

Fig. D.29: Cross plot of the hydrogen index (HI) versus maximum of temperatures (Tmax) for marls corresponding to the Late Hauterivian – earliest Barremian interval of the Angles section. The shading and sizing of the bubbles corresponds to the total organic carbon (TOC) content. The evolution of kerogens and the correspondence of the diagenetic stages with respect to the reflectance of vitrinite is after Espitalié et al. (1985), and Kübler and Jaboyedoff (2000), respectively.

that the sedimentary succession underwent diagenetic overprint from the transition between stage 2 and 3 to the middle of the stage 4.

At Eclépens, the mineralogy of the clay fraction is more diversified, and includes some true smectites. This implies that diagenesis had a relatively low impact on the sedimentary succession, as is suggested by the rapid exhumation of the succession after a maximum burial depth of approximately 2500 m (Burkhard and Sommaruga, 1998). Moreover, the IC ranges between 0.25 and 0.3 °2θ (Blanc-Aletru, 1995); this implies that the majority of the mica from Eclépens has a detrital origin. Finally, the relative high content of smectite layers in R0 I/S (average value of approximately 71 %; see Table D.9) is another argument to conclude that the intensity of diagenesis did not exceed the middle of the diagenetic stage 2 of Kübler and Jaboyedoff (2000).

D.4.5.2.Climate change during the Late Hauterivian – Early Aptian

A correlation based of the stratigraphic evolution of kaolinite is proposed between the Western Swiss Jura, the Subalpine Chains, and the Vocontian Trough, for the time period from the Early Hauterivian to the earliest Aptian (Fig. D.30). Kaolinite / smectite and smectite / mica ratios curves are also reported, where appropriate. In southeastern France and in the vicinity of Neuchâtel, clay-mineral assemblages

are dominated by smectite during the Hauterivian. The lack of good age control at the base of the Cluses section, as well as diagenetic processes that may have transformed eventually present smectite into mixed-layer minerals, do not allow a firm correlation of this section with the two other domains for this interval.

In general, the dominance of "smectites" from the base of the Hauterivian stage to the *B. balearis* ammonite zone (mean value of 59%; extreme values of smectite for this interval: 20 to 81%), suggests the presence of a dry but seasonally contrasted climate (*e.g.*, Chamley, 1989; Weaver, 1989).

Upwards, the evolution in kaolinite contents follows a threefold division, with low values in part I and III and an increase in part II; the same behaviour is reported for the evolution of the kaolinite / mica and the kaolinite / (quartz + feldspar + plagioclase) ratios. Kaolinite constitutes therefore the main mineral of the clay assemblage in the sections of Angles and Combe-Lambert for most of the Barremian. This conclusion is supported by the clay-mineral evolution from the Cluses section (Fig. D.26).

The presence of kaolinite implies warm or humid climates, under which well-drained continental areas may undergo intense biogeochemical weathering leading to the concentration of Al_2O_3 and the genesis of bauxite and associated kaolinite (*e.g.*, Chamley, 1989; Weaver, 1989; Thiry *et al.*, 1999). In the time interval from the *P. mortilleti* to the *Imerites giraudi* ammonite zones, the development of such soils may have been important on the southern European continent bordering the northern Tethyan margin, due to a shift from a seasonally well contrasted to a warmer and more humid climate during the latest Hauterivian (Fig. D.30). The stratigraphically highest peak in kaolinite content is observed in marly sediments near the SbB4 and this may reflect the predominance of humid conditions during the deposition of marls. However, an intensification of humid conditions during the *H. sayni* and the *H. feraudianus* ammonite zones is also suggested by the symmetric shape of this increase around the SbB4.

A comparison with the $\delta^{18}O$ measured on bulk-rock limestone samples from the Angles section (Godet *et al.*, 2006) suggests a possible link between the variations in temperature mirrored by the main trends of the $\delta^{18}O$ curve and the evolution of the kaolinite content (Fig. D.31). Effectively, Godet *et al.* (2006) described a four-fold evolution, with two maxima in $\delta^{18}O$ values at the base of the *N. pulchella* and in particular in the *I. giraudi* ammonite zones. Whereas the first maximum in the $\delta^{18}O$ record corresponds to a period characterized by stable but relatively moderate kaolinite contents, the second maximum follows immediately after the highest values recorded in the kaolinite evolution. The genesis of kaolinite requires a humid and warm climate; in the part II of the Angles section, the augmentation in kaolinite content may mirror an increased continental runoff, which may have constituted a sink for atmospheric CO_2. Subsequently, the greenhouse effect may have decreased and the temperature as well. As a consequence, the $\delta^{18}O$ values may shift toward more positive values after episodes of high continental runoff, as the one recorded from the end of the *H. sayni* to the *I. giraudi* ammonite zones at Angles. Thereafter, the $\delta^{18}O$ returns to lighter values, reflecting an increase of temperature. Alternatively, the evolution of kaolinite is compatible with the $\delta^{18}O$ record, if the latter reflects salinity rather than temperature; during time of kaolinite dominance, the input of freshwater in the ocean may increase, as kaolinite genesis requires an increased rainfall. Consequently, the salinity of the surface ocean may decrease by dilution and the $\delta^{18}O$ may shift toward more negative values.

D.4.5.3. Kaolinite evolution from the Vocontian Trough to the western Swiss Jura: Evidence for differential settling

The evolution of kaolinite contents along the northern Tethyan margin from the late Early Barremian to the earliest Aptian reveals an ambiguous behaviour of this clay mineral: whereas the latest Barremian - earliest Aptian sedimentary record in the Western Swiss Jura is characterized by high kaolinite contents (Fig. D.28 and Table D.8), contemporaneous sediments deposited in the Vocontian trough are relatively impoverished in this mineral (Fig. D.26 and

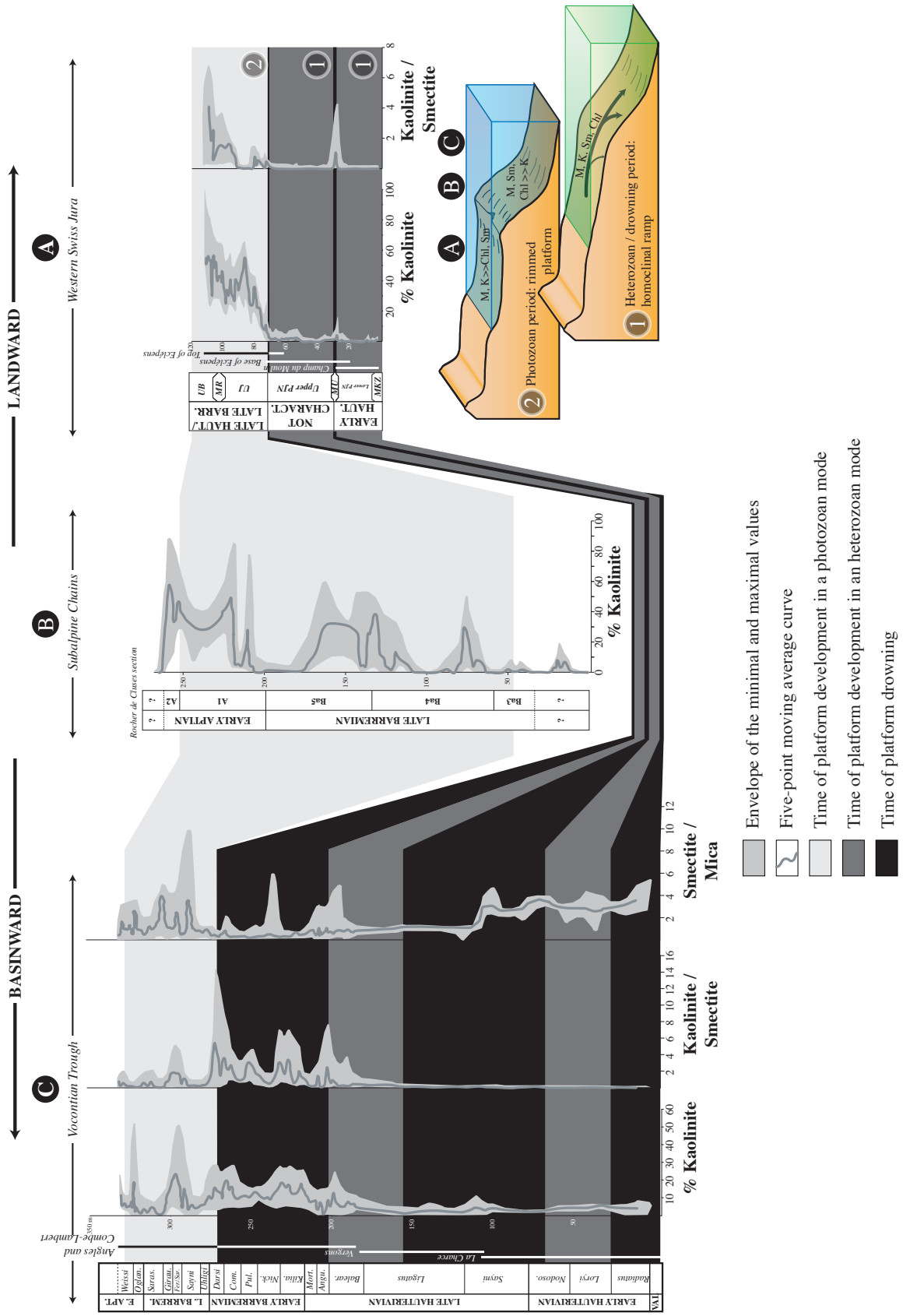

Fig. D.30: Correlation between the Vocontian Trough (Angles and Combe-Lambert sections), the Subalpine Chains (Cluses section), and the Western Swiss Jura (Champ du Moulin and Eclépens sections), based on the kaolinite evolution. Both the relative abundance of kaolinite, as well as the kaolinite/smectite ratio are used, where appropriate. Bloc diagrams on the right side of the figure illustrate the morphology of the platform and the subsequent differential settling of clay-minerals during times of heterozoan and drowned platform (1), and photozoan platform (2); on the top on these two transects, the letters A, B and C indicate the theoretical position of the three studied regions along the margin. Note that data from Champ du Moulin (after Rumley, 1993; see Fig. D.23 for a location) complete the data from Eclépens for the lower PJN.

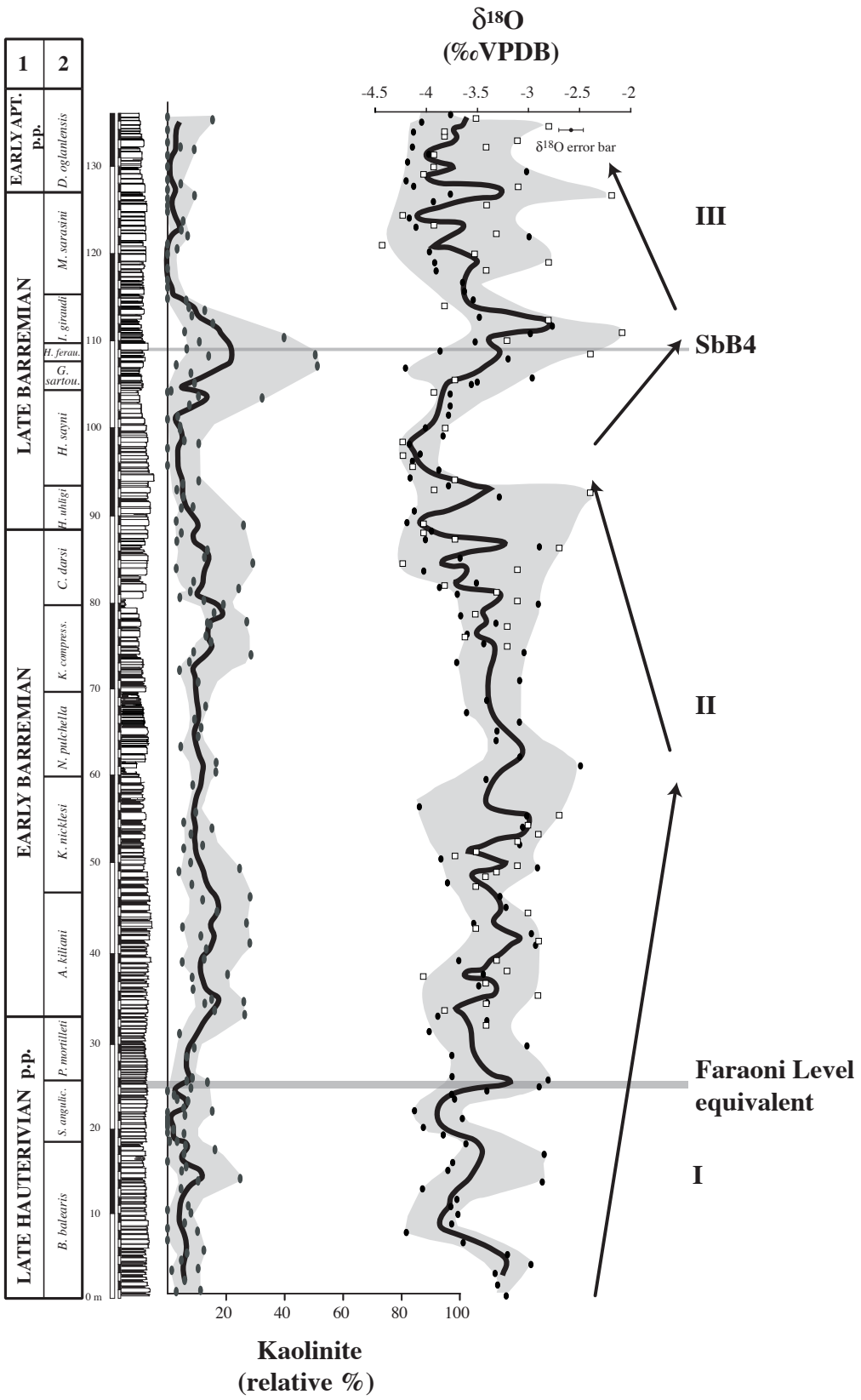

*Fig. D.31: Comparison of the kaolinite and the $\delta^{18}O$ (measured on bulk-rock limestone samples) evolution in the Angles section. On the left side of the figure, the numbers on the top of the columns corresponds to the stratigraphic stage **(1)** and the ammonite zone **(2)**. The $\delta^{18}O$ values are after Wissler et al. (2002; white squares), and Godet et al. (2006; black circles).*

Table D.8). As the kaolinite content displays intermediate values in Aptian sediments from the Cluses section (Table D.8), a link between sea-level fluctuation, a change in the morphology

of the carbonate platform, and migration of the depo-centre of kaolinite as a function of the distance from the coastline through sea-level change may explain this apparent decrease in kaolinite in distal directions along the northern Tethyan margin.

During the Hauterivian, a heterozoan assemblage dominated the carbonate-producing community along the northern Tethyan margin, whereas during the period between the *C. darsi* ammonite zone (late Early Barremian) and the *Deshayesites weissi* ammonite zone (Early Aptian), this assemblage progressively evolved into a photozoan ecosystem (Föllmi *et al.*, 1994; 2006). In the period between the latest Hauterivian and late Early Barremian (*P. mortilleti* to the *C. darsi* ammonite zone), the Helvetic platform underwent a major drowning phase (Bodin *et al.*, 2006b). An important difference between these two regimes of carbonate production is associated with the platform morphology: the Hauterivian heterozoan platform is interpreted as a ramp structure with a good connection to the ocean, whereas the late Early Barremian to Early Aptian photozoan platform developed a marginal rim consisting of patch reefs and oolitic shoals (*e.g.*, Arnaud-Vanneau, 1980). The heterozoan platform structure was, for this reason, particularly favourable to the bypass of detrital continental material, such as clay minerals and quartz particles, into the open sea. The photozoan platform structure may, on the contrary, have functioned as a barrier for larger detrital particles such as kaolinite, and may have fractioned the clay-mineral assemblage transferred to the ocean in a way that the larger, less reactive kaolinite particles were trapped on the platform (see below).

In the Vocontian Trough, kaolinite is absent in sediments older than the latest Hauterivian (data from van de Schootbrugge, 2001), appears in sediments attributed to the *B. balearis* ammonite zone and reaches more than 30-40% in Early Barremian sediments (Fig. D.30). The absence of kaolinite and the dominance of smectite in most of the Hauterivian sediments may reflect a true climatic signal, which is in agreement with the type of carbonate platform that developed at that time, under high nutrient conditions (*e.g.*, van de Schootbrugge *et al.*, 2003; Bodin *et al.*, 2006a). During the latest Hauterivian, the appearance of kaolinite indicates a change from a seasonally contrasted towards a more humid and warm (intertropical) climate that can be linked to an acceleration of the hydrologic cycle, and with that an increase in continental run-off. The related enhanced supply of phosphorus and of Dissolved Inorganic carbon (DIC) to the ocean may have been triggered by intensified biogeochemical weathering, as already suggested by Bodin *et al.* (2006) and Godet *et al.* (2006). The latter linked the very stable evolution of the $\delta^{13}C$ record observed from the base of the *P. mortilleti* to the top of the *C. darsi* ammonite zone to an increase of the oceanic DIC volume in the ocean, which may have buffered the $\delta^{13}C$ signal against paleoceanographic change (see Bartley and Kah (2004) for a detailed explanation of the DIC buffering effect on the $\delta^{13}C$ record). As a consequence of the change towards a warmer and wetter climate during the latest Hauterivian and a corresponding increase in phosphorus input into the ocean, the northern Tethyan carbonate platform drowned (during the period between the *S. angulicostatum* and the *C. darsi* ammonite zones; Arnaud-Vanneau and Arnaud, 1990; Bodin *et al.*, 2006b).

Then, from the *Gerhadtia sartousiana* ammonite zone onward, carbonate production took up again on the platforms of the northern Tethys, and this especially in the Vercors and the Helvetic Alps (Arnaud-Vanneau and Arnaud, 1990; Föllmi *et al.*, 1994; 2006; Bodin *et al.*, 2006c); corals, green algae, stromatoporoids and associated rudists recovered in the platform sediments of this period are typical of a photozoan assemblage (*e.g.*, James, 1997; Mutti and Hallock, 2003). During the time of carbonate production in a photozoan mode, the presence of a barrier or a reef that separated the platform from the basin, as well as the morphology of the platform may have led to a fractionation of clay minerals during its transfer to the ocean. This is related to the size of kaolinite crystals (and consequently its weight) as well as its high capacity to flocculate (Ruffell *et al.*, 2002), which both may have favoured the deposition of this mineral after a relatively brief transport in the ocean (*e.g.* Gibbs, 1977; Hallam, 1984), and may have led to a decrease of the

kaolinite content toward the basin. Moreover, this differential settling of clay particles may have been enhanced by changes in sea-level. During sea-level rise and subsequent sea-level highstand, the shelf area increases and the distance between the continent where kaolinite was formed and the basin becomes more important. Moreover, the diversity and the development of facies susceptible to trap detrital particles are the highest within highstand deposits. This implies that kaolinite may be deposited in proximal shelf settings rather than in hemipelagic environments during periods of high sea-level. This may also explain the difference in the quantity of kaolinite deposited along the northern Tethyan margin during the latest Barremian and earliest Aptian, as this time span corresponds to a long-term maximum in eustatic sea level (Haq *et al.*, 1987; Arnaud, 2005).

This fractionation pattern with regards to the kaolinite distribution in clay-mineral assemblages has already been suggested for the Valanginian-Hauterivian carbonate platform (Adatte and Rumley, 1989), and for the middle Jurassic succession (Bolle *et al.*, 1996) of the Western Swiss Jura. Sediments from a platform developing in a photozoan mode may as a consequence record a faithful climatic signal, whereas in the adjacent hemipelagic setting the preserved clay-mineral assemblage may have been fractionated and the climate signal correspondingly altered. Consequently, looking at the clay-minerals evolution along a platform to basin transect may be more useful than considering only pelagic sections when attempting to trace climate change.

D.4.6. Conclusions

The evolution of clay-mineral assemblages during the Hauterivian, Barremian and earliest Aptian along a platform-basin transect in the northern Tethys highlights the dominance of smectite and the quasi absence of kaolinite in sediments up to the latest Hauterivian. During the latest Hauterivian to the Early Aptian, kaolinite becomes abundant, which may indicate a general change from a seasonally contrasted, temperate climate prevailing during the Hauterivian to a warmer and wetter climate in the period from the latest Hauterivian to the earliest Aptian for the southern European realm adjacent to the Northern Tethys. The increased humidity and enhanced continental runoff may have triggered elevated input of nutrients and DIC in the ocean. The latter may have contributed to initiate the anoxia characteristic of the Faraoni Level, and also to buffer the $\delta^{13}C$ signal.

The distribution of clay minerals along this transect was not only influenced by climate change, but also by the morphology of the platform and by sea-level change. During the Hauterivian, the ramp-type morphology of the northern Tethyan platform may have favoured a direct transport of clay particles into the basin without major fractionation. From the *B. balearis* to the *C. darsi* ammonite zone, the Helvetic platform underwent a major phase of drowning, which may have also facilitated the transport of clay toward the basin. The re-installation of the carbonate platform in a photozoan mode near the Early - Late Barremian boundary and the development of a marginally rimmed platform topography – together with general sea-level rise - may have fractionated the clay-mineral assemblages during their transport into the basin, with the preferred deposition of kaolinite in proximal settings, and the subsequent depletion of this mineral in distal environments. This highlights the importance of comparing several sections distributed along a proximal – distal transect, in order to better constrain climatic changes by means of clay mineralogy.

D.4.7. Acknowledgements

The authors acknowledge Laureline Scherler and Laurent Chalumeau (University of Neuchâtel) for the preparation of the samples from Angles with regards to the clay-mineral analysis, Philipp Steinmann (University of Neuchâtel) for performing the Rock Eval analyses, and Stéphane Westermann (University of Neuchâtel) for the help in sampling and measuring the Combe-Lambert section. We thank the staff of the Eclépens quarry (Holcim company), for allowing us to sample the Eclépens section. This research is financially supported by the Swiss National Fund (projects n°2100-067807/1 and 200020-105206/1). The reviews of Cédric John, Thomas Pletsch and Alastair Ruffell greatly improved the quality

of this manuscript.

D.4.8. References

Adatte, T. and Rumley, G. (1989). "Sedimentology and mineralogy of the Valanginian and Hauterivian in the stratotypic region (Jura mountains, Switzerland)". *In:* Wiedmann, J., (*Ed.*). Cretaceous of the Western Tethys: proceedings of the 3rd International Cretaceous Symposium, Tübingen 1987. Stuttgart, E. Schweizerbart'sche Verlagsbuchhandlung (Nägele u. Obermiller): 329-351.

Adatte, T., Stinnesbeck, W. and Keller, G. (1996). «Lithostratigraphic and mineralogic correlations of near K/T boundary sediments in northeastern Mexico: Implications for origin and nature of deposition». *In:* Ryder, G., Fastovsky, D. and Gartner, S., (*Eds*). The Cretaceous-Tertiary Event and Other Catastrophes in Earth History. Boulder, Colorado, **Geological Society of America Special Paper 307**: 211-226.

Arnaud, H. (2005). «The South-East France Basin (SFB) and Its Mesozoic Evolution.» Géologie Alpine **Série Spéciale «Colloques et Excursions» N°7**: 5-28.

Arnaud-Vanneau, A. (1980). «Micropaléontologie, paléoécologie et sédimentologie d'une plate-forme carbonatée de la marge passive de la Téthys: l'Urgonien du Vercors septentrional et de la Chartreuse (Alpes occidentales).» Géologie Alpine **Grenoble Mém HS 10**: 874 p.

Arnaud-Vanneau, A. and Arnaud, H. (1990). «Hauterivian to Lower Aptian carbonate shelf sedimentation and sequence stratigraphy in the Jura and northern Subalpine chains (southeastern France and Swiss Jura)». *In:* Tucker, M. E., Wilson, J. L., Crevello, P. D., Sarg, J. R. and Read, J. F., (*Eds*). Carbonate Platforms: Facies, Sequences and Evolution. Blackwell Scientific Publications, Special Publication of the International Association of Sedimentologists, **9**: 203-233.

Bartley, J. K. and Kah, L. C. (2004). «Marine carbon reservoir, C_{org} - C_{carb} coupling, and the evolution of the Proterozoic carbon cycle.» Geology **32** (*2*): 129-132.

Baudin, F. (2005). «A Late Hauterivian short-lived anoxic event in the Mediterranean Tethys: the «Faraoni Event».» Comptes Rendus de l'Académie des Sciences de Paris.

Baudin, F., Bulot, L. G., Cecca, F., Coccioni, R., Gardin, S. and Renard, M. (1999). «Un équivalent du «Niveau Faraoni» dans le Bassin du Sud-Est de la France, indice possible d'un événement anoxique fini-hauterivien étendu à la Téthys méditerranéenne.» Bull. Soc. géol. France **170** (*4*): 487-498.

Behar, F., Beaumont, V. and De B. Penteado, H. L. (2001). «Rock-Eval 6 technology: performances and developments.» Oil & Gas Science and Technology - Rev. IFP **56** (*2*): 111-134.

Blanc-Aletru, M. C. (1995). Importance des discontinuités dans l'enregistrement sédimentaire de l'Urgonien jurassien. Micropaléontologie, Sédimentologie, Minéralogie et Stratigraphie Séquentielle. Géologie Alpine. Ph.D. Thesis Grenoble, Laboratoire de Géologie de l'Université I de Grenoble. Mémoire HS n°24: 299 pp.

Bodin, S., Godet, A., Vermeulen, J., Arnaud, H., Strasser, A., Fiet, N., Adatte, T. and Föllmi, K. B. (2006). «The late Hauterivian Faraoni oceanic anoxic event in the western Tethys: Evidence from phosphorus burial rates.» Palaeogeography, Palaeoclimatology, Palaeoecology **235**: 245-264.

Bodin, S., Godet, A., Vermeulen, J., Linder, P. and Föllmi, K. B. (2006). «Biostratigraphy, sedimentology and sequence stratigraphy of the latest Hauterivian - early Barremian drowning episode of the Northern Tethyan margin (Altmann Member, Helvetic Nappes, Switzerland).» Eclogae Geologicae Helveticae, in press.

Bolle, M.-P., Adatte, T., Mangold, C. and Remane, J. (1996). «Microfaciès, minéralogie, stratigraphie du Dogger de la région du Furcil (NE).» Bulletin de la Société neuchâteloise des Sciences Naturelles **119**: 123-144.

Bulot, L. G., Thieuloy, J.-P., Blanc, E. and Klein, J. (1992). «Le cadre stratigraphique du Valanginien supérieur et de l'Hauterivien du Sud-Est de la France; définition des biochronozones et caractérisation de nouveaux biohorizons.» Géologie Alpine **68**: 13-56.

Burkhard, M. (1988). «L'Helvétique de la bordure occidentale du massif de l'Aar (évolution tectonique et métamorphique).» Eclogae

Geologicae Helvetiae **81** (*1*): 63-114.

Burkhard, M. and Sommaruga, A. (1998). «Evolution of the western Swiss Molasse basin: structural relations with the Alps and the Jura belt». *In:* Mascle, A., Puigdefàbregas, C., Luterbacher, H. P. and Fernàndez, M., (*Eds*). Cenozoic foreland Basins of Western Europe. Geological Society Special Publications, **134**: 279-298.

Cecca, F., Faraoni, P., Marini, A. and Pallini, G. (1995). «Field-trip across the representative sections for the Upper Hauterivian-Barremian ammonite biostratigraphy in the Maiolica exposed at Monte Nerone, Monte Petrano and Monte Catria (Umbria-Marche, Apennines).» Memorie Descrittive della Carta Geologica d'Italia **51**: 187-211.

Chamley, H. (1981). «Long-term trends in clay deposition in the ocean.» Oceanologica Acta **n°SP Proceedings 26th International Geological Congress, Geology of Oceans Symposium, Paris, July 7-17, 1980**: 105-110.

Chamley, H. (1989). «Clay sedimentology», Springer Verlag, Berlin, 623.

de Montmollin, A. (1835). «Mémoire sur le terrain Crétacé du Jura.» Mémoires de la Société des Sciences Naturelles de Neuchâtel **tome I**: 49-65.

Deconinck, J.-F. (1987). «Identification de l'origine détritique ou diagénétique des assemblages argileux: le cas des alternances marne-calcaire du Crétacé inférieur subalpin.» Bulletin de la Société Géologique de France **(8) t. III** (*1*): 139-145.

Deconinck, J.-F. and Chamley, H. (1983). «Héritage et diagenèse des minéraux argileux dans les alternances marno-clacaires du Crétacé inférieur du domaine subalpin.» Comptes Rendus de l'Académie des Sciences de Paris **297** (*24 octobre 1983*): 589-594.

Deconinck, J.-F. and Debrabant, P. (1985). «Diagenèse des argiles dans le domaine subalpin: rôles respectifs de la lithologie, de l'enfouissement et de la surcharge tectonique.» Revue de Géologie Dynamique et de Géographie Physique **26** (*5*): 321-330.

Delanoy, G. (1997). «Biostratigraphie des faunes d'Ammonites à la limite Barrémien-Aptien dans la région d'Angles-Barrême-Castellane. Etude particulière de la famille des Heteroceratina Spath, 1922 (Ancyloceratina, Ammonoidea).» Annales du Muséum d'Histoire Naturelle de Nice **Tome XII**: 1-270.

Espitalié, J., Deroo, G. and Marquis, F. (1985). «La pyrolyse Rock-Eval et ses applications.» Revue de l'Institut Français du Pétrole **40** (*5*): 563-579.

Ferrero, J. (1965). «Dosage des principaux minéraux des roches par diffraction de Rayon X.» Rapport C.F.P. (Bordeaux), inédit.

Ferrero, J. (1966). «Nouvelle méthode empirique pour le dosage des minéraux par diffraction R.X.» Rapport C.F.P. (Bordeaux), inédit.

Ferry, S., Cotillon, P. and Rio, M. (1983). «Diagenèse croissante des argiles dans des niveaux isochrones de l'alternance calcaire-marne valanginienne du bassin vocontien. Zonation géographique.» Comptes Rendus de l'Académie des Sciences de Paris Série II **297** (*4 juillet 1983*): 51-56.

Föllmi, K. B., Godet, A., Bodin, S. and Linder, P. «Interactions between environmental change and shallow-water carbonate build-up along the northern Tethyan margin and their impact on the early Cretaceous carbon-isotope record.» Submitted to Paleoceanography.

Föllmi, K. B., Weissert, H., Bisping, M. and Funk, H. (1994). «Phosphogenesis, carbon-isotope stratigraphy, and carbonate-platform evolution along the Lower Cretaceous northern Tethyan margin.» Geological Society of America Bulletin **106** (*II*): 729-746.

Gibbs, R. J. (1977). «Clay mineral segregation in the marine environment.» Journal of Sedimentary Petrology **47** (*1*): 237-243.

Godet, A., Blanc-Aletru, M.-C., Bodin, S., Adatte, T. and Föllmi, K. B. (2005). «The Hauterivian-Barremian of the Western Swiss Jura around Neuchâtel.» Géologie Alpine **Série Spéciale «Colloques et Excursions» n°7**: 79-96.

Godet, A., Bodin, S., Föllmi, K. B., Vermeulen, J., Gardin, S., Fiet, N., Adatte, T., Berner, Z., Stüben, D. and van de Schootbrugge, B. (2006). «Evolution of the marine stable carbone-isotope record during the early Cretaceous: A focus on

the late Hauterivian and Barremian in the Tethyan realm.» Earth and Planetary Science Letters **242** (*3-4 doi:10.1016/j.epsl.2005.12.011*): 254-271.

Hallam, A. (1984). «Continental humid and arid zones during the Jurassic and Cretaceous.» Palaeogeography, Palaeoclimatology, Palaeoecology **47**: 195-223.

Haq, B. U., Hardenbol, J. and Vail, P. R. (1987). «The chronology of fluctuating sea level since the Triassic.» Science **235**: 1156-1167.

Hillier, S. (1989). «Clay mineral diagenesis and organic maturity indicators in Devonian lacustrine mudrock from the Orcadian Basin, Scotland.» *PhD thesis*, University of Southampton, United Kingdom, 298 pp.

Huon, S., Burkhard, M. and Hunziker, J.-C. (1994). «Mineralogical, K-Ar, stable and Sr isotope systematics of K-white micas during very low-grade metamorphism of limestones (Helvetic nappes, western Switzerland).» Chemical Geology (Isotope Geoscience Section) **113**: 347-376.

James, N. P. (1997). «The cool-water carbonate depositional realm». *In:* James, N. P. and Clarke, J. A. D., (*Eds*). Cool-water carbonates. Tulsa, Oklahoma, Society for Sedimentary Geology, **SEPM Special Publication N° 56**: 1-20.

Klug, H. P. and Alexander, L. (1974). «X-ray Diffraction Procedures for Polycrystalline and Amorphous Materials», John Wiley and Sons, Inc., New York, 992.

Kübler, B. (1983). «Dosage quantitatif des minéraux majeurs des roches sédimentaires par diffraction X.» Cahiers de l'Institut de Géologie, Université de Neuchâtel, Suisse **Série AX n°1.1 and 1.2**: 13 p.

Kübler, B. (1987). «Cristallinité de l'illite: méthodes normalisées de préparation, méthode normalisée de mesure, méthode automatique normalisée de mesure.» Cahiers de l'Institut de Géologie, Université de Neuchâtel, Suisse **Série ADX n° 2**.

Kübler, B. (1997). «Concomitant Alteration of Clay Minerals and Organic Matter During Burial Diagenesis». *In:* Paquet, H. and Clauer, N., (*Eds*). Soils and Sediments. Mineralogy and Geochemistry. Springer-Verlag, **Berlin**: 327-362.

Kübler, B. and Goy-Eggenberger, D. (2001). «La cristallinité de l'illite revisitée: un bilan des connaissances acquises ces trente dernières années.» Clay Minerals **36**: 143-157.

Kübler, B. and Jaboyedoff, M. (2000). «Illite Cristallinity.» C.R. Ac. Sc. Paris, Sciences de la terre et des planètes / Earth & Planetary Sciences **331**: 75-89.

Lafargue, E., Marquis, F. and Pillot, D. (1998). «Rock-Eval 6 Applications in Hydrocarbon Exploration, Production and Soils Contamination Studies.» Oil & Gas Science and Technology **53** (*4*): 421-437.

Larson, R. L. and Erba, E. (1999). «Onset of the mid-Cretaceous greenhouse in the Barremian-Aptian: Igneous events and the biological, sedimentary and geochemical responses.» Paleoceanography **14** (*6*): 663-678.

Moore, D. M. and Reynolds, R. C. J. (1997). «X-Ray diffraction and the Identification and Analysis of Clay Minerals», Oxford University Press, New York, 378 pp.

Mutti, M. and Hallock, P. (2003). «Carbonate systems along nutrient and temperature gradients: some sedimentological and geochemical constraints.» Int. J. Earth Sci. (Geol. Rundsch.) **92**: 465-475.

Persoz, F. (1982). «Inventaire minéralogique, diagenèse des argiles et minéralostratigraphie des séries jurassiques et crétacées inférieures du Plateau suisse et de la bordure sud-est du Jura entre les lacs d'Annecy et de Constance.» Matériaux pour la Carte Géologiaue de la Suisse **Nouvelle Série 155**: 1-52.

Ruffell, A., Mc Kinley, J. and Worden, R. (2002). «Comparison of clay mineral stratigraphy to other proxy palaeoclimate indicators in the Mesozoic of NW Europe.» Phil. Trans. R. Soc. Lond. **360**: 675-693.

Ruffell, A. H. and Batten, D. J. (1990). «The Barremian-Aptian arid phase in western Europe.» Palaeogeography, Palaeoclimatology, Palaeoecology **80** (*3-4*): 197-212.

Rumley, G. (1993). «Sédimentologie, minéralogie et stratigraphie de l'Hauterivien dans le Jura neuchâtelois et vaudois (Suisse).» *thesis*, Université de Neuchâtel, 207 pp.

Schlanger, S. O. and Jenkyns, H. C. (1976). «Cretaceous oceanic anoxic events: causes and consequences.» Geologie en Mijnbouw **55** (*3-4*):

179-184.

Scholle, P. A. and Arthur, M. A. (1980). «Carbon Isotope Fluctuations in Cretaceous Pelagic Limestones: Potential Stratigraphic and Petroleum Exploration Tool.» American Association of Petroleum Geologists Bulletin **64** (*1*): 67-87.

Środoń, J. (1980). «Precise identification of illite / smectite interstratification by X-Ray powder diffraction.» Clays and Clay Minerals **28** (*6*): 401-411.

Thiry, M., Simon-Coinçon, S. and Schmitt, J.-M. (1999). «Paléoaltérations kaoliniques: signification climatique et signature dans la colonne sédimentaire.» Comptes Rendus de l'Académie des Sciences de Paris, Sciences de la terre et des planètes **329**: 853-863.

Trabold, G. L. (1996). «Development of the Urgonian limestones in the Delphino Helvetic Realm (Northern Subalpine Chains, Haute-Savoie, France). Sedimentology, Sequence Stratigraphy and Biostratigraphy.» Université de Genève, Publications du Département de Géologie et Paléontologie **20**: 1-187.

van de Schootbrugge, B. (2001). «Influence of paleo-environmental changes during the Hauterivian (early Cretaceous) on carbonate deposition along the northern margin of the Tethys: Evidence from geochemical records (C, O and Sr-isotopes, P, Fe, Mn).» *Ph.D. thesis*, Université de Neuchâtel, 291 pp.

van de Schootbrugge, B., Föllmi, K. B., Bulot, L. G. and Burns, S. J. (2000). «Paleoceanographic changes during the early Cretaceous (Valanginian-Hauterivian): evidence from oxygen and carbon stable isotopes.» Earth and Planetary Science Letters **181**: 15-31.

van de Schootbrugge, B., Kuhn, O., Adatte, T., Steinmann, P. and Föllmi, K. (2003). «Decoupling of P- and Corg-burial following Early Cretaceous (Valanginian-Hauterivian) platform drowning along the NW Tethyan margin.» Palaeogeography, Palaeoclimatology, Palaeoecology **199** (*3-4 SU* -): 315-331.

Vermeulen, J. (2002). «Etude stratigraphique et paléontologique de la famille des Pulchelliidae (Ammonoidea, Ammonitina, Endomocerataceae).» Géologie Alpine **Mémoire H.S. N°42**: 333 pp.

Weaver, C. E. (1989). «Clays, Muds, and Shales», Developments in Sedimentology **44**, Elsevier Science Publishers B. V., Amsterdam, 819.

Weissert, H. (1989). «C-Isotope stratigraphy, a monitor of paleoenvironmental change: a case study from the Early Cretaceous.» Surveys in Geophysics **10** (*1*): 1-61.

Weissert, H., Lini, A., Föllmi, K. B. and Kuhn, O. (1998). «Correlation of Early Cretaceous carbon isotope stratigraphy and platform drowning events: a possible link?» Palaeogeography, Palaeoclimatology, Palaeoecology **137**: 189-203.

Wermeille, S. (1996). «Etude sédimentologique, minéralogique et micropaléontologique des calcaires urgoniens de la région subalpine (Savoie, France). Coupes du Rocher de Cluses, du Borne et d'Andey.» *Unpublished diploma thesis*, University of Neuchâtel, 129 pp.

Wissler, L., Weissert, H., Masse, J.-P. and Bulot, L. G. (2002). «Chemostratigraphic correlation of Barremian and lower Aptian ammonite zones and magnetic reversals.» Int. J. Earth Sci. (Geol. Rundsch.) **91** (*2*): 272-279.

D.5.
Interactions between environmental change and shallow-water carbonate build-up along the northern Tethyan margin and their impact on the Early Cretaceous carbon-isotope record

Karl B. Föllmi, Alexis Godet, Stéphane Bodin, and Pascal Linder

Geological Institute, University of Neuchâtel, CH-2007 Neuchâtel, Switzerland

Accepted in Paleoceanography

Abstract

The evolution of the Early Cretaceous, northern Tethyan carbonate platform was not only influenced by changes in sea level, detrital influx, and surface-water temperature, but also by changes in trophic levels. We distinguish between phases of carbonate production dominated by oligotrophic photozoan communities and by mesotrophic and eventually colder water heterozoan communities. Superimposed on this bimodal trend in platform evolution were phases of platform demise for which we provide improved age control based on ammonite biostratigraphy. The initial phase of these episodes of platform demise corresponds in time to episodes of oceanic anoxic events (OAE's) and environmental change in general.

Based on a comparison between the temporal changes in an Early Cretaceous, ammonite-calibrated, $\delta^{13}C$ record from southeastern France and coeval changes in the platform record, we suggest that the history of carbon fractionation along the northern Tethyan margin was not only influenced by changes in the oceanic carbon cycle such as in the rate of production and preservation of organic and carbonate carbon, and in the size of the oceanic dissolved inorganic carbon (DIC) reservoir, but also by the above-mentioned changes in the ecology and geometry of the adjacent carbonate platform. Phases of photozoan carbonate production induced positive trends in the hemipelagic carbonate $\delta^{13}C$ record. Phases of heterozoan carbonate production pushed the $\delta^{13}C$ system towards more negative values. Platform drowning episodes implied an initial increase in $\delta^{13}C$ values, followed by longer-term decrease in $\delta^{13}C$ values.

D.5.1. Introduction

Shallow-water carbonate successions of Early Cretaceous age are widespread in the western Carpathians, the Alps, southeastern France, the Pyrenees, and the Betic Cordillera (*e.g.*, Garcia-Hernandez, 1979; Pascal, 1982; Arnaud-Vanneau and Arnaud, 1990; Masse, 1993; Funk *et al.*, 1993; Michalík, 1994; Föllmi *et al.*, 1994; Bernaus *et al.*, 2003). They embody the remains of an extensive shallow-water carbonate platform, which developed along the northern Tethyan margin along a distance of over 2500 km (*e.g.*, Golonka, 2004). The central European portion of the platform is presently locked up in the northern, Helvetic Alps, which extend from southeastern Germany and western Austria through Switzerland to eastern France (Fig. D.24). The structural architecture of the Helvetic nappe and thrust belt allows for the palinspastic reconstruction of proximal-distal transects across the former platform for distances surpassing

80 km (Fig. D.25), and the Early Cretaceous platform sediments preserved therein provide, therefore, excellent insight into the spatial and temporal evolution of this platform. Furthermore, the presence of ammonites in marker horizons within the Helvetic succession is the key to excellent time control.

Of special interest is the observation that the Helvetic platform succession does not only document the influence of regional environmental change such as relative sea-level fluctuations, variations in ambient sea-surface water temperature, and the type and intensity of detrital influx, but also the impact of global

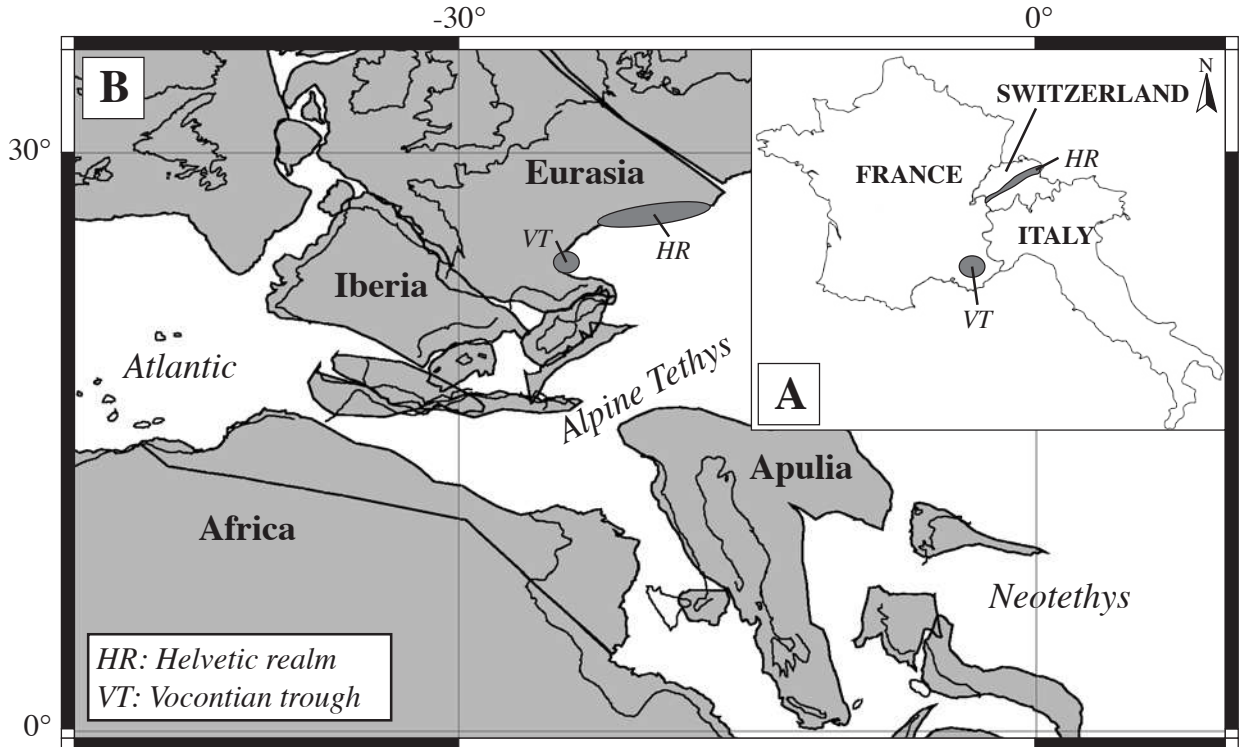

Figure D.24: **A**. *Geographic location of the studied areas.* **B**. *Paleogeographic map of the northern Tethyan margin during the Late Hauterivian – Early Barremian showing the position of the studied areas (modified from Bodin et al., 2006).*

paleoceanographic and paleoenvironmental change, such as modifications in the carbon and phosphorus cycles in association with global oceanic anoxic events (Föllmi *et al.*, 1994; Weissert *et al.*, 1998; Wissler *et al.*, 2003; van de Schootbrugge *et al.*, 2003; Bodin *et al.*, 2006a). One important indicator of the paleoceanographic influence on the evolution of this carbonate platform system is the near-coincidence in timing of the phases of platform demise with episodes of major paleoceanographic change during the Valanginian, Hauterivian, Aptian, and Albian (Schlanger and Jenkyns, 1976; Arthur and Schlanger, 1979; Jenkyns, 1980; Weissert *et al.*, 1979; Weissert, 1981; Schlager, 1981; Hallock and Schlager, 1986; Erbacher *et al.*, 2001; Leckie *et al.*, 2002; Höfling and Scott, 2002; Erba *et al.*, 2004).

The changes in carbonate-platform growth and the phases of platform demise in association with the global anoxic events had a probable, but poorly quantifiable influence on the marine carbon cycle and associated $\delta^{13}C$ record, in that carbonate-carbon burial may have generally been diminished in neritic domains, whereas organic-carbon burial may have been increased in general (*e.g.*, Weissert *et al.*, 1998; Weissert and Erba, 2004). Triggering mechanisms for these events proposed so far include modifications in the global output rate of primordial CO_2 by episodes of intense volcanic activity, and eventually by the increased release of methane (*e.g.*, Jenkyns, 2003; but compare also Heimhofer *et al.*, 2004).

With this contribution, we give an update on the temporal record of the northern Tethyan carbonate platform exposed in the Helvetic Alps and provide improved time control on the episodes of platform demise by ammonite biostratigraphy,

thereby using new data obtained from recently published and ongoing Ph.D. thesises (Kuhn, 1996; van de Schootbrugge, 2001; Linder *et al.*, submitted; Bodin *et al.*, 2006b, 2006c). We also present a new, high-resolution compilation of $\delta^{13}C$ records for the Early Cretaceous, which has been derived from hemipelagic sections invariably belonging to the Vocontian basin (southeastern France) and its immediate surroundings (Figs. D.24 and D.26). The here presented record is obtained from a single region, thereby precluding the potentially blurring effect related to the accumulation of records from different basins with different environmental and depositional

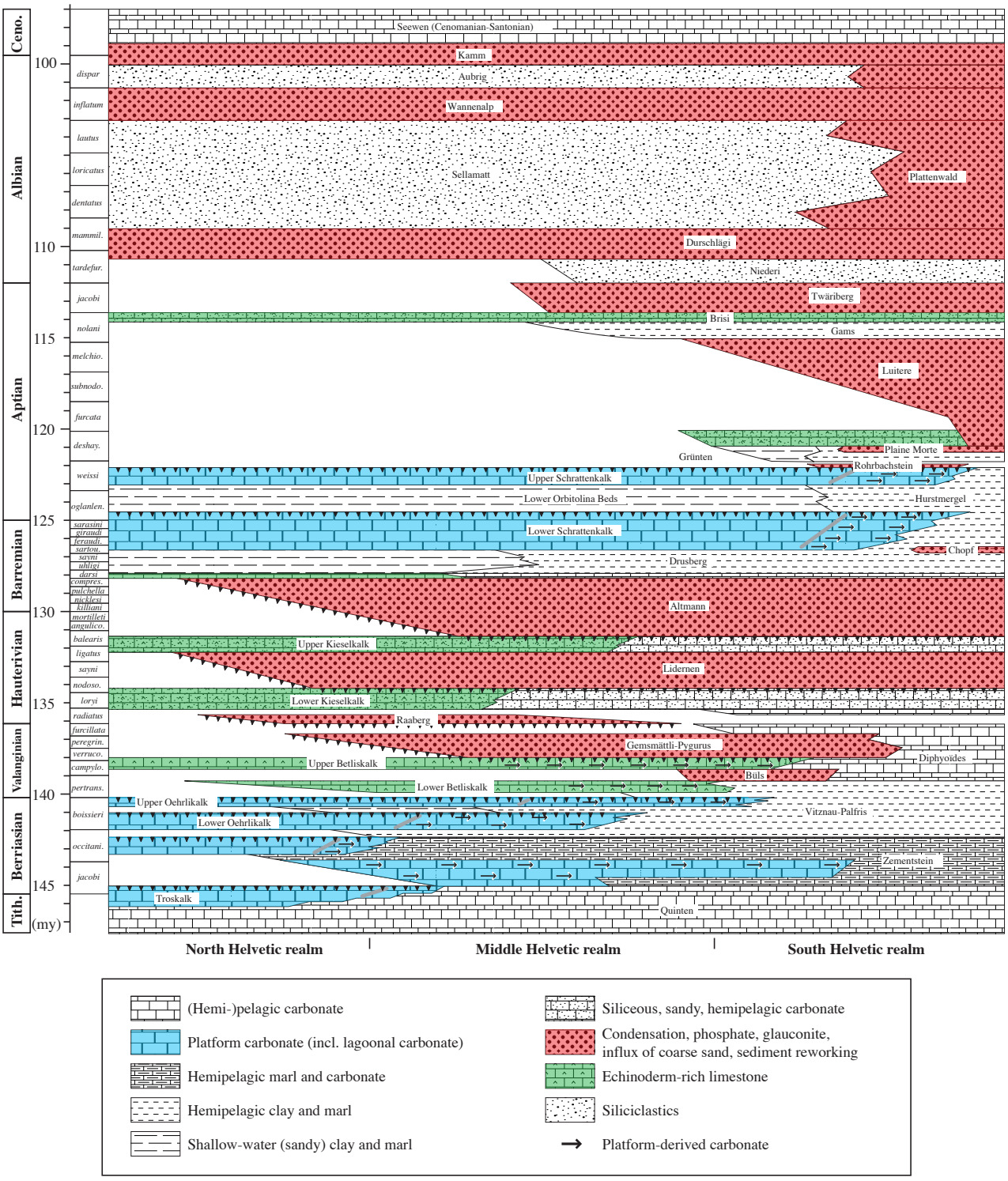

Figure D.25 Time-space diagram showing the temporal evolution of the distal portion of the northern Tethyan carbonate platform during the Early Cretaceous, based on occurrences in the Helvetic Alps of central and eastern Switzerland (modified from Föllmi et al., 1994). Time scale after Gradstein et al. (2004).

histories. Furthermore, it is derived from a marginal epicontinental basin indented into the northern Tethyan margin, bordered to the north, west, and south by the northern Tethyan carbonate platform (*e.g.*, Bréhéret, 1997). Its proximity to this platform is, for this reason, ideal for a study of the potential interactions between the northern Tethyan platform and the adjacent basin in terms of the carbon cycle. A further important advantage of this record is its calibration by ammonite biostratigraphy, which facilitates its correlation with the record from the Early Cretaceous northern Tethyan shelf environment.

We also propose a novel interpretation of the changes in the here presented $\delta^{13}C$ record, which we view not only as the consequence of ocean-wide changes in the ratio of C_{carb} to C_{org} burial flux rates, and changes in continental output of DIC and oceanic DIC reservoir size, but also as the result of changes in the ecology and geometry of the adjacent shallow-water carbonate platform. We thereby follow up on earlier publications, in which a close link between the Tethyan whole-rock $\delta^{13}C$ record and the evolution of the northern Tethyan carbonate platform was already suggested (Föllmi *et al.*, 1994; Weissert *et al.*, 1998; Godet *et al.*, 2006).

D.5.2. Methodology

The sediments of the Helvetic platform have been investigated by a combination of traditional fieldwork consisting of detailed logging and sampling of key sections, the analysis of sedimentological features and determination of biostratigraphically significant fossils (mostly ammonites), and different types of geochemical and mineralogical laboratory analyses (stable carbon and oxygen isotopes, organic matter contents, XRD, XRF, etc.). The data discussed here are extracted from a selection of publications which resulted from a long tradition of research in the Helvetic zone (*e.g.*, Heim, 1910-1916; Fichter, 1934), and are also based on the results of more recent and still ongoing research projects at the ETH Zürich, and the Universities of Berne, Geneva, and Neuchâtel.(*e.g.*, Mohr, 1992; Kuhn, 1996; van de Schootbrugge, 2001).

The here proposed compilation of stable carbon isotopes is based on earlier published work. All data were extracted from whole-rock samples of limestone beds within hemipelagic carbonate and carbonate-marl alternating sections (Emmanuel and Renard, 1993; Moullade *et al.*, 1998; Hennig *et al.*, 1999; van de Schootbrugge *et al.*, 2000; Herrle *et al.*, 2004; Godet *et al.*, 2006). A small series of stable carbon isotope measurements of Early Cretaceous calcite after aragonite were performed for this study at the geochemistry laboratory, University of Orsay-Paris Sud, by using a VG SIRA 10 triple collector instrument and the methods described by Godet *et al.* (2006). The presence of calcite was confirmed at our laboratory (GEA laboratory, University of Neuchâtel) by using a Scintag 2000 XRD device and the methods described by Adatte *et al.* (1996).

D.5.3. Evolution of the Early Cretaceous northern Tethyan carbonate platform succession in the Helvetic Alps

During the Early Cretaceous, the northern Tethyan carbonate platform witnessed a series of profound changes in its carbonate-producing platform ecology, which were superimposed by different episodes of platform demise. The external portion of this platform is well documented and dated by ammonite biostratigraphy in the Helvetic zone of the central European Alps (Wyssling, 1986; Föllmi, 1989b; Mohr, 1992; Kuhn, 1996; van de Schootbrugge, 2001; Bodin *et al.*, 2006b, 2006c), and its distal position determines it as an excellent recorder of the interactions between regional environmental and paleoceanographic change within the Tethyan basin.

Temporal changes in platform paleoecology were essentially between photozoan and heterozoan carbonate-producing communities (Lees and Buller, 1972, Carannante *et al.*, 1988; James, 1997; Mutti and Hallock, 2003). The preserved photozoan ecosystem includes hermatypic corals, rudists, chaetetids, stromatoporoids, and green algae, whereas the preserved heterozoan community is dominated by sessile crinoids, and includes bryozoans, bivalves, and brachiopods, in addition to variable amounts of siliceous sponge spicules.

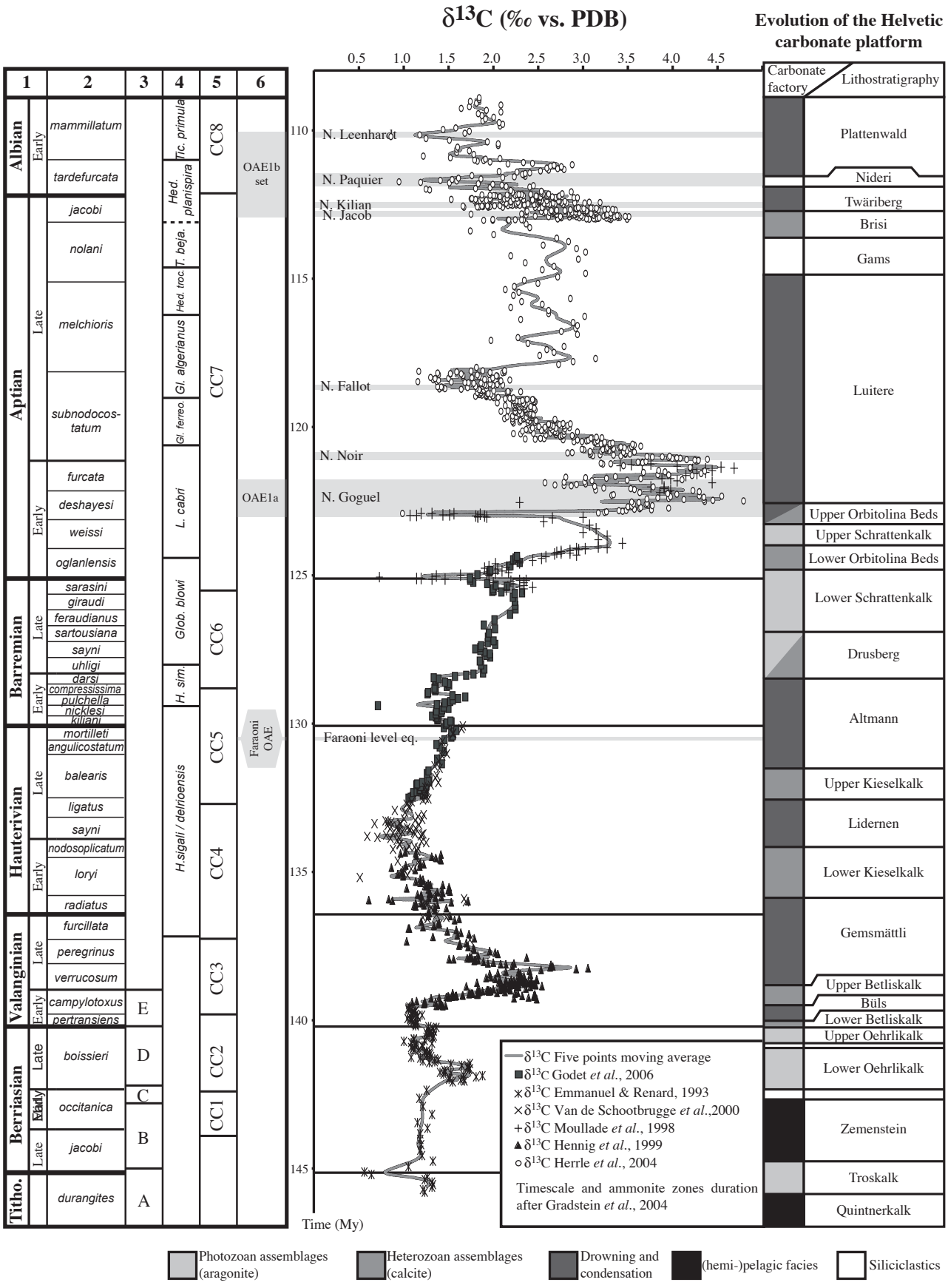

Figure D.26: Whole-rock carbonate $\delta^{13}C$ record from southeastern France. The general trends in the evolution of the northern Tethyan carbonate platform are from Figure D.25. On the left side of the figure, the numbers on the top of columns refer to **1:** *stages and sub-stages;* **2:** *ammonite zones;* **3:** *calpionellid zones;* **4:** *planktonic foraminifera zones;* **5:** *calcareous nannoplankton zones;* **6:** *Oceanic Anoxic Events (all according to Gradstein et al., 2004). Shown is also the timing of the occurrence of organic-rich layers resulting from oceanic anoxic events in the Vocontian basin (after Bréhéret, 1997; Herrle et al., 2004; Bodin et al., 2006).*

Phases of important photozoan carbonate production are discerned for the time periods between the latest Jurassic and the Berriasian-Valanginian boundary (Tros member, Oehrli Formation; Fig. D.25), and the Late Barremian and Early Aptian (*sartousiana* to *weissi* zone: the Urgonian Schrattenkalk Formation; Bodin *et al*., 2006b; Linder *et al*., submitted). These phases are associated with significant build-up and build-out of the platform by aggradation and progradation (indicated in blue in Fig. D.25).

Episodes of carbonate production and distribution by heterozoan communities are documented from the Valanginian (*pertransiens* to *verrucosum* zone: Betlis Formation; Fig. D.25), the Hauterivian (*radiatus* to *nodosoplicatum* zone: lower Kieselkalk member; *ligatus* to *balearis* zone: upper Kieselkalk member; Fig. D.25), and the Aptian (*deshayesi* zone: Grünten member; *nolani* zone: Brisi Beds; Fig. D.25). These phases of heterozoan platform production have led to the aggradation and progradation of large volumes of carbonate (indicated in green in Fig. D.25). Undecompacted accumulation rates are approximately 50% higher than for those in the photozoan mode (Föllmi *et al*., 1994).

The construction of the northern Tethyan carbonate platform was interrupted by a series of episodes of platform demise, which each lasted up to several million years (indicated in red in Fig. D.25). These episodes are registered by hiatuses and erosion surfaces in proximal parts of the Helvetic succession, and by the presence of centimeter to several meters thick glauconite- and phosphate-rich beds in distal parts, which are either highly condensed or allochthonous. These occurrences suggest that carbonate growth was highly reduced during these episodes and that the platform was subjected to important erosion instead (Heim 1910-1916, 1924, 1934; Heim and Seitz, 1934; Ganz, 1912; Fichter, 1934; Schaub, 1936, 1948; Haldimann, 1977; Föllmi. 1989a; Föllmi and Delamette, 1991; Föllmi *et al*., 1994; Kuhn, 1996; van de Schootbrugge, 2001).

Episodes of platform demise are observed and dated for the periods of the Early Valanginian to Early Hauterivian (*pertransiens* to *campylotoxus* zone zone: Büls Bed; *verrucosum* to *radiatus* zone: Gemsmättli-Pygurus and Raaberg Beds; Figs. D.25 and D.27 A-B), late Early to early Late Hauterivian (*nodosoplicatum* to *ligatus* zone: Lidernen Bed; Figs. D.25 and D.27 C), latest Hauterivian to latest Early Barremian (*balearis* to *darsi* zone: Altmann member; Figs. D.25 and D.27 D), middle Late Barremian (*sartousiana* zone: Chopf Bed; Fig. D.25), Early Aptian to middle Late Aptian (*deshayesi* zone to *melchioris* zone: Rohrbachstein, Plaine Morte, and Luitere Beds: Figs. D.25 and D.27 E-F), and latest Aptian to earliest Albian (*jacobi* to *tardefurcata* zones: Twäriberg Bed; Fig. D.25).

The episode of demise associated with the Twäriberg Bed corresponds to the final phase of platform demise in the history of the central European region of the northern Tethyan carbonate platform. Shallow-water carbonates younger than the Brisi Beds are not documented. Additional condensed phosphate- and glauconite-rich beds occur in sediments of Albian and Early Cenomanian age, which are greatly reduced in thickness and of siliciclastic and hemipelagic facies (Garschella Formation; Fig. D.25; Föllmi and Ouwehand, 1987). These episodes are dated as *tardefurcata* to *mammillatum* zone (Durschlägi Bed), *inflatum* zone (Wannenalp Bed), and *dispar* zone to middle Early Cenomanian (Kamm Bed) (Fig. D.25). In the distal part of the Helvetic succession, one single condensed phosphate bed occurs, which bundles these former beds and covers most of the Albian and partly also the Early Cenomanian (Plattenwald Bed; Fig. D.25).

D.5.4. An ammonite-calibrated $\delta^{13}C$ reference record from southeastern France

In order to compare the temporal changes in style and intensity of platform carbonate production on the northern Tethyan margin with general changes in the carbon cycle of the Tethyan ocean, we compiled a high-resolution $\delta^{13}C$ whole-rock record from hemipelagic successions which were deposited in or near the Vocontian basin. This basin represents a regional depression within the northern Tethyan margin during the Jurassic and Cretaceous, which was bordered by the northern Tethyan carbonate platform (Figs. D.24 and D.26; *e.g*., Bréhéret, 1997). The data for this

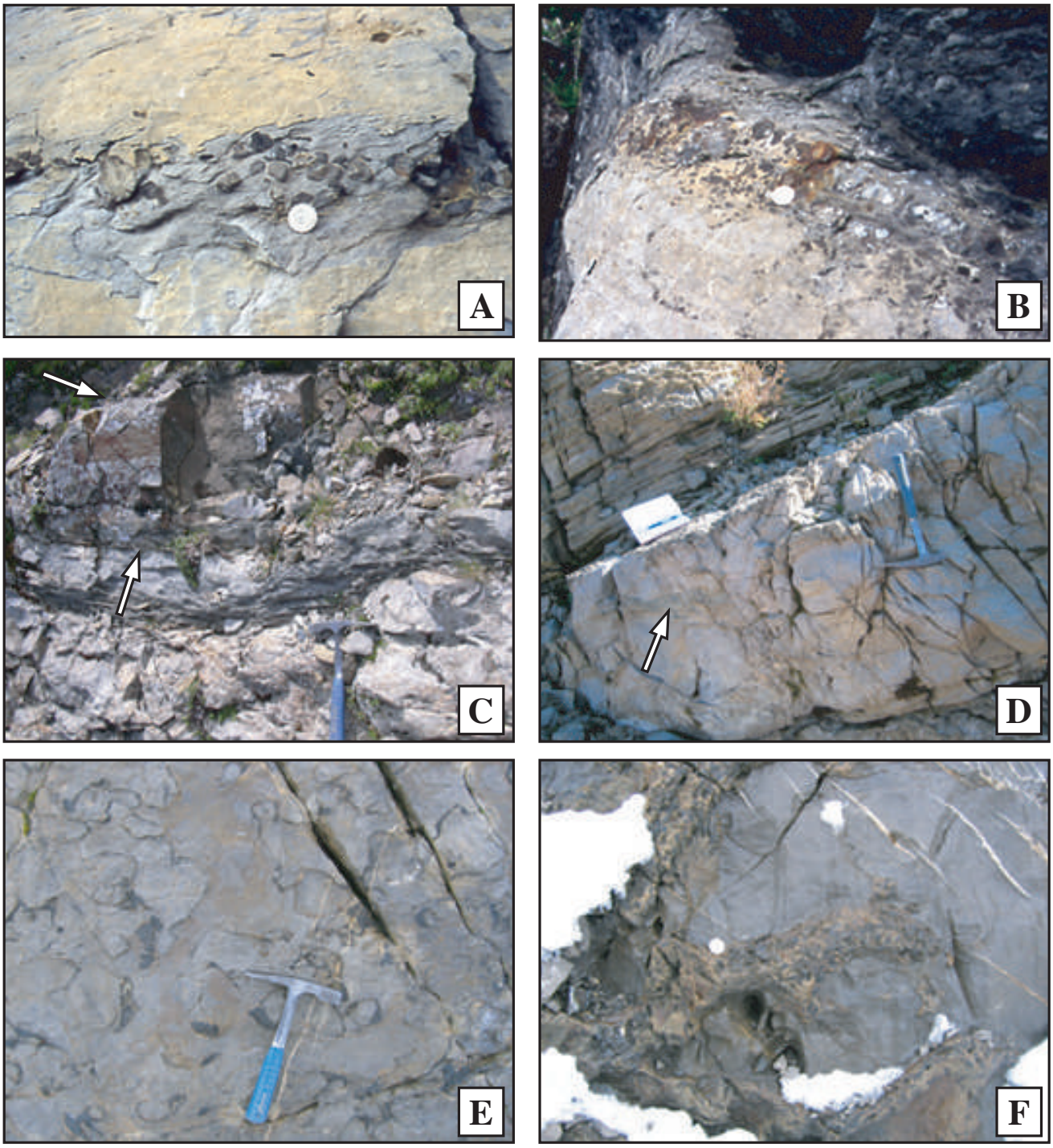

Figure D.27: Outcrop photos of phosphate- and glauconite rich beds which formed during the episodes of platform demise along the northern Tethyan margin: **A)** *Büls Bed (pertransiens zone; Early Valanginian; Kuhn, 1996): a thin and probably reworked phosphate nodular layer in hemipelagic limestone of the Palfris and Diphyoides Formations, Büls near Walenstadt, eastern Switzerland;* **B)** *Gemsmättli Bed (verrucosum to radiatus zone; late Early Valanginian to early Hauterivian): a nodular phosphatic bed intercalated in heterozoan platform carbonates of the upper Betlis Member and lower Kieselkalk Member, north of Lake Walen, eastern Switzerland;* **C)** *Lidernen Bed (nodosoplicatum to ligatus zone; late Early to early Late Hauterivian): here developed as a glauconite-rich bed (base and top indicated by arrows) following a marly interval on top of the lower Kieselkalk Member, Pilatus, central Switzerland;* **D)** *Altmann Bed (balearis to darsi zone; Late Hauterivian to late Early Barremian): a thin layer rich in nodular phosphate which reaches down into the underlying top of the upper Kieselkalk Member by bioturbation (arrow), Rawil, central Switzerland;* **E)** *Pleine Morte Bed (deshayesi zone; middle Early Aptian): shown here in plain view is the surface of this bed, which consists of nodules of heterozoan carbonate of the Grünten Member, which are peripherically phosphatized, Rawil, central Switzerland;* **F)** *Luitere Bed (furcata to melchioris zone; late Early to middle Late Aptian); a sandy and nodular phosphate rich bed on top of the Grünten Member, with extends locally down into the top layer of the heterozoan Grünten Member through burrow-like structures, Rawil, central Switzerland.*

compilation were obtained by our research group for the Hauterivian and Barremian intervals (van de Schootbrugge *et al.*, 2000; Godet *et al.*, 2006), and completed by published records for the Berriasian, Valanginian, and Aptian (Emmanuel and Renard, 1993; Moullade *et al.*, 1998; Hennig *et al.*, 1999; Herrle *et al.*, 2004; compare also Wissler *et al.*, 2002). A detailed description and interpretation of the short- and long-term trends in the here compiled northern Tethyan $\delta^{13}C$ records is provided in chapter D.5.5.6.

The $\delta^{18}O$ records show significant offsets in the absolute values and trends between different sections and we refrain, therefore, from a specific discussion of these data sets (cf. van de Schootbrugge *et al.*, 2000, for a discussion of this problem).

D.5.5. Discussion and interpretations

D.5.5.1. Correlation between episodes of platform demise and paleoceanographic change

We observe a fairly good correspondence in time between the phases of platform demise and general paleoceanographic change, such as is documented by the occurrence of the oceanic anoxic events (Fig. D.28). The oldest episode of platform demise started in the earliest Valanginian (*pertransiens* zone) and lasted until the earliest Hauterivian (*campylotoxus* to *radiatus* zone). The onset of this episode appears to predate the onset of the Valanginian «anoxic» event, which was defined to start at the onset of the Valanginian $\delta^{13}C$ positive excursion dated as *campylotoxus* zone (Erba *et al.*, 2004; Weissert and Erba, 2004). The phase of most intense phosphogenesis during

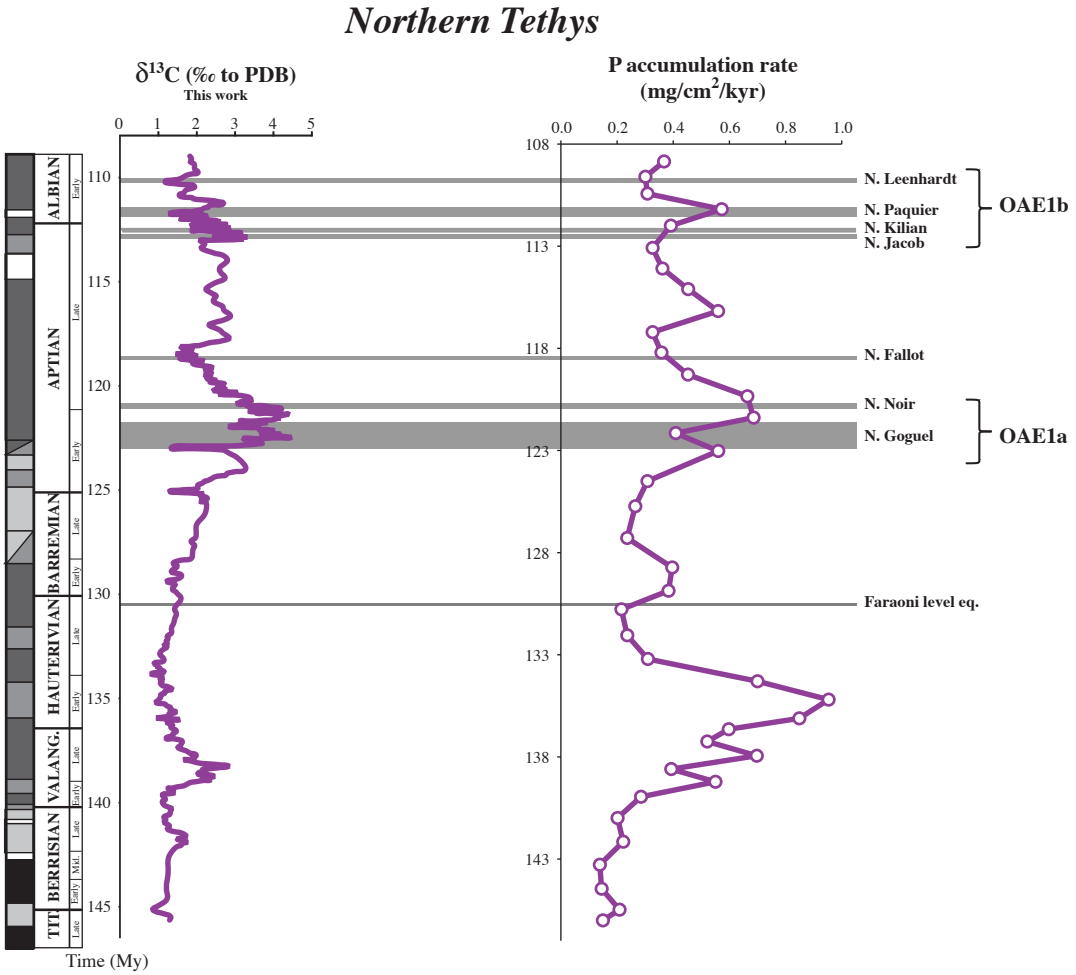

Figure D.28: Correlation plot of the general trends in the evolution of the northern Tethyan carbonate platform (from Figure D.25; see Figure D.26 for the legend), the northern Tethyan $\delta^{13}C$ record (from Figure D.26), and the phosphorus accumulation curve (after Föllmi, 1995; adapted to the timescale of Gradstein et al., 2004). Shown is also the occurrence of organic-rich layers resulting from oceanic anoxic events in the Vocontian basin (after Bréhéret, 1997; Herrle et al., 2004; Bodin et al., 2006).

this episode of demise took, however, place during the *verrucosum* zone (Kuhn, 1996), which corresponds exactly to the period of maximum $\delta^{13}C$ values during the Valanginian «anoxic» event.

A second episode of platform demise is dated as late Early to early Late Hauterivian (*nodosoplicatum* to *ligatus* zone), and this phase corresponds to a phase of important sea-level change and cold-water inflow into the northern Tethyan realm (*e.g.*, van de Schootbrugge *et al*. 2003). A truly anoxic event is, however, not documented from this time period.

The third phase of platform demise started in the latest Hauterivian and lasted until the late Early Barremian (*balearis* to *darsi* zone). Also here, the onset of the drowning phase appears to predate the Faraoni oceanic anoxic event, but a major phase of condensation, phosphogenesis and glauconite formation appears to coincide with this anoxic event (Bodin *et al.*, 2006c).

Also the onset of the fourth phase of drowning in the history of the northern Tethyan carbonate platform (*deshayesi* zone to *melchioris* zone) appears to slightly predate OAE1a, but this event itself is nicely documented by the presence of a phosphate horizon in distal occurrences of the Helvetic platform (Plaine Morte bed, Fig. D.25).

The final drowning episode near the Aptian-Albian boundary coincides with OAE 1b, and younger condensed phosphatic beds (*tardefurcata* to *mammillatum* zone, *inflatum* zone, and *dispar* zone to middle Early Cenomanian) all have their equivalent in oceanic anoxic events (OAE 1b upper part, OAE 1c and d; *e.g.*, Leckie *et al.*, 2002).

With the exception of the late Early to early Late Hauterivian phase of platform demise, all phases of erosion, condensation, phosphogenesis and platform demise appear to have their counterpart in a paleoceanographic anoxic event, and especially the early intervals in each episode appear to coincide with periods of widespread dysaerobic conditions. The time lag between the onset of platform demise and the start of Early Cretaceous OAE's was already observed earlier (Föllmi *et al.*, 1994) and it is interpreted here as a lag in the response times of both environments to environmental change: the highly sensitive ecological systems of the northern Tethyan platform appears to have responded rapidly to environmental change, whereas it may have taken up to 1 million year for the establishment of conditions in the deeper basins which allowed for the increased accumulation of organic matter.

D.5.5.2. Changes in trophic levels and changes in platform ecology and morphology

As was already outlined in Föllmi *et al.* (1994) and Weissert *et al.* (1998), we conceive changes in trophic levels as one of the important mechanisms driving the changes in style, architecture, and the efficiency of the northern Tethyan platform and linking the platform evolution with overall paleoceanographic change.

During the Valanginian and Aptian, phases of platform demise start in distal portions of the platform and proceed by onlap of drowning-related sedimentary bodies onto the platform (Fig. D.25). During the Valanginian, for example, a first pulse of platform demise is registered by the Büls Bed in the distal-most sections, and younger sediment bodies related to consequent drowning episodes expand onto the platform in the form of the Gemsmättli and the Raaberg Beds (Kuhn, 1996). These highly condensed phosphate-rich beds formed during periods of progressive sea-level rise as part of one or several transgressive system tracts covering major sequence boundaries. In most cases they bundle the effect of a series of successive transgressions into one single and highly condensed bed. The formation of these highly condensed and phosphate-rich beds is related to the influence of deeper-water currents, which arrived onto the platform during times of sea-level rise by upwelling, and which were powerful enough to induce a sedimentary regime dominated by erosion and condensation on top of the platform (Delamette, 1988; Ouwehand, 1988; Föllmi, 1989a; Föllmi and Delamette, 1991). These currents are thought to have consisted of cooler water, enriched in nutrients and especially phosphate, and eventually also dissolved CO_2. Their arrival on the platform pushed the platform into phases of carbonate production in a

heterozoan mode and into the episodes of platform demise. Finally, they arrived from an essentially eastern direction, obliquely onto the platform, whereas the transfer of platform material and water from the platform into the outer shelf and basin occurred in truly proximal-distal directions, approximately perpendicular to the platform, as is indicated in the orientation of channel structures and the direction of turbidites (Föllmi, 1989a; Föllmi and Delamette, 1991).

An independent confirmation of the importance of trophic levels is the overall good correlation between the record of oceanic phosphorus accumulation and the state of carbonate production on the shelf (Fig. D.28; Föllmi, 1995; van de Schootbrugge *et al.*, 2003; Bodin *et al.*, 2006a). A further indication of a link between platform evolution and trophic levels is the coincidence of major positive excursions in the northern Tethyan $\delta^{13}C$ record during the Early Valanginian and Early Aptian with periods in which the northern Tethyan carbonate platform shifted into a mixed heterozoan – demise mode (indicated by the green and red zones in Figs. D.25, D.26, and D.28). These phases of major change in the evolution of the northern Tethyan carbonate platform appear to be marked by major transformations in the ocean carbon cycle, which were highly likely induced by a nutrient-driven change in the ratio of carbonate carbon (Ccarb) to organic carbon (Corg) burial (see below; cf. also Immenhauser *et al.*, 2005).

D.5.5.3. Quality and correlation of the northern Tethyan $\delta^{13}C$ record

The here proposed compilation of the northern Tethyan $\delta^{13}C$ record show values typical of Early Cretaceous open-marine carbonates (*e.g.*, Jenkyns and Wilson, 1999; Erba *et al.*, 1999). The stratigraphic continuity of data derived from different sections is an indication of the general quality of the $\delta^{13}C$ signal; the only exception is a jump in absolute values at the base of the Late Aptian *melchioris* zone, which is likely induced by a change in diagenetic conditions between two sections (Herrle *et al.*, 2004; personal communication). Furthermore, the good correlation of the general trend between the here proposed $\delta^{13}C$ curve and other published curves is also an indication of its quality as a recorder of original paleoceanographic change rather than diagenetic overprint (Fig. D.29). The lack of correlation in a $\delta^{18}O$-$\delta^{13}C$ cross plot for all data ($R^2 = 0.0264$) appears to confirm this interpretation (Fig. D.30; *e.g.*, Godet *et al.*, 2006).

A comparison between the northern Tethyan $\delta^{13}C$ curve and the $\delta^{13}C$ records of the central Tethyan and the Pacific realms (*e.g.*, Weissert and Channell, 1989; Lini *et al.*, 1992; Adatte *et al.*, 1996; Erbacher *et al.*, 1996; Erba *et al.*, 1999; Jenkyns and Wilson, 1999; Bartolini, 2003) reveals that the long-term trend in the northern Tethyan record fits well with those in the other records, and that especially the two positive excursions during the Early Valanginian and Early Aptian are well reproduced (Fig. D.29). The evolution of the intervals between the major positive excursions is characterized by rather irregular and locally noisy trends, which are, in general, not very well correlated, neither between sections between different oceans nor within the same basin.

We suggest here that whereas the large positive excursions of the Early Valanginian and Early Aptian are well correlated between the Tethys and the Pacific realms and appear to be a truly global phenomenon, the smaller-scale excursions of the remaining intervals in the Early Cretaceous represent most likely a response to local to regional changes in the carbon cycle.

D.5.5.4. Potential mechanisms driving the marine $\delta^{13}C$ record

The (hemi-)pelagic $\delta^{13}C$ record provides an important tracer of reorganization within the marine carbon cycle (*e.g.*, Kump and Arthur, 1999; Veizer *et al.*, 1999), and temporal changes therein are traditionally interpreted as an approximation of changes in the ratio of burial fluxes of C_{carb} and C_{org} (*e.g.*, Scholle and Arthur, 1980; Arthur *et al.*, 1988; Weissert, 1989; Hoefs, 1997; Weissert *et al.*, 1998). Additional factors of important influence on the marine $\delta^{13}C$ record consist in the quality and flux of externally derived carbon species into the (hemi-)pelagic marine realm, such as terrestrial and platform-derived Corg and dissolved inorganic carbon (DIC), atmospheric

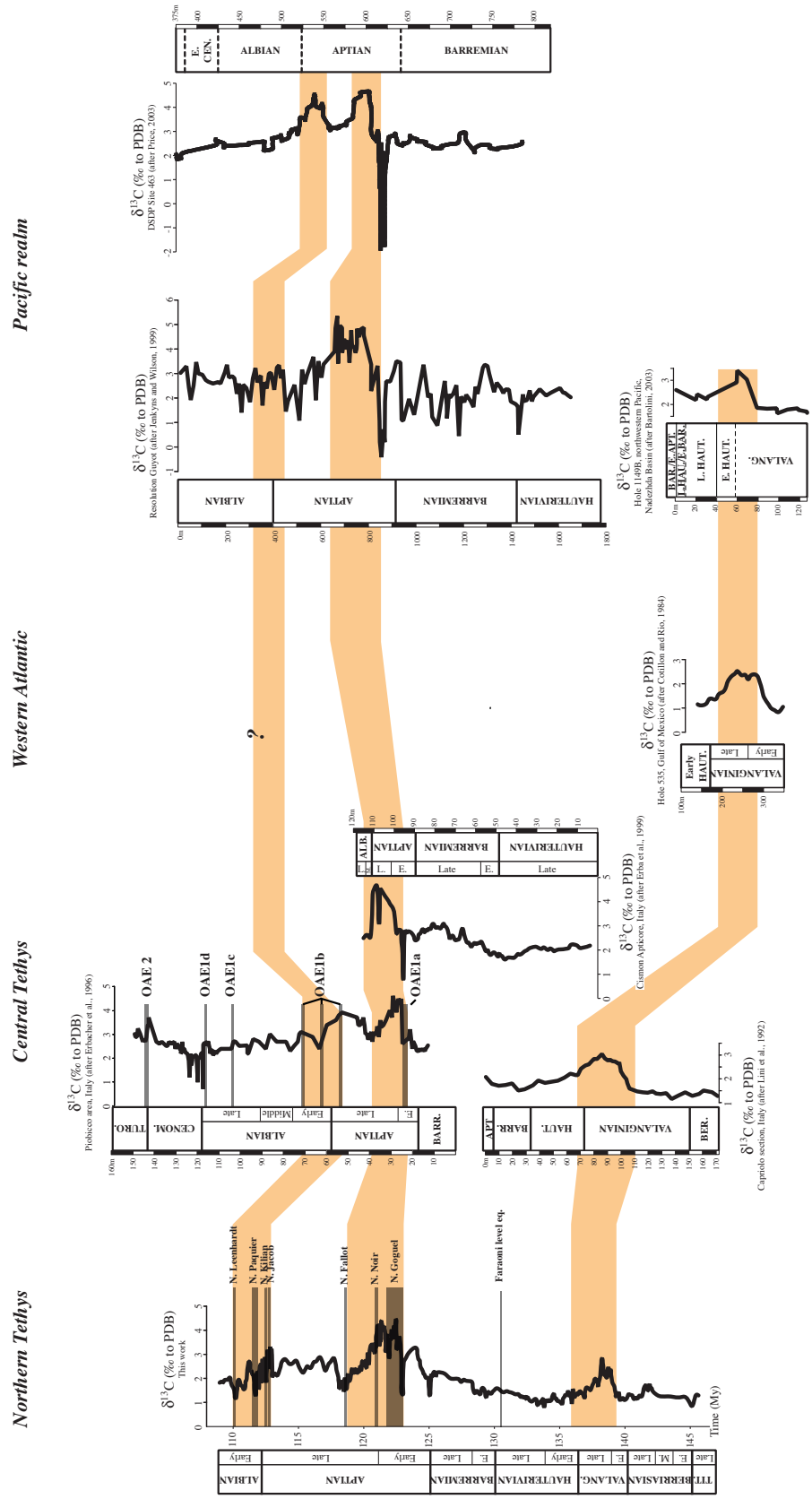

Figure D.29 Correlation of the northern Tethyan $\delta^{13}C$ record with $\delta^{13}C$ records from the central Tethys, the western Atlantic, and the Pacific realms (from Cotillon and Rio, 1984; Lini et al., 1992; Adatte et al., 1996; Erbacher et al., 1996; Erba et al., 1999; Jenkyns and Wilson, 1999; Bartolini, 2003; Price, 2003). Note that whereas the northern Tethyan $\delta^{13}C$ record is calibrated against Early Cretaceous time (Gradstein et al., 2004), the other records shown here are plotted against their lithostratigraphy. Note also that for the northern Tethyan $\delta^{13}C$ record, the central Tethyan record by Erba et al. (1999), and the Pacific record by Price et al. (2003) a five-point moving average is shown, whereas for the remaining records, all measured data are shown.

CO_2, or methane derived from the dissociation of clathrates (Cerlings *et al.*, 1993; Dickens *et al.*, 1995; Kump and Arthur, 1999; Immenhauser *et al.*, 2003; Weissert and Erba, 2004; Swart and Eberli, 2005; Panchuk *et al.*, 2005, 2006). Furthermore, Bartley and Kah (2004) recently suggested a close relationship between the size of the marine DIC reservoir and the sensitivity of the marine $\delta^{13}C$ system to changes in the carbon cycle.

As we will detail out in the following, a combination of these factors influenced the northern Tethyan Early Cretaceous $\delta^{13}C$ record, whereby the precise identification of the relative importance of each factor remains a difficult task. In our interpretation, we especially pay attention to the potential effect of the export of particulate and dissolved inorganic carbon (PIC and DIC) from the northern Tethyan carbonate platform and adjacent European continent, and changes therein, on the here described $\delta^{13}C$ record. We postulate that the smaller temporal shifts in the northern Tethyan $\delta^{13}C$ record, which are not correlated on a wider scale and for which a local or regional cause is to be sought, were influenced by this phenomenon.

There are several reasons for this assumption:

1) Based on a quantification of calcareous nannofossils in the hemipelagic carbonates of the Vocontian basin, Reboulet *et al.* (2003) were able to show that for the Valanginian sections, hemipelagic carbonate accumulation in this marginal basin was for a large part controlled by the export rate of platform-derived carbonate ooze, rather than by depositional rates of pelagic calcareous plankton (cf. also Colombié and Strasser, 2003, for a similar interpretation of Late Jurassic carbonate beds in Vocontian sections). The influence of shedding of shallow-water carbonate mud into the adjacent basin is also indicated by the important decrease in carbonate accumulation in the Vocontian basin during periods of platform demise, such as during the pertransiens and verrucosum zone (Valanginian; *e.g.*, Reboulet *et al.*, 2003), and the late Early to early Late Aptian (*e.g.*, Bréhéret, 1997).

2) As will be shown below, the timing and the negative or positive character of the shifts

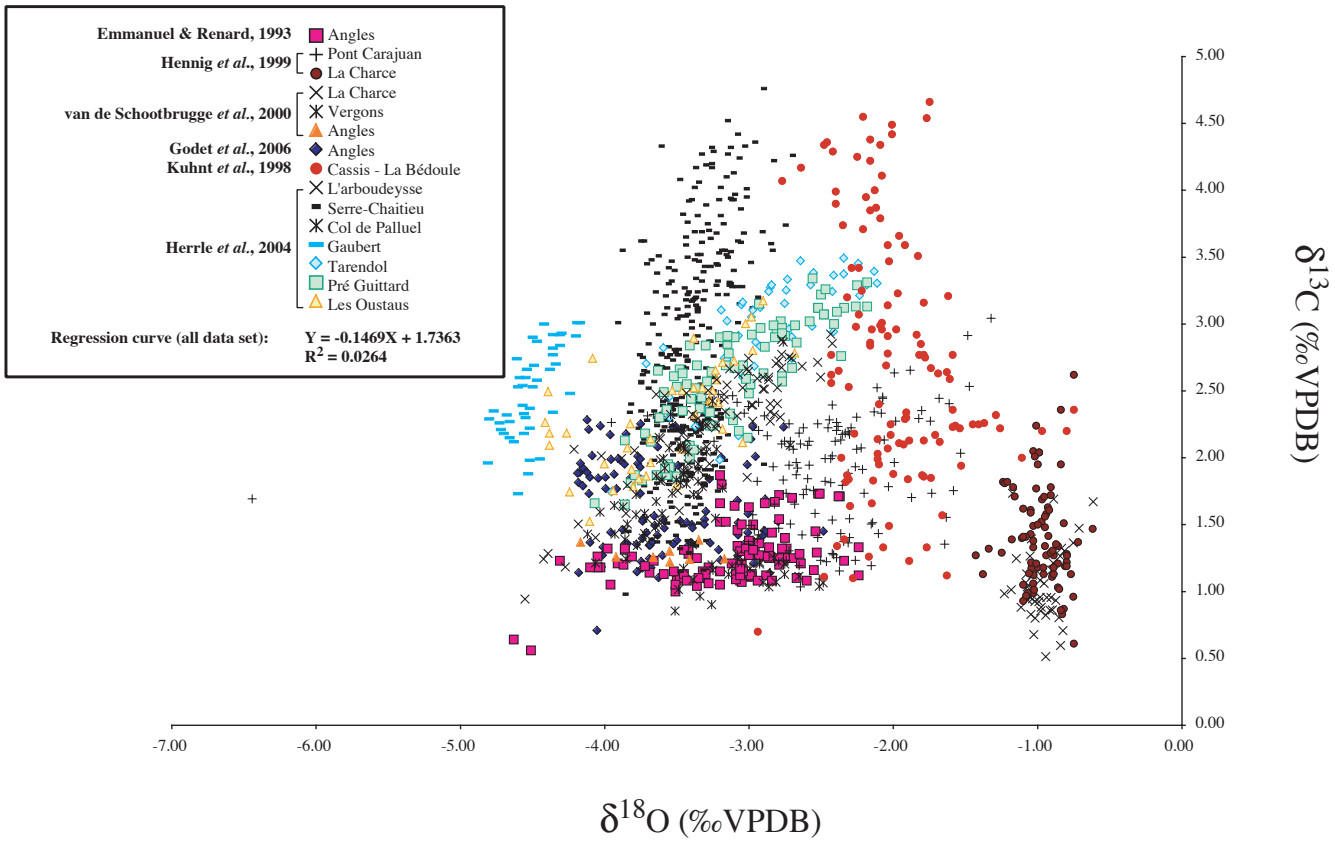

Figure D.30: $\delta^{13}C$-$\delta^{18}O$ cross plot of all data used in the $\delta^{13}C$ compilation of Figure D.26.

in the northern Tethyan $\delta^{13}C$ record appear to be correlated to changes in the style and intensity in carbonate production on the northern Tethyan platform.

3) A numerical model published by Godet *et al*. (2006) suggests that the export of platform-derived carbonate and especially aragonite may have an impact on the $\delta^{13}C$ record in adjacent basins

D.5.5.5. Changes in the ecology and geometry of the northern Tethyan carbonate platform and its influence on the northern Tethyan $\delta^{13}C$ record

There are several mechanisms related to the predominant ecosystem and geometry of the Early Cretaceous northern Tethyan carbonate platform, which may have influenced the hemipelagic $\delta^{13}C$ record described here (Fig. D.31). The northern Tethyan carbonate platform was constituted by photozoan and/or heterozoan ecosystems. The photozoan community included hermatypic corals, rudists, stromatoporoids, chaetitids, and green algae as its main constituents (*e.g*., Bollinger, 1988; Mohr, 1992; Föllmi *et al*., 1994). Of interest here is that these organisms precipitated their hard parts predominantly in aragonite (*e.g*., Morycowa, 1980; Wefer and Berger, 1991). This is also true for the Early Cretaceous rudists, which had relatively thick aragonite shells covered by a thin calcitic layer (Steuber, 2002). The participation of photosynthetic organisms in the form of green and zooxanthellic algae was important and the overall high photosynthetic rates in photozoan communities may have increased $\delta^{13}C$ values in skeletal aragonite. Fractionation towards more positive $\delta^{13}C$ values was likely also related to the geometry of the photozoan platform, which was confined by marginal reef build-ups and oolitic shoals (Linder *et al*., submitted; Godet *et al*., submitted), thereby promoting carbon recycling within the platform (*e.g*., Swart and Eberli, 2005; Panchuk *et al*., 2005, 2006). Furthermore, in single carbonate systems, aragonite $\delta^{13}C$ values tend generally to be higher than calcite $\delta^{13}C$ values (Romanek *et al*., 1992). For instance, Swart and Eberli (2005) reported $\delta^{13}C$ values of maximal +5‰ for aragonite on the present-day Bahamian platform. A preliminary isotopic survey of platform-derived skeletal material which consists of calcitized aragonite appears to confirm the high initial values for Early Cretaceous aragonite for samples from the Gargano platform (Italy; sample obtained from Jean-Pierre Masse: $\delta^{13}C$ value = +5‰) and the north Mexican and Texan carbonate platforms (Woo *et al*., 1993: $\delta^{13}C$ values between 2.3-4.3‰; n=24, mean value = +3.3‰).

The Early Cretaceous was characterized by broad epicontinental seas and widespread carbonate platforms (*e.g*., Philip, 2003) and aragonite production rates may have been significant in photozoan shallow-water communities in generally. The export of this mineral into adjacent basins during, for example, storm events and probably also more generally through the process of platform build-out by the formation of progradational carbonate wedges influenced the northern Tethyan $\delta^{13}C$ signal as a whole either by direct incorporation into pelagic sediments or by dissolution and transfer into the marine DIC reservoir (*e.g*., Droxler *et al*., 1983; Swart and Eberli, 2005; Godet *et al*., 2006). The potential influence of aragonite shedding on the $\delta^{13}C$ signature in carbonates of the Vocontian basin has been modeled by Godet *et al*. (2006). They were able to show that the presence of 20% aragonite in the total depositional rate of carbonate may increase the $\delta^{13}C$ signature by 0.2‰, in the case the initial value is at 2‰, and the initial aragonite $\delta^{13}C$ value is set at 5‰.

In analogy to modern tropical carbonate platforms (Kawahata *et al*., 1997; Suzuki *et al*., 2001; Suzuki and Kawahata, 2003, 2004), the confined geometry of photozoan platforms may also have had an effect on the air-sea exchange of CO_2. We assume that most CO_2 derived from respiration of organic matter, precipitation of carbonate, and river influx was directly returned to the atmosphere, rather than transported laterally into deeper waters. This means that photozoan platforms were a likely source of CO_2 to the atmosphere. This also signifies that a non-negligible part of continentally derived DIC was returned to the atmosphere as CO_2 or stored as platform carbonate, rather than transferred into the deep basin. All by all, the dominance of photozoan carbonate platforms may have pushed the oceanic $\delta^{13}C$ system towards more positive

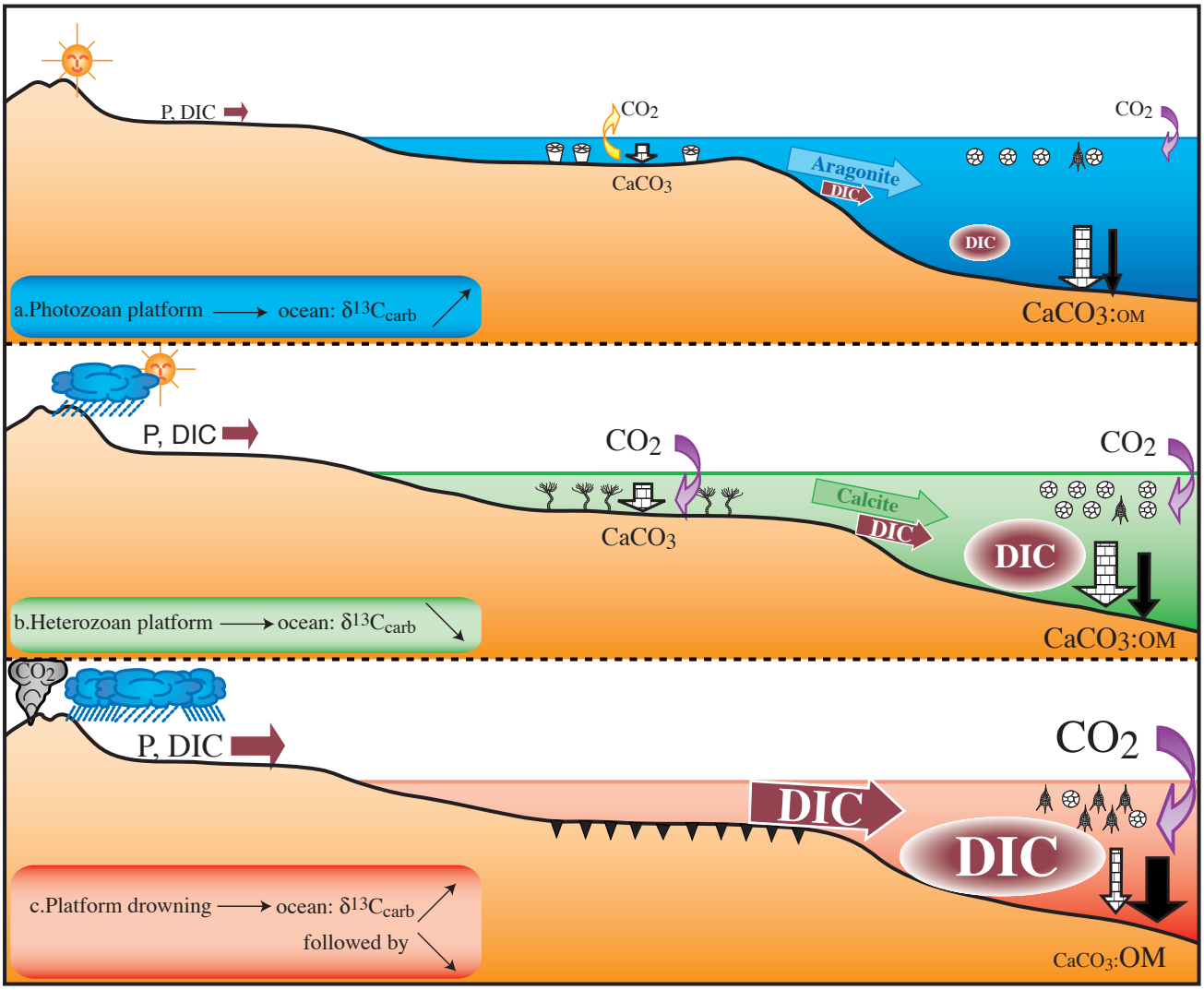

Figure D.31: Schematic overview of the potential impact of the different stages in the evolution of the northern Tethyan platform on the oceanic carbon cycle and $\delta^{13}C$ record. Differences in flux rates of DIC into the ocean and burial rates of C_{carb} and C_{org} are indicated by different sizes in arrows and characters.

values both by increased aragonite exportation and by decreased output of platform-derived DIC and throughput of continentally derived DIC (Fig. D.31). The possibility that the Early Cretaceous photozoan platform acted as a source of CO_2 to the atmosphere rather than a sink signifies also that this system was less vulnerable towards changes in atmospheric pCO_2 (cf. Wissler *et al.*, 2003; Weissert and Erba, 2004).

Early Cretaceous heterozoan ecosystems consisted predominantly of respiring organisms such as crinoids, thick shelly bivalves, brachiopods, and bryozoans, which precipitated their hard parts mainly in calcite (*e.g.*, Sprinkle and Kier, 1987; Smith *et al.*, 1998; Flügel, 2004). Early Cretaceous heterozoan platforms consisted of homoclinal or distally steepened ramps with good connections to the adjacent basin (*e.g.*, James, 1997; Linder *et al.*, submitted). Very few benthic photosynthetic organisms are preserved from the heterozoan assemblages and benthos-related photosynthetic processes may have been less important - at least in comparison to the photozoan carbonate platform. Due to the specific fractionation pattern of heterozoan organisms and the open-platform architecture, the overall $\delta^{13}C$ signal of precipitated calcite is less positive in comparison to that of aragonite in photozoan platforms (*e.g.*, Wefer and Berger, 1991; Swart and Eberli, 2005). In addition, the heterozoan mode of platform carbonate production along the Early Cretaceous northern Tethyan margin was associated with important detrital input, higher nutrient levels and eventually colder waters (Föllmi *et al.*, 1994). This implies that

phytoplankton productivity was important, thereby favoring the suspension-feeding mode exercised by an important part of the heterozoan community (crinoids, brachiopods, bryozoans). Since almost no organic matter is preserved in the heterozoan carbonate deposits, it is assumed that most of it was efficiently decomposed and reintegrated into the DIC pool, whereas ^{13}C-enriched C_{carb} was efficiently buried. This induced a decrease in the $\delta^{13}C$ signal of platform DIC and subsequently also of precipitated calcite (*e.g.*, Immenhauser *et al.*, 2003). To this comes that the import of terrestrially-derived DIC in association with high detrital flux rates may have reinforced the trend towards a more negative $\delta^{13}C$ signal on top of the heterozoan platform.

Heterozoan platforms may also have acted as a pump of atmospheric CO_2, which was consequently exported into adjacent basins, analogous to the present-day North Sea (Thomas *et al.*, 2004): the open, ramp-like architecture of heterozoan platforms probably allowed for a better vertical separation of photosynthetic (by planktonic organisms) and respiration processes (by benthic, carbonate-producing organisms) in its external, deeper part. This leads to a corresponding increase of respired CO_2 in subsurface waters, which was ultimately exported into the adjacent basin rather than transferred back to the atmosphere (Fig. D.31). The absence of aragonite and the increased export of both calcite as well as platform-derived and continentally-derived DIC likely influenced the marine $\delta^{13}C$ system and induced lower values in open-marine carbonates. The corresponding increase in the marine DIC reservoir may also have attenuated the sensitivity of the open-ocean $\delta^{13}C$ record (Bartley and Kah, 2004).

The repeated phases of platform demise during the Early Cretaceous occurred in close relation with oceanic anoxic events (Figs. D.26 and D.28). Such phases had an important impact on the $\delta^{13}C$ system, in that carbonate production and export were greatly diminished on shelves and also in open-marine systems through the competition with siliceous organisms, whereas C_{org} production and preservation were enhanced. This situation generates a general shift in the $\delta^{13}C$ record towards more positive values. The greatly reduced output of carbonates and the increased throughput of continentally derived DIC accompanied by an increase in re-mineralized C would automatically have led to an increase in the oceanic DIC reservoir. The environmental conditions leading to oceanic anoxia and platform drowning also induced an increase of this reservoir by increased humidity and weathering on the continent (*e.g.*, Föllmi *et al.*, 1994; Föllmi, 1995; Weissert *et al.*, 1998). The increase in size of the oceanic DIC reservoir may have also led to a more negative $\delta^{13}C$ signal by its increased recycling into the photic zone (*e.g.*, van de Schootbrugge *et al.*, 2005) and may have also attenuated short-term shifts in the signal (Bartley and Kah, 2004). Oceanic anoxic events and corresponding platform drowning episodes may therefore first have led to a rather rapid positive excursion in $\delta^{13}C$ followed by a longer term trend towards a more negative $\delta^{13}C$ record, which was less sensitive towards short-term change.

D.5.5.6. Correlation of changes in carbonate platform ecology along the northern Tethyan margin and trends in the northern Tethyan $\delta^{13}C$ record

A direct comparison of the evolution in the northern Tethyan $\delta^{13}C$ record with the changes in platform ecology along the northern Tethyan margin allows us to infer temporal correlations, which are consistent with the above described influences of platform carbonate production and morphology on basinal $\delta^{13}C$ records. In the Helvetic realm, the minimum in the northern Tethyan $\delta^{13}C$ record at the Jurassic-Cretaceous boundary corresponds to a halt in the growth of a photozoan platform (Tros Member) and the onset of the deposition of marly, hemi-pelagic sediments (Zementstein Formation). The negative excursion as such is interpreted as the result of diminished aragonite shedding and an increase in continental DIC input.

The two positive excursions in the early and late *boissieri* zone correspond to two phases of platform growth in a photozoan mode (lower and upper Oehrlikalk members), which were interrupted by a phase of detrital input (Mohr, 1992; Mohr and Funk, 1993). Here, an eventual increase in aragonite shedding and a concomittant decrease in DIC output from the platform may

have been influential.

During the Early Valanginian, the $\delta^{13}C$ record is first shifted to slightly more negative values and subsequently rapidly toward heavier values. A first maximum in $\delta^{13}C$ values corresponds to the early *verrucosum* zone. Thereafter, $\delta^{13}C$ values show a slight regression, before they culminate again in the late *verrucosum* zone. This trend corresponds to the well-known Valanginian positive excursion, which has been established in the Apulian basin and elsewhere (Lini *et al*., 1992; Föllmi *et al*., 1994; Hennig *et al*., 1999; Erba *et al*., 2004). A comparison with the Helvetic realm suggests that the slight negative shift at the base of the Valanginian correlates to a change from a photozoan to a heterozoan platform mode (lower Betlis member). The rapid shift toward heavier values during the Early Valanginian is coeval with a first platform drowning phase (Büls Beds). The following negative shift corresponds to a return of the platform in a heterozoan mode (upper Betlis member) and the second positive shift is the result of renewed platform drowning (Gemsmättli Bed).

For the remainder of the Late Valanginian and the entire Hauterivian, the $\delta^{13}C$ record is remarkably stable with regards to short-term changes and shows only a long-term change towards more negative values. This started in the *verrucosum* zone and lasted until the late *loryi* zone and was followed by a long-term increase towards more positive values ending at the Hauterivian-Barremian boundary (van de Schootbrugge *et al*., 2000). The drowning phases during the Hauterivian and near the Hauterivian-Barremian boundary are not obvious in the $\delta^{13}C$ record with the possible exception that an eventual increase in organic-carbon burial during the Late Hauterivian (culminating in the Faraoni anoxic event) may have pushed the $\delta^{13}C$ record slowly to more positive values. The relative stability of the Hauterivian-Early Barremian record is probably related to the increased size of the oceanic DIC reservoir, which induced the trend towards more negative values during the Late Valanginian and Early Hauterivian and attenuated the sensitivity of the $\delta^{13}C$ signal in general (Godet *et al*., 2006).

The Late Barremian is characterized by a positive shift in $\delta^{13}C$ values, which is correlated with the progressive installation of the photozoan Urgonian platform (Drusberg Member and lower Schrattenkalk Member; Godet *et al*., 2006; Bodin *et al*., 2006b). The Barremian-Aptian boundary is marked by a well-defined negative peak in the $\delta^{13}C$ record, which may - amongst others - be related to the increased output of continental detritus and DIC, leading to a corresponding increase in the oceanic DIC reservoir. The minimum of this negative excursion appears close to the onset of a widely documented interruption in photozoan platform growth along the northern Tethyan margin accompanied by an increase in detrital input («lower Orbitolina Beds»).

The Aptian shows a rather unsteady short-term evolution in $\delta^{13}C$, which starts off with an important positive shift during the *oglanlensis* zone. This shift is well correlated with a significant phase of photozoan carbonate production (upper Schrattenkalk member). This first maximum in $\delta^{13}C$ values during the Aptian is followed by a decrease, which becomes accelerated near the boundary between the *weissi* and *deshayesi* zones and forms a negative spike. This decrease in $\delta^{13}C$ values corresponds to a change to a heterozoan platform mode in the Helvetic zone (Grünten member; Linder *et al*., submitted), which is followed by the demise of the Urgonian Schrattenkalk platform (Luitere Bed). The negative spike occurs near the base of the Goguel level - an anoxic bed which corresponds to OAE 1a. It was first described by Menegatti *et al*. (1998) in the Apulian basin and has been interpreted to represent a short period of increased uptake of recycled ^{12}C–enriched carbon and/or increased release of methane (Menegatti *et al*., 1998; Jenkyns, 2003). The Early Aptian negative spike is followed by a positive excursion towards an Early Aptian twofold maximum in $\delta^{13}C$ values, which lasts until the top of the *furcata* zone. Subsequently, the $\delta^{13}C$ record slowly returns to more negative values, and arrives at a minimum near the top of the *subnodosocostatum* zone. This trend in $\delta^{13}C$ is paralleled on the Helvetic shelf by a long-lasting drowning episode, and is interpreted to have resulted from increased output of C_{org} relative to C_{carb} during OAE 1a, followed by an increase in the oceanic DIC reservoir, which was due to the prolonged diminution in platform

carbonate production paralleled by increased input of continental DIC.

The base of the minimum in the Late Aptian $\delta^{13}C$ record near the boundary of the *subnodosocostatum* and *melchioris* zones corresponds to a regional anoxic event (Fallot level; Herrle *et al*., 2004). The subsequent excursion towards more positive $\delta^{13}C$ values is probably artificial and related to different diagenetic conditions in the set of sections measured by Herrle *et al*. (2004, personal communication). A final phase of shallow-water carbonate production in a heterozoan mode (Brisi Beds) is documented from the *nolani* zone, and appears to trace an irregular trend towards more negative values in the $\delta^{13}C$ record. In the latest Aptian and earliest Albian, an ultimate drowning phase occurred on the Helvetic platform which is documented by the Twäriberg Bed. The positive shift in $\delta^{13}C$ values in sediments of the latest Aptian (*jacobi* zone) appears to register the final demise of the platform. On the Helvetic shelf, the Early Albian witnessed a phase of increased detrital input (Nideri beds), followed by a renewed phase of condensation (Plattenwald Bed), which - for its onset - correlates to OAE 1b represented in the Vocontian basin by the Paquier level (*e.g*., Herrle *et al*., 2004). The onset of OAE 1b is paralleled by an increase in $\delta^{13}C$ values of the Vocontian realm, which is followed by a renewed decrease in values.

The good temporal coincidence between changes in the northern Tethyan $\delta^{13}C$ record and changes in platform ecology and morphology opens the possibility to explain almost all minor and major changes in this curve. This was hitherto not possible in using changes in Tethyan paleoceanography as the exclusive driver of carbon isotope fractionation patterns.

D.5.6. Conclusions

The Helvetic zone preserves a distal portion of the Early Cretaceous northern Tethyan carbonate platform and its transition into the deeper outer shelf. The succession recovered in the Alps is not only the result of regional environmental conditions on the shelf, but also of global paleoceanographic conditions as is shown by the temporal correspondence between drowning episodes, OAE's, and the here presented Early Cretaceous $\delta^{13}C$ reference record of SE France. The link between paleoceanographic changes and coeval modulations in the style and architecture on the platform is provided by the upwelling of deeper and colder waters - rich in nutrients and likely in dissolved CO_2 - onto the platform.

Furthermore, virtually every change in the northern Tethyan $\delta^{13}C$ record makes sense, if correlated with the evolution of the northern Tethyan platform. This indicates that reciprocally, the northern Tethyan platform system exerted an influence on northern Tethyan ocean chemistry. We propose that this occurred by the production and storage of shallow-water carbonates, and by the existing platform geometry and intensity of photosynthetic activity which both were decisive for the degree of CO_2 return into the atmosphere and/or ocean, and the degree of output of platform-derived DIC and throughput of continental DIC. Furthermore, the changes within the platform ecosystem between photozoan, aragonite-based carbonate production mode and heterozoan, calcite-based carbonate production mode may have also played an important role in the oceanic carbon budget, especially if corresponding carbonates became exported into the adjacent basin. The high-resolution $\delta^{13}C$ record of SE France reflects both the complexity of such changes on the adjacent northern Tethyan platform, as well as coeval changes in paleoceanographic conditions, which episodically culminated in anoxic events, thereby engaging the northern Tethyan carbonate platform in mutual feedback.

D.5.7. Acknowledgements

We are grateful to Thierry Adatte, Bas van de Schootbrugge, Haydon Mort, Annie Arnaud-Vanneau, Hubert Arnaud, Thomas Steuber, Adrian Immenhauser, Helmut Weissert, Hanspeter Funk, Robert Skelton, and Jean-Pierre Masse for insightful discussions and advise. We also thank Jean-Pierre Masse and Elzbietta Morycowa for providing sample material, and Nicolas Fiet for analyzing this material for its stable carbon-isotope contents. We very much appreciated the insightful and highly constructive comments from

Karla Panchuk and an anonymous reviewer. We acknowledge the financial support of the Swiss National Fund for this project (projects 2100-067807/1 and 200020-105206/1).

D.5.8. References

Adatte, T., Stinnesbeck, W., and Keller, G. (1996). "Lithostratigraphic and mineralogic correlations of near K/T boundary sediments in northeastern Mexico: Implications for origin and nature of deposition". *In* Ryder, G., Fastovsky, D., and Gartner. S., *(Eds)*. The Cretaceous-Tertiary Event and Other Catastrophes in Earth History. Geol. Soc. Amer. Spec. Paper, **vol. 307,** GSA, Boulder, Colorado: 211-226.

Adatte, T., Stinnesbeck, W., Remane, J., and Hubberten, H.. (1996). "Paleoceanographic changes at the Jurassic-Cretaceous boundary in the western Tethys, northeastern Mexico." Cret. Research, **17:** 671-689.

Arnaud-Vanneau, A. and Arnaud, H. (1990). «Hauterivian to Lower Aptian carbonate shelf sedimentation and sequence stratigraphy in the Jura and northern Subalpine chains (southeastern France and Swiss Jura)». *In:* Tucker, M. E., Wilson, J. L., Crevello, P. D., Sarg, J. R. and Read, J. F., (*Eds*). Carbonate Platforms: Facies, Sequences and Evolution. Blackwell Scientific Publications, Special Publication of the International Association of Sedimentologists, **9**: 203-233.

Arthur, M. A., and Schlanger, S. O. (1979). ""Cretaceous «Oceanic Anoxic Events» as causal factors in development of reef-reservoired giant oil fields." Amer. Ass. Petrol. Geol. Bull., **63:** 870-885.

Arthur, M. A., Dean, W. E., and Pratt, L. M. (1988). "Geochemical and climatic effects of increased marine organic carbon burial at the Cenomanian/Turonian boundary." Nature, **335:** 714-717.

Bartley, J. K. and Kah, L. C. (2004). «Marine carbon reservoir, C_{org} - C_{carb} coupling, and the evolution of the Proterozoic carbon cycle.» Geology 32 (*2*): 129-132.

Bartolini, A. (2003). «Cretaceous Radiolarian Biochronology and Carbon Isotope Stratigraphy of ODP Site 1149 (Northwestern Pacific, Nadezhda Basin)». *In:* Luddern, J. N., Plank, T. and Escutia, C., (*Eds*). Proceedings of the Ocean Drilling Program, Scientific Results. **185**: 1-17.

Bernaus, J. M., Arnaud-Vanneau, A. and Caus, E. (2003). «Carbonate platform sequence stratigraphy in a rapidly subsiding area: the Late Barremian-Early Aptian of the Organya basin, Spanish Pyrenees.» Sedimentary Geology **159** (*3-4*): 177-201.

Bodin, S., Godet, A., Vermeulen, J., Arnaud, H., Strasser, A., Fiet, N., Adatte, T. and Föllmi, K. B. (2006a). «The late Hauterivian Faraoni oceanic anoxic event in the western Tethys: Evidence from phosphorus burial rates.» Palaeogeography, Palaeoclimatology, Palaeoecology **235**: 245-264.

Bodin, S., Vermeulen, J., Godet, A. and Föllmi, K. B. (2006b). «New data on the age of the installation of Urgonian-type carbonates along the northern Tethyan margin: biostratigraphy of the Chopf Member (Helvetic Alps, eastern Switzerland).» Comptes Rendus Géosciences **338**: 727-733.

Bodin, S., Godet, A., Vermeulen, J., Linder, P. and Föllmi, K. B. (2006c). «Biostratigraphy, sedimentology and sequence stratigraphy of the latest Hauterivian - early Barremian drowning episode of the Northern Tethyan margin (Altmann Member, Helvetic Nappes, Switzerland).» Eclogae Geologicae Helveticae, in press.

Bollinger, D. (1988). "Die Entwicklung des distalen osthelvetischen Schelfs im Barremian und Früh-Aptian." *Ph.D. thesis,* ETH Zürich, Zürich, Switzerland.

Bréhéret, J.-G. (1997). «L'Aptien et l'Albien de la Fosse vocontienne (des bordures au bassin). Evolution de la sédimentation et enseignements sur les événements anoxiques.» Société géologique du Nord **25**: 1-164.

Carannante, G., Esteban, M., Milliman, J. D. and Simone, L. (1998). «Carbonate lithofacies as paleolatitude indicators: problems and limitations». *In:* Nelson, C. S., (*Ed.*). Non-Tropical Shelf Carbonates - Modern and Ancient. Sedimentary Geology, **60**: 333-346.

Cerlings, T. E., Wang, Y. and Quade, J. (1993). «Expansion of C4 ecosystems as an indicator of global ecological change in the late Miocene.» Nature **361**: 344-345.

Colombié, C. and Strasser, A. (2003). «Depositiona sequences in the Kimmeridgian of the vocontian Basin (France) controlled by carbonate export from shallow-water platforms.» Geobios **36**: 675-683.

Cotillon, P. and Rio, M. (1984). «6. Cyclic sedimentation in the Cretaceous of Deep Sea Drilling Project Sites 535 and 540 (Gulf of Mexico), 534 (central Atlantic), and in the Vocontian Basin (France)». *In:* Buffler, R. T., Schlager, W. and *et al.*, (*Eds*). Initial Reports of the Deep Sea Drilling Project. Washington, **Vol. 77**: 339-376.

Delamette, M. (1988). "L'Evolution du domaine helvétique (entre Bauges et Morcles) de l'Aptien supérieur au Turonien: séries condensées, phosphorites, et circulations océaniques, Publ. Dep. Géol. Paléont., Univ. Genève, **5:** 1-316.

Dickens, G. R., O'Neil, J. R., Rea, D. K. and Oven, R. M. (1995). «Dissociation of oceanic methane hydrate as a cause of the carbon isotope excursion at the end of the Paleocene.» Paleoceanography **10** (*6*): 965-971.

Droxler, A. W., Schlager, W. and Whallon, C. C. (1983). «Quaternary aragonite cycles and oxygen isotope record in Bahamian carbonate ooze.» Geology **11**: 235-239.

Emmanuel, L. and Renard, M. (1993). «Carbonate geochemistry (Mn, $\delta^{13}C$, $\delta^{18}O$) of the late Tithonian - Berriasian pelagic limestones of the Vocontian trough (SE France).» Bulletin des Centres de Recherche Exploration-Production Elf-Aquitaine **17** (*1*): 205-221.

Erba, E., Bartolini, A. and Larson, R. L. (2004). «Valanginian Weissert oceanic anoxic event.» Geology **32** (*2*): 149-152.

Erba, E., Channell, J. E. T., Claps, M., Jones, C. E., Larson, R. L., Opdyke, B., Premoli-Silva, I., Riva, A., Salvini, G. and Torriceli, S. (1999). «Integrated stratigraphy of the Cismon APTICORE (Southern Alps, Italy): A «reference section» for the Barremian-Aptian interval at low latitudes.» Journal of Foraminiferal Research **29** (*4*): 371-391.

Erbacher, J., Thurow, J. and Littke, R. (1996). «Evolution patterns of radiolaria and organic matter variations: A new approach to identify sea-level changes in mid-Cretaceous pelagic environments.» Geology **24** (*6*): 499-502.

Erbacher, J., Huber, B. T., Norris, R. D. and Markey, M. (2001). «Increased thermohaline stratification as a possible cause for an ocean anoxic event in the Cretaceous period.» Nature **409** (*18 January 2001*): 325-327.

Fichter, H. J. (1934). "Geologie der Bauen-Brisen-Kette." Beitr. Geol. Karte Schweiz, Neue Folge, **69:** 1-128.

Flügel, E. (2004). "Microfacies of Carbonate Rocks." Springer-Verlag, Berlin, 976 pp.

Föllmi, K. B. (1989a). "Evolution of the Mid-Cretaceous triad." Lecture Notes Earth Sci., **23**: 1-153.

Föllmi, K. B. (1989b). "Beschreibung neugefundener Ammonoidea aus der Vorarlberger Garschella-Formation (Aptian-Albian)." Jahrb. Geol. Bundesanstalt, **132:** 105-189.

Föllmi, K. B. (1995). "160 m.y. record of marine sedimentary phosphorus burial: Coupling of climate and continental weathering under greenhouse and icehouse conditions." Geology, **23**: 859-862.

Föllmi, K. B., and M. Delamette (1991). "Comment on: Model simulation of mid-Cretaceous ocean circulation." Science, **251**: 94.

Föllmi, K. B., and Ouwehand, P. J. (1987). "Garschella-Formation und Götzis-Schichten (Aptian-Coniacian): Neue stratigraphische Daten aus dem Helvetikum der Ostschweiz und des Vorarlbergs." Eclog. geol. Helv., **80**: 141-191.

Föllmi, K. B., Weissert, H., Bisping, M. and Funk, H. (1994). «Phosphogenesis, carbon-isotope stratigraphy, and carbonate-platform evolution along the Lower Cretaceous northern Tethyan margin.» Geological Society of America Bulletin **106** (*II*): 729-746.

Funk, H., Föllmi, K. B. and Mohr, H. (1993). «Evolution of the Tithonian-Aptian carbonate platform along the northern Tethyan margin, eastern Helvetic Alps.» *In:* Simo, J. A. T., Scott, R. W. and Masse, J. P., (*Eds*). Cretaceous carbonates platforms. Tulsa, OK, United States., **AAPG (American Association of Petroleum Geologists) Memoir 56**: 387-407.

Ganz, E. (1912). "Stratigraphie der mittleren Kreide (Gargasien, Albien) der

oberen helvetischen Decken in den nördlichen Schweizeralpen." Denkschr. Schweiz. Naturf. Ges., **42/1**: 1-148.

Garcia-Hernandez, M. (1979). "Les faciès urgoniens pendant la sédimentation barrémo-albienne dans les Sierras de Cazorla et du Segura (zone prébétique, S-E de l'Espagne)." Mém. Spéc. Géobios, **3**: 57-69.

Godet, A., Bodin, S., Föllmi, K. B., Vermeulen, J., Gardin, S., Fiet, N., Adatte, T., Berner, Z., Stüben, D. and van de Schootbrugge, B. (2006). «Evolution of the marine stable carbone-isotope record during the early Cretaceous: A focus on the late Hauterivian and Barremian in the Tethyan realm.» Earth and Planetary Science Letters **242** (*3-4 doi:10.1016/j.epsl.2005.12.011*): 254-271.

Godet, A., Bodin, S., Adatte, T. and Föllmi, K. B (submitted). «Platform-induced clay-mineral fractionation along a northern Tethyan basin-platform transect: implications for the interpretation of Early Cretaceous climate change (Late Hauterivian-Early Aptian).» Cretaceous Research.

Golonka, J. (2004). "Plate tectonic evolution of the southern margin of Eurasia in the Mesozoic and Cenozoic." Tectonophysics, **381**: 235-273.

Gradstein, F. M., Ogg, J. G. and Smith, A. M. (2004). «A Geological Time Scale 2004», Cambridge University Press, 600 pp.

Haldimann, P. (1977). "Sedimentologische Entwicklung der Schichten an einer Zyklengrenze der helvetischen Unterkreide." Mitt. Geol. Inst. ETH Univ. Zürich, Neue Folge, **219:** 1-183.

Hallock, P. and Schlager, W. (1986). "Nutrient excess and the demise of coral reefs and carbonate platforms." Palaios, **1:** 389-398.

Heim, A. (1910-1916). "Monographe der Churfirsten-Mattstock-Gruppe." Beitr. Geol. Karte Schweiz, Neue Folge, **20**/*1-3*: 573 p.

Heim, A. (1924). "Über submarine Denudation und chemische Sedimente." Geol. Rundschau, **15**: 1-47.

Heim, A. (1934). "Stratigraphische Kondensation." Eclog. geol. Helv., **27**: 372-383.

Heim, A., and Seitz, O. (1934). "Die mittlere Kreide in den helvetischen Alpen von Rheintal und Vorarlberg und das Problem der Kondensation." Denkschr. Schweiz. Naturf. Ges., **69**/*2*: 185-310.

Heimhofer, U., Hochuli, P. A., Herrle, J. O., Andersen, N. and H. Weissert (2004). "Absence of major vegetation and palaeoatmospheric pCO_2 changes associated with oceanic anoxic event 1a (early Aptian, SE France)." Earth Planet. Sci. Letters, **223**: 303-318.

Hennig, S., Weissert, H. and Bulot, L. (1999). «C-isotope stratigraphy, a calibration tool between ammonite- and magnetostratigraphy.» Geologica Carpathica **50**: 91-96.

Herrle, J. O., Kößler, P., Friedrich, O., Erlenkeuser, H. and Hemleben, C. (2004). «High-resolution carbon isotope records of the Aptian to Lower Albian from SE France and the Mazagan Plateau (DSDP Site 545): a stratigraphic tool for paleoceanographic and paleobiologic reconstruction.» Earth and Planetary Science Letters **218** (*1-2*): 149-161.

Hoefs, J. (1997). "Stable Isotope Geochemistry." Springer-Verlag, Berlin: 201 pp.

Höfling, R., and Scott, R. W. (2002). "Early and mid-Cretaceous build-ups." *In* Kiessling, W., Flügel, E. and Golonka J., (*Eds*.) "Phanerozoic Reef Patterns." SEPM (Soc. Sedim. Geol.) **Spec. Publ. 72**: 521-548.

Immenhauser, A., Della Porta, G., Kenter, J. A. M. and Bahamonde, J. R. (2003). «An alternative model for positive shifts in shallow-marine carbonate $\delta^{13}C$ and $\delta^{18}O$.» Sedimentology **50**: 953-959.

Immenhauser, A., Hillgärtner, H. and van Bentum, E. (2005). "Microbial-foraminiferal episodes in the early Aptian of the southern Tethyan margin: ecological significance and possible relation to oceanic anoxic event 1a." Sedimentology, **52**: 77-99.

James, N. P. (1997). «The cool-water carbonate depositional realm». *In:* James, N. P. and Clarke, J. A. D., (*Eds*). Cool-water carbonates. Tulsa, Oklahoma, Society for Sedimentary Geology, **SEPM Special Publication N° 56**: 1-20.

Jenkyns, H. C. (1980). «Cretaceous anoxic events: from continents to oceans.» Journal of the Geological Society, London **137**: 171-188.

Jenkyns, H. C. (2003). «Evidence for rapid climate change in the Mesozoic-Paleogene greenhouse world.» Philosophical Transactions of

the Royal Society of London **361**: 1885-1916.

Jenkyns, H. C. and Wilson, P. A. (1999). «Stratigraphy, paleoceanography, and evolution of Cretaceous pacific guyots: relics from a greenhouse Earth.» American Journal of Science **299**: 341-392.

Kawahata, H., Suzuki, A. and Goto, K. (1997). "Coral reef ecosystems as a source of atmospheric CO_2: evidence from pCO_2 measurements of surface waters." Coral Reefs, **16**: 261-266.

Kuhn, O. (1996). "Der Einfluss von Verwitterung auf die Paläozeanographie zu Beginn des Kreide-Treibhausklimas (Valanginian und Hauterivian) in der West-Tethys." *Ph.D. thesis,* ETH Zürich, Zürich, Switzerland.

Kump, L. R. and Arthur, M. A. (1999). «Interpreting carbon-isotope excursions: carbonates and organic matter.» Chemical Geology **161** (*1-3*): 181-198.

Leckie, M. R., Bralower, T. J. and Cashman, R. (2002). «Oceanic anoxic events and plankton evolution: Biotic response to tectonic forcing during the mid-Cretaceous.» Paleoceanography **17** (*3*):10.1029/2001pa000623.

Lees, A. and Buller, A. T. (1972). «Modern temperate-water and warm-water shelf carbonate sediments contrasted.» Marine Geology **13** (*5*): M67-M73.

Linder, P., Gigandet, J., Hüsser, J. L., Gainon, F. and Föllmi, K. B. (submitted). "The early Aptian Grünten member." Eclog. geol. Helv.

Lini, A., Weissert, H. and Erba, E. (1992). «The Valanginian carbon isotope event: a first episode of greenhouse climate conditions during the Cretaceous.» Terra Nova **4** (*Global Change Spec. Issue (ed. by F.-C. Wezel)*): 374-384.

Masse, J.-P. (1993). «Valanginian-Early Aptian Carbonate Platforms from Provence, Southeastern France». *In:* Simo, J. A. T., Scott, R. W. and Masse, J.-P., (*Eds*). Cretaceous Carbonate Platforms. Tulsa, Oklahoma, U.S.A., American Association of Petroleum Geologists, **Memoir 56**: 363-375.

Menegatti, A. P., Weissert, H., Brown, R. S., Tyson, R. V., Farrimond, P., Strasser, A. and Caron, M. (1998). «High-resolution $\delta^{13}C$ stratigraphy through the early Aptian «Livello Selli» of the Alpine Tethys.» Paleoceanography **13** (*5*): 530-545.

Michalík, J. (1994). "Lower Cretaceous carbonate platform facies, western Carpathians." Palaeogeogr., Palaeoclimatol., Palaeoecol., **111**: 263-277.

Mohr, H. (1992). "Der helvetische Schelf der Ostschweiz am Übergang vom späten Jura zur frühen Kreide." *Ph.D. thesis*, ETH Zürich, Zürich, Switzerland.

Mohr, H. and Funk, H. (1995). "Die Entwicklung der helvetischen Karbonatplattform in der Ostschweiz (Tithonian-Berriasian): eine sequenzstratigraphische Annäherung." Eclog. geol. Helv., **88**: 281-320.

Moullade, M., Kuhnt, W., Bergen, J. A., Masse, J.-P. and Tronchetti, G. (1998). «Correlation of biostratigraphic and stable isotope events in the Aptian historical stratotype of La Bedoule (southeast France).» Comptes Rendus de l'Academie des Sciences - Series IIA - Earth and Planetary Science **327** (*10*): 693-698.

Mutti, M. and Hallock, P. (2003). «Carbonate systems along nutrient and temperature gradients: some sedimentological and geochemical constraints.» Int. J. Earth Sci. (Geol. Rundsch.) **92**: 465-475.

Ouwehand, P. J. (1987). "Die Garschella-Formation («Helvetischer Gault», Aptian-Cenomanian) der Churfirsten-Alvier Region (Ostschweiz)." Mitt. Geol. Inst. ETH Univ. Zürich, Neue Folge, **275**: 1-296.

Panchuk, K. M., Holmden, C. and Kump, L. R. (2005). «Sensitivity of the epeiric sea carbon isotope record to local-scale carbon cycle processes: Tales from the Mohawkian Sea.» Palaeogeography, Palaeoclimatology, Palaeoecology **228**: 320-337.

Panchuk, K. M., Holmden, C. E. and Leslie, S. A. (2006). "Local controls on carbon cycling in the Ordovician midcontinent region of North America, with implications for carbon isotope secular curves." Journ. Sedim. Res., **76**: 200-211.

Pascal, A. (1982). "Evolution des systèmes biosédimentaires urgoniens en Espagne du Nord." N. Jb. geol. Paläont. Abh., **165**/*1*: 77-86.

Philip, J. (2003). «Peri-Tethyan neritic carbonate areas: distribution through time and driving factors.» Palaeogeography,

Palaeoclimatology, Palaeoecology **196** (*1-2*): 19-37.

Price, G. D. (2003). «New constraints upon isotope variations during the early Cretaceous (Barremian-Cenomanian) from the Pacific Ocean.» Geol. Mag. **140** (*5*): 513-522.

Reboulet, S., Mattioli, E., Pittet, B., Baudin, F., Olivero, D. and Proux, O. (2003). «Ammonoid and nannoplankton abundance in Valanginian (early Cretaceous) limestone-marl successions from the southeast France Basin: carbonate dilution or productivity?» Palaeogeography, Palaeoclimatology, Palaeoecology **201** (*1-2*): 113-139.

Romanek, C. S., Grossman, E. L. and Morse, J. W. (1992). «Carbon isotopic fractionation in synthetic aragonite and calcite: Effects of temperature and precipitation rate.» Geochimica et Cosmochimica Acta **56** (*1*): 419-430.

Schaub, H. P. (1936). "Geologie des Rawilgebietes." Eclog. geol. Helv., **29**: 337-407.

Schaub, H. P. (1948). "Über Aufarbeitung und Kondensation." Eclog. geol. Helv., **41**: 89-94.

Schlager, W. (1981). "The paradox of drowned reefs and carbonate platforms." Geol. Soc. Amer. Bull., **92**: 197-211.

Schlanger, S. O. and Jenkyns, H. C. (1976). «Cretaceous oceanic anoxic events: causes and consequences.» Geologie en Mijnbouw **55** (*3-4*): 179-184.

Scholle, P. A. and Arthur, M. A. (1980). «Carbon Isotope Fluctuations in Cretaceous Pelagic Limestones: Potential Stratigraphic and Petroleum Exploration Tool.» American Association of Petroleum Geologists Bulletin **64** (*1*): 67-87.

Smith, A. M., Nelson, C. S. and Spencer, H. G. (1998). «Skeletal carbonate mineralogy of New Zealand bryozoans.» Marine Geology **151** (*1-4*): 27-46.

Sprinkle, J. and. Kier, P. M (1987). "Phylum Echinodermata." *In* Boardman, R. S., Cheetham, A. H. and Rowell, A. J. (*Eds*.). "Fossil Invertrebrates." Blackwell Scientific Publications, Oxford, 550-611.

Steuber, T. (2002). «Plate tectonic control on the evolution of Cretaceous platform-carbonate production.» Geology **30** (*3*): 259-262.

Suzuki, A. and Kawahata, H. (2003). "Carbon budget of coral reef systems: an overview of observations in fringing reefs, barrier reefs and atolls in the Indo-Pacific regions." Tellus, **55B**: 428-444.

Suzuki, A. and Kawahata, H. (2004). «Reef Water CO_2 System and Carbon Production of Coral Reefs: Topographic Control of System-Level Performance». *In:* Shiyomi**,** M., Kawahata**,** H., Koizumi**,** H. and Awaya**,** Y., (*Eds*). Global Environmental Change in the Ocean and on Land. TERRAPUB: 229-248.

Suzuki, A., Kawahata, A., Ayukai, T. and Goto, K. (2001). "The oceanic CO_2 system and carbon budget in the Great Barrier Reef, Australia." Geophys. Res. Lett., **28**: 1243-1246.

Swart, P. K. and Eberli, G. (2005). «The Nature of the $\delta^{13}C$ of Periplatform Sediments: Implications for stratigraphy and the global carbon cycle.» Sedimentary Geology **175**: 115-129.

Thomas, H., Bozec, Y., Elkalay, K. and de Baar, H. J. W. (2004). «Enhanced open ocean storage of CO_2 from shelf sea pumping.» Science **304**: 1005-1008.

van de Schootbrugge, B. (2001). «Influence of paleo-environmental changes during the Hauterivian (early Cretaceous) on carbonate deposition along the northern margin of the Tethys: Evidence from geochemical records (C, O and Sr-isotopes, P, Fe, Mn).» *Ph.D. thesis*, Université de Neuchâtel, 291 pp.

van de Schootbrugge, B., Föllmi, K. B., Bulot, L. G. and Burns, S. J. (2000). «Paleoceanographic changes during the early Cretaceous (Valanginian-Hauterivian): evidence from oxygen and carbon stable isotopes.» Earth and Planetary Science Letters **181**: 15-31.

van de Schootbrugge, B., Kuhn, O., Adatte, T., Steinmann, P. and Föllmi, K. (2003). «Decoupling of P- and Corg-burial following Early Cretaceous (Valanginian-Hauterivian) platform drowning along the NW Tethyan margin.» Palaeogeography, Palaeoclimatology, Palaeoecology **199** (*3-4 SU* -): 315-331.

van de Schootbrugge, B., Mc Arthur, J. M., Bailey, T. R., Rosenthal, Y., Wright, J. D. and Miller, K. G. (2005). «The Toarcian oceanic

anoxic event (T-OAE): an assessment of global causes using belemnite C-isotope records.» Paleoceanography, **20**, PA3008, doi: 10.1029/2004PA001102.

Veizer, J., Ala, D., Azmy, K., Bruckschen, P., Buhl, D., Bruhn, F., Carden, G. A. F., Diener, A., Ebneth, S. and Godderis, Y. (1999). «$^{87}Sr/^{86}Sr$, $\delta^{13}C$ and $\delta^{18}O$ evolution of Phanerozoic seawater.» Chemical Geology **161** (*1-3*): 59-88.

Wefer, G. and Berger, W. H. (1991). «Isotope paleontology: growth and composition of extant calcareous species.» Marine Geology **100**: 207-248.

Weissert, H. (1981). "The environment of deposition of black shales in the early Cretaceous: an ongoing controversy." *In* Warme, J. E., Douglas, R. G. and Winterer, E. L. (*Eds*.). The Deep Sea Drilling Project: a decade of progress. Soc. Econ. Paleont. Mineral., **Spec. Vol. 32**: 547-560.

Weissert, H. (1989). «C-Isotope stratigraphy, a monitor of paleoenvironmental change: a case study from the Early Cretaceous.» Surveys in Geophysics **10** (*1*): 1-61.

Weissert, H. and Channell, J. E. T. (1989). "Tethyan carbonate carbon isotope stratigraphy across the Jurassic-Cretaceous boundary: an indicator of decelerated global carbon cycling?" Paleoceanography, **4**: 483-494.

Weissert, H., McKenzie, J. A. and Hochuli, P. (1979). "Cyclic anoxic events in the early Cretaceous Tethys ocean." Geology, **7**: 147-151.

Weissert, H., Lini, A., Föllmi, K. B. and Kuhn, O. (1998). «Correlation of Early Cretaceous carbon isotope stratigraphy and platform drowning events: a possible link?» Palaeogeography, Palaeoclimatology, Palaeoecology **137**: 189-203.

Weissert, H. and Erba, E. (2004). «Volcanism, CO_2 and palaeoclimate: a Late Jurassic-Early Cretaceous carbon and oxygen isotope record.» Journal of the Geological Society, London **161**: 695-702.

Wissler, L., Weissert, H., Masse, J.-P. and Bulot, L. G. (2002). «Chemostratigraphic correlation of Barremian and lower Aptian ammonite zones and magnetic reversals.» Int. J. Earth Sci. (Geol. Rundsch.) **91** (*2*): 272-279.

Wissler, L., Funk, H. and Weissert, H. (2003). «Response of Early Cretaceous carbonate platforms to changes in atmospheric carbon dioxide levels.» Palaeogeography, Palaeoclimatology, Palaeoecology **200** (*1-4*): 187-205.

Woo, K. S., Anderson, T. F. and Sandberg, P. A. (1993). "Diagenesis of skeletal and nonskeletal components of mid-Cretaceous limestones." Journ. Sedim. Petrol., **63**: 18-32.

Wyssling, G. W. (1986). "Der frühkretazische helvetische Schelf im Vorarlberg und Allgäu." Jahrb. Geol. Bundesanstalt, **129**: 161-265.

D.6. THE HEMIPELAGIC AND PELAGIC RECORD: MAIN CONCLUSIONS

Geochemical and mineralogical analyses are usually performed on sediments from basinal settings, in order to reconstruct paleoceanographic changes; *ad priori*, such sections are supposed to have a good age control (*e.g.*, by ammonite and/or nannofossils biostratigraphy), and also to hold the more complete sedimentary record compared to more proximal environments, such as platforms.

Our analyses performed on several (hemi-)pelagic sections from different basins from Italy, France and Switzerland clearly showed that the Late Hauterivian –earliest Aptian times were marked by a major paleoceanographic change, the Faraoni anoxic event, which started in the Late Hauterivian *Pseudothurmannia mortilleti* ammonite zone. Even if the Faraoni event gathers all the sedimentological characteristics of other Oceanic Anoxic Events, such as the Bonarelli Level of the OAE2 (Cenomanian – Turonian boundary; *e.g.*, Coccioni *et al.*, 1991; Luciani *et al.*, 1999; Mort *et al.*, in press), its anoxic character was not yet clearly established, and geochemical evidence rather pointed out to dysoxic conditions during the time of deposition of the Faraoni level (*e.g.*, Baudin *et al.*, 2002). However, the enrichment in redox sensitive trace elements highlighted in sediments from the Faraoni level tends to prone for anoxia near the water-sediment interface. The latter may have been sustained by a decrease of the preservation of phosphorus in the sediment, which may have favoured the anoxia through a positive feedback mechanism. In return, the installation of dysoxic to anoxic conditions in the northern Tethys may have led to the demise of northern Tethyan carbonate platforms.

The return to oligotrophic conditions that began in the latestmost Early Barremian allowed the onset of the Urgonian carbonate platform which is representative of a photozoan-dominated carbonate platform. The installation of this ecosystem had consequences: Indeed, organisms constituting photozoan ecosystems are thought to produce predominantly aragonite, and the input of such ^{13}C-enriched material into the ocean may have pushed the $\delta^{13}C$ toward more positive values.

Similar environmental disturbances occurred several times during the Cretaceous, and they are in many cases linked to volcanism (*e.g.*, Weissert and Erba, 2004). However, it seems that there is no evidence for a volcanic event during the Late Hauterivian, which may explain the unfolding of the Faraoni anoxic event (*e.g.*, Courtillot and Renne, 2003). Consequently, an alternative starting point for this environmental crisis has to be found. One piece of answer is given by the evolution of clay minerals during the studied period. Whereas the Early and partly the Late Hauterivian were dominated by a seasonally-contrasted climate, the time span from the Late Hauterivian *Balearites balearis* ammonite zone to the earliest Aptian is characterised by an increased content in kaolinite, which corresponds to a more humid climate on land. Under such intertropical conditions, continental weathering, as well as the delivery of detrital material and nutrients into the oceans, may have increased. The augmentation of the phosphorus input may have thus triggered a phase of generally increased productivity and with that the anoxic conditions of the Faraoni event.

Last but not least, how may this climate change have occurred? Classically, the installation of more humid conditions is linked to an enhanced

greenhouse effect, which could be triggered, by example, by volcanism. However, as previously said, there is no evidence for Hauterivian volcanism. Changes in tectonic processes may constitute another way to change climate and increase, for example, humidity. During the Early Cretaceous, the opening of the southern Atlantic Ocean created larger shallow-water areas (see Fig. 2 in Philip, 2003). The release of vapour into the atmosphere via evaporation of epicontinental seas may constitute a source of humidity which may have ultimately triggered the Late Hauterivian – Early Barremian Faraoni anoxic event.

References

Baudin, F., Cecca, F., Galeotti, S. and Coccioni, R. (2002). «Palaeoenvironmental controls of the distribution of organic matter within a Corg-rich marker bed (Faraoni level, uppermost Hauterivian, central Italy).» Eclogae geol. Helv. **95**: 1-13.

Coccioni, R., Erba, E. and Premoli-Silva, I. (1991). «Litho- and biostratigraphy of the Livello Bonarelli close to the Cenomanian/Turonian boundary (Umbria-Marche Apennines, Italy) and possible paleoceanographic significance.» Géologie Alpine, Mémoire Hors Série **17**: 25-26.

Courtillot, V. E. and Renne, P. R. (2003). «On the ages of flood basalt events.» C.R. Geoscience **335**: 113-140.

Luciani, V. and Cobianchi, M. (1999). «The Bonarelli Level and other black shales in the Cenomanian-Turonian of the northeastern Dolomites (Italy): calcareous nannofossil and foramniniferal data.» Cretaceous Research **20**: 135-167.

Mort, H. P., Jaquat, O., Adatte, T., Steinmann, P., Follmi, K., Matera, V., Berner, Z. and Stuben, D. (in press). «The Cenomanian-Turonian anoxic event in Italy and Spain: enhanced productivity and/or better preservation.» Cretaceous Research.

Philip, J. (2003). «Peri-Tethyan neritic carbonate areas: distribution through time and driving factors.» Palaeogeography, Palaeoclimatology, Palaeoecology **196** (*1-2*): 19-37.

Weissert, H. and Erba, E. (2004). «Volcanism, CO_2 and palaeoclimate: a Late Jurassic-Early Cretaceous carbon and oxygen isotope record.» Journal of the Geological Society, London **161**: 695-702.

Chapter E.

Main Conclusions

Marnes d'Uttins and overlying packstone with bivalves (quarry of Eclépens, VD, Switzerland)

E.
Main Conclusions

E. 1. The Western Swiss Jura

In order to solve the dilemma that rests upon the age of the Urgonian from the Western Swiss Jura for more than twenty years, we developed a multidisciplinary approach in which we emphasize the use of sedimentological and geochemical techniques. Even if the latter were, sometimes, hard to implement, they succeed in giving new support to date the Eclépens Fm as Late Hauterivian to Late Barremian, in the case we assumed that the base of the lower Eclépens Fm unit represents an equivalent of the Altmann Member of the Helvetic area, which basal part is attributed to the *Pseudothurmannia seitzi* ammonite zone (see Annexe 4.1), and that the Marnes de la Russille informal unit corresponds to the maximum flooding surface of the B3 depositional sequence (*Gerhardtia sartousiana* ammonite zone, after Arnaud, 2005). Moreover, the systematic use of sequence stratigraphy clarifies the organization of the sedimentary record in the Western Swiss Jura itself; it is also useful for correlation purposes between this area and other regions of the Northern Tethyan margin, such as the Helvetic realm, the Subalpine Chains and the Northern Vercors. Based on these correlations, it can be suggested that sequence boundary B3 played a major role in the history of the Urgonian Platform, as this sedimentary architecture began to rise during the depositional sequence B3, at least in this part of the Northern Tethys.

However, the Late Barremian age of the Urgonian from the Neuchâtel area calls the accuracy of the biostratigraphy of specific shallow-water groups into question. Depending on the used taxon, the calibration of the range of species can be shifted by one stratigraphic stage, which is somewhat longer than the total duration of the deposition of the Urgonien Jaune and the Urgonien Blanc, which can be approximated to be of or less than 1.2 Ma (duration of the B3 sequence, after Arnaud, 2005). Moreover, the validity of the calibration of benthic organisms against ammonites has to be scrupulously checked before using them to date shallow-water carbonates.

We finally want to underline that sequence stratigraphic schemes of the Western Swiss Jura, the Helvetic realm and even the Northern Vercors represent a logical evolution from distal to proximal settings. Effectively, the Western Swiss Jura represents the most proximal part of the Urgonian platform; omissions and erosions will thus be most pronounced in this environment, and sediments may have been deposited only during times of high sea level, as it is the case during the depositional sequence B3: Arnaud (2005) reported that the maximum flooding surface B3 of the *Gerhardtia sartousiana* may represent the highest sea level of the Barremian. Consequently, it may have created enough accommodation space to allow the deposition of the Eclépens Fm in the Neuchâtel area. Then, at the time of the maximum flooding surfaces B4 and B5, the sea level may not have reached comparable levels; as all the accommodation space may have been previously filled by sediments constituting the Eclépens Fm, the Urgonian platform may have had no other choice than prograding into more distal regions, such as the Subalpine Chains, the Northern Vercors and the Helvetic realm, where the depositional sequences B4, B5 and A1 were preserved.

E.2. Paleoceanographic impact of the rise of the Urgonian Platform

Besides the “in-situ” dating of the Urgonian of the Western Swiss Jura, other elements tend to point out a Late Barremian age.

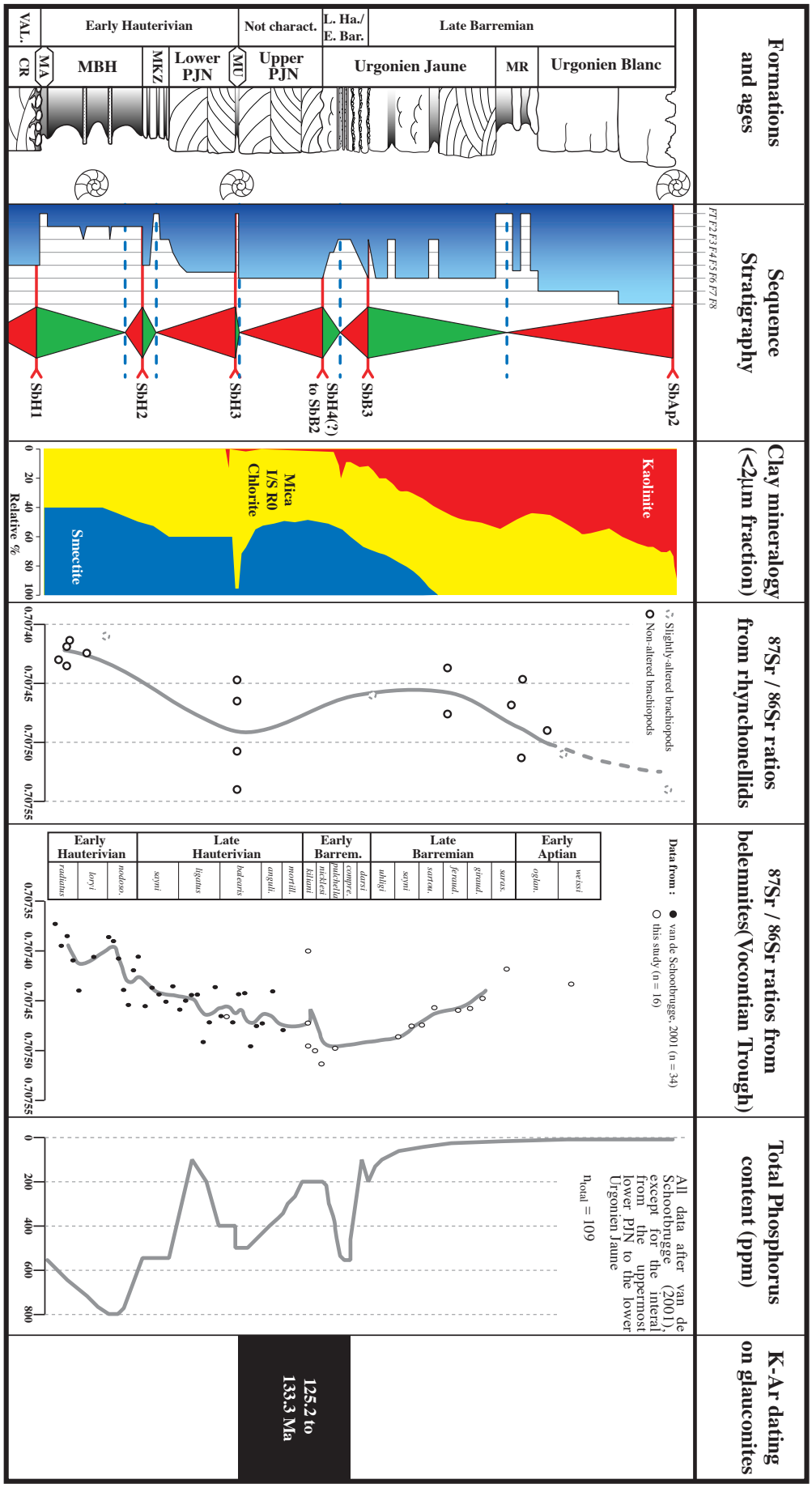

Abbreviations of the names of the formations: **CR:** Calcaire Roux; **MA:** Marnes à Astieria; **MBH:** Marne Bleue d'Hauterive; **MKZ:** Mergelkalk zone; **PJN:** Pierre Jaune de Neuchâtel; **MU:** Marnes d'Uttins; **MR:** Marnes de la Russille.

Fig. E.1: Overview of the results obtained from the different approaches applied to the Western Swiss Jura, and the deduced stratigraphic framework.

First, it can be noted that in the Helvetic, Subalpine and Vercors areas the Urgonian platform began to rise during the Late Barremian. Paleoecological and paleoceanographic conditions may have triggered this phenomenon, as it seems to be a supraregional phenomenon, at least at the scale of the northern Tethys. A change both in the clay mineral assemblages, as well as in the continental detritus and the phosphorus mass accumulation rates is reported from the period between the Late Hauterivian and the Late Barremian; especially, the arrival of a more humid climate from the latest Hauterivian onward may have increased continental particulate input into the ocean. Consequently, as a response, carbonate factories from the northern Tethyan margin ceased their rise and began to decline - a phase which lasted up to the Late Barremian, where the return to more oligotrophic conditions under a more seasonally-contrasted climate allowed the genesis of the photozoan Urgonian carbonate platform. We thus concluded that all these paleoenvironmental parameters acted as limiting factors on the installation of the Urgonian platform, and were especially responsible for the high trophic levels observed during the Late Hauterivian.

On the other hand, the Late Barremian age of the Urgonian helps to explain several features observed in the evolution of two proxies. First, the relatively stable evolution of the $\delta^{13}C$ during the Early Barremian may be linked to the drowning of Northern Tethyan carbonate platforms recorded, in particular, in the Helvetic realm. On the contrary, the positive shift initiated in the *Coronites darsi* ammonite zone may be the consequence of the export of ^{13}C-enriched material from the platform to the basin; the production of aragonite by benthic organisms may represent a non-negligible source of this mineral. Moreover, the Urgonian platform may have acted as a barrier for the export of fine-grained particles during the Late Barremian, in particular for kaolinite which was preferentially deposited in proximal environments (*e.g.*, the Neuchâtel area), whereas contemporaneous (hemi-) pelagic sediments were depleted in this mineral.

Finally, Urgonian platforms are also known from other parts of the Tethys, especially in Oman (*e.g.*, Masse *et al.*, 1998; Hillgärtner *et al.*, 2003), and Mexico (Cupido and Coahuila carbonate platforms; *e.g.*, Bralower *et al.*, 1999; Lehman *et al.*, 1999). Their history is relatively similar to the one of the Urgonian platform from the Northern Tethyan margin. In all these regions, limestones deposited in lagoonal environments (and thus comparable to some facies of the Eclépens Fm) are dated from the Late Barremian, and thus suggest that the installation of urgonian-type facies was a widespread phenomenon within the Tethys.

E.3. Integration of the Western Swiss Jura into the geochemical and sedimentological history of the Northern Tethyan margin

Thanks to the multiproxy approach performed on (hemi-)pelagic sections (and in particular on the Angles section), it is possible to describe the unfolding of paleoceanographic and paleoclimatic changes that occurred during the Late Hauterivian – earliest Aptian period, and to include the Western Swiss Jura into the evolution of the Northern Tethyan margin in the light of these paleoenvironmental events.

Whereas the main part of the Hauterivian (from its base to the *B. balearis* zone) was characterized by a seasonally contrasted climate – as deducted from the dominance of smectitic minerals – coupled with mesotrophic oceans, the latest Hauterivian experimented a change toward a more humid climate (increased kaolinite content), which may have been accompanied by an enhanced continental runhoff and a subsequent higher delivery of phosphorus and dissolved inorganic carbon (DIC) into the ocean. The augmentation of the oceanic trophic level may have constituted a limiting factor for the growth of carbonate factories, which may have became less and less healthy. This phenomenon may have culminated in the *P. mortilleti* zone, with the installation of bottom-water anoxia, as suggested by enrichments in redox-sensitive trace-elements (e.g., U, V, Mo; see Fig. E.2), and the deposition of organic-rich sediments, the Faraoni Level. It may also have led to the demise of the Northern Tethyan

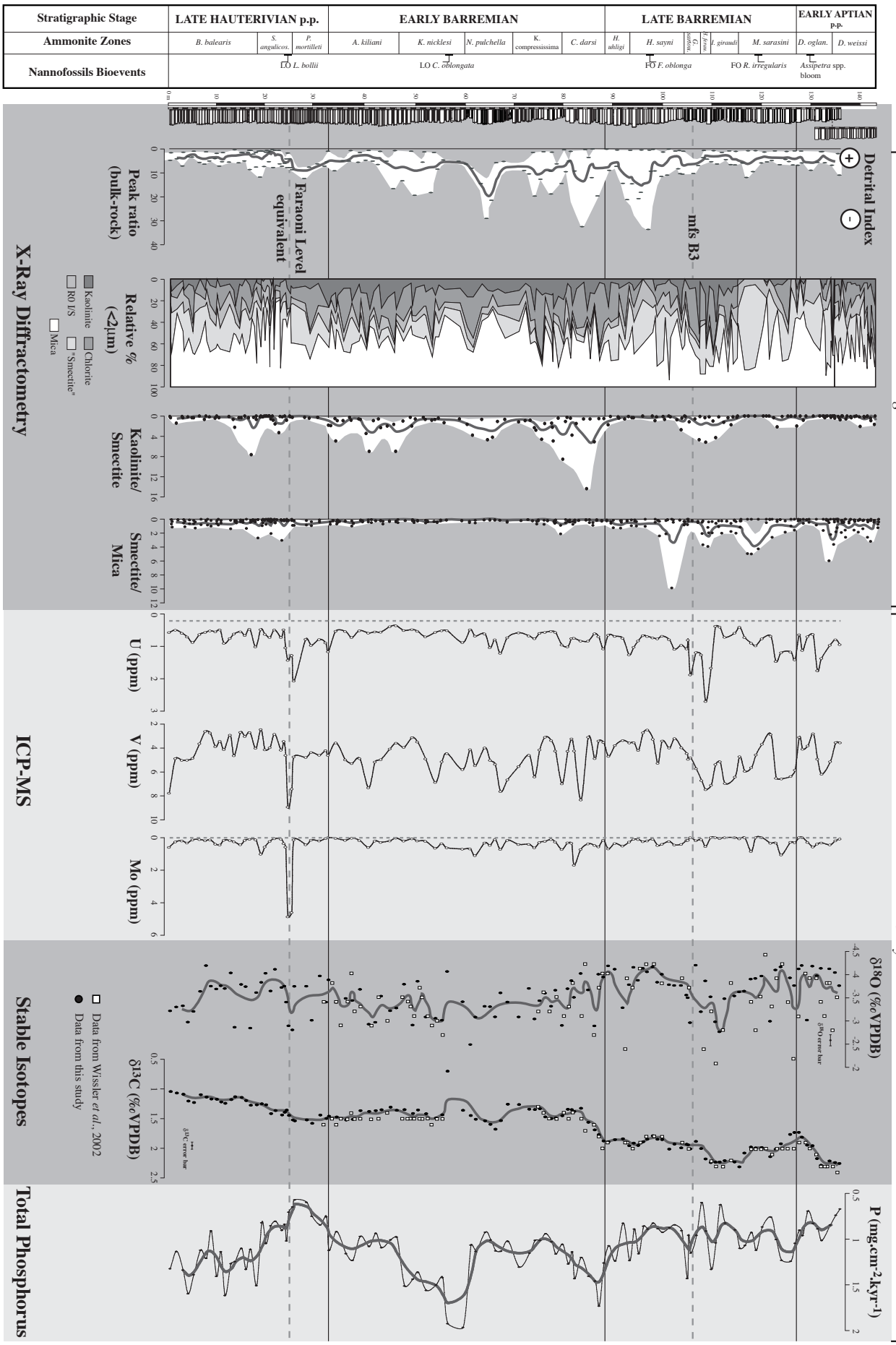

Fig. E.2: XRD (bulk rock and clay fraction), ICP-MS, stable isotopes (C and O) and Phosphorus Mass Accumulation Rates results for the Angles section.

carbonate platform, such as the Helvetic platform; the Altmann Mb of the latter area documents this drowning phase, and ammonite biostratigraphy indicates that this episode lasted until the *C. darsi* ammonite zone of the latest Early Barremian. This implies that during the Early Barremian, the DIC flux into the Tethys was not regulated anymore by benthic organisms constituting the carbonate platform, and the resulting increase in the DIC reservoir in the adjacent basins may have buffered perturbations of the carbon cycle (e.g., Bartley and Kah, 2004). This may explain why the $\delta^{13}C$ did not record a positive excursion associated with the Faraoni OAE, whereas other Cretaceous OAE's are linked to such variations. On the contrary, the $\delta^{13}C$ curve remained abnormally calm during the Early Barremian; it only begins to record fluctuations from the sequence boundary B3 located in the *C. darsi* zone, which corresponds in time to the end of the Altmann Mb and the rise of the Urgonian carbonate platform along the Northern Tethyan margin. The installation of the Urgonian platform in a photozoan mode is also synchronous with the settling of oligotrophic conditions, as is suggested by the decrease of the Phosphorus Mass Accumulation Rates (PMAR) observed between the Early and the Late Barremian at Angles.

The same trend in the total phosphorus content is noticeable in the Western Swiss Jura: whereas sediments from the Marne Bleue d'Hauterive are characterized by relatively high phosphorus contents, the main part of the Urgonien Jaune and the Urgonien Blanc exhibit low concentrations in phosphorus (see Fig. E.1). This may suggest that the main part of the Urgonian from the Neuchâtel area was deposited during the Late Barremian, when the Northern Tethys was characterized by waters depleted in nutrients. This age is coherent with high $^{87}Sr/^{86}Sr$ values obtained from brachiopods (rhynchonellids) sampled in the upper Urgonien Jaune, the Marnes de la Russille and the Urgonien Blanc. However, reworked sediments coupled with glauconite-rich sediments, as well as high phosphorus contents at the base of the Urgonien Jaune suggest a phase of condensation which may correlate with the Altmann Mb of the Helvetic area. This hypothesis is supported by sequence stratigraphic arguments: the correlation of third-order depositional sequences between the Western Swiss Jura, the Helvetic ramp, the Subalpine Chains and the Northern Vercors highlights the stacking of the sequence boundaries (Sb) H4? (*S. sayni* ammonite zone) to B2 (base of the *C. darsi* ammonite zone; Arnaud, 2005) in the first fifteen meters of the Urgonien Jaune at Eclépens; the last erosional boundary of the basal part of the Urgonien Jaune –i.e., where reworking processes are the strongest - may thus correspond to the SbB3 (top of the *C. darsi* ammonite zone), and the Marnes de la Russille to the maximum flooding surface of the depositional sequence B3 (*G. sartousiana* ammonite zone). On the other hand, this correlation emphasizes that sediments deposited above the SbB3 represent only one depositional sequence, and thus that the main part of the Urgonian from the Western Swiss Jura correlates with the "Masse Urgonienne inférieure" and the Lower Schrattenkalk Fm, which both embodies the first sequence of in the Urgonian Formations preserved from the Northern Vercors and the Helvetic realm, respectively. This finally implies that the depositional sequences B4 to A1 that constitute the remainder of the Urgonian Fm from the Vercors are not preserved in the Western Swiss Jura. This may be explained by the very proximal setting of the Neuchâtel area within the Northern Tethyan margin during the Barremian, which may have prevent the creation of accommodation space; in this case, the Urgonian platform may have had no other choice than to prograde toward more distal environments. Alternatively, the depositional sequence B4 to A1 may have been deposited in the Western Swiss Jura thanks to the creation of accommodation space by synsedimentary faults, but subsequent erosion did not allowed their preservation.

E.4. Outlook

Although this study helps to better constrain the age of the Urgonian from the Western Swiss Jura, it also calls several problems into question.

The K-Ar dating performed on glauconitic layers delivered two ages, which are in the same interval of error. Moreover, the attribution of the analysed sediments to a stratigraphic stage depends on the used stratigraphic chart. One way to test the reliability of this approach may consist in the use of another chronometer in contemporaneous sediments, such as for example the absolute dating of brachiopod sample $EC_{II}58$ using the

Rb-Sr chronometer may confirm (or infirm) the K-Ar dating of glauconites from sample $EC_{II}57$. Moreover, the K-Ar and Rb-Sr of both glauconites and brachiopods, respectively, from the Marne Bleue d'Hauterive may help to choose the most appropriate stratigraphic chart, as the age of this formation is well- constrained by ammonite biostratigraphy (Early Hauterivian).

An other outlook may be the detailed study of the karst in the uppermost Urgonien Blanc. Effectively, even if the basal limit of the Urgonien Jaune is clearly defined, as is also the Late Barremian age of the main part of the Urgonian from the Western Swiss Jura, the history and unfolding of the upper boundary of this formation calls another problem into question. As only one depositional sequence is recorded in the main part of the Urgonien Jaune and the Urgonien Blanc, and as an Early Aptian fauna has been found in the karst (ammonites and orbitolina such as *Palorbitolina lenticularis*), the presence of several phases of karstification is suspected, and a detailed sedimentological study is required in order to improve the sequence stratigraphic model of the development of the upper limit of the Urgonien Blanc. This could be performed in sections such as La Lance or even Eclépens, where the karsts are well-developed and have a good exposure.

Finally, the comparison of the redox-sensitive trace-element concentration with the type and content of clay minerals within the Angles section may hint at a possible link. In particular, smectitic minerals may better integrate trace-elements within their interlayer space and may thus constitute a non-negligible contributor to trace-element enrichments. This may help to differentiate between climatic and anoxic signals.

E.5. References

Arnaud, H. (2005). «The South-East France Basin (SFB) and Its Mesozoic Evolution». *In:* Adatte, T., Arnaud-Vanneau, A., Arnaud, H., Blanc-Aletru, M.-C., Bodin, S., Carrio-Schaffhauser, E., Föllmi, K. B., Godet, A., Raddadi, M. C. and Vermeulen, J., (*Eds*). The Hauterivian-Lower Aptian sequence stratigraphy from Jura Platform to Vocontian Basin: A multidisciplinary approach. Géologie Alpine, **Série Spéciale «Colloques et Excursions» N°7**: 5-28.

Bartley, J. K. and Kah, L. C. (2004). «Marine carbon reservoir, C_{org} - C_{carb} coupling, and the evolution of the Proterozoic carbon cycle.» **Geology** 32(*2*): 129-132.

Bralower, T. J., CoBabe, E., Clement, B., Sliter, W. V., Osburn, C. L. and Longoria, J. (1999). «The record of global change in mid-Cretaceous (Barremian-Albian) sections from the Sierra Madre, northeastern Mexico.» Journal of Foraminiferal Research **29** (*4*): 418-137.

Hillgärtner, H., Van Buchem, F. S. P., Gaumet, F., Razin, P., Pittet, B., Grötsch, J. and Droste, H. (2003). «The Barremian-Aptian evolution of the eastern Arabian carbonate platform margin (northern Oman).» Journal of Sedimentary Research **73** (*5*): 756-773.

Lehman, C., Osleger, D. A., Montanez, I. P., Arnaud-Vanneau, A. and Banner, J. (1999). «Evolution of Cupido and Coahuila carbonate platforms, Early Cretaceous, northeastern Mexico.» GSA Bulletin **111** (*7*): 1010-1029.

Masse, J.-P., Borgomano, J. and Al Maskiry, S. (1998). «A platform-to-basin transition for lower Aptian carbonates (Shuaiba Formation) of the northeastern Jebel Akhdar (Sultanate of Oman).» Sedimentary Geology **119** (*3-4*): 297-309.

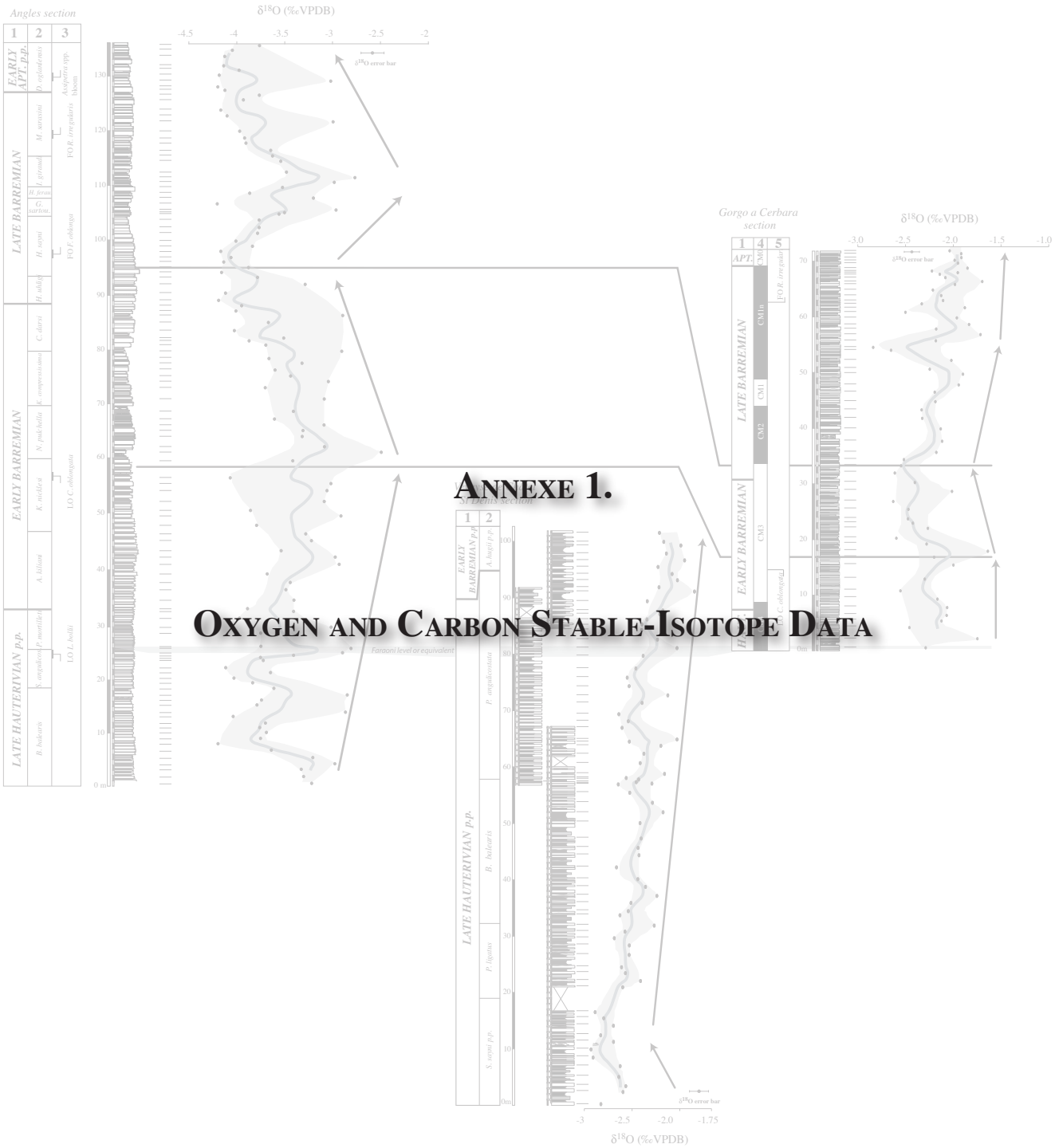

ANNEXE 1.

OXYGEN AND CARBON STABLE-ISOTOPE DATA

Sample ID	Depth (m)	Stage	Ammonite Zone	Non-treated data (‰VPDB)		Five points moving average (‰VPDB)	
				$\delta^{13}C$	$\delta^{18}O$	$\delta^{13}C$ smooth	$\delta^{18}O$ smooth
AN 2	0.34	Late Hauterivian	*B. balearis*	1.05	-3.21		
AN 4	1.68	Late Hauterivian	*B. balearis*	1.07	-3.29		
AN 6	2.85	Late Hauterivian	*B. balearis*	1.09	-3.31	1.12	-3.20
AN 8	4.03	Late Hauterivian	*B. balearis*	1.21	-2.97	1.16	-3.19
AN 10	4.87	Late Hauterivian	*B. balearis*	1.23	-3.19	1.17	-3.34
AN 13	6.38	Late Hauterivian	*B. balearis*	1.10	-3.62	1.16	-3.61
AN 15.1	7.38	Late Hauterivian	*B. balearis*	1.14	-4.18	1.15	-3.81
AN 16	8.39	Late Hauterivian	*B. balearis*	1.17	-3.74	1.16	-3.82
AN 18	9.56	Late Hauterivian	*B. balearis*	1.18	-3.68	1.19	-3.75
AN 20	10.40	Late Hauterivian	*B. balearis*	1.22	-3.74	1.21	-3.74
AN 23	11.90	Late Hauterivian	*B. balearis*	1.24	-3.69	1.21	-3.71
AN 26	12.42	Late Hauterivian	*B. balearis*	1.18	-4.02	1.19	-3.60
AN 27.2	13.26	Late Hauterivian	*B. balearis*	1.13	-2.85	1.16	-3.52
AN 29	14.43	Late Hauterivian	*B. balearis*	1.14	-3.77	1.17	-3.47
AN 31	15.60	Late Hauterivian	*B. balearis*	1.20	-3.73	1.21	-3.43
AN 33	16.44	Late Hauterivian	*B. balearis*	1.28	-2.84	1.24	-3.41
AN 35	17.95	Late Hauterivian	*B. balearis*	1.27	-3.60	1.26	-3.51
AN 38	18.79	Late Hauterivian	*S. anguliscotatum*	1.25	-3.82	1.28	-3.71
AN 40	19.63	Late Hauterivian	*S. anguliscotatum*	1.27	-4.01	1.31	-3.84
AN 43	20.64	Late Hauterivian	*S. anguliscotatum*	1.42	-3.63	1.35	-3.87
AN 46	21.48	Late Hauterivian	*S. anguliscotatum*	1.36	-4.10	1.39	-3.85
AN 49.1	22.82	Late Hauterivian	*S. anguliscotatum*	1.44	-3.71	1.40	-3.78
AN 50	23.32	Late Hauterivian	*S. anguliscotatum*	1.39	-3.74	1.40	-3.60
AN 51	23.83	Late Hauterivian	*S. anguliscotatum*	1.36	-3.39	1.41	-3.33
AN 52	24.70	Late Hauterivian	*S. anguliscotatum*	1.45	-2.89	1.45	-3.13
AN 53.2	25.00	Late Hauterivian	*S. anguliscotatum*	1.52	-2.80	1.49	-3.18
AN 55	25.34	Late Hauterivian	*S. mortiletti*	1.54	-3.73	1.53	-3.37
AN 62.1	27.85	Late Hauterivian	*S. mortiletti*	1.52	-3.73	1.53	-3.49
AN 65.1	28.86	Late Hauterivian	*S. mortiletti*	1.58	-3.00	1.52	-3.52
AN 68	30.54	Late Hauterivian	*S. mortiletti*	1.44	-3.96	1.50	-3.55
AN 71	32.93	Late Hauterivian	*S. mortiletti*	1.50	-3.39	1.48	-3.62
AN 72	33.45	Early Barremian	*A. kiliani*	1.46	-3.87	1.48	-3.61
AN 75	34.06	Early Barremian	*A. kiliani*	1.47	-3.39	1.49	-3.53
AN 78	35.74	Early Barremian	*A. kiliani*	1.52	-3.47	1.49	-3.49
AN 81	37.08	Early Barremian	*A. kiliani*	1.51	-3.43	1.46	-3.45
AN 84	38.93	Early Barremian	*A. kiliani*	1.37	-3.67	1.42	-3.35
AN 87	40.44	Early Barremian	*A. kiliani*	1.38	-2.92	1.38	-3.21
AN 89	41.95	Early Barremian	*A. kiliani*	1.37	-2.96	1.36	-3.17
AN 90 haut	42.95	Early Barremian	*A. kiliani*	1.35	-3.52	1.35	-3.23
AN 92	44.80	Early Barremian	*A. kiliani*	1.31	-3.21	1.34	-3.33
AN 93 haut	46.14	Early Barremian	*A. kiliani*	1.36	-3.27	1.35	-3.37
AN 95 bas	47.99	Early Barremian	*K. nicklesi*	1.35	-3.78	1.37	-3.39
AN 97	49.50	Early Barremian	*K. nicklesi*	1.41	-2.90	1.38	-3.40
AN 98 haut	50.50	Early Barremian	*K. nicklesi*	1.36	-3.84	1.40	-3.34
AN 101	52.18	Early Barremian	*K. nicklesi*	1.42	-3.07	1.42	-3.24
AN 103	53.86	Early Barremian	*K. nicklesi*	1.49	-3.05	1.38	-3.19
AN 104	55.20	Early Barremian	*K. nicklesi*	1.44	-3.01	1.26	-3.32
AN 105	56.38	Early Barremian	*K. nicklesi*	0.71	-4.05	1.18	-3.41
AN 108	59.56	Early Barremian	*K. nicklesi*	1.36	-3.40	1.24	-3.27
AN 109.4	61.07	Early Barremian	*N. pulchella*	1.45	-2.48	1.39	-3.06
AN 110.1b	62.25	Early Barremian	*N. pulchella*	1.51	-3.07	1.50	-3.03
AN 110.3c	64.09	Early Barremian	*N. pulchella*	1.54	-3.30	1.55	-3.16
AN 110.4	65.27	Early Barremian	*N. pulchella*	1.60	-3.30	1.59	-3.25
AN 111.2	66.28	Early Barremian	*N. pulchella*	1.68	-3.08	1.57	-3.31
AN 111.5	67.28	Early Barremian	*N. pulchella*	1.53	-3.59	1.48	-3.35
AN 112.2	68.79	Early Barremian	*N. pulchella*	1.26	-3.40	1.37	-3.36
AN 112.7	71.64	Early Barremian	*K. compressissima*	1.26	-3.08	1.31	-3.35
AN 114.2	72.99	Early Barremian	*K. compressissima*	1.34	-3.69	1.32	-3.33
AN 115	73.99	Early Barremian	*K. compressissima*	1.35	-3.03	1.35	-3.34
AN 117	75.17	Early Barremian	*K. compressissima*	1.33	-3.42	1.39	-3.38
AN 119	76.34	Early Barremian	*K. compressissima*	1.47	-3.59	1.44	-3.43
AN 121	78.36	Early Barremian	*K. compressissima*	1.50	-3.31	1.47	-3.44
AN 123	78.52	Early Barremian	*K. compressissima*	1.49	-3.65	1.47	-3.37
AN 125	79.70	Early Barremian	*C. darsi*	1.45	-2.89	1.43	-3.39
AN 127	80.70	Early Barremian	*C. darsi*	1.34	-3.68	1.39	-3.51
AN 128	81.54	Early Barremian	*C. darsi*	1.35	-3.85	1.36	-3.65
AN 129	82.21	Early Barremian	*C. darsi*	1.38	-3.50	1.37	-3.74
AN 131	83.39	Early Barremian	*C. darsi*	1.33	-4.01	1.43	-3.69
AN 133	84.90	Early Barremian	*C. darsi*	1.56	-3.65	1.54	-3.57
AN 136.2	86.24	Early Barremian	*C. darsi*	1.69	-2.88	1.66	-3.53
AN 138	87.50	Early Barremian	*C. darsi*	1.77	-3.99	1.77	-3.69
AN 139d	88.09	Early Barremian	*C. darsi*	1.87	-3.93	1.83	-3.93
AN 141.1	89.09	Late Barremian	*H. uhligi*	1.89	-4.17	1.86	-4.00
AN 143.1a	90.44	Late Barremian	*H. uhligi*	1.85	-4.10	1.87	-3.87

Table An.1.1: Carbon and oxygen stable-isotope data for the Angles section.

Sample ID	Depth (m)	Stage	Ammonite Zone	Non-treated data (‰VPDB)		Five points moving average (‰VPDB)	
				$\delta^{13}C$	$\delta^{18}O$	$\delta^{13}C$ smooth	$\delta^{18}O$ smooth
AN 144	91.95	Late Barremian	*H. uhligi*	1.84	-3.27	1.88	-3.75
AN 147.1	93.29	Late Barremian	*H. uhligi*	1.95	-3.77	1.90	-3.77
AN 148	94.13	Late Barremian	*H. sayni*	1.91	-4.14	1.92	-3.90
AN 149.3	95.13	Late Barremian	*H. sayni*	1.95	-3.86	1.92	-4.00
AN 151.1	96.00	Late Barremian	*H. sayni*	1.89	-4.12	1.89	-4.04
AN 151.3	96.98	Late Barremian	*H. sayni*	1.84	-4.04	1.85	-4.05
AN 153.2	97.00	Late Barremian	*H. sayni*	1.79	-4.15	1.83	-4.02
AN 155.1a	98.99	Late Barremian	*H. sayni*	1.84	-3.82	1.85	-3.96
AN 156.1	99.83	Late Barremian	*H. sayni*	1.85	-3.99	1.89	-3.89
AN 156.4	101.17	Late Barremian	*H. sayni*	2.01	-3.77	1.93	-3.82
AN 156.6	102.35	Late Barremian	*H. sayni*	1.93	-3.75	1.96	-3.76
AN 158	102.80	Late Barremian	*H. sayni*	1.99	-3.75	1.96	-3.68
AN 160.3	103.50	Late Barremian	*G. sartousiana*	1.93	-3.54	1.95	-3.55
AN 161.1	105.03	Late Barremian	*G. sartousiana*	1.94	-3.49	1.95	-3.45
AN 161.2	105.54	Late Barremian	*G. sartousiana*	2.01	-2.95	1.95	-3.46
AN 163.1b	106.40	Late Barremian	*G. sartousiana*	1.88	-4.19	1.97	-3.54
AN 164.2	107.72	Late Barremian	*H. feraudianus*	2.00	-3.19	2.03	-3.61
AN 166 b	108.46	Late Barremian	*H. feraudianus*	2.17	-3.85	2.13	-3.55
AN 168.1	109.73	Late Barremian	*H. feraudianus*	2.23	-3.51	2.20	-3.37
AN 170 c	110.57	Late Barremian	*I. giraudi*	2.23	-2.97	2.22	-3.17
AN 172.1	111.41	Late Barremian	*I. giraudi*	2.23	-2.76	2.22	-3.12
AN 173	112.58	Late Barremian	*I. giraudi*	2.20	-3.47	2.23	-3.28
AN 176.1	114.43	Late Barremian	*I. giraudi*	2.22	-3.53	2.23	-3.48
AN 177	115.44	Late Barremian	*M. sarasini*	2.31	-3.61	2.19	-3.61
AN 179.1	116.28	Late Barremian	*M. sarasini*	2.08	-3.63	2.11	-3.70
AN 181	117.79	Late Barremian	*M. sarasini*	1.98	-3.89	2.03	-3.81
AN 183	118.62	Late Barremian	*M. sarasini*	1.99	-3.90	2.00	-3.81
AN 185	119.97	Late Barremian	*M. sarasini*	1.98	-3.95	2.03	-3.70
AN 188	121.64	Late Barremian	*M. sarasini*	2.14	-2.98	2.04	-3.67
AN 190	122.82	Late Barremian	*M. sarasini*	2.01	-4.08	2.00	-3.80
AN 192	123.83	Late Barremian	*M. sarasini*	1.92	-4.15	1.91	-3.94
AN 195	125.50	Late Barremian	*M. sarasini*	1.76	-3.92	1.81	-3.96
AN 196.2	126.68	Late Barremian	*M. sarasini*	1.73	-3.75	1.76	-3.95
AN 197	127.35	Early Aptian	*D. oglanlensis*	1.73	-4.11	1.77	-3.93
AN 198	128.19	Early Aptian	*D. oglanlensis*	1.81	-4.18	1.83	-3.83
AN 200	129.19	Early Aptian	*D. oglanlensis*	1.94	-3.01	1.91	-3.76
AN 202 c	130.37	Early Aptian	*D. oglanlensis*	1.95	-4.17	2.02	-3.82
AN 204	131.88	Early Aptian	*D. oglanlensis*	2.17	-3.96	2.13	-3.98
AN 206	133.22	Early Aptian	*D. oglanlensis*	2.28	-4.12	2.20	-4.07
AN 211	134.72	Early Aptian	*D. oglanlensis*	2.21	-4.11	2.23	-4.05
AN 214	136.22	Early Aptian	*D. oglanlensis*	2.23	-4.03		
AN 216	137.72	Early Aptian	*D. oglanlensis*	2.25	-3.75		

Table An1.1 (continued): Carbon and oxygen stable-isotope data for the Angles section.

				Non-treated data (‰VPDB)		Five points moving average (‰VPDB)	
Sample ID	**Depth (m)**	**Stage**	**Ammonite Zone**	**$\delta^{13}C$**	**$\delta^{18}O$**	**$\delta^{13}C$ smooth**	**$\delta^{18}O$ smooth**
FB2	0.24	Late Hauterivian	-	1.76	-2.35		
FB5	1.71	Late Hauterivian	-	1.71	-2.44		
FB8	3.29	Late Hauterivian	-	1.77	-2.41	1.70	-2.44
FB12	4.61	Late Hauterivian	-	1.56	-2.59	1.70	-2.38
FB15	5.98	Late Hauterivian	-	1.78	-2.13	1.74	-2.26
FB18	7.11	Late Hauterivian	-	1.85	-2.17	1.80	-2.14
FB21	8.37	Late Hauterivian	-	1.84	-1.93	1.81	-2.12
FB28	9.41	Late Hauterivian	-	1.77	-2.25	1.79	-2.19
FB33	10.37	Late Hauterivian	-	1.76	-2.35	1.75	-2.30
FB41	11.48	Late Hauterivian	-	1.71	-2.31	1.71	-2.38
FB45	12.66	Late Hauterivian	-	1.68	-2.58	1.68	-2.42
FB50	13.72	Late Hauterivian	-	1.62	-2.34	1.66	-2.42
FB55	14.64	Late Hauterivian	-	1.68	-2.42	1.66	-2.41
FB59	15.31	Late Hauterivian	-	1.65	-2.42	1.68	-2.40
FB65	16.38	Late Hauterivian	-	1.72	-2.40	1.71	-2.35
FB71	17.75	Late Hauterivian	*B. balearis - P. ligatus*	1.77	-2.27	1.74	-2.27
FB79	18.82	Late Hauterivian	*B. balearis - P. ligatus*	1.76	-2.12	1.75	-2.18
FB89	19.92	Late Hauterivian	*B. balearis - P. ligatus*	1.69	-2.16	1.76	-2.12
FB94	20.84	Late Hauterivian	*B. balearis - P. ligatus*	1.86	-1.95	1.76	-2.14
FB99	21.77	Late Hauterivian	*B. balearis - P. ligatus*	1.73	-2.34	1.73	-2.20
FB104	22.73	Late Hauterivian	*B. balearis - P. ligatus*	1.63	-2.30	1.69	-2.24
FB109	23.78	Late Hauterivian	*B. balearis - P. ligatus*	1.65	-2.17	1.70	-2.24
FB115	24.68	Late Hauterivian	*B. balearis - P. ligatus*	1.78	-2.21	1.75	-2.27
FB123	25.81	Late Hauterivian	*B. balearis - P. ligatus*	1.82	-2.38	1.81	-2.30
FB128A	26.71	Late Hauterivian	*P. angulicostata* auct.	1.83	-2.43	1.87	-2.24
FB134A	27.81	Late Hauterivian	*P. angulicostata* auct.	1.90	-1.99	1.93	-2.14
FB136	28.36	Late Hauterivian	*P. angulicostata* auct.	2.09	-1.85	1.97	-2.15
FB139	28.93	Late Hauterivian	*P. angulicostata* auct.	1.93	-2.53	1.96	-2.26
FB371	29.07	Late Hauterivian	*P. angulicostata* auct.	1.90	-2.37	1.92	-2.34
FB373A	29.17	Late Hauterivian	*P. catulloi*	1.89	-2.28	1.90	-2.31
FB373D	29.47	Late Hauterivian	*P. catulloi*	1.91	-2.32	1.91	-2.27
FB375	29.53	Late Hauterivian	*P. catulloi*	1.92	-2.06	1.92	-2.26
FB378	29.64	Late Hauterivian	*P. catulloi*	1.91	-2.59	1.94	-2.21
FB380A	29.68	Late Hauterivian	*P. catulloi*	1.99	-1.87	1.97	-2.13
FB380B	29.80	Late Hauterivian	*P. catulloi*	2.00	-1.99	2.01	-2.12
FB382A	30.00	Late Hauterivian	*P. catulloi*	2.05	-2.26	2.03	-2.24
FB382C	30.12	Late Hauterivian	*P. catulloi*	2.05	-2.52	2.04	-2.38
FB385	30.39	Late Hauterivian	*P. catulloi*	2.04	-2.41	2.03	-2.45
FB387B	30.79	Late Hauterivian	*P. catulloi*	1.98	-2.48	2.05	-2.43
FB391	31.14	Late Hauterivian	*P. catulloi*	2.11	-2.44	2.09	-2.33
FB396B	32.60	Late Hauterivian	*P. catulloi*	2.15	-2.12	2.14	-2.23
FB402B	33.56	Late Hauterivian	*P. catulloi*	2.23	-2.00	2.15	-2.20
FB410	34.64	Late Hauterivian	*P. catulloi*	2.08	-2.44	2.13	-2.27
FB417	35.80	Early Barremian	*S. hugii*	2.09	-2.32	2.10	-2.35
FB424	37.20	Early Barremian	*S. hugii*	2.08	-2.44	2.07	-2.35
FB430A	38.27	Early Barremian	*S. hugii*	2.09	-2.24	2.02	-2.32
FB433	39.43	Early Barremian	*S. hugii*	1.90	-2.28	1.98	-2.30
FB440A	40.43	Early Barremian	*S. hugii*	1.91	-2.40	1.97	-2.26
FB448B	41.71	Early Barremian	*S. hugii*	2.10	-2.10	1.97	-2.22
FB451A	42.73	Early Barremian	*S. hugii*	1.92	-2.16	1.95	-2.22
FB454B	43.91	Early Barremian	*S. hugii*	1.88	-2.32	1.91	-2.29
FB459B	44.68	Early Barremian	*S. hugii*	1.92	-2.29	1.86	-2.38
FB464A	45.73	Early Barremian	*S. hugii*	1.77	-2.73	1.82	-2.37
FB469	46.75	Early Barremian	*S. hugii*	1.78	-2.09	1.80	-2.27
FB473B	47.69	Early Barremian	*S. hugii*	1.77	-2.11	1.82	-2.16
FB480A	48.62	Early Barremian	*S. hugii*	1.89	-2.12	1.89	-2.13
FB487	49.54	Early Barremian	*S. hugii*	1.99	-2.16	1.96	-2.20
FB494B	50.59	Early Barremian	*S. hugii*	2.12	-2.20		
FB499A	51.35	Early Barremian	*S. hugii*	1.82	-2.63		

Table An.1.2: Carbon and oxygen stable-isotope data for the Fiume-Bosso section.

Sample ID	Depth (m)	Stage	Ammonite Zone	Non-treated data (‰VPDB)		Five points moving average (‰VPDB)	
				$\delta^{13}C$	$\delta^{18}O$	$\delta^{13}C$ smooth	$\delta^{18}O$ smooth
VCD1A	0.20	Late Hauterivian	*S.sayni*	0.85	-2.82		
VCD3A	2.57	Late Hauterivian	*S.sayni*	0.86	-2.59		
VCD4A	3.62	Late Hauterivian	*S.sayni*	0.99	-2.56	0.91	-2.61
VCD6A	5.26	Late Hauterivian	*S.sayni*	0.88	-2.63	0.90	-2.63
VCD9A	7.17	Late Hauterivian	*S.sayni*	0.89	-2.62	0.87	-2.71
VCD13A	8.68	Late Hauterivian	*S.sayni*	0.79	-2.90	0.86	-2.80
VCD15A	10.13	Late Hauterivian	*S.sayni*	0.88	-2.93	0.88	-2.83
VCD18A	11.48	Late Hauterivian	*S.sayni*	0.96	-2.69	0.92	-2.80
VCD21A	12.63	Late Hauterivian	*S.sayni*	0.92	-2.82	0.96	-2.76
VCD24A	14.31	Late Hauterivian	*S.sayni*	1.04	-2.69	0.97	-2.77
VCD27A	15.66	Late Hauterivian	*S.sayni*	0.95	-2.79	0.96	-2.78
VCD29A	16.71	Late Hauterivian	*S.sayni*	0.89	-2.88	0.95	-2.73
SDII1	21.12	Late Hauterivian	*S.sayni*	1.00	-2.59	0.96	-2.63
SDII3	22.23	Late Hauterivian	*S.sayni*	0.99	-2.41	0.97	-2.55
SDII5	23.62	Late Hauterivian	*S.sayni*	0.90	-2.56	0.97	-2.53
SDII6	24.67	Late Hauterivian	*S.sayni*	1.03	-2.60	0.99	-2.55
SDII7C	26.84	Late Hauterivian	*S.sayni*	0.97	-2.53	1.02	-2.56
SDII10	28.55	Late Hauterivian	*S.sayni*	1.12	-2.52	1.03	-2.57
SDII11	29.80	Late Hauterivian	*S.sayni*	0.97	-2.68	1.03	-2.57
SDII13A	30.98	Late Hauterivian	*S.sayni*	1.00	-2.57	1.02	-2.52
SDII14	32.04	Late Hauterivian	*S.sayni*	1.09	-2.26	1.03	-2.49
SDII15	33.88	Late Hauterivian	*S.sayni*	0.98	-2.62	1.04	-2.50
SDII16B	34.60	Late Hauterivian	*S.sayni*	1.11	-2.53	1.05	-2.50
SDII18	36.05	Late Hauterivian	*B. balearis*	1.01	-2.51	1.06	-2.44
SDII19	37.30	Late Hauterivian	*B. balearis*	1.08	-2.23	1.07	-2.37
SDII21	38.91	Late Hauterivian	*B. balearis*	1.11	-2.35	1.08	-2.38
SDII23	40.26	Late Hauterivian	*B. balearis*	1.06	-2.43	1.08	-2.45
SDII25	42.36	Late Hauterivian	*B. balearis*	1.08	-2.66	1.08	-2.50
SDII27	44.50	Late Hauterivian	*B. balearis*	1.09	-2.42	1.10	-2.48
SDII28	45.82	Late Hauterivian	*B. balearis*	1.14	-2.43	1.10	-2.44
SDII30	47.46	Late Hauterivian	*B. balearis*	1.07	-2.40	1.11	-2.39
SDII33	50.19	Late Hauterivian	*B. balearis*	1.14	-2.41	1.13	-2.34
SDII34	52.10	Late Hauterivian	*B. balearis*	1.17	-2.17	1.14	-2.31
SDII36	53.78	Late Hauterivian	*B. balearis*	1.16	-2.28	1.13	-2.35
SDII40	55.55	Late Hauterivian	*B. balearis*	1.08	-2.52	1.11	-2.44
VCDII51A	57.03	Late Hauterivian	*B. balearis*	1.07	-2.64	1.10	-2.48
SDII42	57.20	Late Hauterivian	*B. balearis*	1.12	-2.29	1.12	-2.45
VCDII50A	57.46	Late Hauterivian	*B. balearis*	1.17	-2.45	1.15	-2.43
SDII43	57.92	Late Hauterivian	*P. angulicostata*	1.17	-2.42	1.16	-2.43
VCDII49A	58.18	Late Hauterivian	*P. angulicostata*	1.14	-2.56	1.15	-2.40
VCDII48A	58.91	Late Hauterivian	*P. angulicostata*	1.14	-2.15	1.12	-2.36
VCDII46A	60.82	Late Hauterivian	*P. angulicostata*	1.08	-2.41	1.08	-2.33
VCDII44A	62.46	Late Hauterivian	*P. angulicostata*	1.02	-2.37	1.07	-2.33
VCDII42A	63.87	Late Hauterivian	*P. angulicostata*	1.06	-2.19	1.07	-2.32
VCDII40A	64.63	Late Hauterivian	*P. angulicostata*	1.19	-2.52	1.06	-2.31
SDII51	64.99	Late Hauterivian	*P. angulicostata*	0.93	-2.02	1.04	-2.35
VCDII37A	67.07	Late Hauterivian	*P. angulicostata*	1.01	-2.60	1.04	-2.44
VCDII35A	68.22	Late Hauterivian	*P. angulicostata*	1.10	-2.53	1.07	-2.52
VCDII33A	69.47	Late Hauterivian	*P. angulicostata*	1.08	-2.63	1.11	-2.50
VCDII30A	71.47	Late Hauterivian	*P. angulicostata*	1.15	-2.39	1.15	-2.41
VCDII27A	72.82	Late Hauterivian	*P. angulicostata*	1.22	-2.12	1.17	-2.37
VCDII25A	74.43	Late Hauterivian	*P. angulicostata*	1.14	-2.53	1.19	-2.41
VCDII22A	75.95	Late Hauterivian	*P. angulicostata*	1.28	-2.55	1.19	-2.47
VCDII19A	77.56	Late Hauterivian	*P. angulicostata*	1.09	-2.45	1.20	-2.43
VCDII16A	79.79	Late Hauterivian	*P. angulicostata*	1.24	-2.38	1.27	-2.31
VCDII12A	81.18	Late Hauterivian	*P. angulicostata*	1.43	-2.02	1.35	-2.23
VCDII10A	82.69	Late Hauterivian	*P. angulicostata*	1.45	-2.23	1.40	-2.24
VCDII8A	84.40	Late Hauterivian	*P. angulicostata*	1.37	-2.39	1.39	-2.32
SD42	85.39	Late Hauterivian	*P. angulicostata*	1.34	-2.39	1.38	-2.35
VCDII6A	86.24	Late Hauterivian	*P. angulicostata*	1.42	-2.34	1.38	-2.31
SD38	87.19	Late Hauterivian	*P. angulicostata*	1.35	-2.20	1.40	-2.26
SD36	87.85	Late Hauterivian	*P. angulicostata*	1.45	-2.17	1.40	-2.21
SD32	89.46	Late Hauterivian	*P. angulicostata*	1.37	-2.34	1.39	-2.15
SD29	91.17	Late Hauterivian	*P. angulicostata*	1.39	-1.84	1.37	-2.10
SD27	91.93	Late Hauterivian	*P. angulicostata*	1.33	-2.21	1.35	-2.07
SD24	93.18	Late Hauterivian	*P. angulicostata*	1.38	-2.02	1.32	-2.08
SD21	94.30	Late Hauterivian	*P. angulicostata*	1.26	-2.07	1.27	-2.10
SD19	95.55	Early Barremian	*A. hugii*	1.15	-2.22	1.24	-2.09
SD16	96.70	Early Barremian	*A. hugii*	1.31	-1.94	1.22	-2.07
SD12	97.92	Early Barremian	*A. hugii*	1.20	-2.13	1.21	-2.06
SD8	99.33	Early Barremian	*A. hugii*	1.14	-1.98	1.18	-2.08
SD5	99.99	Early Barremian	*A. hugii*	1.19	-2.16		
SD1	101.57	Early Barremian	*A. hugii*	1.07	-2.21		

Tavle An.1.1: Carbon and oxygen stable-isotope data for the Veveyse de Châtel Saint Denis section.

ANNEXE 2.

XRD DATA (BULK ROCK AND CLAY FRACTION)

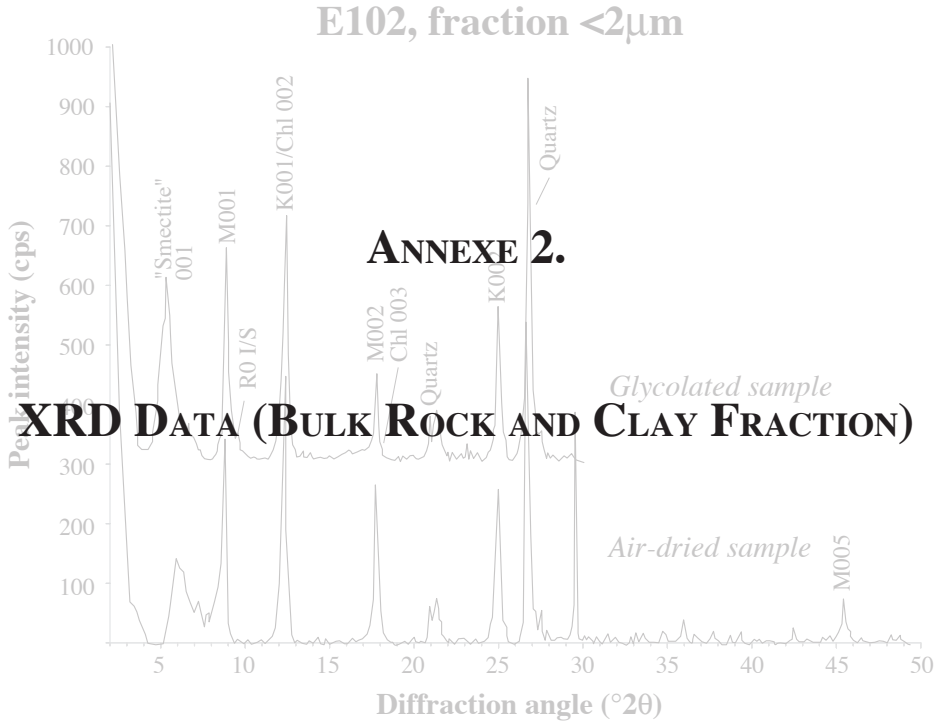

Table An.2.1: data of XRD analysis of bulk-rock samples from the Angles section.

Sample ID	Depth (m)	Stage	Ammonite Zone	Lithology	Peak Intensity (cps)								Quantification (%)						Detritism Index
					Phyllo-silicates *19.8°2θ*	Quartz *26.65°2θ*	K-Feldspar *27.5°2θ*	Na-Plagioclase *27.9°2θ*	Calcite *29.43°2θ*	Ankerite-Dolomite *30.83-30.9°2θ*	Pyrite *56.3°2θ*	Goethite *21.2°2θ*	Phyllo-silicates	Quartz	K-Feldspar	Na-Plagioclase	Calcite	Unquan.	*Cc / (Qz + Phy)* [cps]
AN2	0.34	Late Hauterivian	*B.balearis*	limestone	22	778	0	0	6455	0	0	0	5.17	5.43	0.00	0.00	88.84	0.57	8.07
AN2b	0.50	Late Hauterivian	*B.balearis*	marlstone	28	559	0	24	2452	0	0	0	13.71	8.62	0.00	0.97	65.53	11.17	4.18
AN4	1.68	Late Hauterivian	*B.balearis*	limestone	18	741	0	0	5516	0	0	0	5.00	6.48	0.00	0.00	83.64	4.87	7.26
AN6	2.85	Late Hauterivian	*B.balearis*	limestone	2	678	0	0	5391	0	0	0	0.55	5.87	0.00	0.07	80.88	12.63	7.93
AN6b	3.02	Late Hauterivian	*B.balearis*	marlstone	33	640	16	28	2478	0	0	0	16.20	9.90	0.84	1.13	66.41	5.51	3.68
AN8	4.03	Late Hauterivian	*B.balearis*	limestone	30	559	8	20	5199	0	0	0	8.11	4.76	0.23	0.45	76.73	9.71	8.82
AN10	4.87	Late Hauterivian	*B.balearis*	limestone	29	578	0	16	5229	0	0	0	7.86	4.93	0.00	0.36	77.37	9.47	8.62
AN10b	5.20	Late Hauterivian	*B.balearis*	marlstone	39	790	22	22	2118	14	0	0	18.08	11.53	1.09	0.84	53.61	14.68	2.55
AN13	6.38	Late Hauterivian	*B.balearis*	limestone	12	608	0	0	5694	0	0	0	3.39	5.41	0.00	0.00	87.85	3.35	9.19
AN15.1	7.38	Late Hauterivian	*B.balearis*	limestone	6	643	0	0	5392	0	0	0	1.65	5.57	0.00	0.00	80.92	11.86	8.31
AN15.1b	7.72	Late Hauterivian	*B.balearis*	marlstone	34	827	15	19	2616	0	0	0	17.03	13.04	0.80	0.78	66.50	1.85	3.04
AN16	8.39	Late Hauterivian	*B.balearis*	limestone	15	503	0	10	4973	0	0	0	3.85	4.20	0.00	0.21	72.05	19.69	9.61
AN18	9.56	Late Hauterivian	*B.balearis*	limestone	24	514	0	0	5315	0	0	0	6.56	4.42	0.00	0.00	79.32	9.69	9.88
AN18b	9.90	Late Hauterivian	*B.balearis*	marlstone	25	551	0	17	2711	0	0	14	13.01	9.03	0.00	0.73	75.00	1.05	4.71
AN20	10.40	Late Hauterivian	*B.balearis*	limestone	8	516	0	0	5624	0	0	0	2.25	4.57	0.00	0.00	86.28	6.91	10.73
AN23	11.00	Late Hauterivian	*B.balearis*	limestone	17	482	0	0	5481	0	0	0	4.58	4.21	0.00	0.00	83.04	8.17	11.00
AN23b	11.20	Late Hauterivian	*B.balearis*	marlstone	30	612	0	27	2565	0	0	0	14.94	9.60	0.00	1.11	69.74	4.61	4.00
AN26	12.42	Late Hauterivian	*B.balearis*	limestone	12	599	5	0	5521	0	0	0	3.34	5.25	0.15	0.00	83.87	7.40	9.04
AN27.2b	13.59	Late Hauterivian	*B.balearis*	marlstone	40	725	29	38	924	0	0	0	15.67	8.95	1.21	1.23	19.76	53.18	1.21
AN29	14.43	Late Hauterivian	*B.balearis*	limestone	15	300	0	0	4967	0	0	0	3.85	3.18	0.00	0.00	72.03	20.94	15.82
AN 29b	14.93	Late Hauterivian	*B.balearis*	marlstone	0	789	0	0	4227	0	0	0	13.68	6.18	0.00	0.43	57.38	22.33	5.36
AN 30b	15.25	Late Hauterivian	*B.balearis*	marlstone	0	1044	0	0	3596	0	0	0	10.39	7.76	0.30	0.72	51.36	29.36	3.44
AN31	15.60	Late Hauterivian	*B.balearis*	limestone	20	380	0	6	4831	0	0	0	5.12	2.67	0.00	0.13	69.26	22.81	12.10
AN 31b	16.35	Late Hauterivian	*B.balearis*	marlstone	0	715	0	0	3210	0	0	0	11.18	5.24	0.00	1.09	45.80	36.04	4.49
AN32b	16.55	Late Hauterivian	*B.balearis*	marlstone	100	1703	0	72	2357	0	0	0	21.36	11.46	0.89	1.27	37.48	27.55	1.31
AN33	16.70	Late Hauterivian	*B.balearis*	limestone	10	323	0	0	5540	0	0	0	2.79	2.78	0.00	0.00	84.50	9.93	16.63
AN 33b	16.95	Late Hauterivian	*B.balearis*	marlstone	84	1410	0	68	2966	0	0	0	18.81	9.94	0.74	1.26	36.26	32.99	1.99
AN 34b	17.45	Late Hauterivian	*B.balearis*	marlstone	0	808	0	0	5301	0	0	0	13.35	6.93	0.46	0.00	78.83	0.43	6.56
AN35	17.95	Late Hauterivian	*B.balearis*	limestone	13	316	0	0	5582	0	0	0	3.65	2.74	0.00	0.00	85.47	8.14	16.98
AN 35b	17.95	Late Hauterivian	*B.balearis*	marlstone	0	1146	0	0	4344	0	0	0	13.43	9.14	0.35	0.84	60.09	15.34	3.79
AN 37b	18.50	Late Hauterivian	*S. angulicostatum*	marlstone	77	1434	0	0	3363	0	0	0	17.78	10.42	1.08	0.97	47.37	22.37	2.23
AN38	18.79	Late Hauterivian	*S. angulicostatum*	limestone	0	310	0	0	4775	0	0	0	0.00	3.29	0.06	0.00	68.12	28.54	15.38
AN38b	18.96	Late Hauterivian	*S. angulicostatum*	marlstone	76	1333	0	67	3280	0	0	0	17.44	9.63	0.68	1.27	41.08	29.89	2.33
AN39b	19.30	Late Hauterivian	*S. angulicostatum*	marlstone	100	1563	0	82	4642	0	0	0	22.65	12.62	0.96	1.73	61.99	0.71	2.79
AN40	19.63	Late Hauterivian	*S. angulicostatum*	limestone	7	399	2	0	5526	0	0	0	1.95	4.53	0.00	0.00	84.04	9.48	13.60
AN40b	19.97	Late Hauterivian	*S. angulicostatum*	marlstone	0	1016	0	0	2446	0	0	0	10.84	6.94	0.37	0.61	43.95	37.29	2.41
AN41b	20.13	Late Hauterivian	*S. angulicostatum*	marlstone	75	1711	79	61	2213	0	0	0	15.89	11.41	1.78	1.07	35.59	34.18	1.24
AN42b	20.47	Late Hauterivian	*S. angulicostatum*	marlstone	77	1446	0	62	2840	0	0	0	17.08	10.10	0.47	1.13	40.39	30.82	1.86
AN43	20.64	Late Hauterivian	*S. angulicostatum*	limestone	15	516	0	25	6183	0	0	0	4.44	5.05	0.00	0.61	89.82	0.09	11.64
AN43b	20.64	Late Hauterivian	*S. angulicostatum*	marlstone	0	1022	0	0	4035	0	0	0	12.95	7.86	0.36	0.79	53.80	24.25	3.95
AN44b	20.97	Late Hauterivian	*S. angulicostatum*	marlstone	0	1687	0	0	4322	0	0	0	16.89	13.20	0.53	0.64	58.61	10.13	2.56
AN45b	21.31	Late Hauterivian	*S. angulicostatum*	marlstone	164	2033	102	126	1272	0	0	0	32.62	12.73	2.16	2.07	31.81	18.28	0.58
AN46	21.48	Late Hauterivian	*S. angulicostatum*	limestone	7	542	0	0	5800	0	0	0	2.00	4.60	0.00	0.00	90.42	2.98	10.57
AN46b	21.81	Late Hauterivian	*S. angulicostatum*	marlstone	92	1463	84	105	1176	0	0	0	18.18	9.10	1.77	1.71	32.69	36.48	0.76
AN48b	22.65	Late Hauterivian	*S. angulicostatum*	marlstone	91	1974	0	0	3450	0	0	0	21.01	14.35	0.49	1.28	43.48	19.39	1.67
AN49.1	22.82	Late Hauterivian	*S. angulicostatum*	limestone	16	511	0	0	6086	0	0	0	4.70	3.57	0.00	0.00	91.54	0.20	11.54
AN50	23.32	Late Hauterivian	*S. angulicostatum*	limestone	15	386	0	0	5672	0	0	0	4.24	2.60	0.00	0.00	87.57	5.58	14.14
AN51	23.83	Late Hauterivian	*S. angulicostatum*	limestone	19	292	0	8	5549	0	0	0	5.31	2.68	0.33	0.18	84.70	6.79	17.84
AN51b	24.16	Late Hauterivian	*S. angulicostatum*	marlstone	0	302	0	0	4980	0	0	0	7.19	2.53	0.00	0.00	72.39	17.78	16.49
AN52	24.34	Late Hauterivian	*S. angulicostatum*	limestone	15	304	11	0	5456	0	0	0	4.16	1.83	0.00	0.00	82.67	11.34	17.10
AN 52b	24.50	Late Hauterivian	*S. angulicostatum*	marlstone	0	716	0	0	3907	0	0	0	11.16	5.47	0.67	0.56	51.75	30.39	5.46
AN53.1b	24.83	Late Hauterivian	*S. angulicostatum*	marlstone	0	357	0	0	5002	0	0	0	6.93	2.99	0.00	0.24	72.74	17.10	14.01
AN53.2	25.00	Late Hauterivian	*S. angulicostatum*	limestone	13	209	0	0	5028	0	0	0	3.48	1.84	0.00	0.00	73.39	21.30	22.64
AN55	25.34	Late Hauterivian	*P.mortilleti*	limestone	10	218	0	0	5874	0	0	0	2.88	3.16	0.00	0.00	92.33	1.63	25.72
AN62.1	27.85	Late Hauterivian	*P.mortilleti*	limestone	4	349	0	0	5457	0	0	0	1.11	2.70	0.00	0.00	82.62	13.57	15.46
AN65.1	28.86	Late Hauterivian	*P.mortilleti*	limestone	14	309	0	0	5261	0	0	0	3.68	2.16	0.00	0.00	78.34	15.82	16.31
AN68	30.54	Late Hauterivian	*P.mortilleti*	limestone	16	251	0	5	5563	0	0	0	4.48	3.20	0.00	0.12	84.99	7.22	20.80
AN71	32.00	Late Hauterivian	*P.mortilleti*	limestone	13	363	0	0	5719	0	0	0	3.69	3.26	0.00	0.00	88.63	4.42	15.22
AN72	32.50	Early Barremian	*A.kiliani*	limestone	19	365	0	0	5080	0	0	0	5.10	2.68	0.00	0.00	74.43	17.79	13.23
AN72b	32.72	Early Barremian	*A.kiliani*	marlstone	99	1583	0	0	4640	0	0	0	22.28	12.73	0.54	0.67	62.67	1.11	2.76

Sample ID	Depth (m)	Stage	Ammonite Zone	Lithology	Peak Intensity (cps)								Quantification (%)						Detritism Index
					Phyllo-silicates *19.8°2θ*	Quartz *26.65°2θ*	K-Feldspar *27.5°2θ*	Na-Plagioclase *27.9°2θ*	Calcite *29.43°2θ*	Ankerite-Dolomite *30.83-30.9°2θ*	Pyrite *56.3°2θ*	Goethite *21.2°2θ*	Phyllo-silicates	Quartz	K-Feldspar	Na-Plagioclase	Calcite	Unquan.	*Cc / (Qz + Phy)* [cps]
AN75	34.06	Early Barremian	*A.kiliani*	limestone	6	317	0	0	6111	0	0	0	1.77	4.07	0.00	0.00	94.13	0.04	18.92
AN78	35.74	Early Barremian	*A.kiliani*	limestone	18	439	0	0	6169	0	0	0	5.32	4.84	0.00	0.00	89.55	0.29	13.49
AN81	37.08	Early Barremian	*A.kiliani*	limestone	18	519	0	0	6231	0	0	0	5.35	4.52	0.00	0.07	89.16	0.89	11.59
AN81b	37.42	Early Barremian	*A.kiliani*	marlstone	56	568	0	13	1861	0	0	0	25.07	8.01	0.00	0.48	45.47	20.98	2.98
AN84	38.93	Early Barremian	*A.kiliani*	limestone	16	482	0	0	5842	0	0	0	4.59	4.57	0.00	0.00	90.43	0.41	11.73
AN84b	39.26	Early Barremian	*A.kiliani*	limestone	34	514	0	18	2690	0	0	0	17.32	8.25	0.00	0.76	71.82	1.86	4.91
AN87	40.44	Early Barremian	*A.kiliani*	limestone	25	507	0	0	5500	0	0	0	6.96	2.99	0.00	0.00	83.57	6.47	10.34
AN87b	41.11	Early Barremian	*A.kiliani*	marlstone	43	1016	13	26	1720	0	0	11	19.00	14.13	0.61	0.95	41.47	23.05	1.62
AN89	41.95	Early Barremian	*A.kiliani*	limestone	22	342	0	10	5892	0	0	0	6.34	3.63	0.00	0.24	89.69	0.10	16.20
AN90 haut	42.95	Early Barremian	*A.kiliani*	limestone	10	400	0	15	4598	0	0	0	2.57	3.06	0.05	0.32	64.62	29.38	11.21
AN90b	43.46	Early Barremian	*A.kiliani*	marlstone	35	659	0	72	1984	20	0	0	15.90	9.42	0.00	2.70	49.18	22.57	2.86
AN92	44.80	Early Barremian	*A.kiliani*	limestone	22	377	2	0	5992	0	0	0	6.40	3.43	0.00	0.00	89.19	0.97	15.01
AN93 haut	46.14	Early Barremian	*A.kiliani*	limestone	0	374	0	0	5360	0	0	0	0.00	2.76	0.00	0.00	80.46	16.78	14.32
AN93b	46.48	Early Barremian	*A.kiliani*	marlstone	41	852	15	41	1723	0	0	0	17.86	11.69	0.70	1.47	40.97	27.31	1.93
AN95 bas	47.99	Early Barremian	*K.nicklesi*	limestone	0	319	0	0	5277	0	0	0	0.00	3.36	0.00	0.00	78.59	18.05	16.53
AN97b	49.83	Early Barremian	*K.nicklesi*	marlstone	40	678	10	19	2051	0	0	0	18.38	9.81	0.49	0.72	51.43	19.18	2.86
AN98 haut	50.50	Early Barremian	*K.nicklesi*	limestone	0	391	0	0	4885	0	0	0	0.00	2.07	0.00	0.00	70.44	27.50	12.49
AN101	52.18	Early Barremian	*K.nicklesi*	limestone	20	120	0	0	5059	0	0	0	5.36	2.20	0.00	0.00	74.03	18.41	36.14
AN101b	52.52	Early Barremian	*K.nicklesi*	marlstone	40	584	0	14	2402	0	0	0	19.43	8.93	0.00	0.56	63.70	7.37	3.85
AN103	53.86	Early Barremian	*K.nicklesi*	limestone	0	249	0	0	4994	0	0	0	0.00	2.27	0.00	0.00	72.66	25.07	20.09
AN103b	54.53	Early Barremian	*K.nicklesi*	marlstone	35	379	0	24	2359	0	0	0	16.94	5.78	0.00	0.96	62.33	13.99	5.70
AN104	55.20	Early Barremian	*K.nicklesi*	limestone	11	260	0	0	6291	0	0	0	3.30	2.95	0.00	0.00	92.86	0.89	23.18
AN105	56.38	Early Barremian	*K.nicklesi*	limestone	27	271	0	6	5712	0	0	0	7.66	3.07	0.00	0.14	88.46	0.67	19.20
AN108	59.56	Early Barremian	*K.nicklesi*	limestone	24	312	0	0	5605	0	0	0	6.75	2.65	0.00	0.00	86.01	4.60	16.66
AN109.4	61.07	Early Barremian	*N.pulchella*	limestone	20	343	0	0	5921	0	0	0	5.79	2.47	0.00	0.00	91.54	0.20	16.30
AN110.1b	62.25	Early Barremian	*N.pulchella*	limestone	13	300	0	0	5113	0	0	0	3.50	1.78	0.00	0.00	75.19	19.53	16.36
AN110.3c	64.09	Early Barremian	*N.pulchella*	limestone	7	271	0	0	5555	0	0	0	1.96	1.38	0.00	0.00	84.97	11.69	19.95
AN110.4	65.27	Early Barremian	*N.pulchella*	limestone	0	210	0	0	5354	0	0	0	0.00	1.58	0.00	0.00	80.42	18.00	25.51
AN111.2	66.28	Early Barremian	*N.pulchella*	limestone	0	157	0	0	5326	0	0	0	0.00	2.12	0.00	0.00	79.77	18.11	34.00
AN111.5	67.28	Early Barremian	*N.pulchella*	limestone	21	183	0	0	5178	0	0	0	5.69	1.85	0.00	0.00	76.57	15.89	25.41
AN112.2	68.79	Early Barremian	*N.pulchella*	limestone	25	246	0	12	5662	0	0	0	7.06	2.31	0.00	0.28	87.34	3.01	20.93
AN114.2	72.99	Early Barremian	*K.compressissima*	limestone	10	217	0	7	4762	0	0	0	2.61	1.66	0.00	0.15	67.97	27.61	20.95
AN115	73.99	Early Barremian	*K.compressissima*	limestone	8	260	0	0	4368	0	0	0	2.03	1.26	0.00	0.00	60.39	36.33	16.30
AN116b	74.83	Early Barremian	*K.compressissima*	marlstone	27	671	0	22	2336	0	0	0	12.96	10.14	0.00	0.87	61.18	14.86	3.35
AN117	75.17	Early Barremian	*K.compressissima*	limestone	1	128	0	0	5679	0	0	0	0.28	2.26	0.15	0.09	87.77	9.44	43.95
AN119	76.34	Early Barremian	*K.compressissima*	limestone	5	202	0	0	5362	0	0	0	1.38	2.24	0.00	0.02	80.55	15.82	25.95
AN119b	77.01	Early Barremian	*K.compressissima*	marlstone	25	648	10	31	1796	13	0	0	11.07	9.04	0.47	1.13	43.41	34.73	2.67
AN121	78.36	Early Barremian	*K.compressissima*	limestone	12	158	0	0	6259	0	0	0	3.59	2.19	0.00	0.00	94.10	0.12	36.88
AN123	78.52	Early Barremian	*K.compressissima*	limestone	0	254	5	0	5671	0	0	0	0.00	2.65	0.12	0.00	87.54	9.69	22.33
AN123b	78.69	Early Barremian	*K.compressissima*	marlstone	27	522	10	43	1970	0	0	0	12.27	7.47	0.48	1.61	48.87	29.29	3.59
AN125	79.70	Early Barremian	*C.darsi*	limestone	15	258	0	0	5139	0	0	0	4.05	2.78	0.06	0.00	75.65	17.46	18.80
AN127	80.70	Early Barremian	*C.darsi*	limestone	5	233	0	0	4340	0	0	0	1.26	1.10	0.00	0.00	59.88	37.75	18.25
AN127b	81.21	Early Barremian	*C.darsi*	marlstone	98	658	22	66	1473	0	0	0	41.31	8.73	0.99	2.29	33.89	12.78	1.95
AN128	81.54	Early Barremian	*C.darsi*	limestone	14	297	4	0	5579	0	0	0	3.93	1.17	0.00	0.07	85.52	9.31	17.93
AN129	82.21	Early Barremian	*C.darsi*	limestone	21	328	2	0	5072	0	0	0	5.50	2.89	0.00	0.00	74.24	17.37	14.56
AN129b	82.55	Early Barremian	*C.darsi*	marlstone	34	611	0	18	1893	0	0	0	15.27	8.64	0.00	0.67	46.41	29.00	2.93
AN131	83.39	Early Barremian	*C.darsi*	limestone	7	138	0	0	4858	0	0	0	1.84	2.46	0.36	0.00	69.85	25.48	33.39
AN133	84.90	Early Barremian	*C.darsi*	limestone	0	132	0	0	5744	0	0	0	0.00	1.57	0.18	0.00	89.36	8.89	43.56
AN134b	85.57	Early Barremian	*C.darsi*	marlstone	68	1447	24	28	1183	13	27	19	28.57	19.15	1.07	0.97	27.13	20.90	0.78
AN136.2	86.24	Early Barremian	*C.darsi*	limestone	29	343	0	0	5010	0	0	0	7.73	3.74	0.09	0.09	72.86	15.50	13.48
AN138	86.90	Early Barremian	*C.darsi*	limestone	7	296	13	5	5582	0	0	0	1.96	2.10	0.00	0.12	85.51	10.31	18.42
AN138b	87.08	Early Barremian	*C.darsi*	marlstone	63	1232	44	60	361	141	29	0	23.58	14.52	1.75	1.85	7.37	48.86	0.28
AN139d	88.09	Early Barremian	*C.darsi*	limestone	3	175	6	0	6132	0	0	0	0.89	1.92	0.00	0.00	96.86	0.33	34.45
AN142.2b	89.93	Late Barremian	*H.uhligi*	marlstone	45	838	48	52	434	13	0	0	16.55	9.71	1.88	1.58	8.71	61.45	0.49
AN143.1a	90.44	Late Barremian	*H.uhligi*	limestone	12	446	3	0	5425	0	0	0	3.32	1.89	0.00	0.07	81.97	12.75	11.84
AN144	91.95	Late Barremian	*H.uhligi*	limestone	14	238	0	0	5404	0	0	0	3.87	2.46	0.00	0.02	81.47	12.19	21.47
AN144b	92.11	Late Barremian	*H.uhligi*	marlstone	42	836	0	33	1118	0	43	0	17.33	10.86	0.00	1.12	25.18	44.29	1.27
AN147.1	93.29	Late Barremian	*H.uhligi*	limestone	4	207	0	0	4448	0	0	0	1.02	1.43	0.00	0.06	61.89	35.60	21.09
AN148	94.13	Late Barremian	*H.sayni*	limestone	3	161	6	0	5723	0	0	0	0.85	1.54	0.00	0.00	88.87	8.74	34.91
AN148b	94.80	Late Barremian	*H.sayni*	marlstone	47	639	20	144	1321	0	0	0	19.31	8.26	0.88	4.88	29.62	37.06	1.93

Table An.2.1 (continued): data of XRD analysis of bulk-rock samples from the Angles section.

Sample ID	Depth (m)	Stage	Ammonite Zone	Lithology	Peak Intensity (cps)								Quantification (%)						Detritism Index
					Phyllo-silicates *19.8°2θ*	Quartz *26.65°2θ*	K-Feldspar *27.5°2θ*	Na-Plagioclase *27.9°2θ*	Calcite *29.43°2θ*	Ankerite-Dolomite *30.83-30.9°2θ*	Pyrite *56.3°2θ*	Goethite *21.2°2θ*	Phyllo-silicates	Quartz	K-Feldspar	Na-Plagioclase	Calcite	Unquan.	*Cc / (Qz + Phy)* [cps]
AN149.3	95.13	Late Barremian	*H.sayni*	limestone	6	217	0	0	5667	0	0	0	1.70	1.72	0.00	0.00	87.53	9.05	25.39
AN151.1	96.50	Late Barremian	*H.sayni*	limestone	1	283	0	0	4660	0	0	0	0.26	1.55	0.04	0.00	65.96	32.19	16.43
AN151.3	96.98	Late Barremian	*H.sayni*	limestone	3	178	0	0	5051	0	0	0	0.80	1.52	0.11	0.04	73.89	23.62	27.83
AN151.3b	97.10	Late Barremian	*H.sayni*	marlstone	46	533	12	61	1015	0	30	0	18.66	6.81	0.52	2.04	22.47	48.68	1.75
AN153.2	98.50	Late Barremian	*H.sayni*	limestone	0	172	0	0	5996	0	0	0	0.00	1.62	0.06	0.02	95.46	2.84	34.90
AN153.2b	98.70	Late Barremian	*H.sayni*	marlstone	48	703	34	92	1273	0	0	0	19.64	9.06	1.48	3.10	28.43	38.29	1.70
AN155.1a	98.99	Late Barremian	*H.sayni*	limestone	9	194	0	0	5365	0	0	0	2.48	2.42	0.06	0.00	80.61	14.44	26.48
AN155.2b	99.50	Late Barremian	*H.sayni*	marlstone	49	878	32	53	654	0	16	0	18.68	10.54	1.30	1.67	13.61	53.79	0.71
AN156.1	99.83	Late Barremian	*H.sayni*	limestone	14	190	1.5	0	5784	0	0	0	4.00	1.58	0.00	0.00	90.30	4.11	28.33
AN156.4	101.17	Late Barremian	*H.sayni*	limestone	8	181	4	5	5913	0	0	0	2.31	2.30	0.00	0.12	93.35	1.91	31.36
AN156.4b	101.51	Late Barremian	*H.sayni*	marlstone	35	592	32	86	2404	0	21	0	17.15	9.13	1.67	3.47	64.28	3.60	3.83
AN156.6	102.35	Late Barremian	*H.sayni*	limestone	7	176	2	0	5466	0	0	0	1.94	2.36	0.09	0.00	82.87	12.74	29.85
AN157.1b	102.68	Late Barremian	*H.sayni*	marlstone	61	661	25	79	444	0	21	0	22.81	7.78	1.00	2.44	9.06	56.38	0.61
AN158b	104.03	Late Barremian	*H.sayni*	marlstone	40	519	22	82	1733.5	0	0	0	17.53	7.16	1.03	2.96	41.46	29.87	3.10
AN160.3	104.65	Late Barremian	*G.sartousiana*	limestone	11	280	2	5	5846	0	0	0	3.16	3.11	0.00	0.12	91.64	1.97	20.09
AN160.3b	104.87	Late Barremian	*G.sartousiana*	marlstone	43	867	27	23	1703	0	35	10	19.40	12.31	1.30	0.86	41.93	22.40	1.87
AN161.1	105.03	Late Barremian	*G.sartousiana*	limestone	6	176	0	0	4487	0	0	0	1.53	1.91	0.00	0.00	62.60	33.96	24.72
AN161.2	105.54	Late Barremian	*G.sartousiana*	limestone	9	253	0	0	4346	0	0	0	2.28	0.96	0.00	0.00	59.99	36.77	16.58
AN161.2b	105.70	Late Barremian	*G.sartousiana*	marlstone	50	566	0	31	2257	0	0	0	23.73	8.46	0.00	1.21	58.47	8.13	3.66
AN164.2	107.72	Late Barremian	*H.feraudianus*	limestone	10	270	3	9	4847	0	0	0	2.63	1.23	0.00	0.20	69.69	26.25	17.30
AN166b	108.72	Late Barremian	*H.feraudianus*	marlstone	14	130	0	0	4912	0	0	0	3.71	2.07	0.00	0.04	70.97	23.20	34.13
AN168.1	109.73	Late Barremian	*I.giraudi*	limestone	29	344	0	0	6619	0	0	0	8.96	4.29	0.00	0.05	86.62	0.08	17.75
AN168.1b	109.90	Late Barremian	*I.giraudi*	marlstone	35	1049	10	52	1525	18	0	0	14.78	13.95	0.45	1.81	35.15	33.68	1.41
AN170c	110.57	Late Barremian	*I.giraudi*	limestone	21	237	0	0	4849	0	0	0	5.52	3.64	0.00	0.09	69.56	21.19	18.80
AN172.1	111.41	Late Barremian	*I.giraudi*	limestone	20	121	0	0	5698	0	0	0	5.66	3.63	0.00	0.00	88.08	2.62	40.38
AN172.1b	111.91	Late Barremian	*I.giraudi*	marlstone	37	1015	0	15	1770	0	52	18	17.18	14.84	0.00	0.57	44.86	19.55	1.68
AN173	112.58	Late Barremian	*I.giraudi*	limestone	14	154	6	0	6451	0	0	0	4.26	3.93	0.42	0.00	91.07	0.32	38.36
AN174.1b	113.59	Late Barremian	*I.giraudi*	marlstone	30	658	0	0	2942	0	0	0	15.93	11.00	0.00	0.00	72.27	0.80	4.28
AN176.1	114.43	Late Barremian	*I.giraudi*	limestone	18	148	0	0	5166	0	0	0	4.86	4.75	0.14	0.00	76.08	14.16	31.16
AN176.1b	115.10	Late Barremian	*I.giraudi*	marlstone	47	1013	24	24	2341	0	0	0	22.44	15.23	1.22	0.95	59.00	1.16	2.21
AN177	115.44	Late Barremian	*M.sarasini*	limestone	9	249	0	0	4944	0	0	0	2.38	3.81	0.00	0.00	71.50	22.31	19.18
AN179.1	116.28	Late Barremian	*M.sarasini*	limestone	14	441	0	0	5644	0	0	0	3.95	3.42	0.00	0.07	86.84	5.72	12.42
AN179.1b	116.44	Late Barremian	*M.sarasini*	marlstone	44	594	23	14	2194	11	0	13	21.10	8.97	1.18	0.55	57.44	9.62	3.44
AN181	117.79	Late Barremian	*M.sarasini*	limestone	13	439	0	0	5375	0	0	0	3.57	4.15	0.21	0.02	80.68	11.37	11.88
AN 183	118.62	Late Barremian	*M.sarasini*	limestone	3	407	0	0	4526	0	0	0	0.77	2.49	0.16	0.00	68.30	28.47	11.03
AN183b	119.00	Late Barremian	*M.sarasini*	marlstone	43	1042	0	13	2013	0	0	0	19.51	14.88	0.00	0.49	49.85	15.27	1.86
AN 185	119.97	Late Barremian	*M.sarasini*	limestone	4	411	13	0	5617	0	0	0	1.12	4.02	0.00	0.00	86.15	8.70	13.55
AN186b	120.50	Late Barremian	*M.sarasini*	marlstone	44	752	0	23	1725	0	0	0	19.23	10.35	0.00	0.83	41.15	28.45	2.17
AN188	121.64	Late Barremian	*M.sarasini*	limestone	15	559	5	0	5301	0	0	0	4.10	3.54	0.00	0.00	79.09	13.27	9.23
AN188b	122.32	Late Barremian	*M.sarasini*	marlstone	35	614	0	0	2437	0	0	0	17.10	9.45	0.00	0.00	65.00	8.44	3.76
AN190	122.82	Late Barremian	*M.sarasini*	limestone	14	457	0	0	5171	0	0	0	3.78	4.18	0.20	0.00	76.43	15.61	10.97
AN192	123.83	Late Barremian	*M.sarasini*	limestone	20	386	0	0	5934	0	0	0	5.78	4.53	0.00	0.00	89.10	0.59	14.63
AN193b	124.50	Late Barremian	*M.sarasini*	marlstone	40	624	14	73	1739	11	68	0	18.29	8.98	0.68	2.75	43.40	23.65	2.62
AN195	125.50	Late Barremian	*M.sarasini*	limestone	8	479	7	14	4797	0	0	0	2.09	3.85	0.39	0.30	69.17	24.89	9.84
AN196.2	126.68	Late Barremian	*M.sarasini*	limestone	20	309	6	0	5825	0	0	0	5.72	5.55	0.00	0.00	87.63	1.10	17.71
AN196.2b	126.90	Late Barremian	*M.sarasini*	marlstone	33	856	20	12	2172	0	0	0	15.40	12.58	0.99	0.46	55.32	15.24	2.44
AN197	127.35	Early Aptian	*D.oglanlensis*	limestone	7	454	0	0	6086	0	0	0	2.05	7.59	0.00	0.00	90.20	0.17	13.19
AN198	128.19	Early Aptian	*D.oglanlensis*	limestone	10	411	0	0	5218	7	0	6	2.71	3.80	0.00	0.00	77.29	16.14	12.39
AN198b	128.52	Early Aptian	*D.oglanlensis*	marlstone	49	619	12	26	2015	0	0	0	22.40	8.91	0.58	0.98	50.29	16.83	3.02
AN200	129.19	Early Aptian	*D.oglanlensis*	limestone	15	492	7	0	6987	6	0	0	4.82	2.70	0.00	0.00	90.50	1.93	13.79
AN201b	129.87	Early Aptian	*D.oglanlensis*	marlstone	41	647	0	42	1898	73	0	0	18.52	9.20	0.00	1.56	46.79	23.11	2.76
AN202a	130.00	Early Aptian	*D.oglanlensis*	limestone	3	497	1	0	5379	7	0	0	0.82	6.95	0.00	0.00	80.55	11.62	10.75
AN204	131.88	Early Aptian	*D.oglanlensis*	limestone	2	467	14	0	4822	0	0	0	0.52	3.86	0.00	0.00	69.01	26.60	10.27
AN206	133.22	Early Aptian	*D.oglanlensis*	limestone	14	617	0	5	5831	0	0	0	4.01	5.11	0.00	0.12	90.23	0.65	9.24
AN206b	133.89	Early Aptian	*D.oglanlensis*	marlstone	40	550	0	26	2201	0	0	11	19.12	8.28	0.00	1.03	57.44	13.28	3.73
AN210b	134.20	Early Aptian	*D.oglanlensis*	marlstone	39	830	0	24	2514	0	0	0	19.20	12.86	0.00	0.97	66.04	0.93	2.89
AN211	134.72	Early Aptian	*D.oglanlensis*	limestone	8	823	0	5	5894	0	0	7	2.30	6.47	0.00	0.12	90.15	1.08	7.09
AN214	136.22	Early Aptian	*D.oglanlensis*	limestone	5	445	0	13	4198	6	0	0	1.24	4.35	0.00	0.27	67.29	27.08	9.33
AN215b	137.40	Early Aptian	*D.oglanlensis*	marlstone	17	540	0	22	2213	0	0	0	8.02	8.02	0.00	0.86	57.00	26.10	3.97
AN216	137.72	Early Aptian	*D.oglanlensis*	limestone	0	267	0	9	5575	0	0	13	0.00	4.44	0.27	0.21	85.61	9.94	20.88

Table An.2.1 (continued): data of XRD analysis of bulk-rock samples from the Angles section.

Sample ID	Depth (m)	Stage	Ammonite Zone	Lithology	Peak Intensity, <2µm fraction (cps)														
					"Smectite" 001 5.2°2θ	Mica 001 8.8°2θ	R0 I/S 002 9-9.5°2θ	Kaolinite/ Chlorite 001/002 12.34°2θ	Mica 002 17.92°2θ	Chlorite 003 18.56°2θ	Quartz 20.85°2θ	Goethite 21.2°2θ	Kaolinite 002 24.9°2θ	Chlorite 004 25.2°2θ	K-Feldspar 27.5°2θ	Na-Plagioclase 27.9°2θ	Pyrite 28.12°2θ	Mica 005 45.68°2θ	K001* K002*(K001,C002)/ (K002+C004)	C002* C004*(K001,C002)/(K002+C004)
AN 2	0.34	Late Hauterivian	*B.balearis*	limestone	156	222	54	55	183	11	183	0	13	37	54	83	11	91	14	41
AN2b	0.50	Late Hauterivian	*B.balearis*	marlstone	644	566	269	283	244	30	85	0	175	74	110	133	50	295	199	84
AN4	1.68	Late Hauterivian	*B.balearis*	limestone	10	162	24	42	57	0	121	0	12	24	38	40	18	59	14	28
AN 6	2.85	Late Hauterivian	*B.balearis*	limestone	109	208	56	30	84	0	289	0	13	55	23	76	29	43	6	24
AN6b	3.02	Late Hauterivian	*B.balearis*	marlstone	178	168	87	73	122	0	83	0	35	13	18	110	0	107	53	20
AN8	4.03	Late Hauterivian	*B.balearis*	limestone	44	72	14	30	43	0	123	15	6	18	27	56	0	50	8	23
AN 10	4.87	Late Hauterivian	*B.balearis*	limestone	60	94	24	123	15	12	158	19	13	67	51	59	48	38	20	103
AN10b	5.20	Late Hauterivian	*B.balearis*	marlstone	693	544	342	225	299	40	67	0	237	0	110	160	14	288	225	0
AN13	6.38	Late Hauterivian	*B.balearis*	limestone	133	171	48	63	48	0	295	0	0	41	25	61	31	41	0	63
AN 15.1	7.38	Late Hauterivian	*B.balearis*	limestone	46	187	18	59	67	0	332	0	14	12	49	119	10	37	32	27
AN15.1b	7.72	Late Hauterivian	*B.balearis*	marlstone	537	649	182	150	261	12	107	0	0	81	0	130	93	171	0	150
AN16	8.39	Late Hauterivian	*B.balearis*	limestone	103	107	41	79	19	0	264	12	18	56	19	53	17	17	19	60
AN18	9.56	Late Hauterivian	*B.balearis*	limestone	65	114	33	105	87	0	225	0	24	75	28	67	30	29	25	80
AN18b	9.90	Late Hauterivian	*B.balearis*	marlstone	326	390	128	144	205	28	70	0	0	77	131	71	48	150	0	144
AN20	10.40	Late Hauterivian	*B.balearis*	limestone	48	87	41	72	42	0	167	0	17	53	23	49	15	51	17	55
AN26	12.42	Late Hauterivian	*B.balearis*	limestone	121	89	33	32	43	0	196	0	10	15	33	68	18	42	13	19
AN27.2	13.26	Late Hauterivian	*B.balearis*	limestone	40	118	25	55	123	25	118	14	43	52	57	147	0	69	25	30
AN27.2b	13.59	Late Hauterivian	*B.balearis*	marlstone	124	545	142	314	273	66	55	0	330	41	142	157	108	198	279	35
AN29	14.43	Late Hauterivian	*B.balearis*	limestone	73	203	24	211	72	0	311	0	10	76	34	96	19	76	25	186
AN 29b	14.93	Late Hauterivian	*B.balearis*	marlstone	356	797	210	279	327	77	82	0	77	128	112	98	21	81	105	174
AN31	15.60	Late Hauterivian	*B.balearis*	limestone	329	250	49	170	109	0	389	0	0	88	0	164	0	42	0	170
AN 33	16.44	Late Hauterivian	*B.balearis*	limestone	57	134	20	98	56	0	321	10	14	65	27	99	25	36	17	81
AN 33b	16.95	Late Hauterivian	*B.balearis*	marlstone	29	859	164	314	368	44	76	0	204	85	1105	131	74	327	222	92
AN 34b	17.45	Late Hauterivian	*B.balearis*	marlstone	139	356	68	72	211	0	94	10	66	56	60	83	18	126	39	33
AN35	17.95	Late Hauterivian	*B.balearis*	limestone	593	223	126	81	76	0	282	0	7	72	36	145	34	37	7	74
AN 35b	17.95	Late Hauterivian	*B.balearis*	marlstone	55	781	112	117	397	41	74	0	21	49	67	161	49	276	35	82
AN38	18.79	Late Hauterivian	*S.angulicostatum*	limestone	57	62	12	37	22	16	152	0	16	46	13	79	27	19	10	27
AN38b	18.96	Late Hauterivian	*S.angulicostatum*	marlstone	315	605	193	75	206	0	52	0	0	44	87	88	0	129	0	75
AN39b	19.30	Late Hauterivian	*S.angulicostatum*	marlstone	116	759	42	112	355	11	54	17	12	50	93	80	0	275	22	90
AN40	19.63	Late Hauterivian	*S.angulicostatum*	limestone	39	54	18	15	40	0	402	0	0	13	0	67	27	47	0	15
AN40b	19.97	Late Hauterivian	*S.angulicostatum*	limestone	83	611	92	60	312	13	43	0	0	28	118	105	0	240	0	60
AN41b	20.13	Late Hauterivian	*S.angulicostatum*	marlstone	208	1090	170	90	471	38	59	12	0	39	172	135	109	342	0	90
AN42b	20.47	Late Hauterivian	*S.angulicostatum*	marlstone	208	602	188	84	303	46	39	0	0	31	98	180	50	234	0	84
AN43	20.64	Late Hauterivian	*S.angulicostatum*	limestone	108	53	41	83	20	0	135	0	0	81	13	70	25	30	0	83
AN43b	20.64	Late Hauterivian	*S.angulicostatum*	marlstone	106	258	55	128	197	12	70	0	0	65	98	106	74	192	0	128
AN44b	20.97	Late Hauterivian	*S.angulicostatum*	marlstone	65	408	60	61	317	0	26	0	15	11	53	63	0	401	35	26
AN45b	21.31	Late Hauterivian	*S.angulicostatum*	marlstone	32	711	150	162	322	0	49	20	0	0	251	150	87	413	0	0
AN46	21.48	Late Hauterivian	*S.angulicostatum*	limestone	85	158	0	213	114	0	625	0	41	84	0	95	37	41	70	143
AN46b	21.81	Late Hauterivian	*S.angulicostatum*	marlstone	26	565	57	74	413	32	37	0	49	41	41	108	26	354	40	34
AN48b	22.65	Late Hauterivian	*S.angulicostatum*	marlstone	20	755	55	106	488	37	71	0	55	34	126	99	82	468.5	66	40
AN49.1	22.82	Late Hauterivian	*S.angulicostatum*	limestone	466	154	74	196	28	25	205	0	18	101	31	67	37	55	30	166
AN50	23.32	Late Hauterivian	*S.angulicostatum*	limestone	50	197	17	51	108	0	298	0	11	68	23	106	38	46	7	44
AN51	23.83	Late Hauterivian	*S.angulicostatum*	limestone	74	279	35	57	175	0	227	0	0	57	18	146	38	33	0	57
AN51b	24.16	Late Hauterivian	*S.angulicostatum*	marlstone	21	120	14	60	83	15	74	0	19	47	0	301	0	62	17	43
AN53.1b	24.83	Late Hauterivian	*S.angulicostatum*	marlstone	0	138	0	50	43	12	123	0	61	58	25	39	42	13	26	24
AN53.2	25.00	Late Hauterivian	*S.angulicostatum*	limestone	207	231	39	93	77	15	120	0	32	48	12	111	29	0	37	56
AN55	25.34	Late Hauterivian	*P.mortilleti*	limestone	146	162	20	71	59	0	257	42	37	40	29	170	48	43	34	37
AN62.1	27.85	Late Hauterivian	*P.mortilleti*	limestone	121	149	30	87	58	10	139	18	28	67	33	122	38	44	26	61
AN65.1	28.86	Late Hauterivian	*P.mortilleti*	limestone	119	131	16	242	93	18	205	0	25	105	172	33	12	56	47	195
AN68	30.54	Late Hauterivian	*P.mortilleti*	limestone	58	146	20	73	66	0	54	11	5	25	28	57	28	64	12	61
AN72b	32.72	Early Barremian	*A.kiliani*	marlstone	114	292	182	211	281	38	58	0	241	0	128	201	96	290	211	0
AN73b	33.22	Early Barremian	*A.kiliani*	marlstone	126	916	142	292	405	38	31	0	145	33	116	97	58	75	238	54
AN75	34.06	Early Barremian	*A.kiliani*	limestone	132	191	51	172	85	21	197	0	59	87	56	52	38	71	70	102
AN75b	34.23	Early Barremian	*A.kiliani*	marlstone	51	515	121	283	251	22	37	0	244	29	82	107	35	259	253	30
AN76b	34.56	Early Barremian	*A.kiliani*	marlstone	184	578	132	227	206	0	32	0	147	50	86	117	64	144	169	58
AN78	35.74	Early Barremian	*A.kiliani*	limestone	67	232	59	347	91	0	69	0	26	121	63	125	28	49	61	286
AN81	37.08	Early Barremian	*A.kiliani*	limestone	271	272	65	254	106	22	86	0	37	92	80	0	0	67	73	181
AN81b	37.42	Early Barremian	*A.kiliani*	marlstone	404	634	212	361	264	13	64	0	310	28	181	136	92	301	331	30
AN84	38.93	Early Barremian	*A.kiliani*	limestone	60	311	34	326	129	28	138	0	20	157	68	94	42	75	37	289
AN84b	39.26	Early Barremian	*A.kiliani*	marlstone	156	406	110	165	106	0	21	0	98	56	178	83	12	319	105	60

Table An.2.2: peak intensities for the minerals identified in the <2 µm fraction of samples from the Angles section.

Sample ID	Depth (m)	Stage	Ammonite Zone	Lithology	Peak Intensity, <2µm fraction (cps)														
					"Smectite"	Mica	R0 I/S	Kaolinite/ Chlorite	Mica	Chlorite	Quartz	Goethite	Kaolinite	Chlorite	K-Feldspar	Na-Plagioclase	Pyrite	Mica	K001*	C002*
					001 **5.2°2θ**	*001* **8.8°2θ**	*002* **9-9.5°2θ**	*001/002* **12.34°2θ**	*002* **17.92°2θ**	*003* **18.56°2θ**	**20.85°2θ**	**21.2°2θ**	*002* **24.9°2θ**	*004* **25.2°2θ**	**27.5°2θ**	**27.9°2θ**	**28.12°2θ**	*005* **45.68°2θ**	K002*(K001,C002)/ (K002+C004)	C004*(K001,C002)/(K002+C004)
AN87	40.44	Early Barremian	*A.kiliani*	limestone	29	262	25	447	213	58	203	0	110	377	27	202	40	31	101	346
AN87b	41.11	Early Barremian	*A.kiliani*	marlstone	34	478	41	297	205	0	42	0	177	43	81	100	14	244	239	58
AN89	41.95	Early Barremian	*A.kiliani*	limestone	96	397	52	196	139	0	100	0	77	101	41	186	47	59	85	111
AN90 haut	42.95	Early Barremian	*A.kiliani*	limestone	71	303	80	386	165	92	120	0	32	257	80	149	50	113	43	343
AN90b	43.46	Early Barremian	*A.kiliani*	marlstone	105	365	119	302	155	28	82	0	234	59	78	93	23	233	241	61
AN92	44.80	Early Barremian	*A.kiliani*	limestone	41	230	38	179	82	18	89	10	66	77	42	123	37	64	83	96
AN93 haut	46.14	Early Barremian	*A.kiliani*	limestone	58	249	24	450	156	89	189	11	69	262	82	227	75	130	94	356
AN93b	46.48	Early Barremian	*A.kiliani*	marlstone	51	735	74	408	260	0	31	0	271	38	101	172	61	206	358	50
AN95 bas	47.99	Early Barremian	*K.nicklesi*	limestone	56	293	72	270	107	31	87	0	37	137	85	138	32	67	57	213
AN97	49.50	Early Barremian	*K.nicklesi*	limestone	75	312	27	141	201	35	268	0	30	167	49	206	47	143	21	120
AN97b	49.83	Early Barremian	*K.nicklesi*	marlstone	68	264	28	184	166	0	51	0	192	71	58	94	31	139	134	50
AN98 haut	50.50	Early Barremian	*K.nicklesi*	limestone	50	171	19	124.5	1220	13	146	0	33	109	75	72	22	84	29	96
AN101	52.18	Early Barremian	*K.nicklesi*	limestone	185	359	58	204	128	28	161	0	40	143	40	159	62	39	45	159
AN101b	52.52	Early Barremian	*K.nicklesi*	marlstone	214	536	103	285	174	12	36	0	121	130	138	149	39	132	137	148
AN103	53.86	Early Barremian	*K.nicklesi*	limestone	30	87	23	174	48	21	47	0	31	182	46	46	37	41	25	149
AN103b	54.53	Early Barremian	*K.nicklesi*	marlstone	137	277	72	112	127	0	59	0	99	23	79	115	14	76	91	21
AN104	55.20	Early Barremian	*K.nicklesi*	limestone	124	463	121	291	191	50	180	0	31	133	41	202	78	70	55	236
AN105	56.38	Early Barremian	*K.nicklesi*	limestone	45	400	28	129	188	20	124	0	46	56	101	160	51	89	58	71
AN108	59.56	Early Barremian	*K.nicklesi*	limestone	144	544	71	216	191	42	134	0	92	144	69	201	34	32	84	132
AN109.4	61.07	Early Barremian	*N.pulchella*	limestone	66	233	68	296	116	40	137	0	139	235	56	147	47	92	110	186
AN110.1b	62.25	Early Barremian	*N.pulchella*	marlstone	42	305	81	522	192	82	140	0	150	346	87	185	49	116	158	364
AN 110.3c	64.09	Early Barremian	*N.pulchella*	limestone	56	498	48	212	165	51	344	0	26	123	68	140	54	134	37	175
AN110.4	65.27	Early Barremian	*N.pulchella*	limestone	19	546	58	221	256	59	228	0	58	87	73	127	91	60	88	133
AN111.2	66.28	Early Barremian	*N.pulchella*	limestone	15	395	59	80	136	14	115	0	63	17	72	59	39	116	63	17
AN111.5	67.28	Early Barremian	*N.pulchella*	limestone	61	432	50	187	204	85	161	0	63	112	56	118	0	49	67	120
AN112.2	68.79	Early Barremian	*N.pulchella*	limestone	96	210	46	114	117	25	77	18	25	22	44	68	28	52	61	53
AN112.7	71.64	Early Barremian	*K.compressissima*	limestone	44	244	73	113	103	22	124	0	44	56	86	78	39	53	50	63
AN114.2	72.99	Early Barremian	*K.compressissima*	limestone	23	369	51	56	139	14	189	11	15	26	66	129	44	100	20	36
AN115	73.99	Early Barremian	*K.compressissima*	limestone	90	406	127	396	168	85	288	0	51	213	32	245	56	47	77	320
AN116b	74.83	Early Barremian	*K.compressissima*	marlstone	88	298	56	265	139	0	72	0	228	71	42	124	50	99	202	63
AN117	75.17	Early Barremian	*K.compressissima*	limestone	26	326	32	426	90	83	141	0	47	231	45	219	52	68	72	354
AN119	76.34	Early Barremian	*K.compressissima*	limestone	45	277	36	1034	128	133	228	0	86	342	14	166	30	109	208	826
AN119b	77.01	Early Barremian	*K.compressissima*	marlstone	60	374	118	113	169	0	49	0	110	32	103	134	54	158	88	25
AN 121	78.36	Early Barremian	*K.compressissima*	limestone	75	271	74	279	117	43	202	0	45	77	44	197	0	73	103	176
AN123	78.52	Early Barremian	*K.compressissima*	limestone	33	125	112	268	246	34	290	0	68	179	72	276	47	107	74	194
AN123b	78.69	Early Barremian	*K.compressissima*	marlstone	55	553	73	315	197	0	51	0	208	34	84	94	25	125	271	44
AN125	79.70	Early Barremian	*C.darsi*	limestone	314	148	69	285	44	36	106	11	123	146	74	108	34	18	130	155
AN127	80.70	Early Barremian	*C.darsi*	limestone	22	367	80	514	177	126	323	12	183	318	46	215	60	115	188	326
AN127b	81.21	Early Barremian	*C.darsi*	marlstone	36	136	77	56	51	10	38	0	78	37	39	117	27	36	38	18
AN128	81.54	Early Barremian	*C.darsi*	limestone	124	329	85	183	114	52	492	12	17	86	53	272	55	89.5	30	153
AN129	82.21	Early Barremian	*C.darsi*	limestone	91	126	33	227	87	58	130	0	31	159	41	133	75	44	37	190
AN129b	82.55	Early Barremian	*C.darsi*	marlstone	42	372	38	198	138	0	44	0	162	41	56	97	18	87	158	40
AN131	83.39	Early Barremian	*C.darsi*	limestone	52	367	40	388	130	62	285	17	58	238	46	303	53	74	76	312
AN133	84.90	Early Barremian	*C.darsi*	limestone	60	491	112	531	150	77	537	26	24	339	56	278	52	89	35	496
AN134b	85.57	Early Barremian	*C.darsi*	marlstone	29	829	69	502	373	17	45	0	376	76	30	124	26	214	418	84
AN136.2	86.24	Early Barremian	*C.darsi*	limestone	208	231	59	395	120	66	133	0	118	294	79	167	71	107	113	282
AN138b	87.08	Early Barremian	*C.darsi*	marlstone	27	734	12	239	282	38	30	0	155	113	76	116	34	242	138	101
AN139d	88.09	Early Barremian	*C.darsi*	limestone	59	204	40	536	66	130	511	0	25	472	119	167	66	79	27	509
AN141.1	89.09	Late Barremian	*H.uhligi*	limestone	105	408	91	410	119	92	1828	0	38	289	21	211	31	81	48	362
AN142.2b	89.93	Late Barremian	*H.uhligi*	marlstone	58	164	20	137	61	11	15	0	100	39	58	51	28	51	99	38
AN143.1a	90.44	Late Barremian	*H.uhligi*	limestone	312	254	60	419	88	102	468	0	23	285	114	131	62	69	31	388
AN144	91.95	Late Barremian	*H.uhligi*	limestone	293	230	72	320	108	58	395	0	44	281	45	190	37	42	43	277
AN144b	92.11	Late Barremian	*H.uhligi*	marlstone	36	86	29	27	31	0	0	0	19	14	39	18	0	41	16	11
AN147.1	93.29	Late Barremian	*H.uhligi*	limestone	27	92	32	117	48	28	232	13	13	91	53	141	39	36	15	102
AN148	94.13	Late Barremian	*H.sayni*	limestone	133	141	41	22	61	17	904	0	13	14	28	199	43	35	11	11
AN148b	94.80	Late Barremian	*H.sayni*	marlstone	39	136	18	54	39	12	20	0	13	41	15	49	20	46	13	41
AN149.3	95.13	Late Barremian	*H.sayni*	limestone	68	70	32	60	20	0	86	0	29	42	19	36	21	23	25	35
AN151.3	96.98	Late Barremian	*H.sayni*	limestone	32	31	15	16	0	0	69	0	0	0	29	25	12	0	0	0
AN155.1a	98.99	Late Barremian	*H.sayni*	limestone	34	76	21	19	51	0	477.5	16	0	35	14	69	52	16	0	19
AN155.2b	99.50	Late Barremian	*H.sayni*	marlstone	38	202	22	54	96	0	0	0	49	29	28	64	17	114	34	20

Table An.2.2 (continued): peak intensities for the minerals identified in the <2 µm fraction of samples from the Angles section.

Sample ID	Depth (m)	Stage	Ammonite Zone	Lithology	Peak Intensity, <2µm fraction (cps)															
					"Smectite"	Mica	R0 I/S	Kaolinite/ Chlorite	Mica	Chlorite	Quartz	Goethite	Kaolinite	Chlorite	K-Feldspar	Na-Plagioclase	Pyrite	Mica	K001*	C002*
					001 ***5.2°2θ***	*001* ***8.8°2θ***	*002* ***9-9.5°2θ***	*001/002* ***12.34°2θ***	*002* ***17.92°2θ***	*003* ***18.56°2θ***	***20.85°2θ***	***21.2°2θ***	*002* ***24.9°2θ***	*004* ***25.2°2θ***	***27.5°2θ***	***27.9°2θ***	***28.12°2θ***	*005* ***45.68°2θ***	K002*(K001,C002)/ (K002+C004)	C004*(K001,C002)/(K002+C004)
AN156.1	99.83	Late Barremian	*H.sayni*	limestone	349	146	84	186	38	23	569	42	41	132	32	165	47	32	44	142
AN 156.4	101.17	Late Barremian	*H.sayni*	limestone	181	87	43	44	11	0	321	0	14	26	0	77	26	18	15	29
AN156.4b	101.51	Late Barremian	*H.sayni*	marlstone	38	370	73	92	130	0	38	0	16	44	62	55	20	77	25	67
AN156.6	102.35	Late Barremian	*H.sayni*	limestone	305	31	102	59	58	0	1198	0	0	33	58	145	38	48	0	59
AN157.1b	102.68	Late Barremian	*H.sayni*	marlstone	152	350	59	204	149	35	46	0	14	93	84	179	64	96	27	177
AN158b	104.03	Late Barremian	*H.sayni*	limestone	82	513	98	127	216	11	14	0	57	61	76	798	115	181	61	66
AN160.3b	104.87	Late Barremian	*G.sartousiana*	marlstone	162	518	150	510	186	65	34	0	428	75	108	177	56	123	434	76
AN161.1	105.03	Late Barremian	*G.sartousiana*	limestone	35	52	17	46	0	0	344	0	11	21	0	125	41	21	16	30
AN161.2	105.54	Late Barremian	*G.sartousiana*	limestone	170	218	45	129	102	33	795	0	0	63	14	91	31	88	0	129
AN161.2b	105.70	Late Barremian	*G.sartousiana*	marlstone	87	337	68	63	111	33	44	0	5	40	53	196	14	146	7	56
AN163.1b	106.54	Late Barremian	*G.sartousiana*	marlstone	14	72	10	75	28	11	368	16	15	56	35	221	36	31	16	59
AN164.2	107.72	Late Barremian	*H.feraudianus*	limestone	81	168	26	298	91	40	1082	0	35	192	24	437	68	42	46	252
AN165b	108.56	Late Barremian	*H.feraudianus*	marlstone	117	270	51	637	103	0	24	0	460	72	52	127	20	90	551	86
AN166b	108.72	Late Barremian	*H.feraudianus*	marlstone	378	104	50	338	26	49	143	0	17	203	17	99	77	36	26	312
AN168.1	109.73	Late Barremian	*I.giraudi*	limestone	746	190	52	602	67	58	155	0	193	325	53	175	59	53	224	378
AN168.1b	109.90	Late Barremian	*I.giraudi*	marlstone	76	199	28	474	134	0	27	0	468	97	92	79	17	139	393	81
AN170c	110.57	Late Barremian	*I.giraudi*	limestone	631	327	154	601	104	49	111	0	70	301	117	106	76	68	113	488
AN172.1	111.41	Late Barremian	*I.giraudi*	limestone	81	138	28	488	112	46	297	0	58	297	35	124	40	123	80	408
AN172.1b	111.91	Late Barremian	*I.giraudi*	marlstone	108	428	61	554	179	31	35	0	351	73	30	60	0	167.5	459	95
AN173	112.58	Late Barremian	*I.giraudi*	limestone	525	264	98	279	67	26	150	0	45	140	55	76	32	42	68	211
AN174.1b	113.59	Late Barremian	*I.giraudi*	marlstone	74	301	52	145	154	0	50	0	106	67	66.5	45	12	99	89	56
AN176.1	114.43	Late Barremian	*I.giraudi*	limestone	180	103	87	377	43	32	89	0	52	265	53	51	29	54	62	315
AN176.1b	115.10	Late Barremian	*I.giraudi*	marlstone	44	377	39	142	202	22	56	0	65	55	82	61	10	137	77	65
AN177	115.44	Late Barremian	*M.sarasini*	limestone	358	177	73	231	64	22	234	0	48	133	52	84	69	40	61	170
AN179.1	116.28	Late Barremian	*M.sarasini*	limestone	105	92	61	88	34	20	347	15	37	111	24	108	24	32	22	66
AN179.1b	116.44	Late Barremian	*M.sarasini*	marlstone	44	186	67	18	127	15	42	17	0	16	45	58	57	93	0	18
AN181	117.79	Late Barremian	*M.sarasini*	limestone	369	75	34	0	27	0	439	0	0	38	39	44	33	23	0	0
AN183	118.62	Late Barremian	*M.sarasini*	limestone	784.5	158	62	0	36	0	583	24	0	7	16	51	22	39	0	0
AN185	119.97	Late Barremian	*M.sarasini*	limestone	322	76	22	0	30	0	432	0	0	17	30	27	33	23	0	0
AN188	121.64	Late Barremian	*M.sarasini*	limestone	41	82	20	0	20	0	379	0	0	21	17	38	26	39	0	0
AN188b	122.32	Late Barremian	*M.sarasini*	marlstone	0	262	38	20	141	22	46	0	22	20	53	52	0	67	10	10
AN190	122.82	Late Barremian	*M.sarasini*	limestone	82	32	12	0	0	12	100	0	0	0	0	37	0	0	0	0
AN192	123.83	Late Barremian	*M.sarasini*	limestone	33	92	23	11	18	0	305	0	37	0	25	55	30	39	11	0
AN193b	124.50	Late Barremian	*M.sarasini*	marlstone	11	356	60	77	172	0	61	0	19	43	32	61	43	71	24	53
AN195	125.50	Late Barremian	*M.sarasini*	limestone	86	47	18	47	0	0	86	42	11	38	33	65	32	17	11	36
AN 196.2	126.68	Late Barremian	*M.sarasini*	limestone	64	67	22	110.5	18	0	156	20	0	74	18	44	24	38	0	111
AN197	127.35	Early Aptian	*D.oglanlensis*	limestone	127	82	20	0	14	0	306	0	0	25	42	25	14	25	0	0
AN 198	128.19	Early Aptian	*D.oglanlensis*	limestone	14	57	19	0	41	27	345	0	24	0	31	21	0	23	0	0
AN198b	128.52	Early Aptian	*D.oglanlensis*	marlstone	15	207	11	89	159	0	44	0	24	48	30	112	55	80	30	59
AN200	129.19	Early Aptian	*D.oglanlensis*	limestone	31	52	0	19	38	0	208	0	0	0	31	36	16	14	0	0
AN201b	129.87	Early Aptian	*D.oglanlensis*	marlstone	34	414	30	117	146	0	56	0	26	88	30	38	29	38	27	90
AN 202c	130.37	Early Aptian	*D.oglanlensis*	limestone	34	78	27	0	0	0	392	24	0	30	0	24	0	24	0	0
AN204	131.88	Early Aptian	*D.oglanlensis*	limestone	61	72	40	0	24	0	382	0	0	0	47	41	66	43	0	0
AN 206	133.22	Early Aptian	*D.oglanlensis*	limestone	110	69	27	0	36	0	535	17	0	14	27	47	0	47	0	0
AN206b	133.89	Early Aptian	*D.oglanlensis*	marlstone	0	167	25	44	94	0	69	0	35	36	49	52	0	111	22	22
AN210b	134.20	Early Aptian	*D.oglanlensis*	marlstone	26	105	18	36	82	18	50	17	11	38	57	72	34	110	8	28
AN211	134.72	Early Aptian	*D.oglanlensis*	limestone	86	39	26	24	0	0	158	0	0	13	36	43	21	0	0	24
AN 214	136.22	Early Aptian	*D.oglanlensis*	limestone	178	0	57	0	0	0	491	12	0	0	24	33	0	33	0	0
AN215b	137.40	Early Aptian	*D.oglanlensis*	marlstone	36	76	19	38	49	0	44	0	37	17	0	43	0	119	26	12
AN216	137.72	Early Aptian	*D.oglanlensis*	limestone	39	25	22	0	0	0	229	0	0	0	20	44	36	11	0	0

Table An.2.2 (continued): peak intensities for the minerals identified in the <2 µm fraction of samples from the Angles section.

Sample ID	Depth (m)	Stage	Ammonite Zone	Lithology	Peak Intensity, 2-16 µm fraction (cps)														
					Mica *001* ***8.8°2θ***	R0 I/S *002* ***9-9.5°2θ***	Kaolinite/ Chlorite *001/002* ***12.34°2θ***	Mica *002* ***17.92°2θ***	Chlorite *003* ***18.56°2θ***	Quartz ***20.85°2θ***	Goethite ***21.2°2θ***	Kaolinite *002* ***24.9°2θ***	Chlorite *004* ***25.2°2θ***	K-Feldspar ***27.5°2θ***	Na-Plagioclase ***27.9°2θ***	Pyrite ***28.12°2θ***	Mica *005* ***45.68°2θ***	K001* K002*(K001,C002)/ (K002+C004)	C002* C004*(K001,C002)/(K002+C004)
AN 2	0.34	Late Hauterivian	*B.balearis*	limestone	315	21	63	229	0	982	18	10	56	44	343	36	143	10	53
AN2b	0.50	Late Hauterivian	*B.balearis*	marlstone	611	52	396	662	79	91	0	263	124	135	122	61	207	269	127
AN4	1.68	Late Hauterivian	*B.balearis*	limestone	104	23	45	77	0	903	0	24	93	16	171	33	104.5	9	36
AN 6	2.85	Late Hauterivian	*B.balearis*	limestone	163	31	43	99	0	970	0	32	40	12	24	33	118	19	24
AN6b	3.02	Late Hauterivian	*B.balearis*	marlstone	454	36	173	363	13	495	0	136	83	132	139	31	168	107	66
AN8	4.03	Late Hauterivian	*B.balearis*	limestone	105	23	52	83.5	0	574	19	19	19	24	152	17	104	26	26
AN 10	4.87	Late Hauterivian	*B.balearis*	limestone	89	34	74	110	0	678	0	66	74	18	278	21	109	35	39
AN10b	5.20	Late Hauterivian	*B.balearis*	marlstone	503	49	392	677	18	327	0	649.5	86	163	134	14	445	346	46
AN13	6.38	Late Hauterivian	*B.balearis*	limestone	134	23	58	94	0	932	0	0	51	16	248	35	93	0	58
AN 15.1	7.38	Late Hauterivian	*B.balearis*	limestone	332	33	41	177	0	1574	18	0	33	0	750	69	148	0	41
AN15.1b	7.72	Late Hauterivian	*B.balearis*	marlstone	324	84	103	385	78	374	0	20	106	102	141	27	274	16	87
AN16	8.39	Late Hauterivian	*B.balearis*	limestone	84	14	64	72	0	903	16	0	53	22	300	29	83	0	64
AN18	9.56	Late Hauterivian	*B.balearis*	limestone	442	16	77	231	0	770	14	13	81	24	622	53	69	11	66
AN18b	9.90	Late Hauterivian	*B.balearis*	marlstone	362	52	95	383	21	443	0	0	101	120	115	43	254	0	95
AN20	10.40	Late Hauterivian	*B.balearis*	limestone	185	41	53	111	0	777	0	0	32	20	523	29	83	0	53
AN26	12.42	Late Hauterivian	*B.balearis*	limestone	164	0	22	129	0	835	22	16	43	28	435	25	99	6	16
AN27.2	13.26	Late Hauterivian	*B.balearis*	limestone	178	34	99	148	18	609	15	50	69	35	376	36	83	42	57
AN27.2b	13.59	Late Hauterivian	*B.balearis*	marlstone	848	61	607	466	0	533	10	599	25	139	215	43	350	583	24
AN29	14.43	Late Hauterivian	*B.balearis*	limestone	573	28	81	295.5	0	1118	14	10	35	16	1116	93	221	18	63
AN 29b	14.93	Late Hauterivian	*B.balearis*	marlstone	416	17	142	444	60	405	0	134	107	107	219	24	415	79	63
AN31	15.60	Late Hauterivian	*B.balearis*	limestone	304	50	78	182	12	1131	0	0	46	14	1434	115	98	0	78
AN 33	16.44	Late Hauterivian	*B.balearis*	limestone	580	31	54	243	23	997	14	15	70	21	2216	167	192	10	44
AN 33b	16.95	Late Hauterivian	*B.balearis*	marlstone	866	99	331	527	31	458	14	360	126	118	198	61	434	245	86
AN 34b	17.45	Late Hauterivian	*B.balearis*	marlstone	374	27	80	371	29	517	19	0	62	87	393	53	396	0	80
AN35	17.95	Late Hauterivian	*B.balearis*	limestone	389	35	52	227	0	696	0	0	42	32	1016	73	68	0	52
AN 35b	17.95	Late Hauterivian	*B.balearis*	marlstone	445	47	69	432	41	443	0	77	97	133	203	51	424	31	38
AN38	18.79	Late Hauterivian	*S.angulicostatum*	limestone	125	20	60	58	0	747	0	67	56	12	62	18	85	33	27
AN38b	18.96	Late Hauterivian	*S.angulicostatum*	marlstone	908	56	111	556	32	449	0	40	104	152	277	73	495	31	80
AN39b	19.30	Late Hauterivian	*S.angulicostatum*	marlstone	689	36	140	447	28	442	0	31	98	61	215	62	354	34	106
AN40	19.63	Late Hauterivian	*S.angulicostatum*	limestone	309	16	0	159	0	1082	18	10	18	0	931	76	90	0	0
AN40b	19.97	Late Hauterivian	*S.angulicostatum*	limestone	382	103	51	329	17	328	0	0	59	152	220	57	322	0	51
AN41b	20.13	Late Hauterivian	*S.angulicostatum*	marlstone	537	38	56	442	16	350	0	0	106	183	214	78	398	0	56
AN42b	20.47	Late Hauterivian	*S.angulicostatum*	marlstone	399	30	52	491	31	309	10	15	88	82	182	70	374	8	44
AN43	20.64	Late Hauterivian	*S.angulicostatum*	limestone	109	10	105	74	0	752	11	17	50	0	402	11	79	27	78
AN44b	20.97	Late Hauterivian	*S.angulicostatum*	marlstone	654	48	71	513	11	501	0	23	90	93	294	62	425	14	57
AN45b	21.31	Late Hauterivian	*S.angulicostatum*	marlstone	1244	113	433	637	18	441	10	595	107	254	340	108	107	367	66
AN46	21.48	Late Hauterivian	*S.angulicostatum*	limestone	393	25	109	267	14	1276	0	0	70	51	1139	82	132	0	109
AN46b	21.81	Late Hauterivian	*S.angulicostatum*	marlstone	527	80	165	382	23	322	0	268	60	138	281	77	68	135	30
AN48b	22.65	Late Hauterivian	*S.angulicostatum*	marlstone	1860	31	319.5	1013	19	424	0	264	104	137	415	96	1005	229	90
AN49.1	22.82	Late Hauterivian	*S.angulicostatum*	limestone	269	20	88	137	0	477	0	27	64	56	615	53	121	26	62
AN50	23.32	Late Hauterivian	*S.angulicostatum*	limestone	419	29	47	259	0	804	0	14	40	40	1504	114	67	12	35
AN51	23.83	Late Hauterivian	*S.angulicostatum*	limestone	602	64	66	311	0	977	0	25	82	23	1764	140	117	15	51
AN51b	24.16	Late Hauterivian	*S.angulicostatum*	marlstone	270	36	38	107	0	596	15	11	17	49	1121	79	32	15	23
AN53.1b	24.83	Late Hauterivian	*S.angulicostatum*	marlstone	115	14	18	59	0	669	0	0	28	42	1435	102	58	0	18
AN53.2	25.00	Late Hauterivian	*S.angulicostatum*	limestone	184	35	109	142	0	670	0	34	65	29	317.32	39	61	37	72
AN55	25.34	Late Hauterivian	*P.mortilleti*	limestone	382	27	69	190	19	952	22	15	55	15	1604	103	71	15	54
AN62.1	27.85	Late Hauterivian	*P.mortilleti*	limestone	192	18	27	93	0	1010	0	12	25	36	957	66	96	9	18
AN65.1	28.86	Late Hauterivian	*P.mortilleti*	limestone	264	12	177	178	17	1021	0	12	68	33	1236	63	96	27	150
AN68	30.54	Late Hauterivian	*P.mortilleti*	limestone	222	26	59	158	0	663	12	0	44	0	1121	104	191	0	59
AN72b	32.72	Early Barremian	*A.kiliani*	marlstone	406	66	258	457	23	431	0	341	105	111	126	44	320	197	61
AN73b	33.22	Early Barremian	*A.kiliani*	marlstone	808	82	462	533	31	452	15	422	194	171	161	61	381	317	146
AN75	34.06	Early Barremian	*A.kiliani*	limestone	306	35	83	174	31	1708	6	10	51	77	1712	160	108	14	69
AN75b	34.23	Early Barremian	*A.kiliani*	marlstone	633	50	463	476	31	485	0	565	87	116	285	58	333	401	62
AN76b	34.56	Early Barremian	*A.kiliani*	marlstone	659	73	328	469	15	501	0	307	81	82	437	84	345	260	68
AN78	35.74	Early Barremian	*A.kiliani*	limestone	262	37	590	177	58	687	47	229	391	50	133	68	162	218	372
AN81	37.08	Early Barremian	*A.kiliani*	limestone	376	22	99	237	0	1087	0	28	100	34	1187	101	204	22	77
AN81b	37.42	Early Barremian	*A.kiliani*	marlstone	417	53	225	435	14	385	0	297	64	124	115	44	327	185	40
AN84	38.93	Early Barremian	*A.kiliani*	limestone	246	39	129	176	17	1126	11	14	77	21	809	107	115	20	109
AN84b	39.26	Early Barremian	*A.kiliani*	marlstone	714	40	382	268	0	55	0	282	76	53	201	60	204	301	81

Table An.2.3: peak intensities for the minerals identified in the 2-16 µm fraction of samples from the Angles section.

Sample ID	Depth (m)	Stage	Ammonite Zone	Lithology	Peak Intensity, 2-16 µm fraction (cps)														
					Mica *001* *8.8°2θ*	R0 I/S *002* *9-9.5°2θ*	Kaolinite/ Chlorite *001/002* *12.34°2θ*	Mica *002* *17.92°2θ*	Chlorite *003* *18.56°2θ*	Quartz *20.85°2θ*	Goethite *21.2°2θ*	Kaolinite *002* *24.9°2θ*	Chlorite *004* *25.2°2θ*	K-Feldspar *27.5°2θ*	Na-Plagioclase *27.9°2θ*	Pyrite *28.12°2θ*	Mica *005* *45.68°2θ*	K001* K002*(K001,C002)/ (K002+C004)	C002* C004*(K001,C002)/(K002+C004)
AN87	40.44	Early Barremian	*A.kiliani*	limestone	463	46	635	293	60	187	13	57	382	68	224	53	122	82	553
AN87b	41.11	Early Barremian	*A.kiliani*	marlstone	269	74	253	203	14	62	0	221	68	67	82	46	123	193	60
AN89	41.95	Early Barremian	*A.kiliani*	limestone	142	13	108	98	11	774	0	44	60	28	389	44	108	46	62
AN90 haut	42.95	Early Barremian	*A.kiliani*	limestone	327	60	175	249	25	1056	0	65	123	55	724	38	167	61	114
AN90b	43.46	Early Barremian	*A.kiliani*	marlstone	312	26	241	152	0	41	0	224	35	60	134	63	162	208	33
AN92	44.80	Early Barremian	*A.kiliani*	limestone	295	17	101	179	14	960	16	44	59	43	1122	87	121	43	58
AN93 haut	46.14	Early Barremian	*A.kiliani*	limestone	340	12	155	286	25	1691	0	27	150	47	1771	216	199	24	131
AN93b	46.48	Early Barremian	*A.kiliani*	marlstone	240	43	143	221	0	35	0	116	83	69	94	62	75	83	60
AN95 bas	47.99	Early Barremian	*K.nicklesi*	limestone	209	23	125	161	0	952	0	17	98	28	671	87	127	18	107
AN97	49.50	Early Barremian	*K.nicklesi*	limestone	240	14	141	196	0	111	0	66	108	67	157	54	72	53	88
AN97b	49.83	Early Barremian	*K.nicklesi*	marlstone	457	22	223	278	16	486	0	289	70	73	195	37	194	180	43
AN98 haut	50.50	Early Barremian	*K.nicklesi*	limestone	170	20	51	143	10	2066	0	23	72	0	1459	123	88	12	39
AN101	52.18	Early Barremian	*K.nicklesi*	limestone	291	36	80	182	0	998	0	40	88	43	1710	158	120	25	55
AN101b	52.52	Early Barremian	*K.nicklesi*	marlstone	313	20	362	123	12	248	0	296	66	139	220	88	134	296	66
AN103	53.86	Early Barremian	*K.nicklesi*	limestone	281	20	229	159	27	761	0	20	139	25	1183	105	86	29	200
AN103b	54.53	Early Barremian	*K.nicklesi*	marlstone	101	0	101	181	13	308	0	11	35	98	356	57	134	24	77
AN104	55.20	Early Barremian	*K.nicklesi*	limestone	511	61	196	302	0	1836	0	37	118	51	3587	326	174	47	149
AN105	56.38	Early Barremian	*K.nicklesi*	limestone	145	19	64	137	0	719	12	31	45	27	807	97	86	26	38
AN108	59.56	Early Barremian	*K.nicklesi*	limestone	342	27	121	197	0	1219	21	756	75	52	1902	191	97	110	11
AN109.4	61.07	Early Barremian	*N.pulchella*	limestone	345	18	266	139	25	800	11	101	68	36	1514	175	107	159	107
AN110.1b	62.25	Early Barremian	*N.pulchella*	marlstone	559	36	318	271	47	1346	0	2949	171	38	3192	296	84	301	17
AN 110.3c	64.09	Early Barremian	*N.pulchella*	limestone	837	45	139	320	19	4795	39	228	61	48	2430	240	225	110	29
AN110.4	65.27	Early Barremian	*N.pulchella*	limestone	1548	14	89	75	0	4929	15	64	106	37	6581	622	108	34	55
AN111.2	66.28	Early Barremian	*N.pulchella*	limestone	417	26	72	227	21	1699	0	32	54	25	1811	179	185	27	45
AN111.5	67.28	Early Barremian	*N.pulchella*	limestone	494	26	88	250.5	0	1535	0	126	101	27	2146	156	79	49	39
AN112.2	68.79	Early Barremian	*N.pulchella*	limestone	137	12	43	110	0	618	0	44.5	24	13	621	54	63	28	15
AN112.7	71.64	Early Barremian	*K.compressissima*	limestone	61	16	56	85	0	903	34	216	55	30	118	25	75	45	11
AN114.2	72.99	Early Barremian	*K.compressissima*	limestone	324	27	42	177	0	1760	17	25	30	34	1295	182	99	19	23
AN115	73.99	Early Barremian	*K.compressissima*	limestone	494	34	128	243	18	2078	0	31	125	38	2200	210.5	68	25	103
AN116b	74.83	Early Barremian	*K.compressissima*	marlstone	182	0	100	114	17	367	0	136	75	85	191	61	102	64	36
AN117	75.17	Early Barremian	*K.compressissima*	limestone	261	15	182	150	19	2192	0	36	124	13	1473	144	117	41	141
AN119	76.34	Early Barremian	*K.compressissima*	limestone	938	28	451	383	80	5791	53	74	283	32	2558	216	214	93	358
AN119b	77.01	Early Barremian	*K.compressissima*	marlstone	229	13	82	196	0	384	0	99	63	147	193	47	167	50	32
AN 121	78.36	Early Barremian	*K.compressissima*	limestone	456	34	117	195	14	2636	14	15	45	69	2037	191	147	29	88
AN123	78.52	Early Barremian	*K.compressissima*	limestone	730	36	104	356	23	2328	28	46	81	20	2361	246	228	38	66
AN123b	78.69	Early Barremian	*K.compressissima*	marlstone	356	20	180	188	13	414	0	192	71	111	147	40	189	131	49
AN125	79.70	Early Barremian	*C.darsi*	limestone	190	15	367	94	27	897	35	308	205	58	828	61	102	220	147
AN127	80.70	Early Barremian	*C.darsi*	limestone	615	26	164	238	25	4169	17	19	99	40	2310	222	173	26	138
AN127b	81.21	Early Barremian	*C.darsi*	marlstone	186	11	91	84	27	573	0	0	70	40	1073	94	63	0	91
AN128	81.54	Early Barremian	*C.darsi*	limestone	446	12	87	186	39	7156	40	18	61	37	3554	282	139	20	67
AN129	82.21	Early Barremian	*C.darsi*	limestone	278	23	345	197	44	367	0	71	276	57	220	61	107	71	274
AN129b	82.55	Early Barremian	*C.darsi*	marlstone	390	23	191	215	0	444	0	123	74	59	132	32	147	119	72
AN131	83.39	Early Barremian	*C.darsi*	limestone	445	18	145	176	44	2980	31	27	111	49	2254	174	182	28	117
AN133	84.90	Early Barremian	*C.darsi*	limestone	228	65	151	134	0	160	0	17	76	46	156	36	37	28	123
AN134b	85.57	Early Barremian	*C.darsi*	marlstone	647	46	503	273	26	401	0	506	84	179	137	67	241	431	72
AN136.2	86.24	Early Barremian	*C.darsi*	limestone	193	13	265	127	30	663	0	44	172	35	451	51	74	54	211
AN138b	87.08	Early Barremian	*C.darsi*	marlstone	593	49	145	356	51	291	0	122	108	108	391	70	310	77	68
AN139d	88.09	Early Barremian	*C.darsi*	limestone	254	19	133	112	78	10174	51	41	132	0	3653	207	85	32	101
AN141.1	89.09	Late Barremian	*H.uhligi*	limestone	554	44	80	252	98	18391	173	33	82	38	4409	280	172	23	57
AN142.2b	89.93	Late Barremian	*H.uhligi*	marlstone	940	30	303	351	0	161	0	256	47	60	688	117	281	256	47
AN143.1a	90.44	Late Barremian	*H.uhligi*	limestone	263	16	51	79	33	5853	47	17	67	13	3625	248	78	10	41
AN144	91.95	Late Barremian	*H.uhligi*	limestone	343	26	242	185	53	1434	0	19	121	47	2061	204	101	33	209
AN144b	92.11	Late Barremian	*H.uhligi*	marlstone	274	17	68	197	29	205	0	51	51	114	186	39	152	34	34
AN147.1	93.29	Late Barremian	*H.uhligi*	limestone	233	34	147	116	10	1304	0	0	121	124	2347	192	84	0	147
AN148	94.13	Late Barremian	*H.sayni*	limestone	178	14	37	88	19	3294	0	30	53	0	4405	249	73	13	24
AN148b	94.80	Late Barremian	*H.sayni*	marlstone	198	22	61	62	0	58	0	14	37	35	264	37	32	17	44
AN149.3	95.13	Late Barremian	*H.sayni*	limestone	108	44	112	51	43	1323	0	0	107	15	2869	173	62	0	112
AN155.2b	99.50	Late Barremian	*H.sayni*	marlstone	508	34	87	210	23	102	0	60	35	55	409	54	179	55	32

Table An.2.3 (continued): peak intensities for the minerals identified in the 2-16 µm fraction of samples from the Angles section.

Sample ID	Depth (m)	Stage	Ammonite Zone	Lithology	Peak Intensity, 2-16 µm fraction (cps)														
					Mica *001* *8.8°2θ*	R0 I/S *002* *9-9.5°2θ*	Kaolinite/ Chlorite *001/002* *12.34°2θ*	Mica *002* *17.92°2θ*	Chlorite *003* *18.56°2θ*	Quartz *20.85°2θ*	Goethite *21.2°2θ*	Kaolinite *002* *24.9°2θ*	Chlorite *004* *25.2°2θ*	K-Feldspar *27.5°2θ*	Na-Plagioclase *27.9°2θ*	Pyrite *28.12°2θ*	Mica *005* *45.68°2θ*	K001* K002*(K001,C002)/ (K002+C004)	C002* C004*(K001,C002)/(K002+C004)
AN156.1	99.83	Late Barremian	*H.sayni*	limestone	328	44	141	132	0	1231	0	19	100	25	4634	283	77	23	118
AN 156.4	101.17	Late Barremian	*H.sayni*	limestone	75	18	61	40	0	825	0	0	36	43	1472	102	44	0	61
AN156.4b	101.51	Late Barremian	*H.sayni*	marlstone	688	55	103	260	25	102.5	30	11	83	92	1209	205	166	12	91
AN156.6	102.35	Late Barremian	*H.sayni*	limestone	389	16	43	161	0	2182	19	15	46	33	3424	292	105	11	32
AN157.1b	102.68	Late Barremian	*H.sayni*	marlstone	308	45	161	132	11	212	0	39	91	59	679	119	100	48	113
AN160.3b	104.87	Late Barremian	*G.sartousiana*	marlstone	208	44	126	157	0	330	0	83	96	66	204	46	132	58	68
AN161.1	105.03	Late Barremian	*G.sartousiana*	limestone	69	10	48	39	0	839	0	27	36	14	722	88	63	21	27
AN161.2	105.54	Late Barremian	*G.sartousiana*	limestone	257	11	40	124	0	3614.5	30	0	53	0	1371	93	54	0	40
AN161.2b	105.70	Late Barremian	*G.sartousiana*	marlstone	159	18	74	117	0	442	0	53	37	73	177	34	111	44	30
AN163.1b	106.54	Late Barremian	*G.sartousiana*	marlstone	52	16	27	0	0	1502	0	17	17	10	468	41	61	14	14
AN164.2	107.72	Late Barremian	*H.feraudianus*	limestone	126	18	39	60	42	6215	16	339	108	0	3658	232	108	30	9
AN165b	108.56	Late Barremian	*H.feraudianus*	marlstone	349	19	566	135	0	147	0	423	46	49	572.5	76	105	510	56
AN166b	108.72	Late Barremian	*H.feraudianus*	marlstone	62	19	162	28	33	1409	13	31	103	32	609	48	57	37	125
AN168.1	109.73	Late Barremian	*I.giraudi*	limestone	172	25	304	104	16	1616	16	148	216	24	902	107	78	124	180
AN168.1b	109.90	Late Barremian	*I.giraudi*	marlstone	288.5	45	508	158	12	278	12	471	49	72	285	37	118	460	48
AN170c	110.57	Late Barremian	*I.giraudi*	limestone	296	20	196	168	41	1084	0	87	111	57	319	72	112	86	110
AN172.1	111.41	Late Barremian	*I.giraudi*	limestone	575	24	213	288	0	3213	0	39	125	38	1471	125	221	51	162
AN172.1b	111.91	Late Barremian	*I.giraudi*	marlstone	186	24	271	237	0	349	16	329	68	38	89	21	160	225	46
AN173	112.58	Late Barremian	*I.giraudi*	limestone	201	25	84	71	0	1220	22	23	54	21	684	92	84	25	59
AN174.1b	113.59	Late Barremian	*I.giraudi*	marlstone	192	21	57	116	0	384	0	33	30	42	79	16	73	30	27
AN176.1	114.43	Late Barremian	*I.giraudi*	limestone	484	27	268	292	24	1441	0	26	142	44	1191	158	223	41	227
AN176.1b	115.10	Late Barremian	*I.giraudi*	marlstone	544	20	216	505	20	384	13	264	81	87	161	26	510	165	51
AN177	115.44	Late Barremian	*M.sarasini*	limestone	193	22	79	108	0	1314	23	20	72	43	293	35	87	17	62
AN179.1	116.28	Late Barremian	*M.sarasini*	limestone	356	26	47	176	0	762	0	23	48	13	1395	132	101	15	32
AN179.1b	116.44	Late Barremian	*M.sarasini*	marlstone	839	33	66	551	52	437	0	31	63	62	389	72	418	22	44
AN181	117.79	Late Barremian	*M.sarasini*	limestone	131	12	19	88	0	1269	13	0	29	23	475	65	72	0	19
AN183	118.62	Late Barremian	*M.sarasini*	limestone	302	17	25	125	0	1156	13	0	42	44	677	101	85	0	25
AN185	119.97	Late Barremian	*M.sarasini*	limestone	121	12	0	38	0	1201	0	0	16	16	169	13	134	0	0
AN188	121.64	Late Barremian	*M.sarasini*	limestone	177	19	27	86	0	1457	15	0	17	47	372	48	127	0	27
AN188b	122.32	Late Barremian	*M.sarasini*	marlstone	451	39	58	323	15	285	22	23	52	61	140	36	207	18	40
AN190	122.82	Late Barremian	*M.sarasini*	limestone	108	11	10	51	0	641	17	10	13	25	186	42	68	4	6
AN192	123.83	Late Barremian	*M.sarasini*	limestone	100	18	13	51	20	1130	12	0	0	21	370	39	129	0	0
AN193b	124.50	Late Barremian	*M.sarasini*	marlstone	223	33	48	180	13	248	0	14	36	57	226	28	102	13	35
AN195	125.50	Late Barremian	*M.sarasini*	limestone	91	26	63	73	0	664	0	33	31	43	132	40	73	32	31
AN 196.2	126.68	Late Barremian	*M.sarasini*	limestone	60	14	173	56	0	725	0	20	123	21	178	18	49	24	149
AN197	127.35	Early Aptian	*D.oglanlensis*	limestone	123	27	11	46	0	870	11	10	16	25	148	41	190	4	7
AN 198	128.19	Early Aptian	*D.oglanlensis*	limestone	146	17	0	59	0	1032	0	0	25	30	186	19	105	0	0
AN198b	128.52	Early Aptian	*D.oglanlensis*	marlstone	157	15	36	136	0	341	10	0	40	57	184	44	81	0	36
AN200	129.19	Early Aptian	*D.oglanlensis*	limestone	138	0	11	60	0	481	0	0	34	57	587	93	78	0	11
AN201b	129.87	Early Aptian	*D.oglanlensis*	marlstone	288	43	56	162	14	280	0	10	31	67	214	56	93	14	42
AN 202c	130.37	Early Aptian	*D.oglanlensis*	limestone	189	15	25	131	19	1015	0	0	20	0	257	191	93	0	25
AN204	131.88	Early Aptian	*D.oglanlensis*	limestone	78	16	0	47	0	586	0	14	0	18	152	53	35	0	0
AN 206	133.22	Early Aptian	*D.oglanlensis*	limestone	279	17	22	126	15	1023	13	0	0	24	264	44	99	0	0
AN206b	133.89	Early Aptian	*D.oglanlensis*	marlstone	314	46	30	163	0	251	0	18	57	42	164	39	84	7	23
AN210b	134.20	Early Aptian	*D.oglanlensis*	marlstone	221	37	79	218	19	187	0	0	61	66	155	52	103	0	79
AN211	134.72	Early Aptian	*D.oglanlensis*	limestone	101	11	55	38	0	802	0	18	27	28	80	30	0	22	33
AN 214	136.22	Early Aptian	*D.oglanlensis*	limestone	97	13	0	45	0	892	11	0	0	37	145	16	80	0	0
AN215b	137.40	Early Aptian	*D.oglanlensis*	marlstone	1999	29	29	159	0	204	0	14	76	78	103	33	123	5	24
AN216	137.72	Early Aptian	*D.oglanlensis*	limestone	89	11	0	17	17	683	33	12	0	13	276	52	50	0	0

Table An.2.3 (continued): peak intensities for the minerals identified in the 2-16 µm fraction of samples from the Angles section.

					Quantification, <2μm fraction (relative %)					Five-Point Moving Average (relative %)				
Sample ID	**Depth (m)**	**Stage**	**Ammonite Zone**	**Lithology**	**"Smectite"**	**Mica**	**R0 I/S**	**Kaolinite**	**Chlorite**	**"Smectite"**	**Mica**	**R0 I/S**	**Kaolinite**	**Chlorite**
AN 2	0.34	Late Hauterivian	*B.balearis*	limestone	32.0	45.6	11.1	2.9	8.4					
AN2b	0.50	Late Hauterivian	*B.balearis*	marlstone	36.5	32.1	15.3	11.3	4.8					
AN4	1.68	Late Hauterivian	*B.balearis*	limestone	4.2	68.1	10.1	5.9	11.8	22.9	50.2	13.0	6.3	7.6
AN 6	2.85	Late Hauterivian	*B.balearis*	limestone	27.0	51.6	13.9	1.4	6.0	24.2	48.9	13.5	5.9	7.5
AN6b	3.02	Late Hauterivian	*B.balearis*	marlstone	35.2	33.2	17.2	10.5	3.9	27.4	43.5	12.9	6.1	10.2
AN8	4.03	Late Hauterivian	*B.balearis*	limestone	27.5	45.0	8.8	4.7	14.1	28.4	37.9	11.9	7.0	14.7
AN 10	4.87	Late Hauterivian	*B.balearis*	limestone	19.9	31.2	8.0	6.6	34.2	28.7	35.4	12.0	7.4	16.5
AN10b	5.20	Late Hauterivian	*B.balearis*	marlstone	38.4	30.2	19.0	12.5	0.0	29.3	36.9	12.4	7.1	14.3
AN13	6.38	Late Hauterivian	*B.balearis*	limestone	32.0	41.2	11.6	0.0	15.2	28.6	42.5	11.7	6.2	10.9
AN 15.1	7.38	Late Hauterivian	*B.balearis*	limestone	14.8	60.3	5.8	10.2	8.8	27.6	46.3	10.4	4.9	10.7
AN15.1b	7.72	Late Hauterivian	*B.balearis*	marlstone	35.4	42.8	12.0	0.0	9.9	27.7	43.9	10.4	4.7	13.4
AN16	8.39	Late Hauterivian	*B.balearis*	limestone	31.2	32.4	12.4	5.8	18.1	28.4	38.8	11.3	4.8	16.7
AN18	9.56	Late Hauterivian	*B.balearis*	limestone	20.5	36.0	10.4	8.0	25.1	27.4	36.4	12.2	4.7	19.2
AN18b	9.90	Late Hauterivian	*B.balearis*	marlstone	33.0	39.5	13.0	0.0	14.6	27.2	36.3	13.1	4.6	18.7
AN20	10.40	Late Hauterivian	*B.balearis*	limestone	19.4	35.1	16.5	7.1	22.0	28.8	36.8	13.5	5.1	15.9
AN26	12.42	Late Hauterivian	*B.balearis*	limestone	44.0	32.4	12.0	4.7	7.0	27.4	39.3	12.9	8.0	12.5
AN27.2	13.26	Late Hauterivian	*B.balearis*	limestone	16.8	49.6	10.5	10.5	12.6	22.2	43.0	11.4	11.8	11.6
AN27.2b	13.59	Late Hauterivian	*B.balearis*	marlstone	11.0	48.4	12.6	24.8	3.1	16.9	45.2	10.1	13.0	14.8
AN29	14.43	Late Hauterivian	*B.balearis*	limestone	14.3	39.7	4.7	4.8	36.5	17.8	44.2	9.3	10.3	18.4
AN 29b	14.93	Late Hauterivian	*B.balearis*	marlstone	21.7	48.5	12.8	6.4	10.6	23.6	41.6	8.6	5.9	20.4
AN31	15.60	Late Hauterivian	*B.balearis*	limestone	41.2	31.3	6.1	0.0	21.3	25.1	42.0	8.3	4.8	19.9
AN 33	16.44	Late Hauterivian	*B.balearis*	limestone	18.4	43.4	6.5	5.6	26.1	20.6	46.7	8.7	7.0	17.0
AN 33b	16.95	Late Hauterivian	*B.balearis*	marlstone	2.1	62.9	12.0	16.2	6.8	19.1	50.2	9.8	8.4	12.5
AN 34b	17.45	Late Hauterivian	*B.balearis*	marlstone	21.9	56.1	10.7	6.1	5.2	24.3	49.6	11.1	7.0	8.0
AN35	17.95	Late Hauterivian	*B.balearis*	limestone	58.0	21.8	12.3	0.7	7.2	29.1	47.9	11.0	4.4	7.6
AN 35b	17.95	Late Hauterivian	*B.balearis*	marlstone	5.2	73.3	10.5	3.3	7.7	28.7	48.0	10.6	3.2	9.4
AN38	18.79	Late Hauterivian	*S.angulicostatum*	limestone	33.9	36.9	7.1	5.7	16.3	25.0	51.3	10.4	3.0	10.3
AN38b	18.96	Late Hauterivian	*S.angulicostatum*	marlstone	26.5	50.9	16.2	0.0	6.3	23.1	54.3	10.3	2.2	10.0
AN39b	19.30	Late Hauterivian	*S.angulicostatum*	marlstone	11.3	73.8	4.1	2.1	8.8	21.8	57.1	10.5	1.2	9.4
AN40	19.63	Late Hauterivian	*S.angulicostatum*	limestone	31.0	42.9	14.3	0.0	11.9	18.9	60.9	10.8	0.5	8.9
AN40b	19.97	Late Hauterivian	*S.angulicostatum*	limestone	9.8	72.2	10.9	0.0	7.1	16.9	63.1	11.7	0.2	8.2
AN41b	20.13	Late Hauterivian	*S.angulicostatum*	marlstone	13.4	70.0	10.9	0.0	5.8	17.4	60.4	13.1	0.0	9.1
AN42b	20.47	Late Hauterivian	*S.angulicostatum*	marlstone	19.2	55.6	17.4	0.0	7.8	21.7	50.6	13.9	0.0	13.9
AN43	20.64	Late Hauterivian	*S.angulicostatum*	limestone	37.9	18.6	14.4	0.0	29.1	24.3	43.5	13.4	0.5	18.3
AN43b	20.64	Late Hauterivian	*S.angulicostatum*	marlstone	19.4	47.2	10.1	0.0	23.4	20.6	48.8	12.3	1.5	16.8
AN44b	20.97	Late Hauterivian	*S.angulicostatum*	marlstone	10.9	68.7	10.1	5.9	4.3	14.1	59.0	11.3	3.3	12.3
AN45b	21.31	Late Hauterivian	*S.angulicostatum*	marlstone	3.6	79.6	16.8	0.0	0.0	10.5	62.8	9.6	5.8	11.3
AN46	21.48	Late Hauterivian	*S.angulicostatum*	limestone	18.6	34.6	0.0	15.3	31.4	9.1	63.5	7.5	7.6	12.4
AN46b	21.81	Late Hauterivian	*S.angulicostatum*	marlstone	3.6	78.3	7.9	5.6	4.7	11.1	63.0	6.2	7.7	12.0
AN48b	22.65	Late Hauterivian	*S.angulicostatum*	marlstone	2.1	80.7	5.9	7.0	4.3	17.6	58.9	6.5	6.0	11.1
AN49.1	22.82	Late Hauterivian	*S.angulicostatum*	limestone	52.4	17.3	8.3	3.3	18.7	23.6	53.3	6.9	3.9	12.3
AN50	23.32	Late Hauterivian	*S.angulicostatum*	limestone	15.9	62.5	5.4	2.3	13.9	23.5	52.2	6.9	2.8	14.5
AN51	23.83	Late Hauterivian	*S.angulicostatum*	limestone	16.6	62.7	7.9	0.0	12.8	16.3	58.0	6.3	4.0	15.4
AN51b	24.16	Late Hauterivian	*S.angulicostatum*	marlstone	9.8	55.8	6.5	8.0	19.9	11.8	61.2	5.2	6.8	15.0
AN53.1b	24.83	Late Hauterivian	*S.angulicostatum*	marlstone	0.0	73.4	0.0	13.6	13.0	16.0	57.2	4.4	8.9	13.6
AN53.2	25.00	Late Hauterivian	*S.angulicostatum*	limestone	36.3	40.5	6.8	6.5	9.8	24.7	49.9	4.7	8.9	11.8
AN55	25.34	Late Hauterivian	*P.mortilleti*	limestone	36.6	40.6	5.0	8.6	9.2	31.0	41.6	5.6	8.0	13.8
AN62.1	27.85	Late Hauterivian	*P.mortilleti*	limestone	31.3	38.5	7.8	6.6	15.9	30.1	36.9	5.8	7.5	19.7
AN65.1	28.86	Late Hauterivian	*P.mortilleti*	limestone	23.4	25.8	3.1	9.2	38.5	24.7	36.9	7.0	8.6	22.7
AN68	30.54	Late Hauterivian	*P.mortilleti*	limestone	19.5	49.2	6.7	4.1	20.5	19.2	40.3	10.2	12.2	18.1
AN72b	32.72	Early Barremian	*A.kiliani*	marlstone	14.3	36.5	22.8	26.4	0.0	15.7	45.1	12.7	15.7	10.8
AN73b	33.22	Early Barremian	*A.kiliani*	marlstone	8.5	62.1	9.6	16.1	3.7	14.5	47.1	12.8	17.7	7.9
AN75	34.06	Early Barremian	*A.kiliani*	limestone	24.2	35.0	9.3	12.7	18.8	14.1	47.8	11.5	18.3	8.4
AN75b	34.23	Early Barremian	*A.kiliani*	marlstone	5.3	53.1	12.5	26.1	3.1	13.4	47.2	10.9	17.7	10.7
AN76b	34.56	Early Barremian	*A.kiliani*	marlstone	16.4	51.6	11.8	15.1	5.1	13.8	44.2	10.5	15.5	15.9
AN78	35.74	Early Barremian	*A.kiliani*	limestone	9.5	32.9	8.4	8.7	40.5	17.7	39.5	9.8	12.7	20.5
AN81	37.08	Early Barremian	*A.kiliani*	limestone	31.4	31.6	7.5	8.5	21.0	21.2	36.4	9.3	11.8	21.3
AN81b	37.42	Early Barremian	*A.kiliani*	marlstone	25.1	39.4	13.2	20.6	1.9	20.6	38.4	9.2	12.0	19.7
AN84	38.93	Early Barremian	*A.kiliani*	limestone	8.2	42.5	4.7	5.0	39.6	16.6	41.6	9.0	11.8	21.0
AN84b	39.26	Early Barremian	*A.kiliani*	marlstone	18.6	48.5	13.1	12.5	7.2	11.6	43.4	7.9	12.8	24.3
AN87	40.44	Early Barremian	*A.kiliani*	limestone	3.8	34.3	3.3	13.2	45.4	8.7	45.6	6.6	15.9	23.2
AN87b	41.11	Early Barremian	*A.kiliani*	marlstone	4.0	56.2	4.8	28.1	6.8	7.8	47.8	6.1	17.0	21.4
AN89	41.95	Early Barremian	*A.kiliani*	limestone	13.0	53.6	7.0	11.4	15.0	8.7	47.2	7.3	15.5	21.3
AN90 haut	42.95	Early Barremian	*A.kiliani*	limestone	8.5	36.1	9.5	5.1	40.9	10.0	44.3	9.3	15.1	21.3
AN90b	43.46	Early Barremian	*A.kiliani*	marlstone	11.8	41.0	13.4	27.1	6.8	9.8	41.6	9.6	16.5	22.5
AN92	44.80	Early Barremian	*A.kiliani*	limestone	8.4	47.1	7.8	16.9	19.8	8.6	41.8	8.0	18.2	23.4
AN93 haut	46.14	Early Barremian	*A.kiliani*	limestone	7.4	31.9	3.1	12.0	45.6	7.2	43.8	6.4	18.2	24.3
AN93b	46.48	Early Barremian	*A.kiliani*	marlstone	4.0	58.0	5.8	28.2	4.0	7.0	46.5	6.4	16.2	23.9
AN95 bas	47.99	Early Barremian	*K.nicklesi*	limestone	8.1	42.4	10.4	8.3	30.8	8.7	49.4	6.8	13.9	21.2
AN97	49.50	Early Barremian	*K.nicklesi*	limestone	13.5	56.2	4.9	3.9	21.5	11.1	50.2	6.4	12.6	19.7
AN97b	49.83	Early Barremian	*K.nicklesi*	marlstone	12.5	48.5	5.1	24.7	9.1	13.6	49.2	5.7	12.3	19.2
AN98 haut	50.50	Early Barremian	*K.nicklesi*	limestone	13.7	46.9	5.2	7.9	26.2	16.1	47.5	6.0	11.5	18.8
AN101	52.18	Early Barremian	*K.nicklesi*	limestone	23.0	44.5	7.2	5.5	19.8	17.6	44.7	7.0	9.6	21.1
AN101b	52.52	Early Barremian	*K.nicklesi*	marlstone	18.8	47.1	9.1	12.1	13.0	17.4	41.5	8.1	9.4	23.6
AN103	53.86	Early Barremian	*K.nicklesi*	limestone	9.6	27.7	7.3	8.1	47.3	16.6	40.2	9.3	10.4	23.5
AN103b	54.53	Early Barremian	*K.nicklesi*	marlstone	22.9	46.3	12.0	15.2	3.5	15.3	43.4	10.0	10.3	21.0
AN104	55.20	Early Barremian	*K.nicklesi*	limestone	12.4	46.3	12.1	5.5	23.6	13.8	50.6	9.4	9.4	16.8
AN105	56.38	Early Barremian	*K.nicklesi*	limestone	7.5	66.4	4.7	9.7	11.8	12.0	54.5	8.3	9.4	15.8
AN108	59.56	Early Barremian	*K.nicklesi*	limestone	14.8	55.8	7.3	8.6	13.5	10.7	50.5	7.9	11.3	19.6
AN109.4	61.07	Early Barremian	*N.pulchella*	limestone	10.0	35.1	10.3	16.6	28.1	9.3	44.3	8.2	13.0	25.1
AN110.1b	62.25	Early Barremian	*N.pulchella*	marlstone	4.4	32.1	8.5	16.6	38.3	7.1	44.8	8.1	12.4	27.6
AN 110.3c	64.09	Early Barremian	*N.pulchella*	limestone	6.9	61.2	5.9	4.5	21.5	5.0	53.5	7.6	10.6	23.3
AN110.4	65.27	Early Barremian	*N.pulchella*	limestone	2.3	64.7	6.9	10.5	15.7	4.2	62.5	7.7	9.6	15.9
AN111.2	66.28	Early Barremian	*N.pulchella*	limestone	2.7	71.9	10.7	11.5	3.1	5.9	63.8	8.3	10.2	11.8
AN111.5	67.28	Early Barremian	*N.pulchella*	limestone	8.4	59.2	6.8	9.2	16.4	9.6	58.7	9.3	10.9	11.5

Table An.2.4: semi-quantitative estimation of the amount of the identified minerals in the <2 μm fraction of samples from the Angles section.

Sample ID	Depth (m)	Stage	Ammonite Zone	Lithology	Quantification, <2μm fraction (relative %)					Five-Point Moving Average (relative %)				
					"Smectite"	Mica	R0 I/S	Kaolinite	Chlorite	"Smectite"	Mica	R0 I/S	Kaolinite	Chlorite
AN112.2	68.79	Early Barremian	*N.pulchella*	limestone	20.6	45.1	9.9	13.0	11.5	11.9	54.8	10.6	10.6	12.1
AN112.7	71.64	Early Barremian	*K.compressissima*	limestone	9.3	51.5	15.4	10.5	13.4	10.8	55.2	11.8	9.2	13.1
AN114.2	72.99	Early Barremian	*K.compressissima*	limestone	4.6	73.9	10.2	4.1	7.1	8.8	54.7	11.9	9.3	15.2
AN115	73.99	Early Barremian	*K.compressissima*	limestone	8.8	39.8	12.5	7.5	31.4	8.2	49.9	10.3	12.3	19.2
AN116b	74.83	Early Barremian	*K.compressissima*	marlstone	12.4	42.1	7.9	28.6	8.9	7.8	41.9	7.8	15.2	27.3
AN117	75.17	Early Barremian	*K.compressissima*	limestone	3.2	40.2	4.0	8.9	43.7	6.5	36.9	6.5	15.6	34.6
AN119	76.34	Early Barremian	*K.compressissima*	limestone	3.2	19.9	2.6	14.9	59.4	6.1	37.5	7.8	14.1	34.5
AN119b	77.01	Early Barremian	*K.compressissima*	marlstone	9.0	56.2	17.7	13.2	3.8	7.3	38.7	11.3	13.7	29.1
AN 121	78.36	Early Barremian	*K.compressissima*	limestone	10.7	38.8	10.6	14.7	25.2	8.1	39.1	14.0	15.1	23.7
AN123	78.52	Early Barremian	*K.compressissima*	limestone	6.1	23.2	20.8	13.7	36.1	10.1	37.5	13.6	17.5	21.3
AN123b	78.69	Early Barremian	*K.compressissima*	marlstone	5.5	55.5	7.3	27.2	4.4	14.1	35.2	11.3	19.3	20.1
AN125	79.70	Early Barremian	*C.darsi*	limestone	38.5	18.1	8.5	16.0	19.0	16.3	34.9	10.5	19.1	19.2
AN127	80.70	Early Barremian	*C.darsi*	limestone	2.2	37.3	8.1	19.1	33.2	15.2	36.6	12.7	16.1	19.4
AN127b	81.21	Early Barremian	*C.darsi*	marlstone	11.8	44.6	25.2	12.5	5.9	13.6	39.3	14.7	12.0	20.5
AN128	81.54	Early Barremian	*C.darsi*	limestone	17.2	45.6	11.8	4.2	21.2	14.2	40.8	13.1	10.1	21.8
AN129	82.21	Early Barremian	*C.darsi*	limestone	19.1	26.4	6.9	7.8	39.8	13.8	41.8	9.2	11.5	23.7
AN129b	82.55	Early Barremian	*C.darsi*	marlstone	6.5	57.2	5.8	24.3	6.2	10.3	43.7	6.6	12.9	26.4
AN131	83.39	Early Barremian	*C.darsi*	limestone	6.1	43.3	4.7	9.0	36.8	6.7	46.1	6.4	12.9	28.0
AN133	84.90	Early Barremian	*C.darsi*	limestone	5.0	41.1	9.4	2.9	41.5	6.2	46.0	6.6	13.6	27.7
AN134b	85.57	Early Barremian	*C.darsi*	marlstone	2.0	58.0	4.8	29.2	5.9	8.5	45.7	6.1	15.5	24.1
AN136.2	86.24	Early Barremian	*C.darsi*	limestone	23.3	25.9	6.6	12.7	31.6	9.9	46.7	4.9	15.5	23.0
AN138b	87.08	Early Barremian	*C.darsi*	marlstone	2.7	72.5	1.2	13.7	10.0	9.5	44.9	4.4	11.4	29.8
AN139d	88.09	Early Barremian	*C.darsi*	limestone	7.0	24.3	4.8	3.2	60.7	8.8	42.1	5.1	8.9	35.1
AN141.1	89.09	Late Barremian	*H.uhligi*	limestone	10.4	40.2	9.0	4.7	35.7	11.7	38.4	6.1	10.3	33.5
AN142.2b	89.93	Late Barremian	*H.uhligi*	marlstone	15.3	43.3	5.3	26.0	10.1	18.4	34.7	6.5	11.3	29.2
AN143.1a	90.44	Late Barremian	*H.uhligi*	limestone	29.9	24.3	5.7	3.0	37.1	24.3	32.6	7.3	9.8	26.0
AN144	91.95	Late Barremian	*H.uhligi*	limestone	32.0	25.1	7.9	4.7	30.2	25.3	33.0	9.6	7.1	25.0
AN144b	92.11	Late Barremian	*H.uhligi*	marlstone	20.2	48.3	16.3	8.7	6.4	23.0	36.5	11.9	6.0	22.6
AN147.1	93.29	Late Barremian	*H.uhligi*	limestone	10.1	34.3	11.9	5.5	38.2	22.3	40.7	12.4	5.6	19.1
AN148	94.13	Late Barremian	*H.sayni*	limestone	39.5	41.8	12.2	3.1	3.4	23.8	42.9	11.4	5.3	16.7
AN148b	94.80	Late Barremian	*H.sayni*	marlstone	15.8	55.1	7.3	5.3	16.6	26.8	42.6	11.5	5.7	13.4
AN149.3	95.13	Late Barremian	*H.sayni*	limestone	29.6	30.4	13.9	10.7	15.4	29.2	41.6	13.4	5.1	10.6
AN151.3	96.98	Late Barremian	*H.sayni*	limestone	41.0	39.7	19.2	0.0	0.0	29.1	43.4	14.6	4.0	8.9
AN155.1a	98.99	Late Barremian	*H.sayni*	limestone	22.7	50.7	14.0	0.0	12.7	27.1	46.9	13.3	4.1	8.6
AN155.2b	99.50	Late Barremian	*H.sayni*	marlstone	12.0	63.9	7.0	10.7	6.4	28.7	44.1	11.2	5.4	10.6
AN156.1	99.83	Late Barremian	*H.sayni*	limestone	45.6	19.1	11.0	5.8	18.6	33.4	38.1	10.7	6.0	11.8
AN 156.4	101.17	Late Barremian	*H.sayni*	limestone	51.0	24.5	12.1	4.3	8.1	36.2	34.9	12.3	4.9	11.8
AN156.4b	101.51	Late Barremian	*H.sayni*	marlstone	6.6	64.6	12.7	4.3	11.8	35.8	34.6	14.0	3.3	12.4
AN156.6	102.35	Late Barremian	*H.sayni*	limestone	61.4	6.2	20.5	0.0	11.9	32.2	36.9	14.0	2.9	14.0
AN157.1b	102.68	Late Barremian	*H.sayni*	marlstone	19.9	45.8	7.7	3.5	23.2	26.0	41.1	12.7	6.1	14.1
AN158b	104.03	Late Barremian	*H.sayni*	limestone	10.0	62.6	12.0	7.5	8.0	18.4	45.4	11.4	12.3	12.5
AN160.3b	104.87	Late Barremian	*G.sartousiana*	marlstone	12.1	38.7	11.2	32.4	5.7	16.5	44.2	10.9	15.6	12.8
AN161.1	105.03	Late Barremian	*G.sartousiana*	limestone	23.3	34.7	11.3	10.5	20.1	20.5	41.2	10.6	12.3	15.4
AN161.2	105.54	Late Barremian	*G.sartousiana*	limestone	30.2	38.8	8.0	0.0	23.0	21.5	43.5	10.0	6.4	18.6
AN161.2b	105.70	Late Barremian	*G.sartousiana*	marlstone	15.7	60.7	12.3	1.3	10.1	18.0	45.8	8.9	4.3	23.1
AN163.1b	106.54	Late Barremian	*G.sartousiana*	marlstone	8.2	42.1	5.8	9.3	34.6	13.6	41.9	7.2	9.7	27.6
AN164.2	107.72	Late Barremian	*H.feraudianus*	limestone	14.1	29.3	4.5	8.0	44.0	14.4	32.6	5.7	18.2	29.1
AN165b	108.56	Late Barremian	*H.feraudianus*	marlstone	10.9	25.1	4.7	51.2	8.0	22.6	23.2	4.9	21.8	27.5
AN166b	108.72	Late Barremian	*H.feraudianus*	marlstone	43.4	12.0	5.7	3.0	35.8	30.9	17.8	4.6	22.2	24.4
AN168.1	109.73	Late Barremian	*I.giraudi*	limestone	46.9	11.9	3.3	14.1	23.8	32.9	17.1	4.6	22.9	22.5
AN168.1b	109.90	Late Barremian	*I.giraudi*	marlstone	9.8	25.6	3.6	50.5	10.5	28.7	18.9	5.1	23.2	24.2
AN170c	110.57	Late Barremian	*I.giraudi*	limestone	36.8	19.1	9.0	6.6	28.5	22.2	21.6	5.6	22.0	28.7
AN172.1	111.41	Late Barremian	*I.giraudi*	limestone	11.0	18.8	3.8	10.8	55.5	19.8	24.3	5.8	19.9	30.1
AN172.1b	111.91	Late Barremian	*I.giraudi*	marlstone	9.4	37.2	5.3	39.8	8.3	21.3	28.7	6.3	19.3	24.4
AN173	112.58	Late Barremian	*I.giraudi*	limestone	45.0	22.6	8.4	5.8	18.1	23.5	32.7	7.7	17.4	18.7
AN174.1b	113.59	Late Barremian	*I.giraudi*	marlstone	12.9	52.6	9.1	15.5	9.8	23.0	35.0	9.0	13.1	19.9
AN176.1	114.43	Late Barremian	*I.giraudi*	limestone	24.1	13.8	11.6	8.3	42.2	20.4	37.1	9.2	10.9	22.4
AN176.1b	115.10	Late Barremian	*I.giraudi*	marlstone	7.3	62.6	6.5	12.8	10.8	22.7	36.2	9.5	10.0	21.6
AN177	115.44	Late Barremian	*M.sarasini*	limestone	42.7	21.1	8.7	7.3	20.2	26.8	35.4	11.7	7.9	18.2
AN179.1	116.28	Late Barremian	*M.sarasini*	limestone	30.3	26.6	17.6	6.4	19.1	31.3	35.4	14.5	5.0	13.7
AN179.1b	116.44	Late Barremian	*M.sarasini*	marlstone	14.0	59.0	21.3	0.0	5.7	41.6	33.3	14.5	2.2	8.4
AN181	117.79	Late Barremian	*M.sarasini*	limestone	77.2	15.7	7.1	0.0	0.0	57.7	27.6	11.1	0.5	3.0
AN183	118.62	Late Barremian	*M.sarasini*	limestone	78.1	15.7	6.2	0.0	0.0	68.1	23.4	8.1	0.0	0.5
AN185	119.97	Late Barremian	*M.sarasini*	limestone	76.7	18.1	5.2	0.0	0.0	58.7	32.4	8.4	0.3	0.2
AN188	121.64	Late Barremian	*M.sarasini*	limestone	28.7	57.3	14.0	0.0	0.0	40.7	47.5	10.2	0.8	0.7
AN188b	122.32	Late Barremian	*M.sarasini*	marlstone	0.0	81.9	11.9	3.3	3.0	31.6	54.3	11.5	1.7	1.0
AN190	122.82	Late Barremian	*M.sarasini*	limestone	65.1	25.4	9.5	0.0	0.0	29.5	54.1	11.9	2.9	1.6
AN192	123.83	Late Barremian	*M.sarasini*	limestone	20.8	57.9	14.5	6.9	0.0	27.4	52.1	11.9	4.2	4.4
AN193b	124.50	Late Barremian	*M.sarasini*	marlstone	2.2	70.6	11.9	4.7	10.6	24.2	48.2	11.3	4.6	11.6
AN195	125.50	Late Barremian	*M.sarasini*	limestone	43.4	23.7	9.1	5.3	18.4	27.4	39.7	10.0	3.5	19.3
AN 196.2	126.68	Late Barremian	*M.sarasini*	limestone	24.3	25.4	8.3	0.0	41.9	34.3	34.5	10.0	1.7	19.5
AN197	127.35	Early Aptian	*D.oglanlensis*	limestone	55.5	35.8	8.7	0.0	0.0	32.5	41.5	11.3	1.2	13.6
AN 198	128.19	Early Aptian	*D.oglanlensis*	limestone	15.6	63.3	21.1	0.0	0.0	25.4	53.5	10.8	2.3	8.1
AN198b	128.52	Early Aptian	*D.oglanlensis*	marlstone	4.7	64.3	3.4	9.2	18.4	19.9	61.7	7.6	3.4	7.4
AN200	129.19	Early Aptian	*D.oglanlensis*	limestone	37.3	62.7	0.0	0.0	0.0	18.4	64.3	5.5	3.4	8.4
AN201b	129.87	Early Aptian	*D.oglanlensis*	marlstone	5.7	69.6	5.0	4.5	15.2	20.7	61.7	8.7	2.3	6.6
AN 202c	130.37	Early Aptian	*D.oglanlensis*	limestone	24.5	56.1	19.4	0.0	0.0	26.0	54.5	14.6	1.1	3.8
AN204	131.88	Early Aptian	*D.oglanlensis*	limestone	35.3	41.6	23.1	0.0	0.0	31.7	48.0	17.1	1.1	2.1
AN 206	133.22	Early Aptian	*D.oglanlensis*	limestone	53.4	33.5	13.1	0.0	0.0	29.8	48.7	15.2	2.7	3.6
AN206b	133.89	Early Aptian	*D.oglanlensis*	marlstone	0.0	70.8	10.6	9.2	9.5	23.9	51.5	12.4	4.2	8.1
AN210b	134.20	Early Aptian	*D.oglanlensis*	marlstone	14.1	56.8	9.7	4.4	15.1	27.7	45.0	12.7	3.8	10.8
AN211	134.72	Early Aptian	*D.oglanlensis*	limestone	49.1	22.3	14.9	0.0	13.7	40.6	31.3	15.3	3.1	9.7
AN 214	136.22	Early Aptian	*D.oglanlensis*	limestone	75.7	0.0	24.3	0.0	0.0	47.8	24.0	17.6	4.2	6.5
AN215b	137.40	Early Aptian	*D.oglanlensis*	marlstone	21.3	45.0	11.2	15.4	7.1					
AN216	137.72	Early Aptian	*D.oglanlensis*	limestone	45.3	29.1	25.6	0.0	0.0					

Table An.2.4 (continued): semi-quantitative estimation of the amount of the identified minerals in the <2 μm fraction of samples from the Angles section.

Sample ID	Depth (m)	Stage	Ammonite Zone	Lithology	Quantification 2-16 μm fraction (relative %)				Five-Point Moving Average (relative %)			
					Mica	R0 I/S	Kaolinite	Chlorite	Mica	R0 I/S	Kaolinite	Chlorite
AN 2	0.34	Late Hauterivian	*B.balearis*	limestone	78.9	5.3	2.4	13.4				
AN2b	0.50	Late Hauterivian	*B.balearis*	marlstone	57.7	4.9	25.4	12.0				
AN4	1.68	Late Hauterivian	*B.balearis*	limestone	60.5	13.4	5.4	20.8	64.1	9.8	11.7	14.4
AN 6	2.85	Late Hauterivian	*B.balearis*	limestone	68.8	13.1	8.1	10.1	64.8	10.5	11.4	13.2
AN6b	3.02	Late Hauterivian	*B.balearis*	marlstone	68.5	5.4	16.2	9.9	63.4	10.8	13.0	12.8
AN8	4.03	Late Hauterivian	*B.balearis*	limestone	58.3	12.8	14.4	14.4	58.0	11.5	17.0	13.5
AN 10	4.87	Late Hauterivian	*B.balearis*	limestone	45.2	17.3	17.7	19.9	53.9	11.6	20.0	14.5
AN10b	5.20	Late Hauterivian	*B.balearis*	marlstone	53.3	5.2	36.7	4.9	56.3	10.5	17.9	15.4
AN13	6.38	Late Hauterivian	*B.balearis*	limestone	62.3	10.7	0.0	27.0	63.6	9.7	10.9	15.8
AN 15.1	7.38	Late Hauterivian	*B.balearis*	limestone	81.8	8.1	0.0	10.1	67.5	10.6	3.9	18.0
AN15.1b	7.72	Late Hauterivian	*B.balearis*	marlstone	63.4	16.4	3.2	17.0	66.6	10.8	1.2	21.3
AN16	8.39	Late Hauterivian	*B.balearis*	limestone	51.9	8.6	0.0	39.5	66.5	9.3	1.3	22.9
AN18	9.56	Late Hauterivian	*B.balearis*	limestone	82.6	3.0	2.0	12.4	69.1	8.3	0.9	21.7
AN18b	9.90	Late Hauterivian	*B.balearis*	marlstone	71.1	10.2	0.0	18.7	72.6	8.5	0.8	18.1
AN20	10.40	Late Hauterivian	*B.balearis*	limestone	66.3	14.7	0.0	19.0	73.6	8.6	2.1	15.7
AN26	12.42	Late Hauterivian	*B.balearis*	limestone	88.2	0.0	3.2	8.6	70.9	7.6	7.6	13.9
AN27.2	13.26	Late Hauterivian	*B.balearis*	limestone	57.2	10.9	13.4	18.5	67.6	6.2	15.1	11.1
AN27.2b	13.59	Late Hauterivian	*B.balearis*	marlstone	55.9	4.0	38.4	1.6	67.3	5.3	18.2	9.1
AN29	14.43	Late Hauterivian	*B.balearis*	limestone	84.0	4.1	2.6	9.2	70.7	5.0	15.0	9.3
AN 29b	14.93	Late Hauterivian	*B.balearis*	marlstone	72.3	3.0	13.7	11.0	74.6	5.6	8.6	11.2
AN31	15.60	Late Hauterivian	*B.balearis*	limestone	70.4	11.6	0.0	18.1	75.9	6.7	5.6	11.8
AN 33	16.44	Late Hauterivian	*B.balearis*	limestone	87.2	4.7	1.4	6.7	75.9	7.1	6.4	10.7
AN 33b	16.95	Late Hauterivian	*B.balearis*	marlstone	66.8	7.6	18.9	6.6	76.2	6.7	6.7	10.5
AN 34b	17.45	Late Hauterivian	*B.balearis*	marlstone	77.8	5.6	0.0	16.6	76.9	6.7	5.3	11.1
AN35	17.95	Late Hauterivian	*B.balearis*	limestone	81.7	7.4	0.0	10.9	77.2	7.4	4.3	11.2
AN 35b	17.95	Late Hauterivian	*B.balearis*	marlstone	79.3	8.4	5.4	6.9	75.6	8.0	6.0	10.4
AN38	18.79	Late Hauterivian	*S.angulicostatum*	limestone	61.0	9.8	15.9	13.3	74.7	7.6	7.7	10.0
AN38b	18.96	Late Hauterivian	*S.angulicostatum*	marlstone	84.5	5.2	2.9	7.5	77.8	6.3	6.4	9.5
AN39b	19.30	Late Hauterivian	*S.angulicostatum*	marlstone	79.7	4.2	3.9	12.3	82.5	6.3	3.3	7.9
AN40	19.63	Late Hauterivian	*S.angulicostatum*	limestone	95.1	4.9	0.0	0.0	83.6	8.4	1.2	6.8
AN40b	19.97	Late Hauterivian	*S.angulicostatum*	limestone	71.3	19.2	0.0	9.5	82.4	10.0	0.5	7.2
AN41b	20.13	Late Hauterivian	*S.angulicostatum*	marlstone	85.1	6.0	0.0	8.9	78.9	9.2	1.4	10.6
AN42b	20.47	Late Hauterivian	*S.angulicostatum*	marlstone	83.0	6.2	1.6	9.2	74.1	6.8	3.7	15.4
AN43	20.64	Late Hauterivian	*S.angulicostatum*	limestone	48.7	4.5	11.9	35.0	71.0	5.6	6.5	16.8
AN44b	20.97	Late Hauterivian	*S.angulicostatum*	marlstone	84.6	6.2	1.9	7.3	70.9	5.7	8.9	14.6
AN45b	21.31	Late Hauterivian	*S.angulicostatum*	marlstone	69.5	6.3	20.5	3.7	72.7	6.1	9.7	11.5
AN46	21.48	Late Hauterivian	*S.angulicostatum*	limestone	74.6	4.7	0.0	20.7	73.4	6.4	10.5	9.7
AN46b	21.81	Late Hauterivian	*S.angulicostatum*	marlstone	68.3	10.4	17.5	3.9	74.2	6.0	10.7	9.2
AN48b	22.65	Late Hauterivian	*S.angulicostatum*	marlstone	84.1	1.4	10.4	4.1	76.2	5.3	9.8	8.8
AN49.1	22.82	Late Hauterivian	*S.angulicostatum*	limestone	71.4	5.3	6.9	16.4	78.5	5.2	7.1	9.2
AN50	23.32	Late Hauterivian	*S.angulicostatum*	limestone	84.6	5.9	2.5	7.0	80.2	6.5	4.3	9.1
AN51	23.83	Late Hauterivian	*S.angulicostatum*	limestone	82.2	8.7	2.1	6.9	80.7	8.2	3.0	8.1
AN51b	24.16	Late Hauterivian	*S.angulicostatum*	marlstone	78.5	10.5	4.3	6.7	78.0	9.4	3.1	9.4
AN53.1b	24.83	Late Hauterivian	*S.angulicostatum*	marlstone	78.2	9.5	0.0	12.2	73.2	9.7	4.4	12.7
AN53.2	25.00	Late Hauterivian	*S.angulicostatum*	limestone	56.1	10.7	11.4	21.8	71.5	8.9	5.2	14.4
AN55	25.34	Late Hauterivian	*P.mortilleti*	limestone	79.9	5.6	3.1	11.3	72.3	7.5	5.3	14.9
AN62.1	27.85	Late Hauterivian	*P.mortilleti*	limestone	81.0	7.6	3.7	7.7	72.3	6.2	4.4	17.1
AN65.1	28.86	Late Hauterivian	*P.mortilleti*	limestone	58.3	2.6	5.9	33.2	69.1	6.1	5.4	19.4
AN68	30.54	Late Hauterivian	*P.mortilleti*	limestone	72.3	8.5	0.0	19.2	64.3	6.9	10.5	18.3
AN72b	32.72	Early Barremian	*A.kiliani*	marlstone	55.6	9.0	27.0	8.3	62.4	7.6	15.6	14.4
AN73b	33.22	Early Barremian	*A.kiliani*	marlstone	59.8	6.1	23.4	10.8	62.5	7.4	18.3	11.8
AN75	34.06	Early Barremian	*A.kiliani*	limestone	72.2	8.3	3.2	16.4	62.6	6.7	20.0	10.7
AN75b	34.23	Early Barremian	*A.kiliani*	marlstone	55.2	4.4	35.0	5.4	59.4	6.1	22.6	11.9
AN76b	34.56	Early Barremian	*A.kiliani*	marlstone	62.2	6.9	24.5	6.5	54.2	5.5	23.7	16.6
AN78	35.74	Early Barremian	*A.kiliani*	limestone	29.5	4.2	24.5	41.9	53.9	5.2	20.5	20.4
AN81	37.08	Early Barremian	*A.kiliani*	limestone	75.7	4.4	4.4	15.6	57.7	5.8	16.7	19.8
AN81b	37.42	Early Barremian	*A.kiliani*	marlstone	60.0	7.6	26.6	5.7	61.5	6.6	15.4	16.5
AN84	38.93	Early Barremian	*A.kiliani*	limestone	59.4	9.4	4.8	26.4	60.2	6.6	15.8	17.3
AN84b	39.26	Early Barremian	*A.kiliani*	marlstone	62.9	3.5	26.5	7.1	54.7	6.2	16.8	22.4
AN87	40.44	Early Barremian	*A.kiliani*	limestone	40.5	4.0	7.2	48.3	49.9	6.5	19.0	24.6
AN87b	41.11	Early Barremian	*A.kiliani*	marlstone	45.1	12.4	32.5	10.0	48.7	7.6	20.1	23.6
AN89	41.95	Early Barremian	*A.kiliani*	limestone	54.0	4.9	17.4	23.7	51.7	8.1	20.2	20.0
AN90 haut	42.95	Early Barremian	*A.kiliani*	limestone	58.2	10.7	10.8	20.4	56.1	7.3	20.5	16.1
AN90b	43.46	Early Barremian	*A.kiliani*	marlstone	53.9	4.5	36.0	5.6	60.5	5.8	19.1	14.6
AN92	44.80	Early Barremian	*A.kiliani*	limestone	71.4	4.1	10.4	14.0	63.6	4.8	16.2	15.4
AN93 haut	46.14	Early Barremian	*A.kiliani*	limestone	67.1	2.4	4.7	25.9	63.7	5.3	12.5	18.6
AN93b	46.48	Early Barremian	*A.kiliani*	marlstone	56.3	10.1	19.6	14.0	61.2	6.2	11.0	21.6
AN95 bas	47.99	Early Barremian	*K.nicklesi*	limestone	58.5	6.4	5.2	29.8	59.8	6.0	12.5	21.7
AN97	49.50	Early Barremian	*K.nicklesi*	limestone	60.8	3.5	13.5	22.2	61.7	5.1	14.3	18.9
AN97b	49.83	Early Barremian	*K.nicklesi*	marlstone	65.1	3.1	25.6	6.2	65.4	5.3	14.1	15.2
AN98 haut	50.50	Early Barremian	*K.nicklesi*	limestone	70.5	8.3	5.1	16.0	66.5	6.3	14.3	12.9
AN101	52.18	Early Barremian	*K.nicklesi*	limestone	71.5	8.8	6.1	13.5	62.6	6.3	16.6	14.6
AN101b	52.52	Early Barremian	*K.nicklesi*	marlstone	45.0	2.9	42.6	9.5	56.2	4.8	18.5	20.5
AN103	53.86	Early Barremian	*K.nicklesi*	limestone	53.0	3.8	5.4	37.8	52.9	3.4	16.5	27.2
AN103b	54.53	Early Barremian	*K.nicklesi*	marlstone	50.0	0.0	12.0	38.0	55.6	3.9	11.4	29.2
AN104	55.20	Early Barremian	*K.nicklesi*	limestone	66.5	7.9	6.1	19.4	60.8	5.5	10.2	23.5
AN105	56.38	Early Barremian	*K.nicklesi*	limestone	63.6	8.3	11.4	16.6	64.0	6.4	14.1	15.5
AN108	59.56	Early Barremian	*K.nicklesi*	limestone	69.8	5.5	22.5	2.2	63.5	5.6	19.9	10.9
AN109.4	61.07	Early Barremian	*N.pulchella*	limestone	54.8	2.9	25.3	17.0	63.2	4.4	24.1	8.3
AN110.1b	62.25	Early Barremian	*N.pulchella*	marlstone	61.2	3.9	32.9	1.9	68.2	3.7	22.0	6.1
AN 110.3c	64.09	Early Barremian	*N.pulchella*	limestone	82.0	4.4	10.7	2.9	77.4	3.3	14.9	4.4
AN110.4	65.27	Early Barremian	*N.pulchella*	limestone	93.8	0.8	2.0	3.4	83.9	3.3	8.1	4.7
AN111.2	66.28	Early Barremian	*N.pulchella*	limestone	81.0	5.0	5.2	8.8	83.5	3.9	6.4	6.3

Table An.2.5: semi-quantitative estimation of the amount of the identified minerals in the 2-16 μm fraction of samples from the Angles section.

Sample ID	Depth (m)	Stage	Ammonite Zone	Lithology	Quantification 2-16 μm fraction (relative %)				Five-Point Moving Average (relative %)			
					Mica	R0 I/S	Kaolinite	Chlorite	Mica	R0 I/S	Kaolinite	Chlorite
AN111.5	67.28	Early Barremian	*N.pulchella*	limestone	81.3	4.3	8.0	6.4	76.8	5.3	10.6	7.3
AN112.2	68.79	Early Barremian	*N.pulchella*	limestone	71.4	6.3	14.5	7.8	69.2	7.2	16.1	7.6
AN112.7	71.64	Early Barremian	*K.compressissima*	limestone	45.9	12.0	33.6	8.5	66.8	8.1	17.0	8.1
AN114.2	72.99	Early Barremian	*K.compressissima*	limestone	82.4	6.9	4.9	5.8	69.1	7.1	14.1	9.7
AN115	73.99	Early Barremian	*K.compressissima*	limestone	75.3	5.2	3.9	15.6	70.4	4.7	11.8	13.1
AN116b	74.83	Early Barremian	*K.compressissima*	marlstone	64.5	0.0	22.9	12.6	67.0	2.9	11.8	18.4
AN117	75.17	Early Barremian	*K.compressissima*	limestone	57.0	3.3	8.9	30.8	63.8	2.4	12.0	21.8
AN119	76.34	Early Barremian	*K.compressissima*	limestone	66.2	2.0	6.6	25.2	65.6	2.9	10.6	20.8
AN119b	77.01	Early Barremian	*K.compressissima*	marlstone	70.7	4.0	15.5	9.8	70.6	3.8	9.1	16.4
AN 121	78.36	Early Barremian	*K.compressissima*	limestone	75.1	5.6	4.8	14.5	74.5	4.4	9.1	12.0
AN123	78.52	Early Barremian	*K.compressissima*	limestone	83.9	4.1	4.3	7.6	71.4	4.2	13.1	11.3
AN123b	78.69	Early Barremian	*K.compressissima*	marlstone	64.0	3.6	23.6	8.7	63.3	3.6	19.3	13.9
AN125	79.70	Early Barremian	*C.darsi*	limestone	33.2	2.6	38.5	25.6	58.6	3.2	19.9	18.3
AN127	80.70	Early Barremian	*C.darsi*	limestone	76.4	3.2	3.3	17.1	62.1	3.2	13.0	21.8
AN127b	81.21	Early Barremian	*C.darsi*	marlstone	64.6	3.8	0.0	31.6	67.4	3.1	5.9	23.6
AN128	81.54	Early Barremian	*C.darsi*	limestone	81.8	2.2	3.6	12.3	65.9	3.2	5.9	25.0
AN129	82.21	Early Barremian	*C.darsi*	limestone	43.0	3.6	10.9	42.5	62.4	3.3	9.9	24.4
AN129b	82.55	Early Barremian	*C.darsi*	marlstone	64.6	3.8	19.7	11.9	61.7	4.3	11.3	22.7
AN131	83.39	Early Barremian	*C.darsi*	limestone	73.2	3.0	4.7	19.2	61.5	6.2	12.0	20.4
AN133	84.90	Early Barremian	*C.darsi*	limestone	51.4	14.6	6.2	27.8	57.7	7.1	14.9	20.3
AN134b	85.57	Early Barremian	*C.darsi*	marlstone	54.1	3.8	36.1	6.0	53.5	6.4	17.6	22.5
AN136.2	86.24	Early Barremian	*C.darsi*	limestone	41.0	2.8	11.5	44.8	55.5	5.0	16.4	23.0
AN138b	87.08	Early Barremian	*C.darsi*	marlstone	75.3	6.2	9.8	8.7	62.3	4.8	11.4	21.5
AN139d	88.09	Early Barremian	*C.darsi*	limestone	62.6	4.7	7.8	25.0	69.7	5.2	8.5	16.6
AN141.1	89.09	Late Barremian	*H.uhligi*	limestone	81.7	6.5	3.4	8.4	74.3	4.8	9.2	11.7
AN142.2b	89.93	Late Barremian	*H.uhligi*	marlstone	73.8	2.4	20.1	3.7	74.9	4.4	9.4	11.4
AN143.1a	90.44	Late Barremian	*H.uhligi*	limestone	79.7	4.8	3.1	12.3	72.2	4.2	8.5	15.1
AN144	91.95	Late Barremian	*H.uhligi*	limestone	56.1	4.3	5.4	34.2	68.6	4.7	6.6	20.1
AN144b	92.11	Late Barremian	*H.uhligi*	marlstone	76.3	4.7	9.5	9.5	66.7	5.6	5.2	22.5
AN147.1	93.29	Late Barremian	*H.uhligi*	limestone	56.3	8.2	0.0	35.5	67.8	6.5	4.8	20.9
AN148	94.13	Late Barremian	*H.sayni*	limestone	77.7	6.1	5.8	10.3	67.4	7.8	4.2	20.6
AN148b	94.80	Late Barremian	*H.sayni*	marlstone	70.5	7.8	6.0	15.7	64.6	9.4	4.2	21.8
AN149.3	95.13	Late Barremian	*H.sayni*	limestone	40.9	16.7	0.0	42.4	63.2	10.1	4.5	22.1
AN155.2b	99.50	Late Barremian	*H.sayni*	marlstone	80.8	5.4	8.7	5.1	63.1	9.7	4.5	22.7
AN156.1	99.83	Late Barremian	*H.sayni*	limestone	63.9	8.6	4.4	23.1	63.9	9.1	3.8	23.3
AN 156.4	101.17	Late Barremian	*H.sayni*	limestone	48.7	11.7	0.0	39.6	66.5	8.4	2.4	22.7
AN156.4b	101.51	Late Barremian	*H.sayni*	marlstone	81.3	6.5	1.4	10.8	71.3	7.4	2.2	19.0
AN156.6	102.35	Late Barremian	*H.sayni*	limestone	86.8	3.6	2.4	7.2	72.9	6.9	4.8	15.4
AN157.1b	102.68	Late Barremian	*H.sayni*	marlstone	59.9	8.8	9.4	21.9	66.7	7.9	9.1	16.3
AN160.3b	104.87	Late Barremian	*G.sartousiana*	marlstone	55.0	11.6	15.5	17.9	61.1	8.6	11.7	18.5
AN161.1	105.03	Late Barremian	*G.sartousiana*	limestone	54.3	7.9	16.2	21.6	63.0	7.8	11.5	17.8
AN161.2	105.54	Late Barremian	*G.sartousiana*	limestone	83.4	3.6	0.0	13.0	66.4	7.3	10.9	15.4
AN161.2b	105.70	Late Barremian	*G.sartousiana*	marlstone	63.3	7.2	17.4	12.1	65.9	9.0	12.0	13.1
AN163.1b	106.54	Late Barremian	*G.sartousiana*	marlstone	54.7	16.8	14.2	14.2	61.4	10.3	17.7	10.6
AN164.2	107.72	Late Barremian	*H.feraudianus*	limestone	68.9	9.8	16.2	5.1	53.4	9.2	25.3	12.0
AN165b	108.56	Late Barremian	*H.feraudianus*	marlstone	37.4	2.0	54.7	5.9	43.5	6.9	29.4	20.3
AN166b	108.72	Late Barremian	*H.feraudianus*	marlstone	25.5	7.8	15.4	51.2	35.0	5.6	30.9	28.5
AN168.1	109.73	Late Barremian	*I.giraudi*	limestone	34.3	5.0	24.7	36.0	34.3	5.5	31.7	28.5
AN168.1b	109.90	Late Barremian	*I.giraudi*	marlstone	34.3	5.3	54.7	5.7	42.5	4.9	30.4	22.2
AN170c	110.57	Late Barremian	*I.giraudi*	limestone	57.8	3.9	16.8	21.5	51.6	4.2	26.8	17.4
AN172.1	111.41	Late Barremian	*I.giraudi*	limestone	70.8	3.0	6.2	20.0	56.0	4.3	23.2	16.5
AN172.1b	111.91	Late Barremian	*I.giraudi*	marlstone	38.7	5.0	46.7	9.7	57.5	5.4	21.5	15.6
AN173	112.58	Late Barremian	*I.giraudi*	limestone	64.8	8.1	8.1	19.0	60.1	6.4	18.1	15.3
AN174.1b	113.59	Late Barremian	*I.giraudi*	marlstone	71.1	7.8	11.1	10.1	64.5	6.1	12.7	16.7
AN176.1	114.43	Late Barremian	*I.giraudi*	limestone	62.1	3.5	5.3	29.1	66.8	5.0	11.0	17.2
AN176.1b	115.10	Late Barremian	*I.giraudi*	marlstone	69.7	2.6	21.2	6.5	68.0	4.7	11.1	16.1
AN177	115.44	Late Barremian	*M.sarasini*	limestone	65.6	7.5	5.8	21.0	72.7	5.2	8.8	13.3
AN179.1	116.28	Late Barremian	*M.sarasini*	limestone	83.0	6.1	3.5	7.4	79.0	5.6	5.0	10.4
AN179.1b	116.44	Late Barremian	*M.sarasini*	marlstone	89.4	3.5	2.3	4.7	83.6	5.6	2.1	8.7
AN181	117.79	Late Barremian	*M.sarasini*	limestone	80.9	7.4	0.0	11.7	85.8	5.8	0.9	7.5
AN183	118.62	Late Barremian	*M.sarasini*	limestone	87.8	4.9	0.0	7.3	86.3	6.8	0.2	6.8
AN185	119.97	Late Barremian	*M.sarasini*	limestone	91.0	9.0	0.0	0.0	85.7	7.6	0.3	6.4
AN188	121.64	Late Barremian	*M.sarasini*	limestone	79.4	8.5	0.0	12.1	84.1	8.0	1.1	6.8
AN188b	122.32	Late Barremian	*M.sarasini*	marlstone	82.3	7.1	3.2	7.3	82.8	8.7	1.9	6.6
AN190	122.82	Late Barremian	*M.sarasini*	limestone	83.7	8.5	3.4	4.4	82.4	10.0	2.3	5.3
AN192	123.83	Late Barremian	*M.sarasini*	limestone	84.7	15.3	0.0	0.0	78.6	11.7	3.7	6.0
AN193b	124.50	Late Barremian	*M.sarasini*	marlstone	73.4	10.9	4.4	11.4	67.3	12.2	7.1	13.4
AN195	125.50	Late Barremian	*M.sarasini*	limestone	50.6	14.4	18.0	17.0	54.7	11.6	9.8	23.9
AN 196.2	126.68	Late Barremian	*M.sarasini*	limestone	24.3	5.7	9.8	60.2	53.4	11.5	8.8	26.3
AN197	127.35	Early Aptian	*D.oglanlensis*	limestone	76.4	16.8	2.6	4.2	64.4	11.4	4.8	19.3
AN 198	128.19	Early Aptian	*D.oglanlensis*	limestone	89.6	10.4	0.0	0.0	77.6	9.9	1.5	11.0
AN198b	128.52	Early Aptian	*D.oglanlensis*	marlstone	75.5	7.2	0.0	17.3	83.3	7.3	0.5	8.9
AN200	129.19	Early Aptian	*D.oglanlensis*	limestone	92.6	0.0	0.0	7.4	82.7	6.0	0.9	10.4
AN201b	129.87	Early Aptian	*D.oglanlensis*	marlstone	74.4	11.1	3.5	10.9	81.8	7.4	1.2	9.7
AN 202c	130.37	Early Aptian	*D.oglanlensis*	limestone	82.5	6.6	0.0	10.9	82.4	9.7	0.9	7.0
AN204	131.88	Early Aptian	*D.oglanlensis*	limestone	83.0	17.0	0.0	0.0	84.8	10.7	0.4	4.1
AN 206	133.22	Early Aptian	*D.oglanlensis*	limestone	94.3	5.7	0.0	0.0	84.6	10.6	0.5	4.3
AN206b	133.89	Early Aptian	*D.oglanlensis*	marlstone	80.5	11.8	1.8	5.8	78.8	10.1	1.7	9.5
AN210b	134.20	Early Aptian	*D.oglanlensis*	marlstone	65.6	11.0	0.0	23.4	72.3	9.7	3.8	14.2
AN211	134.72	Early Aptian	*D.oglanlensis*	limestone	60.5	6.6	13.2	19.8	73.4	9.0	4.6	13.0
AN 214	136.22	Early Aptian	*D.oglanlensis*	limestone	88.2	11.8	0.0	0.0	81.7	7.8	3.3	7.2
AN215b	137.40	Early Aptian	*D.oglanlensis*	marlstone	97.2	1.4	0.2	1.2				
AN216	138.90	Early Aptian	*D.oglanlensis*	limestone	89.0	11.0	0.0	0.0				

Table An.2.5 (continued): semi-quantitative estimation of the amount of the identified minerals in the 2-16 μm fraction of samples from the Angles section.

Sample ID	Depth (m)	Stage	Ammonite Zone	Lithology	Peak Intensity (cps)																
					"Smectite" 001 5.2°2θ	R1 I/S 001 ≈6.5°2θ	Mica 001 8.8°2θ	R0 I/S 002 9-9.5°2θ	Kaolinite / Chlorite 001/002 12.34°2θ	Mica 002 17.92°2θ	Chlorite 003 18.56°2θ	Quartz 20.85°2θ	Goethite 21.2°2θ	Kaolinite 002 24.9°2θ	Chlorite 004 25.2°2θ	K-Feldspar 27.5°2θ	Na-Plagioclas 27.9°2θ	Pyrite 28.12°2θ	Mica 005 45.68°2θ	K001* K002*(K001,C002)/(K002+C004)	C002* C004*(K001,C002)/(K002+C004)
COM 104	2.09	Early Aptian	*D. oglanlensis*	limestone	955	0	161	109	315	31	0	564	0	53	156	89	23	44	26	79.88	235.12
COM 106	3.07	Early Aptian	*D. oglanlensis*	limestone	1066	0	295	292	0	87	0	818	14	0	0	233	71	0	150	0.00	0.00
COM 106*	3.19	Early Aptian	*D. oglanlensis*	marlstone	152	0	401	133	255	132	0	109	0	22	118	99	106	0	98	40.07	214.93
COM 107*	3.51	Early Aptian	*D. oglanlensis*	marlstone	0	100	148	35	325	10	0	22	0	164	38	80	162	27	44	263.86	61.14
COM 108	3.77	Early Aptian	*D. weissi*	limestone	232	0	194	103	133	54	0	546	0	0	51	92	46	40	47	0.00	133.00
COM 108*	3.94	Early Aptian	*D. weissi*	marlstone	198	0	591	179	280	343	21	128	0	108	266	271	166	129	408	80.86	199.14
COM 110	4.64	Early Aptian	*D. weissi*	limestone	73	0	38	21	34	13	0	118	16	10	32	35	46	0	0	8.10	25.90
COM 110*	4.81	Early Aptian	*D. weissi*	marlstone	85	0	176	20	141	49	0	122	0	14	55	48	27	0	21	28.61	112.39
COM 112	5.51	Early Aptian	*D. weissi*	limestone	373	0	144	103	37	41	0	465	0	0	43	31	42	0	43	0.00	37.00
COM 114	6.20	Early Aptian	*D. weissi*	limestone	122	0	231	41	212	97	22	644	0	60	126	117	46	0	34	68.39	143.61
COM 114*	6.46	Early Aptian	*D. weissi*	marlstone	0	0	272	92	155	114	0	93	0	15	126	76	54	34	53	16.49	138.51
COM 116	7.19	Early Aptian	*D. weissi*	limestone	281	0	179	99	129	50	0	749	39	13	71	54	59	13	66	19.96	109.04
COM 116*	7.33	Early Aptian	*D. weissi*	marlstone	179	0	550	114	301	256	38	135	15	50	223	187	105	116	146	55.13	245.87
COM 118	8.06	Early Aptian	*D. weissi*	limestone	331	0	177	112	147	39	0	357	0	29	108	141	33	44	32	31.12	115.88
COM 118*	8.35	Early Aptian	*D. weissi*	marlstone	0	0	564	138	131	297	23	149	0	53	88	192	101	0	239	49.24	81.76
COM 120	8.99	Early Aptian	*D. weissi*	limestone	290	0	210	146	110	54	0	698	0	37	58	96	44	46	57	42.84	67.16
COM 120*	9.16	Early Aptian	*D. weissi*	marlstone	45	0	538	92	148	217	0	115	0	90	56	103	82	67	100	91.23	56.77
COM 122h	9.94	Early Aptian	*D. weissi*	limestone	695	0	268	100	105	63	0	507	0	48	64	237	61	0	43	45.00	60.00
COM 122*	10.00	Early Aptian	*D. weissi*	marlstone	234	0	590	183	515	280	35	203	0	42	358	237	158	94	221	54.08	460.93
COM 124	10.55	Early Aptian	*D. weissi*	limestone	832	0	263	69	410	78	22	294	0	36	234	71	64	0	48	54.67	355.33
COM 124*	10.67	Early Aptian	*D. weissi*	marlstone	0	0	209	16	201	175	50	44	0	28	116	47	43	40	45	39.08	161.92
COM 126	11.25	Early Aptian	*D. weissi*	limestone	129	0	282	28	652	109	18	221	0	40	478	55	70	18	63	50.35	601.65
COM 126*	11.36	Early Aptian	*D. weissi*	marlstone	60	0	365	167	190	112	25	72	0	34	81	94	80	95	65	56.17	133.83
COM 128	12.06	Early Aptian	*D. weissi*	limestone	169	0	225	125	702	135	53	196	0	120	182	156	82	48	52	278.94	423.06
COM 128*	12.23	Early Aptian	*D. weissi*	marlstone	0	0	284	42	653	256	54	229	0	88	442	75	64	76	93	108.42	544.58

Table A2.6: peak intensities of the identified minerals in the <2 µm fraction of samples from the Combe-Lambert section.

Sample ID	Depth (m)	Stage	Ammonite Zone	Lithology	Quantification (%)						Five-point Moving Average (%)					
					"Smectite"	Mica	R0 I/S	Kaolinite	Chlorite	R1 I/S	"Smectite"	Mica	R0 I/S	Kaolinite	Chlorite	R1 I/S
COM 104	2.09	Early Aptian	*D. oglanlensis*	limestone	62.01	10.45	7.08	5.19	15.27	0.00						
COM 106	3.07	Early Aptian	*D. oglanlensis*	limestone	64.49	17.85	17.66	0.00	0.00	0.00						
COM 106*	3.19	Early Aptian	*D. oglanlensis*	marlstone	16.15	42.61	14.13	4.26	22.84	0.00	29.59	28.07	12.45	12.70	13.07	4.11
COM 107*	3.51	Early Aptian	*D. oglanlensis*	marlstone	0.00	24.34	5.76	43.40	10.06	16.45	19.50	31.53	12.01	16.07	15.41	5.48
COM 108	3.77	Early Aptian	*D. weissi*	limestone	35.05	29.31	15.56	0.00	20.09	0.00	20.66	33.15	12.44	13.23	16.40	4.11
COM 108*	3.94	Early Aptian	*D. weissi*	marlstone	15.87	47.36	14.34	6.48	15.96	0.00	26.72	34.34	12.71	7.56	17.30	1.37
COM 110	4.64	Early Aptian	*D. weissi*	limestone	43.98	22.89	12.65	4.88	15.61	0.00	31.31	34.16	11.59	4.94	17.99	0.00
COM 110*	4.81	Early Aptian	*D. weissi*	marlstone	20.14	41.71	4.74	6.78	26.63	0.00	34.90	32.23	10.42	4.96	17.49	0.00
COM 112	5.51	Early Aptian	*D. weissi*	limestone	56.77	21.92	15.68	0.00	5.63	0.00	32.66	33.54	10.63	5.19	17.98	0.00
COM 114	6.20	Early Aptian	*D. weissi*	limestone	20.13	38.12	6.77	11.28	23.70	0.00	25.99	36.93	12.20	5.36	19.52	0.00
COM 114*	6.46	Early Aptian	*D. weissi*	marlstone	0.00	52.41	17.73	3.18	26.69	0.00	21.28	39.34	13.33	5.01	21.04	0.00
COM 116	7.19	Early Aptian	*D. weissi*	limestone	40.84	26.02	14.39	2.90	15.85	0.00	22.80	38.89	13.50	4.24	20.56	0.00
COM 116*	7.33	Early Aptian	*D. weissi*	marlstone	15.65	48.08	9.97	4.82	21.49	0.00	26.22	38.31	13.43	4.10	17.95	0.00
COM 118	8.06	Early Aptian	*D. weissi*	limestone	43.16	23.08	14.60	4.06	15.11	0.00	24.90	41.12	14.31	4.75	14.92	0.00
COM 118*	8.35	Early Aptian	*D. weissi*	marlstone	0.00	67.71	16.57	5.91	9.81	0.00	22.14	44.74	15.76	5.73	11.64	0.00
COM 120	8.99	Early Aptian	*D. weissi*	limestone	38.36	27.78	19.31	5.67	8.88	0.00	22.71	46.36	15.30	6.80	8.83	0.00
COM 120*	9.16	Early Aptian	*D. weissi*	marlstone	5.47	65.37	11.18	11.09	6.90	0.00	27.57	43.34	13.08	6.86	9.15	0.00
COM 122h	9.94	Early Aptian	*D. weissi*	limestone	59.50	22.95	8.56	3.85	5.14	0.00	32.65	37.39	10.63	5.71	13.63	0.00
COM 122*	10.00	Early Aptian	*D. weissi*	marlstone	15.37	38.76	12.02	3.55	30.28	0.00	33.67	32.37	8.49	4.70	20.76	0.00
COM 124	10.55	Early Aptian	*D. weissi*	limestone	52.86	16.71	4.38	3.47	22.58	0.00	27.41	31.59	6.33	5.05	29.62	0.00
COM 124*	10.67	Early Aptian	*D. weissi*	marlstone	0.00	49.06	3.76	9.17	38.01	0.00	18.09	34.11	5.77	5.97	36.05	0.00
COM 126	11.25	Early Aptian	*D. weissi*	limestone	11.82	25.85	2.57	4.61	55.15	0.00	11.42	35.48	8.35	7.82	36.93	0.00
COM 126*	11.36	Early Aptian	*D. weissi*	marlstone	7.67	46.68	21.36	7.18	17.11	0.00	8.97	33.13	10.99	10.95	35.96	0.00
COM 128	12.06	Early Aptian	*D. weissi*	limestone	13.84	18.43	10.24	22.85	34.65	0.00						
COM 128*	12.23	Early Aptian	*D. weissi*	marlstone	0.00	29.01	4.29	11.07	55.63	0.00						

Table An.2.7: semi-quantitative estimation of the amount of the identified minerals in the <2 µm fraction of samples from the Combe-Lambert section.

Sample ID	Depth (m)	Stage	Ammonite Zone	Lithology	Peak Intensity (cps)								Quantification (%)								Detritism Index
					Phyllo-silicates *19.8°2θ*	Quartz *26.65°2θ*	K-Feldspar *27.5°2θ*	Na-Plagioclase *27.9°2θ*	Calcite *29.43°2θ*	Ankerite-Dolomite *30.83-30.9°2θ*	Pyrite *56.3°2θ*	Goethite *21.2°2θ*	Phyllo-silicates	Quartz	K-Feldspar	Na-Plagioclase	Calcite	Pyrite	Ankerite	Unquan.	*Cc / (Qz + Phy)* [cps]
FB 2	0.24	Late Hauterivian	-	limestone	0	59	0	0	5982	6	0	0	0.0	0.5	0.0	0.0	95.2	0.0	0.0	4.2	101.1
FB 3	0.35	Late Hauterivian	-	limestone	96	1487	23	67	4337	17	12	228	23.9	11.7	0.6	1.4	59.2	0.2	0.1	2.9	2.7
FB 5	1.71	Late Hauterivian	-	limestone	2	41	0	0	6110	0	0	0	0.6	0.4	0.0	0.0	98.4	0.0	0.0	0.6	142.1
FB 8	3.29	Late Hauterivian	-	limestone	0	49	0	0	6477	0	0	0	0.0	0.5	0.0	0.0	99.1	0.0	0.0	0.5	132.2
FB 12	4.61	Late Hauterivian	-	limestone	6	49	7	6	5771	0	0	0	1.7	0.4	0.2	0.1	90.1	0.0	0.0	7.4	104.9
FB 15	5.98	Late Hauterivian	-	limestone	0	48	0	0	5717	0	0	0	0.0	0.4	0.0	0.0	88.8	0.0	0.0	10.8	119.1
FB 21	8.37	Late Hauterivian	-	limestone	9	71	6	5	6327	0	0	0	2.7	0.7	0.2	0.1	96.0	0.0	0.0	0.3	79.1
FB 28	9.41	Late Hauterivian	-	limestone	7	50	0	0	5859	0	0	0	2.0	0.5	0.0	0.0	92.2	0.0	0.0	5.3	102.8
FB 33	10.37	Late Hauterivian	-	limestone	3	44	0	0	5561	0	0	0	0.8	0.4	0.0	0.0	85.2	0.0	0.0	13.6	118.3
FB 41	11.48	Late Hauterivian	-	limestone	0	65	0	0	6639	0	0	0	0.0	0.6	0.0	0.0	98.5	0.0	0.0	0.8	102.1
FB 45	12.66	Late Hauterivian	-	limestone	0	78	0	7	5429	0	0	6	0.0	0.7	0.0	0.2	82.1	0.0	0.0	17.0	69.6
FB 46	12.79	Late Hauterivian	-	marlstone	108	1336	78	47	1207	36	0	18	21.6	8.4	1.7	0.8	13.1	0.0	0.2	54.4	0.8
FB 48	13.19	Late Hauterivian	-	marlstone	105	1367	40	42	1641	15	22	114	21.6	8.9	0.9	0.7	18.5	0.3	0.1	49.1	1.1
FB 50	13.72	Late Hauterivian	-	limestone	7	75	5	0	6045	0	0	0	2.1	0.7	0.2	0.0	96.8	0.0	0.0	0.3	73.7
FB 51	13.80	Late Hauterivian	-	marlstone	153	2400	74	49	262	30	0	0	28.3	14.0	1.5	0.8	2.7	0.0	0.1	52.7	0.1
FB 55	14.64	Late Hauterivian	-	limestone	5	68	0	0	5739	0	0	0	1.4	0.6	0.0	0.0	89.3	0.0	0.0	8.7	78.6
FB 56	14.82	Late Hauterivian	-	marlstone	121	1426	55	58	1150	16	0	11	24.0	8.9	1.2	1.0	12.4	0.0	0.1	52.6	0.7
FB 58	15.12	Late Hauterivian	-	marlstone	70	1673	74	61	1933	18	0	0	14.6	11.0	1.7	1.1	21.9	0.0	0.1	49.8	1.1
FB 59	15.31	Late Hauterivian	-	limestone	7	42	0	0	2626	0	100	8	1.6	0.3	0.0	0.0	33.0	1.6	0.0	63.6	53.6
FB 60	15.41	Late Hauterivian	-	marlstone	113	74	32	47	2118	7	0	0	24.3	0.5	0.7	0.8	24.8	0.0	0.0	48.8	11.3
FB 63	16.08	Late Hauterivian	-	marlstone	141	1925	91	67	522	0	0	0	26.7	11.4	1.8	1.1	5.4	0.0	0.0	53.7	0.3
FB 65	16.38	Late Hauterivian	-	limestone	10	101	3	0	5526	6	0	0	2.8	0.9	0.1	0.0	84.4	0.0	0.0	11.8	49.8
FB 68	17.03	Late Hauterivian	-	marlstone	138	1359	47	76	1823	17	0	21	28.6	8.9	1.0	1.3	20.6	0.0	0.1	39.6	1.2
FB 71	17.75	Late Hauterivian	*B. balearis - P. ligatus*	limestone	6	132	0	8	6005	5	0	0	1.8	1.2	0.0	0.2	95.7	0.0	0.0	1.1	43.6
FB 73	18.11	Late Hauterivian	*B. balearis - P. ligatus*	marlstone	133	1587	126	111	678	0	0	0	25.4	9.5	2.6	1.8	7.1	0.0	0.0	53.7	0.4
FB 75	18.35	Late Hauterivian	*B. balearis - P. ligatus*	marlstone	97	1469	68	66	1244	22	7	0	19.4	9.2	1.5	1.1	13.5	0.1	0.1	55.1	0.8
FB 77	18.56	Late Hauterivian	*B. balearis - P. ligatus*	marlstone	127	939	88	114	397	18	6	0	24.2	5.6	1.8	1.8	4.1	0.1	0.1	62.4	0.4
FB 79	18.82	Late Hauterivian	*B. balearis - P. ligatus*	limestone	1	142	0	0	5500	0	0	0	0.3	1.3	0.0	0.0	83.7	0.0	0.0	14.8	38.4
FB 83	19.35	Late Hauterivian	*B. balearis - P. ligatus*	marlstone	115	1452	82	74	535	23	0	0	21.8	8.7	1.7	1.2	5.6	0.0	0.1	61.0	0.3
FB 85	19.57	Late Hauterivian	*B. balearis - P. ligatus*	marlstone	47	1236	70	115	725	6	19	0	9.1	7.5	1.5	1.8	7.7	0.3	0.0	72.1	0.6
FB 88	19.76	Late Hauterivian	*B. balearis - P. ligatus*	marlstone	88	1162	70	77	1737	0	0	0	18.1	7.5	1.5	1.3	19.5	0.0	0.0	52.0	1.4
FB 89	19.92	Late Hauterivian	*B. balearis - P. ligatus*	limestone	17	199	0	0	6196	0	0	0	5.1	1.9	0.0	0.0	92.5	0.0	0.0	0.6	28.7
FB 94	20.84	Late Hauterivian	*B. balearis - P. ligatus*	limestone	3	100	8	6	5934	0	0	9	0.9	0.9	0.3	0.1	94.0	0.0	0.0	3.8	57.8
FB 99	21.77	Late Hauterivian	*B. balearis - P. ligatus*	limestone	1	203	11	0	6971	0	0	0	0.3	2.1	0.4	0.0	97.1	0.0	0.0	0.2	34.2
FB 104	22.73	Late Hauterivian	*B. balearis - P. ligatus*	limestone	2	165	0	0	6651	0	0	6	0.6	1.6	0.0	0.0	97.3	0.0	0.0	0.5	39.9
FB 109	23.78	Late Hauterivian	*B. balearis - P. ligatus*	limestone	3	83	0	0	5344	0	0	0	0.8	0.7	0.0	0.0	80.3	0.0	0.0	18.2	62.1
FB 110	23.90	Late Hauterivian	*B. balearis - P. ligatus*	limestone	96	968	145	123	354	32	0	154	18.1	5.8	2.9	1.9	3.7	0.0	0.2	67.5	0.3
FB 112	24.15	Late Hauterivian	*B. balearis - P. ligatus*	marlstone	108	1492	24	65	1870	12	0	14	22.4	9.7	0.5	1.1	21.1	0.0	0.1	45.1	1.2
FB 116	24.78	Late Hauterivian	*B. balearis - P. ligatus*	marlstone	108	1038	72	88	986	13	6	10	21.3	6.4	1.5	1.4	10.6	0.1	0.1	58.6	0.9
FB 118	25.06	Late Hauterivian	*B. balearis - P. ligatus*	marlstone	98	864	16	91	948	21	11	163	19.4	5.4	0.3	1.5	10.2	0.2	0.1	63.0	1.0
FB 120	25.31	Late Hauterivian	*B. balearis - P. ligatus*	marlstone	86	1156	21	74	1945	16	0	0	17.9	7.6	0.5	1.3	22.2	0.0	0.1	50.5	1.6
FB 123	25.81	Late Hauterivian	*B. balearis - P. ligatus*	limestone	1	71	0	7	6160	0	0	0	0.3	0.7	0.0	0.2	98.7	0.0	0.0	0.2	85.6
FB 126	26.28	Late Hauterivian	*P. angulicostata* auct.	marlstone	53	966	17	45	4209	0	0	0	13.1	7.5	0.5	0.9	56.9	0.0	0.0	21.0	4.1
FB 128a	26.71	Late Hauterivian	*P. angulicostata* auct.	limestone	0	106	0	0	5887	0	0	0	0.0	1.0	0.0	0.0	92.8	0.0	0.0	6.2	55.5
FB 129	27.18	Late Hauterivian	*P. angulicostata* auct.	marlstone	98	949	51	48	2334	11	0	8	21.1	6.4	1.2	0.9	27.5	0.0	0.1	43.0	2.2
FB 131	27.46	Late Hauterivian	*P. angulicostata* auct.	marlstone	103	1573	0	59	1817	0	9	9	21.2	10.2	0.0	1.0	20.5	0.1	0.0	46.9	1.1
FB 133	27.73	Late Hauterivian	*P. angulicostata* auct.	marlstone	88	1551	14	49	2363	74	0	5	18.9	10.5	0.3	0.9	27.7	0.0	0.4	41.3	1.4
FB 134a	27.81	Late Hauterivian	*P. angulicostata* auct.	limestone	8	128	7	0	5361	13	0	0	2.2	1.1	0.2	0.0	80.7	0.0	0.1	15.7	39.4
FB 136	28.36	Late Hauterivian	*P. angulicostata* auct.	limestone	12	99	0	0	6862	6	0	0	3.8	1.0	0.0	0.0	94.9	0.0	0.1	0.2	61.8
FB 138	28.86	Late Hauterivian	*P. angulicostata* auct.	marlstone	137	1724	57	128	1379	9	0	0	27.3	10.8	1.2	2.1	15.0	0.0	0.1	43.6	0.7
FB 139	28.93	Late Hauterivian	*P. angulicostata* auct.	limestone	1	100	0	0	5843	0	0	0	0.3	0.9	0.0	0.0	91.8	0.0	0.0	7.0	57.8
FB 371	29.07	Late Hauterivian	*P. angulicostata* auct.	limestone	0	91	0	0	5978	0	0	0	0.0	0.8	0.0	0.0	95.1	0.0	0.0	4.1	65.7
FB 372	29.15	Late Hauterivian	*P. angulicostata* auct.	marlstone	105	1093	87	57	264	24	0	0	19.8	6.5	1.7	0.9	2.7	0.0	0.1	68.3	0.2
FB 373 a	29.17	Late Hauterivian	*P. catulloi*	limestone	0	167	0	10	5736	0	0	0	0.0	1.5	0.0	0.2	89.2	0.0	0.0	9.1	34.3
FB 373d	29.47	Late Hauterivian	*P. catulloi*	limestone	6	53	0	0	5120	0	0	0	1.6	0.5	0.0	0.0	75.5	0.0	0.0	22.5	86.8
FB 374	29.51	Late Hauterivian	*P. catulloi*	marlstone	98	600	41	59	281	0	0	89	18.5	3.6	0.8	0.9	2.9	0.0	0.0	73.3	0.4
FB 375	29.53	Late Hauterivian	*P. catulloi*	limestone	0	55	0	0	5793	0	0	0	0.0	0.5	0.0	0.0	90.6	0.0	0.0	8.9	105.3
FB 377	29.60	Late Hauterivian	*P. catulloi*	marlstone	21	158	5	5	5196	0	0	11	5.7	1.4	0.1	0.1	77.0	0.0	0.0	15.7	29.1
FB 378	29.64	Late Hauterivian	*P. catulloi*	limestone	11	55	0	0	6131	0	0	0	3.3	0.5	0.0	0.0	96.0	0.0	0.0	0.3	92.9
FB 379	29.66	Late Hauterivian	*P. catulloi*	marlstone	82	723	56	41	1061	0	0	120	16.3	4.5	1.2	0.7	11.5	0.0	0.0	65.9	1.3

Table An.2.8: Results of XRD analysis of bulk-rock samples from the Fiume-Bosso section.

Sample ID	Depth (m)	Stage	Ammonite Zone	Lithology	Peak Intensity (cps)								Quantification (%)								Detritism Index
					Phyllo-silicates *19.8°2θ*	Quartz *26.65°2θ*	K-Feldspar *27.5°2θ*	Na-Plagioclase *27.9°2θ*	Calcite *29.43°2θ*	Ankerite-Dolomite *30.83-30.9°2θ*	Pyrite *56.3°2θ*	Goethite *21.2°2θ*	Phyllo-silicates	Quartz	K-Feldspar	Na-Plagioclase	Calcite	Pyrite	Ankerite	Unquan.	*Cc / (Qz + Phy)* [cps]
FB 380b	29.80	Late Hauterivian	*P. catulloi*	limestone	3	61	0	0	6090	0	0	0	0.9	0.6	0.0	0.0	97.9	0.0	0.0	0.6	95.2
FB 381b	29.86	Late Hauterivian	*P. catulloi*	marlstone	40	312	0	5	3976	8	0	22	9.8	2.4	0.0	0.1	*53.2*	0.0	0.1	34.4	11.3
FB 382a	30.00	Late Hauterivian	*P. catulloi*	limestone	5	68	0	0	5985	0	0	0	1.5	0.6	0.0	0.0	95.3	0.0	0.0	2.6	82.0
FB 382c	30.12	Late Hauterivian	*P. catulloi*	limestone	5	104	0	0	7593	0	0	0	1.7	1.1	0.0	0.0	97.1	0.0	0.0	0.1	69.7
FB 384	30.33	Late Hauterivian	*P. catulloi*	marlstone	110	1491	32	74	3010	9	0	0	24.8	10.5	0.8	1.4	36.9	0.0	0.1	25.6	1.9
FB 385	30.39	Late Hauterivian	*P. catulloi*	limestone	2	92	0	7	5250	0	0	0	0.6	0.8	0.0	0.2	78.2	0.0	0.0	20.3	55.8
FB 386	30.53	Late Hauterivian	*P. catulloi*	marlstone	103	1030	18	103	519	13	14	9	19.7	6.2	0.4	1.6	5.4	0.2	0.1	66.5	0.5
FB 387b	30.79	Late Hauterivian	*P. catulloi*	limestone	2	64	0	0	7137	0	0	9	0.7	0.7	0.0	0.0	98.3	0.0	0.0	0.4	108.1
FB 391	31.14	Late Hauterivian	*P. catulloi*	limestone	6	56	0	0	5489	0	0	0	1.7	0.5	0.0	0.0	83.5	0.0	0.0	14.3	88.5
FB 396b	32.60	Late Hauterivian	*P. catulloi*	limestone	0	85	0	0	6593	0	0	0	0.0	0.8	0.0	0.0	98.5	0.0	0.0	0.0	77.6
FB 397	32.64	Late Hauterivian	*P. catulloi*	marlstone	124	1799	60	81	749	0	0	0	23.8	10.8	1.2	1.3	7.8	0.0	0.0	55.0	0.4
FB 399	32.97	Late Hauterivian	*P. catulloi*	marlstone	94	1199	82	52	912	8	0	0	18.4	7.4	1.7	0.8	9.7	0.0	0.0	62.0	0.7
FB 401	33.23	Late Hauterivian	*P. catulloi*	marlstone	122	1190	82	43	1218	17	9	0	24.4	7.5	1.7	0.7	13.3	0.1	0.1	52.2	0.9
FB 402b	33.56	Late Hauterivian	*P. catulloi*	limestone	0	108	0	0	5602	0	0	0	0.0	1.0	0.0	0.0	86.1	0.0	0.0	13.0	51.9
FB 407	34.29	Late Hauterivian	*P. catulloi*	marlstone	96	1622	60	115	681	0	0	0	18.4	9.7	1.2	1.8	7.1	0.0	0.0	61.8	0.4
FB 410	34.64	Late Hauterivian	*P. catulloi*	limestone	0	128	0	0	6169	10	0	0	0.0	1.2	0.0	0.0	99.9	0.0	0.1	0.0	48.0
FB 411	34.86	Late Hauterivian	*P. catulloi*	marlstone	94	1309	61	73	1244	17	12	0	18.9	8.3	1.3	1.2	13.6	0.2	0.1	56.6	0.9
FB 414	35.47	Early Barremian	*S. hugii*	marlstone	116	1226	62	67	984	20	11	9	22.9	7.6	1.3	1.1	10.6	0.2	0.1	56.3	0.7
FB 417	35.80	Early Barremian	*S. hugii*	limestone	6	130	0	0	6760	6	0	0	1.9	1.3	0.0	0.0	96.0	0.0	0.1	0.8	49.6
FB 420	36.08	Early Barremian	*S. hugii*	marlstone	113	1016	58	65	1372	11	16	0	23.0	6.5	1.3	1.1	15.2	0.2	0.1	52.7	1.2
FB 424	37.20	Early Barremian	*S. hugii*	limestone	0	52	0	0	5935	0	0	0	0.0	0.5	0.0	0.0	94.1	0.0	0.0	5.5	114.1
FB 430a	38.27	Early Barremian	*S. hugii*	limestone	5	59	10	7	5982	0	0	0	1.5	0.5	0.3	0.2	95.2	0.0	0.0	2.3	93.3
FB 433	39.43	Early Barremian	*S. hugii*	limestone	96	1487	0	0	4337	0	0	0	23.9	11.7	0.0	0.0	59.1	0.0	0.0	5.4	2.7
FB 435	39.72	Early Barremian	*S. hugii*	marlstone	96	1595	66	62	587	16	11	11	18.3	9.6	1.3	1.0	6.1	0.1	0.1	63.4	0.3
FB 440a	40.43	Early Barremian	*S. hugii*	limestone	14	91	0	0	6110	0	0	0	4.1	0.9	0.0	0.0	94.4	0.0	0.0	0.6	58.2
FB 442	40.90	Early Barremian	*S. hugii*	marlstone	118	1522	84	58	296	0	0	0	22.0	9.0	1.7	0.9	3.0	0.0	0.0	63.4	0.2
FB 451a	42.73	Early Barremian	*S. hugii*	limestone	0	92	0	0	5771	0	0	0	0.0	0.8	0.0	0.0	90.1	0.0	0.0	9.1	62.7
FB 454b	43.91	Early Barremian	*S. hugii*	limestone	0	114	0	0	6032	0	0	0	0.0	1.1	0.0	0.0	96.4	0.0	0.0	2.6	53.1
FB 455	43.95	Early Barremian	*S. hugii*	marlstone	144	952	68	62	1224	0	20	202	28.9	6.0	1.5	1.0	13.4	0.3	0.0	48.8	1.1
FB 459b	44.68	Early Barremian	*S. hugii*	limestone	4	52	5	0	6327	0	0	0	1.2	0.5	0.2	0.0	98.1	0.0	0.0	0.1	113.0
FB 463	45.59	Early Barremian	*S. hugii*	marlstone	108	1307	54	75	538	0	7	0	20.6	7.8	1.1	1.2	5.6	0.1	0.0	63.6	0.4
FB 464a	45.73	Early Barremian	*S. hugii*	limestone	0	3116	0	7	3951	0	0	0	0.0	23.3	0.0	0.1	51.3	0.0	0.0	25.2	1.3
FB 465	45.94	Early Barremian	*S. hugii*	marlstone	128	1148	65	123	1112	0	0	0	25.3	7.1	1.4	2.0	12.0	0.0	0.0	52.3	0.9
FB 469	46.75	Early Barremian	*S. hugii*	limestone	0	112	0	0	6031	0	0	0	0.0	1.0	0.0	0.0	96.4	0.0	0.0	2.6	54.0
FB 473b	47.69	Early Barremian	*S. hugii*	limestone	0	102	0	0	6639	0	0	0	0.0	1.0	0.0	0.0	98.5	0.0	0.0	0.5	65.1
FB 480a	48.62	Early Barremian	*S. hugii*	limestone	0	106	0	0	5429	0	0	0	0.0	0.9	0.0	0.0	82.1	0.0	0.0	16.9	51.2
FB 487	49.54	Early Barremian	*S. hugii*	limestone	0	86	0	0	6045	0	0	0	0.0	0.8	0.0	0.0	96.8	0.0	0.0	2.5	70.3
FB 490a	50.17	Early Barremian	*S. hugii*	marlstone	54	578	0	35	5139	13	0	0	14.5	4.9	0.0	0.8	75.4	0.0	0.1	4.3	8.1
FB 491	50.25	Early Barremian	*S. hugii*	marlstone	127	1410	73	105	1453	10	0	286	25.6	8.9	1.6	1.8	16.0	0.0	0.1	46.2	0.9
FB 494b	50.59	Early Barremian	*S. hugii*	limestone	0	137	0	0	6035	0	0	0	0.0	1.3	0.0	0.0	96.5	0.0	0.0	2.3	44.1

Table An.2.8 (continued): Results of XRD analysis of bulk-rock samples from the Fiume-Bosso section.

Sample ID	Depth (m)	Peak Intensity (cps)															
		"Smectite"	Mica	R0 I/S	Kaolinite / Chlorite	Mica	Chlorite	Quartz	Goethite	Kaolinite	Chlorite	K-Feldspar	Na-Plagioclase	Pyrite	Mica	K001*	C002*
		001	*001*	*002*	*001/002*	*002*	*003*			*002*	*004*				*005*	K002*(K001,C002)/(K002+C004)	C004*(K001,C002)/(K002+C004)
		5.2°2θ	8.8°2θ	9-9.5°2θ	12.34°2θ	17.92°2θ	18.56°2θ	20.85°2θ	21.2°2θ	24.9°2θ	25.2°2θ	27.5°2θ	27.9°2θ	28.12°2θ	45.68°2θ		
ECII1	0.00	451.00	324.00	83.00	33.00	102.00	0.00	112.00	0.00	20.00	31.00	63.00	0.00	22.00	94.00	12.94	20.06
ECII3	1.70	426.00	203.00	67.00	16.00	79.00	14.00	147.00	0.00	0.00	12.00	29.00	0.00	0.00	52.00	0.00	16.00
ECII5	2.20	0.00	116.00	0.00	0.00	55.00	0.00	72.00	27.00	0.00	30.00	16.00	18.00	24.00	34.00	0.00	0.00
ECII8	2.70	352.00	267.00	93.00	0.00	81.00	0.00	109.00	59.00	15.00	26.00	37.00	16.00	0.00	0.00	0.00	0.00
ECII10	3.55	0.00	147.00	23.00	27.00	34.00	0.00	36.00	17.00	12.00	18.00	21.00	11.00	36.00	0.00	10.80	16.20
ECII13	4.75	58.00	130.00	25.00	0.00	62.00	0.00	76.00	38.00	12.00	32.00	11.00	18.00	22.00	0.00	0.00	0.00
ECII15	5.75	18.00	71.00	22.00	0.00	49.00	0.00	100.00	30.00	0.01	0.00	16.00	11.00	32.00	0.00	0.00	0.00
ECII18	6.95	10.00	179.00	45.00	42.00	36.00	0.00	359.00	0.00	0.01	0.00	50.00	37.00	14.00	0.00	42.00	0.00
ECII19	7.55	47.00	134.00	20.00	19.00	30.00	10.00	365.00	19.00	24.00	46.00	35.00	25.00	30.00	0.00	6.51	12.49
ECII21	8.15	65.00	179.00	31.00	11.00	83.00	0.00	12.00	21.00	25.00	19.00	21.00	11.00	0.00	119.00	6.25	4.75
ECII22	8.33	97.00	407.00	62.00	48.00	180.00	17.00	10.00	0.00	19.00	26.00	31.00	23.00	25.00	154.00	20.27	27.73
ECII23	8.50	190.00	435.00	22.00	52.00	210.00	20.00	48.00	0.00	19.00	49.00	63.00	34.00	17.00	107.00	14.53	37.47
ECII25	13.40	64.00	221.00	20.00	0.00	90.00	11.00	110.00	41.00	22.00	10.00	28.00	18.00	31.00	80.00	0.00	0.00
ECII27	15.20	68.00	146.00	41.00	10.00	86.00	17.00	94.00	44.00	0.01	0.00	41.00	23.00	17.00	84.00	10.00	0.00
ECII28	16.20	65.00	199.00	49.00	0.00	98.50	21.00	153.00	96.00	35.00	0.00	29.00	27.00	21.00	55.00	0.00	0.00
ECII30	17.90	46.00	154.00	34.00	0.00	104.00	0.00	136.00	52.00	27.00	13.00	50.00	13.00	38.00	91.00	0.00	0.00
ECII33	19.30	49.00	130.00	17.00	0.00	46.00	0.00	177.00	62.00	20.00	16.00	34.00	0.00	37.00	34.00	0.00	0.00
ECII35	20.35	0.00	132.00	14.00	0.00	57.00	0.00	70.00	104.00	19.00	24.00	25.00	12.00	21.00	43.00	0.00	0.00
ECII36	21.70	138.00	354.00	62.00	0.00	200.00	0.00	399.00	148.00	18.00	10.00	53.00	25.00	11.00		0.00	0.00
ECII38	23.90	94.00	211.00	28.00	12.00	123.00	0.00	166.00	186.00	30.00	37.00	38.00	0.00	26.00	85.00	5.37	6.63
ECII40	25.20	72.00	99.00	18.00	13.00	42.00	0.00	58.00	62.00	0.00	12.00	32.00	17.00	33.00	30.00	0.00	13.00
ECII42	26.50	44.00	147.00	42.00	0.00	67.00	0.00	73.00	102.00	0.00	15.00	38.00	17.00	32.00	45.00	0.00	0.00
ECII45	28.55	49.00	115.00	26.00	0.00	39.00	0.00	129.00	95.00	18.00	34.00	37.00	42.00	21.00	29.00	0.00	0.00
ECII48	30.75	60.00	131.00	33.00	0.00	79.00	0.00	77.00	127.00	0.00	21.00	38.00	20.00	29.00	38.00	0.00	0.00
ECII50	32.35	56.00	84.00	23.00	22.00	37.00	0.00	36.00	74.00	23.00	13.00	32.00	27.00	20.00		14.06	7.94
ECII52	34.55	106.00	111.00	22.00	0.00	126.00	0.00	78.00	99.00	0.01	0.00	68.00	25.00	29.00	91.00	0.00	0.00
ECII53	36.45	142.00	196.00	62.00	0.00	150.00	0.00	128.00	126.00	23.00	11.00	43.00	31.00	19.00	57.00	0.00	0.00
ECII54	37.10	248.00	183.00	72.00	36.00	142.00	0.00	156.00	160.00	21.00	0.00	84.00	66.00	37.00	109.00	36.00	0.00
ECII55	37.20	850.00	310.00	201.00	27.00	190.00	41.00	150.00	214.00	0.01	0.00	69.00	53.00	98.00	178.00	27.00	0.00
ECII56	37.65	150.00	267.00	46.00	13.00	165.00	0.00	87.00	57.00	12.00	12.00	53.00	37.00	31.00	95.00	6.50	6.50
ECII57	37.70	1678.00	777.00	207.00	54.00	344.00	16.00	470.00	80.00	0.00	40.00	94.00	103.00	52.00	378.00	0.00	54.00
ECII58	37.80	251.00	260.00	60.00	30.00	143.00	34.00	129.00	84.00	17.00	24.00	68.00	50.00	20.00	100.00	12.44	17.56
ECII59	38.15	157.00	202.00	33.00	12.00	113.00	0.00	152.00	69.00	14.00	13.00	47.00	19.00	0.00	114.00	6.22	5.78
ECII60	38.40	785.00	534.00	109.00	62.00	273.00	18.00	132.00	54.00	0.01	0.00	82.00	43.00	49.00	185.00	62.00	0.00
ECII62	39.10	89.00	111.00	29.00	12.00	90.00	0.00	103.00	61.00	12.00	14.00	61.00	51.00	24.50	55.00	5.54	6.46
ECII65	40.80	370.00	328.00	57.00	19.00	164.00	11.00	119.00	45.00	19.00	11.00	54.00	32.00	38.00	87.00	12.03	6.97
ECII67	42.20	510.00	359.00	68.00	17.00	196.00	0.00	157.00	72.00	0.01	0.00	64.00	20.00	14.00	116.00	17.00	0.00
ECII70	44.25	122.00	163.00	16.00	15.00	118.00	0.00	122.00	53.00	0.00	14.00	51.00	32.00	12.00	58.00	0.00	15.00
ECII72	45.20	294.00	252.00	86.00	26.00	171.00	0.00	62.00	33.00	11.00	25.00	52.00	46.00	18.00	98.00	7.94	18.06
ECII72b	46.35	274.00	399.00	31.00	41.00	271.00	12.00	104.00	0.00	43.00	66.00	83.00	0.00	13.00	170.00	16.17	24.83
ECII73	47.10	376.00	299.00	31.00	0.00	149.50	0.00	147.00	44.00	0.00	24.00	32.00	12.00	0.00	83.00	0.00	0.00
ECII74	47.75	830.00	395.00	76.00	39.00	189.00	0.00	114.00	81.00	17.00	0.00	41.00	41.00	18.00	147.00	39.00	0.00
ECII76	49.00	272.00	358.00	46.00	52.00	198.00	0.00	143.00	30.00	38.00	53.00	51.00	20.00	38.00	123.00	21.71	30.29
ECII78	50.30	106.00	140.00	28.00	30.00	132.00	0.00	68.00	46.00	0.01	0.00	62.00	35.00	14.00	0.00	30.00	0.00
ECII79	51.00	794.00	728.00	87.00	174.00	350.00	50.00	203.00	0.00	113.00	48.00	86.00	46.00	136.00	203.00	122.12	51.88
ECII81 j	52.05	150.00	221.00	43.00	91.00	185.00	0.00	123.00	81.00	67.00	16.00	96.00	11.00	22.00	153.00	73.46	17.54
ECII81 n	52.05	64.00	260.00	35.00	110.00	179.00	0.00	64.00	0.00	78.00	74.00	98.00	24.00	157.00	242.00	56.45	53.55
ECII82	52.30	678.00	417.00	52.00	160.00	222.00	21.00	181.00	124.00	125.00	0.00	57.00	39.00	16.00	201.00	160.00	0.00

Table An.2.9: peak intensities of the identified minerals in the <2 µm fraction of samples from the lower part of the Eclépens section.

Sample ID	Depth (m)	Quantification (relative %)					Five-point Moving Average (relative%)				
		"Smectite"	Mica	R0 I/S	Kaolinite	Chlorite	"Smectite"	Mica	R0 I/S	Kaolinite	Chlorite
ECII1	0.00	50.62	36.36	9.32	1.45	2.25					
ECII3	1.70	59.83	28.51	9.41	0.00	2.25					
ECII5	2.20	0.00	100.00	0.00	0.00	0.00	31.54	59.08	7.37	0.58	1.43
ECII8	2.70	49.44	37.50	13.06	0.00	0.00	23.73	63.62	9.03	1.37	2.24
ECII10	3.55	0.00	74.62	11.68	5.48	8.22	20.52	63.17	11.74	1.83	2.74
ECII13	4.75	27.23	61.03	11.74	0.00	0.00	17.55	63.52	14.23	2.64	2.06
ECII15	5.75	16.22	63.96	19.82	0.00	0.00	14.90	64.09	15.35	4.51	1.16
ECII18	6.95	3.62	64.86	16.30	15.22	0.00	14.77	63.14	14.54	5.99	1.56
ECII19	7.55	21.36	60.91	9.09	2.96	5.68	16.38	63.02	12.31	5.61	2.68
ECII21	8.15	22.73	62.59	10.84	2.19	1.66	19.43	63.25	10.03	3.74	3.55
ECII22	8.33	15.80	66.29	10.10	3.30	4.52	21.27	64.41	8.17	2.41	3.73
ECII23	8.50	27.18	62.23	3.15	2.08	5.36	22.29	65.24	7.41	2.01	3.05
ECII25	13.40	20.98	72.46	6.56	0.00	0.00	23.25	64.31	8.99	1.74	1.72
ECII27	15.20	25.66	55.09	15.47	3.77	0.00	22.89	63.04	12.18	1.43	0.45
ECII28	16.20	20.77	63.58	15.65	0.00	0.00	22.08	62.98	13.99	0.94	0.00
ECII30	17.90	19.66	65.81	14.53	0.00	0.00	20.13	66.54	13.01	0.31	0.00
ECII33	19.30	25.00	66.33	8.67	0.00	0.00	17.05	71.79	11.16	0.00	0.00
ECII35	20.35	0.00	90.41	9.59	0.00	0.00	16.39	73.27	10.05	0.13	0.16
ECII36	21.70	24.91	63.90	11.19	0.00	0.00	20.17	68.80	9.62	0.39	1.02
ECII38	23.90	27.25	61.16	8.12	1.56	1.92	25.79	61.41	10.03	0.52	2.25
ECII40	25.20	35.64	49.01	8.91	0.00	6.44	27.64	57.77	11.58	0.39	2.63
ECII42	26.50	18.88	63.09	18.03	0.00	0.00	26.16	58.38	13.56	0.13	1.77
ECII45	28.55	25.79	60.53	13.68	0.00	0.00	25.51	58.44	14.53	0.63	0.89
ECII48	30.75	26.79	58.48	14.73	0.00	0.00	28.21	55.10	13.71	1.90	1.07
ECII50	32.35	30.27	45.41	12.43	7.60	4.29	32.98	50.49	12.56	2.53	1.43
ECII52	34.55	44.35	46.44	9.21	0.00	0.00	37.29	46.79	12.39	2.46	1.07
ECII53	36.45	35.50	49.00	15.50	0.00	0.00	42.05	42.08	13.05	2.46	0.36
ECII54	37.10	46.01	33.95	13.36	6.68	0.00	45.84	37.70	13.52	2.83	0.11
ECII55	37.20	61.24	22.33	14.48	1.95	0.00	47.90	36.42	12.51	2.66	0.51
ECII56	37.65	31.51	56.09	9.66	1.37	1.37	48.57	37.87	10.69	1.67	1.20
ECII57	37.70	61.78	28.61	7.62	0.00	1.99	47.25	40.40	9.34	1.15	1.85
ECII58	37.80	41.76	43.26	9.98	2.07	2.92	46.10	41.73	8.69	1.54	1.94
ECII59	38.15	38.86	50.00	8.17	1.54	1.43	44.79	42.66	8.69	2.26	1.60
ECII60	38.40	52.68	35.84	7.32	4.16	0.00	43.97	43.10	8.93	2.65	1.35
ECII62	39.10	36.93	46.06	12.03	2.30	2.68	45.13	42.21	8.96	2.47	1.24
ECII65	40.80	47.80	42.38	7.36	1.55	0.90	46.14	42.33	8.28	1.89	1.37
ECII67	42.20	53.46	37.63	7.13	1.78	0.00	46.22	43.06	7.57	1.27	1.86
ECII70	44.25	38.61	51.58	5.06	0.00	4.75	44.45	44.17	7.70	1.06	2.62
ECII72	45.20	44.68	38.30	13.07	1.21	2.74	42.63	45.72	7.62	1.09	2.93
ECII72b	46.35	36.78	53.56	4.16	2.17	3.33	45.12	44.77	6.65	1.27	2.19
ECII73	47.10	53.26	42.35	4.39	0.00	0.00	49.27	42.17	5.54	1.62	1.41
ECII74	47.75	61.94	29.48	5.67	2.91	0.00	49.27	41.01	5.68	2.72	1.32
ECII76	49.00	37.36	49.18	6.32	2.98	4.16	44.81	42.21	6.60	4.76	1.63
ECII78	50.30	34.87	46.05	9.21	9.87	0.00	39.73	43.96	7.05	7.20	2.06
ECII79	51.00	44.53	40.83	4.88	6.85	2.91	35.24	44.78	7.21	9.64	3.14
ECII81 j	52.05	29.70	43.76	8.51	14.55	3.47	31.67	45.15	7.02	11.41	4.74
ECII81 n	52.05	13.65	55.44	7.46	12.04	11.42					
ECII82	52.30	51.87	31.91	3.98	12.24	0.00					

Table An.2.10: semi-quantitative estimation of the amount of the identified minerals in the <2 µm fraction of samples from the lower part of the Eclépens section.

Table An.2.11: peak intensities of the identified minerals in the <2 µm fraction of samples from the Gorge de l'Areuse section.

ID	Depth (m)	Peak Intensity, <2 µm fraction (cps)															
		Smectite	**Mica**	**R0 I/S**	**Kaolinite/ Chlorite**	**Mica**	**Chlorite**	**Quartz**	**Goethite**	**Kaolinite**	**Chlorite**	**K-Feldspar**	**Na-Plagioclase**	**Pyrite**	**Mica**	**K002***	**C004***
		001 5.2°2θ	*001* 8.8°2θ	*002* 9-9.5°2θ	*001-002* 12.34°2θ	*002* 17.92°2θ	*003* 18.56°2θ	20.85°2θ	21.2°2θ	*002* 24.9°2θ	*004* 25.2°2θ	27.5°2θ	27.9°2	28.12°2θ	*005* 45.68°2θ	K002*(K001,C002)/ (K002+C004)	C004*(K001,C002)/(K002+C004)
GA1	0.00	316	301	59	634	151	0	94	103.5	376	0	42	16	0	101	634.00	0.00
GA2	0.35	184	177	31	787	88	0	53	57	438	81	27	65	24	69	664.17	122.83
GA3	0.60	63	82	16	223	57	0	89	119	150	25	26	22	0	58	191.14	31.86
GA4	0.75	0	153	12	24	82	17	55	52	29	29	32	11	16	69	12.00	12.00
GA5	1.25	56	159	34	0	113	0	10	91	17	0	0	0	1	62	0.00	0.00
GA6	1.25	32	127	50	0	88	0	25	68	27	11	11	18	12	77	0.00	0.00
GA7	1.75	64	253	37	10	122	0	56	29	30	20	36	46	10	97	6.00	4.00
GA8	2.25	93	226	62	0	90	22	44	47	15	17	36	25	22	94	0.00	0.00
GA9	2.65	44	375	42	44	137	0	28	0	31	18	79	18	22	131	27.84	16.16
GA10	3.05	41	223	38	0	114	0	46	68	24	11.5	33	29	0	56	0.00	0.00
GA11	3.15	42	80	0	10	42	0	32	48	17	14	15	17	24	53	5.48	4.52
GA12	3.15	53	271	43.5	37	147	21	113	51	29	17	41	47	34	69	23.33	13.67
GA13	3.45	70	202	25	19	87	0	63	0	24	26	42	0	0	58	9.12	9.88
GA14	3.85	58	171	68	18	50	0	63	33	15	26	37	10	20	46	6.59	11.41
GA15	3.95	0	233	57	31	76	0	58	26	59	10	35	56	10	55	26.51	4.49
GA16	4.35	38	143	18	20	63	0	12	36	21	21	33	29	28	39	10.00	10.00
GA17	4.75	0	236	27	79	96	16	26	37	29	23	38	39	36	48	44.06	34.94
GA18	5.15	25	143	41	440	169	12	82	88	255	42	82	37	27	113	377.78	62.22
GA19	5.40	61	199	26	634	111	0	47	84	393	71	42	12	13	49	536.99	97.01
GA20	5.65	213	247	57	197	190	13	106	112	119	57	63	53	15	76	133.20	63.80
GA21	5.90	150	142	53	203	112	38	36	96	124	78	67	22	0	62	124.61	78.39
GA22	6.35	43	72	30	156	44	0	38	70	120	0	56	25	15	37	156.00	0.00
GA23	6.40	0	49	15	10	59	0	111	140	0	0	67	26	14	92	0.00	0.00
GA24	6.40	0	86	26	0	52	0	63	32	0	0	51	20	31	52	0.00	0.00
GA25	6.55	23	71	13	34	0	19	13	25	59	33	25	16	19	26	21.80	12.20
GA26	6.55	17	161	0	227	60	0	29	96	118	0	19	24	10	50	227.00	0.00
GA27	6.70	18	47	12	23	52	0	12	74	28	17	10	28	14	45	14.31	8.69
GA28	7.05	0	54	21	146	54	0	36	77	105	23	54	38	10	71	119.77	26.23
GA29	7.40	0	153	0	58.5	38	0	84	34	131	18	59	18	22	60	51.43	7.07
GA30	7.80	19	53	0	54	0	0	20	89	38	11	21	28	10	16	41.88	12.12
GA31	8.15	17	67	0	31	23	0	19	52	22	10	23	21	16	13	21.31	9.69
GA32	8.30	18	51	17	0	43	0	17	32	17	11	26	12	10	45	0.00	0.00
GA36	9.60	24	33	17	0	21	0	0	27	0	0	24	12	10	21	0.00	0.00
GA37	9.90	31	28	10	0	22	0	23	19	0	0	26	14	0	23	0.00	0.00
GA38	10.30	10	62	16	0	47	0	21	24	0	0	21	11	13	36	0.00	0.00
GA39	10.80	18	0	11	0	22	0	23	32	0	0	22	0	0	32	0.00	0.00
GA40	10.80	0	54	20	0	48	0	37	22	0	0	38	14	33	29	0.00	0.00
GA41	11.30	26	53	17	0	52	0	18	36	0	0	33	21	15	23	0.00	0.00
GA42	11.50	15	44	24	0	56	0	23	21	0	0	22	15	0	25	0.00	0.00
GA43	12.10	31	72	0	0	33	0	38	27	0	0	33	45	26	30	0.00	0.00
GA44	12.35	20	41	0	0	0	0	18	44	0	0	23	20	13	23	0.00	0.00
GA45	12.45	32	86	23	0	46	0	59	75	0	0	37	13	0	38	0.00	0.00
GA46	12.80	38	23	12	0	23	0	29	18	0	0	20	25	20	26	0.00	0.00
GA47	13.30	21	55	16	0	31	0	53	29	0	0	37	0	13	66	0.00	0.00
GA48	13.90	21	55	0	0	31	0	53	29	0	0	37	24	15		0.00	0.00
GA50	14.70	21	61	26	0	64	0	72	29	0	0	38	33	27	45	0.00	0.00
GA51	15.10	17	67	19	0	39	0	49	82	0	0	27	40	0		0.00	0.00
GA52	15.50	11	71	18	0	38	0	48	10	0	0	32	11	12	34	0.00	0.00
GA53	16.00	0	34	0	0	84	0	69	62	0	0	47	23	14	43	0.00	0.00
GA54	16.35	27	20	15	0	38	0	43	48	0	0	17	20	11	36	0.00	0.00
GA55	16.80	31	17	0	0	75	0	48	21	0	0	33	30	28	63	0.00	0.00

Sample ID	Depth (m)	Quantification (relative%)					Five-Point Moving Average (relative %)				
		Smectite	Mica	R0 I/S	Kaolinite	Chlorite	Smectite	Mica	R0 I/S	Kaolinite	Chlorite
GA1	0.00	24.1	23.0	4.5	48.4	0.0					
GA2	0.35	15.6	15.0	2.6	56.3	10.4					
GA3	0.60	16.4	21.4	4.2	49.8	8.3	13.3	38.3	5.1	36.3	7.0
GA4	0.75	0.0	81.0	6.3	6.3	6.3	12.3	54.6	8.8	19.3	5.1
GA5	1.25	22.5	63.9	13.7	0.0	0.0	14.2	64.3	13.3	5.9	2.4
GA6	1.25	15.3	60.8	23.9	0.0	0.0	17.2	65.3	15.8	0.9	0.8
GA7	1.75	17.6	69.5	10.2	1.6	1.1	18.4	64.7	15.3	1.0	0.6
GA8	2.25	24.4	59.3	16.3	0.0	0.0	17.1	66.9	13.1	1.8	1.1
GA9	2.65	8.7	74.3	8.3	5.5	3.2	16.5	68.9	10.8	2.3	1.4
GA10	3.05	13.6	73.8	12.6	0.0	0.0	17.8	68.9	8.5	2.9	1.9
GA11	3.15	31.8	60.6	0.0	4.2	3.4	19.8	66.9	7.2	3.5	2.5
GA12	3.15	13.1	67.0	10.8	5.8	3.4	20.5	64.1	8.4	3.9	3.1
GA13	3.45	22.2	63.9	7.9	2.9	3.1	17.9	62.7	12.2	4.0	3.2
GA14	3.85	18.4	54.3	21.6	2.1	3.6	14.2	63.2	15.2	4.3	3.0
GA15	3.95	0.0	72.6	17.8	8.3	1.4	10.8	65.2	14.7	5.7	3.6
GA16	4.35	17.4	65.3	8.2	4.6	4.6	7.6	63.5	11.5	11.8	5.5
GA17	4.75	0.0	69.0	7.9	12.9	10.2	5.9	52.7	8.0	25.5	7.9
GA18	5.15	3.9	22.0	6.3	58.2	9.6	6.9	38.3	6.1	39.2	9.5
GA19	5.40	6.6	21.6	2.8	58.4	10.5	12.9	29.3	6.0	41.6	10.2
GA20	5.65	29.8	34.6	8.0	18.7	8.9	20.0	27.2	7.1	35.7	10.0
GA21	5.90	27.4	25.9	9.7	22.7	14.3	20.7	31.4	9.9	30.1	7.9
GA22	6.35	14.3	23.9	10.0	51.8	0.0	14.1	42.9	14.2	24.5	4.3
GA23	6.40	0.0	76.6	23.4	0.0	0.0	7.2	57.1	17.7	16.1	1.9
GA24	6.40	0.0	76.8	23.2	0.0	0.0	5.6	62.6	16.7	12.9	2.2
GA25	6.55	16.3	50.4	9.2	15.5	8.6	8.0	56.2	11.8	20.4	3.6
GA26	6.55	4.2	39.8	0.0	56.0	0.0	10.0	46.0	8.0	30.6	5.3
GA27	6.70	18.0	47.0	12.0	14.3	8.7	8.4	41.9	7.1	35.6	6.9
GA28	7.05	0.0	24.4	9.5	54.2	11.9	6.1	44.8	6.2	35.2	7.8
GA29	7.40	0.0	72.3	0.0	24.3	3.3	6.5	49.5	3.4	32.7	7.9
GA30	7.80	15.1	42.1	0.0	33.2	9.6	10.5	53.6	2.4	26.3	7.1
GA31	8.15	14.8	58.3	0.0	18.5	8.4	16.6	54.5	6.9	16.5	5.5
GA32	8.30	20.9	59.3	19.8	0.0	0.0	23.8	52.4	13.5	7.4	2.9
GA36	9.60	32.4	44.6	23.0	0.0	0.0	29.5	50.6	17.7	1.5	0.7
GA37	9.90	44.9	40.6	14.5	0.0	0.0	32.8	47.2	19.9	0.0	0.0
GA38	10.30	11.4	70.5	18.2	0.0	0.0	33.2	43.4	23.3	0.0	0.0
GA39	10.80	62.1	0.0	37.9	0.0	0.0	29.5	43.8	26.6	0.0	0.0
GA40	10.80	0.0	73.0	27.0	0.0	0.0	24.7	48.4	26.8	0.0	0.0
GA41	11.30	27.1	55.2	17.7	0.0	0.0	21.2	55.7	23.0	0.0	0.0
GA42	11.50	18.1	53.0	28.9	0.0	0.0	23.1	60.6	16.3	0.0	0.0
GA43	12.10	30.1	69.9	0.0	0.0	0.0	26.9	63.0	10.1	0.0	0.0
GA44	12.35	32.8	67.2	0.0	0.0	0.0	30.0	62.2	7.9	0.0	0.0
GA45	12.45	22.7	61.0	16.3	0.0	0.0	33.2	55.8	11.0	0.0	0.0
GA46	12.80	52.1	31.5	16.4	0.0	0.0	33.8	52.3	13.9	0.0	0.0
GA47	13.30	22.8	59.8	17.4	0.0	0.0	31.0	55.7	13.3	0.0	0.0
GA48	13.90	27.6	72.4	0.0	0.0	0.0	25.5	61.2	13.3	0.0	0.0
GA50	14.70	19.4	56.5	24.1	0.0	0.0	20.3	64.1	15.6	0.0	0.0
GA51	15.10	16.5	65.0	18.4	0.0	0.0	15.4	67.9	16.7	0.0	0.0
GA52	15.50	11.0	71.0	18.0	0.0	0.0	13.0	72.3	14.6	0.0	0.0
GA53	16.00	0.0	100.0	0.0	0.0	0.0	20.4	67.5	12.1	0.0	0.0
GA54	16.35	43.5	32.3	24.2	0.0	0.0					
GA55	16.80	64.6	35.4	0.0	0.0	0.0					

Table An.2.12: semi-quantitative estimation of the amount of the identified minerals in the <2 µm fraction of samples from the Gorge de l'Areuse section.

Sample ID	Depth (m)	Stage*	Depositionnal Sequence*	Peak Intensity (cps)															
				Corrensite	Rectorite	Mica	R0 I/S	Kaolinite/ Chlorite	Mica	Chlorite	Quartz	Goethite	Kaolinite	Chlorite	K-Feldspar	Na-Plagioclase	Pyrite	Mica	K001*	C002*
				002 5.5-6.0°2θ	*002* 6.0°2θ	*001* 8.8°2θ	*002* 9-9.5°2θ	*001/002* 12.34°2θ	*002* 17.92°2θ	*003* 18.56°2θ	20.85°2θ	21.2°2θ	*002* 24.9°2θ	*004* 25.2°2θ	27.5°2θ	27.9°2θ	28.12°2θ	*005* 45.68°2θ	K002*(K001,C002)/ (K002+C004)	C004*(K001,C002)/ (K002+C004)
C 18	10.57	-	-	0	0	302	13	0	111	0	619	0	0	0	49	30	17	86	0	0
C 21	11.95	-	-	0	56	253	63	0	81	0	213	0	0	0	57	40	0	61	0	0
C 60	30.19	-	-	0	0	308	30	0	117	0	125	0	0	0	42	0	37	49	0	0
C 65	32.20	-	-	0	0	205	52	0	68	0	116	0	0	0	49	15	0	37	0	0
C 70	34.77	-	-	0	0	337	73	0	148	0	66	0	0	0	79	21	0	83	0	0
C 153	91.45	Late Barremian	Ba4	0	0	881	46	43	331	0	44	0	0	0	92	0	0	123	0	0
C 162	98.54	Late Barremian	Ba4	0	25	656	36	0	262	0	0	0	0	0	40	0	14	154	0	0
C 168	102.31	Late Barremian	Ba4	0	53	921	55	30	436	21	19	0	0	0	51	27	0	224	0	0
C 175	107.92	Late Barremian	Ba4	244	33	1098	72	46	464	56	0	0	0	52	99	10	19	223	0	46
C 176	109.56	Late Barremian	Ba4	0	0	209	29	0	80	0	41	0	0	0	33	0	0	53	0	0
C 185	117.11	Late Barremian	Ba4	0	0	659	82	38	387	13	8	0	19	3	56	32	0	216	33	5
C 245	158.74	Late Barremian	Ba0	89	146	777	31	119	392	11	0	0	112	32	44	24	0	205	93	26
C 255	163.45	Late Barremian	Ba1	0	0	675	131	1309	378	41	0	24	1289	44	39	24	0	171	1266	43
C 260	166.54	Late Barremian	Ba2	63	364	280	17	36	137	51	39	0	51	63	27	15	31	105	16	20
C 265	171.82	Late Barremian	Ba3	0	81	418	55	0	141	0	0	0	0	0	15	13	0	58	0	0
C 270	176.48	Late Barremian	Ba4	0	58	425	52	19	161	0	20	0	20	16	14	36	0	87	11	8
C 280	184.78	Late Barremian	Ba5	0	44	249	23	12	80	0	13	0	13	23	31	10	17	45	4	8
C 290	193.08	Early Aptian	A1	20	40	157	0	0	57	0	0	14	0	0	13	26	13	28	0	0
C 295	196.98	Early Aptian	A2	72	362.5	333	45	69	146	53	14	0	29	51	44	10	0	81	25	44
C 340	226.79	Early Aptian	A3	0	0	583	77	731	310	76	10	0	609	19	108	19	0	140	709	22
C 345	235.09	Early Aptian	A4	41	216	913	77	218	389	11	12	0	203	21	58	23	16	184	198	20
C 351	243.27	Early Aptian	A5	0	115	663	86	83	211	0	193	0	57	23	72	12	27	106	59	24

**After Wermeille (1996), unpublished diploma thesis*

Table An.2.13: peak intensities of the identified minerals in the <2 µm fraction of samples from the Cluses section.

Sample ID	Depth (m)	Stage*	Depositionnal Sequence*	Quantification (relative %)						Five-Point Moving Average (relative %)					
				Corrensite	Rectorite	Mica	R0 I/S	Kaolinite	Chlorite	Corrensite	Rectorite	Mica	R0 I/S	Kaolinite	Chlorite
C 18	10.57	-	-	0.0	0.0	95.9	4.1	0.0	0.0						
C 21	11.95	-	-	0.0	15.1	68.0	16.9	0.0	0.0						
C 60	30.19	-	-	0.0	0.0	91.1	8.9	0.0	0.0	0.0	3.8	82.2	14.1	0.0	0.0
C 65	32.20	-	-	0.0	0.0	79.8	20.2	0.0	0.0	0.0	1.3	83.5	15.2	0.0	0.0
C 70	34.77	-	-	0.0	0.0	82.2	17.8	0.0	0.0	0.0	0.3	86.3	13.4	0.0	0.0
C 153	91.45	Late Barremian	Ba4	0.0	0.0	95.0	5.0	0.0	0.0	0.0	1.3	89.2	9.5	0.0	0.0
C 162	98.54	Late Barremian	Ba4	0.0	3.5	91.5	5.0	0.0	0.0	1.4	2.6	89.6	6.1	0.0	0.3
C 168	102.31	Late Barremian	Ba4	0.0	5.2	89.5	5.3	0.0	0.0	4.1	3.1	86.3	5.7	0.0	0.8
C 175	107.92	Late Barremian	Ba4	16.3	2.2	73.5	4.8	0.0	3.1	5.4	2.3	83.5	7.3	0.4	1.1
C 176	109.56	Late Barremian	Ba4	0.0	0.0	87.8	12.2	0.0	0.0	4.7	2.0	81.8	8.6	1.7	1.1
C 185	117.11	Late Barremian	Ba4	0.0	0.0	84.6	10.5	4.2	0.7	3.3	3.3	75.7	8.1	8.4	1.2
C 245	158.74	Late Barremian	Ba0	7.7	12.6	66.9	2.7	8.0	2.3	3.2	8.2	61.8	6.3	18.8	1.7
C 255	163.45	Late Barremian	Ba1	0.0	0.0	31.9	6.2	59.8	2.0	4.0	16.3	49.9	5.0	22.8	2.0
C 260	166.54	Late Barremian	Ba2	8.3	47.9	36.8	2.2	2.1	2.6	3.4	21.5	51.1	5.8	16.5	1.7
C 265	171.82	Late Barremian	Ba3	0.0	14.6	75.5	9.9	0.0	0.0	2.1	20.6	62.5	7.3	6.1	1.4
C 270	176.48	Late Barremian	Ba4	0.0	10.5	76.7	9.4	1.9	1.5	1.5	16.0	72.5	7.6	1.1	1.3
C 280	184.78	Late Barremian	Ba5	0.0	13.4	75.9	7.0	1.3	2.3	3.0	16.3	72.0	5.9	1.2	1.6
C 290	193.08	Early Aptian	A1	9.2	18.4	72.4	0.0	0.0	0.0	5.1	20.7	62.4	4.3	5.4	2.1
C 295	196.98	Early Aptian	A2	8.2	41.1	37.8	5.1	2.8	5.0	5.3	20.7	52.7	4.1	14.9	2.4
C 340	226.79	Early Aptian	A3	0.0	0.0	41.9	5.5	51.0	1.6	3.5	16.5	50.9	5.2	21.6	2.3
C 345	235.09	Early Aptian	A4	2.8	14.7	62.3	5.3	13.5	1.4						
C 351	243.27	Early Aptian	A5	0.0	12.1	70.0	9.1	6.2	2.5						

**After Wermeille (1996), unpublished diploma thesis*

Table An.2.14: semi-quantitative estimation of the amount of the identified minerals in the <2 µm fraction of samples from the Cluses section.

ANNEXE 3.

CATHODOLUMINESCENCE AND SEM PLATES

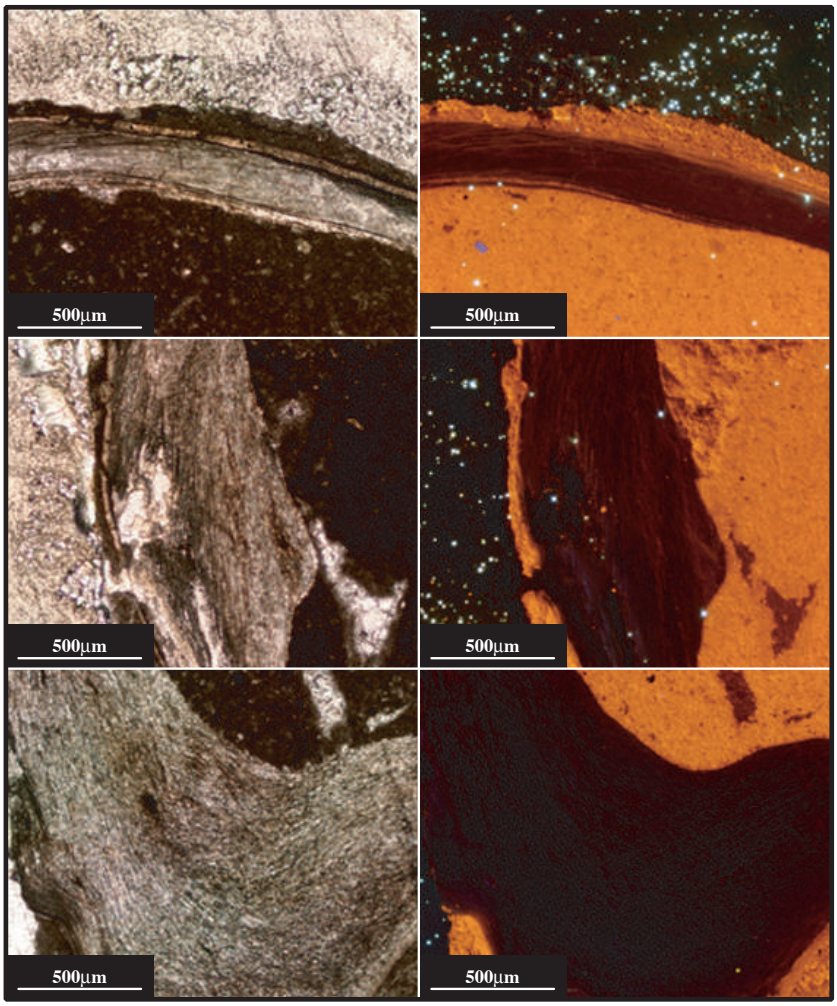

Table An.3.1: Cathodoluminescence micrographs of brachiopod C-40a (Marne Bleue d'Hauterive, Early Hauterivian, Cressier section).

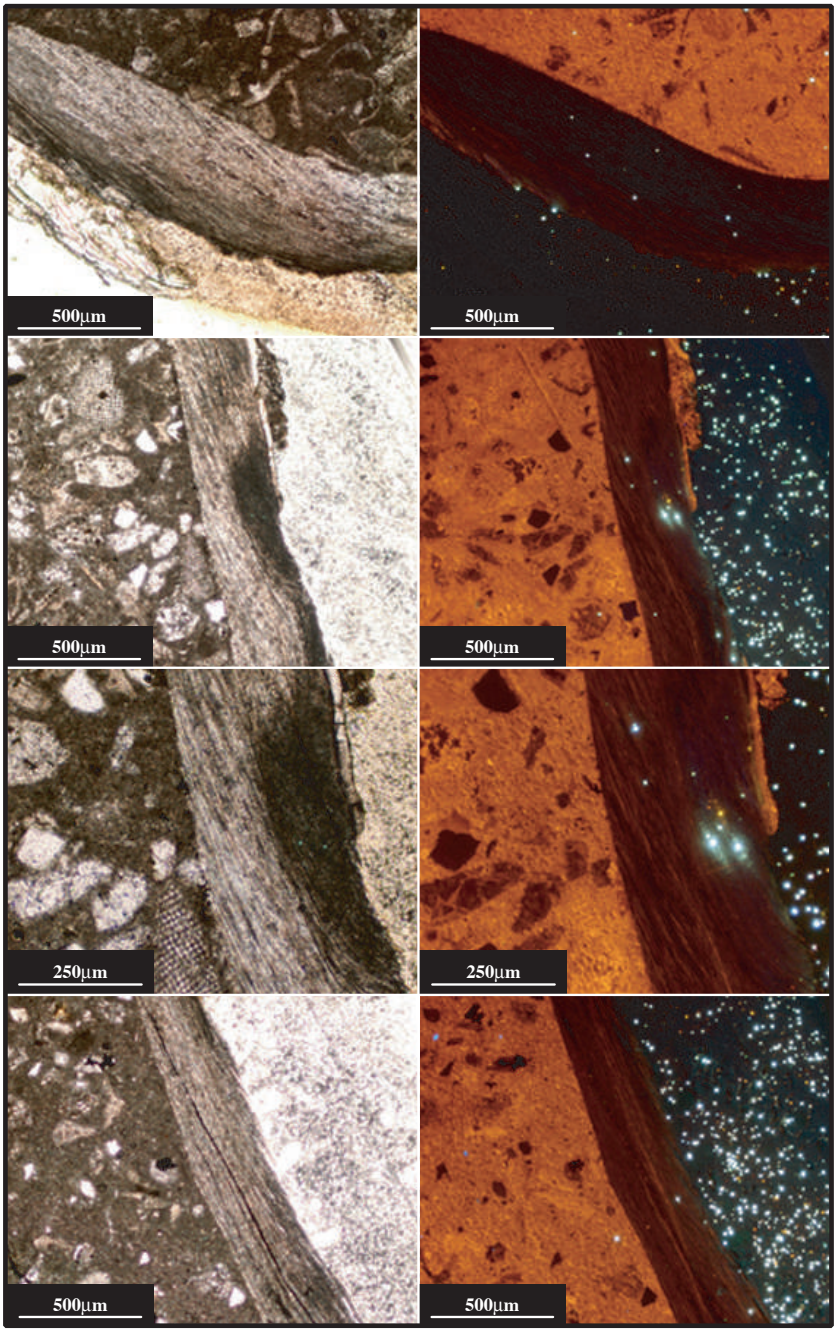

Table An.3.2: Cathodoluminescence micrographs of brachiopod C(0;-30) (Marne Bleue d'Hauterive, Early Hauterivian, Cressier section).

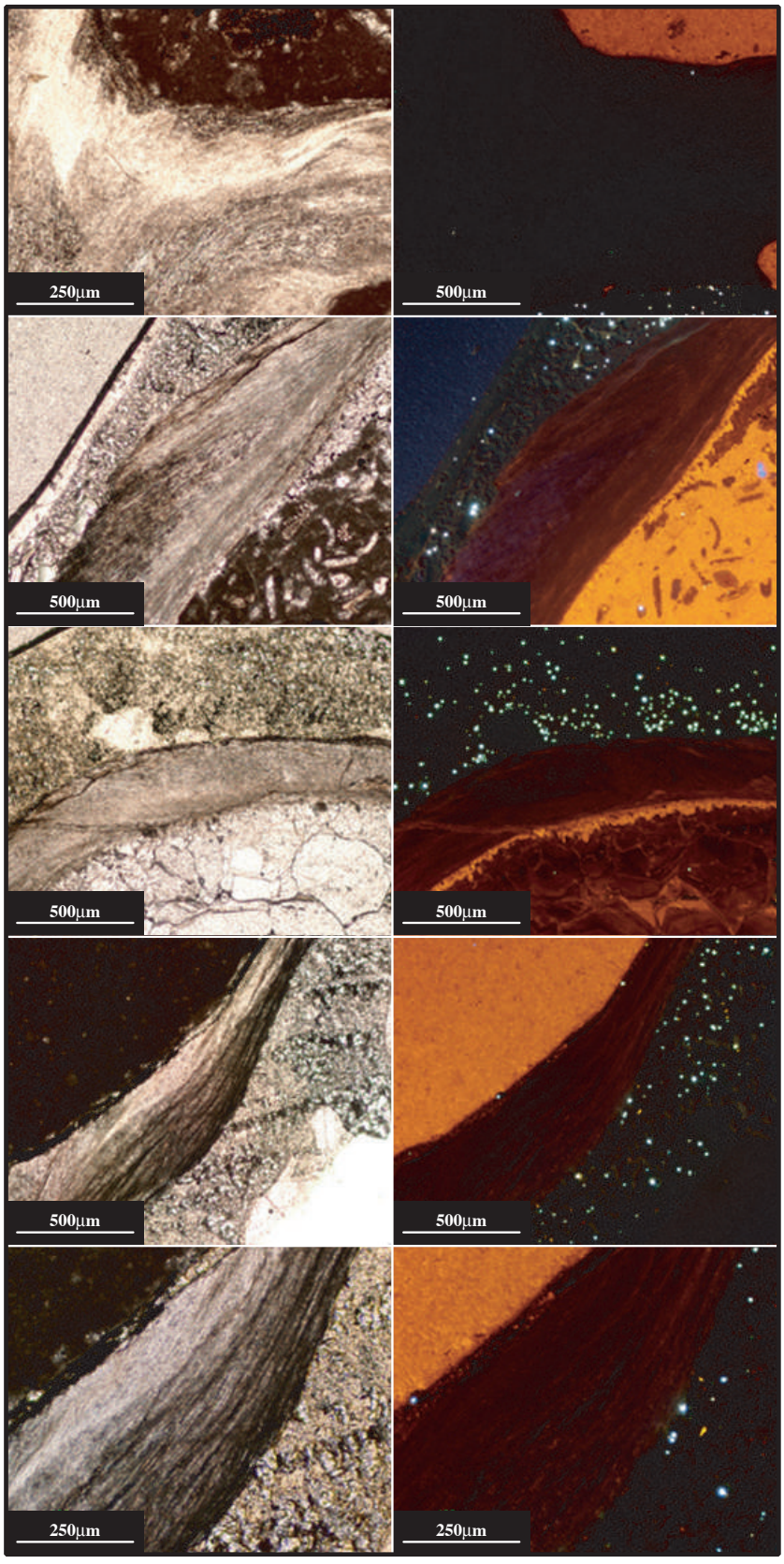

Table An.3.3: Cathodoluminescence micrographs of brachiopod C+100 (Marne Bleue d'Hauterive, Early Hauterivian, Cressier section).

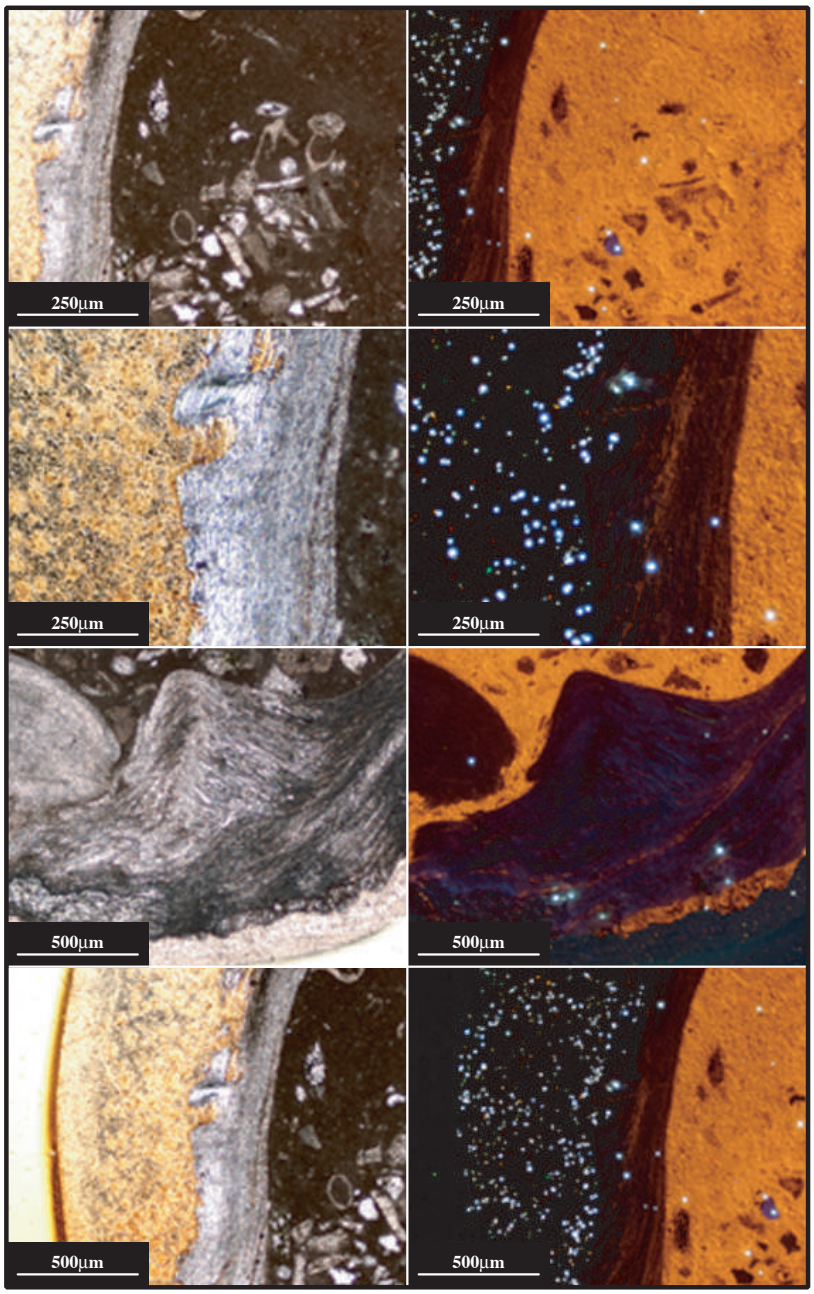

Table An.3.4: Cathodoluminescence micrographs of brachiopod C+120 (Marne Bleue d'Hauterive, Early Hauterivian, Cressier section).

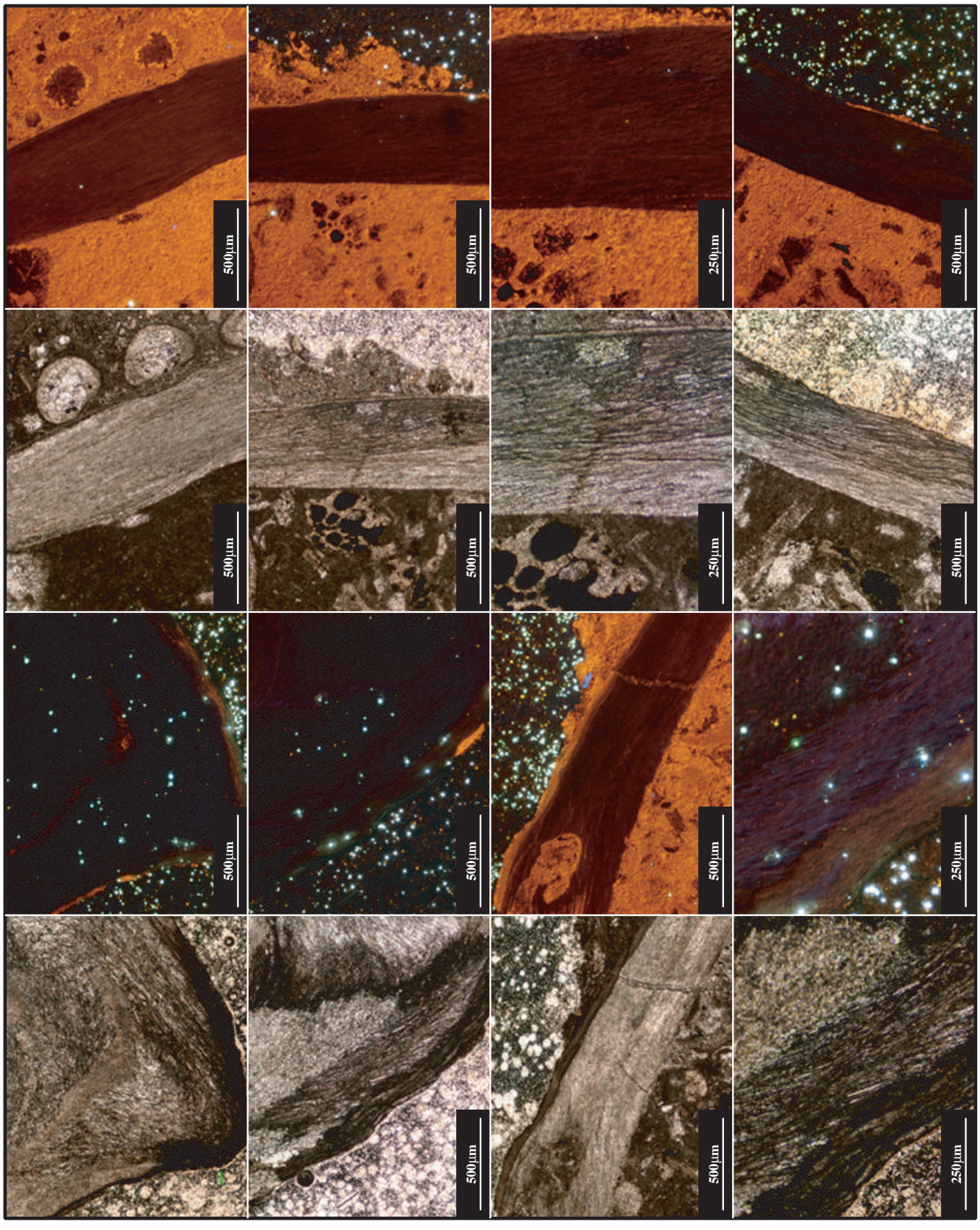

Table An.3.5: Cathodoluminescence micrographs of brachiopod C+160b (Marne Bleue d'Hauterive, Early Hauterivian, Cressier section).

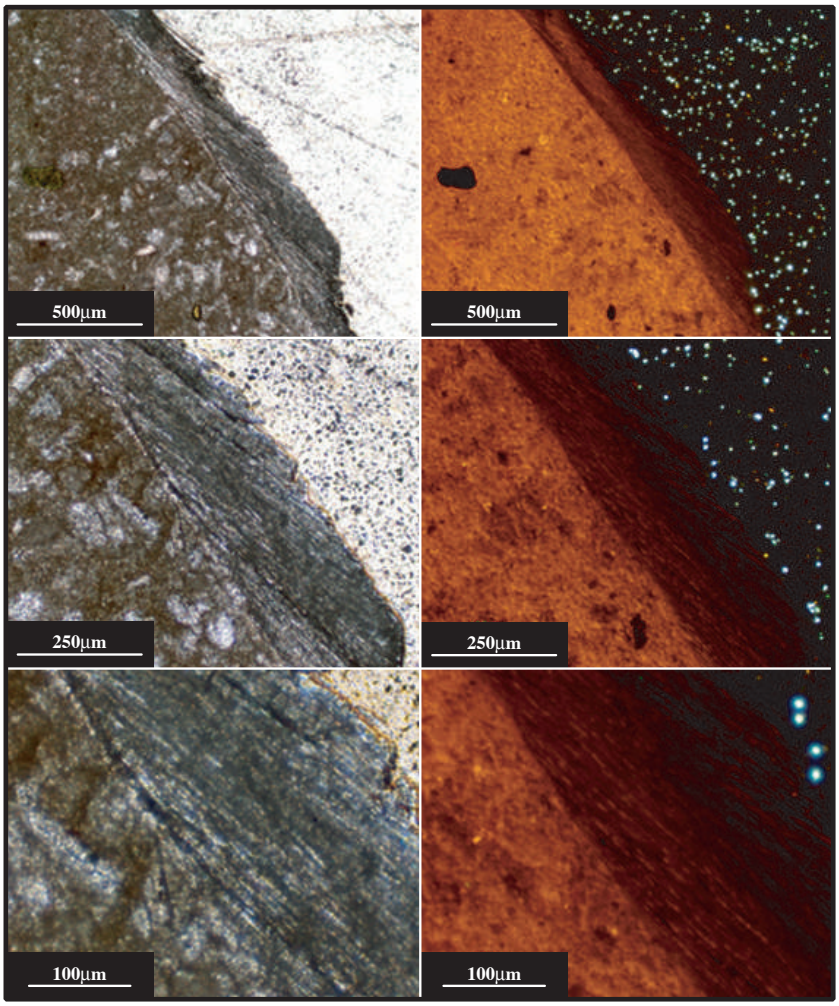

Table An.3.6: Cathodoluminescence micrographs of brachiopod MC1a (Marnes d'Uttins, Early Hauterivian, Mont-Chamblon section).

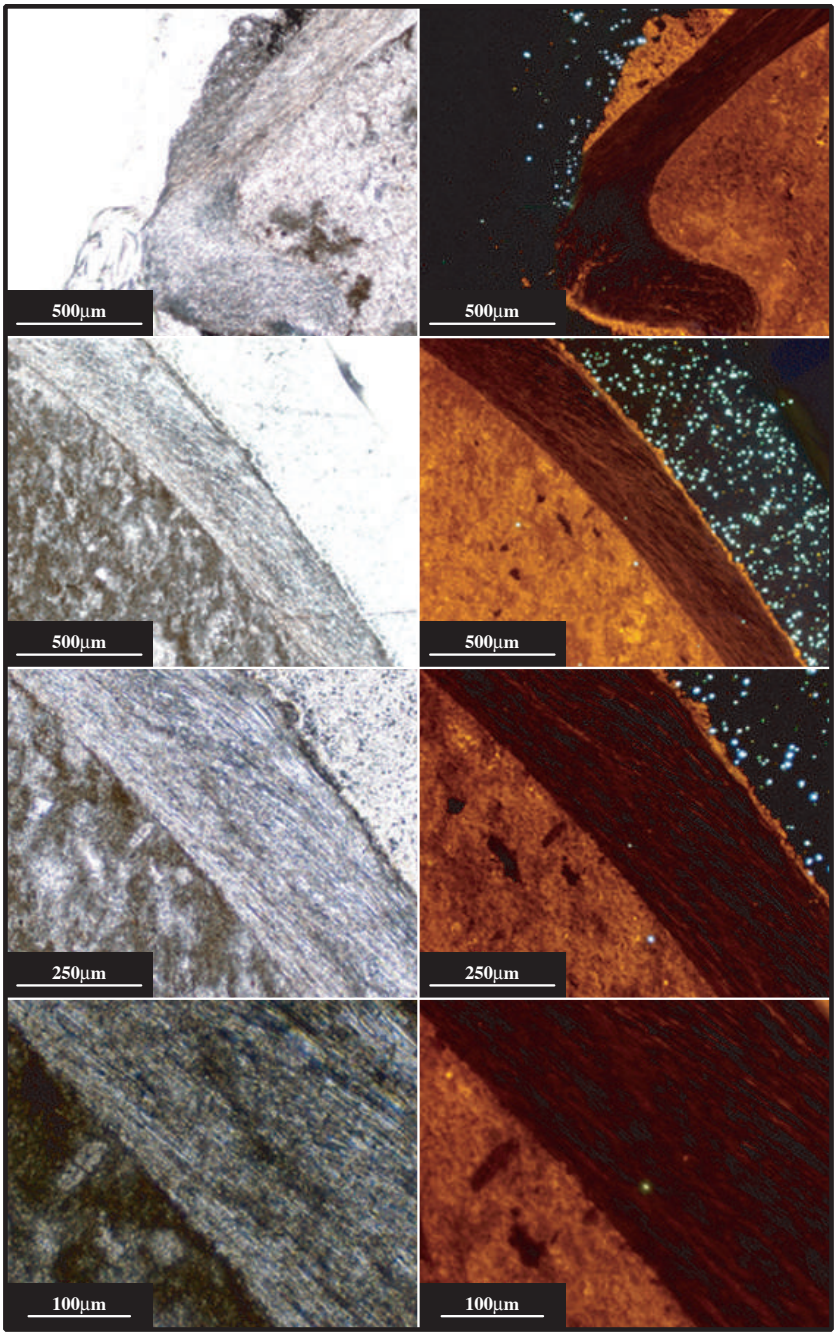

Table An.3.7: Cathodoluminescence micrographs of brachiopod MC1c (Marnes d'Uttins, Early Hauterivian, Mont-Chamblon section).

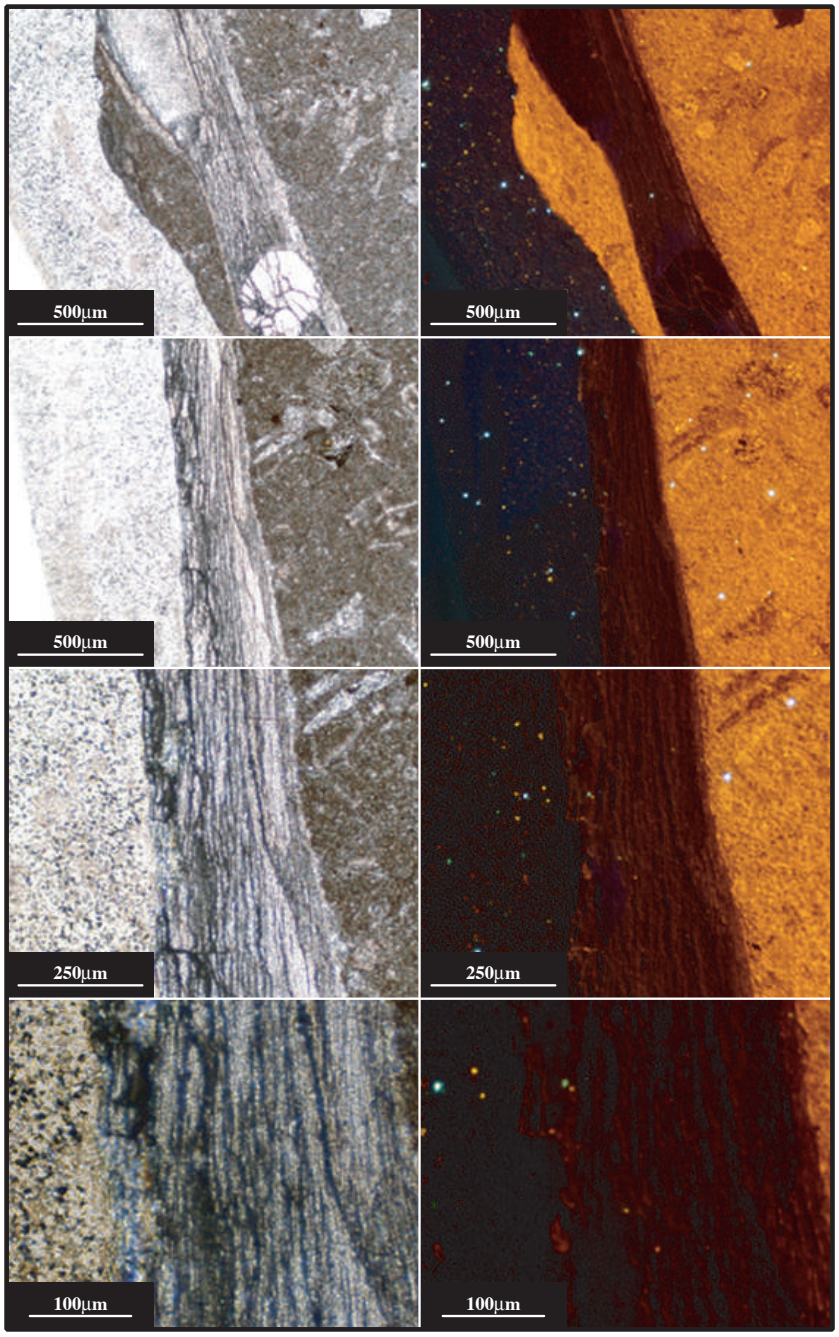

Table An.3.8: Cathodoluminescence micrographs of brachiopod MC3a (Marnes d'Uttins, Early Hauterivian, Mont-Chamblon section).

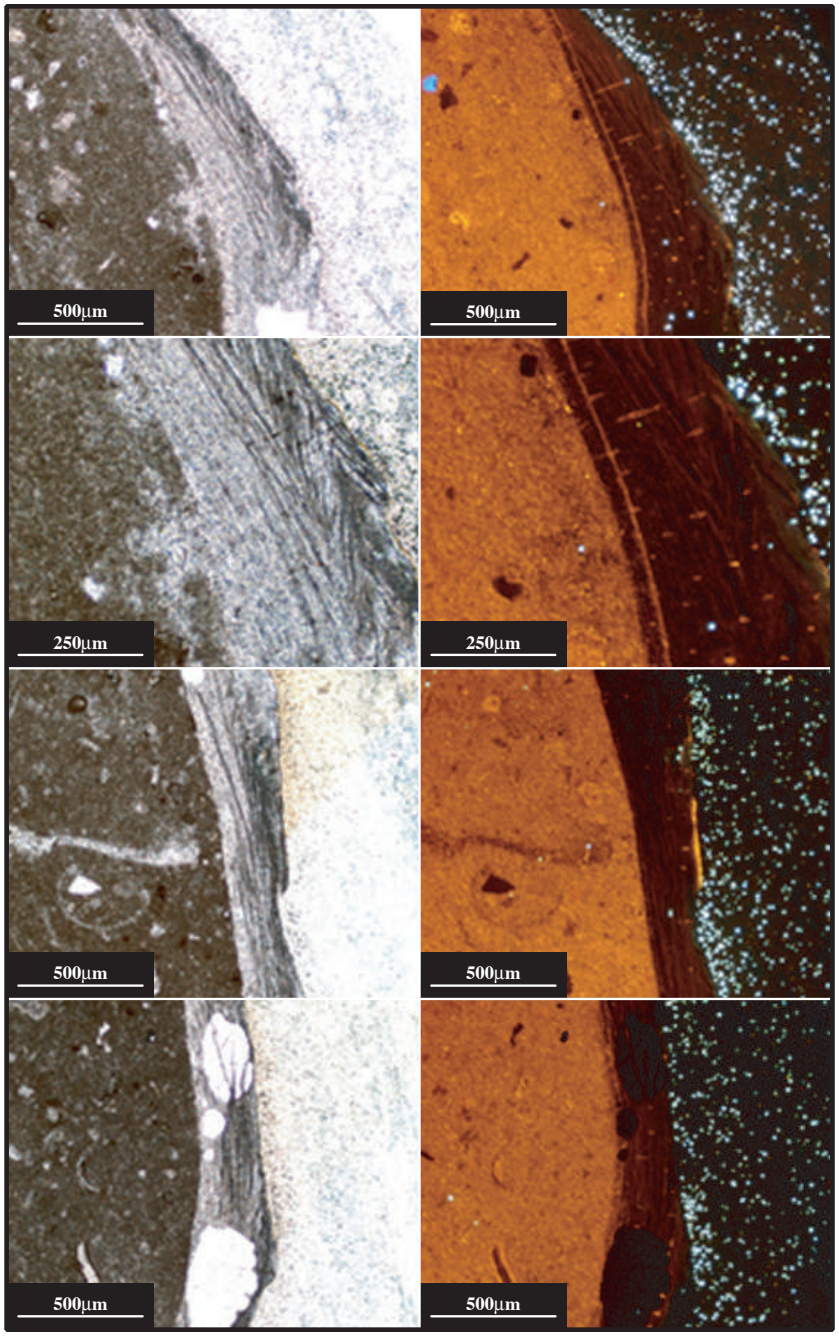

Table An.3.9: Cathodoluminescence micrographs of brachiopod MC4 (Marnes d'Uttins, Early Hauterivian, Mont-Chamblon section).

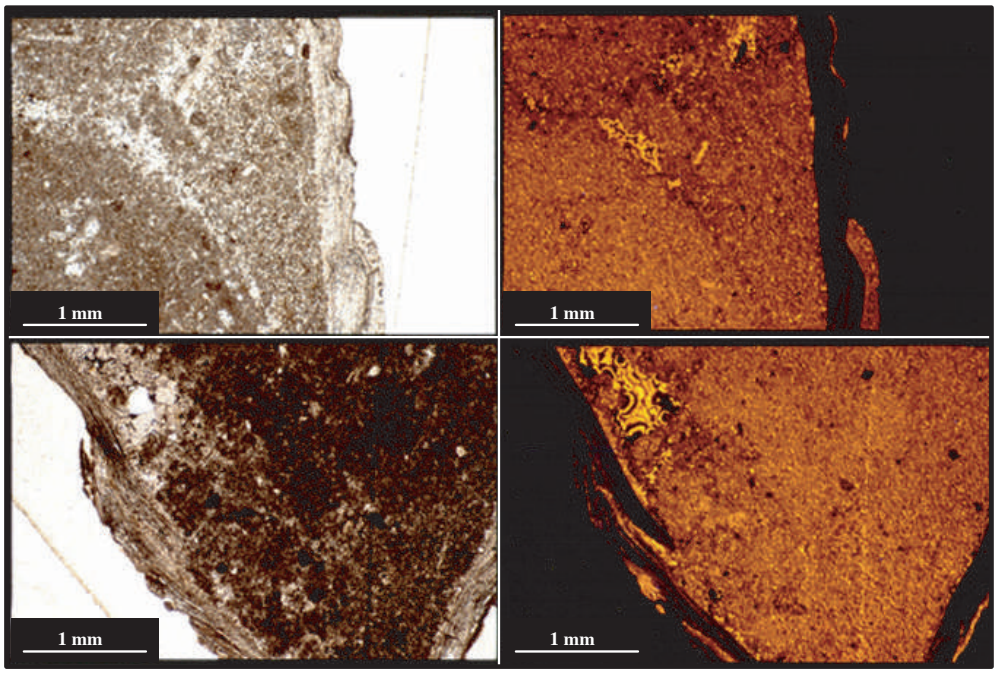

Table An.3.10: Cathodoluminescence micrographs of brachiopod F1b (Urgonien Jaune, Late Barremian, Pourtalès Hospital section).

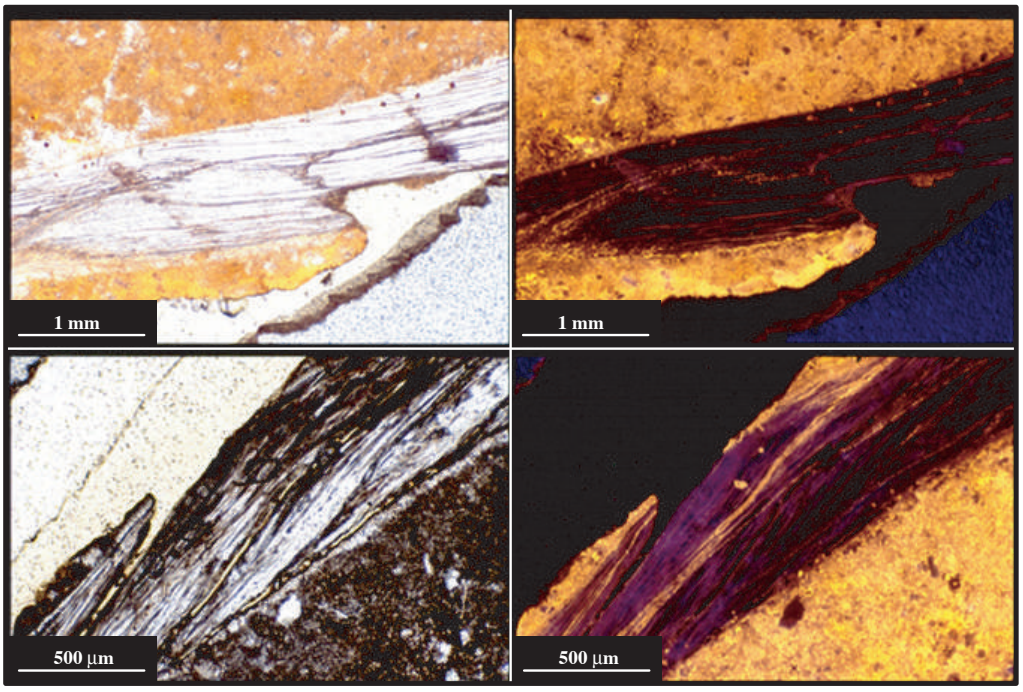

Table An.3.11: Cathodoluminescence micrographs of brachiopod F2a (Urgonien Jaune, Late Barremian, Pourtalès Hospital section).

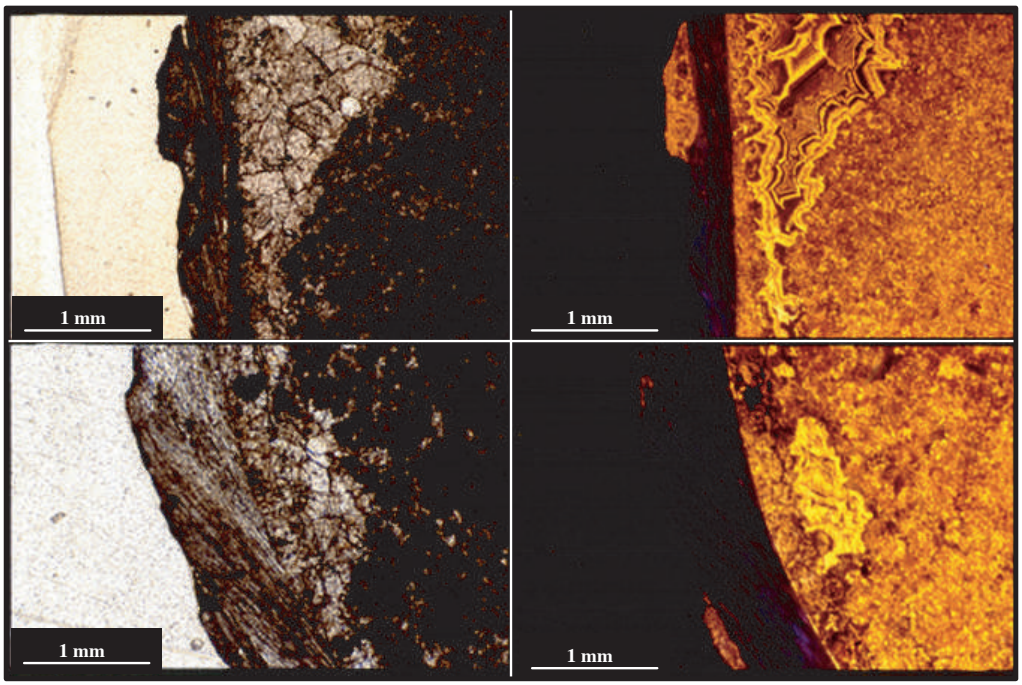

Table An.3.12: Cathodoluminescence micrographs of brachiopod F2b (Urgonien Jaune, Late Barremian, Pourtalès Hospital section).

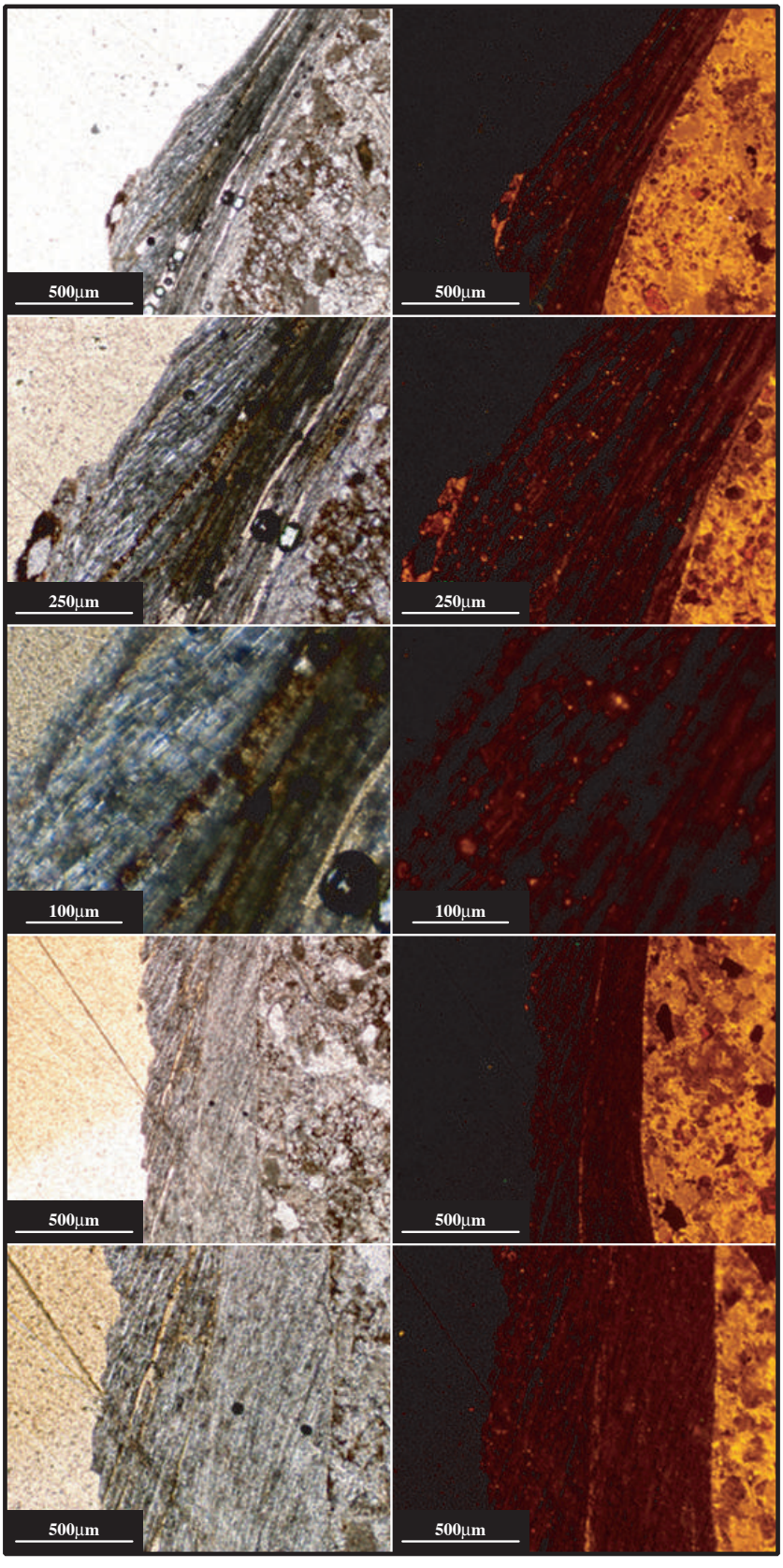

Table An.3.13: Cathodoluminescence micrographs of brachiopod $EC_{II}58$ (Urgonien Jaune, Late Barremian, Eclépens section).

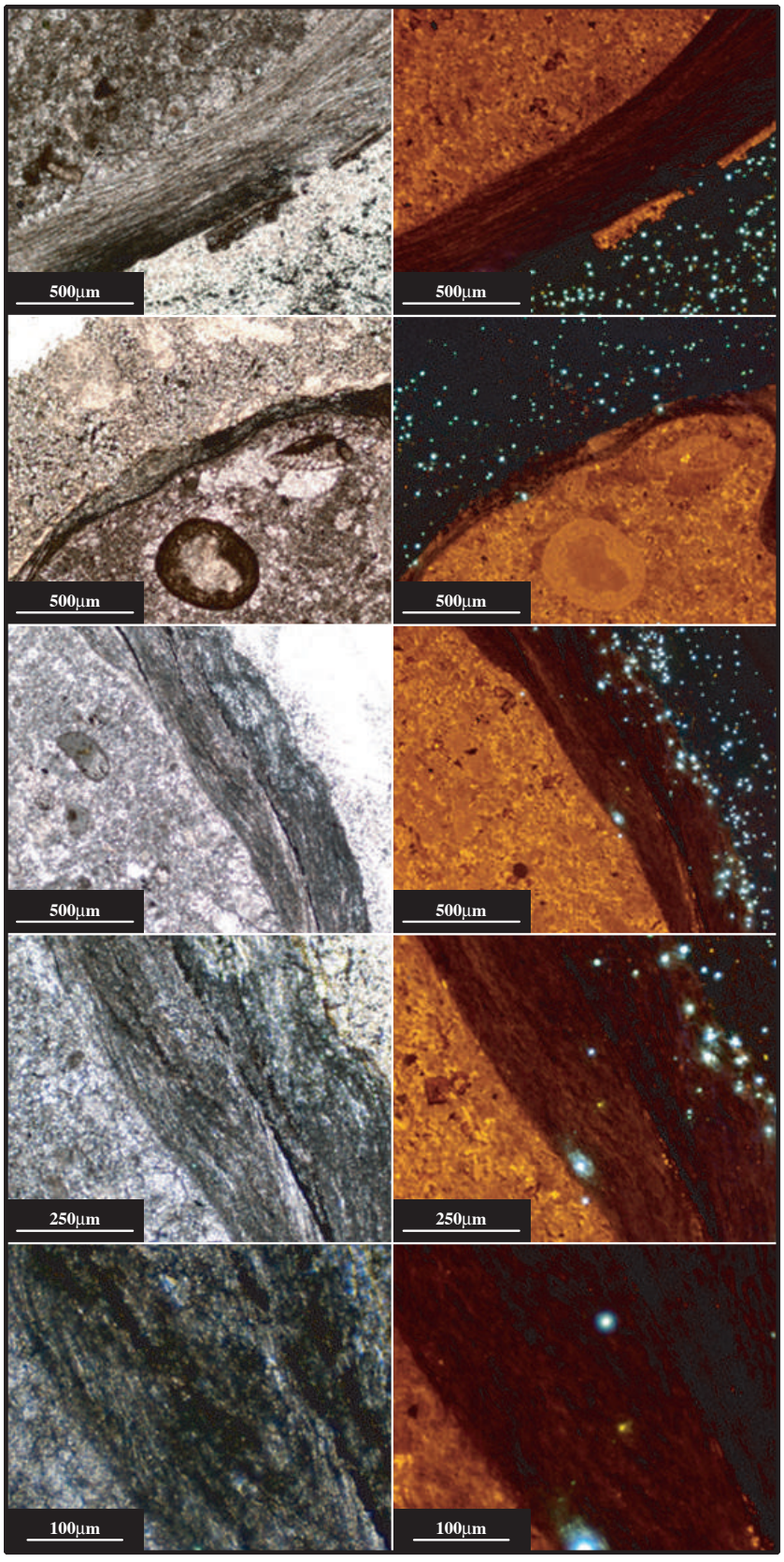

Table An.3.14: Cathodoluminescence micrographs of brachiopod ECb10 (Urgonien Jaune, Late Barremian, Eclépens section).

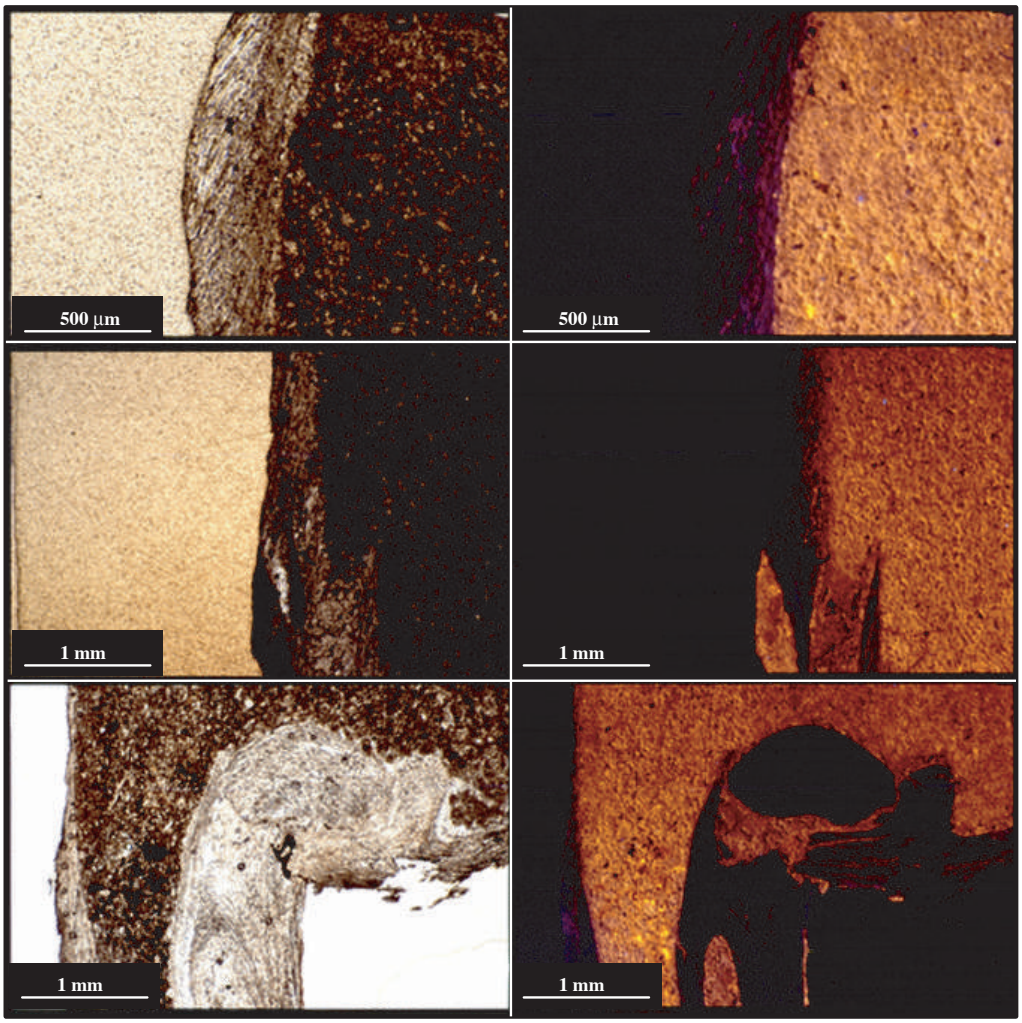

Table An.3.15: Cathodoluminescence micrographs of brachiopod LRu4 (Marnes de la Russille, Late Barremian, La Russille section).

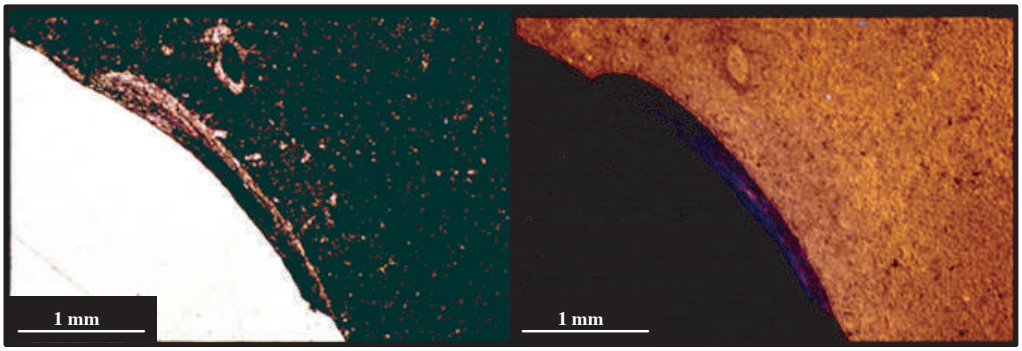

Table An.3.16: Cathodoluminescence micrographs of brachiopod LRu12a (Marnes de la Russille, Late Barremian, La Russille section).

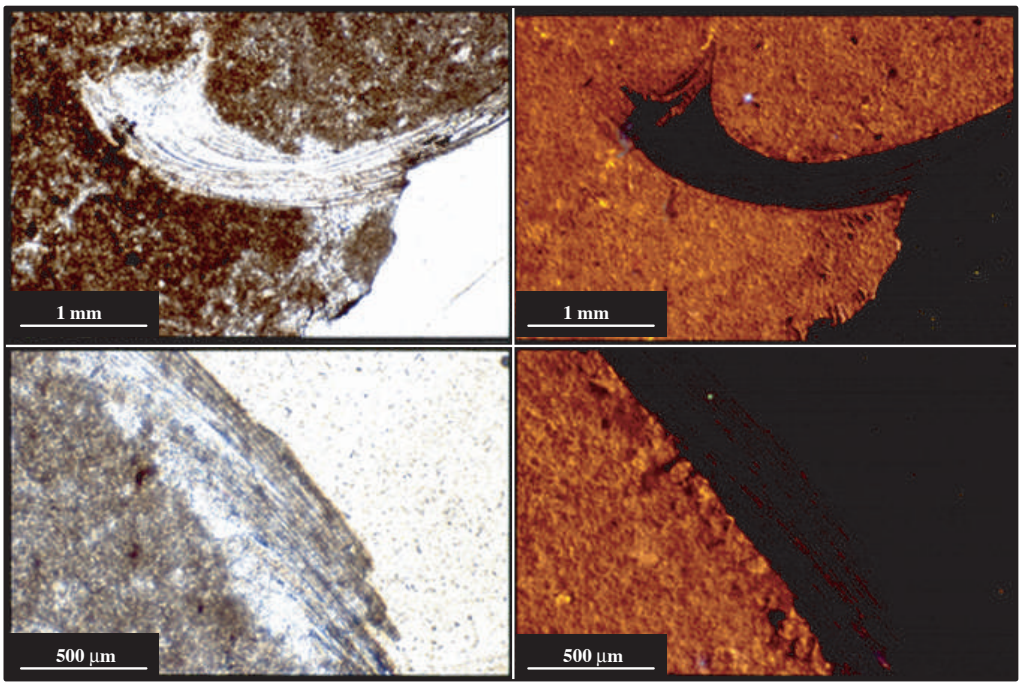

Table An.3.17: Cathodoluminescence micrographs of brachiopod LRu12b (Marnes de la Russille, Late Barremian, La Russille section).

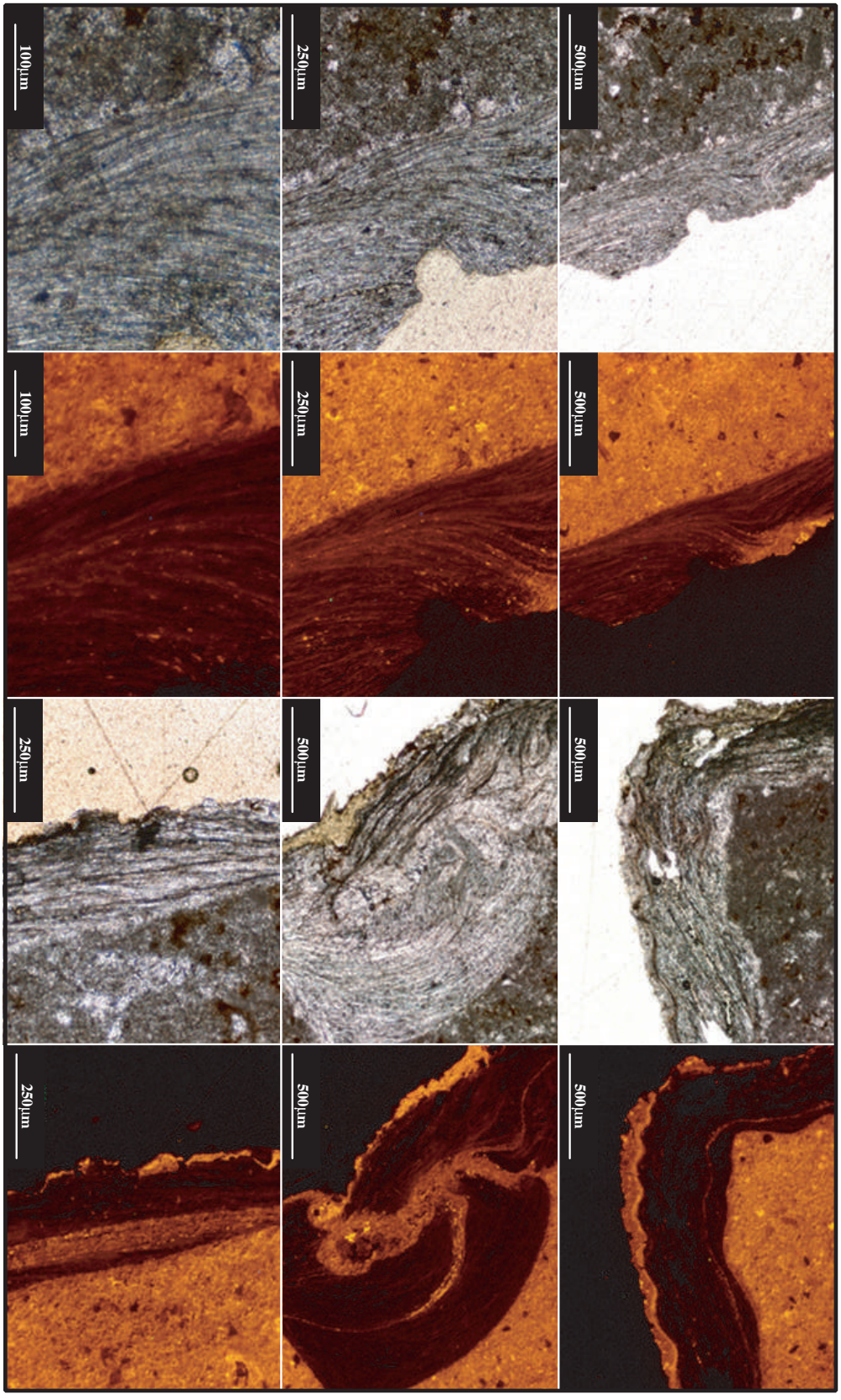

Table An.3.18: Cathodoluminescence micrographs of brachiopod E120Br (Urgonien Blanc, Late Barremian, Eclépens section).

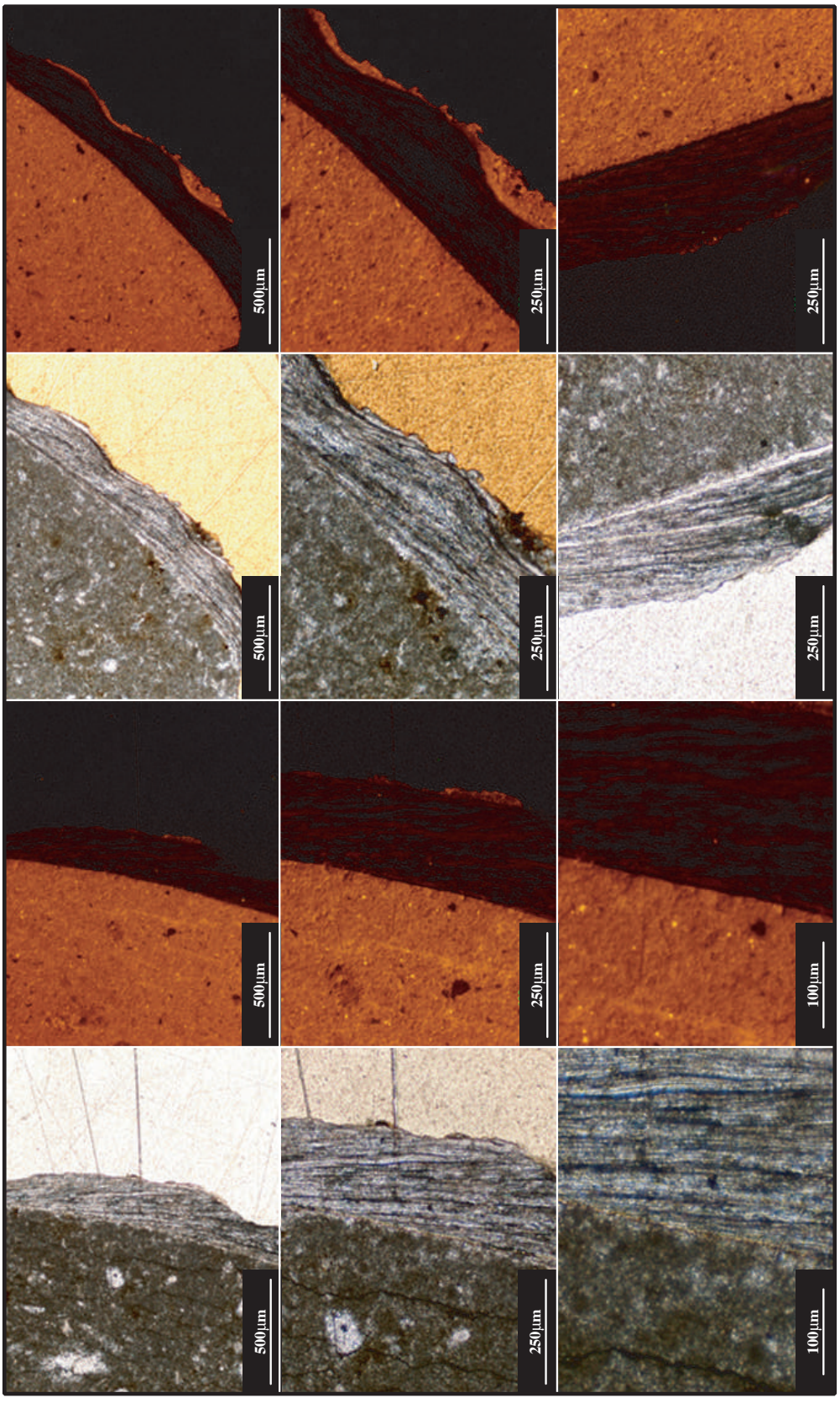

Table An.3.19: Cathodoluminescence micrographs of brachiopod E125Br (Urgonien Blanc, Late Barremian, Eclépens section).

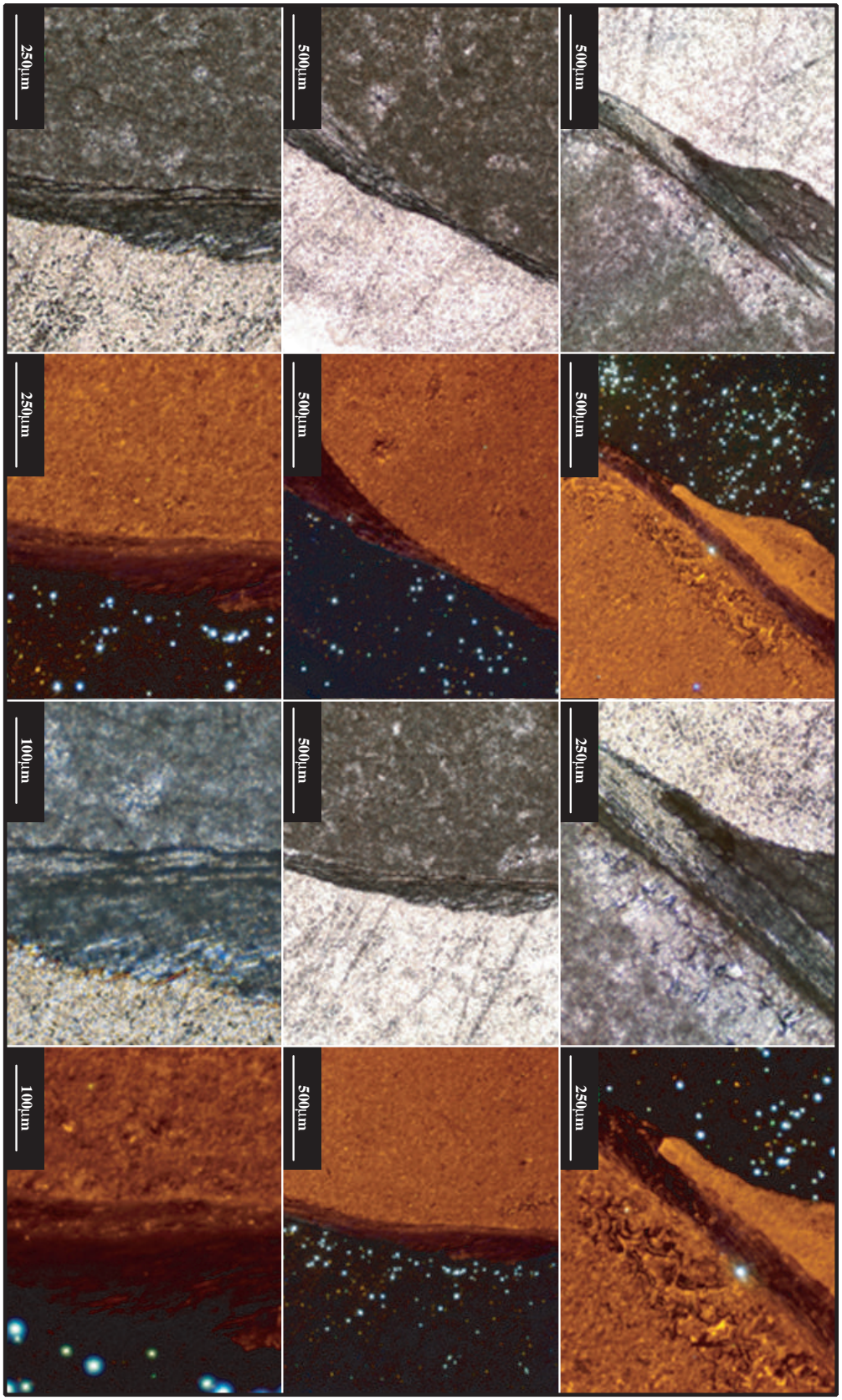

Table An.3.20: Cathodoluminescence micrographs of brachiopod VA61 (Urgonien Blanc, Late Barremian, Vaumarcus section).

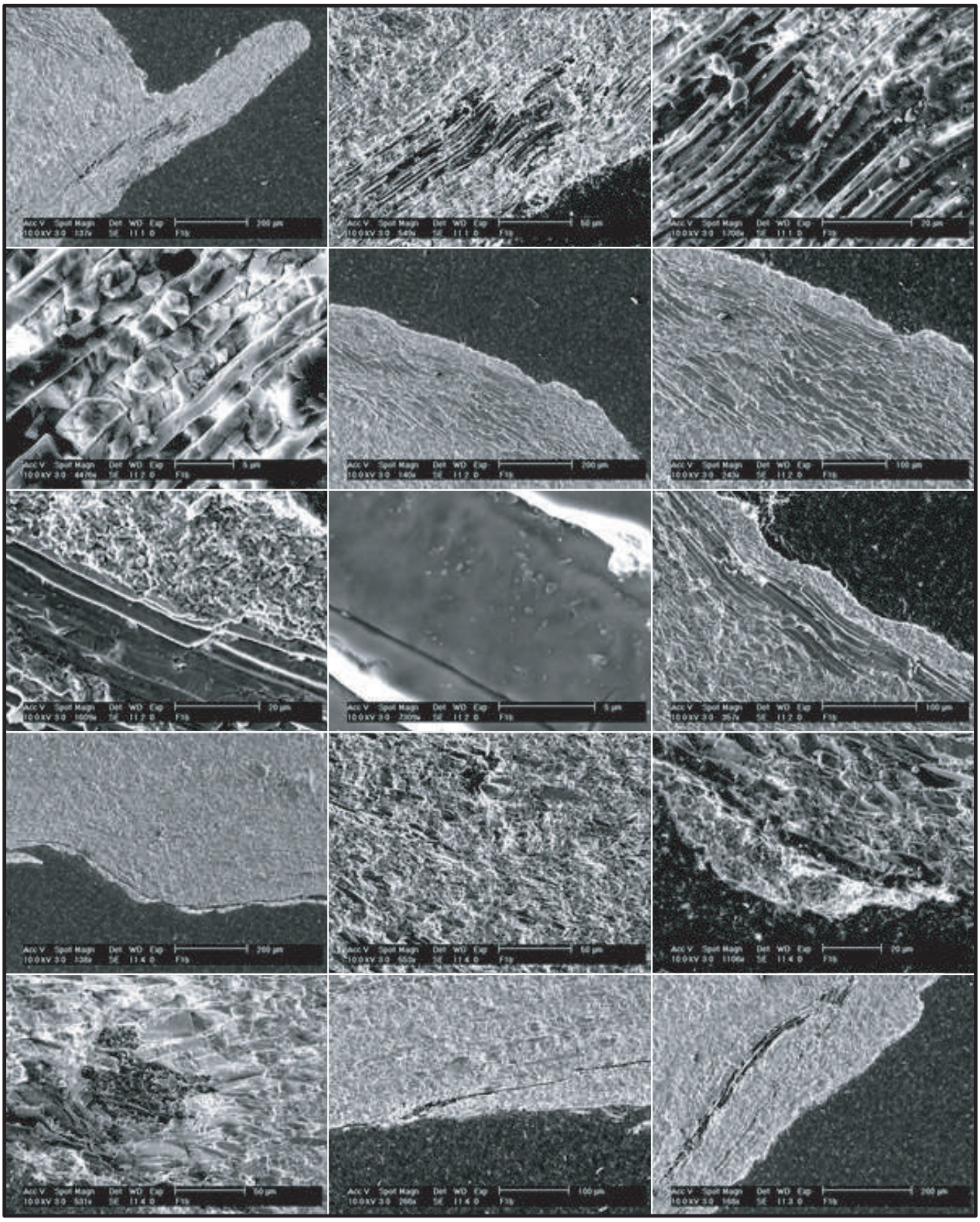

Table An.3.21: SEM micrographs of brachiopod F1b (Urgonien Jaune, Late Barremian, Pourtalès Hospital section).

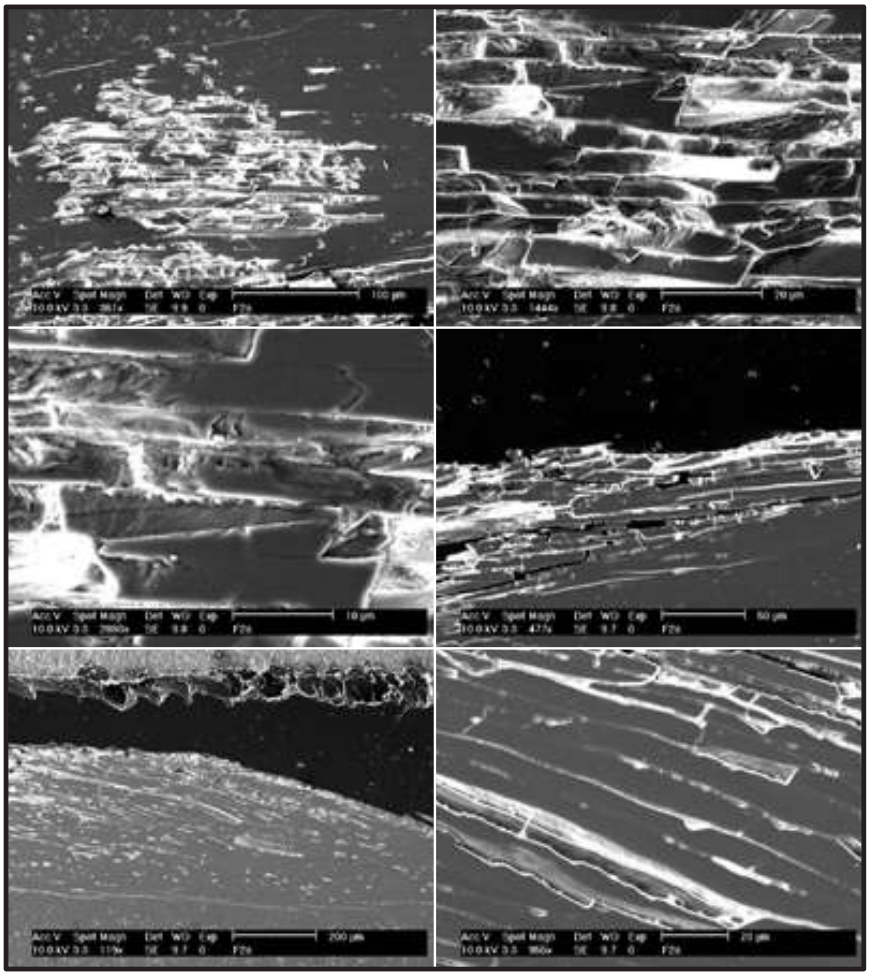

Table An.3.22: SEM micrographs of brachiopod F2a (Urgonien Jaune, Late Barremian, Pourtalès Hospital section).

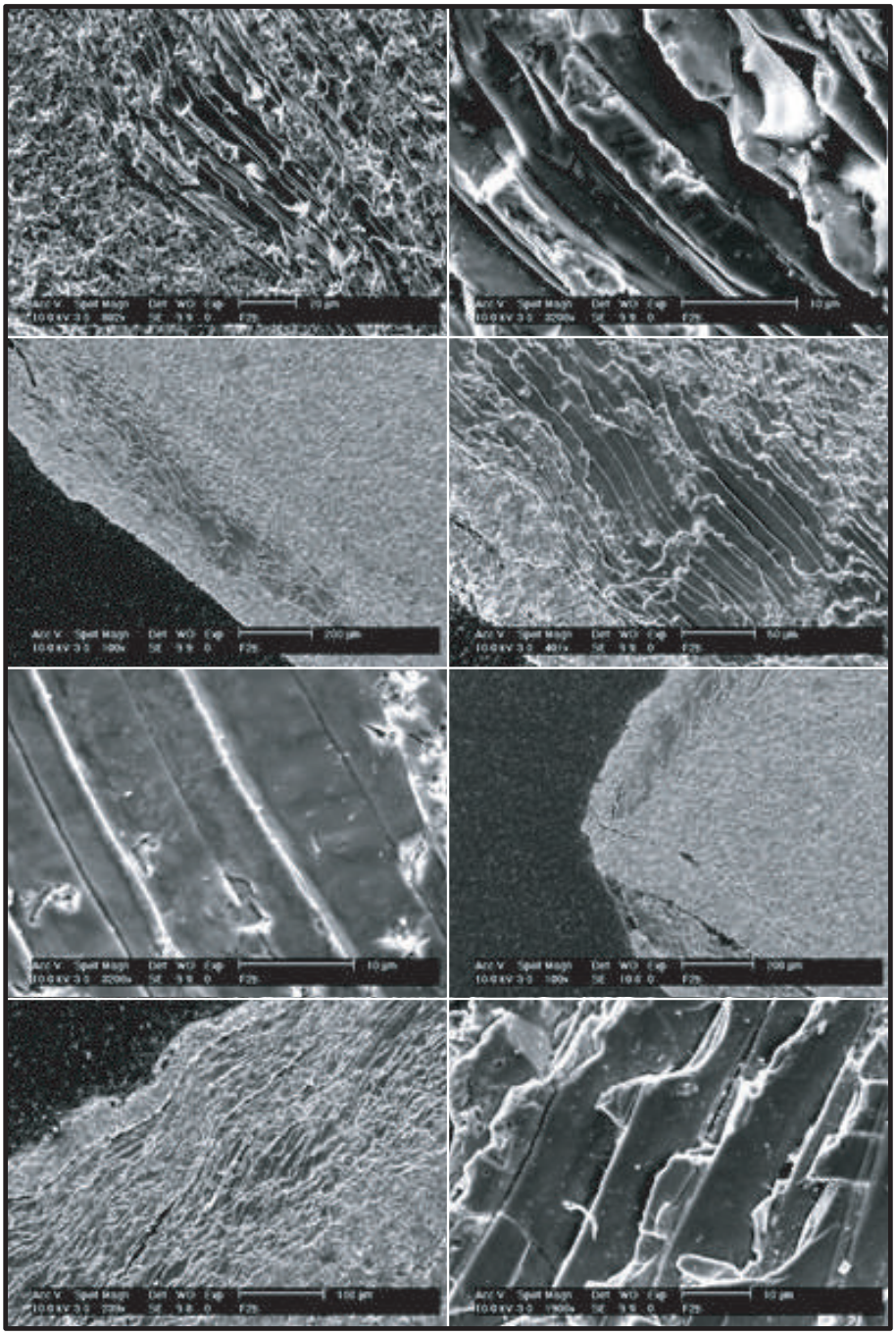

Table An.3.23: SEM micrographs of brachiopod F2b (Urgonien Jaune, Late Barremian, Pourtalès Hospital section).

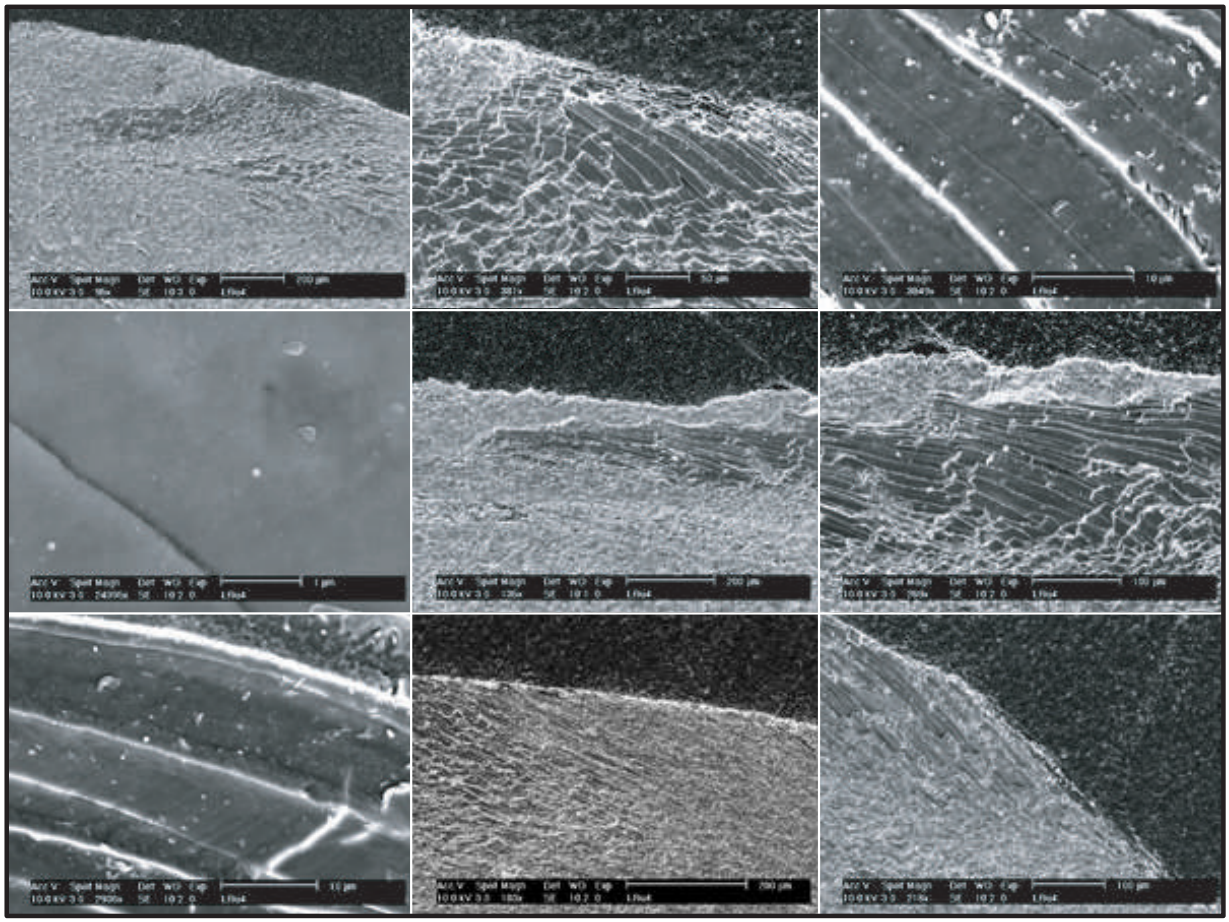

Table An.3.24: SEM micrographs of brachiopod LRu4 (Marnes de la Russille, Late Barremian, La Russille section).

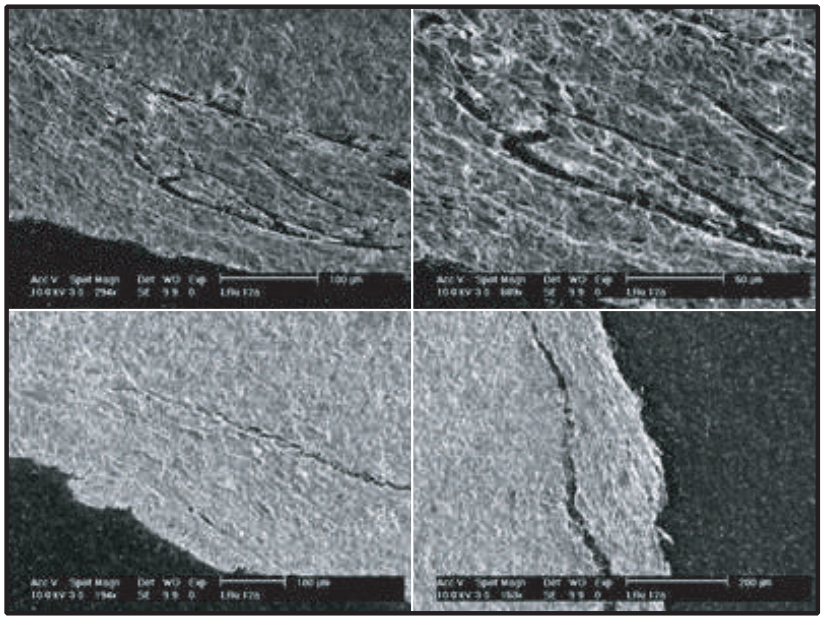

Table An.3.25: SEM micrographs of brachiopod LRu12a (Marnes de la Russille, Late Barremian, La Russille section).

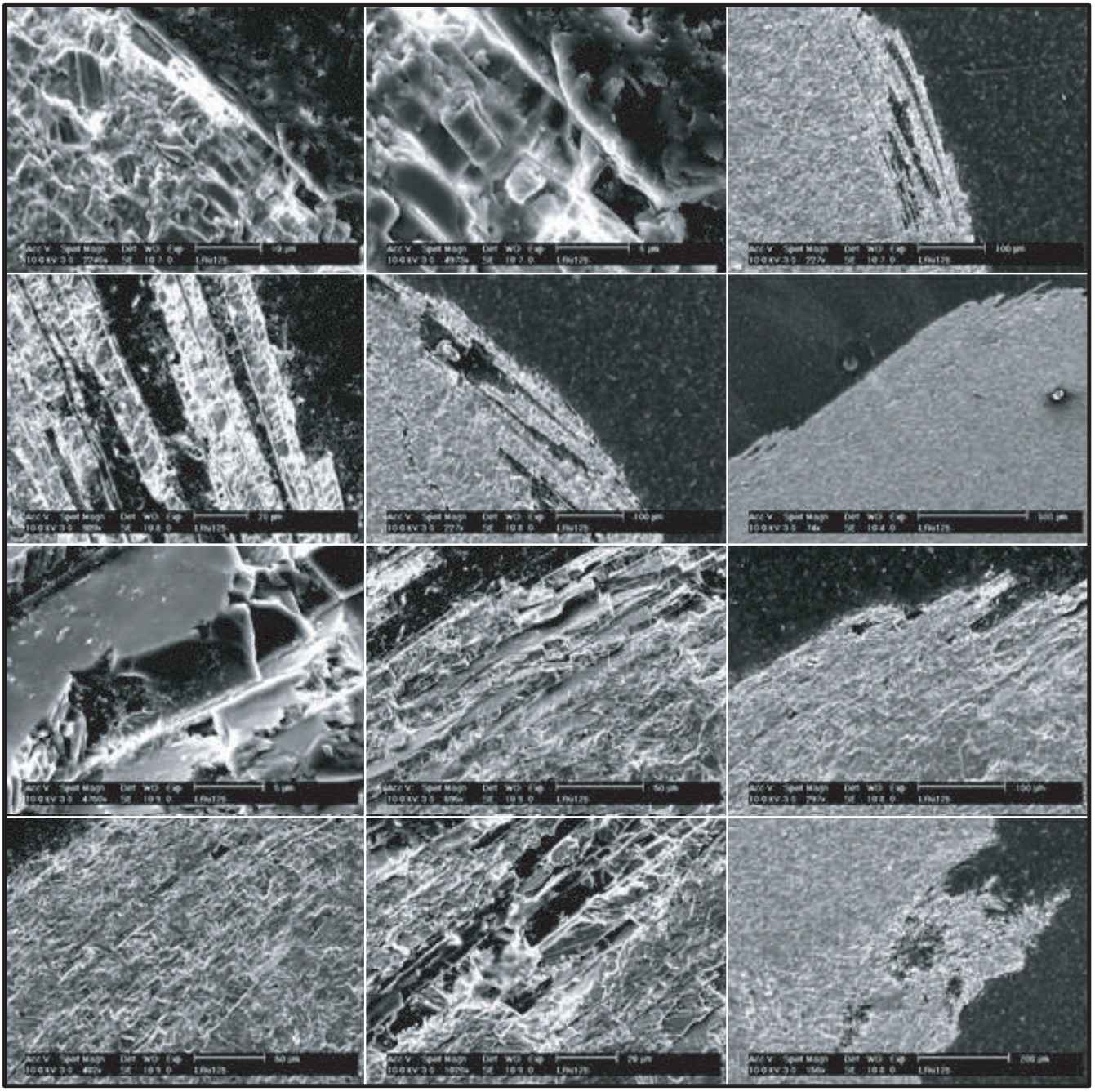

Table An.3.26: SEM micrographs of brachiopod LRu12b (Marnes de la Russille, Late Barremian, La Russille section).

Annexe 4.

Other Manuscripts related to

the SFN Projects n°2100-067807/1 and 200020-105206/1

An. 4.1.
Biostratigraphy, sedimentology and sequence stratigraphy of the latest Hauterivian – Early Barremian drowning episode of the Northern Tethyan margin (Altmann Member, Helvetic nappes, Switzerland)

Stéphane Bodin[1], Alexis Godet[1], Jean Vermeulen[2], Pascal Linder[1] & Karl B. Föllmi[1]

[1]Institut de Géologie, Université de Neuchâtel, Rue Emile Argand 11, CP 158, 2009 Neuchâtel, Switzerland; [2]Grand Rue, 04330 Barrême, France

In press in Eclogae Geologicae Helvetiae.

Abstract

During the Early Cretaceous, major palaeoceanographic changes are mirrored on the northern Tethyan carbonate platform by changes in the carbonate factory and by platform drowning. The Altmann Member of the central European, northern Alpine Helvetic thrust and fold belt, contains the sedimentary record of one of these drowning events which occurred during the Late Hauterivian – Early Barremian. It consists mainly of highly condensed beds, which are rich in glaucony and phosphates. The Altmann Member was hitherto only poorly dated. New ammonite findings and a re-evaluation of existing ammonite fauna allow to precisely date this drowning episode, starting in the Pseudothurmannia seitzi biozone (latest Hauterivian) and lasting until the Coronites darsi biozone (latest Early Barremian). These new age dates, coupled with sequence stratigraphic interpretations allow to better understand the unfolding of the drowning episode, which proceeded in two stages: The first stage consisted in an important phase of marine transgression during the latest Hauterivian, during which carbonate production was highly reduced; the second stage is recorded during the latest Early Barremian by an important sequence boundary, which is associated with a phosphatized hardground, followed by rapid sea-level rise and the deposition of outer ramp sediment associated with the backstepping of the platform. Almost the whole early Barremian is likely to be condensed in this phosphatized hardground, which is associated to a second order sea-level lowstand. The onset of the drowning event is linked to the Faraoni oceanic anoxic event, whereas during the Early Barremian, phosphatization might be the result of important winnowing during a period of highly eutrophic conditions.

Keywords

Early Cretaceous; Platform Drowning; Phosphatization; Condensation; Heterozoan; Northern Tethyan marginv

Résumé

Durant le Crétacé inférieur, les changements paléoceanographiques sont enregistrés sur la marge nord-Téthysienne par des fluctuations du mode de production des carbonates ainsi que des épisodes d'ennoiement de plate-forme. Le Membre d'Altmann, qui affleure en Europe centrale, dans les nappes plissées et charriées du domaine Helvétique, est le résultat d'un de ces ennoiements de la plate-forme carbonatée se déroulant durant l'Hauterivien tardif et le Barrémien précoce. Principalement constitué de couches fortement condensées riches en glauconie et phosphate, le Membre d'Altmann, qui peut être relié à des changements paléocéanographiques majeurs durant le Crétacé inférieur, n'a pour l'instant été que faiblement daté. De nouvelles datations biostratigraphiques basées sur des ammonites nouvellement trouvées, ainsi que sur une réévaluation de celles précédemment publiées, permettent de précisément dater cet épisode d'ennoiement de plate-forme. Celui-ci débute dans la zone d'ammonites à Pseudothurmannia seitzi (Hauterivien tardif) et se termine dans la zone à Coronites darsi (dernière zone du Barrémien inférieur). Ces nouvelles datations, couplées avec des interprétations en stratigraphie séquentielle, permettent de mieux appréhender le déroulement de cet épisode d'ennoiement de plate-forme qui se développe en deux temps : une première étape correspond à une importante phase de transgression marine durant l'Hauterivien terminal, accompagnée par une réduction importante de la production carbonatée. Une seconde étape est enregistrée durant la fin du Barrémien précoce par la formation d'un fond induré phosphaté associé à un bas niveau marin, suivie par une remontée rapide du niveau marin et le dépôt de sédiments de rampe carbonatée externe associé à une forte rétrogradation de la plateforme. De plus, la majeure partie du Barrémien précoce est condensée dans ce fond induré phosphaté associé à un bas niveau marin de second ordre. Le début de cet épisode d'ennoiement de plate-forme semble être lié à l'événement d'anoxie océanique du niveau Faraoni, tandis que durant le Barrémien inférieur, la phosphatogenèse semble être le résultat d'un important vannage des fonds océaniques durant une période d'eutrophie marine.

An.4.1.1. Introduction

The Early Cretaceous record on the Helvetic platform is characterized by several drowning episodes expressed in highly condensed and phosphatized beds (Funk *et al.*, 1993; Föllmi *et al.*, 1994). These beds are relatively rich in macrofossils (ammonites, belemnites, bivalves, brachiopods, sponges and echinoids) and have been the focus of several studies for nearly a century (*e.g.*, Heim, 1910-1916; Goldschmid, 1927; Fichter, 1934; Hantke, 1961; Funk, 1971; Briegel, 1972; Wyssling, 1986; Föllmi, 1989; Kuhn, 1996; van de Schootbrugge, 2001) due to their importance to date the intercalated sediments poor in biostratigraphically significant fossils.

This paper focuses on one of these condensed horizons, the Altmann Member (Mb), which separates the Kieselkalk Formation (Fm; Hauterivian) from the rest of the Drusberg Fm (latest Early to early Late Barremian). Previously, the Altmann Mb has not been dated precisely although a latest Hauterivian to earliest Barremian age was assumed (*e.g.*, Funk, 1969; Briegel, 1972; Rick, 1985; Wyssling, 1986; Funk *et al.*, 1993; Föllmi *et al.*, 1994). Thus, a first goal of this study is to provide a high-resolution biostratigraphy for the Altmann Mb using newly collected ammonites, as well as a reevaluation of those already collected during previous studies and stored in different museums.

The drowning horizons of the early Cretaceous Helvetic platform are of great interest since Föllmi *et al.* (1994) and Weissert *et al.* (1998) (see also Kuhn, 1996; van de Schootbrugge, 2001) have postulated links between these episodes and global palaeoceanographic events, as the carbon-isotope record expresses them. The Altmann Mb documents an episode for which no clear explanation has been yet formulated. On the other hand, major palaeoceanographic changes are present in the Tethyan realm during the Late Hauterivian – Early Barremian, such as the Faraoni oceanic anoxic event (Late Hauterivian; *e.g.*, Cecca *et al.*, 1994; Baudin *et al.*, 1999; Baudin, 2005) and a phase of enhanced phosphorus input during the Early Barremian (Bodin *et al.*, 2006). Using improved biostratigraphy and sedimentology of the Altmann Mb, this study aims at linking the initiation, unfolding and termination of the Altmann Mb drowning event to these major palaeoceanographic events.

An.4.1.2. Geological setting

The studied sections are located in the Helvetic nappes of Switzerland, situated in the northern part of the Alps and representing the northern Tethyan

margin. This domain was thrusted, overthrusted and folded in a northward direction during Alpine orogenesis (Fig. An.4.1). With regards to its age, almost the entire Hauterivian is represented in this tectonic unit by the Kieselkalk Fm (Fig. An.4.2), which is divided into three members; the Lower Kieselkalk, the Lidernen and the Upper Kieselkalk Mbs (Funk, 1969). The Kieselkalk Fm overlays the Gemsmättli Mb (early Late Valanginian to earliest Hauterivian; Kuhn, 1996). The latest Hauterivian to early Late Barremian correspond to the Drusberg formation, which is divided into a lower part (the Altmann Mb) and an upper part (the Drusberg Mb) (cf. Bollinger, 1988; Funk *et al*., 1993). During the Late Barremian – Early Aptian, the Helvetic platform is represented by the Schrattenkalk Fm, which is the equivalent of the Urgonian limestone facies described in many other locations in the world (*e.g*., Arnaud *et al*., 1998; Lehmann *et al*., 1999). Gemsmättli, Lidernen and Altmann Mbs represent three successive phases of incipient Helvetic platform drowning (D1, D2 and D3 respectively, in Föllmi *et al*., 1994; See also Kuhn, 1996 and van de Schootbrugge, 2001).

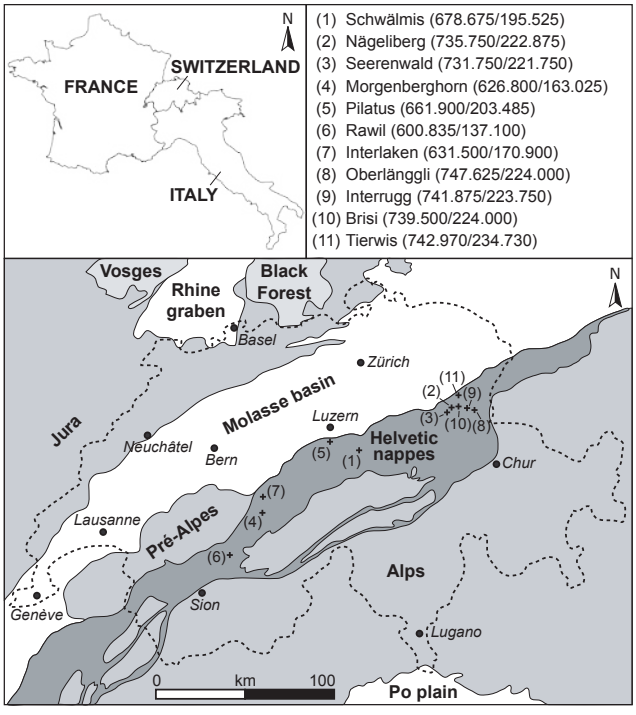

Fig. An.4.1: Location of the studied sections and their geographical coordinates, expressed in the Swiss orthogonal coordinate system. The Helvetic realm is shown in dark grey.

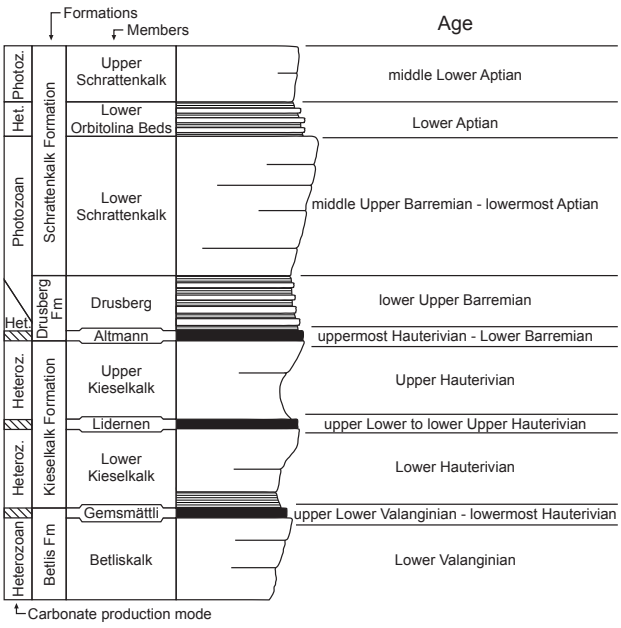

Fig. An.4.2: Synthetic log of Helvetic platform deposits of Valanginian to Early Aptian age.

The Helvetic carbonate platform morphology can be defined as a ramp (sensu Burchette & Wright, 1992). During the Berriasian, the situation was close to a distally steepened carbonate ramp (Kuhn, 1996). Rapid subsidence together with a second order sea level rise during the Early Valanginian resulted in a homoclinal ramp morphology (Kuhn, 1996) until the Late Barremian and the installation of the Urgonian facies, which signaled the return to a distally steepened carbonate ramp morphology. These changes in platform morphology were accompanied by changes of the sediment-producing benthic community, from a photozoan mode (sensu James, 1997; oligotrophic conditions) during the late Tithonian to Berriasian to a heterozoan mode (sensu James, 1997; meso-eutrophic conditions) from the Early Valanginian to the Early Barremian. During the Late Barremian, the installation of the Urgonian platform (Schrattenkalk Fm) underlines the return of photozoans (Föllmi *et al*., 1994). During the Early Cretaceous, reef-related organisms such as corals, stromatoporoids and rudists characterize photozoan assemblages whereas crinoids, bryozoans, abundant sponges and the absence of reef-related organisms mark heterozoan assemblages. The condensed sediments associated with drowning deposits are characterized by the dominance of siliciclastic particles, glaucony

and phosphates (*e.g.*,, Föllmi *et al.*, 1994; van de Schootbrugge, 2001).

An.4.1.3. Materials and methods

Eleven sections are documented (Schwalmis, Nägeliberg, Seerenwald, Morgenberghorn, Pilatus, Rawil, Interlaken, Oberlänggli, Interrugg, Brisi and Tierwis section). The majority of the studied sections is situated in the eastern part of Switzerland (Fig. An.4.1), in the Säntis – Churfirsten – Alvier massif, where the good quality and continuity of the outcrops allow to trace a proximal to distal transect along the northern Tethyan margin. These sections were sampled bed by bed, in order to identify high-frequency microfacies variations along the sedimentary succession. Coupled with stacking-pattern observations, these observations allow sequence-stratigraphic interpretations of the studied section.

To provide a high-resolution biostratigraphy for the Altmann Mb, a large number of ammonites were investigated, including newly collected ammonites as well as previous findings (*e.g.*, Fichter, 1934; Briegel, 1972; Rick, 1985; Wyssling, 1986; and many others…) that are stored in the Museums of Natural History of St. Gallen (Switzerland) and Dornbirn (Austria), and at the ETH Zürich. A total of 211 ammonites were identified. 108 of them provide accurate ages and are listed in Table An.4.1 (see also Fig. An.4.3). The stratigraphic position of the newly collected ammonites was precisely documented within each section in order to allow precise correlations. Combined with sequential stratigraphic interpretations, this allows to establish a markedly improved ammonite biostratigraphy of the Altmann Mb.

Location	Sample	Number
This study		
Tierwis section		
Abrytusites sp.	1	Sa 16a
Balearites sp. gr. mortilleti	1	Sa 16a
Emericiceras gr. koechlini	1	Sa 33
Emericiceras sp.	1	Sa 33
Paraspiticeras gr. percevali	2	Sa 16a
Parathurmannia sp.	1	Sa 16a
Plesiospitidiscus sp.?	1	Sa 16a
Subtorcapella sp.?	2	Sa 38
Torcapella gr. davydovi	1	Sa 33
Torcapella sp.?	2	Sa 36-38
Oberlänggli section		
Barremites sp. juv.	1	Ob 2
Parathurmannia cf. catulloi	1	Ob 2
Interlaken		
Barremites sp.	1	int 2
Dornbirn museum		
Avramidiscus aff. gastaldianus	1	P 11691
Avramidiscus cf. gastaldianus	1	P 6345
Avramidiscus intermedius	1	P 9392
Avramidiscus seunesi	2	P 11675
Balearites aff. mortilleti	1	P9385
Kotetishvilia aff. armenica ??	1	P 9345
Kotetishvilia aff. nicklesi	1	P 9346
Kotetishvilia compressissima	1	P 9370
Metahoplites cf. fallax	2	P 11649
Metahoplites cf. nodosus	1	P 9338
Metahoplites gr. fallax	3	P 9340
Metahoplites nodosus	1	P 11693
Nicklesia pulchella	1	P 11714
Parasaynoceras aff. perezianus	1	P 6332
Torcapella cf. fabrei	1	P 1615
? Metahoplites rarecostatus ?	1	P 11703
St. Gallen museum		
Avramidiscus seunesi	1	52.4
Kotetishvilia cf. compressissima	1	52.2
Pseudothurmanniform fragments	1	51.2
Torcapella sp.?	1	55.2

Location	Sample	Number
ETH Zürich		
Acrioceras sp.	4	F 7102
Anahamulina davidsoni	1	W 2273
Astieridiscus sp.	1	R1
Avramidiscus aff. intermedius	1	F 71007
Avramidiscus aff. kiliani	2	W 4876
Avramidiscus aff. querolensis	1	F 71006
Avramidiscus cf. druentiacus	1	W 4741
Avramidiscus gr. intermedius	2	F 7102.4
Avramidiscus sp.	2	F 71042
Balearites aff. catulloi	1	F 71055
Balearites sp. ?	1	F 71010
Costidiscus sp.	1	W 4518
Davidiceras sp.	1	W 5123
Dissimilites sp. ?	1	W 4955
Hamulina astieri	1	J 1078
Honnoratia sp.	4	F 71008
Karsteniceras aff. beyrichii	1	J 1043
Kotetishvilia cf. compressissima	2	J 1102
Leptoceratoides cf. annulatum	1	C 1042
Leptoceratoides sp.	1	W 5969
Metahoplites aff. fallax	1	J 1044
Metahoplites aff. nicklesi	2	W 4561
Metahoplites cf. fallax	1	J 1101
Metahoplites fallax	2	W 4916.1
Metahoplites gr. fallax	1	W 4860.1
Nickesia aff. nodosa	1	W 5263
Nicklesia cf. didayi	1	J 1039.3
Nicklesia pulchella	2	J 1039.4
Nicklesia pulchella morphotype tardif	2	J 1039.1
Paracrioceras sp.	3	J 1068
Parasaynoceras aff. perezianus	1	F 71005
Parasaynoceras sp.	2	W 4919
Pseudothurmannia aff. catulloi	2	F 71011
Pseudothurmannia aff. ohmi	1	W3 5135
Pseudothurmannia sp. s.l.	1	W 5028
Silesites gr. vulpes	1	W 4232
Taveraidiscus sp.	4	F 71035
Teschenites sp. ?	1	J 1011
Torcapella cf. fabrei	1	W 4971
Torcapella gr. davydovi	7	W 4221
Torcapella gr. fabrei	1	F 71019

Table An.4.1: List of identified ammonites from the Altmann Mb.

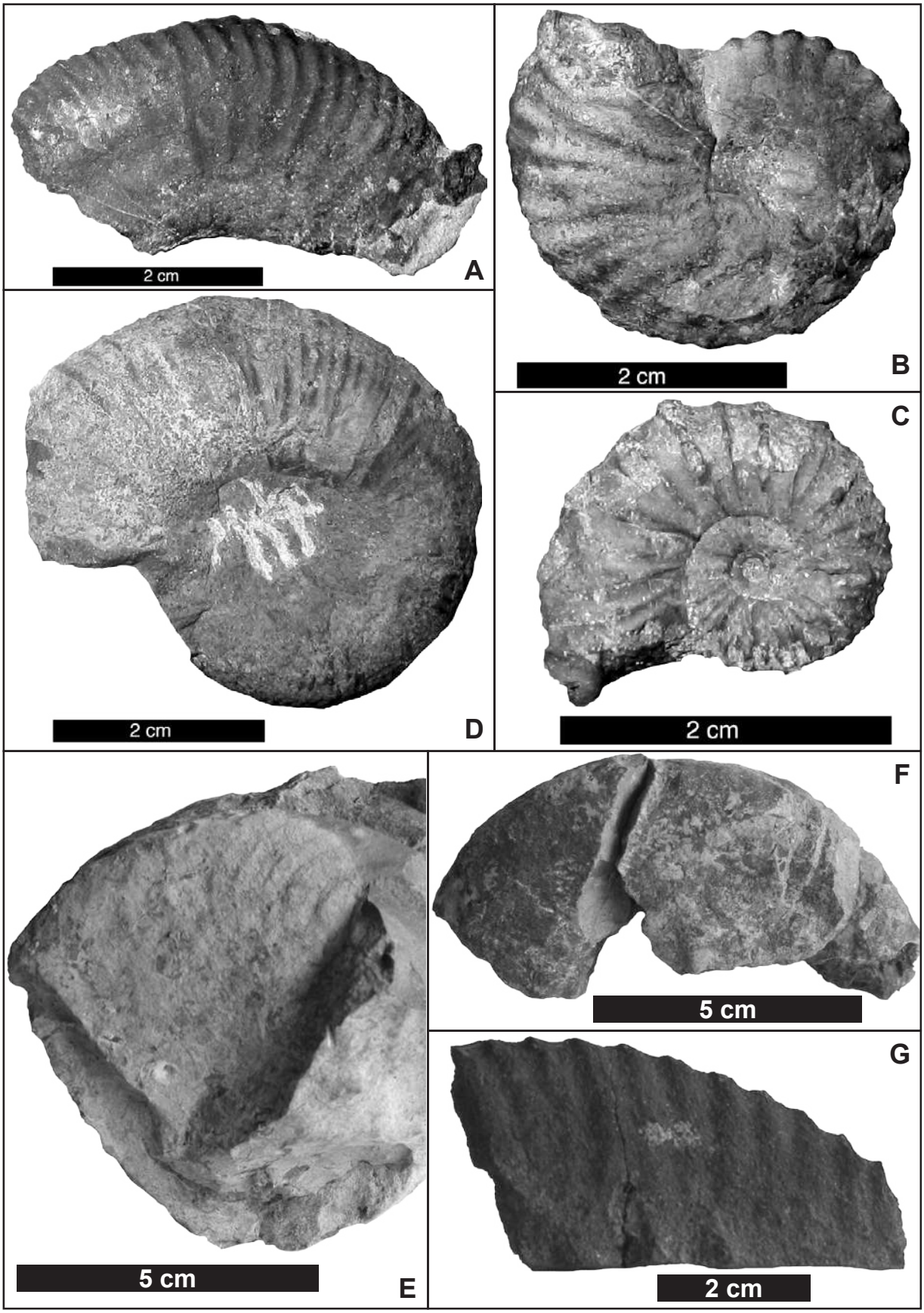

Fig. An.4.3: Examples of well-preserved representative ammonites from the Altmann Mb. A-D: After the study of Wyssling, 1986, re-identified, Vorarlberg region, Austria (stored in the Museum of Natural history of Dornbirn, Austria); E-F: Newly collected ammonites from the Tierwis section (all the newly collected ammonites are stored at the Geological Institute of Neuchâtel). A: Balearites aff. mortilleti, specimen n° P9385. B: Kotetishvilia aff. nicklesi, specimen n° P9346. C: Metahoplites nodosus, specimen n° P11693. D: Avramidiscus cf. gastaldianus, specimen n° P6345. E: Torcapella gr. davydovi, bed Sa 33. F: Emericiceras sp., bed Sa 33. G: Balearites sp. gr. mortilleti, bed Sa 16a.

An.4.1.4. Biostratigraphy

The outcome of the here established improved ammonite biostratigraphy (Fig. An.4.4) suggests that the time documented in the Altmann Mb spans from the latest Hauterivian (P. seitzi biozone) to the latest Early Barremian (C. darsi biozone). This new age determination is different from the previous ones by which a middle Early Barremian age for the end of the Altmann Mb was assumed (*e.g.*, Funk *et al.*, 1993; Föllmi *et al.*, 1994). Moreover, the distribution of these ammonites in time and space suggests that the biostratigraphic ages for the lower and upper limits of the Altmann Mb are synchronous (*i.e.* within the same ammonite zone) for the entire

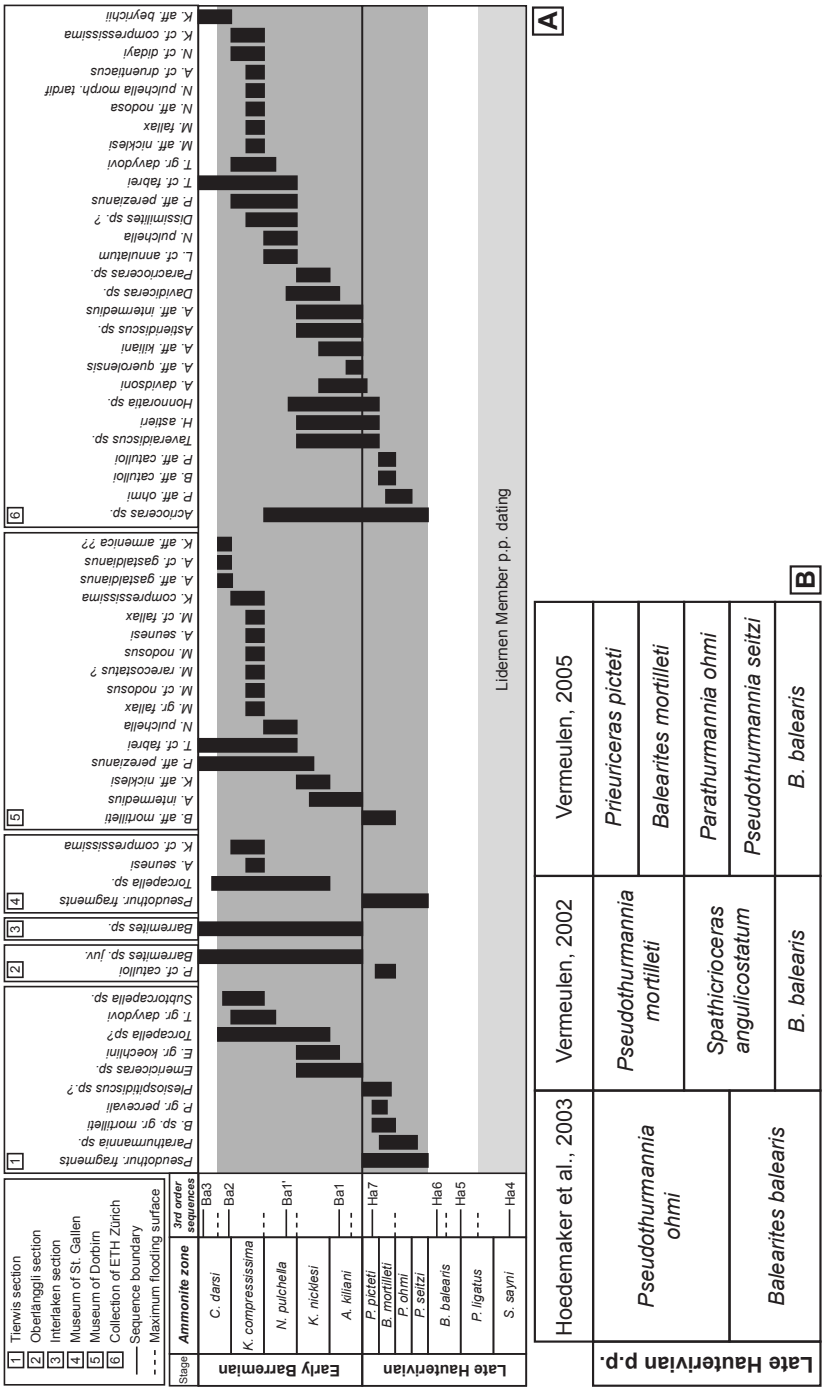

Fig. An.4.4: A. Stratigraphic range of the most significant ammonites identified in the Altmann Mb sections. Ammonite biostratigraphy zonation sensu Vermeulen (2005). Stratigraphic sequences after Hardenbol et al. (1998), modified by Arnaud (2005) for the latest Hauterivian – Barremian. Dating of the Lidernen Mb after van de Schootbrugge (2001). B. Correlation of the ammonite zonation of Vermeulen (2002, 2005) for the late Hauterivian with the current standard zonation (e.g., Hoedemaeker et al., 2003).

studied area. Following cyclo-stratigraphic interpretations of late Hauterivian – Barremian successions from the Vocontian trough (Bodin *et al*., in press), a duration of approximately 3 Myr is estimated for the time preserved in the Altmann Mb. The reduced thickness of the majority of the sections of the Altmann Mb (see below) implies that these sections are highly condensed, and the average sedimentation rate is approximately 1 m/Myr. In comparison, for the Upper Kieselkalk Mb at the Pilatus locality, an average sedimentation rate of 50 m/Myr is estimated (*e.g*., Funk, 1969; Van de Schootbrugge, 2001). This difference is related to the phase of carbonate platform drowning documented by the Altmann Mb and the associated slowdown or stop of the benthic carbonate production.

An.4.1.5. Microfacies

Ten different microfacies types have been recognized in the Upper Hauterivian – Lower Barremian deposits of the Helvetic realm (Upper Kieselkalk, Altmann and Drusberg Mbs). The microfacies HF0 to HF6 are adapted from previous studies focusing on Lower Cretaceous Western Tethyan carbonate platforms (*e.g*., Arnaud-Vanneau, 1980; Schenk, 1992; Wissler *et al*., 2003) because of the meso-eutrophic conditions prevailing on the Helvetic platform during the Hauterivian to Early Barremian. These microfacies are placed on a theoretical proximal to distal transect through the northern Tethyan Helvetic homoclinal ramp (Figs. An.4.5- and An.4.6) using the carbonate ramp depositional system description from Burchette and Wright (1992). The micro-facies HFa, HFb and HFc are specific for the glauconitic- and phosphatic-rich horizons and the gravity-flow deposits within the Altmann Mb, hence a precise localization is not feasible.

An.4.1.5.1. HF0 (marls; marls - micrite)

The rocks corresponding to this facies are finely laminated and composed of radiolaria, calcispheres, rare sponge spicules and rare beds with sparse bivalve fragments, as well as large amounts of very small and unidentifiable bioclasts. If the conditions of preservation are

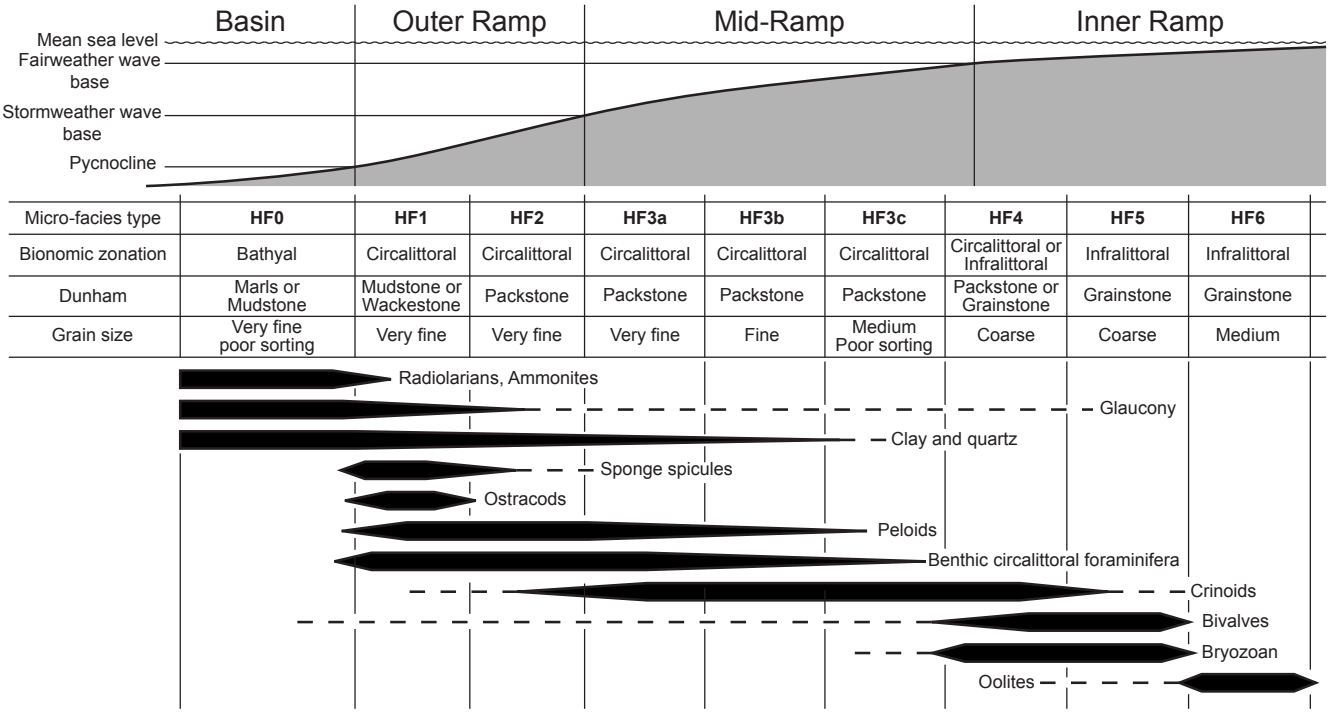

Fig. An.4.5: Distribution of the principal facies types in a schematic transect through the Helvetic ramp during the Hauterivian – Early Barremian. Bionomic zonation after the classification of Pérès (1961).

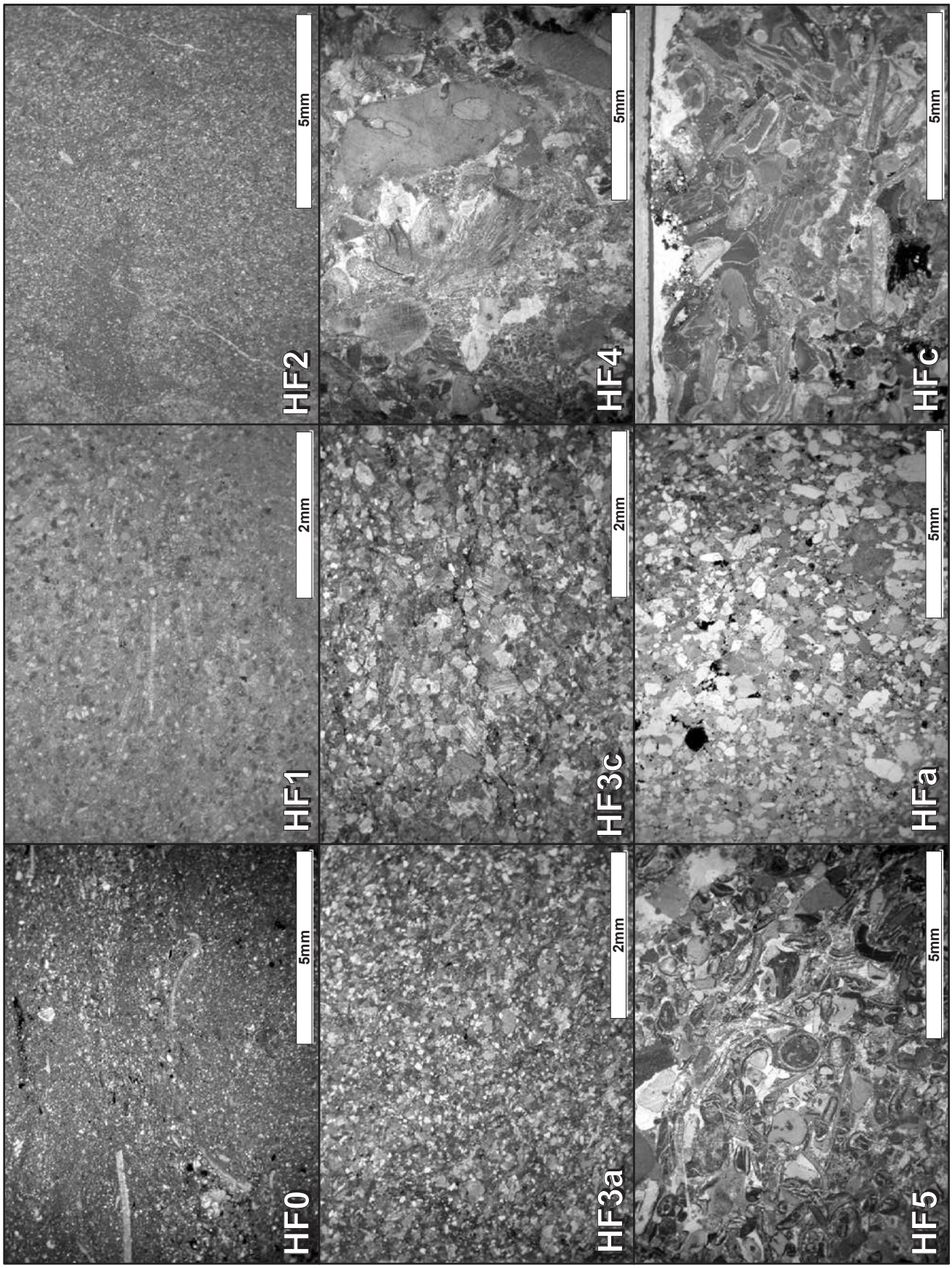

Fig. An.4.6: Photomicrographs of micro-facies HF0-5 and HFa-c. See the text for details. HF0: Sample Sa38. HF1: Sample Sa40. HF2: Sample Sa23. HF3a: Sample Sa30a. HF3c: Sample Sa7. HF4: Sample Pil145. HF5: Sample Pil143. HFa: Sample Schwa1. HFc: Sample Pi1 (note the marine phreatic cement and the phosphatized matrix occurring in the top of this thin-section. Note that this is also the top of the basal hardground in this photomicrograph). Samples Pil145 and Pil143 are taken from the top of the Upper Kieselkalk Mb in the Pilatus section (after van de Schootbrugge, 2001).

good, this facies contains a macro-fauna including ammonites, belemnites or fish teeth.

Interpretation: According to the presence of pelagic fauna, this facies is thought to represent a distal shelf deposit (hemi-pelagic facies).

An.4.1.5.2. HF1 (mudstone or wackestone; spicule-rich biomicrite)

The rocks corresponding to this facies are limestones and marly limestones. It is composed of numerous sponge spicules, in addition to some very small echinoderm fragments, peloids, benthic foraminifera and rare ostracods. Sporadic fish teeth are present.

Interpretation: This facies may represent the outer ramp deposits below the storm-weather wave base (hemi-pelagic facies), as testified by the presence of numerous sponge spicules.

An.4.1.5.3. HF2 (packstone; biopelmicrite)

The rocks corresponding to this facies are limestones and marly limestones. It is composed of large quantities of very small echinoderm fragments, rare sponge spicules, bivalve fragments, peloids, benthic foraminifera and quartz grains.

Interpretation: This facies may represent the upper part of the outer ramp deposits, affected by very rare storm events, as testified by the presence of very small fragments, which were likely derived from shallower regions.

An.4.1.5.4. HF3 (packstone; crinoid-rich biopelmicrite)

The lithology of this facies is typical for the Helvetic Kieselkalk Fm, *i.e.* crinoidal limestone or marly limestone (some chert nodules may also occur). It is mainly composed of angular crinoid fragments, small quartz grains, sparse bivalve fragments, benthic foraminifera and peloids. It is divided into three sub-facies: HF3a, 3b and 3c, taking into account the mean size of the crinoid grains, from very fine to medium grained.

Interpretation: The sorting of the mean size of crinoid grains may reflect redistribution of these grains during storm events. The absence of sparitic cement may, however, reflect the lack of permanent hydrodynamic currents. This facies may thus represent a middle ramp deposit, above the storm wave base and below the fair-weather wave base.

An.4.1.5.5. HF4 (packstone or grainstone; crinoïdal and bryozoan biomicrite or biosparite)

This facies is typical for the "Kieselkalk – Echinodermenbreccie" Mb (Funk, 1969) and is expressed in relatively thick (up to 2-meters-thick) limestone beds, which are sometime cross-stratified. This facies is coarsely grained, poorly sorted, and composed of angular echinodermal and bivalve fragments, bryozoans, gastropods, peloids and rare ooids. Sparitic cements are observed.

Interpretation: The presence of sparitic cement in this facies hints to a deposition under quasi-permanent hydrodynamic currents. This facies is thus attributed to the transition between the upper middle and the lower inner ramp.

An.4.1.5.6. HF5 (grainstone; coarse biosparite with rounded grains)

This facies presents the same allochem assemblage as the previous one, with the main difference being that all the grains are well rounded. Some grains present traces of incipient ooid formation (superficial ooid).

Interpretation: According to the presence of rounded grains and sparitic cement, which suggests deposition under permanent agitation, this facies may have been deposited on the inner ramp, under permanent hydrodynamic currents, above the fair-weather wave base.

An.4.1.5.7. HF6 (grainstone; oosparite or oobiosparite)

This facies was never observed in the Hauterivian – Early Barremian of the Helvetic realm. Only indirect clues for oolithic bars are present (*i.e.* oolithes dispersed in MF4 and MF5 facies). During the Hauterivian, the presence of oolithic bars is, however, observed in the deposits

of the Jura Mountains (Pierre Jaune de Neuchâtel Fm; *e.g.*, Blanc-Aletru, 1995; see Fig. An.4.1 for localization), which represent the upper part of the Helvetic ramp.

Interpretation: According to the presence of oolithes and sparitic cement, this facies may be representative of the inner ramp.

An.4.1.5.8. HFa (glauconitic-rich sandstone)

The lithology of this facies is characteristic for the highly reduced sections of the Altmann Mb (less than 2m thick). It is composed of coarse rounded quartz grains, mature glaucony grains, some phosphate and calcite grains, as well as authigenic pyrite grains. The matrix corresponds to micritic or phosphatized ooze. In the field, oblique stratifications are sometimes recognized.

Interpretation: The presence of numerous mature glauconitic grains, as well as phosphate and pyrite, may point to a highly condensed or an allochthonous deposit derived from a condensed deposit.

An.4.1.5.9. HFb (wackestone or packstone; biomicrite)

The lithology of this facies is recognized in deposits occurring within Altmann Mb sections with phosphatized hardground at their base or with phosphatic nodules. It has the same characteristic as the micro-facies HFa. Quartz grains are, however, rare and smaller and glaucony grains (if present) are well rounded. The sorting is relatively good and many coarse crinoid grains are present. In addition, bryozoans, brachiopods and bivalve fragments, as well as small benthic foraminifera and phosphate grains are observed. The matrix is often phosphatized.

Interpretation: Well-rounded glaucony grains may indicate their parautochtonous origin (*e.g.*, Pasquini *et al.*, 2004). Due to the presence of oblique stratification, as well as an erosive base below the bed presenting this microfacies, theses rocks are interpreted as gravity flow deposits.

An.4.1.5.10. HFc (phosphatized hardground)

The macroscopic aspect of this facies differs between different sections. Similarities include the presence of macrofauna (ammonites, belemnites, bivalves, brachiopods, sponges…), as well as the presence of burrows, encrusting organisms and sometimes burrow infills below the hardground. The matrix is always composed of completely or partially phosphatized ooze. Phosphate grains, glaucony and lithoclasts are frequent, as well as grains or rock fragments reworking.

Interpretation: Hardground surfaces are subaquatic features. The formation of such discontinuity surfaces can be related to the lowering of the effective wave base exposing the sea floor to wave action (*e.g.*, Immenhauser *et al.*, 2000).

An.4.1.6. Macroscopic sedimentological aspects

The Altmann Mb is easily distinguished in the field due to its high content of glauconitic grains and the presence of phosphatic particles and crusts (Funk, 1969). The distinct lithological differences between the dark colored, sandy crinoidal limestones of the subjacent Kieselkalk Fm and the grey colored hemipelagic marl – limestone alternations of the superjacent Drusberg Mb are characteristic properties that assist in the identification of the Altmann Mb. The sections of the Altmann Mb studied here are subdivided into four main types according to their thickness and lithologic pattern.

An.4.1.6.1. Highly reduced sections or hiati

Reduced sections and hiati represent the majority of the Altmann Mb sections. This highly reduced type of section is characterized by the following field aspects: a total thickness < 2 meters, occasionally with an erosive base (*e.g.*, the Schwalmis and the Nägeliberg sections; Fig. An.4.7). In some beds, oblique stratifications are observed, depending on the exposure conditions. Glaucony-rich sandstone and rare phosphatized grains characterize the facies of these beds. No datable ammonites have been found in these sections, even if some of the dispersed phosphate grains, due to their bean-shaped aspect, could be attributed to altered and phosphatized ammonite clasts. The Seerenwald section (Fig. An.4.7) is

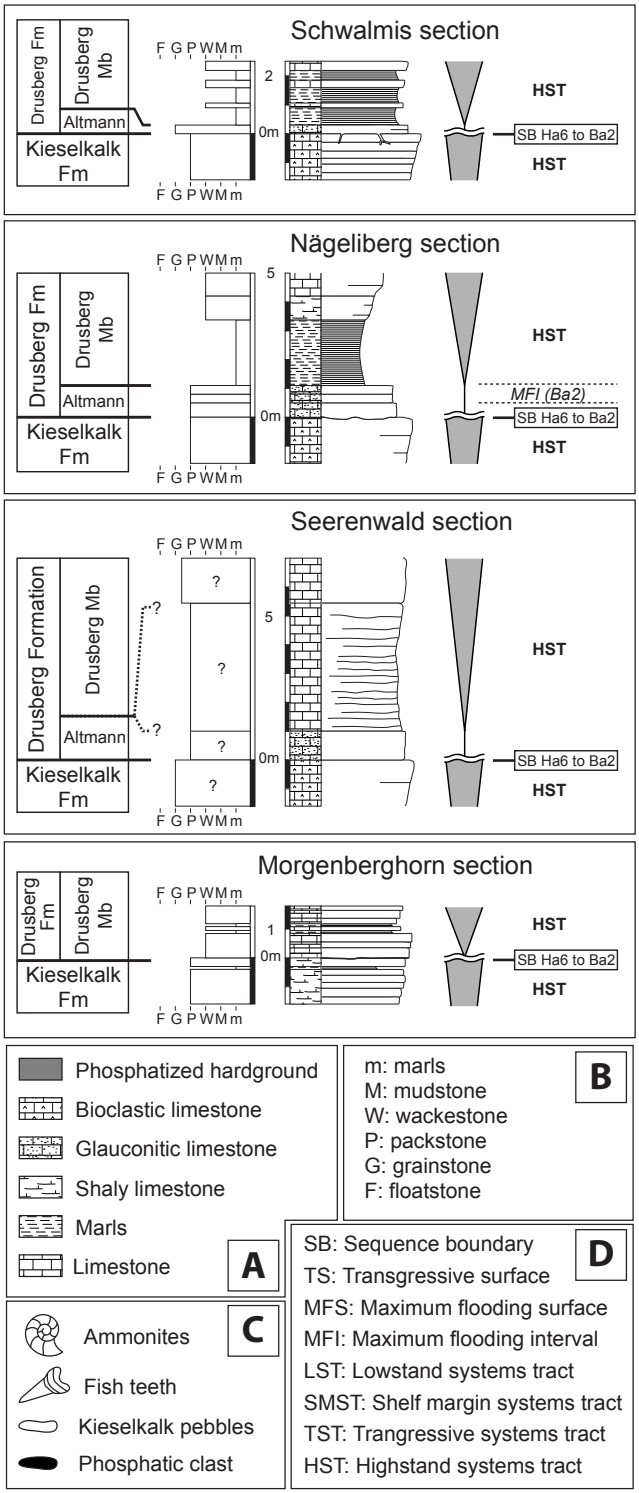

Fig. An.4.7: Highly reduced sections or hiati. The Seerenwald section is drawn after the description of Heim (1910-1916). A: lithology; B: Dunham classification; C: Key to fossils or nodules. D: sequence-stratigraphic terminology.

no more accessible today, and was drawn after the precise descriptions of Heim (1910-1916). In most outcrops situated in proximal settings, the Altmann Mb is not present between the Kieselkalk Fm and the Drusberg Mb, and only an erosive surface is observed (*e.g.*, at the Morgenberghorn section; Fig. An.4.7).

An.4.1.6.2. Sections with a phosphatized hardground at their base

This type of section of the Altmann Mb is characterized by a thickness varying between 1 and 8 meters and by a same stacking pattern, even if some local differences exist. At the base, a phosphatized hardground rich in macrofossils is present (*e.g.*, Pilatus, Rawil, Interlaken and Oberlänggli sections; Fig. An.4.8). The thickness of the phosphatized crust associated to the hardground varies from 2 to 15 cm. Below the hardground, burrows are observed in all sections except the one measured at the Oberlänggli locality. Above this basal horizon, a succession of alternating limestone and marls follows. In the studied sections, the Altmann Mb always ends in a marly interval, which is locally rich in fish teeth and glaucony. In the Pilatus and Oberlänggli sections, a glauconitic-rich bed occurs just below the uppermost marl interval.

An.4.1.6.3. Sections with phosphatic nodules

Sections with phosphatic nodules are found in the Interrugg and the Brisi localities (Fig. An.4.9). This type of section is characterized by the following field aspects: an erosive base, the presence of phosphate nodules and an obliquely stratified glaucony-rich bed (up to 60 cm thick at the Brisi locality) occurring just below an uppermost marly interval. In the Interrugg section, the poor outcrop conditions do not allow to log a complete section.

An.4.1.6.4. Expanded sections

Expanded Altmann Mb sections are found in the Tierwis (Fig. An.4.10), Altmann-Sattel and Fluebrig localities (*e.g.*, Funk, 1969; Rick, 1985). The Altmann-Sattel section is the Altmann Mb type section whereas the Tierwis section is the paratype section of the Altmann Mb (Funk, 1969). At Tierwis, the Altmann Mb is approximately 35 m thick and consists of crinoidal limestones intercalated with two marly intervals; a thin and darkly colored one near the base (ca. 6 m above the Kieselkalk – Altmann boundary) and a thick

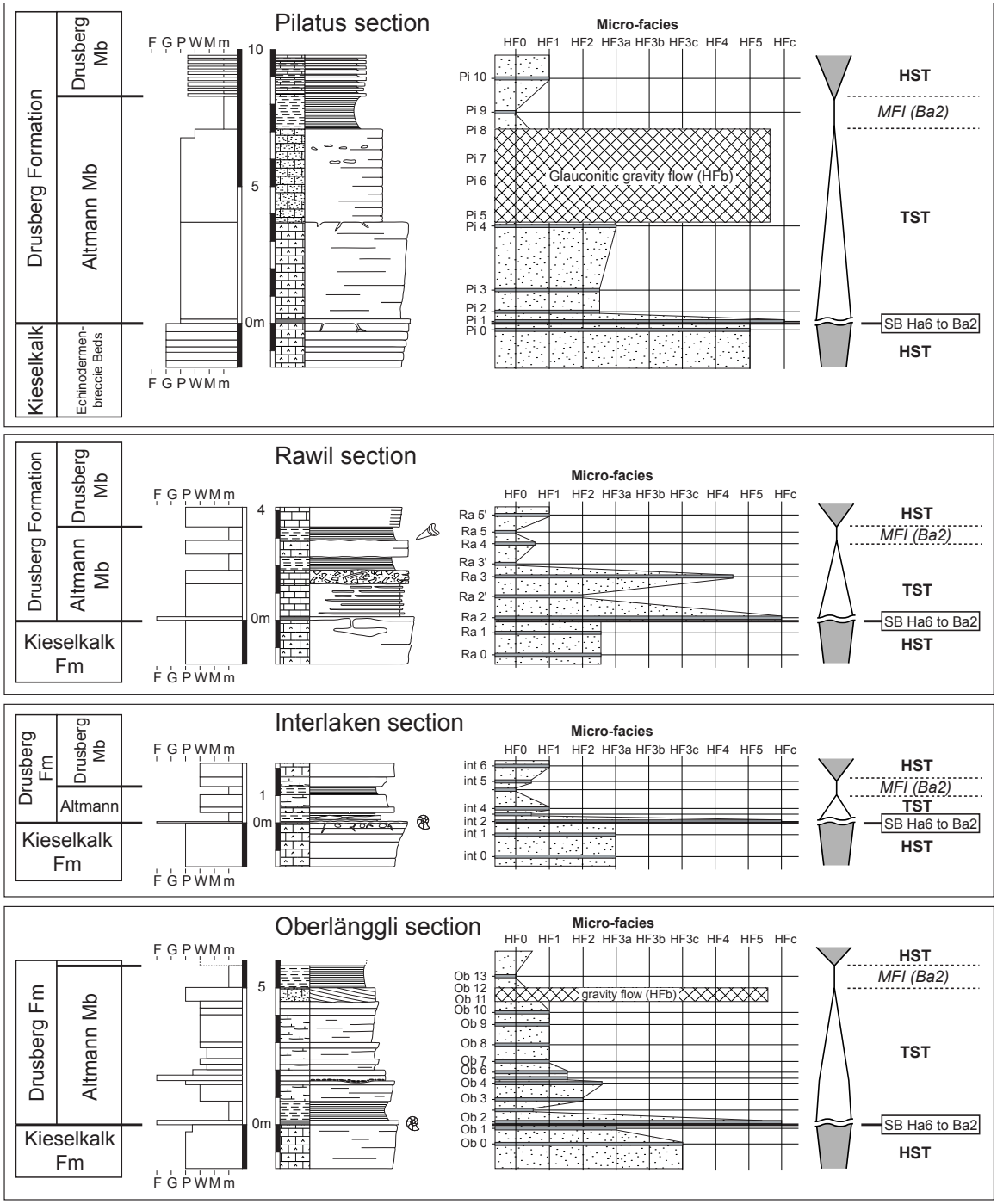

Fig. An.4.8: Sections with a phosphatized hardground at the base. See Fig. B.2.7 for key to abbreviations and symbols.

second one, with intercalated layers rich in fish teeth at the top of the Altmann Mb.

The lowermost four meters of the Altmann Mb section present all the characteristics of the "Kieselkalk – Echinodermenbreccie" facies and were first attributed to the Kieselkalk Fm according to Funk (1969). The discovery of an erosive surface below these beds and the presence of a relatively high amount of glaucony within the limestone (contrary to the Pilatus section, which is the type section for the Kieselkalk Fm) suggest that these beds belong to the Altmann Mb. At their top, an horizon with ferric concretions and glauconitic crusts is observed (Funk, 1969).

The middle part of the section is constituted by a thick crinoidal thickening-upward limestone succession (ca. 25 m) capped by Thalassinoides, Ophiomorpha and Skolithos burrows belonging to the Cruziana – Glossifungites ichnofacies (*e.g.*, Pemberton, 1998; Malpas *et al.*, 2005). A

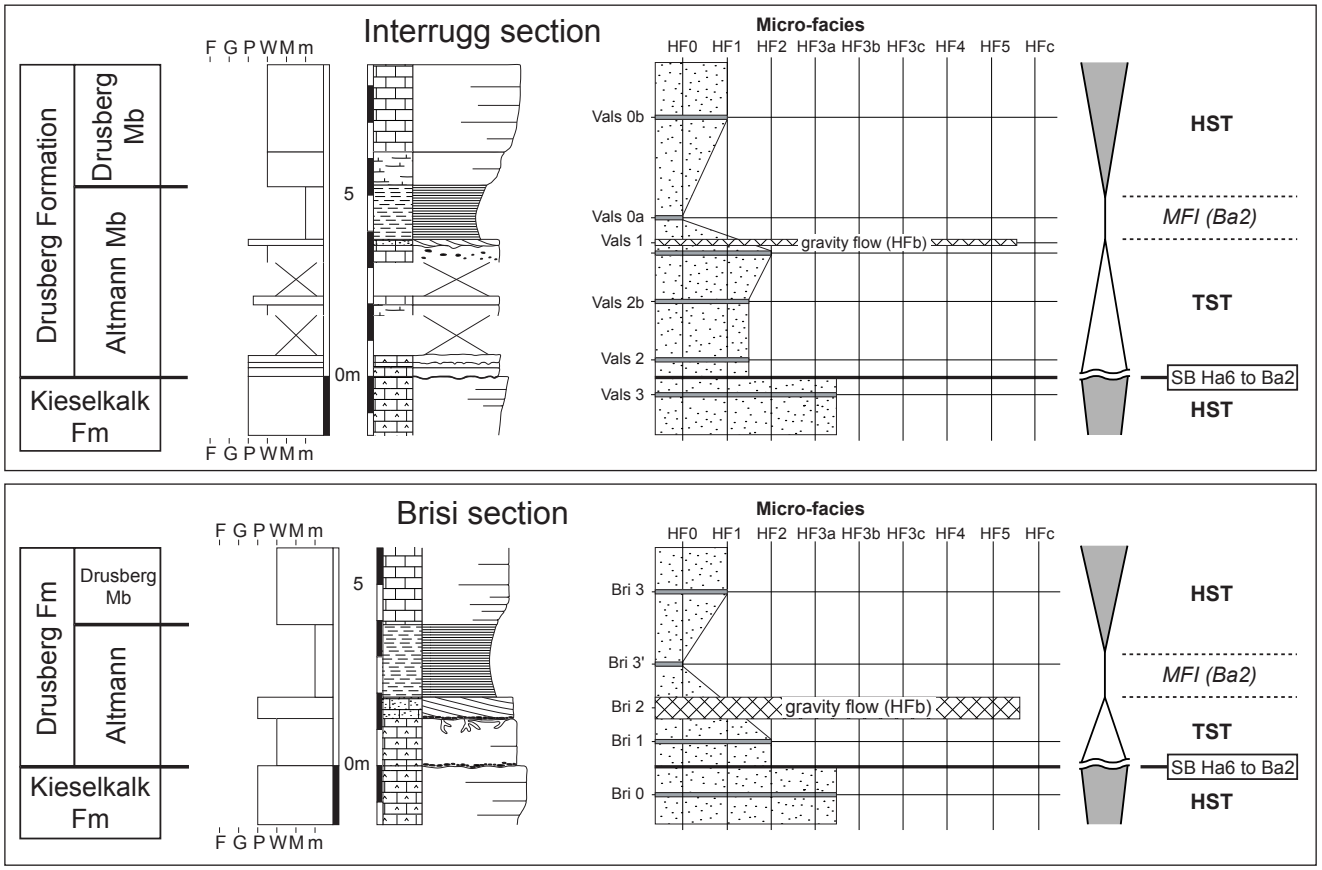

Fig. An.4.9: Sections with phosphatic nodules. See Fig. B.2.7 for key to abbreviations and symbols.

3-meters-thick glauconitic-rich zone follows, presenting Cruziana – Glossifungites ichnofacies in the first meter. This zone precedes ca. 3 m of marly crinoidal limestone capped by a hardground surface. The latter is rich in macrofossils such as ammonites, oysters, sponges, belemnites and incrusting organisms, and presents many reworked rock fragments (with phosphatized outlines), burrows and traces of silicification (see Fig. An.4.11).

The Drusberg Mb is separated from the Altmann Mb by a 1-meters-thick marly interval. The lower part of the Drusberg Mb is characterized by a thickening-upward limestone – marl alternation whereas a thinning-upward marl-dominated deposit characterizes the upper part of the Drusberg Mb.

An.4.1.6.5. Ammonite biostratigraphy in the Altmann Member

Newly collected ammonites come from the basal hardground of the Interlaken and Oberlänggli sections (Fig. An.4.8), and in different levels of the Tierwis section (Fig. An.4.10). The ammonites from the two first sections are phosphatized and belong to the B. mortilleti biozone and to the Early Barremian (Fig. An.4.4), indicating significant periods involved in the condensation or reworking associated with the basal hardground. In the Tierwis section, the bed Sa 16b (Fig. An.4.10), which is particularly rich in ammonites, is dated as belonging to the B. mortilleti biozone by Parathurmannia sp., Balearites sp. gr. mortilleti, Paraspiticeras gr. percevali and Plesiospitidiscus sp. The hardground (bed Sa 33) yields ammonites from the A. kiliani to the K. compressissima biozones (Table An.4.1) indicating again an extended period of condensation or reworking associated to this hardground. In the upper part of the section, ammonites were found in the beds Sa 36 to Sa 38. They belong to the K. compressissima to C. darsi biozones (Table An.4.1).

An.4.1.7. Sequence-stratigraphic interpretation

The analysis of the micro-facies temporal evolution and the stacking pattern leads to a sequence stratigraphic interpretation of the studied sections (Figs. An.4.7-10).

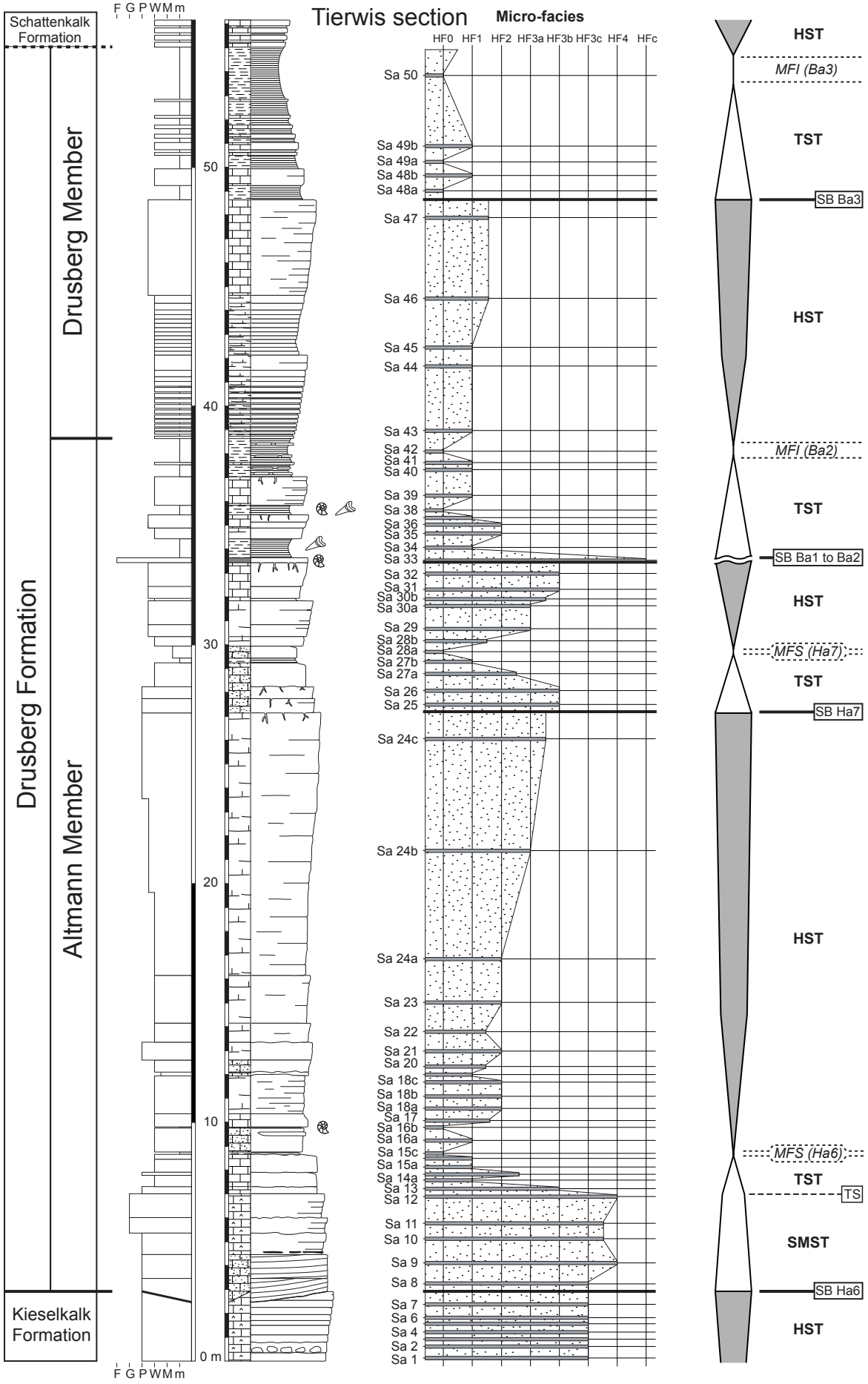

Fig. An.4.10: Tierwis section. See Fig. B.2.7 for key to abbreviations and symbols.

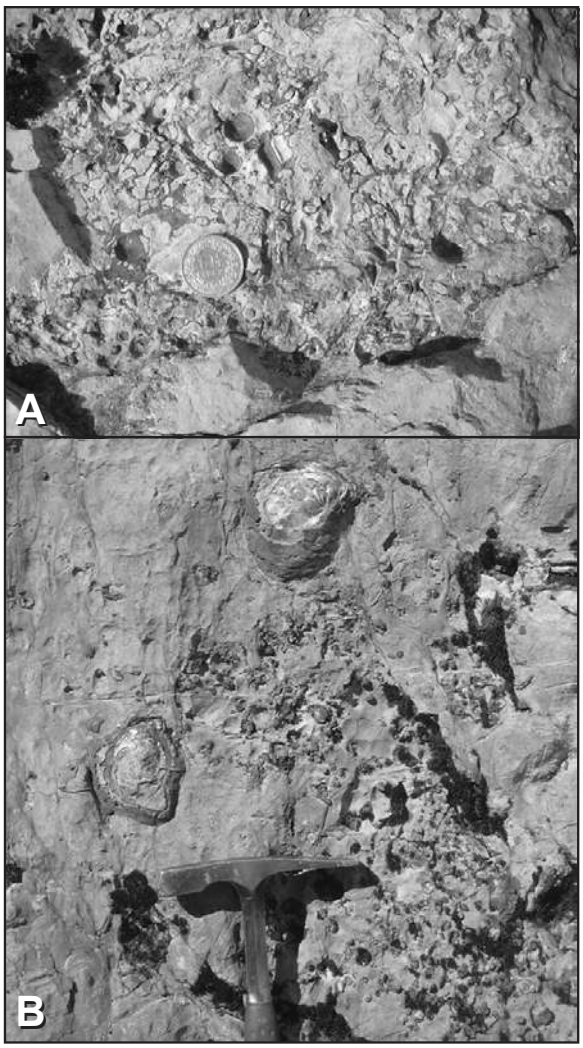

Fig. An.4.11: Details of features at the top of the phosphatized hardground (bed Sa33, Tierwis section). A: Phosphatized burrows; B: Oysters, burrows and phosphatized nodules.

In highly reduced Altmann Mb sections, sequential interpretation of the thin glaucony-rich beds is rather difficult. However, the condensed pattern of these section, as well as the high amount of glaucony, point to a deposit associated with a maximum flooding surface (MFS). In addition, the shallowing-upward stacking of the overlying Drusberg Beds (which are attributed to highstand deposits) supports this interpretation. Due to its shallowing- and thickening-upward pattern, the underlying Upper Kieselkalk Mb is attributed to a highstand deposit. No transgressive systems tract (TST) could be identified in these sections.

In sections with a phosphatized hardground or with phosphatic nodules at their base, an identified trend toward deeper facies as well as a thinning-upward stacking pattern is observed. These beds represent thus a TST. This latter overlies the Upper Kieselkalk Mb, attributed to a highstand systems tract (HST) deposit, without a recognizable sea-level fall or lowstand deposits in between. Following Schlager (1999), this SB can thus be qualified as a type 3 sequence boundary. Due to the presence of Late Hauterivian and Early Barremian ammonites in the phosphate crust of the basal hardground, this latter may be interpreted as the result of a long-period of condensation. In the Oberlänggli section, which is the most distal section studied, as indicated by microfacies variations, the first 1.5 meters consist of shallowing-upward sediments and are overlain by a phosphatic lag. These beds are interpreted as representing a first shallowing-upward parasequence associated to the TST.

In the Altmann Mb of the Tierwis section, the preserved succession is more complete, with three main sequences recorded. The Altmann Mb begins with four meters of aggrading "Echinodermenbreccie – like" limestone overlying an erosive surface. This erosive surface, which lacks any indication of emersion, may be the expression of a type 2 SB. The following deposits are thus attributed to shelf margin systems tract (SMST) deposits. This succession is capped by a thin interval of glaucony-rich marly limestone. The strong shift toward deeper facies, as well as the high content of glaucony of these deposits, is characteristic of the TST (*e.g.*, Chamley, 1989; Amorosi & Centineo, 1997). Between these two systems tracts, the horizon with ferric concretions and glauconitic crusts may thus be attributed to the TS. The MFS is represented by a thin dark-colored marl interval. The following HST is represented by thick shallowing- and thickening-upward marl-limestone succession.

This first main sequence is followed by a thinner second sequence. Here, no lowstand deposits are identified. The TST is thin (ca. 3m), and is marked by an enrichment in glaucony content and a shift to deeper facies. The SB is expressed as a firmground, rich in Cruziana – Glossifungites burrows, which may underline pauses in sedimentation (*e.g.*, Pemberton, 1998) and may be transgressively modified during subsequent relative sea-level rise (*e.g.*, MacEachern *et al.*, 1999). The HST is ca. 3.5

meters thick, and presents one shallowing-upward sequence.

The following phosphatized hardground (bed Sa 33, Fig. An.4.10) represents a SB, above which a ca. 4 m thick TST occurs. The Altmann Mb ends within a marly interval, corresponding to a MFS. The overlying lower part of the Drusberg Mb shows two shallowing-upward deposits, attributed to the following HST.

These interpretations, coupled with sequential stratigraphic interpretations of chronostratigraphically calibrated, fossiliferous basinal sections (Haq *et al.*, 1987; Hardenbol *et al.*, 1998; modified by Arnaud (2005) for the late Hauterivian – Barremian of the Angles section, Vocontian trough, France; Fig. An.4.4), allow to date the identified sequences. Thus, in the Tierwis section, the Altmann Mb begins with the Ha6 sequence. The dark-colored marly interval of the MFS is thus contemporaneous with the Faraoni level documented so far only from basin sections (Cecca *et al.*, 1994; Baudin *et al.*, 1999). By extrapolation, the second sequence may correspond to the Ha7 sequence, even if ammonite biostratigraphy dating within these beds is lacking to confirm this hypothesis. According to the presence of Emericiceras gr. Koechlini and Torcapella gr. Davydovi in the phosphatized hardground (bed Sa 33), this latter represents a time interval associated to the Ba1 and Ba1' sequences. The presence of Subtorcapella sp. (bed Sa 38) in the third sequence indicates that this TST deposit is dated from the K. compressissima – C. darsi biozone interval. In basinal sections from the Vocontian Trough, only one TST is noted during this time interval: the Ba2 TST, dated from the base of the C. darsi biozone. The Torcapella sp. found in the bed Sa 36-38, which belongs to the K. compressissima biozone, may thus be reworked from the underlying hardground. As a result, this confirms that Ba1 and Ba1' sequences are condensed and/or lacking in the phosphatized hardground of this section.

In sections with a phosphatized hardground or with phosphatic nodules at their base (Figs. An.4.8-9), the temporal resolution is less good due to the absence of numerous fossil findings. However, the presence of Barremites sp. in the phosphatized hardground argues in favor of a Barremian age for the overlaying TST deposit. Owing to the general trends in ammonite biostratigraphy in the Altmann Mb, as well as the fact that this TST is overlain by the Drusberg Mb without any evidence of a major hiatus, this TST may thus correspond to the Ba2 TST. Consequently, the sequences Ha6 to Ba1 are lacking in these sections and/or condensed within the basal phosphatized hardground. A notable point is the fact that the Ba2 sequence lacks evidence for a LST deposit in all studied sections, as well as in the basinal section of Angles (*e.g.*, Arnaud, 2005; Bodin *et al.*, 2006). This is compatible with the here-proposed hypothesis that the highly-condensed basal phosphatized hardground is representative of a type 3 SB.

In Fig. An.4.12, a palinspastic transect along the Säntis-Churfirsten-Alvier massif is shown. With the exception of the Tierwis section, a small decrease in thickness of the Altmann Mb is observed toward proximal sections. This thickness decrease is related to the progressive landward disappearance of parasequences. In this transect, the important thickness of the Tierwis section, which is due to the preservation of the sequences Ha6 and Ha7, may be related to a locally, rapidly subsiding area, or the infill of an incised (sub-marine?) valley. No direct clues for both hypothesis were, however, found in the field. The observation of a synsedimentary normal fault at the top of the Altmann Mb of the Fluebrig section may argue in favor of the first hypothesis.

An.4.1.8. Depositional model

The depositional history of the Altmann Mb begins with the sequence Ha6 (Fig. An.4.13). In the Säntis massif, a local depression (probably initiated by normal faults) led to the record of a thin SMST, followed by a very thin TST and a thick HST. The thin transgressive deposits reflect slower rates of sediment production that may be associated to the reduction of carbonate growth potential. Thus, the beginning of the "drowning episode" may correspond to the TS Ha6. During maximum flooding, the Helvetic ramp is drowned and ca. 1-m-thick, dark glauconitic-rich marls and marly limestone are deposited during the B. mortilleti biozone. According to cyclostratigraphic interpretations of Late Hauterivian – Barremian

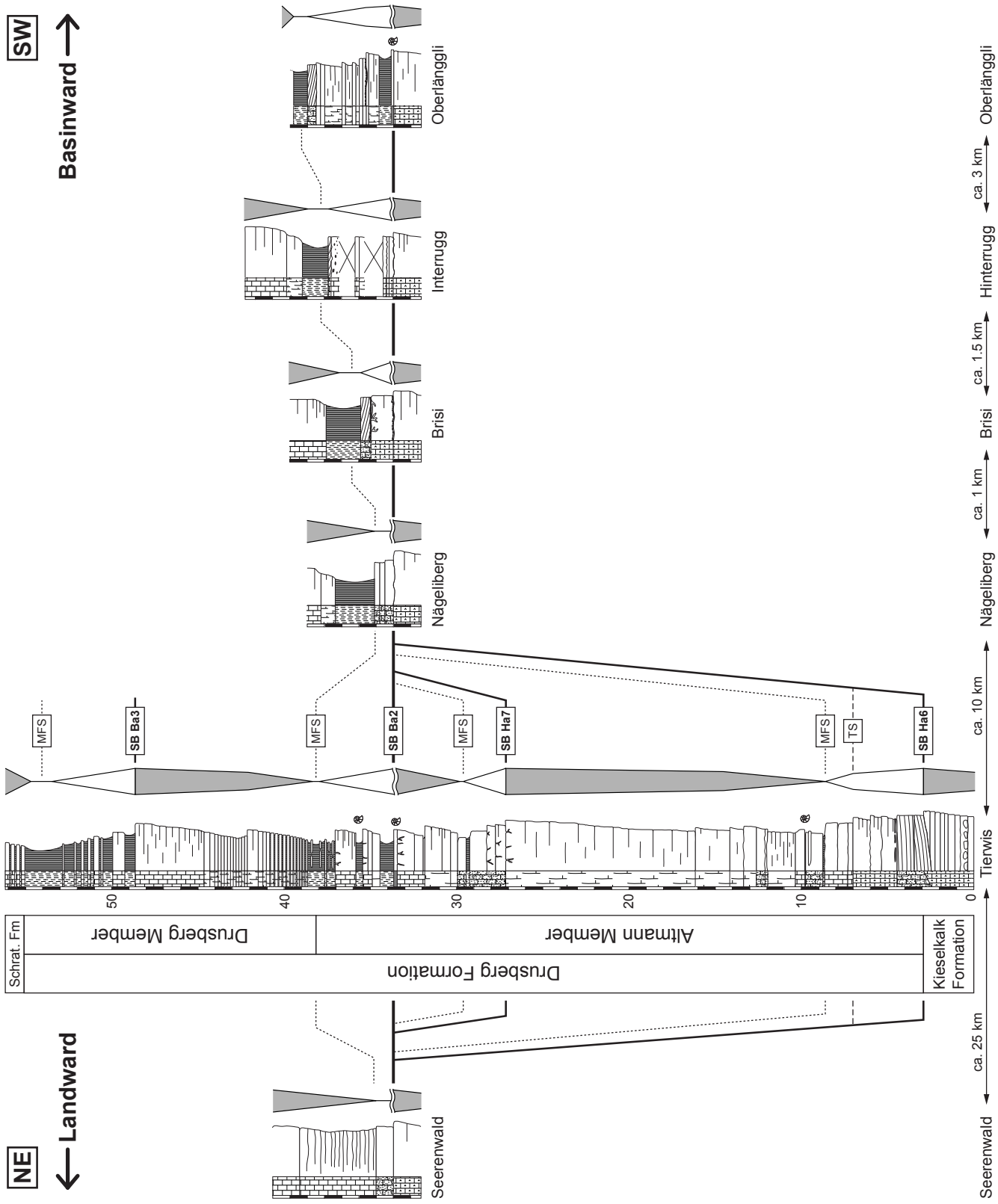

Fig. An.4.12: Palinspastic transect along the Säntis-Churfirsten-Alvier massif with a proposed sequential correlation of sections. Note the decrease in the thickness of the Altmann Mb from basinward to landward positions (except for the Tierwis section; see text for discussion).

successions from the Vocontian trough (Bodin *et al*., 2006), a duration of approximately 300 kyr is likely to be condensed in this interval. During the HST, the important thickness of deposits indicates renewed carbonate production and the end of the first drowning phase in the Säntis massif. The sequence Ha7 is recorded only in the Säntis massif and is characterized by a thin TST followed by a thin HST.

The absence of Upper Hauterivian – lowermost Barremian deposits in other part of the Helvetic ramp, as well as the finding of a well-preserved phosphatized ammonite dated from the Late Hauterivian (Parathurmannia cf. catulloi) of the Oberlänggli section, may point to erosion, sediment starvation and/or winnowing and phosphatization along the other parts of the platform associated with this first drowning step. Following previous sea-level reconstructions (*e.g*., Ruffell, 1991; Hardenbol *et al*., 1998), this first drowning phase is coeval with a second order sea-level rise (Ha6 third order MFS). The observation that at the Säntis locality the carbonate platform has not been drowned during the entire Ha6 and Ha7 sequences, but only during the Ha6 TST and MFS interval, could be related to the peculiar paleogeographical setting of this locality. Indeed, the sediments preserved at this locality were likely to be deposited within a tectonically-induced depression, that could have protected this part of the platform from winnowing currents.

The Helvetic platform preserved no major deposits during the time interval corresponding to sequences Ba1 and Ba1'. In the middle and outer ramp, the platform experienced the development of a phosphatized hardground, which is indicative of important winnowing and sediment starvation (*e.g*., Föllmi, 1996; Trappe, 1998). The excellent preservation of phosphatized fossils such as ammonites or sponges may point to the effect of rapid burial and consequent phosphogenesis (Föllmi, 1996). In places where no phosphatized hardground is present, an erosive surface has been observed. This feature might point to bottom current erosion and reworking. In other parts of the European continent, the Early Barremian

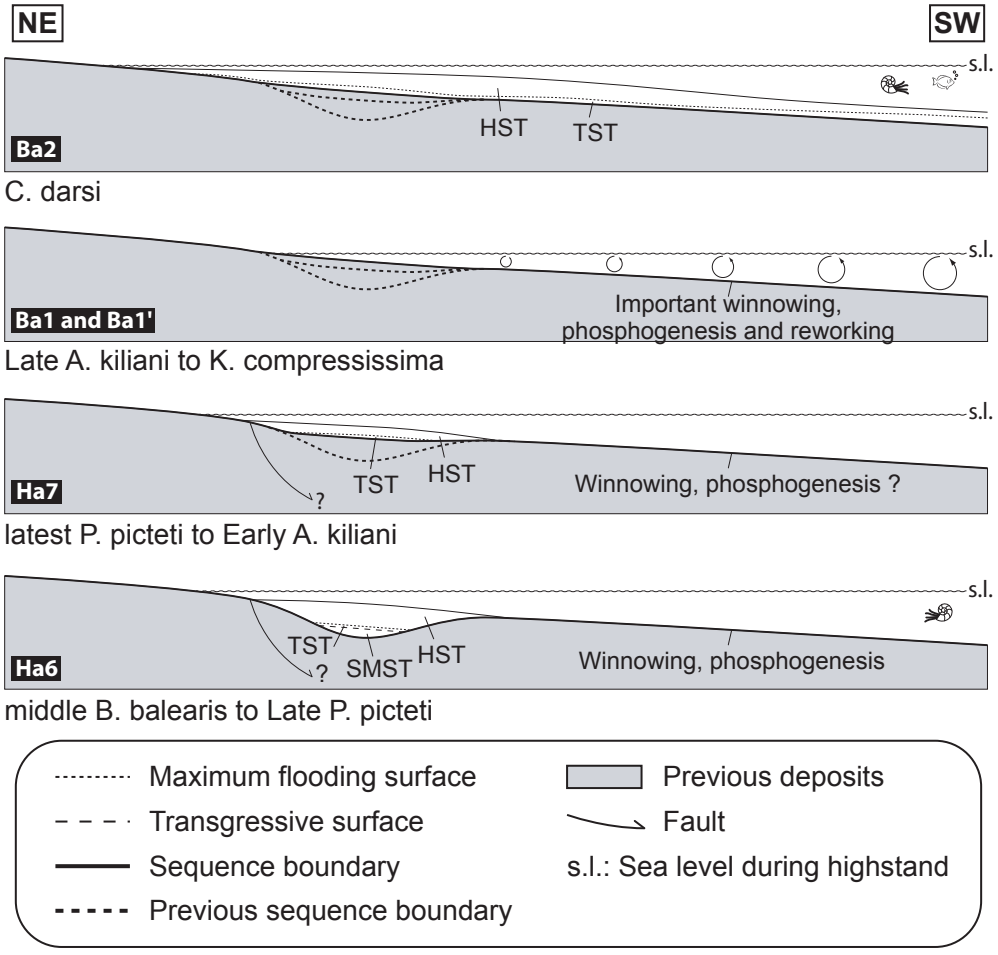

Fig. An.4.13: Depositional model for the Altmann Mb in four successive time steps (see text for details).

corresponds to a second order sea-level lowstand (Ruffel, 1991; Arnaud, 2005). This may imply that winnowing and phosphogenesis along the northern Tethyan realm might have take place during a long sea-level lowstand period. Hardground formation during sea-level lowstand can be related to the lowering of the effective wave base exposing the sea floor to wave action (*e.g.*, Immenhauser *et al.*, 2000).

A second drowning phase took place during the Ba2 sequence. According to the overall backstepping pattern of the platform recorded within the Ba2 and Ba3 sequences, the SB Ba2, which is qualified as a type 3 SB, may thus be related to the TS of this Barremian second order sea-level cycle. The presence of phosphatized nodules in the TST might highlight ongoing phosphogenesis during the transgressive phase. Reworking of sediments is recorded by glauconitic-rich gravity-flow deposits in a majority of the studied sections. The deposit of a thick marly interval related to the MFS BA2, which marks the top of the Altmann Mb and which is associated to pelagic facies (HF0), documents the second drowning of the Helvetic platform. During the Ba2 HST, a great part of the Helvetic platform experienced the deposition of outer-ramp hemi-pelagic facies (HF1). This might indicate a strong decrease of the platform-growth area associated to the second drowning episode (backstepping of the platform). Following Tucker and Wright (1990; p. 57), this episode can be defined as an incipient drowning stage.

Whereas sea-level change plays an important role in the Late Hauterivian – Early Barremian drowning of the Helvetic platform, it alone cannot explain the drowning of the carbonate platform. Indeed, the growth rates of carbonate platforms can easily exceed the fastest sea-level rise (*e.g.*, Schlager, 1981; Hallock & Schlager, 1986; Mallarino *et al.*, 2002). One solution to resolve this apparent paradox is to reduce the growth potential of the carbonate platform through environmental stress, such as the reduction of water transparency, temperature or nutrient excess (Hallock & Schlager, 1981). Bodin *et al.* (2006) have observed significantly high phosphorus levels in the western Tethys during the latest Hauterivian – Early Barremian. This observation might be best explained by high nutrient input correlated with the observed carbonate platform-drowning episode. On the other hand, this drowning might also have a non-negligible effect on the carbon-isotope variations of Tethyan basin sections. Indeed, following Godet *et al.* (2006), the high oceanic DIC resulting from this drowning may explain the rather stable trend of the $\delta^{13}C$ curve during the latest Hauterivian – Early Barremian.

The close relationship between the timing of the onset of the Altmann Mb drowning event and the Faraoni oceanic anoxic event point to a connection between these two events. Indeed, in basinal sections, the bottom water anoxia associated to the Faraoni level led to decreased phosphorus preservation in sediments and a positive feedback that led to a rise in nutrient levels in sea water (Bodin *et al.*, 2006). This mechanism may have highly reduced the growth potential of the carbonate platform through environmental stress by nutrient excess, and induced the first step of this drowning event. During the Early Barremian, winnowing, associated to a second order sea-level lowstand and also to high nutrient level in the ocean (Bodin *et al.*, 2006), may have induced the formation of a phosphatized hardground and the complete stop of platform growth. During the latest Early Barremian (C. darsi zone), the following second order sea-level transgression, which is also associated to high nutrient levels, led to the end of the hardground formation and to a second drowning step. The overall decrease in nutrient levels during the Late Barremian marks the end of the slowdown and demise of carbonate platform growth and the progressive return of a photozoan association (*i.e.* the Schrattenkalk Fm).

An.4.1.9. Conclusions

(1) Ammonite biostratigraphy shows that the Altmann Mb spans the time interval from the P. seitzi (latest Hauterivian) to the C. darsi ammonite zone (latest Early Barremian). Coupled with a detailed sequence stratigraphic interpretation of basin sections, these age data indicate that the Altmann Mb begins at the Sb Ha6 and ends within the MFS Ba2.

(2) The majority of the Altmann Mb sections records only the upper part of the Hauterivian – Barremian transition drowning event. Only some sections, mainly located in the Säntis massif, recorded evidence of a more detailed depositional history of the Altmann Mb.

(3) This may be the result of a twofold drowning. A first drowning phase is recorded in the Tierwis section (representative of the Säntis massif) and documents the Ha6 transgression, leading to the deposition of glaucony-rich black marls during the TST-MFS. These deposits are contemporaneous to the Faraoni event black-shales in basin sections (*e.g.*, Cecca *et al.*, 1994; Baudin *et al.*, 1999; Baudin, 2005). In the other platform areas, reworking, winnowing and phosphogenesis recorded this first drowning stage. A second phase is contemporaneous to the Ba2 transgression and is associated to a following pronounced backstepping of the carbonate factory. With the exception of the Tierwis section, the sequences Ha6, Ha7, Ba1 and Ba1' are either condensed in a phosphatized hardground or lacking. This observation is best explained by strong winnowing and bottom current-induced reworking along the northern Tethyan ramp. The Altmann Mb drowning episode ended with the Ba2 highstand and the beginning of the Drusberg Mb deposition.

(4) There is a strong coupling of this drowning event with a palaeoceanographic changes within the western Tethyan realm: the onset of the drowning episode is linked to the Faraoni oceanic anoxic event (latest Hauterivian) by platform eutrophication. During the Early Barremian, the high nutrient levels in the northern Tethys, associated with current-induced winnowing, preclude carbonate platform growth until the beginning of the Late Barremian and the progressive return of photozoans in association with a significant decrease in seawater nutrient levels (Bodin *et al.*, 2006).

An.4.1.10. Acknowledgments

The authors acknowledge Hans-Peter Funk, Urs Oberli, Ueli Briegel, Hubert Arnaud, Guillaume Cailleau, Christophe Dupraz, Laureline Scherler, Laure Pelletier and Charles Robert-Charrue for their help in the field and/or constructive discussions, and also André Villard for the preparation of thin-sections. We thank the Museums of Natural History of St. Gallen and Dornbirn, and the ETH Zürich, for providing Altmann Mb ammonites from their collections. Critical reviews by Miguel Company and Adrian Immenhauser were much appreciated and helped to considerably improve this manuscript. Financial support from the Swiss National Science Foundation (project 2100-067807/1 and 200020-105206/1) is gratefully acknowledged.

An.4.1.11. References

Amorosi, A. and Centineo, M. C. (1997). "Glaucony from the Eocene of the Isle of Wight (southern UK): implications for basin analysis and sequence-stratigraphic interpretation." Journal of Geological Society of London **154**: 887-896.

Arnaud, H. (2005). Sequence stratigraphy interpretation. *In:* T. Adatte, A. Arnaud-Vanneau, H. Arnaud, M. C. Blanc-Aletru, S. Bodin, E. Carrio-Schaffhauser, K. B. Föllmi, A. Godet, M. C. Raddadi and J. Vermeulen, (*Eds*). The Hauterivian - Lower Aptian sequence stratigraphy from Jura platform to Vocontian basin: a multidisciplinary approach: Géologie Alpine, Série Spéciale «Colloques et Excursions» n°7. 174-179.

Arnaud, H., Arnaud-Vanneau, A., Blanc-Aletru, M. C., Adatte, T., Argot, M., Delanoy, G., Thieuloy, J.-P., Vermeulen, J., Virgone, A., Virlouvet, B. and Wermeille, S. (1998). «Répartition stratigraphique des orbitolinidés de la plate-forme urgonienne subalpine et jurassienne (SE de la France).» Géologie Alpine **74**: 3-89.

Arnaud-Vanneau, A. (1980). «Micropaléontologie, paléoécologie et sédimentologie d'une plate-forme carbonatée de la marge passive de la Téthys; L'Urgonien du Vercors septentrional et de la Chartreuse (Alpes occidentales).» Géologie Alpine, Mémoire Hors-Série **11**(*1-3*).

Baudin, F. (2005). «A Late Hauterivian short-lived anoxic event in the Mediterranean Tethys: the «Faraoni Event».» Comptes Rendus Geoscience **337**: 1532-1540.

Baudin, F., Bulot, L. G., Cecca, F., Coccioni, R., Gardin, S. and Renard, M. (1999). «Un équivalent du «Niveau Faraoni» dans le bassin

du Sud-Est de la France, indice possible d'un événement anoxique fini-hauterivien étendu à la Téthys méditerranéenne.» Bulletin de la Société Géologique de France **170**(*4*): 487-498.

Blanc-Aletru, M. C. (1995). Importance des discontinuités dans l'enregistrement sédimentaire de l'urgonien jurassien: micropaléontologie, sédimentologie, minéralogie et stratigraphie séquentielle.» *Géologie*, Neuchâtel, 299 pp.

Bodin, S., Godet, A., Föllmi, K. B., Vermeulen, J., Arnaud, H., Strasser, A., Fiet, N. and Adatte, T. (2006). «The Late Hauterivian Faraoni oceanic anoxic event in the western Tethys: Evidence from phosphorus burial rates.» Palaeogeography, Palaeoclimatology, Palaeoecology **235**: 245-264.

Bollinger, D. (1988). Der Entwicklung des distalen osthelvetischen Schelfs im Barremian und Früh-Aptian.» ETH Zürich, 136 pp.

Briegel, U. (1972). «Geologie der östlichen Alviergruppe (Helvetische Decken der Ostschweiz) unter besonderer Berücksichtigung der Drusberg- und Schrattenkalkformation (Unterkreide).» Eclogae Geologicae Helvetiae **65**(*2*): 425-483.

Burchette, T. P. and Wright, V. P. (1992). «Carbonate ramp depositional systems.» Sedimentary Geology **79**(*1-4*): 3-57.

Cecca, F., Marini, A., Pallini, G., Baudin, F. and Begouen, V. (1994). «A guide-level of the uppermost Hauterivian (Lower Cretaceous) in the pelagic succession of Umbria-Marche Apennines (Central Italy): the Faraoni Level.» Riv. Ital. Paleontol. Stratigr. **99**: 551-568.

Chamley, H. (1989). Clay Sedimentology. Berlin, Springer-Verlag.

Fichter, H. J. (1934). Geologie der Bauen-Brisen-Kette am Vierwaldstaettersee und die zyklische Gliederung der Kreide und des Malm der helvetischen Decken.

Funk, H. (1969). «Typusprofile der helvetischen Kieselkalk Formation und der Altmann Schichten.» Eclogae geologicae Helvetiae **62**(*1*): 191-203.

Funk, H. (1971). «Zur stratigraphie und lithologie des Helvetischen Kieselkalkes und der Altmannschichten im der Säntis-Churfirsten-Gruppe (Nordostschweiz).» Eclogae geologicae Helvetiae **64**(*2*): 345-433.

Funk, H., Föllmi, K. B. and Mohr, H. (1993). Evolution of the Tithonian-Aptian carbonate platform along the northern Tethyan margin, eastern Helvetic Alps. *In:* Simo J.A.T., Scott R.W. and Masse J.-P., (*Eds*). Cretaceous carbonates platforms. AAPG Memoir, American Association of Petroleum Geologists. Tulsa, OK, United States., **56**: 387-407.

Föllmi, K. B. (1989). Evolution of the Mid-Cretaceous Triad. Platform Carbonates, Phosphatic Sediments, and Pelagic Carbonates along the Northern Tethys margin, Springer-Verlag.

Föllmi, K. B. (1996). «The phosphorus cycle, phosphogenesis and marine phosphate-rich deposits.» Earth-Science Reviews **40**(*1-2*): 55-124.

Föllmi, K. B., Weissert, H., Bisping, M. and Funk, H. (1994). «Phosphogenesis, carbon-isotope stratigraphy, and carbonate-platform evolution along the Lower Cretaceous northern Tethyan margin.» Geological Society of America Bulletin **106**: 729-746.

Godet, A., Bodin, S., Föllmi, K. B., Vermeulen, J., Gardin, S., Fiet, N., Adatte, T., Berner, Z., Stüben, D. and Van de Schootbrugge, B. (2006). «Evolution of the marine stable carbon-isotope record during the early Cretaceous: A focus on the late Hauterivian and Barremian in the Tethyan realm.» Earth and Planetary Science Letters **242**: 254-271.

Goldschmid, K. (1927). «Geologie der Morgenberghorn-Schwalmerengruppe bei Interlaken.» Mitt. Nat. Ges. Bern: 195-268.

Hallock, P. and Schlager, W. (1986). «Nutrient excess and the demise of coral reefs and carbonate platforms.» Palaios **1**: 389-398.

Hantke, R. (1961). Tektonik der helvetschen Kalkalpen zwischen Obwalden und dem St. Galler Rheintal.

Haq, B. U., Hardenbol, J. and Vail, P. R. (1987). «Chronology of fluctuating sea levels since the Triassic.» Science **235**: 1156-1167.

Hardenbol, J., Thierry, J., Farley, M. B., de Graciansky, P.-C. and Vail, P. R. (1998). Mesozoic and Cenozoic Sequence Chronostratigraphic Framework of European Basins. *In:* P.-C. de Graciansky, J. Hardenbol, T. Jacquin and P. R.

Vail, (*Eds*). Mesozoic and Cenozoic Sequence Stratigraphy of European Basins. Special Publication Society for Sedimentary Geology, **60**: 3-13.

Heim, A. (1910-1916). Monographie der Churfirsten-Mattstock-Gruppe. Bern.

Hoedemaeker, P. J., Reboulet, S., Aguirre-Urreta, M. B., Alsen, P., Aoutem, M., Atrops, F., Barragan, R., Company, M., Gonzalez, C., Klein, J., Lukeneder, A., Ploch, I., Raisossadat, N., Rawson, P. F., Ropolo, P., Vasicek, Z., Vermeulen, J. and Wippich, M. G. E. (2003). «Report on the 1st International Workshop of the IUGS Lower Cretaceous Ammonite Working Group, the 'Kilian Group' (Lyon, 11 July 2002).» Cretaceous Research **24**(*1*): 89-94.

Immenhauser, A., Schlager, W., Burns, S. J., Scott, R. W., Geel, T., Lehmann, J., van der Gaast, S. and Bolder-Schrijver, L. J. A. (2000). Origin and correlation of disconformity surfaces and marker beds, Nahr Umr Formation, northern Oman. *In:* A. S. Alsharhan and R. W. Scott, (*Eds*). Middle East models of Jurassic/Cretaceous carbonate systems. SEPM, **69**: 209-225.

James, N. P. (1997). The cool-water carbonate depositional realm. *In:* N. P. James and J. A. D. Clarke, (*Eds*). Cool water carbonates. Society for Sedimentary Geology, **56**: 1-22.

Kuhn, O. (1996). Der Einfluss von Verwitterung auf die Paläozeanographie zu Beginn des Kreide-Treibhausklimas (Valanginian und Hauterivian) in der West-Tethys.» Universität Zürich, 380 pp.

Lehmann, C., Osleger, D. A., Montanez, I. P., Sliter, W. V., Arnaud-Vanneau, A. and Banner, J. (1999). «Evolution of Cupido and Coahuila carbonate platforms, Early Cretaceous, northeastern Mexico.» GSA Bulletin **111**(*7*): 1010-1029.

MacEachern, J. A., Zaitlin, B. A. and Pemberton, S. G. (1999). «A sharp-based sandstone of the Viking Formation, Joffre Field, Alberta, Canada: criteria for regnition of transgressively incised shoreface complexes.» Journal of Sedimentary Research **69**(*4*): 876-892.

Mallarino, G., Goldstein, R. H. and Di Stefano, P. (2002). «New approach for quantifying water depth applied to the enigma of drowning of carbonate platforms.» Geology **30**(*9*): 783-786.

Malpas, J. A., Gawthorpe, R. L., Pollard, J. E. and Sharp, I. R. (2005). «Ichnofabric analysis of the shallow marine Nukhul Formation (Miocene), Suez Rift, Egypt: implications for depositional processes and sequence stratigraphic evolution.» Palaeogeography Palaeoclimatology Palaeoecology **215**: 239-264.

Pasquini, C., Lualdi, A. and Vercesi, P. (2004). «Depositional dynamics of glaucony-rich deposits in the Lower Cretaceous of the Nice arc, southeast France.» Cretaceous Research **25**(*2*): 179-189.

Pemberton, S. G. (1998). «Stratigraphic applications of the Glossifungites ichnofacies: Delineating discontinuities in the rock record.» American Association of Petroleum Geologists Bulletin **82**(*11*): 2155.

Pérès, J. M., Ed. (1961). T1 - La vie benthique. Océanographie biologique et biologie marine, Presses Universitaires de France, Vendôme.

Rick, B. (1985). Geologie des Fluhbrig (Kt. Sz): unter besonderer beruecksichzigung der Altmannschichten und der «Gault»-formation.» *Diplomarbeit*, 83 pp.

Ruffell, A. (1991). «Sea-level events during the Early Cretaceous in western Europe.» Cretaceous Research **12**: 527-551.

Schenk, K. (1992). Die Drusberg- und Schrattenkalk-Formation (Unterkreide) im Helvetikum des Berner Oberlandes.» *Inauguraldissertation der Philosophisch-naturwissenschaftlichen Fakultät*, Universität Bern, 169 pp.

Schlager, W. (1981). «The paradox of drowned reefs and carbonates platforms.» Geological Society of America Bulletin **92**(*1*): 197-211.

Schlager, W. (1999). Type 3 sequence boundaries. *In:* P. M. Harris, A. H. Saller and J. A. T. Simo, (*Eds*). Advances in carbonate sequence stratigraphy: Application to reservoirs, outcrops and models. SEPM, **63**: 35-45.

Trappe, J. (1998). Phanerozoic Phosphorite Depositional Systems: a dynamic model for a sedimentary resource system, Springer.

Tucker, M. E. and Wright, J. D. (1990). Carbonate sedimentology. Oxford, Blackwell Science.

Van de Schootbrugge, B. (2001). Influence of paleo-environmental changes during the Hauterivian (Early Cretaceous) on carbonate deposition along the northern margin of the Tethys: Evidence from geochimical records (C, O, and Sr-isotopes, P, Fe, Mn).» *Thèse de Doctorat ès Sciences, spécialité Géologie*, Université de Neuchâtel, Institut de Géologie, 268 pp.

Vermeulen, J. (2002). Etude stratigraphique et paléontologique de la famille des Pulchelliidae (ammonoidea, Ammonitina, Endemoceratacea). Grenoble, France.

Vermeulen, J. (2005). Boundaries, ammonite fauna and main subdivisions of the stratotype of the Barremian. *In:* T. Adatte, A. Arnaud-Vanneau, H. Arnaud, M. C. Blanc-Aletru, S. Bodin, E. Carrio-Schaffhauser, K. B. Föllmi, A. Godet, M. C. Raddadi and J. Vermeulen, (*Eds*). The Hauterivian - Lower Aptian sequence stratigraphy from Jura platform to Vocontian basin: a multidisciplinary approach: Géologie Alpine, Série Spéciale «Colloques et Excursions» n°7. 147-173.

Weissert, H., Lini, A., Föllmi, K. B. and Kuhn, O. (1998). «Correlation of Early Cretaceous carbon isotope stratigraphy and platform drowning events: a possible link?» Palaeogeography, Palaeoclimatology, Palaeoecology **137**: 189-203.

AN.4.2.
NEW DATA ON THE AGE OF THE INSTALLATION OF URGONIAN-TYPE CARBONATES ALONG THE NORTHERN TETHYAN MARGIN: BIOSTRATIGRAPHY OF THE CHOPF MEMBER (HELVETIC ALPS, EASTERN SWITZERLAND)

Données nouvelles sur la datation de l'installation des calcaires Urgonien le long de la marge nord-téthysienne: Biostratigraphie du Membre du Chopf (nappes Helvétiques, Suisse orientale)

Stéphane Bodin [1], Jean Vermeulen [2], Alexis Godet [1] & Karl B. Föllmi [1]

[1] Institut de Géologie et d'Hydrogéologie, Université de Neuchâtel, Rue Emile Argand 11, Case postale 158, 2009 Neuchâtel, Switzerland; [2] Grand Rue, 04330 Barrême, France

Published in Comptes Rendus Geosciences (2006), 338, 727-733.

Abstract

The Chopf Member is a glauconitic, phosphate-bearing succession that occurs in the distal part of the Helvetic Alps (eastern Switzerland). The recent discovery of age-diagnostic ammonites within this horizon allows for its attribution to the lower part of the *Gerhardtia sartousiana* zone (middle late Barremian). This new age corresponds to a maximal age for the onset of the Schrattenkalk Fm in this area, and is coeval with the onset of the Urgonian facies in other parts of the western Tethyan realm. This new age allows also for a more precise dating of late Barremian $\delta^{13}C$ curves.

Keywords

Helvetic platform; Switzerland; Drusberg Formation; Urgonian limestone; Late Barremian; carbon isotope curve

Résumé

Le Membre du Chopf correspond à un horizon glauconieux déposé dans la partie distale de la plate-forme helvétique. La découverte récente d'ammonites permet de dater précisément cet horizon de la partie inférieure de la zone à *Gerhardtia sartousiana* (Barrémien supérieur moyen). Cette nouvelle datation permet de donner un âge maximal à la Formation du Schrattenkalk dans cette région. Cet âge est cohérent avec ceux qui sont obtenus dans les autres parties de la Téthys occidentale pour l'installation des faciès urgoniens. Cette nouvelle datation permet aussi d'apporter des précisions sur la calibration des courbes du $\delta^{13}C$ du Barrémien supérieur.

Mots-Clés

Plateforme helvétique ; Suisse ; Formation du Drusberg ; Calcaire Urgonien ; Barrémien supérieur ; courbe isotopique du carbone

An.4.2.1. Version française abrégée

An.4.2.1.1. Introduction

Les nappes Helvétiques affleurent dans la partie nord des Alpes suisses (Fig.An.4.14) et documentent les restes de la marge nord Téthysienne. Dans ces unités tectoniques, des carbonates de plate-forme alternent avec des sédiments phosphatés et glauconieux (*e.g.*, Funk *et al.*, 1993; Föllmi *et al.*, 1994). Dans cette note, de nouvelles ammonites appartenant à un de ces intervalles glauconieux (le Membre du Chopf) sont figurées; elles sont attribuées au Barrémien supérieur moyen. Cette importante découverte permet non seulement de dater l'installation des faciès urgoniens (Formation du Schrattenkalk) dans cette partie de la Téthys, mais aussi de discuter la calibration des courbes téthysiennes de référence du $\delta^{13}C$.

An.4.2.1.2. Cadre géographique et géologique

Le Barrémien du domaine Helvétique est composé de deux formations : la Formation (Fm) du Drusberg et la Fm du Schrattenkalk (Fig.An.4.15). En domaine proximal, la Fm du Drusberg peut être divisée en deux membres (Mb) : le Mb d'Altmann et le Mb du Drusberg (*e.g.*, Funk, 1969, 1971). En domaine distal (région de l'Alvier), Briegel (1972) adjoint deux autres membres à la Fm du Drusberg : le Mb du Chopf et le Mb d'Hurst. D'après cet auteur, l'âge de ces deux derniers membres serait Barrémien moyen, sans plus de précision.

An.4.2.1.3. Sedimentologie et biostratigraphie

Le Mb du Chopf a été étudié au lieu dit du « Barbielergrat » (voir Briegel (1972) pour une localisation précise), où son épaisseur atteint environ 2 m ; il affleure sous forme de quatre bancs calcaires intercalés entre les marnes du Mb du Drusberg et du Mb d'Hurst (Fig.An.4.16). La glauconie est présente dans les deux premiers bancs et abondante dans le troisième. Des traces de phosphatogenèse peuvent être également discernées dans les trois derniers bancs. À la base du troisième banc, la présence de nombreux nodules phosphatés et de nombreuses bélemnites est à noter.

Parmi ces nodules, quatre ammonites phosphatées ont été trouvées (Fig.An.4.16). Deux d'entre elles se sont avérées être des *Hemihoplitidae* sp., tandis que les deux autres sont identifiées comme étant une *Ezeiceras* aff. *janus* et une *Hemihoplites* sp. aff. *limentinus* (Fig.An.4.17). Cet assemblage d'ammonites est typique de la partie terminale de la zone à *Heinzia sayni* et de la première moitié de la zone à *Gerhardtia sartousiana* (Barrémien supérieur moyen; Vermeulen, 2002, 2005).

An.4.2.1.4. Discussion

Cette nouvelle datation du Mb du Chopf permet de discuter quelques aspects importants de la sédimentologie du Barrémien tardif dans les nappes Helvétiques, ainsi que d'affiner la corrélation basée sur l'évolution du $\delta^{13}C$ entre cette région et les sections barrémiennes de références (e,g, Cismon Apticore ; Erba *et al.*, 1999), précédemment proposée par Wissler *et al.*, 2003).

La présence relativement élevée de glauconie et la trace de phosphatogenèse dans le Mb du Chopf témoignent en faveur d'une sédimentation condensée, caractéristique des surfaces d'inondations maximales (SIM) de troisième ordre. Dans le domaine Téthysien, une SIM majeure est localisée dans la zone à *G. sartousiana* (*e.g.*, Arnaud, 2005, Arnaud *et al.*, 1998), la SIM Ba3. Par conséquent, cet horizon condensé semble être synchrone avec la SIM Ba3.

De plus, Bodin *et al.* (2006) ont observé que la SIM Ba3 correspond à la transition entre la Fm du Drusberg et celle du Schrattenkalk en domaine plus proximal (coupe de Tierwis, région du Säntis). Ainsi, le membre du Chopf doit correspondre en temps à la limite Drusberg – Schrattenkalk en domaine proximal. Par conséquent, en situation distale, l'installation du Mb du Schrattenkalk, qui est séparé du Mb du Drusberg par le Mb d'Hurst, doit être plus jeune qu'en situation proximale. Cette observation souligne la progradation de la plate-forme urgonienne durant le Barrémien supérieur dans le domaine Helvétique (Fig.An.4.18 ; *e.g.*,

Bollinger, 1988). Il est également important de noter que cet âge est cohérent avec l'installation des faciès urgoniens dans les autres parties de la Téthys occidentale, et particulièrement dans le Vercors (*e.g.*, Arnaud *et al.*, 1998).

Par ailleurs, Wissler *et al.* (2003) ont publié une courbe haute résolution du $\delta^{13}C$ pour cette région, montrant deux excursions positives durant le Barrémien supérieur, le Mb du Chopf étant situé exactement au milieu de ces deux excursions (Fig.An.4.19). En considérant cette nouvelle datation, il apparaît que la première excursion est plus âgée que la zone à *G. sartousiana*. D'après la datation du sommet du Mb de l'Altmann par Bodin *et al.* (2006) et la conséquente datation de la base du Mb du Drusberg (zone à C. darsi), cette première excursion est datée de la partie inférieure du Barrémien supérieur (zone à *H. uhligi – H. sayni*).

An.4.2.1.5. Conclusions

Le Mb du Chopf est daté de la zone à Gerhardtia *sartousiana* (Barrémien supérieur moyen) et correspond à la surface d'inondation maximale Ba3. Il en résulte que la Fm du Schrattenkalk, équivalente de la Fm Urgonienne dans les autres parties du domaine Téthysien, est plus jeune que la zone à *G. sartousiana* dans la partie distale de la plate-forme Helvétique. Cependant, dans les parties internes, l'installation de ces faciès est datée, par corrélation en stratigraphie séquentielle, de cette même zone à *G. sartousiana*. Cette dichotomie souligne donc la progradation de la marge distale de la plate-forme Helvétique durant le Barrémien supérieur.

An.4.2.2. Introduction

The Helvetic fold- and thrust belt is situated in the northern part of the central European Alps (Fig.An.4.14) and includes a sedimentary succession which documents the evolution of the northern Tethyan margin during the Mesozoic and early Tertiary. The lower Cretaceous comprised in this tectonic zone is composed of an alternation of photozoan and heterozoan platform carbonates and highly condensed phosphatized and glauconitic sediments (*e.g.*, Funk *et al.*, 1993; Föllmi *et al.*, 1994). These latter sediments are associated with repetitive drowning episodes, which interfered with the growth of the northern Tethyan carbonate platform. In this paper, we report the discovery of ammonites from one of these glauconitic beds (the Chopf Member), which date from the middle late Barremian. This new age date allows us to attribute a maximal age to the installation of the Schrattenkalk Formation (Fm), which is the equivalent of the Urgonian-type carbonates

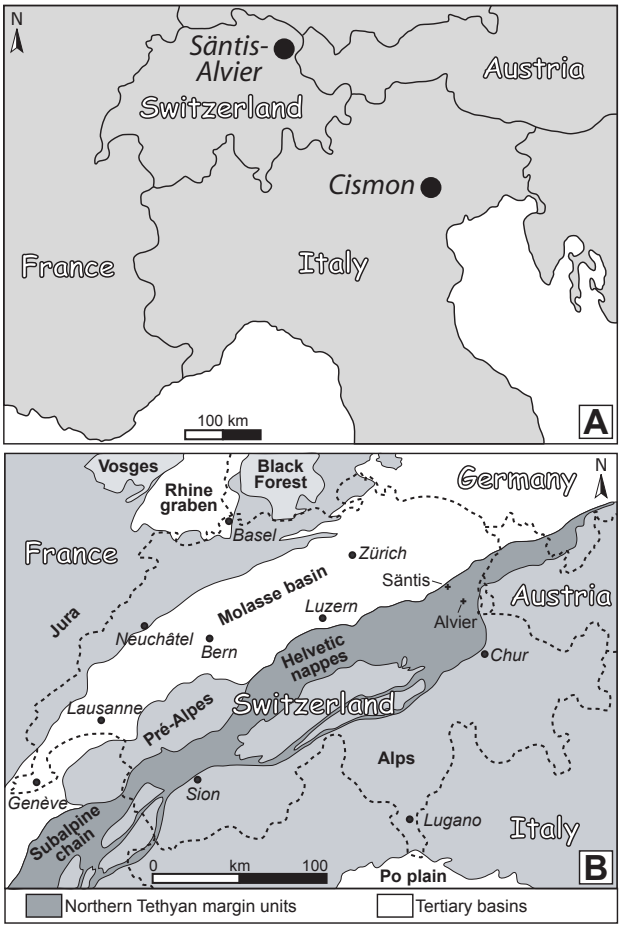

Fig. An.4.14. Location of the different mentioned sections. (A) Location of the Cismon APTICORE drilling and the Säntis and Alvier regions (modified after Wissler et al., 2003). For a precise location of Cismon, see Erba et al., 1999. (B) Tectonic map of Switzerland with the location of the Helvetic realm (dark grey colored) and the Säntis and Alvier regions. For precise location, see Briegel, 1972, and Funk, 1969.

Fig. An.4.14. Localisation des différentes coupes mentionnées. (A) Localisation du forage de Cismon APTICORE et des régions du Säntis et de l'Alvier (modifié d'après Wissler *et al.*, 2003). Pour une localisation précise de Cismon, se reporter à Erba *et al.*, 1999. (B) Carte tectonique de la Suisse avec l'emplacement du domaine Helvétique (gris foncé), ainsi que des régions du Säntis et de l'Alvier. Pour une localisation précise, se reporter à Briegel, 1972, et Funk, 1969.

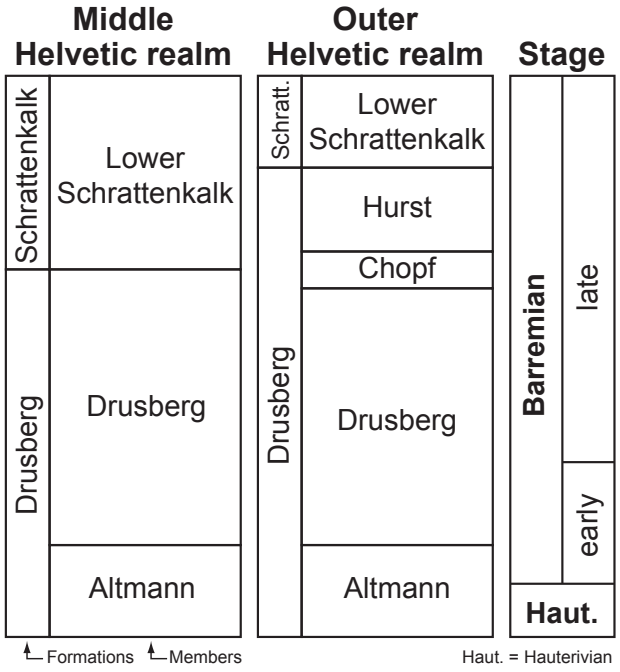

Fig. An.4.15. Barremian Formations and Members from the middle and outer Helvetic shelf.

Fig. An.4.15. Formations et Membres du Barrémien du domaine Helvétique proximal et distal.

known from other parts of the Tethyan realm (*e.g.*, Arnaud *et al.*, 1998; Vermeulen, 2002). Finally, this new age date helps also to refine the dating of $\delta^{13}C$ references curves from the Tethyan realm.

An.4.2.3. Geographical and geological setting

In the Helvetic realm, the Barremian stage is characterized by the deposition of two distinct formations: the Drusberg Fm and the Schrattenkalk Fm (Fig.An.4.15). In proximal settings, the Drusberg Fm is divided into two members (Mb): the Altmann Mb and the Drusberg Mb (*e.g.*, Funk 1968, 1971). In the distal part of the Helvetic platform, and particularly in the Alvier region, Briegel (1972) divided the Drusberg Mb into four members by adding two further members to the top of the Drusberg Mb: the Chopf Mb and the Hurst Mb (Fig.An.4.15). The Chopf Mb represents a thin and glauconite-rich interval, for which no equivalent exists in the more internal part of the helvetic shelf, whereas the Hurst Mb consists of a marly succession which Briegel (1972) considered as a distal equivalent of the lower part of the Schrattenkalk Fm. According to this author, these two latter members are dated as «middle» Barremian, without any further precision.

An.4.2.4. Sedimentology and biostratigraphy

The Chopf Mb was logged and sampled at Barbielergrat, 1 km NE of Alvier, eastern Switzerland (swiss coordinates: 750.650/220.075; Briegel, 1972; Wissler *et al.*, 2003). At this locality, this member is composed of four principal beds and reaches a total thickness of approximately 2m; it is under- and overlain by marly beds corresponding to the Drusberg Mb and the Hurst Mb, respectively (Fig. An.4.16). The base of the Chopf Mb is well-defined and marked by the presence of up to 10 cm thick Thalassinoides burrows. The basal bed is composed of a spicule-rich limestone, whereas the three following beds are characterized by carbonate rich in intraclasts, echinodermal debris, and isolated phosphatized particles. Glaucony is present in the first two beds, and abundant in the third bed. At the base of the third bed, both phosphatized pebbles and fossils, as well as numerous belemnites, are abundant.

Among theses nodules, four well-preserved phosphatized ammonites have been found (Fig.An.4.16). Two of them are identified as Hemihoplitidae sp., whereas the two others are identified as Ezeiceras aff. janus and Hemihoplites sp. aff. limentinus (Fig.An.4.17). This assemblage allows the attribution of the Chopf Mb to the middle late Barremian; more precisely, from the latest Heinzia Sayni and the first half of the

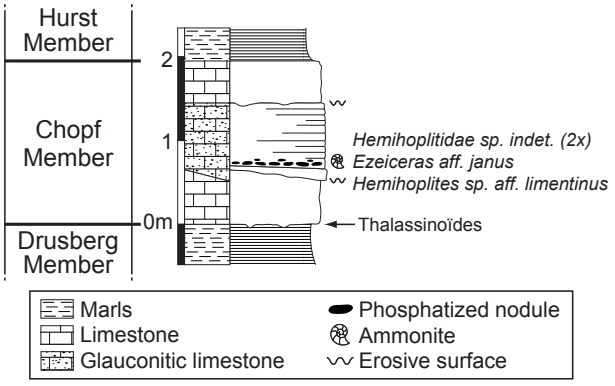

Fig. An.4.16. Sedimentary log of the Chopf Mb at the Barbielergrat locality.

Fig. An.4.16. Colonne sédimentaire du Mb du Chopf au lieu dit du Barbielergrat.

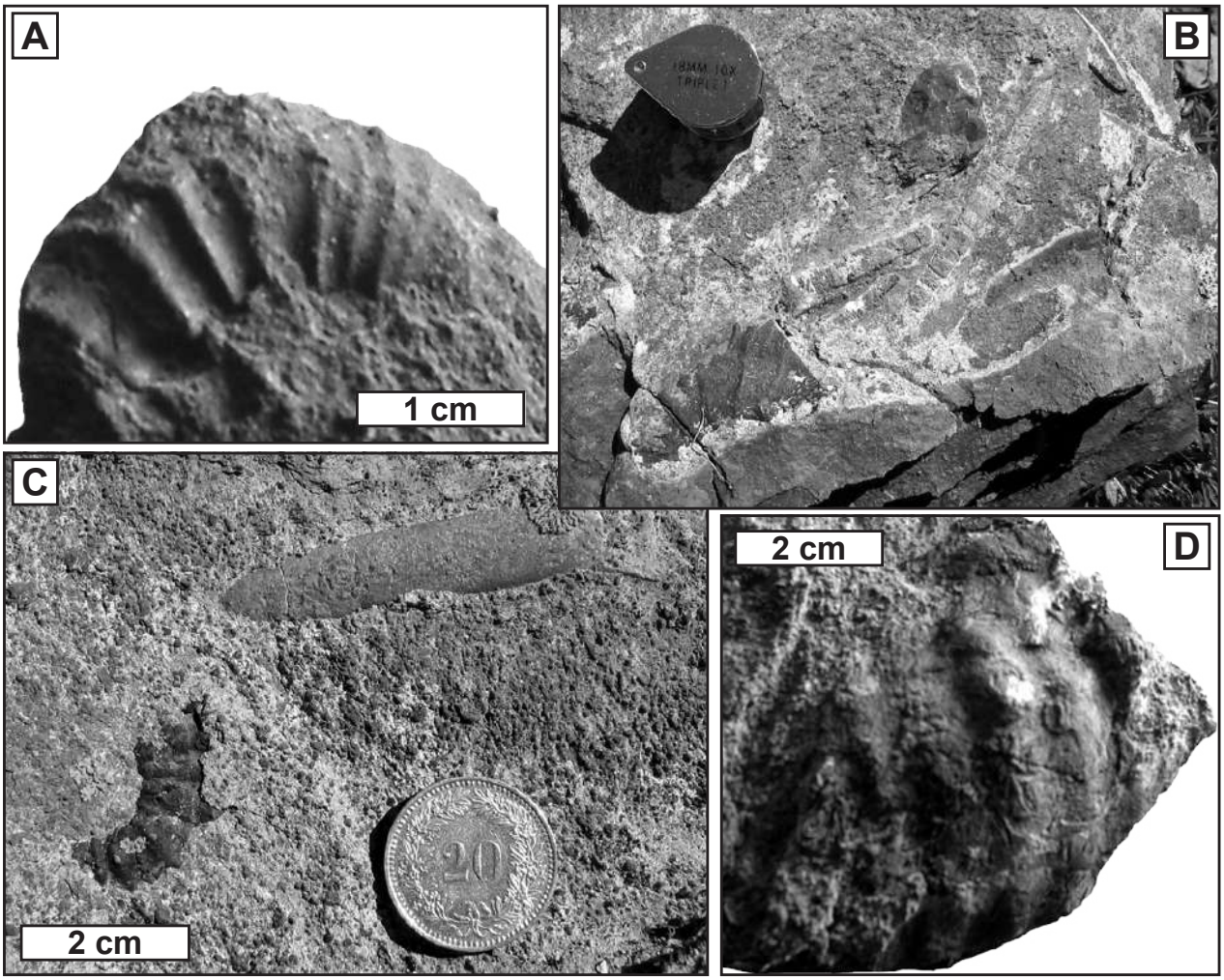

Fig. An.4.17. Photographs of the ammonites of the Chopf Mb. (A) and (B) Hemihoplitidae sp. (C) Ezeiceras aff. janus. (D) Hemihoplites sp. aff. limentinus.

Fig. An.4.17 Photographies des ammonites dans le Mb du Chopfschichten. (A) et (B) Hemihoplitidae sp. (C) Ezeiceras aff. janus. (D) Hemihoplites sp. aff. limentinus.

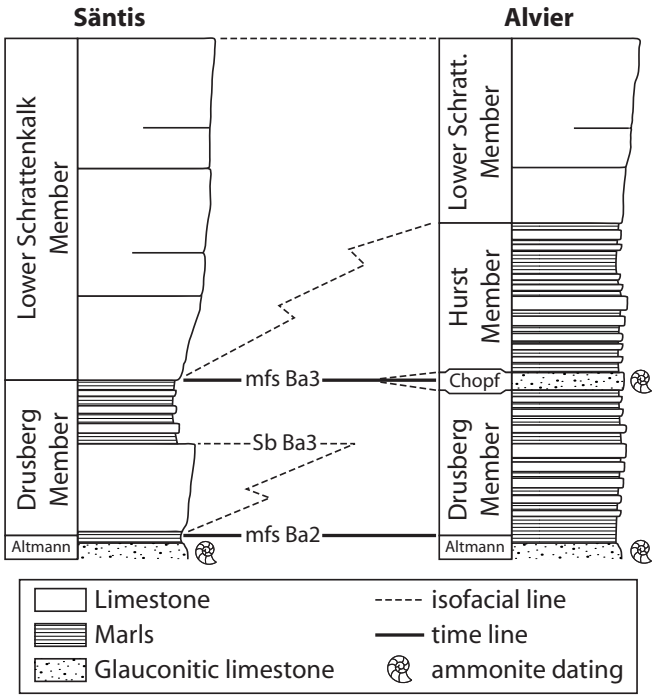

Fig. An.4.18. Synthetic sedimentary columns from the Säntis and the Alvier regions showing the diachronous onset of the Lower Schrattenkalk Mb and the subsequent progradation of the Helvetic margin during the late Barremian.

Fig. An.4.18. Colonnes sédimentaires synthétiques des régions du Säntis et de l'Alvier. On peut y voir l'installation diachronique du Mb inférieur du Schrattenkalk et la conséquente progradation de la marge Helvétique durant le Barrémien supérieur.

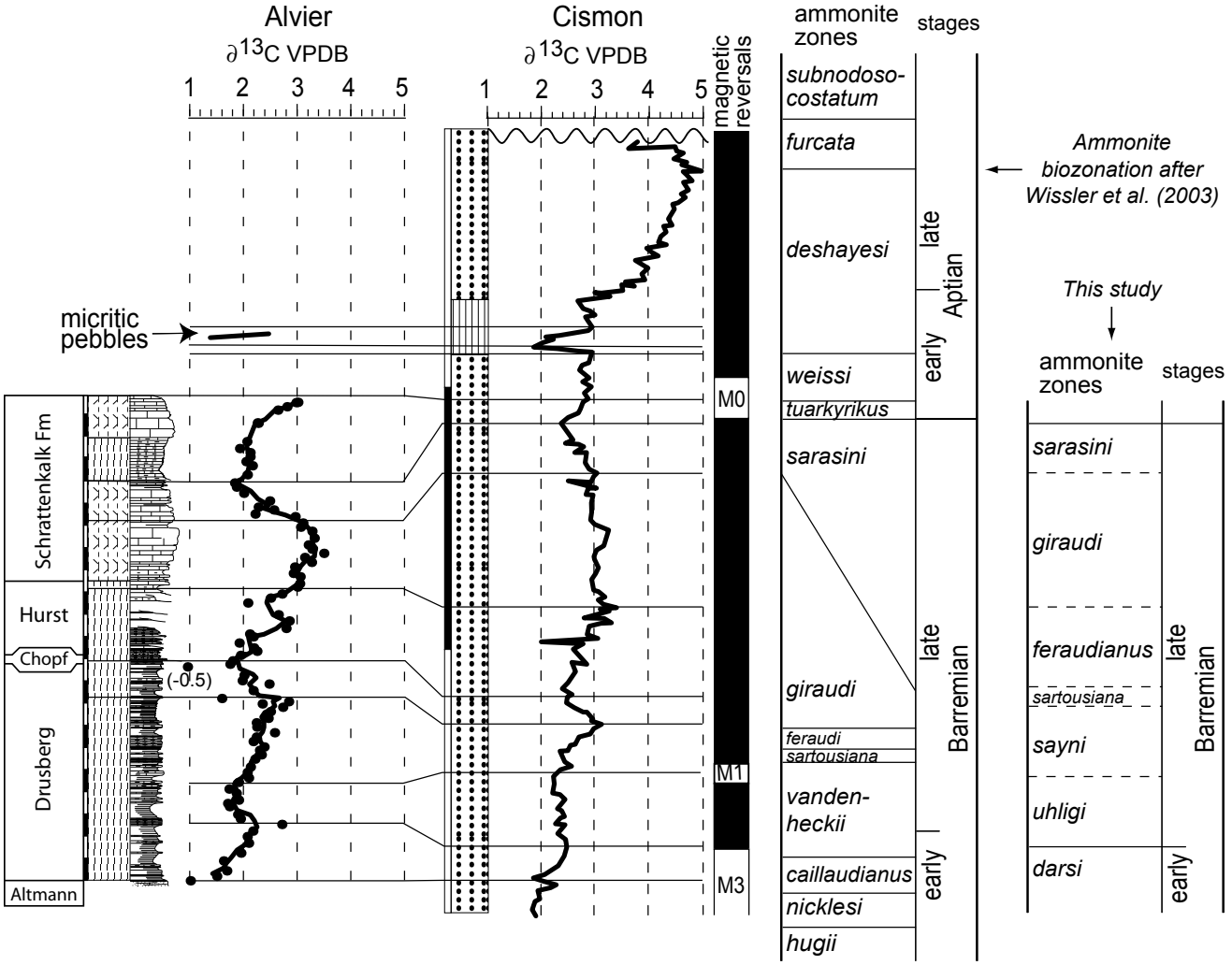

Fig. An.4.19. Carbon isotope correlation between the Alvier region and the Cismon APTICORE drilling (figure modified from Wissler et al., 2003, after the results of Erba et al. 1999, and Wissler et al. 2003), and proposition of a new biostratigraphic framework after the results from Godet et al., 2006, and this study.

Fig. An.4.19. Corrélation des courbes isotopiques du carbone entre la région d'Alvier et le forage de Cismon APTICORE (figure modifiée d'après Wissler *et al.*, 2003, d'après les resultants de Erba *et al.*, 1999, et de Wissler *et al.*, 2003), ainsi que la proposition d'un nouvelle zonation biostratigraphique résultant des travaux de cette note et de Godet *et al.*, 2006.

Gerhardtia sartousiana zones (*e.g.*, Vermeulen, 2002, 2005).

An.4.2.5. Discussion

The newly obtained age of the Chopf Mb allows us to discuss the chronostratigraphic evolution of late Barremian sediments distribution in the Helvetic realm, and also to refine correlations between $\delta^{13}C$ reference curves for this particular section, published by Wissler *et al.* (2003), and other settings in the Tethyan realm.

The presence of glaucony and phosphate within the Chopf Mb relates its origin to a period of condensation during high sea-level, even if subsequent sediment reworking and transport by gravity flow can not be excluded. This horizon may therefore correspond to a maximum flooding surface (mfs) deposit. In the western Tethyan realm, the presence of a major mfs has been identified in sediments corresponding in age to the middle of the G. sartousiana zone (the Ba3 mfs; Arnaud, 2005, Arnaud *et al.*, 1998). Hence, we propose that this horizon corresponds in time to the Ba3 mfs.

Bodin *et al.* (2006) have observed that the transition between the Drusberg Fm and the Schrattenkalk Fm in more proximal areas of the

Helvetic shelf (Tierwis section, Säntis region) corresponds equally to the Ba3 mfs. Indeed, they dated the boundary between the Altmann Mb and Drusberg Mb as middle C. darsi zone and associated it to a mfs (mfs Ba2). The sediments of the Drusberg Mb are characterized by a regressive trend followed by a transgressive trend, which are attributed to the Ba2 highstand and the Ba3 transgressive systems tract, respectively. On top of the Drusberg Fm, the basal part of the Lower Schrattenkalk Mb is characterized by a regressive trend that can be associated with the Ba3 highstand systems tract. The Drusberg – Schrattenkalk boundary may thus correspond to the Ba3 mfs.

The Chopf Mb may therefore represent a distal time-equivalent of the sediments associated with the transition between the Drusberg Fm and Schrattenkalk Fm of more proximal areas. Hence, in distal areas of the Helvetic shelf, the onset of the Lower Schrattenkalk Mb - separated from the Chopf Mb by the Hurst Mb - is therefore younger than in more proximal areas, which is related to the time-transgressive progradation of the "Urgonian" platform during the latest Barremian in the Helvetic realm (Fig.An.4.18; *e.g.*, Bollinger, 1988).

The maximal age obtained here for the onset of the Schrattenkalk Fm is in good agreement with the onset of the Urgonian facies in other parts of the western Tethyan realm, and especially in the Vercors area (*e.g.*, Arnaud *et al.*, 1998). This underlines the close relationships of the sedimentary history between the areas of the northern Tethyan margin, which now are part of France and Switzerland.

Wissler *et al.* (2003) published a high-resolution $\delta^{13}C$ curve for the Alvier region, showing two positive shifts for the late Barremian. The Chopf Mb is situated exactly in the middle of these two positive shifts (Fig.An.4.19). With the new precise age date for the Chopf Mb, it appears that the first positive shift is older than the G. sartousiana zone. According to the new age dates for the lower and upper boundaries of the Altmann Mb by Bodin *et al.* (2006) and the corresponding maximal age for the base of the Drusberg Mb (*C. darsi* zone), this first shift may be dated as early late Barremian (*H. uhligi – H. sayni* zone).

In the Italian Cismon APTICORE drilling, the late Barremian is also characterized by two positive shifts (Erba *et al.*, 1999). In the case these two shifts are correlated with the two excursions observed by Wissler *et al.* (2003) in the Alvier region (Fig.An.4.19), the older shift in Cismon - where precise ammonite stratigraphy is lacking - would also correspond to the early late Barremian.

An.4.2.6. Conclusions

The glaucony-rich and phosphate-bearing Chopf Mb (Helvetic zone, eastern Switzerland) is dated from the Gerhardtia sartousiana ammonite zone (middle late Barremian) and its formation may be linked to the maximum flooding surface Ba3. This new age date indicates that the overlying Schrattenkalk Fm - equivalent of Urgonian carbonates in other parts of the Tethyan realm - is younger than the G. sartousiana zone in distal parts of the Helvetic shelf. In inner parts of the shelf, using sequence-stratigraphic arguments, the onset of the Schrattenkalk Fm dates as *G. sartousiana* zone. This dichotomy underlines the progradation of the distal Helvetic platform margin during the late Barremian.

An.4.2.7. Acknowledgments

The authors acknowledge Urs Oberli and Ueli Briegel for their help in the field and André Villard (Uni Neuchâtel) for the preparation of thin-sections. We thank two anonymous reviewers for their constructive criticism of the manuscript. Financial support from the Swiss National Science Foundation Project 2100-067807/1 and 200020-105206/1 is gratefully acknowledged.

An.4.2.8. References

Arnaud, H. (2005). Sequence stratigraphy interpretation. *In:* T. Adatte, A. Arnaud-Vanneau, H. Arnaud, M. C. Blanc-Aletru, S. Bodin, E. Carrio-Schaffhauser, K. B. Föllmi, A. Godet, M. C. Raddadi and J. Vermeulen, (*Eds*). The Hauterivian - Lower Aptian sequence stratigraphy from Jura platform to Vocontian basin: a multidisciplinary approach. **Géologie Alpine, Série Spéciale «Colloques et Excursions» n°7**: 174-179.

Arnaud, H., Arnaud-Vanneau, A., Blanc-Aletru, M. C., Adatte, T., Argot, M., Delanoy, G., Thieuloy, J.-P., Vermeulen, J., Virgone, A., Virlouvet, B. and Wermeille, S. (1998). «Répartition stratigraphique des orbitolinidés de la plate-forme urgonienne subalpine et jurassienne (SE de la France).» Géologie Alpine **74**: 3-89.

Bodin, S., Godet, A., Vermeulen, J., Linder, P. and Föllmi, K. B. (2006). «Biostratigraphy, sedimentology and sequence stratigraphy of the latest Hauterivian - early Barremian drowning episode of the Northern Tethyan margin (Altmann Member, Helvetic Nappes, Switzerland).» Eclogae Geologicae Helveticae, in press.

Bollinger, D. (1988). Die Entwicklung des distalen osthelvetischen schelfs im Barremian und Früh-Aptian. Drusberg-, Mittagspitz- und Schrattenkalk-Fm im Vorarlberg und Allgäu.

Briegel, U. (1972). «Geologie der östlichen Alviergruppe (Helvetische Decken der Ostschweiz) unter besonderer Berücksichtigung der Drusberg- und Schrattenkalkformation (Unterkreide).» Eclogae Geologicae Helvetiae **65**(*2*): 425-483.

Erba, E., Channell, J. E. T., Claps, M., Jones, C. E., Larson, R. L., Opdyke, B., Premoli-Silva, I., Riva, A., Salvini, G. and Torriceli, S. (1999). «Integrated stratigraphy of the Cismon APTICORE (Southern Alps, Italy): A «reference section» for the Barremian-Aptian interval at low latitudes.» Journal of Foraminiferal Research **29**(*4*): 371-391.

Funk, H. (1969). «Typusprofile der helvetischen Kieselkalk Formation und der Altmann Schichten.» Eclogae geologicae Helvetiae **62**(*1*): 191-203.

Funk, H. (1971). «Zur Stratigraphie und Lithologie des Helvetischen Kieselkalkes und der Altmannschichten im der Säntis-Churfirsten-Gruppe (Nordostschweiz).» Eclogae geologicae Helvetiae **64**(*2*): 345-433.

Funk, H., Föllmi, K. B. and Mohr, H. (1993). Evolution of the Tithonian-Aptian carbonate platform along the northern Tethyan margin, eastern Helvetic Alps. *In:* Simo J.A.T., Scott R.W. and Masse J.-P., (*Eds*). Cretaceous carbonates platforms. AAPG Memoir, American Association of Petroleum Geologists. Tulsa, OK, United States., **56**: 387-407.

Föllmi, K. B., Weissert, H., Bisping, M. and Funk, H. (1994). «Phosphogenesis, carbon-isotope stratigraphy, and carbonate-platform evolution along the Lower Cretaceous northern Tethyan margin.» Geological Society of America Bulletin **106**: 729-746.

Godet, A., Bodin, S., Föllmi, K. B., Vermeulen, J., Gardin, S., Fiet, N., Adatte, T., Berner, Z., Stüben, D. and Van de Schootbrugge, B. (2006). «Evolution of the marine stable carbon-isotope record during the early Cretaceous: A focus on the late Hauterivian and Barremian in the Tethyan realm.» Earth and Planetary Science Letters **242**: 254-271.

Vermeulen, J. (2002). Etude stratigraphique et paléontologique de la famille des Pulchelliidae (ammonoidea, Ammonitina, Endemoceratacea). Grenoble, France.

Vermeulen, J. (2005). Boundaries, ammonite fauna and main subdivisions of the stratotype of the Barremian. *In:* T. Adatte, A. Arnaud-Vanneau, H. Arnaud, M. C. Blanc-Aletru, S. Bodin, E. Carrio-Schaffhauser, K. B. Föllmi, A. Godet, M. C. Raddadi and J. Vermeulen, (*Eds*). The Hauterivian - Lower Aptian sequence stratigraphy from Jura platform to Vocontian basin: a multidisciplinary approach: Géologie Alpine, Série Spéciale «Colloques et Excursions» n°7. 147-173.

Wissler, L., Funk, H. and Weissert, H. (2003). «Response of Early Cretaceous carbonate platforms to changes in atmospheric carbon dioxide levels.» Palaeogeography, Palaeoclimatology, Palaeoecology **200**(*1-4*): 187-205.

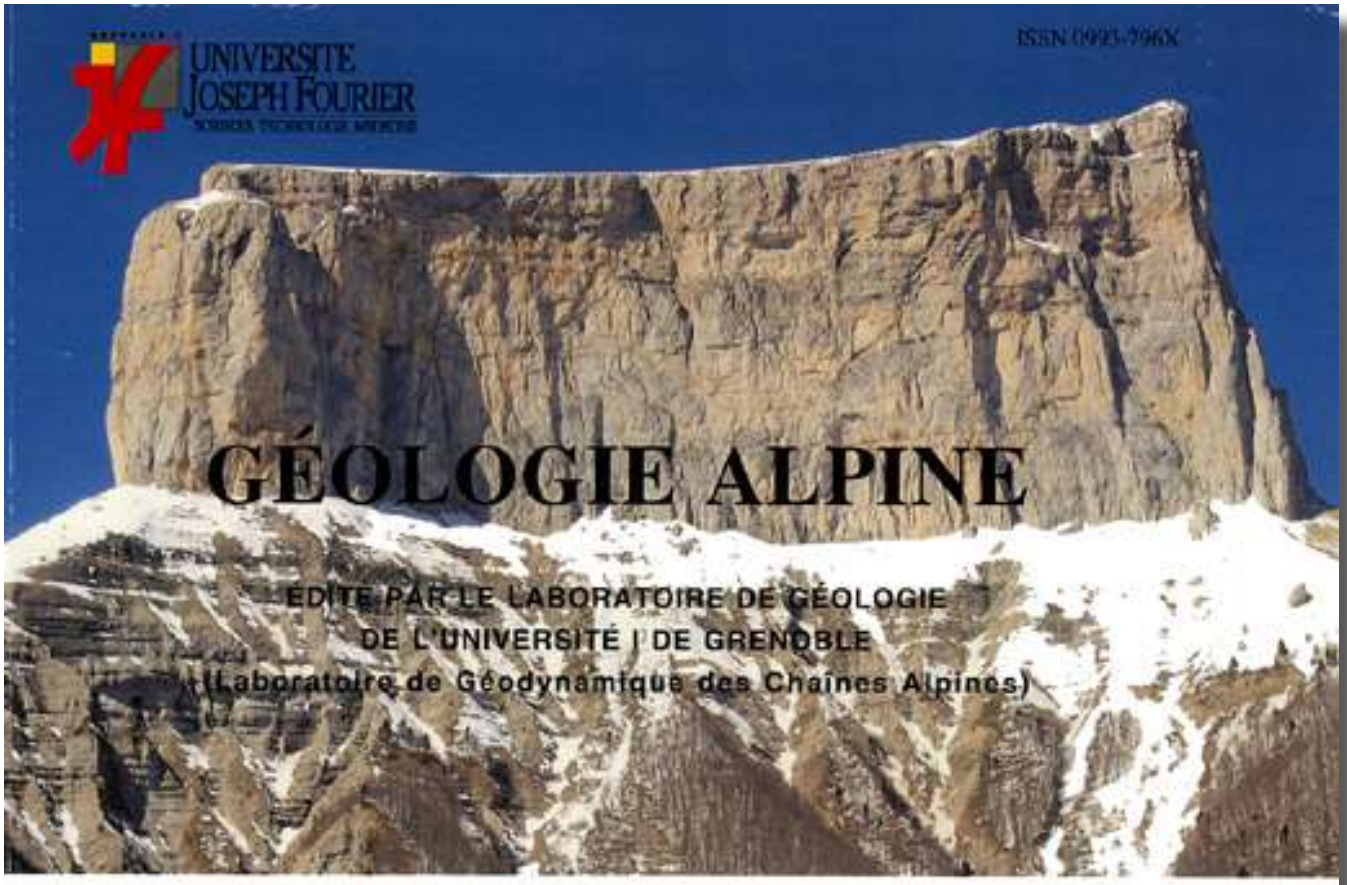

SÉRIE SPÉCIALE «COLLOQUES ET EXCURSIONS» N° 7

THE HAUTERIVIAN - LOWER APTIAN SEQUENCE STRATIGRAPHY FROM JURA PLATFORM TO VOCONTIAN BASIN: A MULTIDISCIPLINARY APPROACH

Field-trip of the 7th International Symposium on the Cretaceous (September 1-4, 2005)

Thierry Adatte, Annie Arnaud-Vanneau, Hubert Arnaud,
Marie-Caroline Blanc-Alétru, Stéphane Bodin, Elisabeth Carrio-Schaffhauser,
Karl B. Föllmi, Alexis Godet, Mohamed Chaker Raddadi et Jean Vermeulen

AN.4.3. THE HAUTERIVIAN - BARREMIAN OF THE WESTERN SWISS JURA AROUND NEUCHÂTEL

Alexis Godet, Marie-Caroline Blanc-Aletru, Stéphane Bodin, Thierry Adatte and Karl B. Föllmi

Published in Géologie Alpine, 2005, série "Colloques et excursions" n°7

An.4.3.1. Introduction: the formations from the early Cretaceous of the western Swiss Jura

An.4.3.1.1. Developments in the historical definition

In 1874, Renevier introduced the Hauterivian stage in the vicinity of Neuchâtel so as to re-establish the Neocomian of Thurmann (1836). Renevier's definition is clearly displayed in the local lithostratigraphy. The newly formed Hauterivian stage it comprised of the following units, from base to top (Fig. An.4.20):

The **"Marne jaune de Morteau à *Ammonites astieranus*"** (synonyms: "Marnes à *Astieria*", "Astieriamergel", "Astieruiaschicht"), which consists of 20-30 cm of yellow clayey marls, restricted only to the vicinity of Neuchâtel. Further from Neuchâtel, the "Marnes à *Astiera*" is sometimes replaced by a condensed bed which always marks the transition between the underlying "Calcaire Roux" (Valanginian) and the "Marne bleue d'Hauterive".

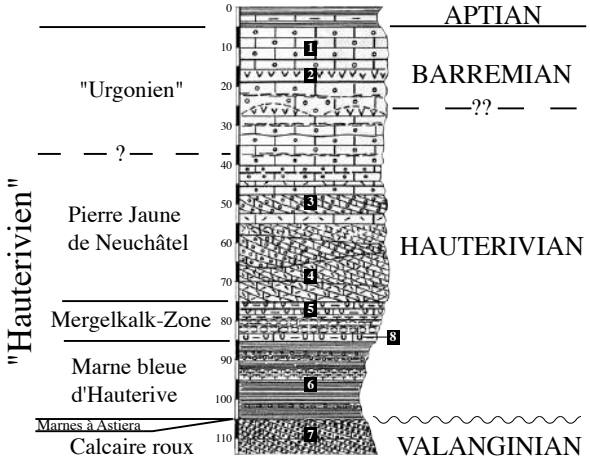

Lithologies: 1) perlsparites; 2) coral limestones (biohermes or biostromes); 3) oosparites; 4) biosparites; 5) marly limestones; 6) calcareous marls and marls; 7) ferrugeneous oolites; 8) burrows.

Fig. An.4.20: Historical succession around Neuchâtel. The local lithostratigraphic units and the ages are reported on the left and the right, respectively (after Remane, 1989).

The **"Marne d'Hauterive à *Ammonites radiatus*"** (synonyms: "Marne bleue", "Marne d'Hauterive") was deposited under open marine sedimentation. This formation can reach more than 20 m, contains several glauconitic-rich layers (*e.g.* the Cressier section located 15 km east of Neuchâtel). and is rich in ammonites and brachiopods. In the Cressier section, Busnardo and Thieuloy (1989) recognized *Teschnites* sp., *Acantodiscus pseudoradiatus*, *Acandodiscus radiatus*, *Acantodiscus* sp. Ind., *Leopoldia leopoldina*, *Leopoldia* sp. Ind., *Leopoldia levigata*, *Saynella neocomiensis* and *Saynella clypeiformis*; this assemblage may imply that the Marne bleue corresponds to the *radiatus* zone (Fig. An.4.21); even if the finding of one *Criocere* belonging to the *loryi* group (Schardt, 1907 in Busnardo and Thieuloy, 1989), and of a *S. clypeiformis* at the top of the Cressier section would indicate that this formation developed until the *Crioceratites loryi* zone (Busnardo and Thieuloy, 1989).

The "Mergelkalkzone" (synonym: "zone marno-calcaire") is the transition between the "Marne Bleue" and the ""Pierre Jaune de Neuchâtel"", which is the last formation of the Hauterivian of Renevier (1874).

Formations	Mean Thickness	Lithology	**Biostratigraphy** (main faunas) after Remane *et al.*(1989), Blanc-Aletru (1995) and this work
Urgonien Blanc	10 to 55 m	Oomicrite to oobiomicrite with builder organisms (rudists, stromatoporoids), orbitolinids and dasycladacae.	**Rudists:** *Agriopleura* sp., *Requiena renevieri*. **Dasycladacae:** *Suppiluliumella* gr. *verae* (Sokac) *corbarica, Falsolikanella* aff. *danilovae* (Radoiac), *Pseudoactinoporella fragilis*. **Orbitolinids:** *Paleodictyoconus cuvillieri, Parakoscinolina* sp., *Praedictyorbitolina carthusianna* (among others).
Marnes de la Russille	2 m	Orange to yellowish marls intercalated with limestones rich in stromatoporoids and corals	**Echinoids:** *Goniopygus* sp. (?)
Urgonien Jaune	30 m	Grainstones with oolites, extraclasts, large bryozoans debris and crinoids. Whereas no current beddings are noted at the bottom of the Urgonien Jaune, its upper part is characterized by well-sorted oolites grainstones with current beddings and even planar bedding organised into thinning-upward parasequences.	**Echinoids:** *Orthopsis* aff *repellini* (?)
Upper PJN	40 m	Orange to yellow oolitic grainstones rich in bryozoans and crinoids debris, with well-marked current bedding. Some marly intervals are clearly enriched in glauconite.	**Ammonites:** *Lyticoceras* sp. ind.
M. Uttins	< 1m	Orange clayey marls rich in glauconite over a hardgroung with burrows and oysters.	**Ammonites:** *Lyticoceras nodosoplicatum*.
Lower PJN	25m	Orange to yellow oolitic grainstones rich in bryozoans and crinoids debris, with well-marked current bedding. Silex are common.	
Mergelkalk zone	< 5 m	Yellowish, more or less marly limestones (wackestones and grainstones with current beddings) with thin marly intercalations.	*Ammonites: Leopoldia* sp. ind., *Cymatoceras pseudoelegans*
Marne Bleue d'Hauterive	30 m	Dark calcareous marls with several glauconite-rich layers, resulting of an open marine sedimentation. Ammonites and brachiopods are easily found.	**Ammonites:** *Teschnites* sp., *Acantodiscus* sp. Ind., *A. pseudoradiatus, A. radiatus, Leopoldia* sp. Ind., *L. leopoldina, L. levigata, Saynella neocomiensis* and *S. clypeiformis*.
M. à Astieria	< 1m	Yellow condensed marly interval, rich in ammonites.	**Ammonites:** *Ammonites astieria, Olcostephanus atherstoni, Dichotomites* gr. *bidichotomoides*.
Calcaire Roux		Current-bedded, ferrugeneous grainstone which becomes nodular upward.	

Fig. An.4.21: Synthetic profile of the early Cretaceous formations around Neuchâtel (not to scale). Facies and significant faunas are described.

The "Pierre Jaune de Neuchâtel" consists of an oolitic grainstone, sometimes enriched in bioclasts and characterized by oblique stratifications. The "Pierre Jaune de Neuchâtel" is divided into two parts by the **"Marnes d'Uttins"**. This is a thin marly interval rich in glauconite; ammonites indicate an early Hauterivian age for the "Marnes d'Uttins" (*Lyticoceras nodosoplicatum* zone).

Above these units, the **"Marnes de la Russille"** divides the Urgonian limestones into two parts. The lower part is represented by the **"Urgonien Jaune",** an oolitic – bioclastic yellow grainstone alternating with marly intervals. In the "Marnes de la Russille", the first cnidarians occur.

Finally, the **"Urgonien Blanc"** is the last formation of the succession. It consists of white oolitic grainstones to slightly recrystallized white limestones and rudists. Some stromatoporoids or corals can also be found.

Whereas the age of the formations under the "Marnes d'Uttins" is well constrained by ammonite biostratigraphy, the lack of such fossils in the upper "Pierre Jaune de Neuchâtel" and the Urgonian limestones is problematic (Fig. An.4.21). In 1901 some controversy arose when Baumberger replaced the lithostratigraphic term "Urgonien" by the stage name Barremian, without any biostratigraphic clues for such an age. So, in the stratigraphic scheme of Baumberger (1901), the upper "Pierre Jaune de Neuchâtel" should belong to the late Hauterivian, and the "Urgonien Jaune" and the "Urgonien Blanc" to the Barremian.

An.4.3.1.2. Recent developments

A study by Remane *et al.* (1989) tried to resolve the questions relating to dating and of the continuity of the historical succession

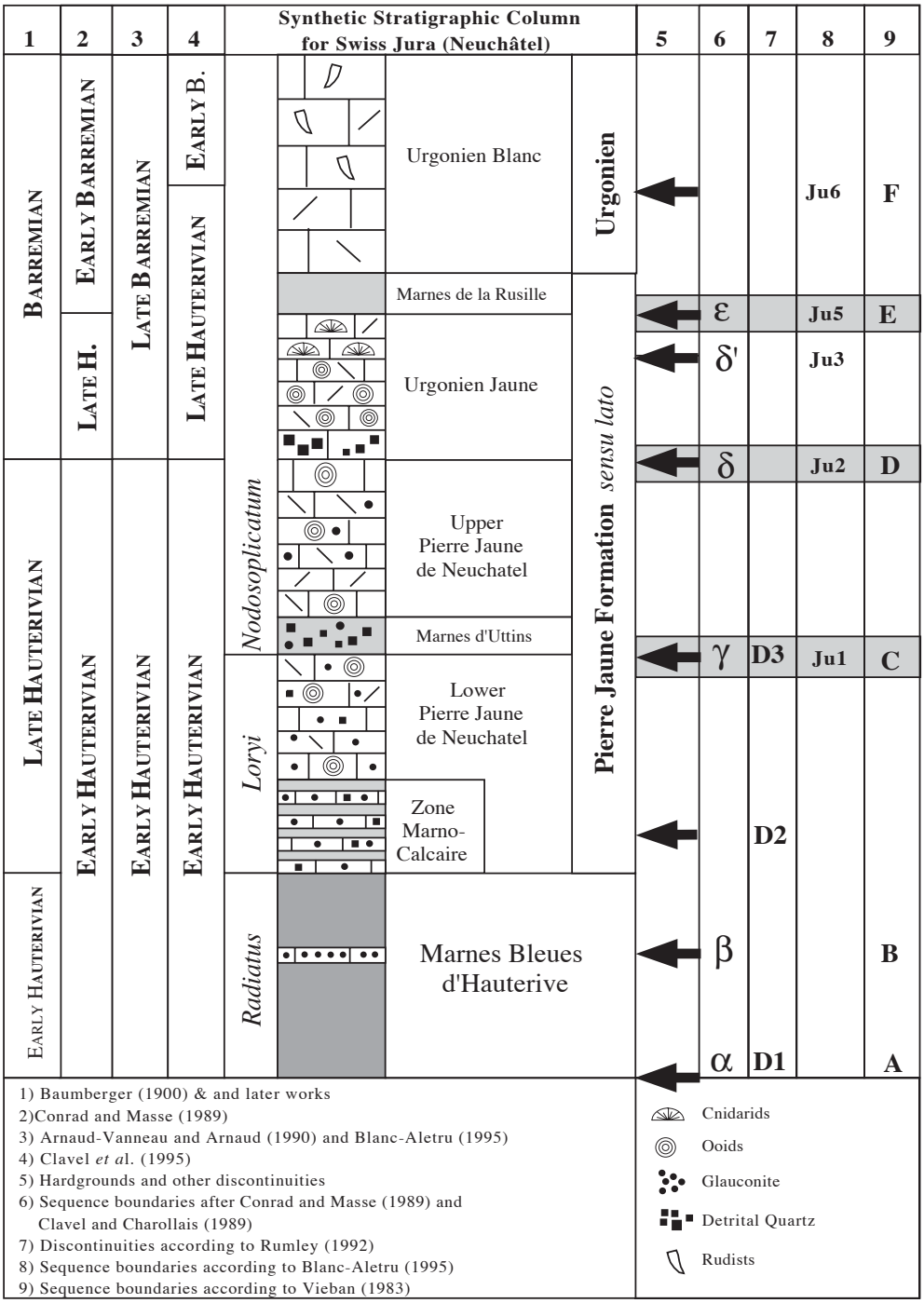

Fig. An.4.22: Synthetic stratigraphic column for the western Swiss Jura. The different proposed ages are reported on the left, as well as the main discontinuities (on the right) according to different authors (after van de Schootbrugge, 2001).

defined around Neuchâtel by Renevier (1874). To do this they studied all the faunas but also the mineralogy and the sequence stratigraphy, in order to try to correlate the western Swiss Jura with the meridional Jura. However, it seems that no consensus could emerge. Two main schools of thought appeared. Based on sequence stratigraphy and orbitolinids biostratigraphy, the conclusions of these two sides are the following (Fig. An.4.22):

1. Arnaud-Vanneau and Arnaud (1990) proposed that a significant hiatus, located at the top of the "Pierre Jaune de Neuchâtel", implies a late Barremian age for both the "Urgonien Jaune" and the "Urgonien Blanc". From their point of view, the Urgonian limestones may have been deposited simultaneously from the Vercors to the vicinity of Neuchâtel, from the maximum flooding surface (mfs) B3

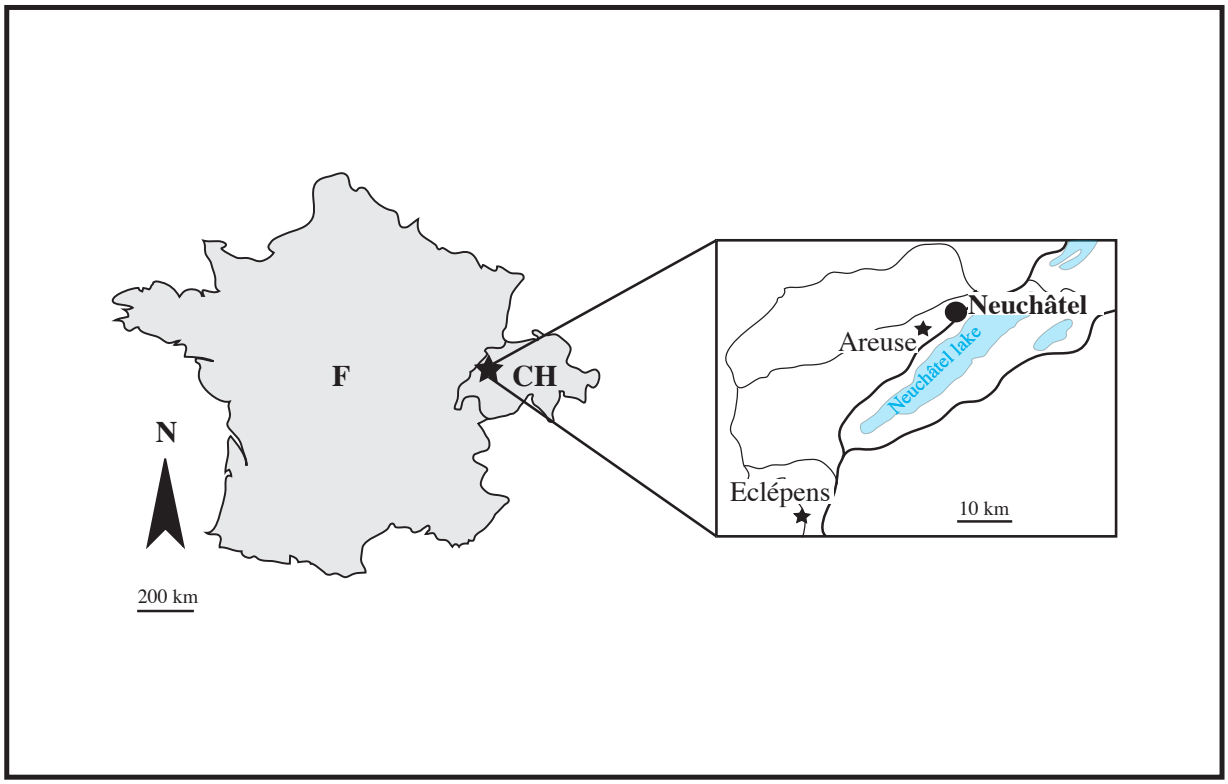

Fig. An.4.23: Location of the Areuse and Eclépens sections.

(*Gerhadtia sartousiana* ammonite zone).

2. On the other hand, Clavel *et al*. (1995) proposed that the sedimentation was continuous from the "Pierre Jaune de Neuchâtel" up to the "Urgonien Blanc". Thus, the "Urgonien Jaune" would belong to the late Hauterivian and the Hauterivian – Barremian boundary may fall within the "Urgonien Blanc".

During this first day of excursion, we will compare the historical succession around Neuchâtel between two sections:

At the Gorges de l'Areuse section (Fig. An.4.23):, we will observe how the sediments from the "Pierre Jaune de Neuchâtel" are arranged in shallowing upward parasequences. We will also discuss the evolution of clay minerals, in particular kaolinite. We will also see how difficult it is to separate the "Pierre Jaune de Neuchâtel" from the overlying "Urgonien Jaune".

At the Eclépens section (Holcim quarry of La Sarraz, canton of Vaud), the succession is more complete and developed than at the Gorges de l'Areuse; this will allow us to examine the "Urgonien Blanc" formation. Moreover, we will discuss of the sequence stratigraphic evolution (based on microfacies analysis) and on the clay mineral evolution. We will finally discuss the age of the "Urgonien Jaune" and "Urgonien Blanc", in view of kaolinite correlation, strontium isotopes stratigraphy, radiochronology and sequence stratigraphy.

An.4.3.2. First stop: Gorges de l'Areuse

An.4.3.2.1. Location

The Gorges de l'Areuse section is located in the village of Boudry, approximately 10 km to the southwest of Neuchâtel (Fig. An.4.23). The section follows the southern edge of the River Areuse beginning at the end of a pedestrian tunnel entering the Val-de-Travers.

An.4.3.2.2. Previous works

The section at the Gorges de l'Areuse, also named the Boudry section, was first studied by Zweidler (1985), then by Rumley in 1993. Finally, Blanc-Aletru in 1995 conducted a high-resolution

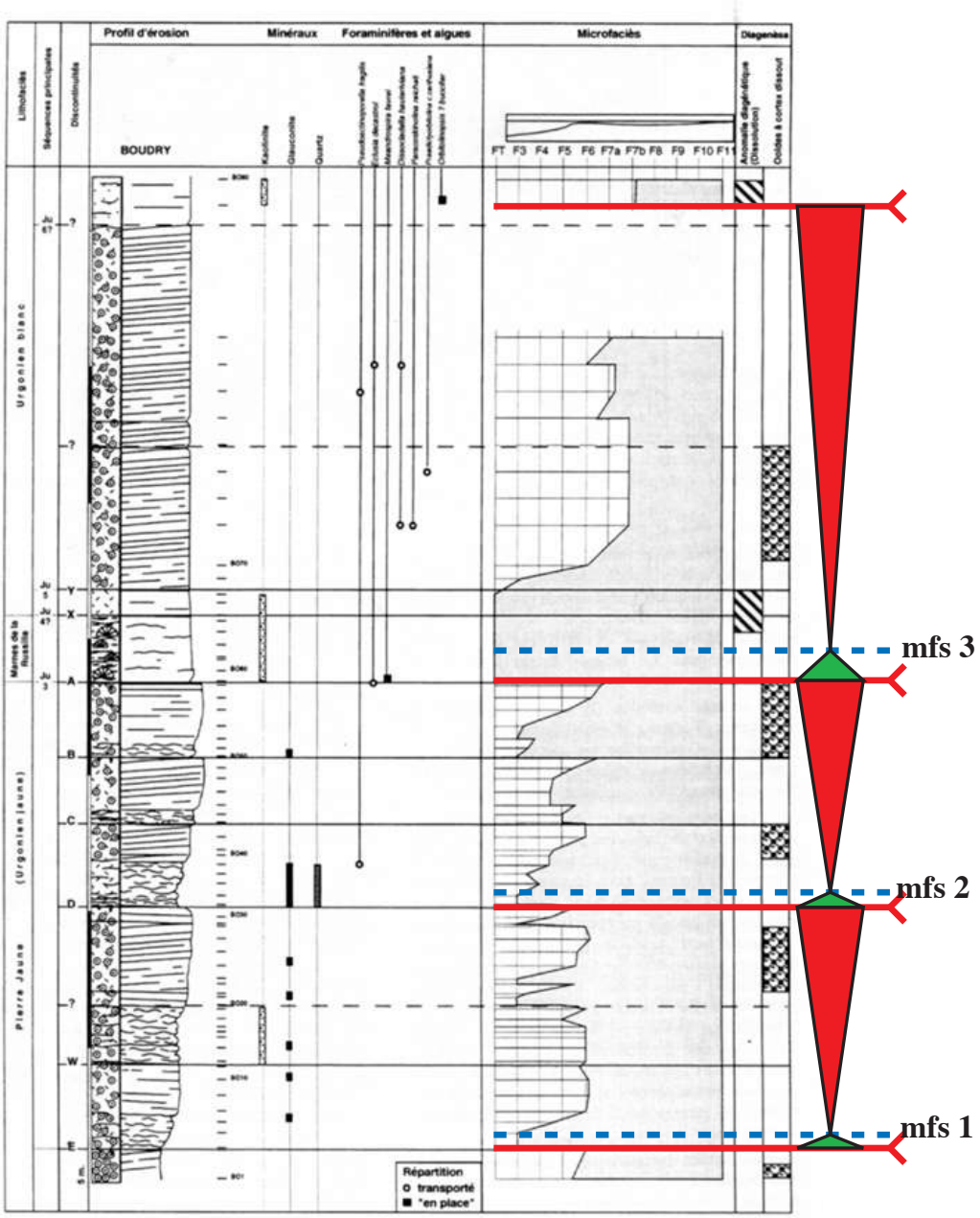

Fig. An.4.24: Profile, repartition of microfossils and microfacies of the Boudry section (after Blanc-Aletru, 1995). From the microfacies curve a sequence stratigraphic scheme is proposed.

study of the biostratigraphy (mainly orbitolinids), the mineralogy and the microfacies (Fig. An.4.24) of the Boudry section.

An.4.3.2.2.1. Description of the section at Boudry

Blanc-Aletru divided the section of Boudry into three main parts.

From the base to the discontinuity "A": this part of the section is composed of oobiopelsparites with much crinoids and bryozoans debris. The amount of quartz, glauconite and iron oxides varies, as do the rocks textures, which range from packstone to grainstone. In "E" and "D", Blanc-Aletru pointed out the presence of perforated surfaces. Unfortunately, Blanc-Aletru did not exactly locate the boundary between the "Pierre Jaune de Neuchâtel" and the "Urgonien Jaune".

Between the discontinuities "A" and "Y": from the discontinuity "A" upward, a major change in the sedimentation occurred as mudstones rich in corals remains and other bioclasts replace the oolitic grainstones. This facies is associated to the "Marnes de la Russille". Blanc-Aletru attributed the discontinuity "A" to

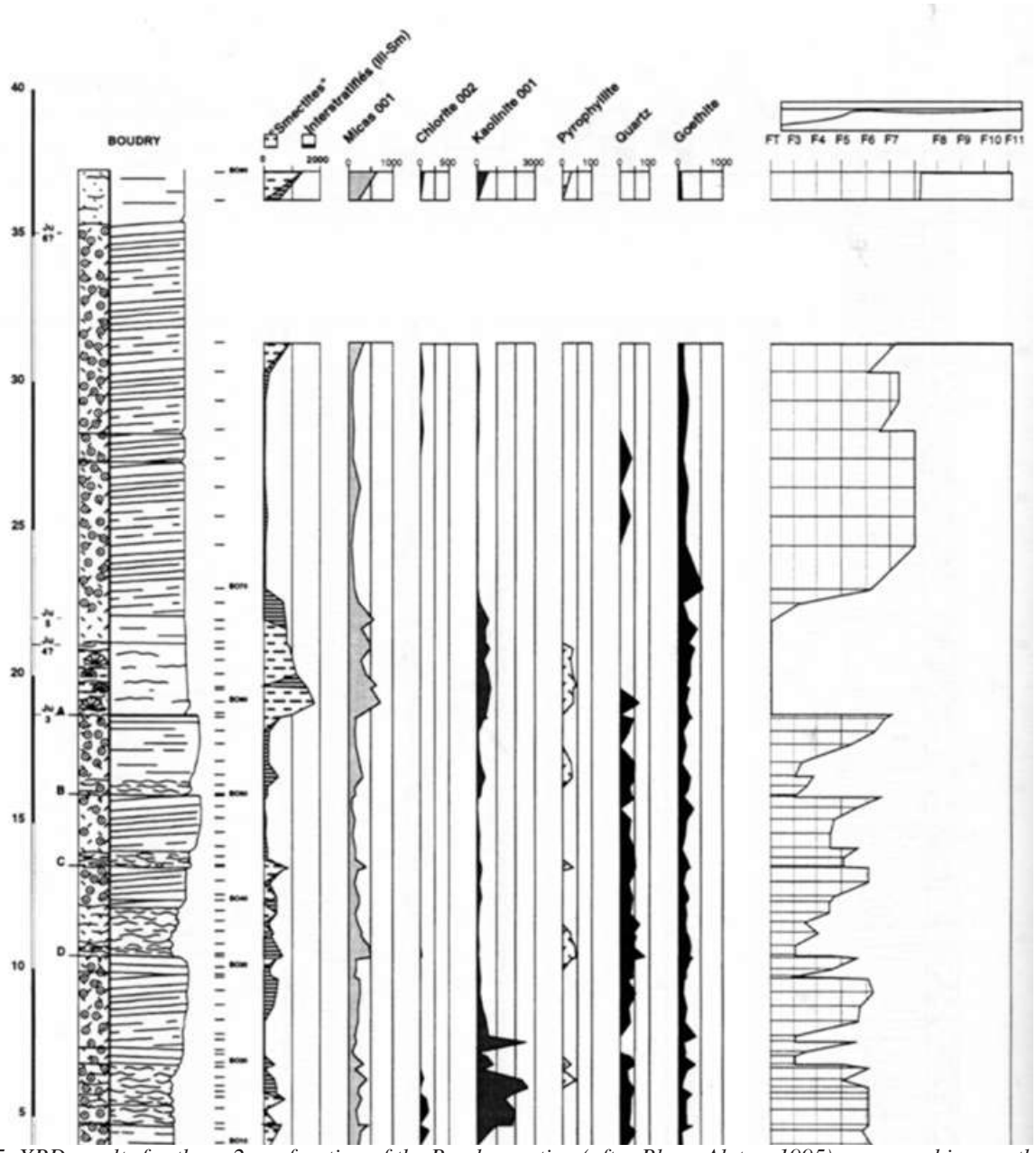

Fig. An.4.25: XRD results for the < 2 µm fraction of the Boudry section (after Blanc-Aletru, 1995), expressed in cps; the microfacies curve is reported on the right.

a major sequence boundary (Ju3 in her sequence stratigraphy scheme), and she observed the presence of bioclastic infill with orbitolinids in "X". Dissolution features observed under "Y" led Blanc-Aletru to deduce the presence of a major sequence boundary (Ju5).

From "Y" to the top: the last part of the section is mainly composed of oobiosparites rich in fragments typical of the internal part of the platform, such as micritised debris and bioclasts. The presence of important intergranular dissolution features, vadose silts and of oxidation could be the consequence of a final sequence boundary occurring at 35 m depth (Ju6 ? after Blanc-Aletru).

An.4.3.2.2.2. Microfacies and sequence stratigraphy of the Boudry section

Based on the presence or absence of micrite, on the type of clasts or lithoclats observed in thin section, Arnaud-Vanneau (1980) defined twelve microfacies (from F0 to F11), which are distributed from pelagic settings to supratidal environments. In the Western Swiss Jura, Blanc-Aletru (1995) recognized the following microfacies (Fig. An.4.26):

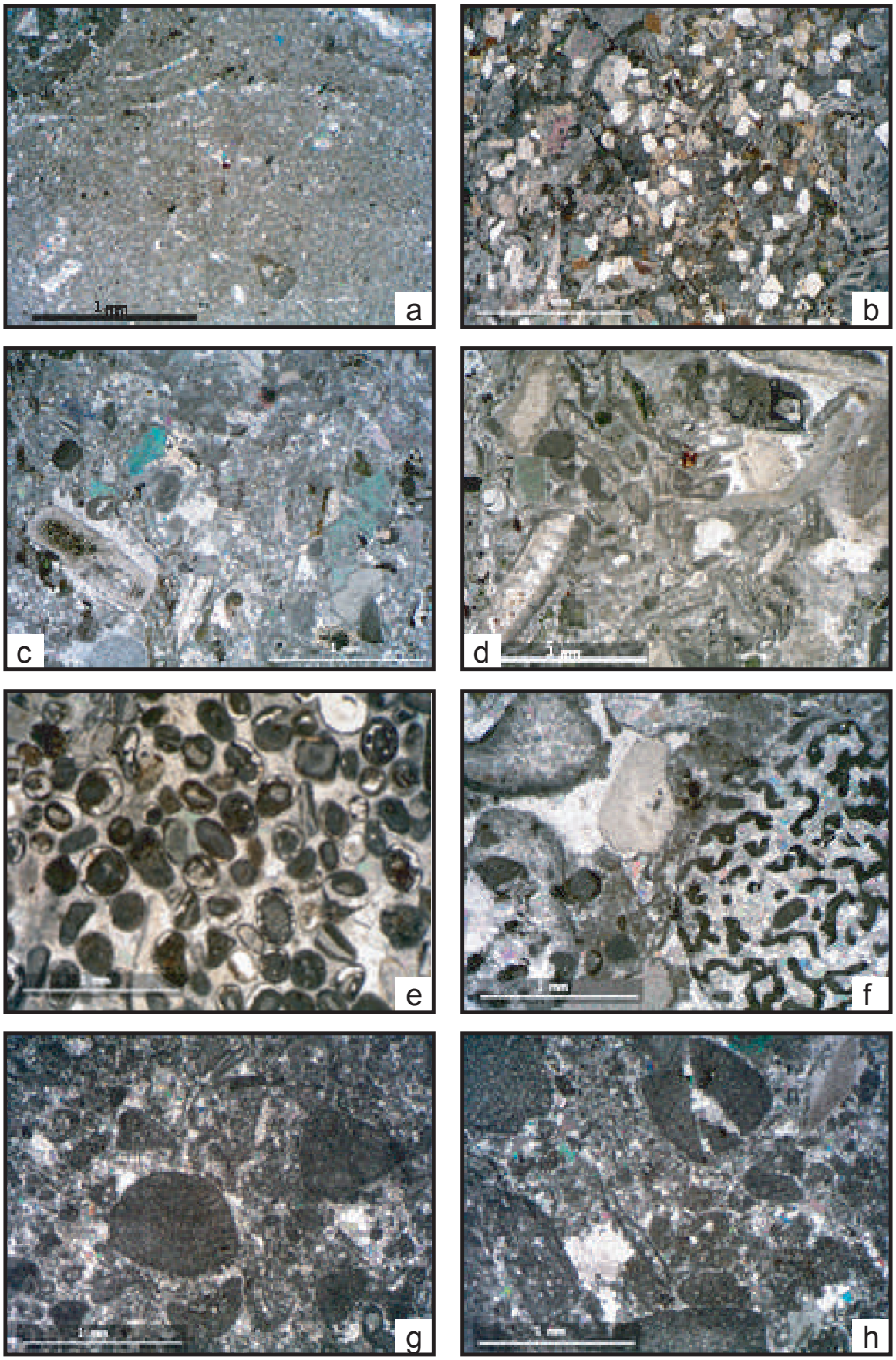

Fig. An.4.26: Micrographs of the microfacies recognized in the studied sections (scale bar: 1 mm). **(a) FT:** *biomicrite with spicules of sponges and cnidarians;* **(b) F3:** *biopelsparite with crinoid remains and small foraminifera;* **(c) F4:** *biosparite and biomicrite with crinoids and bryozoans;* **(d) F5:** *biosparite with large subspherical bioclasts;* **(e) F6:** *oosparite (note the presence of oomoldic porosity on this picture; sample EC$_{II}$50, Eclépens);* **(f) F7:** *biosparite and biomicrite with cnidarians and corals build-up;* **(g and h) F8:** *biosparite and biomicrite with large foraminifera and large rudists.*

- **FT:** biomicrite with spicules of sponges and cnidarians. FT microfacies were deposited in calm environments, under the wave base. When present, the corals can be encrusted by bryozoans or other faunas, such as foraminifera. Iron nodules are recognized in thin section.

- **F3:** biopelsparite with crinoidal remains and small foraminifera deposited in deep environments of the outer platform.

- **F4:** biosparite and biomicrite with crinoids and bryzoans. Whereas such facies are rare on the extern slope of standard platform, they are relatively common on drowned platforms.

- **F5:** biosparite with big subspherical remains. They characterize infralittoral domains with constant hydrodynamism, but also circalittoral regions where the deposits are the results of storm currents.

- **F6:** oosparite. Oolitic deposits are found in shallow water environments where tidal currents are dominant.

- **F7:** biosparites and biomicrites with cnidarians and corals build-up. Such microfacies are characteristic of the platform border, and can be deposited in infralittoral domains with low hydrodynamism where the build-up are preserved, or in high-energy infralittoral environments. In this later case, the F7 microfacies would correspond to the breaking-up of reefs.

- **F8:** biosparites and biomicrites with big foraminifera and big rudists. These facies were deposited in relatively calm environments where sand, muddy sand or mud can settle.

The Boudry section can be split into three 3rd order sequences, each of them being delimited by two sequence boundaries:

The discontinuities “E” and “D” are both characterized by perforations. Morover, F6 microfacies with oomoldic porosity were observed by Blanc-Aletru, so these surface are interpreted as sequence boundaries. Just above “E”, the microfacies curve displays a sharp shift toward FT microfacies, which may correspond to a maximum flooding surface (mfs 1). Consequently, the first meter above “E” and the interval between the mfs 1 and “D” may reflect a transgressive system track (TST) and a highstand system track (HST), respectively.

The microfacies curve indicates a next sequence boundary maybe located at the base of the “Marnes de la Russille” (Ju3 after Blanc-Aletru). This is labelled as the “D” discontinuity. Both perforations and dissolution of the oolites cortex are recovered in Ju3. Regarding the microfacies curve, FT microfacies are observed in a marly interval just after “D”; they are interpreted as a mfs 2. So, the same scheme than between “E” and “D” is recognized, with a TST from “D” to the mfs 2 and a HST from the mfs 2 to the Ju3. However, high frequency microfacies variations observed in this interval may correspond to parasequences and consequently are not discussed in this paragraph (see paragraph 2.3.2.).

Finally, FT microfacies are again present at 5 meters just above Ju3; consequently, the “Marnes de la Russille” are interpreted as a mfs 3. Then, microfacies shift toward F6/F7 in the “Urgonien Blanc”. At the top of the section, clues for the presence of the sequence boundary are noted by Blanc-Aletru (see paragraph 2.2.1.). Consequently, a TST is defined between Ju3 and the mfs 3 whereas the end of the section may reflect a HST.

An.4.3.2.2.3. Mineralogy of the Boudry section

In the Boudry section (Fig. An.4.25), the main clay minerals of the <2μm fraction are smectite, irregular illite smectite mixed-layers, mica, chlorite, kaolinite and pyrophyllite. Small amounts of quartz and goethite are also present.

Mica is present all along the section, whereas the smectite and kaolinite have an antagonistic behaviour. Smectite is present in the 7 first meters of the section, between 12 and 14 m and in the “Marnes de la Russille”. On the contrary,

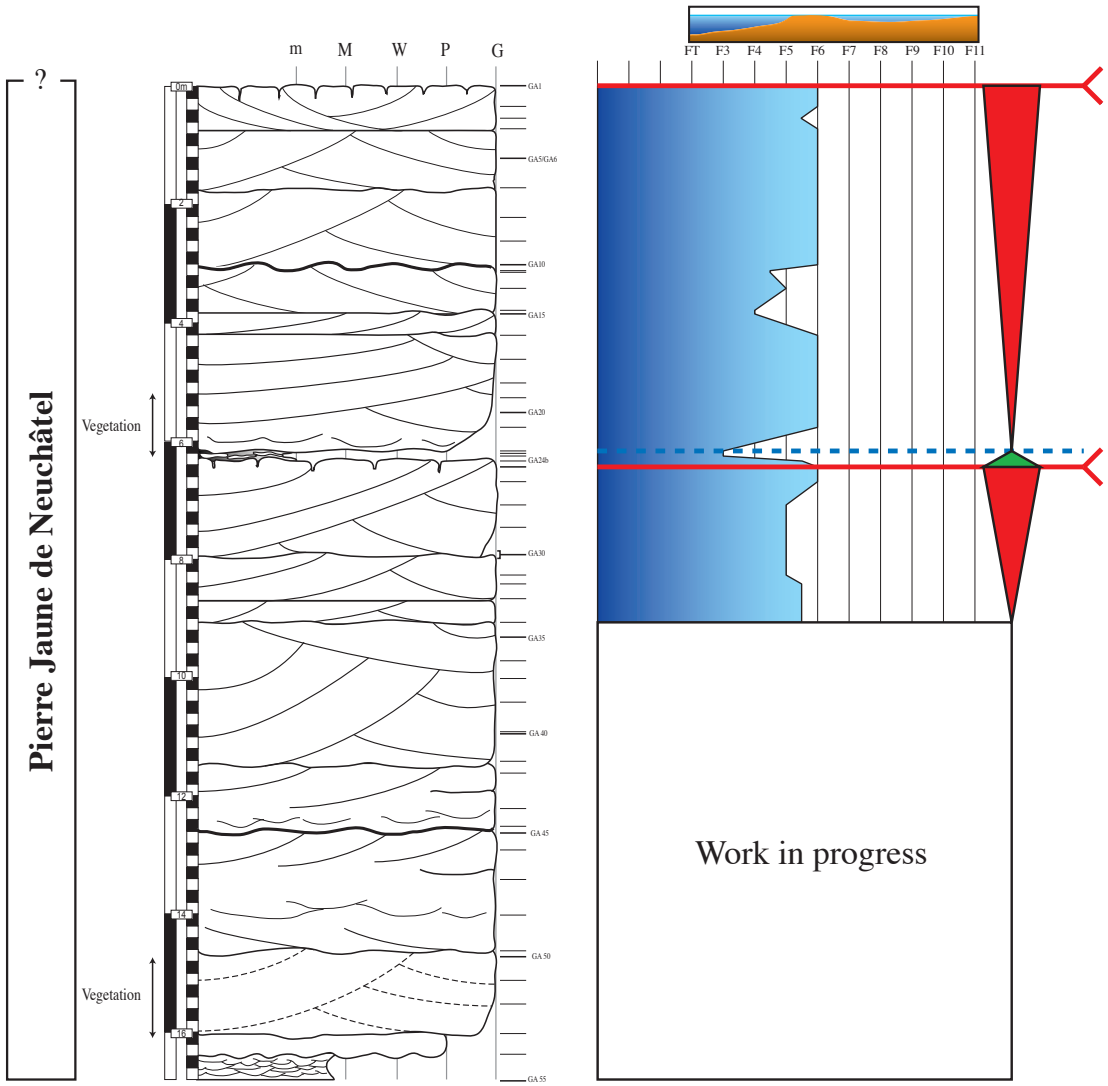

Fig. An.4.27: Microfacies evolution for the Gorges de l'Areuse section (base of the Boudry section).

the kaolinite is present in the whole part of the section, with significant increases between "E" and "D" and in the "Marnes de la Russille" and finally decreases in the "Urgonien Blanc".

An.4.3.2.3. The "Pierre Jaune de Neuchâtel" – "Urgonien Jaune" transition

As shown by Zweidler (1985) and by Blanc-Aletru (1995), the transition between the "Pierre Jaune de Neuchâtel" and the "Urgonien Jaune" is often difficult to recognize in the field, as the facies of both formations are very similar. In the Boudry section, several perforated and erosive surfaces were described in the "Pierre Jaune de Neuchâtel" by these authors.

We propose a high-resolution study on a 16 m thick section and to try to define the boundary between the "Pierre Jaune de Neuchâtel" and the "Urgonien Jaune" with respect to sequence stratigraphy and mineralogy. This section will be called the Gorges de l'Areuse section in the following paragraphs.

An.4.3.2.3.1 Description of the section

The major part of the Gorges de l'Areuse section is composed of oolitic grainstones organised in beds with cross stratifications, which are usually easily recognizable (Fig. An.4.27). In the top of the section, the good quality of the outcrop allows the definition of a basic model.

At 6.40 m, an erosive surface with burrows is described, the laminations of the lower bank displaying toplap features. On this surface, which may corresponds to the discontinuity "ER" of Blanc-Aletru (1995), a marly interval (about 10 cm) contains some bioclastic pebbles. At 6 m

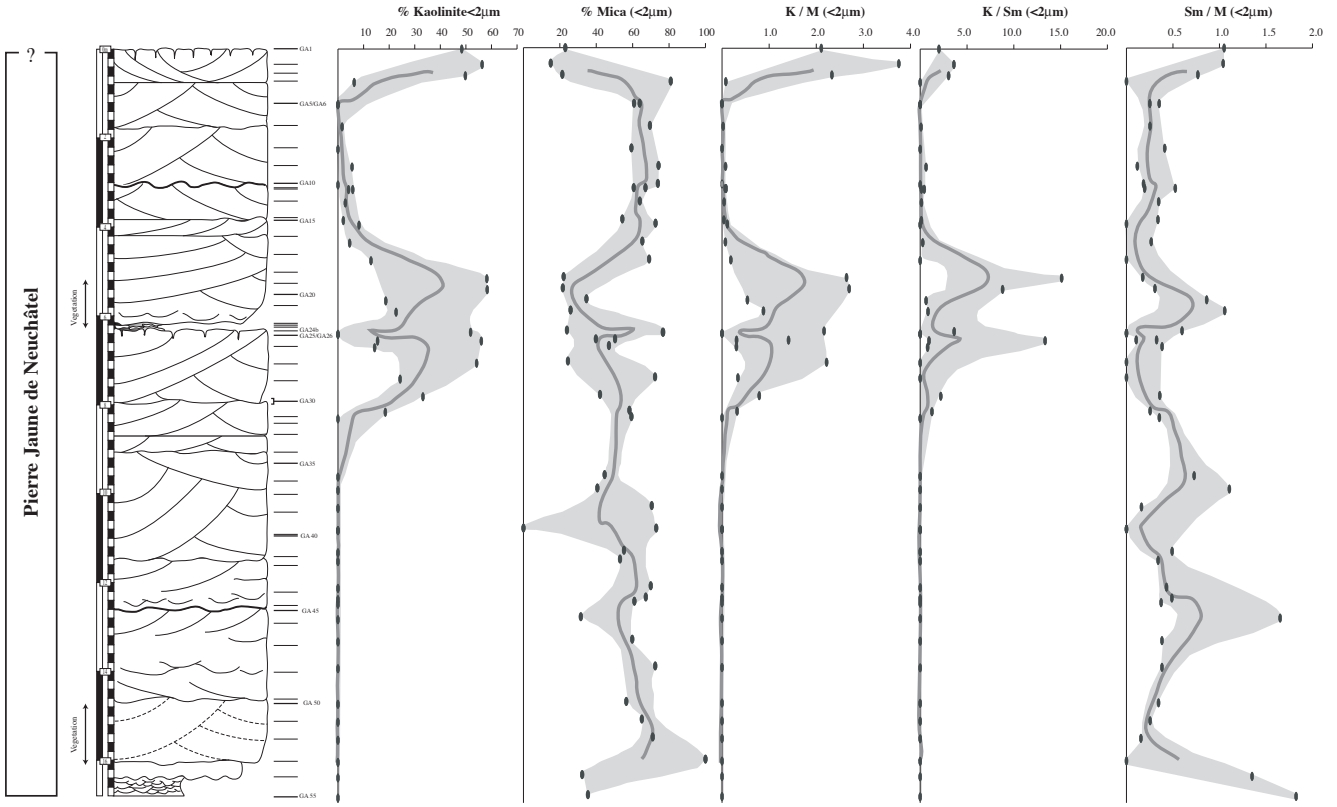

Fig. An.4.28: XRD results for the < 2 µm fraction of the Gorges de l'Areuse section, expressed in relative percents or in cps ratio.

depth, clues for channels were found. Upwards, oolithic banks are present in the following 3 meters. At 3 m depth, a very thin clay layer (less than 5 cm) separates a grainstone with oolites, crinoids, glauconite and some burrows (sample GA 11) from a packestone / grainstones with oolites and bioclastes (sample GA10). Above this, 3 meters of oolitic grainstones are exposed. Finally, a major discontinuity is observed at the top of that part of the section. This erosive surface is perforated erosive overlaid by a conglomerate with a marly matrix.

This kind of succession is repeated in the bottom of the section almost two times, with marly or clayey intervals more or less well-expressed. The section ends in a little depression, where the last bank of oolitic grainstone with cross stratifications surmounts a 50 cm thick interval of marl.

An.4.3.2.3.2. Microfacies and sequence stratigraphy

Thirty six thin sections were analysed in order to determine the main microfacies that occurred in the upper part of the Gorges de l'Areuse section. The results are shown on the Fig. An.4.27. The microfacies range from the F3 to the F6 microfacies (Fig. An.4.26) of Arnaud – Vanneau (1980).

From the determination of the microfacies, a sequence stratigraphical interpretation can be proposed, from base to top.

- From 9.10 m (GA 34) to 6.40 m (GA 25): the evolution of the microfacies is shallowing upward, from F5 to F6. At 6.50 m, the erosive and perforated surface marks a parasequence boundary. In thin section, some oolites cortexes show traces of dissolution (oomoldic porosity). This interval corresponds to a highstand deposits.

- From 6.50 m to 6.20 m (GA 22): the F3 microfacies dominates, implying the presence of a flooding surface. This interval corresponds to transgressive

deposits.

- From 6.20 m to 3.10 m (GA 10 / GA 11): here again, the evolution of the microfacies is shallowing upward, and thin section from the sample GA11 displays dissolution features and recristallisation characteristic of a parasequence boundary. This interval corresponds to highstand deposits.

- From 3.10 m to the top (GA1): except the very thin clay layer described between GA10 and GA11, the microfacies display a general shallowing upward evolution. As previously said (see 2.2), the top of the section is characterized by an erosive and perforated surface, which is interpreted as a parasequence boundary whereas the clay level at 3.10 m could represent a flooding surface. So, the last 3 m of the section represents a complete parasequence with a small interval of transgressive deposits and plurimetric thick highstand deposits.

An.4.3.2.3.3. Mineralogy

The composition of the clay mineral assemblage was determined by X-ray diffractometry on a Scintag XDS 2000 at the Institute of Geology, University of Neuchâtel. The samples were decarbonated by hydrochloric acid digestion using the method described by Kübler (1987). Air-dried (<2μm and 2-16μm fractions) preparations were analysed, as well as glycol saturated preparations (<2μm) in order to determine swelling minerals. Here we present the most important results of the <2μm fraction (Fig. An.4.28).

Mica, kaolinite, smectite, illite-smectite mixed-layers and chlorite were recognized, as well as quartz, pyrite, goethite, potassic feldspar and Na-plagioclase. The kaolinite is not present in the first 8 m of the section and appears abruptly just below the erosive contact observed at 8m (GA30). Then, the kaolinite curve displays a maximum between 4 and 8 meters depth, with a negative peak corresponding to the marly interval at 6 m depth (GA24). Upwards, the section is rather characterized by low contents of kaolinite, the uppermost part excepted, which shows a rapid increase in kaolinite values.

This striking behaviour of the kaolinite is also pointed out by the kaolinite / mica and kaolinite / smectite ratios curves, that show the same maximum between 6 and 8 meters whereas these ratios are close to zero is the rest of the section. Finally, the low values of the smectite / mica ratio (< 1) leads us to conclude that the mica is the main mineral of the clay assemblage, more particularly in the lower part of the section. The kaolinite appearance near the top of the Pierre Jaune is correlatable event over a large area (see section 4.3).

The clay minerals evolution reflects a drastic change between a climate with well-marked seasons, characterized by dominance of the smectite, toward intertropical conditions under kaolinite is produced (see paragraph 3.2.3. for more details).

An.4.3.3. Second stop: Eclépens (Holcim quarry)

An.4.3.3.1. Location

The section of Eclépens crops out in the cement quarry of la Sarraz exploited by Holcim, at 60 km SW of Neuchâtel (Fig. An.4.23). Due to the industrial exploitation of the quarry, the outcrop is very fresh and of a good quality.

An.4.3.3.2. The "Pierre Jaune de Neuchâtel" – "Urgonien Blanc" succession at Eclépens

An.4.3.3.2.1. Description of the section

The Eclépens section is composed of two sub-sections, each measuring more than 50 m. Combining these two parts, the composite section reaches 92 m in thickness (Fig. An.4.29).

The base of the section is situated in the lowermost part of the quarry and begins with 8 m of oolitic grainstones with some flintstones nodules or lenses. At 8 m a glauconitic hardground with oysters and burrows is surmounted by a yellow to reddish marly layer rich in glauconite and with some brachiopods (20 cm), and by a 15 cm thick layer of black marls with bivalves (Panopées);

this interval is thought to be an equivalent of the "Marnes d'Uttins", but ammonite findings are needed to confirm this hypothesis.

Above the black marls, there is a 2 meters thick black packestone to grainstone rich in bivalves and brachiopods. Above, oolitic sedimentation begins again, with relatively well-marked oblique stratification. This type of facies is attributed to the upper (?) "Pierre Jaune de Neuchâtel". At 37 m depth, the glauconite content increases as well as the presence of marly intervals between the oolitic banks. This interval (between the samples $EC_{II}53$ and $EC_{II}58$) is also characterized by the presence of some kind of channels within the oolitic packestone banks. Then, the clay content seems to decrease rapidly, and at 40 m depth, the facies are similar to that recognized in the lower part of the section. Some changes occur at 45 m depth ($EC_{II}72$) with the appearance of a black and massive bank, similar to the one described above the "Marnes d'Uttins equivalent". About 5 meters of bioclastic packestone to grainstone with oolites and glauconite alternating with marly intervals separate this black level from a second one which marks the end of the first part of the Eclépens section, and which can be used to correlate the two studied parts of the quarry. After Blanc-Aletru (1995), the base of this second black bank is erosive, and thus interpreted as a sequence boundary (Ju2 in Blanc-Aletru, 1995).

The upper part of the Eclépens quarry was studied by Blanc-Aletru in 1995; in particular, the repartition of the microfaunas is shown in Fig. An.4.30. She proposed a threefold division:

- From 50 to 71 m: oolitic facies characteristic of the "Pierre Jaune de Neuchâtel" are recognized, but they may belong to the "Urgonien Jaune". Effectively, the transition between the "Pierre Jaune de Neuchâtel" and the "Urgonien Jaune" is sometimes hard to recognized on macroscopic samples. At 71 m, Blanc-Aletru (1995) remarked the presence of dissolution in the cortex of the oolites and of an erosive surface, interpreted as a sequence boundary (Ju3 after Blanc-Aletru, 1995).
- From 71 to 83 m, Blanc-Aletru described three subsets:
- From 71 to 76 m, some mudstones to wackestones with corals fragments, transported foraminifera (with some orbitolinids) and algae, calcareous sponges.
- From 76 to 80 m, a transition from bio-ooclastic facies at the base to oolitic grainstones with dissolution of the cortex at the top which would be the consequence of a major discontinuity (Ju5 in Blanc-Aletru, 1995).
- From 80 to 83 m, the facies is similar to the one described between 71 and 76 m. Blanc-Aletru (1995) attributed these deposits to the "Marnes de la Russille".
- From 83 to 92 m (top of the section): the facies change from a wackestone to packestone rich in foraminifera, particularly in orbitolinids (between 83 and 90 m), toward a rudists-bearing facies (90 to 92 m). The presence of karsts is noted in this part of the section.

An.4.3.3.2.2. Microfacies and sequence stratigraphy

The microfacies recognized in thin sections from the Eclépens section are relatively similar to the ones described in the paragraph 2.3. The main difference is the appearance of microfacies typical of the internal part of the platform.

Based on the microfacies evolution a sequence stratigraphic scheme can be proposed. Only the 3rd order sequences are taken into consideration (Fig. An.4.29).

- From the base of the section to 8 m: the microfacies range from F4 to F5, describing a shallowing upward evolution and ending with a hardground with many glauconite and oysters, which may correspond to a sequence boundary. Thus, this interval is attributed to a highstand system track (HST).

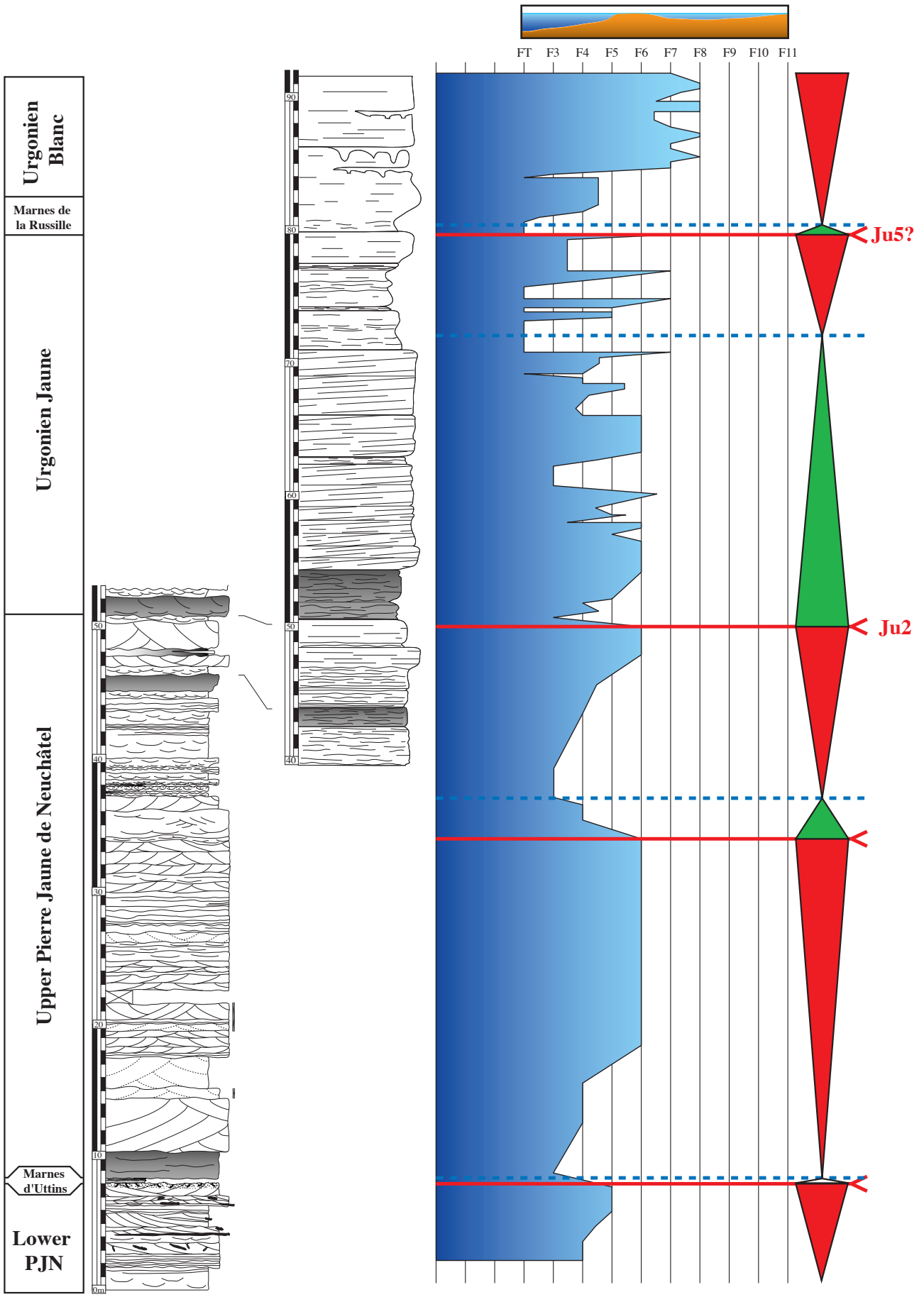

Fig. An.4.29: Microfacies and sequence stratigraphic interpretation of the Eclépens section. The upper part (on the right) is after Blanc-Aletru (1995; see Fig. An.4.25 for more details) and the lower part (on the left) is from this study.

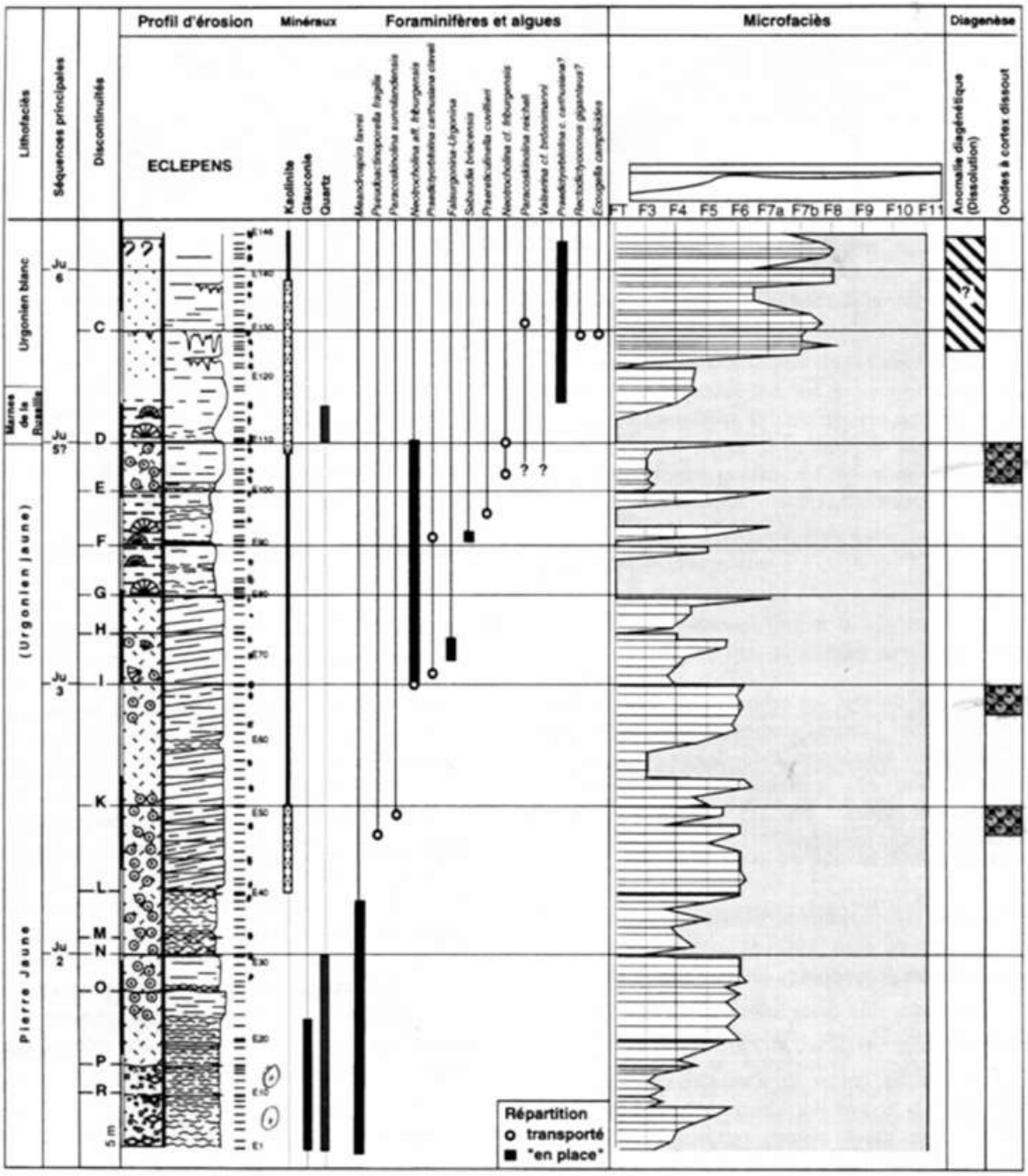

Fig. An.4.30: Profile, repartition of microfossils and microfacies of the upper part of the Eclépens section (after Blanc-Aletru, 1995).

- From 8 to 8.4 m: F5 to F3. The marly interval, which is supposed to be an equivalent of the "Marnes d'Uttins", may correspond to a maximum flooding surface (mfs), so this interval should be a transgressive system track (TST).

- From 8.4 to 34.5 m: the microfacies shift from F3 to F4 (at about 12m), then rapidly from F4 to F6 (between 15.5 and 18 m). Then, F6 microfacies are recognized until 34.5 m. This shallowing upward evolution should correspond to a HST that lasts until a sequence boundary pointed out by erosive features such as reworking and channels.

- From 34.5 to 37.8 m: the evolution is deepening upward, from F6 to F3. Consequently, the marly and glauconitic layers previously described (cf. paragraph 3.2) should correspond to a mfs and this

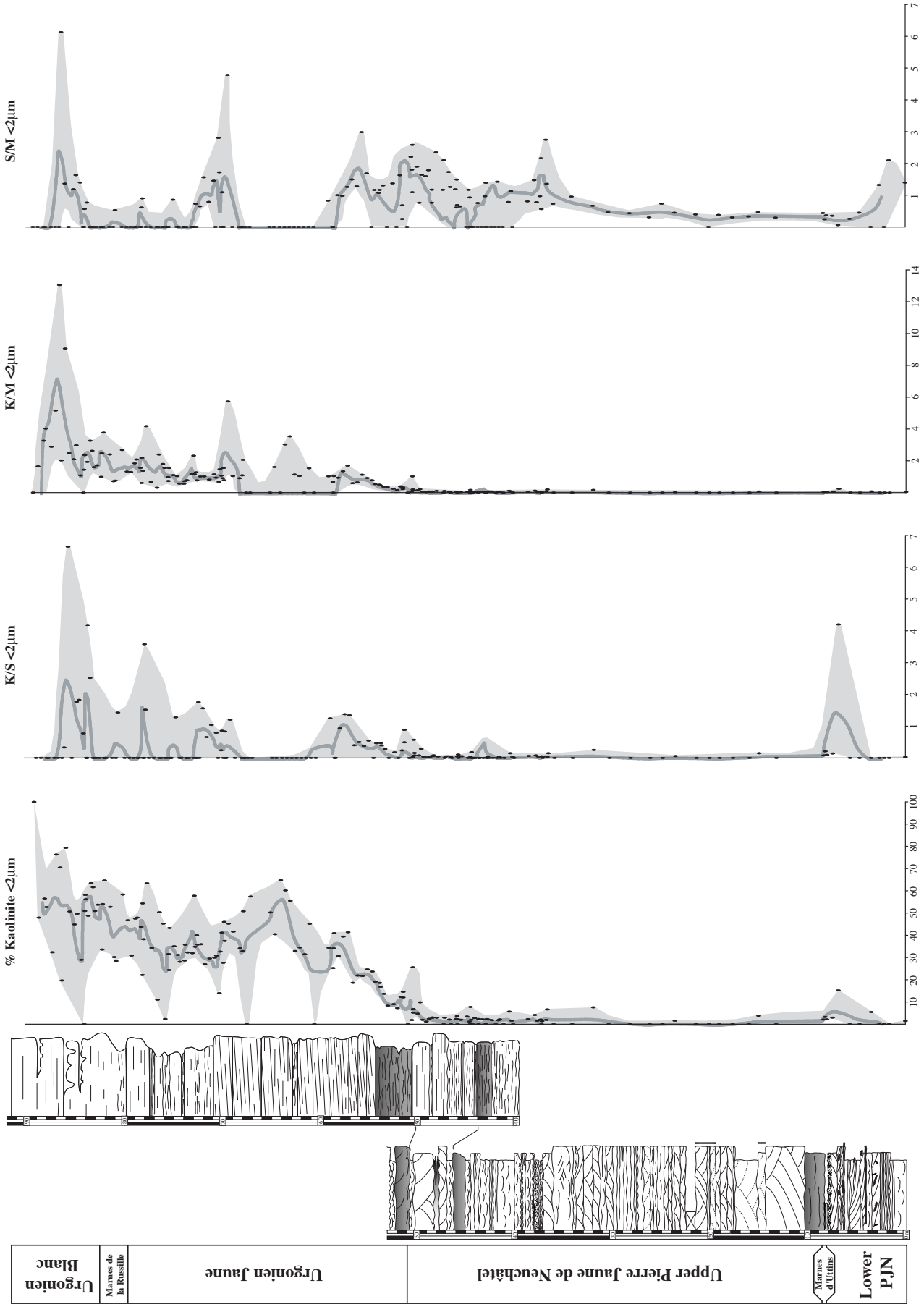

Fig. An.4.31: Kaolinite contents for the < 2 µm fraction for the Eclépens section (upper part after Blanc-Aletru, 1995) expressed in relative percents. Kaolinite / smectite, kaolinite / mica and smectite / mica ratios curves are also reported.

interval to a TST.

- From 37.8 to 50 m: the microfacies evolve gently from F3 to F6 in a two steps fashion, with an acceleration of the evolution at approximately 45 m. This deepening upward progression may be related to a HST. At 50 m, reworking occurs, in particular pebbles with oysters were found. This surface is interpreted as a major sequence boundary (Ju2 in Blanc-Aletru, 1995).

- From 50 to 72.5 m: in detail, the microfacies curve displays high frequency changes from F3 to F7, but the general trend is a deepening upward evolution from F6 to FT microfacies. The high-frequency variations should be related to parasequence deposits. The FT microfacies should mark the mfs, and consequently this interval corresponds to a TST.

- From 72.5 to 80 m: the shallowing upward evolution of the microfacies curve led us to conclude to the presence of a HST, which ends with a sequence boundary marked by the dissolution of oolites cortex (Ju5 in Blanc-Aletru sequence stratigraphy scheme).

- From 80 to 83 m: the "Marnes de la Russille" display FT microfacies and correspond to a mfs. Thus, this small interval could be related to a TST.

- From 83 m to the top: the microfacies curve shows a general shallowing upward trend. At approximately 91.5 m, Blanc-Aletru described an emersive surface with microkarstification, which is interpreted as the sequence boundary Ju6. The presence of karsts in this part of the "Urgonien Blanc" supports this statement. This last part of the section should therefore correspond to a HST.

An.4.3.3.2.3. Mineralogy

At Eclépens, the <2μm clay minerals association is composed of mica, kaolinite, smectite, illite-smectite mixed-layers and chlorite, with mean values of 38, 22.6, 20.2, 14.9 and 4.2 %, respectively. Relative abundance of kaolinite, the kaolinite / smectite, kaolinite / mica and smectite / mica ratios are presented in Fig. An.4.31.

The entire "Pierre Jaune de Neuchâtel" is characterized by the absence of the kaolinite, whereas the smectite / mica ratio reaches values of about 1. Then, from 50 m upward, the kaolinite content increases, with values attaining almost 50% in the upper part of the section. In the same interval, the kaolinite / mica ratio is above 2, so the kaolinite is the dominant mineral of the clay mineral assemblage in the "Urgonien Jaune" and the "Urgonien Blanc". This conclusion is also supported by kaolinite / smectite ratio with values above 2.

This rapid and drastic change in the main clay mineral type can be interpreted in terms of climate changes. Normally clay minerals are formed on continents and the type on clay being accumulated is dependent on the regional climate regime (principally on the rate of hydrolysis) and on the kind of rock that is being altered. The kaolinite is preferentially formed under hot and wet conditions, such under inter-tropical climate. On the other hand, smectite is generated under drier conditions, and its formation happens primarily under climate with well-marked seasons. So, it seems that between the time of deposition of the "Pierre Jaune de Neuchâtel" and of the "Urgonien Jaune" and "Urgonien Blanc", the climate shifted from a relatively dry and seasonal climate, under which the mechanic erosion of land masses was predominant, toward inter-tropical conditions which favoured hydrolysis and thus the formation of kaolinite-rich soils. The later would enrich the oceanic sediments after erosion and transport to the basin.

An.4.3.4. Dating the Urgonian Limestones from the Neuchâtel area

An.4.3.4.1. Strontium isotopes

During the early Cretaceous, the oceanic $^{87}Sr/^{86}Sr$ curve fluctuates. In particular, this curve shows a maximum at about 0.707455 in the late Hauterivian, then a minimum at 0.707450 in

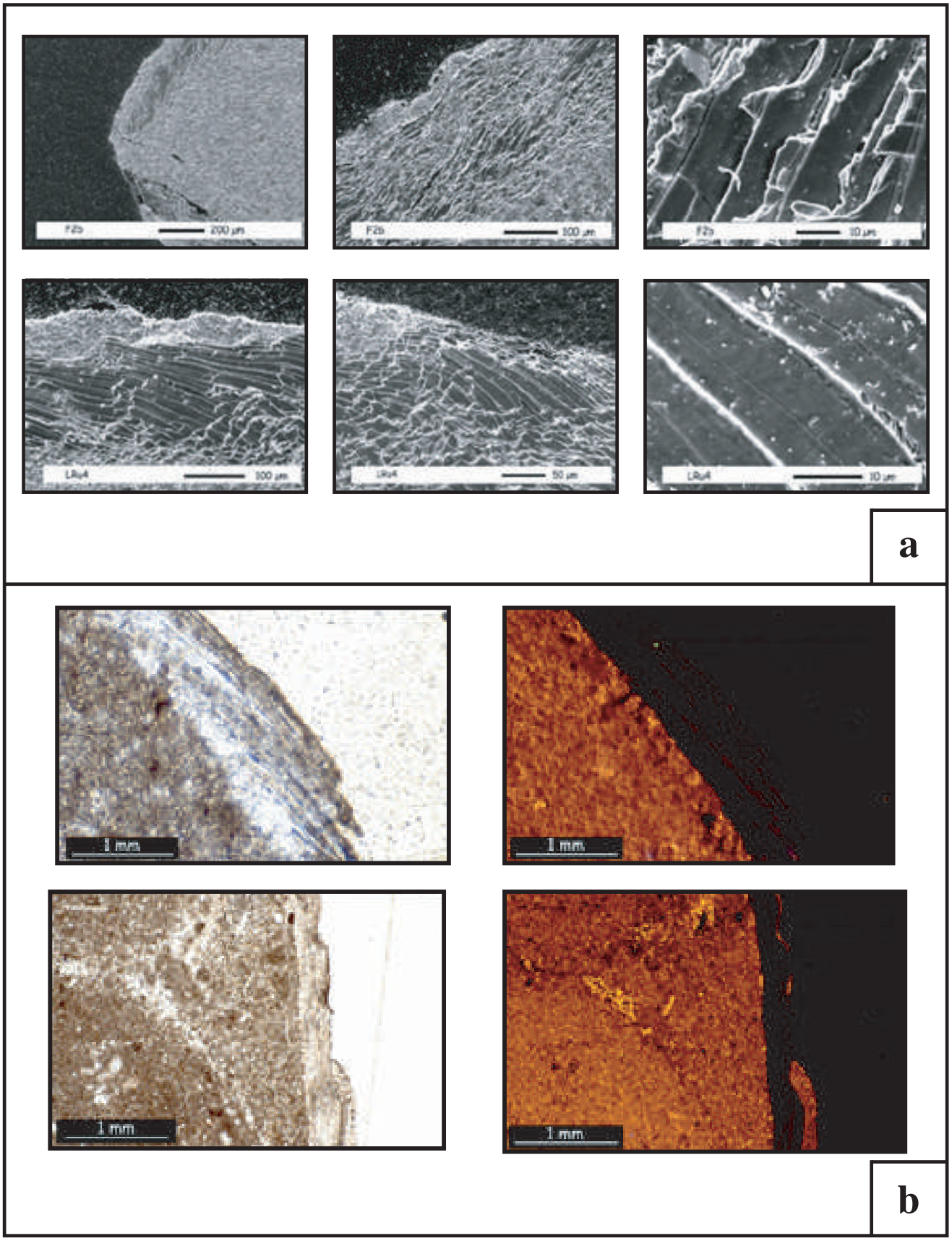

Fig. An.4.32: SEM **(a)** *and cathodoluminescence* **(b)** *observations of rhynchonellids shells; in* **(a)**, *the magnification increases to the right.*

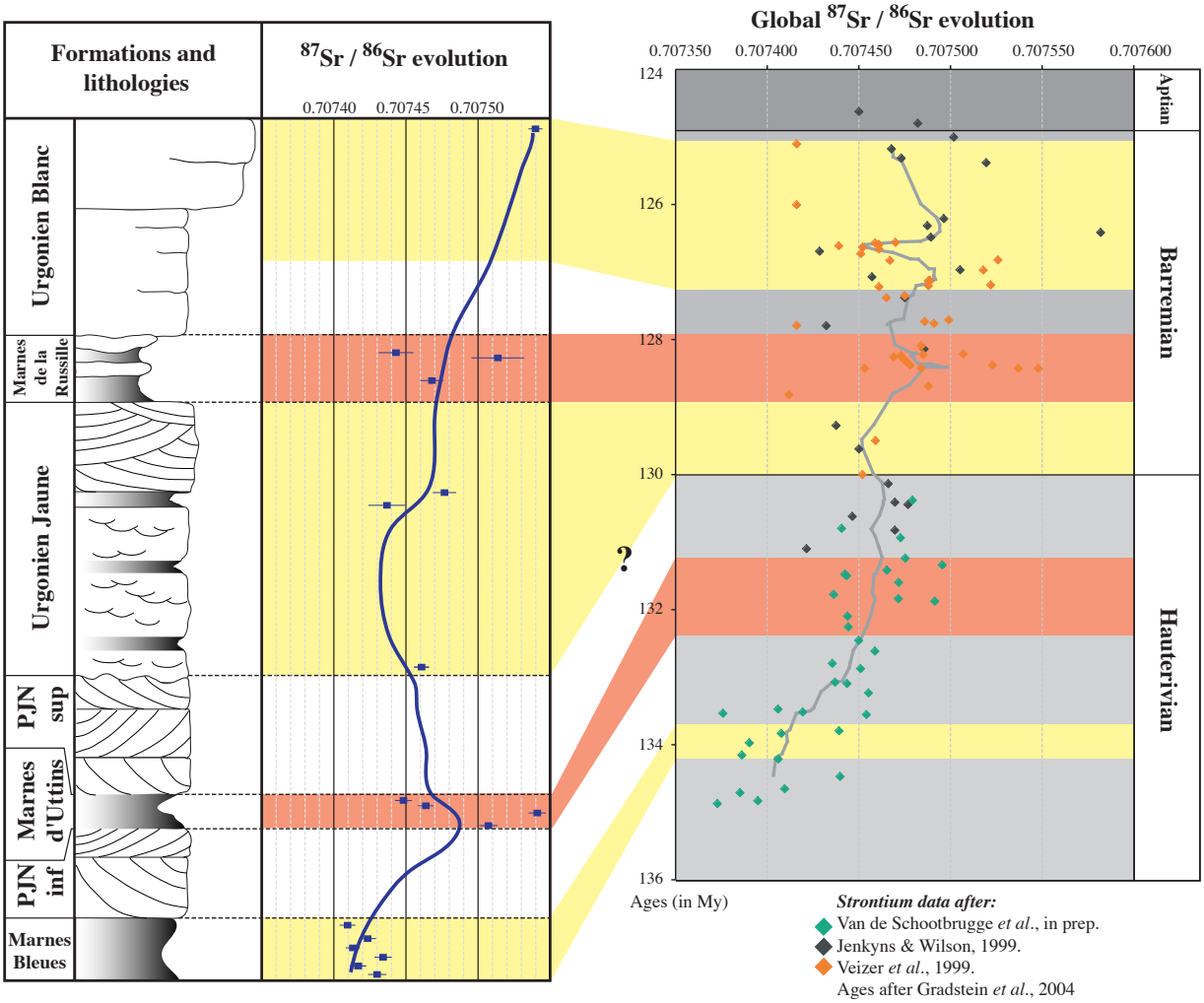

Fig. An.4.33: Comparison of the $^{87}Sr/^{86}Sr$ measured in rhynchonellids shells from the western Swiss Jura with the global oceanic $^{87}Sr/^{86}Sr$ curve. Note that doubts remains for brachiopods of the Urgonien Jaune.

the earliest Barremian. The whole part of the Barremian is characterized by values higher than 0.707455, reaching two maxima (higher than 0.707550) in the end of the early Barremian and in the late Barremian. $^{87}Sr/^{86}Sr$ values then decrease rapidly in the latest Barremian and in the early Aptian (Jenkyns and Wilson, 1999; Veizer *et al.*, 1999; van de Schootbrugge, 2001). With these developments it seems possible to attribute an age to the Urgonian limestones.

Recently $^{87}Sr/^{86}Sr$ isotope work has been carried out at the University of Neuchâtel in order to refine our age estimates. $^{87}Sr/^{86}Sr$ was measured on brachiopods shells (rhynchonellids). The diagenetic state was controlled by both Scannig Electronic Microscope (SEM) analysis and by cathodoluminescence prospecting.

- Regardless of magnification, SEM images (Fig. An.4.32a) show the preservation of the primary lamellar structure of the secondary layer of the rhynchonellids shells, which is supposed to be less sensitive to diagenetic changes (*e.g.* Voigt *et al.*, 2003).

- The secondary layer of all analysed brachiopods was not luminescent (Fig. An.4.32b), revealing no mineralogical change.

From that we conclude that the diagenesis had little or no impact on the isotopic composition of the analysed shells.

The results of the $^{87}Sr/^{86}Sr$ analysis are shown in Fig. An.4.33. Brachiopods from the “Marne Bleue d’Hauterive” and from “Marnes d’Uttins” display similar values to the ones obtained from

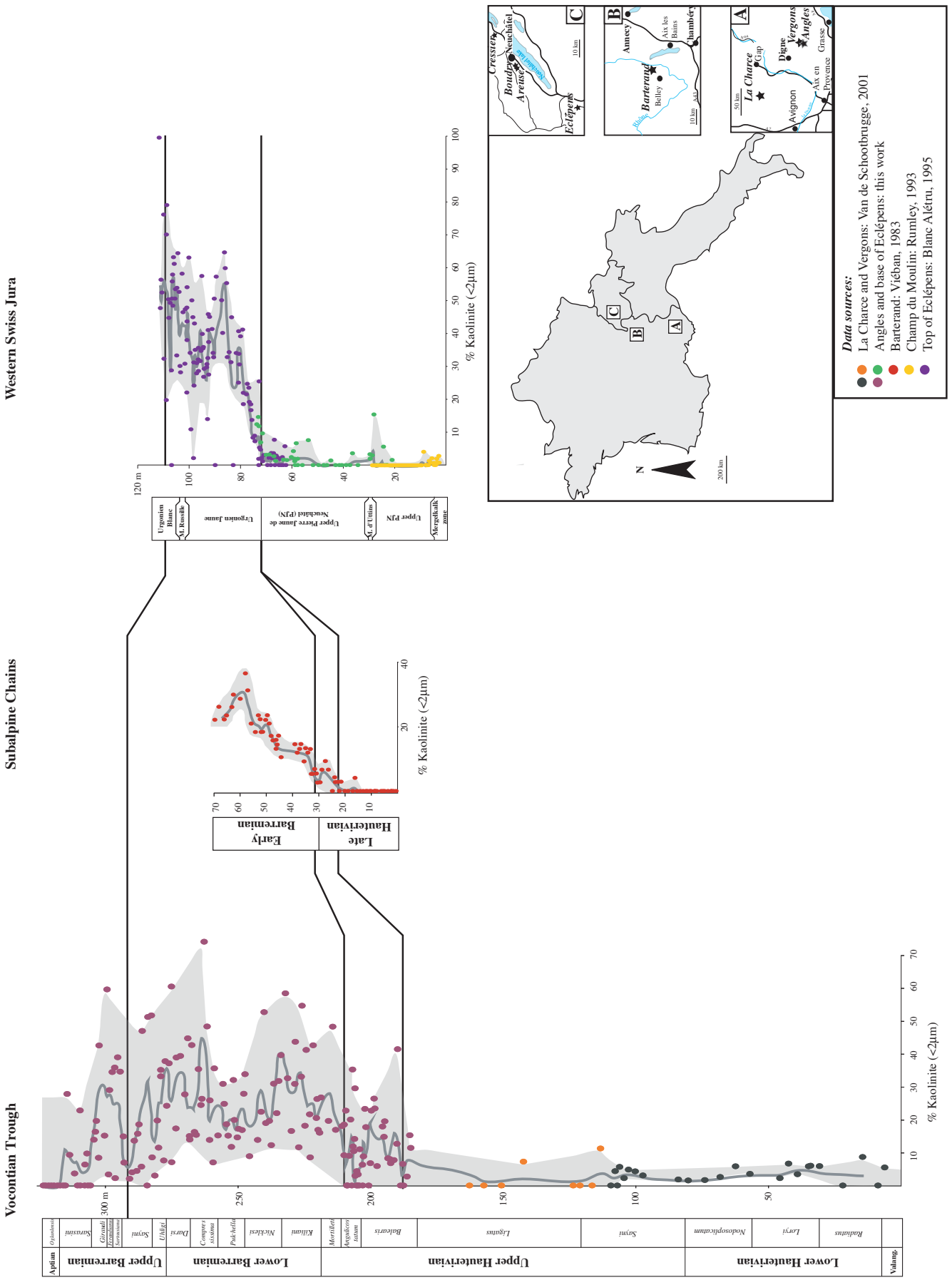

Fig. An.4.34: Comparison of the kaolinite (< 2 µm) evolution between the Neuchâtel area, the subalpine chains and the Vocontian trough. Note the same appearance of the kaolinite between the three domains, and the high values reached during the Barremian.

the base and middle parts of the Hauterivian, respectively, which is in agreement with the dating obtained by ammonite biostratigraphy. Values from the "Urgonien Jaune" are comparable to the ones of the late Hauterivian or of the early Barremian. Finally, brachiopods from the "Marnes de la Russille" and from the top of the "Urgonien Blanc" give values typical for the Barremian, in particular one rhynchonellid from the "Urgonien Blanc" holds value of 0.707554 which is not recorded elsewhere other than in the late Barremian.

As a partial conclusion, even if there are still doubts on the age of the "Urgonien Jaune", the "Urgonien Blanc" could be clearly attributed to the late Barremian.

An.4.3.4.2. K-Ar radiochronology

At Eclépens, two glauconite-rich layers were sampled in order to perform K-Ar dating. The first corresponds to the hardground rich in glauconite and oyster (sample $EC_{II}21$; cf. paragraph 3.2), and the second one to the glauconitic rich interval situated at 37 m (sample $EC_{II}57$). After hand separation, the glauconite grains were digested in an acid cocktail. The potassium content was measured at the Institute of Geology of the University of Neuchâtel by ICP-MS, and the 40Ar was obtained on a VG1200 mass-spectrometer at the "Centre de Géochimie de la Surface" of the University of Strasbourg (France).

Even if XRD analyses of the glauconite revealed that they are relatively well evolved, K-Ar assign too young an age: $EC_{II}21$ is dated at 126.2 +/- 2.5 Ma and $EC_{II}57$ at 123.2 +/- 2.4 Ma, which are ages close to the Barremian – Aptian boundary (after Gradstein *et al.*, 2004).

On the other hand, if we assume a sedimentation rate of 5 cm.yr-1, approximately 150 m of calcareous sediments are deposited in 3 Ma. With a compaction rate of 40 %, the resulting limestones will reach 90 m in thickness. This is therefore quite more, compared with the 30 m measured at Eclépens between the two absolute K-Ar dates. This inconsistency demonstrates that a major discontinuity occurred at some point during the deposition of these sediments.

An.4.3.4.3. Clay mineral correlation

At Eclépens, the evolution of the kaolinite shows a sharp increase from the boundary between the "Pierre Jaune de Neuchâtel" and the "Urgonien Jaune" upward. In the subalpine chains, Viéban (1983) described such an evolution in the Barterand section, where the kaolinite appears just after the discontinuity "D" which corresponds to the Hauterivian – Barremian boundary.

Recently, the mineralogy of the Angles section, the Barremian stratotype, was analysed, and surprisingly, in the $<2\mu$m fraction, the kaolinite appears gradually at the base of the *Balearites balearis* ammonite zone, and reaches amount of 40 to 70 % during the Barremian (see figure 72 of the field-trip guide book). Kaolinite content is compiled in Fig. An.4.34, from the latest Valanginian to the earliest Aptian; whereas this mineral is absent during the Hauterivian, it becomes the dominant clay mineral during the Barremian, and disappears in the earliest Aptian.

The correlation of the kaolinite evolution, from the western Swiss Jura to the subalpine chains and the Vocontian Trough (Fig. An.4.34), indicates that the Urgonian limestones would be not older than late Hauterivian in age. Taking into account the amount of kaolinite and correlating comparable values, then the "Urgonien Jaune" and the "Urgonien Blanc" would be Barremian in age.

Moreover, some nannofossils were recently found directly above the Ju2 at Eclépens. They are typical of the late Barremian; more precisely the nannofossils assemblage belongs to the *Hemihoplites feraudianus* ammonite zone (de Kaenel, personnal communication; work in progress). On the other hand, the absence of kaolinite observed in the upper part of the "Urgonien Blanc" at Boudry may correspond to the sharp decrease of this mineral observed in the latest Barremian of the Vocontian trough. From these observations, it seems that the "Urgonien Jaune" and the "Urgonien Blanc" were deposited during the late Barremian.

An.4.3.5. Conclusion

By using mineralogy, sequence stratigraphy, K-Ar dating and 87Sr/86Sr stratigraphy, ages can be assigned for the "Urgonien Jaune" and of the "Urgonien Blanc".

Whereas the lower "Pierre Jaune de Neuchâtel" belongs undoubtedly to the early Hauterivian, at least one gap in the sedimentary record occurred, leading to a huge hiatus. This later can be located within the "Marnes d'Uttins" and/or at the boundary between the "Pierre Jaune de Neuchâtel".

Our multidisciplinary approach reveals that the urgonian limestones in the vicinity of Neuchâtel were deposited during the Barremian, as shown by the kaolinite correlation from the platform to the basin. If we combine this approach with the $^{87}Sr/^{86}Sr$ measurements in brachiopods shells, then the "Urgonien Jaune" and the "Urgonien Blanc" would be deposited from the early – late Barremian transition onward. This conclusion is consistent with the age of the urgonian limestones from the Vercors or from the Helvetic Alps, where they correspond to the *Gerhadtia sartousiana* ammonite zone.

An.4.3.6.Acknowledgements

The authors would like to acknowledge Peter Stille (University Louis Pasteur, Strasbourg, France) for the ^{40}Ar and $^{87}Sr/^{86}Sr$ measurements, and Jan Kramers (University of Berne, Switzerland) and Viginie Matera (University of Neuchâtel, Switzerland) for the ^{40}K analysis.

We are grateful to Haydon Mort (University of Neuchâtel) for the help on the field in the Gorges de l'Areuse and the improvement of the manuscript, and to André Villard (University of Neuchâtel) for the thin sections preparations.

We thank Claude Brocard, André Caluori and François Girod from Holcim for allowing us to study the La Sarraz quarry.

Finally, we acknowledge the Swiss National Fund for its financial support (projects n°2100-067807/1 and 200020-105206/1).

An.4.3.7. References

Arnaud-Vanneau, A. (1980). "Micropaléontologie, paléoécologie et sédimentologie d'une plate-forme carbonatée de la marge passive de la Tàthys: l'Urgonien du Vercors septentrional et de la Chartreuse (Alpes occidentales).» Géologie Alpine **Grenoble Mém HS 11**: 874 p.

Arnaud-Vanneau, A. and Arnaud, H. (1990). «Hauterivian to Lower Aptian carbonate shelf sedimentation and sequence stratigraphy in the Jura and northern Subalpine chains (southeastern France and Swiss Jura)». *In:* Tucker M. E., Wilson J. L., Crevello P. D., Sarg J. R. and Read J. F., (*Eds*). Carbonate Platforms: Facies, Sequences and Evolution. Blackwell Scientific Publications, Special Publication of the International Association of Sedimentologists, **9**: 203-233.

Baumberger, E. (1901). «Uber Facies und Transgressionen der untern Kreid am Nordrande mediterrano - helvetischen Bucht im westlichen Jura.» Wiss. Beil. Ber. Töchterschule Basel: 1-44.

Blanc-Aletru, M. C. (1995). Importance des discontinuités dans l'enregistrement sédimentaire de l'Urgonien jurassien. Micropaléontologie, Sédimentologie, Minéralogie et Stratigraphie Séquentielle. Géologie Alpine. Ph.D. Thesis Grenoble, Laboratoire de Géologie de l'Université I de Grenoble. Mémoire HS n°24: 299 pp.

Busnardo, R. and Thieuloy, J.-P. (1989). «Les ammonites de l'Hauterivien jurassien: révision des faunes de la région du stratotype historique de l'étage Hauterivien.» Mémoires de la Société neuchâteloise des Sciences naturelles **XI**: 101-147.

Clavel, B., Charollais, J., Schroeder, R. and Busnardo, R. (1995). «Réflexions sur la biostratigraphie du Crétacé inférieur et sur sa complémentarité avec l'analyse séquentielle: exemple de l'Urgonien jurassien et subalpin.» Bull. Soc. géol. France **166** (*6*): 663-680.

Gradstein, F. M., Ogg, J. G., Smith, A. G., Bleeker, W. and Lourens, L. J. (2004). «A new Geologic Time Scale with special reference to Precambrian and Neogene.» Episodes **27** (*2*): 83-100.

Jenkyns, H. C. and Wilson, P. A. (1999). «Stratigraphy, paleoceanography, and evolution

of Cretaceous pacific guyots: relics from a greenhouse Earth.» American Journal of Science **299**: 341-392.

Kübler, B. (1987). «Cristallinité de l'illite: méthodes normalisées de préparation, méthode normalisée de mesure, méthode automatique normalisée de mesure.» Cahiers de l'Institut de Géologie, Université de Neuchâtel, Suisse **Série ADX n° 2**.

Remane, J. (1989). «The historical type Hauterivian of the Jura mountains: original definition, actual concept, lithostratographic subdivision.» Mémoires de la Société neuchâteloise des Sciences naturelles **XI**: 9-18.

Renevier, E. (1874). «Tableau des terrains sédimentaires formés pendant les époques de la phase organique du globe terrestre avec leurs représentants en Suisse et dans les régions classiques, leurs synonymes et les principaux fossiles de chaque étage.» Bull. Soc. vaud. Sci. nat. **13**: 218-252.

Rumley, G. (1993). «Sédimentologie, minéralogie et stratigraphie de l'Hauterivien dans le Jura neuchâtelois et vaudois (Suisse).» *thesis*, Université de Neuchâtel, 207 pp pp.

van de Schootbrugge, B. (2001). «Influence of paleo-environmental changes during the Hauterivian (early Cretaceous) on carbonate deposition along the northern margin of the Tethys: Evidence from geochemical records (C, O and Sr-isotopes, P, Fe, Mn).» *Ph.D. Thesis thesis*, Université de Neuchâtel, 291 p pp.

Veizer, J., Ala, D., Azmy, K., Bruckschen, P., Buhl, D., Bruhn, F., Carden, G. A. F., Diener, A., Ebneth, S. and Godderis, Y. (1999). «$^{87}Sr/^{86}Sr$, $\delta^{13}C$ and $\delta^{18}O$ evolution of Phanerozoic seawater.» Chemical Geology **161** (*1-3*): 59-88.

Viéban, F. (1983). «Installation et évolution de la plate-forme urgonienne (Hauterivian à Bédoulien) du Jura méridional aux chaînes subalpines (Ain, Savoie, Haute-Savoie). Sédimentologie, minéralogie, stratigraphie et paléogéographie.» *PhD Thesis thesis*, Université de Grenoble, 293 pp pp.

Voigt, S., Wilmsen, M., Mortimore, R. N. and Voigt, T. (2003). «Cenomanian palaeotemperatures derived from the oxygen isotopic composition of brachiopods and belemnites: evaluation of Cretaceous palaeotemperatures proxies.» Int. J. Earth Sci. (Geol. Rundsch.) **92**: 285-299.

Zweidler, D. (1985). «Genèse des gisements d'asphalte des formations de la Pierre Jaune de Neuchâtel et des calcaires urgoniens du Jura (Jura neuchâtelois et nord vaudois, Suisse).» *PhD thesis*, Université de Neuchâtel, 108 pp.

Annexe 5.

Paleontological Reports

AN.5.1. DINOFLAGELLATES BY DR. E. GHASEMI-NEJAD

Dr. Karl Foelmi/ Alexis Godet
Institute of Geology, University of Neuchatel
Rue Emile Argand 11, CP 158
2009 Neuchatel, Switzerland

Dr. Ebrahim Ghasemi-Nejad
Dept. of Geology, Faculty of Sciences
University of Tehran, Enghelab Ave.,
Tehran -- Iran.

March, 14, 2006.

Subject: Palynological results of samples # EC 72 and EC 79

Reference: Karl's emil of 01/13/2006 and Alex's letter of Jan. 16/2006.

Dear Karl/Alexis:

The two samples of EC 72 and EC 79 were analyzed for palynological studies in our laboratory of Palynology at the department of Geology of the University of Tehran using almost standard method of sample processing described by Traverse 1989. No oxidant agents were used as the palynomorph specimens were in a bad state of preservation and this agent could have destroyed the remaining and worsen their conditions.

Three palynological slides were finally made for sample numbered EC 72 and five for sample number EC 79 as the residue after processing just allowed for these quantities. The slides were studied under a light photomicroscope (Zeiss, Axioscop 40) possessing a digital camera. Though the palynomorphs are very badly preserved the best preserved ones were photographed and presented in three plates as attachment to this letter. I only studied dinoflagellate cysts and left aside spore and pollen grains though spore and pollen grains are also preserved in the slides. The dinoflagellate cysts are very badly preserved and the majority of them could not be identified to the specific level. Some forms seem to be reworked from Jurassic beds. Many forms are long range indicating only lower Cretaceous. However, based on the presence of some forms such as *Muderongia mcwhaei* and *Muderongia tetracantha* which are the two indices for Aptian stage in sample numbered EC 79 I believe this sample is having an age of early Aptian. I could not find any index taxon in the lower sample (EC 72) however it seems that this could also be of late Barremian to early Aptian as well. To support this conclusion I still

need to prepare thin sections from the limestone samples that are sent to me. I still have not received these samples though I received a notice that the samples are in the central post office in Tehran and one has to go to do custom clearance to get them!

As I will be on a field trip for a period of almost 20 days starting on March 18, I thought would be good to send you this report before departing. I will do the thin section and study them later on when I come back and this may take more time. But I think you can use the palynological results apart from the coming ones from the thin sections if you like.

With all the best wishes

Ebrahim.

Plate 1

Scale bar presents 20 um.

1 – 8. *Crobroperidinium* spp.

9 – 10. *Apteodinium* spp.

11. *Cribroperidinium* sp.

12. Reworking from Jurassic, *Gonyaulacysta eisenackii*

13. *Gonyaulacysta* sp.

14 – 15. *Atopodinium* sp.

16. Reworing from Jurassic. *Rhynchodiniopsis* sp.

Palte 2

Scale bar presents 20 um.

1-2. *Oligosphaeridium* sp.

3. *Achomosphaera* sp.

4. *Oligosphaeridium complex*

5 – 6. *Oligosphaeridium* spp.

7. *Hystrichodinium pulchrum*

8. *Oligosphaeridium* sp.

9. *Oligosphaeridium complex*

10. *Achomosphaera* cf. *sagena*

11. *Oligosphaeridium* sp.

12. *Oligosphaeridium complex*

13. *Achomosphaera* sp.

14. *Hystrichodinium* cf. *pulchrum*

15. cf. *Prolixosphaeridium* sp.

16 – 17. *Cyclonephelium* sp.

18. *Achomosphaera* cf. *sagena*

Plate 3

Scale bar presents 20 um.

1 – 3. *Muderongia* spp.

5. *Muderongia tetracantha*

6 – 7. *Muderongia mcwhaei*

4, 8. *Muderongia* sp.

9. *Muderongia tetracantha*

10 – 11. *Muderongia* sp.

12. *Muderongia* sp.

PLATE 1

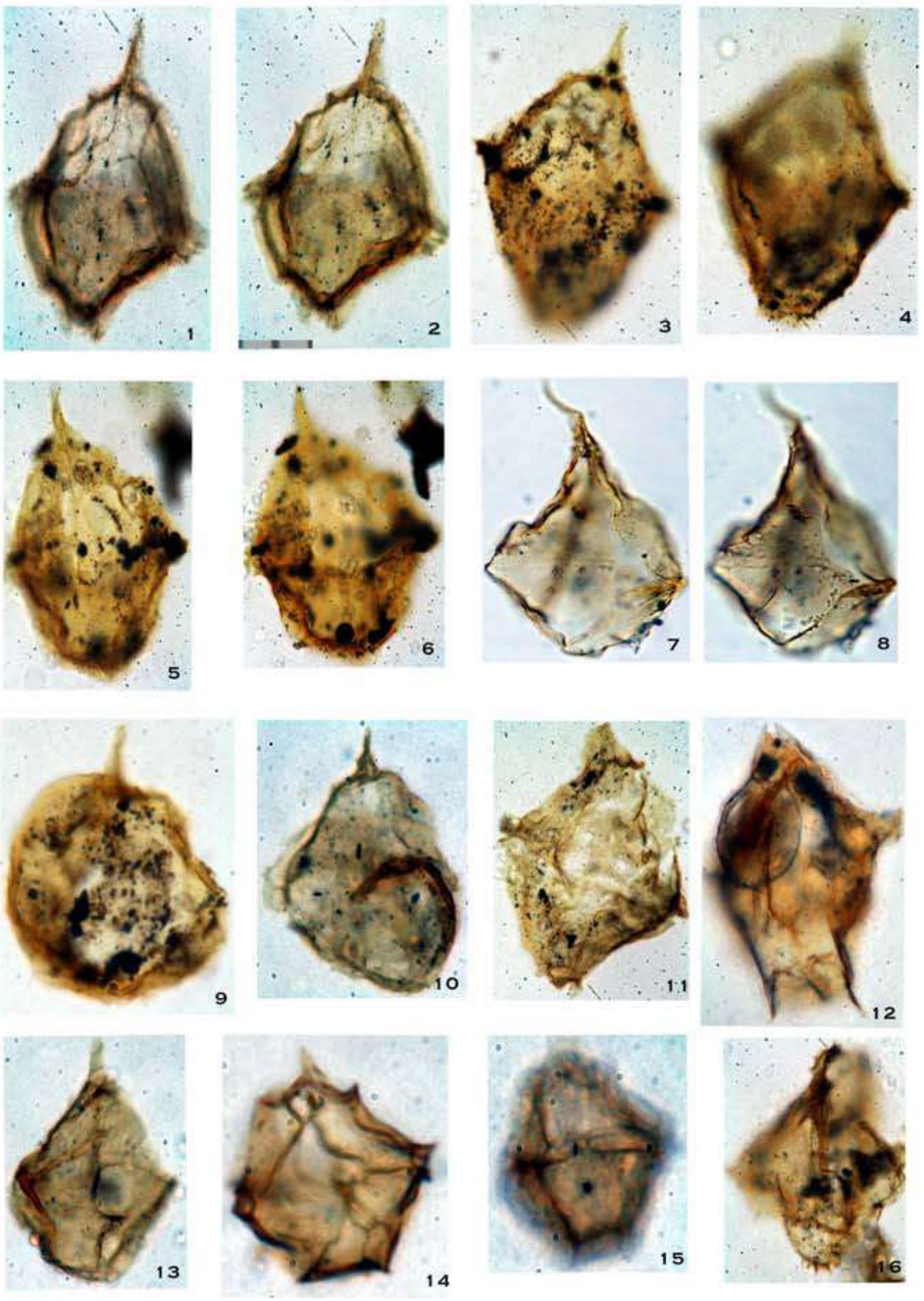

PLATE 2

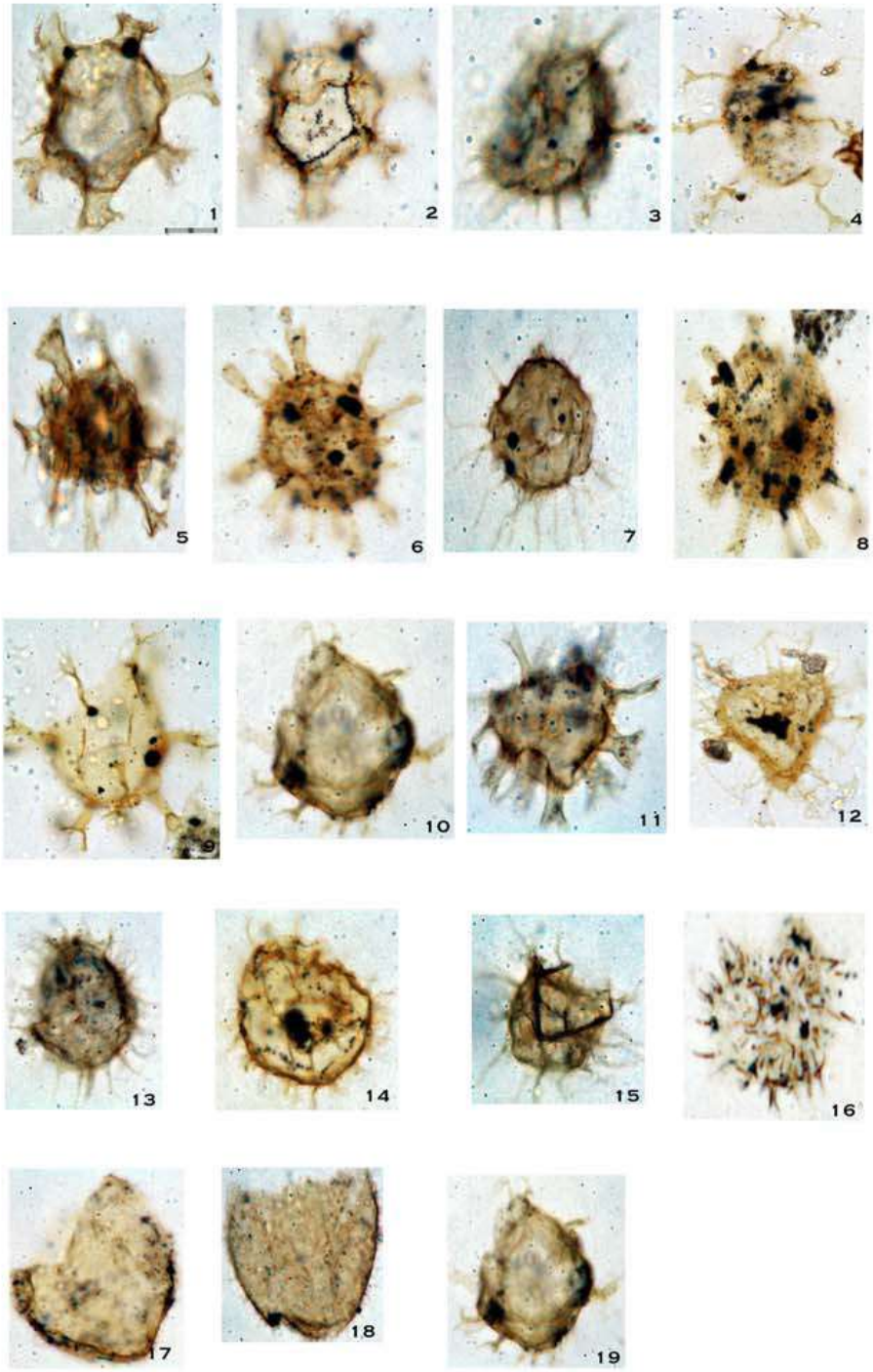

PLATE 3

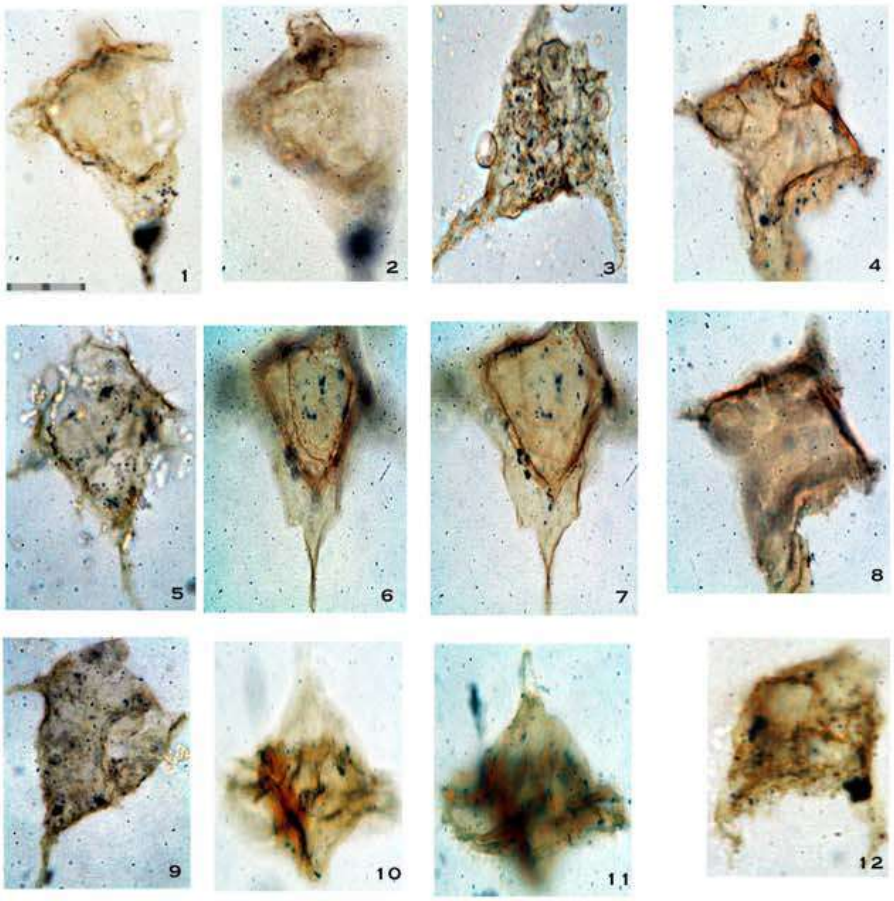

PLATE 4

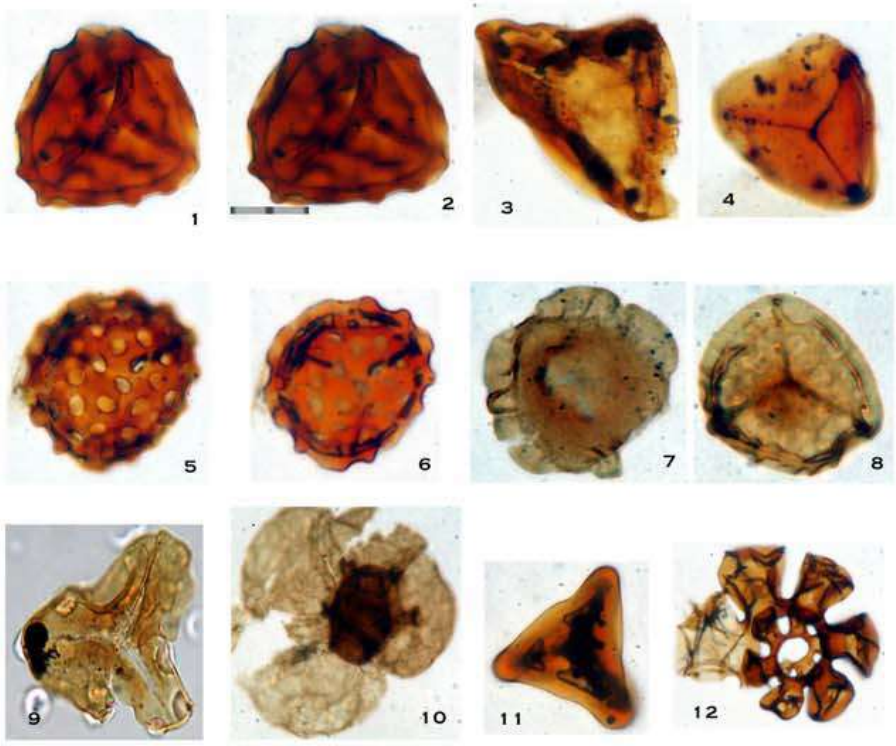

AN.5.2. TAXONOMIC LIST OF NANNOFOSSILS (SUMMER 2006, DR. E. DE KAENEL)

A list of all taxa observed in Samples $EC_{II}72b$ and $EC_{II}79$ is given below. Bibliographic references included in this list could be found in Bown and Concheyro, 2004 :

Assipetra infracretacea (Thierstein, 1973) Roth, 1973
Assipetra terebrodentarius (Applegate, Bralower, Covington & Wise *in* Covington & Wise, 1987) Rutledge & Bergen *in* Bergen, 1994
Axopodorhabdus cylindratus (Noël, 1965) Wind & Wise *in* Wise & Wind, 1977
Axopodorhabdus dietzmannii (Reinhardt, 1965) Wind & Wise, 1983
Bidiscus rotatorius Bukry, 1969
Biscutum constans (Gorka, 1957) Black *in* Black & Barnes, 1959
Biscutum ellipticum (Gorka, 1957) Grün *in* Grün & Allemann, 1975
Biscutum thurowii Burnett, 1998
Bukrylithus ambiguus Black, 1971
Conusphaera mexicana Trejo, 1969
Conusphaera mexicana Trejo, 1969 ssp. *minor* Bralower *in* Bralower *et al*., 1989
Cretarhabdus conicus Bramlette & Martini, 1964
Crucibiscutum trilensis Bown & Concheyro, 2004
Cyclagelosphaera margerelii Noël, 1965
Diazomatolithus lehmanii Noël, 1965
Diloma placinum Wind & Cepek, 1979
Ellipsagelosphaera britannica (Stradner, 1963) Perch-Nielsen, 1968
Flabellites oblongus (Bukry, 1969) Crux *in* Crux *et al*., 1982
Glaucolithus diplogrammus (Deflandre *in* Deflandre & Fert, 1954) Reinhardt, 1964
Gorkae pseudoanthophorus (Bramlette & Martini, 1964) Varol & Girgis, 1994
Hayesites irregularis Thierstein in Roth & Thierstein, 1972
Lithraphidites bollii (Thierstein, 1971) Thierstein, 1973
Lithraphidites carniolensis Deflandre, 1963
Lucianorhabdus salomonii Bergen, 1994
Manivitella pemmatoidea (Deflandre *in* Manivit, 1965) Thierstein, 1971
Micrantholithus hoschulzii (Reinhardt, 1966) Thierstein, 1971
Micrantholithus obtusus Stradner, 1963
Microstaurus chiastius (Worsley, 1971) Grün *in* Grün & Allemann, 1975
Nannoconus bucheri Brönnimann, 1955
Nannoconus globulus Brönnimann, 1955
Nannoconus kamptneri Brönnimann, 1955 ssp. *minor* Bralower *in* Bralower *et al*., 1989
Nannoconus quadriangulus Deflandre & Deflandre, 1957
Nannoconus steinmannii steinmannii Kamptner, 1931
Nannoconus steinmannii Kamptner, 1931 ssp. *minor* Deres & Archéritéguy, 1980
Nannoconus truitti Brönnimann, 1955
Nannoconus wassellii Brönnimann, 1955
Palaeopontosphaera salebrosa (Black, 1971) de Kaenel & Bergen, 1996
Perissocyclus plethotrepus (Wind & Cepek, 1979) Crux, 1989
Reinhardtites scutula Bergen, 1994

Retecapsa octofenestrata (Bralower *in* Bralower *et al*., 1989) Bown *in* Bown & Cooper, 1998
Retecapsa schizobrachiata (Gartner, 1968) Grün *in* Grün & Allemann, 1975
Retecapsa surirella (Deflandre & Fert, 1954) Grün *in* Grün & Allemann, 1975
Rhagodiscus asper (Stradner, 1963) Reinhardt, 1967
Rhagodiscus gallagheri Rutledge & Bown, 1996
*Rotelapillus crenulatus (*Stover, 1966) Perch-Nielsen, 1984
Tegulalithus septentrionalis (Stradner, 1963) Crux, 1986
Tegumentum octiformis (Köthe, 1981) Crux, 1989
Tranolithus gabalus Stover, 1966
Vagalapilla elliptica (Gartner. 1968) Bukry, 1969
Vagalapilla imbricata (Gartner. 1968) Bukry, 1969
Watznaueria barnesae (Black *in* Black & Barnes, 1959) Perch-Nielsen, 1968
Watznaueria fossacincta (Black, 1971) Bown *in* Bown & Cooper, 1989
Watznaueria ovata Bukry, 1969
Zeugrhabdotus choffatii Rood, Hay & Barnard, 1973
Zeugrhabdotus moulladei Bergen, 1998
Zeugrhabdotus trivectis Bergen, 1994
Zygodiscus xenotus (Stover, 1966) Hill, 1976

Reference

Bown, P. R. and Concheyro, A. (2004). «Lower Cretaceous calcareous nannoplankton from the Neuquén Basin, Argentina.» Marine Micropaleontology **52** (*1-4*): 51-84.

AN.5.3.
RESULTS OF THE BLIND TEST ON NANNOFOSSILS FROM ECLÉPENS

Nanno Test (Hauterivian vs Barremian)

There is a controversy regarding the age of the Urgonian limestone between different schools (Grenoble, Geneva, Neuchâtel). As ammonites, dasycladaceans, foraminifera, and dinocysts give no exclusive answer, it was tried to settle the question with nannofossils.

On March 21, 2006, a group composed of Jean Charollais, Marc Weidmann, Roger Jan du Chêne, Karl Föllmi, Alexis Godet, Stéphane Bodin, and André Strasser visited the Eclépens and La Sarraz quarries. A. Strasser took a total of 8 samples from four sites. Each sample was split equally in three parts. No cleaning was done at this stage, but care was taken to avoid contamination between the samples and from outside. Three sets of samples were then sent to Elisabetta Erba, Silvia Gardin, and Eric de Kaenel for determination of the nannoflora and age assignments. The position of the samples was unknown to these experts. The logs drawn by A. Strasser, the position of the samples, and the ages given by each expert are summarized in the following figure. The detailed reports of the experts are in the annex.

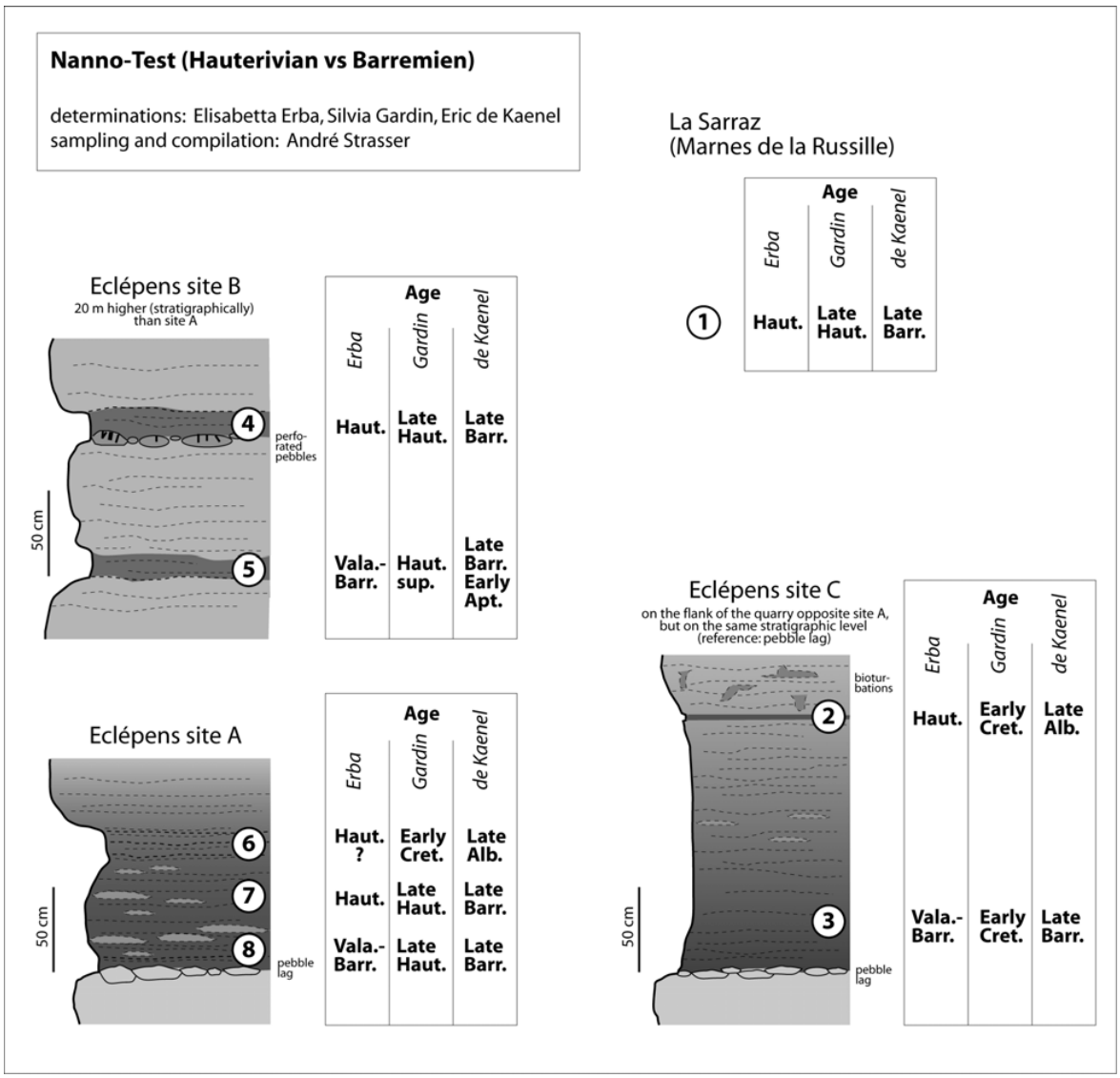

Despite of the generally poor preservation, many species could be identified. However, it is interesting to note that the lists of identified species diverge sometimes strongly between the experts. Also the interpretations vary. While E. Erba and S. Gardin found *T. septentrionalis* and *C. oblongata* in several samples, E. de Kaenel mentions *T. septentrionalis* only in sample 1. For E. Erba and S. Gardin, *T. septentrionalis* is Hauterivian in age, while E. de Kaenel attributes sample 1 to the Late Barremian. E. de Kaenel found *Flabellites* in samples 4, 5, and 8, which he attributes to the Late Barremian. However, according to S. Gardin, this genus may already appear in the Late Hauterivian. *Eifellithus equibiramus* or *E. monechiae* that indicate an Albian age have been found by E. de Kaenel but not by E. Erba or S. Gardin.

According to E. de Kaenel, there are no signs of reworking in the studied samples. From the sedimentological standpoint, there is evidence of condensation (pebble lags, perforated pebbles) but no indication of major erosion or non-deposition. Bioturbation may cause some time averaging but would not affect the results.

The age attributions given by E. Erba and S. Gardin are consistent and suggest a (possibly Late) Hauterivian age for all studied sections. On the other hand, E. de Kaenel places most samples in the Late Barremian, and samples 2 and 6 even in the Late Albian. In the laterally correlated sections A and C, the Late Albian would in both cases overlie the Late Barremian, but there are no signs of condensation or erosion between the samples that would explain such a large time gap. In the case of section B, sample 5 shows evidence of Early Aptian according to E. de Kaenel, but the overlying sample 4 is interpreted as Late Barremian. Also, site B is stratigraphically younger than sites A and C and does not allow to have Late Barremian superposing Late Albian.

As a conclusion, there is **more evidence for an Hauterivian age** of the analyzed sections than for a Barremian age. The presence of Late Albian would pose a serious problem to explain the large time gap within an interval of a few tens of cm where no physical evidence is visible. Reworking of fine-grained, unconsolidated material over a period of some 20 million years (from Hauterivian to Albian times) would certainly leave a signature.

An open question remains the discrepancies in nannofossil determinations and age attributions. This, however, must be solved within the community of nannofossil specialists.

Fribourg, 9 October 2006 André Strasser

ERIC DE KAENEL
RUE MATILE 51
2000 NEUCHATEL
SWITZERLAND
TEL: +41 32 710.15.05
FAX: +41 32 710.15.06
E-Mail: edekaenel @ bluewin.ch

DPR
DEKAENEL
PALEO RESEARCH

BUGWARE VER: **1999.9.2**
AREA: **Swiss Jura**
OPERATOR: **André Strasser**
PALEONTOLOGIST: **Eric de Kaenel (DPR)**
FIRST SAMPLE: **SwissJura-8 (sample processed by ELLINGTON:-EL)**
LAST SAMPLE: **SwissJura-1 (sample processed by ELLINGTON:-EL)**
DATE: **06-05-2006**

@@@@@ Start Sample Data

@SwissJura-8
! Upper Barremian

=Assipetra infracretacea	[1]
=Assipetra terebrodentarius	[1]
=Axopodorhabdus cylindratus	[2]
=Bidiscus rotatorius	[2]
=Biscutum ellipticum	[4]
=Cyclagelosphaera margerelii	[5]
=Diazomatolithus lehmanii	[2]
=Ellipsagelosphaera britannica	[2]
=Flabellites oblongus	[1]
=Glaucolithus choffatii	[3]
=Glaucolithus diplogrammus	[5]
=Glaukolithus bicrescenticus	[1]
=Gorkae pseudoanthophorus	[2]
=Lithraphidites carniolensis	[20]
=Micrantholithus obtusus	[1]
=Nannoconus kamptneri kamptneri	[2]
=Nannoconus st. steinmannii	[1]
=Palaeopontosphaera salebrosa	[5]
=Reinhardtites scutula	[1]
=Retecapsa octofenestrata	[5]
=Retecapsa schizobrachiata	[5]
=Retecapsa surirella	[5]
=Rhagodiscus asper	[5]
=Vagalapilla elliptica	[3]
=Vagalapilla stradneri	[5]
=Watznaueria barnesae	[600]
=Watznaueria fossacincta	[50]
=Watznaueria ovata	[5]
=Zeugrhabdotus trivectis	[3]
# TOTAL FOSSILS: Abundant	{747 }

SAMPLE PRESERVATION: POOR
...
@SwissJura-7

! Upper Barremian

```
=Assipetra terebrodentarius                [1    ]
=Axopodorhabdus cylindratus                [1    ]
=Biscutum ellipticum                       [3    ]
=Cretarhabdus conicus                      [1    ]
=Cyclagelosphaera margerelii               [10   ]
=Diazomatolithus lehmanii                  [2    ]
=Ellipsagelosphaera britannica             [1    ]
=Glaucolithus choffatii                    [3    ]
=Glaucolithus diplogrammus                 [4    ]
=Glaukolithus bicrescenticus               [1    ]
=Gorkae pseudoanthophorus                  [2    ]
=Lithraphidites carniolensis               [10   ]
=Micrantholithus hoschulzii                [1    ]
=Micrantholithus obtusus                   [1    ]
=Microstaurus chiastius                    [1    ]
=Nannoconus st. steinmannii                [1    ]
=Palaeopontosphaera salebrosa              [10   ]
=Retecapsa octofenestrata                  [5    ]
=Retecapsa schizobrachiata                 [5    ]
=Retecapsa surirella                       [1    ]
=Rhagodiscus asper                         [4    ]
=Vagalapilla elliptica                     [1    ]
=Vagalapilla stradneri                     [10   ]
=Watznaueria barnesae                      [600  ]
=Watznaueria fossacincta                   [50   ]
=Watznaueria ovata                         [2    ]
=Zeugrhabdotus moulladei                   [2    ]
=Zeugrhabdotus trivectis                   [3    ]
# TOTAL FOSSILS: Abundant                  {736  }
SAMPLE PRESERVATION: POOR
...
@SwissJura-6
```

! middle Upper Albian-upper Upper Albian

```
=Assipetra infracretacea                   [1    ]
=Assipetra terebrodentarius                [1    ]
=Biscutum ellipticum                       [1    ]
=Biscutum thurowii                         [1    ]
=Crucibiscutum hayi                        [2    ]
=Cyclagelosphaera margerelii               [10   ]
=Eiffellithus equibiramus                  [2    ]
=Eiffellithus monechiae                    [1    ]
=Ellipsagelosphaera britannica             [2    ]
=Glaucolithus diplogrammus                 [3    ]
=Glaukolithus bicrescenticus               [1    ]
=Hayesites irregularis                     [1    ]
=Helicolithus trabeculatus                 [1    ]
=Lithraphidites carniolensis               [5    ]
=Nannoconus truittii                       [1    ]
=Palaeopontosphaera salebrosa              [2    ]
=Placozygus howei                          [1    ]
=Prediscosphaera spinosa                   [1    ]
=Quadrum eneabrachium                      [1    ]
=Retecapsa octofenestrata                  [1    ]
=Retecapsa surirella                       [1    ]
=Rhagodiscus asper                         [1    ]
=Rhagodiscus gallagheri                    [1    ]
=Tranolithus minimus                       [1    ]
=Vagalapilla imbricata                     [1    ]
```

```
=Vagalapilla stradneri                    [5    ]
=Vekshinella angusta                      [1    ]
=Watznaueria barnesae                     [400  ]
=Watznaueria fossacincta                  [10   ]
=Watznaueria ovata                        [5    ]
=Zeugrhabdotus trivectis                  [1    ]
# TOTAL FOSSILS: Abundant                 {466  }
SAMPLE PRESERVATION: POOR
...
@SwissJura-5
! Uppermost Barremian

=Assipetra infracretacea                  [1    ]
=Biscutum ellipticum                      [2    ]
=Cretarhabdus conicus                     [2    ]
=Cyclagelosphaera margerelii              [3    ]
=Ellipsagelosphaera britannica            [2    ]
=Flabellites oblongus                     [5    ]
=Glaucolithus choffatii                   [2    ]
=Glaucolithus diplogrammus                [2    ]
=Micrantholithus hoschulzii               [1    ]
=Micrantholithus obtusus                  [1    ]
=Nannoconus abundans                      [1    ]
=Nannoconus globulus                      [1    ]
=Nannoconus kamptneri kamptneri           [6    ]
=Nannoconus st. steinmannii               [10   ]
=Nannoconus truittii                      [1    ]
=Nannoconus wassalii                      [1    ]
=Palaeopontosphaera salebrosa             [1    ]
=Reinhardtites scutula                    [1    ]
=Retecapsa angustiforata                  [1    ]
=Retecapsa octofenestrata                 [1    ]
=Retecapsa schizobrachiata                [6    ]
=Rhagodiscus asper                        [5    ]
=Rhagodiscus gallagheri                   [1    ]
=Vagalapilla elliptica                    [15   ]
=Vagalapilla stradneri                    [3    ]
=Watznaueria barnesae                     [1000 ]
=Watznaueria fossacincta                  [40   ]
=Watznaueria ovata                        [3    ]
=Zeugrhabdotus moulladei                  [2    ]
=Zeugrhabdotus trivectis                  [1    ]
# TOTAL FOSSILS: Very Abund               {1121 }
SAMPLE PRESERVATION: POOR
...
@SwissJura-4
! Upper Barremian

=Crucicribrum sp. 3                       [1    ]
=Cyclagelosphaera margerelii              [2    ]
=Flabellites oblongus                     [1    ]
=Glaucolithus choffatii                   [1    ]
=Lithraphidites carniolensis              [10   ]
=Micrantholithus hoschulzii               [1    ]
=Nannoconus sp.                           [1    ]
=Palaeopontosphaera salebrosa             [1    ]
=Placozygus howei                         [2    ]
=Reinhardtites scutula                    [1    ]
=Retecapsa schizobrachiata                [1    ]
=Retecapsa surirella                      [1    ]
=Rhagodiscus asper                        [3    ]
```

```
=Vagalapilla elliptica                    [20   ]
=Vagalapilla imbricata                    [1    ]
=Watznaueria barnesae                     [200  ]
=Watznaueria fossacincta                  [30   ]
=Zeugrhabdotus moulladei                  [1    ]
=Zeugrhabdotus trivectis                  [1    ]
# TOTAL FOSSILS: Abundant                 {279  }
SAMPLE PRESERVATION: MODERATE
...
@SwissJura-3
! Upper Barremian

=Assipetra infracretacea                  [1    ]
=Biscutum ellipticum                      [1    ]
=Cyclagelosphaera margerelii              [3    ]
=Glaucolithus choffatii                   [5    ]
=Gorkae pseudoanthophorus                 [1    ]
=Lithraphidites carniolensis              [5    ]
=Nannoconus kamptneri kamptneri           [1    ]
=Palaeopontosphaera salebrosa             [10   ]
=Retecapsa schizobrachiata                [2    ]
=Retecapsa surirella                      [1    ]
=Rhagodiscus asper                        [2    ]
=Rhagodiscus gallagheri                   [1    ]
=Vagalapilla elliptica                    [1    ]
=Vagalapilla stradneri                    [10   ]
=Watznaueria barnesae                     [400  ]
=Watznaueria fossacincta                  [40   ]
=Watznaueria ovata                        [5    ]
=Zeugrhabdotus moulladei                  [1    ]
=Zeugrhabdotus trivectis                  [3    ]
# TOTAL FOSSILS: Abundant                 {493  }
SAMPLE PRESERVATION: POOR
...
@SwissJura-2
! middle Upper Albian-upper Upper Albian

=Assipetra infracretacea                  [2    ]
=Assipetra terebrodentarius               [1    ]
=Biscutum ellipticum                      [1    ]
=Chiastozygus tenuis                      [1    ]
=Cretarhabdus conicus                     [2    ]
=Crucibiscutum hayi                       [5    ]
=Cyclagelosphaera margerelii              [2    ]
=Eiffellithus equibiramus                 [2    ]
=Eiffellithus monechiae                   [2    ]
=Ellipsagelosphaera britannica            [1    ]
=Glaucolithus diplogrammus                [1    ]
=Helicolithus turonicus                   [2    ]
=Lithraphidites alatus                    [1    ]
=Lithraphidites carniolensis              [3    ]
=Nannoconus truittii                      [4    ]
=Palaeopontosphaera salebrosa             [1    ]
=Prediscosphaera spinosa                  [1    ]
=Prediscosphaera stoveri                  [2    ]
=Reinhardtites scutula                    [1    ]
=Retecapsa octofenestrata                 [1    ]
=Retecapsa schizobrachiata                [1    ]
=Rhagodiscus asper                        [4    ]
=Rotelapillus sp.                         [1    ]
=Tegulalithus tessellatus                 [1    ]
```

```
=Tranolithus exiguus                    [1    ]
=Vagalapilla elliptica                  [1    ]
=Vagalapilla stradneri                  [3    ]
=Watznaueria barnesae                   [400  ]
=Watznaueria ovata                      [1    ]
=Zeugrhabdotus trivectis                [1    ]
# TOTAL FOSSILS: Abundant               {450  }
SAMPLE PRESERVATION: POOR
...
@SwissJura-1
! Upper Barremian

=Assipetra infracretacea                [5    ]
=Assipetra terebrodentarius             [1    ]
=Axopodorhabdus cylindratus             [3    ]
=Bidiscus rotatorius                    [2    ]
=Biscutum thurowii                      [1    ]
=Calcicalathina erbae                   [1    ]
=Cretarhabdus conicus                   [5    ]
=Cyclagelosphaera margerelii            [1    ]
=Diazomatolithus lehmanii               [5    ]
=Glaucolithus choffatii                 [20   ]
=Glaucolithus diplogrammus              [3    ]
=Glaukolithus bicrescenticus            [2    ]
=Gorkae pseudoanthophorus               [2    ]
=Lithraphidites carniolensis            [20   ]
=Lucianorhabdus salomonii               [1    ]
=Manivitella pecten                     [1    ]
=Manivitella pemmatoidea                [1    ]
=Micrantholithus hoschulzii             [1    ]
=Micrantholithus obtusus                [1    ]
=Microstaurus chiastius                 [1    ]
=Nannoconus sp.                         [3    ]
=Nannoconus truittii                    [2    ]
=Palaeopontosphaera salebrosa           [1    ]
=Perissocyclus plethotrepus             [1    ]
=Reinhardtites scutula                  [2    ]
=Retecapsa angustiforata                [1    ]
=Retecapsa octofenestrata               [5    ]
=Retecapsa schizobrachiata              [20   ]
=Retecapsa surirella                    [3    ]
=Rhagodiscus achlyostaurion             [1    ]
=Rhagodiscus asper                      [20   ]
=Rhagodiscus gallagheri                 [1    ]
=Rhagodiscus pseudoangustus             [1    ]
=Tegulalithus septentrionalis           [2    ]
=Tegumentum octiformis                  [1    ]
=Vagalapilla elliptica                  [2    ]
=Vagalapilla stradneri                  [4    ]
=Watznaueria barnesae                   [1000 ]
=Watznaueria fossacincta                [200  ]
=Watznaueria ovata                      [5    ]
=Zeugrhabdotus moulladei                [1    ]
# TOTAL FOSSILS: Very Abund             {1353 }
SAMPLE PRESERVATION: POOR
```

Echantillons 8 : Barrémien supérieur
Echantillons 7 : Barrémien supérieur
Echantillons 6 : Albien supérieur supérieur
Echantillons 5 : Barrémien supérieur supérieur (ou base Aptien inférieur)
Echantillons 4 : Barrémien supérieur
Echantillons 3 : Barrémien supérieur
Echantillons 2 : Albien supérieur supérieur
Echantillons 1 : Barrémien supérieur

Une des espèces importante est *Eiffellithus equibiramus* (Watkins and Bergen, 2003). Cette espèce est limitée à la partie supérieure de l'Albien supérieur (101.0 à 99.0 Ma). La présence de *Eiffellithus monechiae* (et d'autres espèces) permet de donner un âge approximatif entre 101.0 et 100.5 Ma pour les deux échantillons Albien (age model of Wison and Noris, 2001 modified by Bellier et al., 2001).

-référence : voir Watkins and Bergen, 2003 : Late Albian adaptative radiation in the calcareous nannofossil genus *Eiffellithus*. Micropaleontology, vol. 49, no. 3.

Le problème n'est plus de savoir si ces échantillons sont Hauterivien ou Barremien, mais de comprendre comment ces marnes albiennes se sont déposées. Je laisse ce travail à Karl et à son équipe. Je n'ai observé aucune espèce remaniée dans aucun échantillon (pas un seul marqueur de l'Hauterivien ou du Barrémien inférieur). Chaque assemblage est bien typique et définit bien l'âge de l'échantillon. La préservation des nannofossiles est généralement pauvre (à modérée parfois), mais cela n'empêche pas de déterminer les espèces avec certitude. Il faut seulement passer beaucoup de temps au microscope.

ECLÉPENS – BLIND TEST
ANALYSES OF CALCAREOUS NANNOFOSSILS (ERBA – June-July 2006)

Sample 1
Abundance FEW preservation MODERATE-POOR

Watznaueria barnesae
Diazomatolithus lehmanii
Calcicalathina oblongata
Tegulalithus septentrionalis
Nannoconus sp.
Micranhtolithus hoschulzii
Cretarhabodus angustiforatus
Rhagodiscus asper
Assipetra infracretacea
Cretarhabdus surirellus
Cyclagelosphaera margerelii
Zeugrhabdotus diplogrammus
Microstaurus chiastius

? L. bollii

Age: based on occurrence of *C. oblongata* : Valanginian to early Barremian. The occurrence of *T.septentrionalis* indicates a Hauterivian age.

Sample 2
Abundance RARE preservation POOR

Watznaueria barnesae
Calcicalathina oblongata
Eiffellithus striatus
Cretarhabdus surirellus
Cyclagelosphaera margerelii

Age: based on occurrence of *C. oblongata* : Valanginian to early Barremian. The occurrence of *E. striatus* indicatea a Hauterivian age (not younger than late Hauterivian).

Sample 3
Abundance RARE preservation POOR

Watznaueria barnesae
Calcicalathina oblongata
Cyclagelosphaera margerelii
Diazomatolithus lehmanii

Age: based on occurrence of *C. oblongata* : Valanginian to early Barremian

Sample 4
Abundance FEW preservation MODERATE-POOR

Watznaueria barnesae
Tegulalithus septentrionalis
Calcicalathina oblongata
Cyclagelosphaera margerelii
Cretarhabdus surirellus
Percivalia fenestrata

Age: based on occurrence of *C. oblongata* : Valanginian to early Barremian. The occurrence of *T.septentrionalis* indicates a Hauterivian age.

Sample 5
Abundance RARE preservation POOR

Watznaueria barnesae
Calcicalathina oblongata
Nannoconus steinmannii
Nannoconus sp.

Age: based on occurrence of *C. oblongata* : Valanginian to earliest Barremian.

Sample 6
Abundance RARE preservation POOR

Watznaueria barnesae
Calcicalathina oblongata
Lithraphidites bollii (?)

Age: based on occurrence of *C. oblongata* : Valanginian to earliest Barremian. Extremely rare and pooròy preservaed specimens are attributed to *L. bollii* that would restrict the age to the Hauterian.

Sample 7
Abundance FEW preservation POOR

Watznaueria barnesae
Calcicalathina oblongata
Clepsilithus maculosus
Crucibiscutum salebrosum
Crucibiscutum neuquenensis
Eiffellithus striatus
Cyclagelosphaera margerelii
Lithraphidites carniolensis
Diazomatolithus lehmanii
Cretarhabdus surirellus

Microstaurus chiastius
Cretarhabdus angustiforatus
Nannoconus bermudezii
Discorhabdus rotatorius

Age: Hauterivian based on the occurrence of *E. striatus, C. salebrosum, C. neuquenensi, C. maculosus.*

Sample 8
Abundance RARE preservation POOR

Watznaueria barnesae
Calcicalathina oblongata
Cyclagelosphaera margerelii
Lithraphidites carniolensis
Nannoconus sp.

Age: based on occurrence of *C. oblongata* : Valanginian to earliest Barremian.

EXPERTISE ON CALCAREOUS NANNOFLORA FROM THE SWISS JURA
(Silvia Gardin)

Introduction

A controversy about the age of the Urgonian Limestones has existed among different schools. The "Génève school" pleads for a late Hauterivian age on the basis of Orbitolinid, Dasycladale, Dinocyst and calcareous nannofossil biostratigraphy (Clavel et al., CR). Recently, the "Neuchatel school" has proposed a late Barremian-early Aptian age on the basis of calcareous nannofossil assemblages (Godet et al ., CRAS).
In order to solve this discrepancy, both schools sampled together an outcrop in the Swiss Jura. Soft lithologies suitable for calcareous nannofossil analysis have been distributed among different specialists. I present herein the results of my expertise.

Methods, abundances, preservation

Simple smear slides from each of the eight samples received were prepared. Each sample was analysed for 1 hour and 40 min and all the nannofossils encountered have been counted. Nannofossils total abundance varies from few to very rare. Preservation is always poor or very poor and species diagnosis is very often hampered because of strong etching and overgrowth. Species richness varies according to the abundance of the assemblage in the sample; it does not seem to be linked to changes in preservation since the latter is always poor.

Results

Table 1 summarizes the findings for each sample examined. To better constrain the age assignment, I have used the stratigraphical distribution of calcareous nannofossils (Fig 1) that I have personally compiled for the Lower Cretaceous Stage Boundary Working Groups (ICS). This biostratigraphic scheme summarizes all the data coming from low latitude sections situated in the Vocontian basin (SE France), Betic cordillera (Spain) and Galicia margin (North Atlantic Ocean) for the late Berriasian to early Barremian time interval.

			A. infracretacea	A. terebrodentarius	Biscutum sp.	C. conicus	C. cuvillieri	C. delicatus	C. margereli	C. mex mex	C. oblongata	C. octofenestr	C. salebrosum	Cretarhabdus spp.	C. silvaradion	C. surirellus	C. trilensis	Chiastozygus sp.	D. lehmanni	E. gallicus	E. primus	E. striatus	Flabellites spp (early morphotipes)	L. bollii	L. camiolensis	M. chiastius	M. circumradiatus	M. hoschulzi	M. obtusus	N. cornuta	N. stein group	N. trutti	Nannoconus spp.	P. fenestrata	R. angustiforata	R. asper (regular)	R. asper (small)	R. lafittei	R. windleyae	T. gabalus	T. octiformis	T. sarmatus	T. septentrionalis	S. angustus	S. colligata	S. ellipticus	S. cf S. imbricatus	S. mutterlosei	Staurolithites spp.	W. barnesae	Zeugrhabdothus spp smal	Z. diplogrammus	Z. embergeri	Z. scutula	Z. trivectis	Z. xenotus	TOTAL
Suisse 1	R	P	4		3				1		2	2	1	3		1								3	3							2		1	4	1		3				1						3	32	5	1				72
Suisse 2	VR	P										3	3			2			2													1			2													3	5				1		22
Suisse 3	VVR	P	1											1																																			4				4		10
Suisse 4	F	P			7				1	2		2	4	8		2	3		2	1			22		2	1		2	1				8			5	3	1	2				2	1	1	3	6		78	71	2	1	2	5	2	253
Suisse 5	F	P	3		3				2			8	1	10		2	2		2				2	2	2								8		2	10	4					1		3		4	4		10	3			2		1	88
Suisse 6	VVR	P			1														1												2																								15
Suisse 7	VR	P	1	?	1				2		1	6	10	5	2	2			2					1				1			2	4			2	1	1	1		1						2		4	6		1				63
Suisse 8	F	P	3		8	1			7		2		10	10		5			15					4	2					1				10	3	3		1							1	1		1	14	62		2		8	1	175

Table1. Quantitative counts of calcareous nannofossils found in the samples analysed.

Sample's age discussion

S1 age : The presence of *Tegulalithus septentrionalis*, *Rucinolithus windleyae, Calcicalathina oblongata* and *L. bolli* indicates a late Hauterivian age .

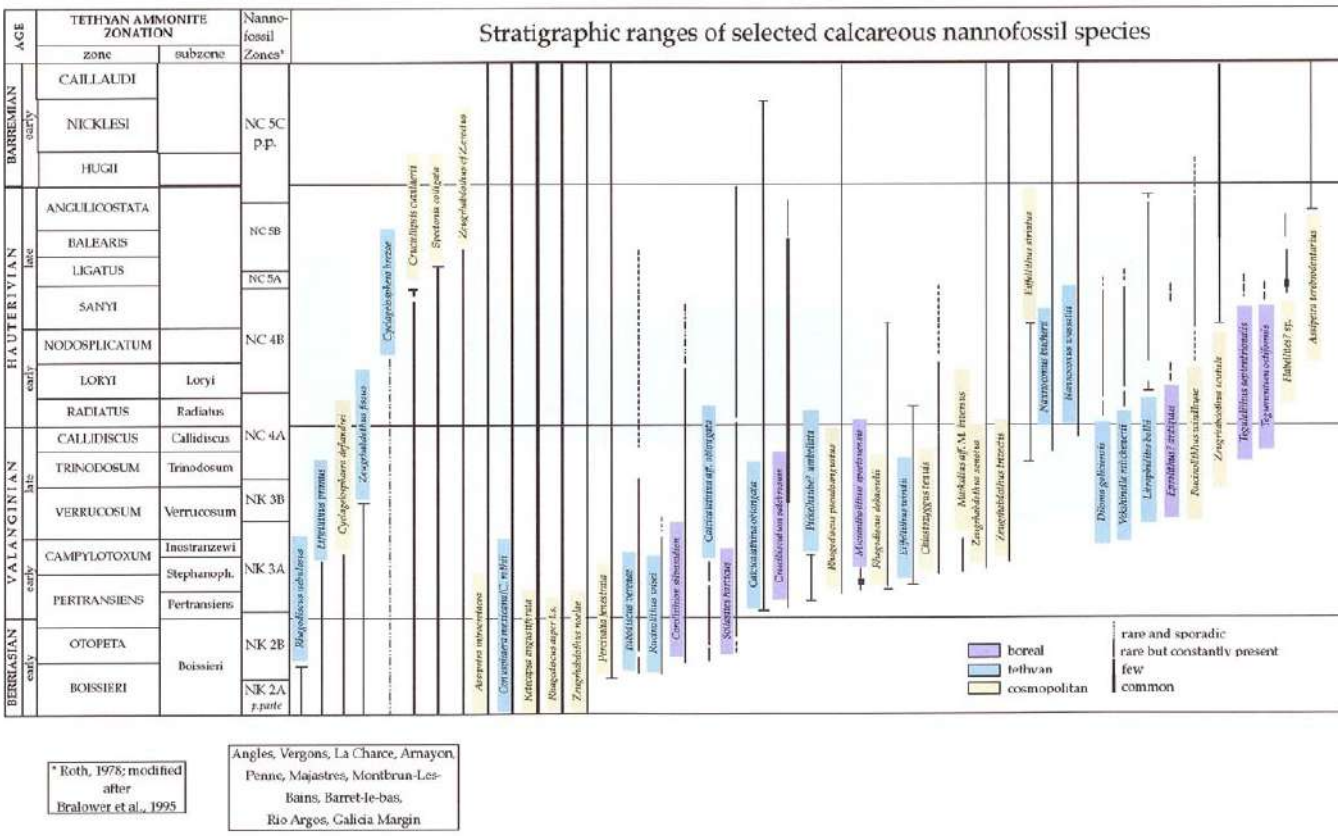

Fig.1 Summary of late Berriasian early Barremian nannofossil distribution. Data from the Vocontian basin, Betic cordillera and North Atlantic.

S2 age : Lower Cretaceous. The assemblage is too poor and scanty for a reliable age assignment.

S3 age : Lower Cretaceous. The assemblage is too poor and scanty for a reliable age assignment.

S4 age : This sample is assigned to late Hauterivian, due to the occurrence of *T. septentrionalis*, *L. bollii*, *C. oblongata*, *R. windleyae* , *Crucibiscutum salebrosum, C. trilensis* and small *Flabellites*? sp. The latter is still left in open nomenclature since no SEM analysis has been performed yet.
The FO of *Flabellites oblonga* (and the FO of genus *Flabellites*) is usually reported from current literature as a late Barremian event. However, different authors (Applegate & Bergen, 1988; Bergen 1994; Gardin et al , 2001) have reported the occurrence genus *Flabellites* (early morphotypes) in the late Hauterivian (see plate 1). According to my personal experience, the co-occurrence of common small *Flabellites*? together with *T. septentrionalis L. bolli*, *N. silvaradion, C. salebrosum* and *C. trilensis*, is a late Hauterivian event, situated around the Ligatus Ammonite zone. This event occurs in the near Vocontian basin, in the betic cordillera and in the Galicia margin (N. Atlantic). I have not found any evidence of late Barremian early Aptian markers such as *R. irregularis* in this sample sofar. The coherent Hauterivian assemblage found and its quantitative analysis is in agreement with late Hauterivian assemblages found in the near Vocontian basin and the other localities mentioned above.

S5 age : this sample contains diagnostic species such as *T. sarmatus*, *C . salebrosum*, *L . bolli*, *Zeugrhabdothus scutula*, *C. oblongata* that indicate a late Hauterivian age.

S6 : age : Lower Cretaceous. The assemblage is too poor and scanty for a reliable biostratigraphy.

S7 age : late Hauterivian due to the presence of *L. bolli*, *C. oblongata*, common *C. salebrosum*, *T. octiformis*, *Corollithion silvaradion.*

S8 age : this sample contains a diagnostic species that indicate a late Hauterivian age (co-occurrence of *R. windleayae*, *L. bolli*, *N. cornuta*, *S. colligata* and common *C. salebrosum*,) comparable to sample S4 though *T. septentrionalis* was not found and *Flabellites* ? spp. are very rare.

Conclusion

Among the eight samples from Swiss Jura the most abundance ones (S1, S4, S5, S7, S8) contain markers indicating a late Hauterivian. Though scanty and poorly preserved, the assemblages are coherent and comparable to those observed in the near Vocontian basin (SE France), betic cordillera (Spain), Galicia Margin (Atlantic ocean) for the same time interval. The occurrence of small *Flabellites?* spp. in some samples is not interpreted as evidence of late Barremian age (*F. oblongus*); instead, it is interpreted as a typical and distinct late Hauterivian event, well correlatable among low latitude sections nearby the Ligatus Ammonite zone. I have not found yet any evidence of a late Barremian - early Aptian age (*R. irregularis*) in any samples. Though the possibility of reworking and mixing of theses assemblages can not be completely ruled out, the Hauterivian component of these assemblage has to be pointed out.

References cited

Applegate J.L & Bergen J.A., 1988 ODP SR, Leg 103, p 293-348.

Bergen J.A., 1994. Journal of Nannoplankton Research, 16, 2, 59-70.

Gardin et al., 2000, 6th Intern. Cretaceous Symposium, August 27th –September 4th Wien, Abstract volume, p34.

Annexe 6.

Abstracts for Congress

Drowning of the northern Tethyan carbonate platform at the Hauterivian-Barremian boundary: expression of a global event?

Alexis Godet[1], Stéphane Bodin[1], Thierry Adatte[1] and Karl B. Föllmi[1]

[1]Institut de Géologie, Université de Neuchâtel, rue Emile Argand 11, CH-2007, Neuchâtel, Switzerland

The evolution of the shallow-water carbonate platform that developed along the northern Tethyan margin during the Jurassic and early Cretaceous is punctuated by a series of drowning events (Föllmi *et al*., 1994; Weissert *et al*., 1998). Our focus is on the event that took place close to the Hauterivian-Barremian boundary (D3 in Föllmi *et al*., 1994), which we will study by the following approaches:

1. A first goal of this study is to identify and date as precisely as possible the formations that were deposited during this drowning event in the historical type areas around Neuchâtel. Here we use biostratigraphic (macro- and microfaunas), chemostratigraphic (stable carbon and strontium isotopes), as well as sequence stratigraphic and sedimentological tools. The formations we investigate comprise (from base to the top) the "Pierre Jaune de Neuchâtel", the "Urgonien jaune", and the "Urgonien blanc" (*e.g*., Remane *et al*., 1989; van de Schootbrugge, 2001). We hope to correlate this important but controversially dated succession to coeval successions in the helvetic, Vercors and vocontian areas.

2. A second goal is to study this drowning episode in the helvetic Alps, were it is documented in the so-called "Altmann Beds" (*e.g*., Funk *et al*., 1993). The Altmann beds are composed of glauconitic and phosphatic sediments, which are generally highly condensed. The purpose of this study is to precisely document the evolution of this drowning event and its effects on the platform. Important here will be the evaluation, if this drowning event occurred in a diachronous, stepwise fashion, or in a synchronous fashion.

3. A third goal will be the correlation of the drowning event with an event of increased organic carbon burial during the latest Hauterivian, which is documented in the "Faraoni level", known from the "Pré-Alpes, vocontian, and apulian areas (Cecca *et al*., 1995; Baudin *et al*., 1999).

With the data to be expected from these surveys, we hope to establish an integral model of platform development during this period, in we put emphasis on the temporal and spatial evolution of platform drowning (regional versus global event?), and on the mechanisms involved in drowning (sea level change, nutrients, temperature, paleo CO_2, etc.).

References

Baudin F., Bulot L.G., Cecca F., Coccioni R., Gardin S. and Renard M. (1999). Un équivalent du "Niveau Faraoni" dans le bassin du Sud-Est de la France, indice possible d'un événement anoxique fini-hauterivien étendu à la Téthys méditerranéenne. Bulletin de la Société Géologique de France **170**(4): 487-498.

Cecca F., Marini A., Pallini G., Baudin F. and Begouen V. (1994). A guide-level of the uppermost Hauterivian (Lower Cretaceous) in the pelagic succession of Umbria-Marche Apennines (Central Italy): the Faraoni Level. Riv. Ital. Paleontol. Stratigr. **99**: 551-568.

Föllmi K.B., Weissert H., Bisping M. and Funk H. (1994). Phosphogenesis, carbon-isotope stratigraphy, and carbonate-platform evolution along the Lower Cretaceous northern Tethyan margin. Geological Society of America Bulletin **106**: 729-746.

Funk H., Föllmi K.B. and Mohr H. (1993). Evolution of the Tithonian-Aptian Carbonate Platform along the Northern Tethyan Margin, Eastern Helvetic Alps. *In* Simo J.A.T., Scott R.W. and Masse J.-P. Cretaceous Carbonate Platforms. American Association of Petroleum Geologists. Tulsa, OK, United States. **56:** 387-407.

Remane, J., Busnardo, R., Charollais, J., Clavel, B., and Thieuloy, J.-P. (1989). Description de profils dans l'Hauterivien de la région Neuchâteloise, du Mont-de-Chamblon et des environs de Sainte-Croix (Cantons de Neuchâtel et de Vaud, Suisse). Mémoires de la Société neuchâteloise des Sciences Naturelles, **11**, 19-48.

van de Schootbrugge B. (2001). Influence of paleo-environmental changes during the Hauterivian (Early Cretaceous) on carbonate deposition along the northern margin of the Tethys: Evidence from geochimical records (C, O, and Sr-isotopes, P, Fe, Mn). PhD Thesis, Neuchâtel (Switzerland), Université de Neuchâtel, Institut de Géologie**,** 268 p.

Weissert H., Lini A., Föllmi K.B. and Kuhn O. (1998). Correlation of Early Cretaceous carbon isotope stratigraphy and platform drowning events: a possible link? Palaeogeography, Palaeoclimatology, Palaeoecology **137**: 189-203.

Abstract for the 11th Meeting of Swiss Sedimentologists, 25th January 2003, Fribourg, Switzerland. *Poster presentation.*

Northern Tethyan carbonate platform drowning D3: a global event near the Hauterivian-Barremian boundary?

Alexis Godet[1], Stéphane Bodin[1], Thierry Adatte[1], Virginie Matera[1], Philip Steinmann[1] and Karl B. Föllmi[1]

[1]Institute of Geology, University of Neuchâtel, rue Emile Argand 11, CH-2007, Neuchâtel, Switzerland

The evolution of the shallow-water carbonate platform that developed along the northern Tethyan margin during the Jurassic and early Cretaceous is punctuated by a series of drowning events (Föllmi *et al*., 1994; Weissert *et al*., 1998). Our focus is on the event that took place close to the Hauterivian-Barremian boundary (D3 in Föllmi *et al*., 1994), which we will study by the following approaches:

1. A first goal of this study is to identify and date as precisely as possible the formations that were deposited during this drowning event in the historical type areas around Neuchâtel. Here we use biostratigraphic (macro- and microfaunas), chemostratigraphic (stable carbon and strontium isotopes), as well as sequence stratigraphic and sedimentological tools. The formations we investigate comprise (from base to the top) the "Pierre Jaune de Neuchâtel", the "Urgonien jaune", and the "Urgonien blanc" (*e.g*., Remane *et al*., 1989; van de Schootbrugge, 2001). We hope to correlate this important but controversially dated succession to coeval successions in the Helvetic, Vercors and Vocontian areas.

2. A second goal is to study this drowning episode in the Helvetic Alps, where it is documented in the so-called "Altmann Beds" (*e.g*., Funk *et al*., 1993). The Altmann beds are composed of glauconitic and phosphatic sediments, which are generally highly condensed. The purpose of this study is to precisely document the evolution of this drowning event and its effects on the platform. Important here will be the evaluation, if this drowning event occurred in a diachronous, stepwise fashion, or in a synchronous fashion.

3. A third goal will be the correlation of the drowning event with an event of increased organic carbon burial during the latest Hauterivian, which is documented in the "Faraoni level", known from the "Pré-Alpes", Vocontian, and Apulian areas (Cecca *et al*., 1994; Baudin *et al*., 1999).

With the data to be expected from these surveys, we hope to establish an integral model of platform development during this period, in we put emphasis on the temporal and spatial evolution of platform drowning (regional versus global event?), and on the mechanisms involved in drowning (sea level change, nutrients, temperature, paleo CO_2, etc.).

References:

Baudin, F., Bulot, L. G., Cecca, F., Coccioni, R., Gardin, S. et Renard, M. (1999). "Un équivalent du "Niveau Faraoni" dans le Bassin du Sud-Est de la France, indice possible d'un événement anoxique fini-hauterivien étendu à la Téthys méditerranéenne." Bull. Soc. géol. France **170**(4): 487-498.

Cecca, F., Pallini, G., Erba, E., Premoli-Silva, I. et Coccioni, R. (1994). "Hauterivian-Barremian chronostratigraphy based on ammonites, nannofossils, planktonic foraminifera and magnetic chrons from the Mediterranean domain." Cretaceous Research **15**(4): 457-467.

Föllmi, K. B., Weissert, H., Bisping, M. et Funk, H. (1994). "Phosphogenesis, carbon-isotope stratigraphy, and carbonate-platform evolution along the Lower Cretaceous northern Tethyan margin." Geological Society of America Bulletin **106**(II): 729-746.

Funk, H., Foellmi, K. B. et Mohr, H. (1993). Evolution of the Tithonian-Aptian carbonate platform along the northern Tethyan margin, eastern Helvetic Alps. Cretaceous carbonates platforms. Simo J.A.T., Scott R.W. and Masse J. P., American Association of Petroleum Geologists. Tulsa, OK, United States.

56: 387-407.

Remane, J. (1989). "The historical type Hauterivian of the Jura mountains : original definition, actual concept, lithostratographic subdivision." Mémoires de la Société neuchâteloise des Sciences naturelles **XI**: 9-18.

van de Schootbrugge, B. (2001) "Influence of paleo-environmental changes during the Hauterivian (Early Cretaceous) on carbonate deposition along the northern margin of the Tethys: Evidence from geochemical records (C, O and Sr-isotopes, P, Fe, Mn)." PhD Thesis in Geology, University of Neuchâtel, Institut of Geology, Neuchâtel (Switzerland): 268 p.

Weissert, H., Lini, A., Föllmi, K. B. et Kuhn, O. (1998). "Correlation of Early Cretaceous carbon isotope stratigraphy and platform drowning events : a possible link ?" Palaeogeography, Palaeoclimatology, Palaeoecology **137**: 189-203.

Abstract for the Paléocéanographie du Mésozoïque, Réunion Spécialisée de la Société Géologique de France, 10th-11th July 2003, Paris, France. *Poster presentation.*

Dating early Cretaceous formations around Neuchâtel: a multi-disciplinary approach

Alexis Godet[1], Stéphane Bodin[1], Thierry Adatte[1], Virginie Matera[1], Philipp Steimann[1], Jean Vermeulen[2] and Karl B. Föllmi[1]

[1]Institut de Géologie, Université de Neuchâtel, rue Emile Argand 11, 2007 Neuchâtel Switzerland; [2]Grand Rue, 04330 Barrême, France

For over a century, the Early Cretaceous formations cropping out around the city of Neuchâtel, Switzerland, have been studied from a biostratigraphical point of view, as they constitute the historical stratotype of the Valanginian and Hauterivian stages. The Hauterivian stratotype was initially formed of the "Marnes à Astiera", the "Marnes d'Hauterive" and the "Pierre Jaune de Neuchâtel". As a consequence, the formations "Urgonien Jaune" and "Urgonien Blanc" which follow on top of these formations were attributed to the Barremian stage. A recent study showed that there is no biostratigraphical evidence for such a date (Remane, Busnardo and Charollais, coord., 1989). This period is seen as an important time during which a significant carbonate platform drowning period occurred (defined as D3 event in the Helvetic realm by Föllmi *et al*., 1994).

During the last year, we investigated a fresh section, cropping out in the canton of Neuchâtel, at Vaumarcus, that allowed us to study the three formations that are controversially dated: the "Pierre Jaune", the "Urgonien Jaune" and the "Urgonien Blanc". Several families of fauna were taken into consideration, but the preliminary results do not allow us to identify the Hauterivian/Barremian boundary in the Vaumarcus section.

Other tools will be used, such as gamma ray prospecting for sequence stratigraphy (La Lance section, canton of Vaud), ICP – MS measurements (Buttes section, canton of Neuchâtel), or $^{87}Sr/^{86}Sr$ measurement on brachiopods (La Russille section, canton of Vaud).

As an alternative, we studied three (hemi-) pelagic sections (Fiume Bosso, Italy; Veveyse Châtel St Denis, Switzerland; Angles, France) for their geochemical and isotopic signals, and for their sequence stratigraphy. Although these sections display ages from Late Hauterivian to Late Barremian, we have focused on the latest Hauterivian, to characterize the Hauterivian – Barremian boundary, and to look for an expression of the D3 event. We hope to be able to correlate pelagic sections, that are extremely well dated by ammonites, with formations of the Neuchâtel area, in order to constrain the age of the lower Cretaceous formations in the Swiss Jura.

Keywords: Early Cretaceous, Swiss Jura, stratigraphy.

Abstract for the 32nd International Geological Congress, 20th-28th August 2004, Florence, Italy.
Oral Presentation

The Hauterivian Historical Stratotype: Comparision of Biostratigaphy and Geochemistry

Alexis Godet[1], Stéphane Bodin[1], Thierry Adatte[1], Virginie Matera[1], Philipp Steimann[1], Jean Vermeulen[2], Silvia Gardin[3] and Karl B. Föllmi[1]

[1]Institut de Géologie, Université de Neuchâtel, Switzerland; [2]Grand rue, 04330 Barrême, France; [3]Université Pierre & Marie Curie (Paris VI) Paléontologie et Stratigraphie - URA 1761, Paris, France

For over a century, the Early Cretaceous formations cropping out around the city of Neuchâtel, Switzerland, have been studied from a biostratigraphical point of view, as they constitute the historical stratotype of the Valanginian and Hauterivian stages. The Hauterivian stratotype was initially formed of the "Marnes à Astiera", the "Marnes d'Hauterive" and the "Pierre Jaune de Neuchâtel". As a consequence, the formations "Urgonien Jaune" and "Urgonien Blanc" which follow on top of these formations were attributed to the Barremian stage. A recent study showed that there is no biostratigraphical evidence for such a date (Remane, Busnardo and Charollais, coord., 1989). This period is seen as an important time during which a significant carbonate platform drowning period occurred (defined as D3 event in the Helvetic realm by Föllmi *et al*., 1994).

During the last year, we investigated a fresh section, cropping out in the canton of Neuchâtel, at Vaumarcus, that allowed us to study the three formations that are controversially dated: the "Pierre Jaune", the "Urgonien Jaune" and the "Urgonien Blanc". Several families of fauna were taken into consideration, but the preliminary results do not allow us to identify the Hauterivian/Barremian boundary in the Vaumarcus section.

Other tools will be used, such as gamma ray prospecting for sequence stratigraphy (La Lance section, canton of Vaud), ICP – MS measurements (Buttes section, canton of Neuchtel), or $^{87}Sr/^{86}Sr$ measurement on brachiopods (La Russille section, canton of Vaud).

As an alternative, we studied three (hemi-) pelagic sections (Fiume Bosso, Italy; Veveyse Châtel St Denis, Switzerland; Angles, France) for their geochemical and isotopic signals, and for their sequence stratigraphy. Although these sections display ages from Late Hauterivian to Late Barremian, we have focused on the latest Hauterivian, to characterize the Hauterivian – Barremian boundary, and to look for an expression of the D3 event. We hope to be able to correlate pelagic sections, that are extremely well dated by ammonites, with formations of the Neuchâtel area, in order to constrain the age of the lower Cretaceous formations in the Swiss Jura.

Abstract for the Joint Earth Sciences Meeting Geological Society of France - Geologische Vereinigung, 20th-25th September 2004, Strasbourg, France. *Poster presentation.*

Mineralogy and geochemistry as key - proxies to determine the precise age of the Hauterivian historical stratotype (Neuchâtel, Switzerland)?

Alexis Godet[1], Stéphane Bodin[1], Jean Vermeulen[2], Peter Stille[3], Thierry Adatte[1] and Karl B. Föllmi[1]*

[1]Institut de Gologie, Université de Neuchâtel, rue Emile Argand 11, CH-2007 Neuchâtel; [2]Grand Rue, F-04330 Barrême; [3]ULP - EOST – CNRS Centre de géochimie de la surface / UMR 7517. 1 rue Blessig, F-67084 Strasbourg CEDEX

In 1874, Renevier defined the historical stratotype of the Hauterivian stage in the canton of Neuchatel, which – according to him – was composed, from base to top, by the Marnes à Astiera, the Marnes bleues d'Hauterive, the Mergelkalkzone and the Pierre Jaune de Neuchâtel. In 1901, Baumberger attributed the succession of the Urgonien Jaune and Urgonien blanc, which follows on top the Pierre Jaune de Neuchâtel, to the Barremian without any biostratigraphic argument.

During the second half of the 20th century, a dispute developed between two schools of thought with regards to the age of the Urgonian limestone. Clavel *et al*. (1995) assumed a late Hauterivian age for the Urgonien Jaune and placed the Hauterivian/Barremian boundary within the Urgonien Blanc, whereas Arnaud-Vanneau and Arnaud (1990) proposed the presence of an important hiatus at the top of the Pierre Jaune and a late Barremian age for the entire Urgonian limestone. They related this hiatus to a phase of emersion, which is dated as approximately early Barremian. In the Helvetic Alps, where the distal prolongation of the Jura carbonate platform system is preserved, a platform drowning phase was identified during the middle Hauterivian (D2 in Föllmi *et al*., 1994) and the latest Hauterivian – latest early Barremian (D3 in Föllmi *et al*., 1994; Bodin, Godet *et al*., in prep.).

The goal of our research is to determine a precise age for the top of the Pierre Jaune de Neuchâtel and the Urgonian limestone, and to determine, if the drowning phases documented in the Helvetic Alps also left their imprint in the successions of the Jura carbonate platform. In order to reach these goals, several approaches are developed. First of all, a re-examination of the biostratigraphic data (orbitolinids, rudists, echinoids, green algae) did not allow us to obtain an accurate age framework. We are presently using an alternative approach that consists of the determination of $^{87}Sr/^{86}Sr$ values in well-preserved rhynchonellids, which will then be compared to the well calibrated $^{87}Sr/^{86}Sr$ curve of Jones and Jenkyns (2001). We also investigating the discontinuities which are present in the middle and at the top of the Pierre Jaune de Neuchâtel, and which suggest that the Pierre Jaune de Neuchâtel consist of two sedimentary sequences. The high amount of fresh glauconite associated with these discontinuities may help to improve age control and correlations between the different sedimentary realms along the northern Tethys. A third approach consists in the study of the clay mineralogy along a paleogeographic transect from the Jura platform into the hemipelagic Vocontian basin. We observe a nearly absence of kaolinite in sediments of Hauterivian age, and its appearance in sediments of early Barremian age for all studied sections along this transect (Route d'Angles, Barterand, Cluses, Cressier, Boudry, Gorges de l'Areuse and Eclépens).

References

Arnaud-Vanneau, A. and Arnaud, H. (1990). "Hauterivian to Lower Aptian carbonate shelf sedimentation and sequence stratigraphy in the Jura and northern Subalpine chains (southeastern France and Swiss Jura)". *In* Tucker M. E., Wilson J. L., Crevello P. D., Sarg J. R. and Read J. F. "Carbonate Platforms: Facies, Sequences and Evolution", Blackwell Scientific Publications, Special Publication of the International Association of Sedimentologists. **9:** 203-233.

Baumberger, E. (1901). "Uber Facies und Transgressionen der untern Kreid am Nordrande mediterrano - helvetischen Bucht im westlichen Jura." Wiss. Beil. Ber. Töchterschule Basel: 1-44.

Bodin, S., Godet, A., Matera, V., Steinmann, P., Vermeulen, J., Gardin, S., Adatte, T., Coccioni, R. and Föllmi, K. B. (in prep.). "Enrichment of redox-sensitive trace metals (U, V, Mo, As) in carbonates associated with the late Hauterivian Faraoni oceanic anoxic event."

Clavel, B., Charollais, J., Schroeder, R. and Busnardo, R. (1995). "Réflexions sur la biostratigraphie du Crétacé inférieur et sur sa complémentarité avec l'analyse séquentielle : exemple de l'Urgonien jurassien et subalpin." Bull. Soc. géol. France **166**(6): 663-680.

Föllmi, K. B., Weissert, H., Bisping, M. and Funk, H. (1994). "Phosphogenesis, carbon-isotope stratigraphy, and carbonate-platform evolution along the Lower Cretaceous northern Tethyan margin." Geological Society of America Bulletin **106**(II): 729-746.

Jones, C. E. and Jenkyns, H. C. (2001). "Seawater strontium isotopes, oceanic anoxic events, and seafloor hydrothermal activity in the Jurassic and Cretaceous." American Journal of Science **301**: 112-149.

Renevier, E. (1874). "Tableau des terrains sédimentaires formés pendant les époques de la phase organique du globe terrestre avec leurs représentants en Suisse et dans les régions classiques, leurs synonymes et les principaux fossiles de chaque étage." Bull. Soc. vaud. Sci. nat. **13**: 218-252.

Abstract for the 13th Meeting of Swiss Sedimentologists, 29th January 2005, Fribourg, Switzerland. *Poster presentation.*

Climate change documented by clay-mineral assemblages from the Barremian stratotype (Angles, France)

Alexis Godet[1], Stephane Bodin[1], Thierry Adatte[1], Jean Vermeulen[2] and Karl B. Föllmi[1]

[1]Institut de Géologie, Université de Neuchâtel, rue Emile Argand 11, 2007 Neuchâtel Switzerland; [2]Grand rue, 04330 Barrême France

In the Helvetic realm, the late Hauterivian and the Barremian are times of major change in the type of carbonate production: the Kieselkalk Formation (Hauterivian) is dominated by heterozoan assemblages, whereas the Urgonian Limestone ("Schrattenkalk"; Barremian and early Aptian) includes the remains of mainly photozoan ecosystems. A similar change is documented in the western Swiss Jura, where the "Pierre Jaune de Neuchâtel" and the "Urgonien blanc" correspond to heterozoan and photozoan facies assemblages, respectively.

In order to test if this major change is linked to climate variations, we analysed the clay-mineral assemblage of the Angles section by XRD. This section is located in the Vocontian trough and consists of limestone-marl alternations. Both bulk rock and decarbonated samples were analysed. The evolution of the detrital index allows to divide the section into three parts: during the late Hauterivian and from the *H. feraudianus* ammonite zone (late Barremian) onward, the detrital influence is higher than in the rest of the section (from the Faraoni level equivalent located at the base of the *P. mortilleti* zone up to the *H. feraudianus* zone). This threefold division is also applicable to the evolution of clay minerals, both for the <2μm and the 2-16μm fractions. Even if the most abundant clay mineral is mica, the kaolinite content increases in the middle part of the section, whereas it is nearly absent in clay assemblages from the latest Barremian and the early Aptian. On the other hand, the smectite evolution displays an antagonistic pattern, with a minimum of the smectite/mica ratio during most of the Barremian. In terms of climate, these trends seem to reflect changes between dry and humid periods. Indeed, the formation of kaolinite requires warm and wet environments, such as those that are characteristic of tropical zones. On the other hand, smectite is a typical clay mineral for temperate climate zones where seasons are well marked. One of the most striking features of this study is that both the detrital index as well as climate evolution coincide with remarkable surfaces in the section. The onset of kaolinite is synchronous with the decrease in the continental detrital input, and they both start at the Faraoni level equivalent, which is representative for a well-known anoxic event of the Tethyan realm. On the other hand, the change from tropical to aride climate is coeval with the B4 sequence boundary that is concomitant with the installation of the Urgonian platform along the northern Tethyan margin.

Moreover, these climatic changes are not only recorded in pelagic settings. A transect from the Vocontian trough, the subalpine chains (Viéban, 1983) and the western Swiss Jura (Rumley, 1993; Blanc-Aletru, 1995) reveals that temporal trends in the occurrence of kaolinite during the Hauterivian and the Barremian is correlated between the three studied regions. This correlation allows us to confirm the late Barremian age of the Urgonian limestones from the Neuchâtel area.

References

Blanc-Aletru, M. C. (1995). Importance des discontinuités dans l'enregistrement sédimentaire de l'Urgonien jurassien. Micropaléontologie, Sédimentologie, Minéralogie et Stratigraphie Séquentielle. Ph.D. Thesis Grenoble, Laboratoire de Géologie de l'Université I de Grenoble. Géologie Alpine **mémoire HS n°24:** 299 pp.

Rumley, G. (1993). Sédimentologie, minéralogie et stratigraphie de l'Hauterivien dans le Jura neuchâtelois et vaudois (Suisse). Ph.D. Thesis Faculté des Sciences, Institut de Géologie. Neuchâtel,

Université de Neuchâtel**:** 207 pp.

Viéban, F. (1983). Installation et évolution de la plate-forme urgonienne (Hauterivian à Bédoulien) du Jura méridional aux chaînes subalpines (Ain, Savoie, Haute-Savoie). Sédimentologie, minéralogie, stratigraphie et paléogéographie. Ph.D. Thesis. Grenoble, Université de Grenoble**:** 293 pp.

Abstract for Sediment 05, 18th-20th July 2005, Gwatt, Lake of Thun, Switzerland. *Oral presentation.*

Sr-isotopes stratigraphy and clay minerals correlation as decisive tools to date the Hauterivian historical stratotype around Neuchâtel, Switzerland

Alexis Godet[1], Stéphane Bodin[1], Thierry Adatte[1], Peter Stille[2], Virginie Matera[1] and Karl B. Föllmi[1]

[1]Institut de Géologie, Université de Neuchâtel, rue Emile Argand 11, 2007 Neuchâtel, Switzerland; [2]ULP-Ecole et Observatoire des Sciences de la Terre-CNRS Centre de Géochimie de la Surface/UMR7517 Cycles Géochimiques et Impacts Anthropiques. 1 rue Blessig, 67084 Strasbourg Cedex France

Defined in 1874 by Renevier, the Hauterivian historical stratotype is composed, from base to top, by the Marnes à Astiera, the Marnes bleues d'Hauterive, the Mergelkalk zone and the Pierre Jaune de Neuchâtel; the dating of these formations is mainly controlled by ammonites whereas the Urgonien Jaune and the Urgonien Blanc, that follow on top the Pierre Jaune de Neuchâtel and are separated by the Marnes de la Russille, are lacking such fossils.

Despite an attempt to revise the age of these formations (Remane *et al.*, 1989), two schools of thought appears in the 90's. On the one hand, Arnaud-Vanneau and Arnaud (1990) supposed that a huge hiatus, located at the top of the Pierre Jaune de Neuchâtel, implies a late Barremian age for both the Urgonien Jaune and the Urgonien Blanc. On the other hand, Clavel *et al.* (1995) attributed the Urgonien Jaune to the late Hauterivian and the major part of the Urgonien Blanc to the early Barremian; after these authors, the Hauterivian-Barremian boundary should fall within the Urgonian Blanc.

Recently, we investigated a fresh and new outcrop at Vaumarcus (20 km south-westward from Neuchâtel). The studied faunas consist of orbitolinids, rudists, echinoids, green algae and nannofossils. Unfortunately, they gave inconsistent age model: the rudists, that are located in a higher stratigraphic position than the orbitolinids, gave the oldest age.

In order to elucidate this dilemma, we developed methods which were never applied to these formations. First of all, selected brachiopod shells were analysed for their $^{87}Sr/^{86}Sr$ ratio. The results were compared to a global $^{87}Sr/^{86}Sr$ curve obtained from published data (Jenkyns and Wilson, 1999; Veizer *et al.*, 1999; van de Schootbrugge, 2001). The correlation of our results with the global curve reveals that the Marnes de la Russille and the Urgonien Blanc display high values characteristic of the Barremian. However, this approach did not help us to date the Urgonien Jaune, as brachiopods from this formation hold $^{87}Sr/^{86}Sr$ ratios similar to the ones of the late Hauterivian or the early Barremian.

An other clue for the age of the Swiss urgonian formations is given by the correlation of clay minerals. In the Vocontian trough, the analysis of pelagic sections revealed a striking behaviour of the kaolinite; this mineral, very common under hot and humid climate, appears from the Faraoni level equivalent recovered in the Angles section, reaches two maxima in the early and the late Barremian (*K. nicklesi* and *H.uhligi* ammonite zones, respectively), and disappears in the lowermost Aptian (*D. oglalensis* zone). This evolution is also recognized in the subalpine chains, more precisely in the Barterand section studied by Viéban (1983). In sections from the Neuchâtel area, the kaolinite is absent from the Marnes bleues d'Hauterive to the Pierre Jaune de Neuchâtel, but appears in the lowermost Urgonien Jaune and reaches amount comparable to the ones observed in pelagic settings in the upper part of the Urgonien Jaune and in the entire Urgonien Blanc.

As a conclusion, it seems that the combination of geochemistry and mineralogy provide good information concerning the age of the urgonian formation from the swiss Jura. From this study it comes that the Urgonien Jaune and the Urgonien Blanc belong to the Barremian.

This study is financially supported by the Swiss National Fund (projects n°2100-067807/1 and

200020-105206/1).

References

Arnaud-Vanneau, A. and Arnaud, H. (1990). “Hauterivian to Lower Aptian carbonate shelf sedimentation and sequence stratigraphy in the Jura and northern Subalpine chains (southeastern France and Swiss Jura)”. *In* Tucker M. E., Wilson J. L., Crevello P. D., Sarg J. R. and Read J. F., eds. "Carbonate Platforms: Facies, Sequences and Evolution", *Blackwell Scientific Publications, Special Publication of the International Association of Sedimentologists*. **9:** 203-233.

Clavel, B., Charollais, J., Schroeder, R. and Busnardo, R. (1995). "Réflexions sur la biostratigraphie du Crétacé inférieur et sur sa complémentarité avec l'analyse séquentielle : exemple de l'Urgonien jurassien et subalpin." Bull. Soc. géol. France **166**(6): 663-680.

Jenkyns, H. C. and Wilson, P. A. (1999). "Stratigraphy, paleoceanography, and evolution of Cretaceous pacific guyots: relics from a greenhouse Earth." American Journal of Science **299**: 341-392.

Remane, J., Busnardo, R. and Charollais, J. (1989). "Révision de l'étage Hauterivien (région - type et environs, Jura franco - suisse)". Neuchâtel (Suisse), Société Neuchâteloise des Sciences Naturelles, Université, 322 pp.

Renevier, E. (1874). "Tableau des terrains sédimentaires formés pendant les époques de la phase organique du globe terrestre avec leurs représentants en Suisse et dans les régions classiques, leurs synonymes et les principaux fossiles de chaque étage." Bull. Soc. vaud. Sci. nat. **13**: 218-252.

van de Schootbrugge, B. (2001). Influence of paleo-environmental changes during the Hauterivian (early Cretaceous) on carbonate deposition along the northern margin of the Tethys: Evidence from geochemical records (C, O and Sr-isotopes, P, Fe, Mn). Ph.D. Thesis Institut de Géologie. Neuchâtel, Université de Neuchâtel**:** 291 p.

Veizer, J., Ala, D., Azmy, K., Bruckschen, P., Buhl, D., Bruhn, F., Carden, G. A. F., Diener, A., Ebneth, S. and Godderis, Y. (1999). "$^{87}Sr/^{86}Sr$, $\delta^{13}C$ and $\delta^{18}O$ evolution of Phanerozoic seawater." Chemical Geology **161**(1-3): 59-88.

Viéban, F. (1983). Installation et évolution de la plate-forme urgonienne (Hauterivian à Bédoulien) du Jura méridional aux chaînes subalpines (Ain, Savoie, Haute-Savoie). Sédimentologie, minéralogie, stratigraphie et paléogéographie. Ph.D. Thesis. Grenoble, Université de Grenoble**:** 293 pp.

Abstract for the 7th International Symposium on the Cretaceous, 5th-7th September 2005, Neuchâtel, Switzerland. *Oral Presentation*

Climate induced stable isotope evolution during the early Cretaceous: example from the Barremian stratotype (Angles section, SE France)

Alexis Godet[1], Stéphane Bodin[1], Karl B. Föllmi[1], Jean Vermeulen[2], Zsolt Berner[3], Doris Stüben[3] and Thierry Adatte[1]

[1]Institut de Géologie, Université de Neuchâtel, rue Emile Argand 11, 2007 Neuchâtel Switzerland; [2]Grand Rue, 04330 Barrême, France; [3]Institut für Mineralogie und Geochemie, Universität Karlsruhe, 76131 Karlsruhe, Germany

The early Cretaceous is punctuated by several major paleoceanographic perturbations, in particular the latest Hauterivian and the early Barremian saw the development of an oceanic anoxic event which is documented in the Faraoni level recovered in pelagic sections from Italy, France and Switzerland. This event is located at the top of the *S. angulicostatum* ammonite zone. Approximately at the same time, the Helvetic carbonate platform underwent a drowning episode; the D3 event (after Föllmi *et al.*, 1994) is documented in the so-called Altmann Beds which cover the time span from the late *B. balearis* to the *C. darsi* ammonite zone.

Surprisingly, the high-resolution $\delta^{13}C$ analysis performed on bulk rock of the Angles section (Vocontian trough, SE France), which is the Barremian stratotype, reveals no major positive shift in $\delta^{13}C$ characteristic of others OAE's (e.g, the Aptian or the Cenomanian - Turonian OAE), but rather a very stable evolution during the whole part of the Barremian. During the same period, XRD analysis points out the presence of kaolinite in both the < 2 μm and the 2 - 16 μm, with amounts reaching 40 or 50 %. This increase in kaolinite content reflects the change from an arid climate during the Hauterivian to humid (intertropical) conditions during the Barremian.

As a consequence of the enhanced humidity, the continental weathering should have increased, implying more Dissolved Inorganic Carbon (DIC) delivered into the ocean. Due to the buffering effect of the increased oceanic DIC pool, the $\delta^{13}C$ record should have become less sensitive to paleoceanographic change.

From the *C. darsi* zone, the rise of carbonate platform under oligotrophic conditions in the Helvetic realm allowed the return to more positive $\delta^{13}C$ values, thanks to the carbon recycling by photosynthetic organisms which built the platform. Moreover, the export of aragonite, which is the main carbonate mineral produced by photozoan assemblages, could also be responsible, at least in part, for the positive shift from 2 to 2.2 ‰ observed during the *C. darsi* zone.

Abstract for the 7th International Symposium on the Cretaceous, 5th-9th September 2005, Neuchâtel, Switzerland. *Poster Presentation*

Age-diagnostic nannofossil assemblages, strontium isotope ratios, and kaolinite distributions in Urgonian sediments from the Swiss Jura mountains: implications for its depositional history and correlation

Alexis Godet[1], Stéphane Bodin[1], Eric de Kaenel[2], Peter Stille[3], Thierry Adatte[1] and Karl B. Föllmi[1]

[1]Institut de Géologie, Université de Neuchâtel, rue Emile Argand 11, CH-2007 Neuchâtel. Email: alexis.godet@unine.ch / +41.032.718.26.25; [2]DeKaenel Paleo-Research, CH-2000 Neuchâtel; [3]ULP - EOST – CNRS Centre de géochimie de la surface / UMR 7517. 1 rue Blessig, F-67084 Strasbourg CEDEX

Since the definition of the historical stratotype of the Hauterivian stage (Renevier, 1874) and the assignment of the Urgonian formation of the Neuchâtel area to the Barremian (Baumberger, 1901), the age attribution of the Urgonien Jaune and Urgonien Blanc has been riddled with incertitude and controversy (*e.g.*, Arnaud-Vanneau and Arnaud, 1990; Clavel *et al.*, 1995; Charollais *et al.*, 2003). Here we propose a new age for these formations, which is based on age-diagnostic nannofossil assemblages, strontium isotope ratios, and kaolinite distributions, and which allows for a firm correlation of this formation with other Urgonian occurrences along the northern Tethyan margin.

Recently in the quarry of Eclépens (canton of Vaud), we identified a well-preserved and age-indicative nannofossil assemblage in two dark and marly intervals near the base of the Urgonien Jaune. The presence of *Flabellites oblongus* together with the absence of *Hayesites irregularis* in the lower marly interval indicate a late Barremian age (NC5D-NC5E nannofossil subzone; *C. sarasini* ammonite zone), whereas the presence of *H. irregularis*, *Nannoconus truitti* and *Rhagodiscus gallagheri* in the upper marly interval is indicative for the earliest Aptian (NC6A nannofossil subzone; *D. oglanlensis* ammonite zone). Consequently, according to these nannofossil assemblages, the main part of the Urgonian limestone from the western Swiss Jura belongs to the early Aptian.

This nannofossil-derived age is coherent with ages obtained by $^{87}Sr/^{86}Sr$ dating. Rhynchonellid brachiopods from the Urgonien Jaune and Urgonien Blanc yield mean Sr-isotope ratios of 0.707458 and 0.707513, respectively, which is coherent with the high values observed for the latest Barremian – earliest Aptian (*e.g.*, Jenkyns and Wilson, 1999). As a control, rhynchonellid brachiopods from the Marnes Bleues d'Hauterive gave a mean ratio of 0.707421, which is coherent with the early Hauterivian age obtained by ammonite biostratigraphy.

The evolution of the kaolinite content (fraction $<2\mu$m) along a north-south transect along the northern Tethyan margin is also compatible with the age indicated by the nannofossils, but its interpretation is more delicate. In the western Swiss Jura (Eclépens section), kaolinite is absent in the Pierre Jaune de Neuchâtel and makes up more than 40% of the total clay mineral assemblage of the Urgonien Jaune and the Urgonien Blanc, describing a positive stratigraphic trend. In more distal settings (Cluses section, subalpine chains, France; Wermeille 1996), the kaolinite content reaches approximately 30% in the late Barremian (Ba5 depositional sequence, *M. sarasini* ammonite zone after Arnaud *et al.*, 1998), and high values continue until the Ap2 sequence (early Aptian, *D. weissi* ammonite zone), which is compatible with the age given by nannofossils in the vicinity of Neuchâtel. However in hemipelagic settings (*e.g.*, Angles and Combe-Lambert sections, Vocontian trough, France), high kaolinite contents are recorded in the Barremian, whereas the early Aptian is rather characterized by values around 15%. A positive trend is observed between the *M. sarasini* and the *D. weissi* ammonite zones, which is coherent with the trend observed in the western Swiss Jura. In order to explain the discrepancy in overall kaolinite contents, we invoke a platform-basin fractionation mechanism which may lower the quantity of kaolinite recorded in the basin.

References

Arnaud, H., Arnaud-Vanneau, A., Blanc-Aletru, M. C., Adatte, T., Argot, M., Delanoy, G., Thieuloy, J.-P., Vermeulen, J., Virgone, A., Virlouvet, B. and Wermeille, S. (1998). "Répartition stratigraphique des orbitolinidés de la plate-forme urgonienne subalpine et jurassienne (SE de la France)." Géologie Alpine **74**: 3-89.

Arnaud-Vanneau, A. and Arnaud, H. (1990). Hauterivian to Lower Aptian carbonate shelf sedimentation and sequence stratigraphy in the Jura and northern Subalpine chains (southeastern France and Swiss Jura). Carbonate Platforms: Facies, Sequences and Evolution. M. E. Tucker, J. L. Wilson, P. D. Crevello, J. R. Sarg and J. F. Read, Blackwell Scientific Publications, Special Publication of the International Association of Sedimentologists. **9:** 203-233.

Baumberger, E. (1901). "Uber Facies und Transgressionen der untern Kreid am Nordrande mediterrano - helvetischen Bucht im westlichen Jura." Wiss. Beil. Ber. Töchterschule Basel: 1-44.

Charollais, J., Clavel, B., Schroeder, R., Busnardo, R., Decrouez, D. and Cherchi, A. (2003). "La migration de la plate-forme urgonienne entre le Jura plissé et les Chaines subalpines septentrionales (France, Suisse): Evolution of the Urgonian platform between the Jura and the Septentrional Subalpine Chains (France, Switzerland)." Geobios **36**(6 SU -): 665-674.

Clavel, B., Charollais, J., Schroeder, R. and Busnardo, R. (1995). "Réflexions sur la biostratigraphie du Crétacé inférieur et sur sa complémentarité avec l'analyse séquentielle: exemple de l'Urgonien jurassien et subalpin." Bull. Soc. géol. France **166**(6): 663-680.

Jenkyns, H. C. and Wilson, P. A. (1999). "Stratigraphy, paleoceanography, and evolution of Cretaceous pacific guyots: relics from a greenhouse Earth." American Journal of Science **299**: 341-392.

Renevier, E. (1874). "Tableau des terrains sédimentaires formés pendant les époques de la phase organique du globe terrestre avec leurs représentants en Suisse et dans les régions classiques, leurs synonymes et les principaux fossiles de chaque étage." Bull. Soc. vaud. Sci. nat. **13**: 218-252.

Wermeille, S., 1996, Etude sédimentologique, minéralogique et micropaléontologique des calcaires urgoniens de la région subalpine (Savoie, France). Coupes du Rocher de Cluses, du Borne et d'Andey: Unpublished diploma thesis, thesis, University of Neuchâtel, Neuchâtel, 129 p.

Abstract for the 14th Meeting of Swiss Sedimentologists, 28th January 2006, Fribourg, Switzerland. *Oral Presentation*

Age, mineralogy and correlation of early Cretaceous sediments from the Western Swiss Jura

Alexis Godet[1], Stéphane Bodin[1], Eric de Kaenel[2], Peter Stille[3], Thierry Adatte[1] and Karl B. Föllmi[1]

[1]Institut de Géologie, Université de Neuchâtel, rue Emile Argand 11, CH-2007 Neuchâtel; [2]DeKaenel Paleo-Research, CH-2000 Neuchâtel; [3]ULP - EOST – CNRS Centre de géochimie de la surface / UMR 7517. 1 rue Blessig, F-67084 Strasbourg CEDEX

Since the definition of the historical stratotype of the Hauterivian stage (Renevier, 1874) and the assignment of the Urgonian formation of the Neuchâtel area to the Barremian (Baumberger, 1901), the age attribution of the Urgonien Jaune and Urgonien Blanc has been riddled with incertitude and controversy (*e.g.*, Arnaud-Vanneau and Arnaud, 1990; Clavel *et al.*, 1995; Charollais *et al.*, 2003). Here we propose a new age for these formations, which is based on age-diagnostic nannofossil assemblages, strontium isotope ratios, and kaolinite distributions, and which allows for a firm correlation of this formation with other Urgonian occurrences along the northern Tethyan margin.

Recently in the quarry of Eclépens (canton of Vaud), a well-preserved and age-diagnostic nannofossil assemblage was identified in two dark and marly intervals near the base of the Urgonien Jaune, which indicates a late Barremian to earliest Aptian age. Consequently, the main part of the Urgonian limestone from the western Swiss Jura belongs to this period.

This nannofossil-derived age is coherent with ages obtained by $^{87}Sr/^{86}Sr$ dating. Rhynchonellid brachiopods from the Urgonien Jaune and Urgonien Blanc indicate a late Barremian – earliest Aptian age. As a control, rhynchonellid brachiopods from the Marnes Bleues d'Hauterive gave a mean ratio of 0.707421, which is coherent with the early Hauterivian age obtained by ammonite biostratigraphy.

The evolution of the kaolinite content (fraction <2μm) along a north-south transect along the northern Tethyan margin is also compatible with the age indicated by the nannofossils, but its interpretation is more delicate. In the western Swiss Jura, kaolinite is absent in the Pierre Jaune de Neuchâtel and makes up more than 40% of the total clay mineral assemblage of the Urgonien Jaune and the Urgonien Blanc, describing a positive stratigraphic trend. In more distal settings (Cluses section, subalpine chains, France; Wermeille 1996), the kaolinite content reaches approximately 30% in the late Barremian (Ba5 depositional sequence, *M. sarasini* ammonite zone after Arnaud *et al.*, 1998), and high values continue until the Ap2 sequence (early Aptian, *D. weissi* ammonite zone). However in hemipelagic settings (*e.g.*, Angles and Combe-Lambert sections, Vocontian trough, France), high kaolinite contents are recorded in the Barremian, whereas the early Aptian is rather characterized by values around 15%. A positive trend is observed between the *M. sarasini* and the *D. weissi* ammonite zones, which is similar to the trend observed in the region of Neuchâtel. In order to explain the discrepancy in overall kaolinite contents, we invoke a platform-basin fractionation mechanism which may lower the quantity of kaolinite recorded in the basin.

References

Arnaud, H., Arnaud-Vanneau, A., Blanc-Aletru, M. C., Adatte, T., Argot, M., Delanoy, G., Thieuloy, J.-P., Vermeulen, J., Virgone, A., Virlouvet, B. and Wermeille, S. (1998). "Répartition stratigraphique des orbitolinidés de la plate-forme urgonienne subalpine et jurassienne (SE de la France)." Géologie Alpine **74**: 3-89.

Arnaud-Vanneau, A. and Arnaud, H. (1990). Hauterivian to Lower Aptian carbonate shelf sedimentation and sequence stratigraphy in the Jura and northern Subalpine chains (southeastern France and Swiss Jura). Carbonate Platforms: Facies, Sequences and Evolution. M. E. Tucker, J. L. Wilson,

P. D. Crevello, J. R. Sarg and J. F. Read, Blackwell Scientific Publications, Special Publication of the International Association of Sedimentologists. **9:** 203-233.

Baumberger, E. (1901). "Uber Facies und Transgressionen der untern Kreid am Nordrande mediterrano - helvetischen Bucht im westlichen Jura." Wiss. Beil. Ber. Töchterschule Basel: 1-44.

Charollais, J., Clavel, B., Schroeder, R., Busnardo, R., Decrouez, D. and Cherchi, A. (2003). "La migration de la plate-forme urgonienne entre le Jura plissé et les Chaines subalpines septentrionales (France, Suisse): Evolution of the Urgonian platform between the Jura and the Septentrional Subalpine Chains (France, Switzerland)." Geobios **36**(6 SU -): 665-674.

Clavel, B., Charollais, J., Schroeder, R. and Busnardo, R. (1995). "Réflexions sur la biostratigraphie du Crétacé inférieur et sur sa complémentarité avec l'analyse séquentielle: exemple de l'Urgonien jurassien et subalpin." Bull. Soc. géol. France **166**(6): 663-680.

Jenkyns, H. C. and Wilson, P. A. (1999). "Stratigraphy, paleoceanography, and evolution of Cretaceous pacific guyots: relics from a greenhouse Earth." American Journal of Science **299**: 341-392.

Renevier, E. (1874). "Tableau des terrains sédimentaires formés pendant les époques de la phase organique du globe terrestre avec leurs représentants en Suisse et dans les régions classiques, leurs synonymes et les principaux fossiles de chaque étage." Bull. Soc. vaud. Sci. nat. **13**: 218-252.

Wermeille, S., 1996, Etude sédimentologique, minéralogique et micropaléontologique des calcaires urgoniens de la région subalpine (Savoie, France). Coupes du Rocher de Cluses, du Borne et d'Andey: Unpublished diploma thesis, thesis, University of Neuchâtel, Neuchâtel, 129 p.

Abstract for the Réunion spécialisée de la société Géologique de France "Histoire et dynamique des plates-formes carbonatées et de leurs biotas durant le Phanérozoïque - Journées Jean Philip", 18th-19th May 2006, Marseille, France. *Oral Presentation*